

9 NOVEMBER 1966

FINAL STUDY REPORT
(MAY THROUGH NOVEMBER 1966)
CONTRACT NO. NASW-1410

VOLUME I

BOOK 3

AN ADVANCED STUDY OF AN APPLICATION
TECHNOLOGY SATELLITE (ATS-4) MISSION

NATIONAL AERONAUTICS AND SPACE ADMINISTRATION
GODDARD SPACE FLIGHT CENTER
GREENBELT, MARYLAND

FACILITY FORM 802

N67-24603

(ACCESSION NUMBER)

468

(PAGES)

CR-81766

(NASA CR OR TMX OR AD NUMBER)

(THRU)

1

(CODE)

31

(CATEGORY)

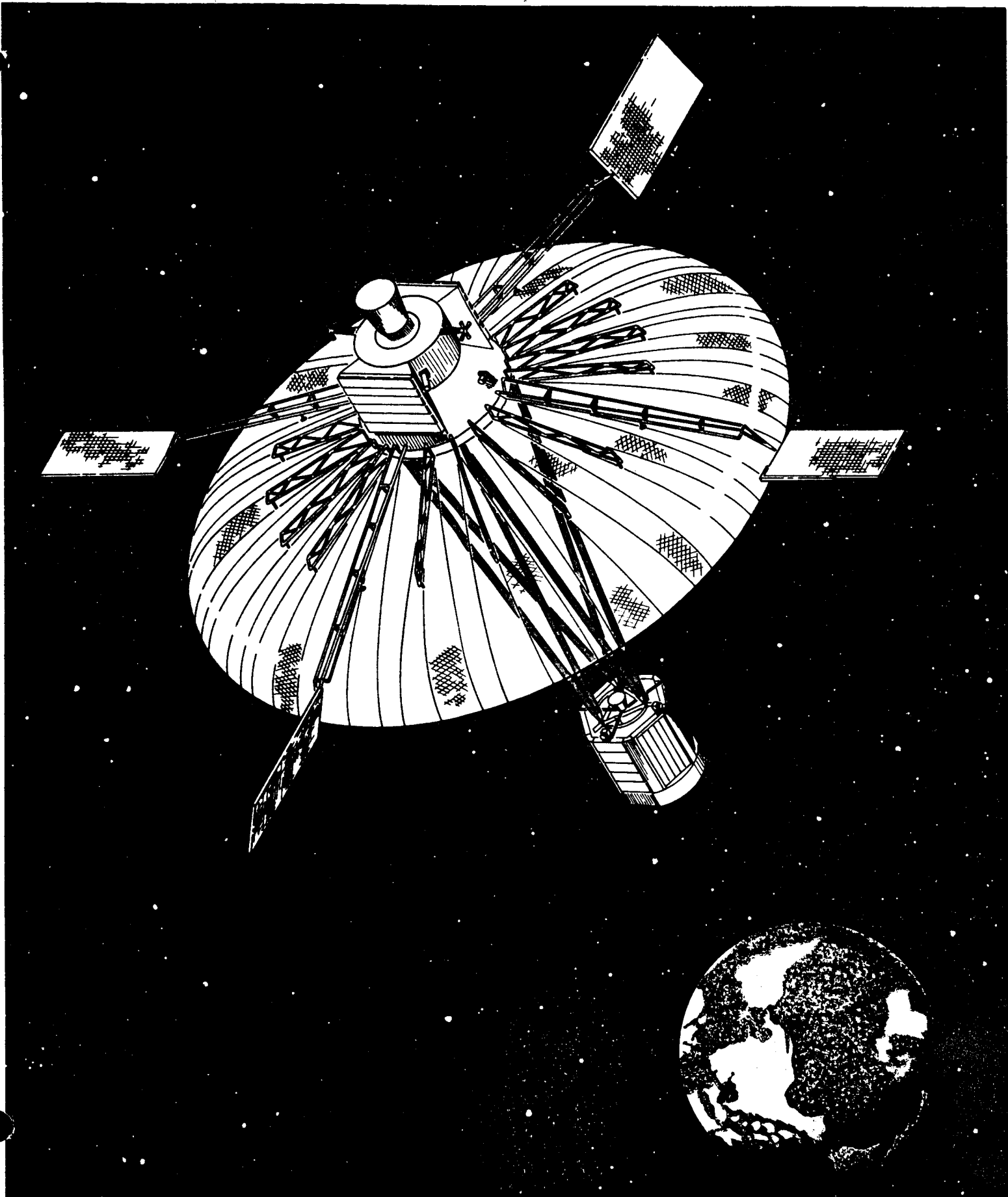


TABLE OF CONTENTS

VOLUME I BOOK 1

<u>Section</u>	<u>Page</u>
1 INTRODUCTION	1-1
2 PROJECT OBJECTIVES	2-1
3 PROJECT FEASIBILITY	3-1
4 EXPERIMENT DESCRIPTION AND JUSTIFICATION	4-1
4.1 General	4-1
4.2 Parabolic Antenna Experiment	4-3
4.2.1 Mechanical	4-3
4.2.2 Electrical	4-4
4.3 Orientation Control Experiment	4-11
4.4 Phased Array Experiment	4-5
4.5 Interferometer Experiment	4-6
4.6 Secondary Experiments	4-7
5 SPACECRAFT DESCRIPTION	5-1
5.1 Introduction	5.1-1
5.2 Operational Concept	5.2-1
5.2.1 Mission Requirements and Constraints	5.2-1
5.2.2 Launch Vehicle and Apogee Motor Selection	5.2-2
5.2.3 Mission Profile	5.2-3
5.2.4 Payload Capability	5.2-5
5.3 System Summary	5.3-1
5.3.1 Configuration Description	5.3-1
5.3.2 Subsystem Summary	5.3-9
5.3.2.1 Power Subsystem	5.3-10
5.3.2.2 Guidance and Control Subsystem	5.3-13
5.3.2.3 TT&C Subsystem	5.3-15
5.3.2.4 Experiments Subsystem	5.3-15
5.3.2.5 Thermal Subsystem	5.3-16
5.3.2.6 Module Interface	5.3-17
5.3.3 System Performance	5.3-18
5.3.3.1 Parabolic Antenna Experiment	5.3-18
5.3.3.2 Orientation Control Experiment	5.3-19
5.3.3.3 Phased Array and Interferometer	5.3-21
5.3.3.4 Command and Telemetry Subsystem	5.3-24
5.3.3.5 Power Subsystem Capability	5.3-25
5.3.3.6 Spacecraft Weight and Balance	5.3-25

TABLE OF CONTENTS (Cont'd)

<u>Section</u>	<u>Page</u>
5.3.4 System Growth Capability	5.3-29
5.4 Parabolic Antenna	5.4-1
5.4.1 Selection of Antenna Concept	5.4-1
5.4.2 Description of Selected Design	5.4-2
5.4.2.1 Reflector and Feed	5.4-2
5.4.2.2 Packaging	5.4-7
5.4.2.3 Deployment	5.4-11
5.4.3 Antenna Performance	5.4-12
5.4.4 Reflector Design	5.4-15
5.4.4.1 Method of Construction	5.4-15
5.4.4.2 Material Selection.	5.4-23
5.4.4.3 Structural Considerations	5.4-28
5.4.4.4 Stowage and Deployment Behavior	5.4-30
5.4.4.5 Performance in 1-g Environment.	5.4-31
5.4.4.6 Spacecraft Interface	5.4-31
5.4.5 Deployment Mechanism Design	5.4-33
5.4.6 Feed Design.	5.4-34
5.4.7 Thermal Design	5.4-36
5.5 Guidance and Control	5.5-1
5.5.1 Summary.	5.5-1
5.5.2 Functional Description	5.5-9
5.5.2.1 Station Acquisition Modes	5.5-9
5.5.2.2 Orientation	5.5-25
5.5.2.3 Orientation Control Operational Modes.	5.5-34
5.5.2.4 Station Capture and Station Change	5.5-42
5.5.2.5 Restabilization.	5.5-45
5.5.3 Component Description	5.5-45
5.5.3.1 Spinup Motors	5.5-48
5.5.3.2 Coning Control Accelerometer.	5.5-48
5.5.3.3 Precession Control Sun Sensor	5.5-49
5.5.3.4 Precession Control Rf POLANG Measurement	5.5-49
5.5.3.5 Station Acquisition Sensor Signal Processor	5.5-51
5.5.3.6 Station Acquisition and Despin Mass Expulsion Subsystem	5.5-51
5.5.3.7 Three Axis Gyro Package	5.5-58
5.5.3.8 Orientation Control Sun Sensors	5.5-60
5.5.3.9 Earth Sensor	5.5-64
5.5.3.10 Polaris Star Sensor	5.5-68
5.5.3.11 Orientation Control Sensor Signal Processor.	5.5-70
5.5.3.12 Flywheel and Jet Controller	5.5-70
5.5.3.13 Mechanical Flywheel.	5.5-70
5.5.3.14 Orientation Control and Stationkeeping Mass Expulsion Subsystem	5.5-73

TABLE OF CONTENTS (Cont'd)

<u>Section</u>	<u>Page</u>
5.5.4 Command, Telemetry, and Programmer Interface	5.5-77
5.5.4.1 Commands	5.5-77
5.5.4.2 Telemetry	5.5-77
5.5.4.3 Programmer	5.5-80
5.5.5 Mounting and Field of View Interface	5.5-81
5.6 Experiment Equipment.	5.6-1
5.6.1 General	5.6-1
5.6.2 Parabolic Antenna.	5.6-2
5.6.2.1 General	5.6-2
5.6.2.2 Electronics and RF Equipment	5.6-4
5.6.2.3 Geometric Instrumentation.	5.6-11
5.6.3 Orientation Control System.	5.6-14
5.6.4 Interferometer Experiment.	5.6-15
5.6.4.1 Introduction.	5.6-15
5.6.4.2 Basis of System Selection	5.6-16
5.6.4.3 Interferometer Fundamentals	5.6-17
5.6.4.4 Detailed Interferometer Design	5.6-21
5.6.4.5 Weight and Power Estimates	5.6-26
5.6.4.6 Thermal Effects	5.6-27
5.6.5 Phase-Steered Array Antenna.	5.6-28
5.7 Telemetry, Tracking and Command	5.7-1
5.7.1 System Requirements	5.7-1
5.7.2 Reference Design Summary	5.7-1
5.7.3 Command Subsystem Operation	5.7-5
5.7.3.1 Star Tracker Memory	5.7-11
5.7.4 Telemetry Subsystem	5.7-12
5.7.4.1 Telemetry Monitor Requiring Additional Circuitry.	5.7-13
5.7.5 Tracking Subsystem Operation	5.7-14
5.7.6 TT&C Antennas	5.7-16
5.7.6.1 Antenna Coverage.	5.7-16
5.7.6.2 Antenna Design.	5.7-18
5.7.7 Margin Calculations	5.7-22
5.7.8 Implementation of Redundancy.	5.7-27
5.7.9 Power, Weight and Size Summary	5.7-27
5.8 Power	5.8-1
5.8.1 Requirements	5.8-1
5.8.1.1 Launch Load Profiles and Spacecraft Sun-orientation.	5.8-1
5.8.1.2 Orbit Load Profile and Spacecraft Sun-orientation.	5.8-3
5.8.2 Subsystem Description	5.8-6

TABLE OF CONTENTS (Cont'd)

<u>Section</u>		<u>Page</u>
	5.8.2.1 Subsystem Selection	5.8-6
	5.8.2.2 Subsystem Block Diagram	5.8-8
	5.8.2.3 General Operational Characteristics	5.8-10
	5.8.2.4 Solar Array Capability	5.8-11
	5.8.2.5 Battery Capability.	5.8-20
	5.8.2.6 Subsystem Efficiency and Margins	5.8-21
	5.8.2.7 Operational Flexibility	5.8-21
	5.8.2.8 Growth Capability	5.8-22
5.8.3	Component Descriptions.	5.8-22
	5.8.3.1 Solar Array.	5.8-22
	5.8.3.2 Batteries.	5.8-29
	5.8.3.3 Voltage Limiter	5.8-30
	5.8.3.4 Battery Charge Regulator	5.8-31
	5.8.3.5 PWM Regulator.	5.8-31
	5.8.3.6 Inverter	5.8-32
	5.8.3.7 Power Control Unit	5.8-32
	5.8.3.8 Summary of Component Characteristics	5.8-32
5.9	Spacecraft Design	5.9-1
	5.9.1 Introduction.	5.9-1
	5.9.2 Launch Phase and Orbital Constraints	5.9-2
	5.9.2.1 Launch Vehicle Constraints	5.9-2
	5.9.2.2 Coast Apogee Firing and Orbital Injection Constraints	5.9-10
	5.9.2.3 Orbital Constraints	5.9-20
5.9.3	Spacecraft Structural Design	5.9-21
	5.9.3.1 Earth Viewing Equipment Module.	5.9-24
	5.9.3.2 Feed Support Truss	5.9-29
	5.9.3.3 Aft Equipment Module	5.9-34
	5.9.3.4 Solar Array Panels and Support Trusses	5.9-36
	5.9.3.5 Spacecraft Adapter	5.9-37
	5.9.3.6 Structure Weight Summary.	5.9-38
5.9.4	Separation and Deployment.	5.9-38
	5.9.4.1 Solar Panel Stowage and Deployment	5.9-38
	5.9.4.2 Combined Purpose Antenna Deployment	5.9-44
	5.9.4.3 Spacecraft/Booster Separation System	5.9-44
5.9.5	Structural Dynamic Considerations	5.9-48
	5.9.5.1 Introduction.	5.9-48
	5.9.5.2 Launch Configuration Behavior	5.9-48
	5.9.5.3 Effect of Structural Damping on Cone Angle	5.9-53
	5.9.5.4 Orbital Configuration Behavior	5.9-53

TABLE OF CONTENTS (Cont'd)

Section

Page

5.9.6	Thermal Control	5.9-58
5.9.6.1	Summary of Selected Configuration	5.9-58
5.9.6.2	Equipment Mounting	5.9-59
5.9.6.3	Semipassive Temperature Control	5.9-59
5.9.6.4	Passive Temperature Control	5.9-61
5.9.6.5	Configuration Thermal Analysis	5.9-62

TABLE OF CONTENTS

VOLUME I BOOK 2

<u>Section</u>	<u>Page</u>
6 SPACECRAFT TRADEOFF AND ANALYSIS.	6.1-1
6.1 Introduction	6.1-1
6.2 Configuration Selection	6.2-1
6.2.1 Approach to Configuration Selection	6.2-1
6.2.2 Launch Vehicle Considerations	6.2-5
6.2.2.1 Atlas/Agena-D Launch Vehicle	6.2-9
6.2.2.2 TITAN III-C Launch Vehicle	6.2-10
6.2.2.3 SLV3C/Centaur Launch Vehicle	6.2-11
6.2.3 Early Conceptual Designs	6.2-22
6.2.3.1 First Stage Designs	6.2-23
6.2.3.2 Major Tradeoffs	6.2-27
6.2.3.3 Second Stage Designs.	6.2-35
6.2.4 Third Stage Designs	6.2-41
6.2.5 Deployed Configuration	6.2-48
6.2.5.1 Structural Considerations	6.2-52
6.2.5.2 Equipment Module Deployment	6.2-56
6.2.6 Alternate Fixed Feed Configuration	6.2-66
6.2.6.1 Alternate Solar Panel Stowage Arrangement	6.2-68
6.2.6.2 Aft Equipment Module Design	6.2-73
6.2.6.3 Apogee Motor Packaging Provisions.	6.2-73
6.3 Paraboloid Antenna	6.3-1
6.3.1 Rationale for Selected Reflector Concept	6.3-1
6.3.1.1 Antenna Requirements	6.3-1
6.3.1.2 Survey of Potential Reflector Concepts	6.3-1
6.3.2 Design Studies of Selected Concept	6.3-26
6.3.2.1 Paraboloid Reflector Configuration	6.3-26
6.3.2.2 Thermal Considerations.	6.3-50
6.3.3 Design Analysis of Selected Configuration	6.3-65
6.3.3.1 Design Criteria	6.3-65
6.3.3.2 Structural Analysis	6.3-67
6.3.3.3 Deployment Analysis.	6.3- 8
6.3.3.4 Dynamic Analysis.	6.3-99
6.3.4 Thermal Distortion Analysis	6.3-104
6.3.4.1 Introduction.	6.3-104
6.3.4.2 Thermal Analysis.	6.3-104
6.3.4.3 Structural Deformation	6.3-105
6.3.5 RF Performance Analysis	6.3-132
6.3.5.1 Introduction.	6.3-132

TABLE OF CONTENTS (Cont'd)

<u>Section</u>		<u>Page</u>
	6.3.5.2 Feed Configuration Studies	6.3-136
	6.3.5.3 Selected Feed Configuration	6.3-144
	6.3.5.4 Monopulse	6.3-146
	6.3.5.5 Beam Steering	6.3-147
	6.3.5.6 RF Loss Budget Cassegrain vs Prime Focus . .	6.3-153
	6.3.5.7 Additional Strut Loss.	6.3-157
	6.3.5.8 Thermal Distortion Loss	6.3-170
	6.3.5.9 RF Loss Budget-Final	6.3-171
	6.3 5.10 References for Section 6	6.3-172
6.4	Guidance and Control	6.4-1
6.4.1	Summary.	6.4-1
6.4.2	Tradeoff Analysis.	6.4-4
6.4.2.1	Spacecraft Configuration Considerations . . .	6.4-4
6.4.2.2	Earth Sensor/Star Trackers	6.4-6
6.4.2.3	Three Axis Control/Spin Stabilization During Station Acquisition Sequence	6.4-8
6.4.2.4	Polaris Star Sensor/Gyrocompassing	6.4-9
6.4.2.5	Momentum Storage Devices	6.4-11
6.4.2.6	On-Off/Proportional Flywheel Control	6.4-15
6.4.2.7	Spacecraft Orientation During Vernier Thrusting	6.4-16
6.4.2.8	Yaw/Roll Axis Stabilization to the Sun	6.4-17
6.4.2.9	Orientation Control/Stationkeeping Mass Expulsion Subsystem.	6.4-18
6.4.2.10	Accelerometer/Gryo for Coning Control	6.4-31
6.4.2.11	Sattion Acquisition and Despin Mass Expulsion Subsystem.	6.4-34
6.4.2.12	Spinup Motor	6.4-42
6.4.3	Design Analysis	6.4-46
6.4.3.1	Transfer Orbit Disturbance Torques	6.4-47
6.4.3.2	On-Station Disturbance Torques	6.4-52
6.4.3.3	Control Static and Dynamic Performance Analysis	6.4-68
6.4.3.4	Earth Pointing Error Analysis	6.4-113
6.5	TT & C Subsystem Tradeoffs and Analysis	6.5-1
6.5.1	VHF vs S-Band Communication Link	6.5-1
6.5.2	Tracking Analysis.	6.5-3
6.5.3	Antenna Configuration Tradeoff	6.5-7
6.5.4	Analysis of Memory Requirements	6.5-11
6.6	Power	6.6-1
6.6.1	Radiation Environment Requirements	6.6-1
6.6.1.1	Trapped Radiation	6.6-1
6.6.1.2	Solar Cosmic Radiation	6.6-2
6.6.1.3	Primary Galactic Cosmic Rays	6.6-4

TABLE OF CONTENTS (Cont'd)

<u>Section</u>	<u>Page</u>
6.6.2 Energy Source Selection	6.6-5
6.6.3 Array Configuration Selection	6.6-6
6.6.3.1 Array Location on Vehicle	6.6-6
6.6.3.2 Array Configuration Studies	6.6-19
6.6.3.3 Comparison of Four-Panel Configuration with Two-Panel Configuration	6.6-30
6.6.4 Array Design	6.6-33
6.6.4.1 Array Sizing and Performance	6.6-33
6.6.4.2 Solar Cell Selection	6.6-33
6.6.4.3 Solar Cell Characteristics	6.6-35
6.6.4.4 Solar Cell Loss Analysis	6.6-35
6.6.4.5 Solar Cell Radiation Degradation Analysis.	6.6-38
6.6.4.6 Cover Thickness Selection	6.6-40
6.6.4.7 Launch Array Power Analysis.	6.6-42
6.6.5 Batteries.	6.6-43
6.6.5.1 Requirements	6.6-43
6.6.5.2 Selection of Battery Type	6.6-43
6.6.5.3 Method of Sizing	6.6-44
6.6.5.4 Effect of Two Paddles Versus Four Paddles	6.6-45
6.6.5.5 Effect of Load Timing on Batteries	6.6-45
6.6.5.6 Battery Description	6.6-47
6.6.5.7 Battery Performance Summary	6.6-47
6.6.6 Power Subsystem Analysis.	6.6-50
6.6.6.1 Power Distribution Selection (DC versus AC).	6.6-50
6.6.6.2 Power Conditioning Equipment Selection	6.6-52
6.6.6.3 Selected Power Subsystem Performance	6.6-61
6.6.7 References	6.6-66
6.7 Spacecraft Design	6.7-1
6.7.1 Structural Analysis	6.7-1
6.7.1.1 Critical Loading	6.7-2
6.7.1.2 Preliminary Design Philosophy	6.7-3
6.7.1.3 Methods of Analysis	6.7-3
6.7.1.4 Selected Configuration Design Rationale and Tradeoffs	6.7-5
6.7.2 Separation and Deployment.	6.7-48
6.7.2.1 Design Criteria	6.7-48
6.7.2.2 Deployment Mechanism Selection.	6.7-48
6.7.2.3 Spacecraft/Booster Separation System	6.7-55
6.7.3 Structural Dynamics	6.7-58
6.7.3.1 Design Criteria	6.7-58
6.7.3.2 Dynamic Environment	6.7-59
6.7.3.3 Methods of Analysis	6.7-61
6.7.3.4 Configuration Selection Support Studies.	6.7-67

TABLE OF CONTENTS (Cont'd)

<u>Section</u>	<u>Page</u>
6.7.4 Electronic Packaging	6.7-88
6.7.4.1 Design Criteria	6.7-88
6.7.4.2 Selected Configurations	6.7-89
6.7.4.3 Alternate Approaches	6.7-91
6.7.4.4 Areas for Further Study.	6.7-96
6.8 Apogee Motor Selection	6.8-1
6.8.1 Introduction.	6.8-1
6.8.2 Apogee Motor Requirements	6.8-2
6.8.3 Apogee Motor Selection - SLV-3A/Agena D	6.8-3
6.8.4 Apogee Motor Selection - SLV-3C/Centaur	6.8-5
6.8.4.1 Final Apogee Motor Selection Tradeoffs for the SLV-3C/Centaur	6.8-11
6.8.4.2 Recommended Apogee Motor for the Atlas/ Centaur Configuration	6.8-13
6.8.4.3 Surveyor Motor Development Requirements	6.8-13

TABLE OF CONTENTS

VOLUME I

BOOK 3

<u>Section</u>	<u>Page</u>
7 FLIGHT DYNAMICS	7-1
7.1 Introduction	7-1
7.2 Reference Design Sequence of Events - Summary.	7-2
7.2.1 Launch Trajectory - General	7-2
7.2.2 Booster/Launch Phase	7-2
7.2.3 Initial/Acquisition Phase	7-5
7.3 Operating Longitude Evaluation.	7-7
7.4 Ascent Trajectory Selection.	7-9
7.4.1 Trajectory Influencing Parameters	7-9
7.4.2 Launch Vehicle Constraints	7-13
7.4.3 Trajectory Selection	7-13
7.5 Initial Acquisition Phase Analyses.	7-15
7.5.1 Spin-Up Motors	7-16
7.5.2 Transfer Trajectory Analysis.	7-16
7.5.2.1 Plane Change Velocity Requirements	7-16
7.5.2.2 Apogee Motor Payload Analysis	7-18
7.5.2.3 Reference Design Orbit Characteristics	7-24
7.5.3 Vernier Velocity Requirements	7-26
7.5.3.1 Reference Design Vernier Velocity Requirements	7-26
7.5.3.2 Preliminary Velocity Requirements Analysis	7-31
7.5.3.3 Injection Bias Analysis	7-46
7.5.3.4 Despin	7-53
7.6 Initial Stabilization and Deployment	7-54
7.7 Synchronous Orbit Stationkeeping Requirements	7-54
7.7.1 Dynamics	7-55
7.7.1.1 Nominal Orbit	7-55
7.7.1.2 Perturbations	7-60
7.7.2 Velocity Requirements	7-63
7.7.2.1 East-West	7-63
7.7.2.2 North-South.	7-65
7.7.3 Tracking for Orbit Determination	7-65
7.8 Operational System.	7-70
7.8.1 Launch and Parking Orbit	7-70
7.8.1.1 Atlas Flight Phase	7-70
7.8.1.2 Centaur Separation	7-70
7.8.1.3 Launch-to-Injection Operations	7-70
7.8.1.4 Perigee Burn	7-71

TABLE OF CONTENTS (Cont'd)

<u>Section</u>	<u>Page</u>
7.8.2 Transfer Orbit	7-71
7.8.3 Vernier Maneuvers	7-73
7.8.4 Despin, Deployment, and Initial Stabilization	7-74
7.8.5 Final Station Acquisition	7-76
7.8.6 Operational Systems Contingency Planning	7-76
8 EXPERIMENT OPERATIONAL PHASE SEQUENCE.	8.1-1
8.1 General	8.1-1
8.2 Experiment Axes Reference	8.2-1
8.3 Parabolic Antenna	8.3-1
8.3.1 General Discussion	8.3-1
8.3.2 Technical Background of Measurements	8.3-2
8.3.2.1 Introduction.	8.3-2
8.3.2.2 Direction and Gain	8.3-2
8.3.3 Selection of Parameters	8.3-7
8.3.3.1 General	8.3-7
8.3.3.2 In-Space Measurements.	8.3-8
8.3.3.3 Ground Testing	8.3-9
8.3.4 In-Space Measurement Techniques	8.3-11
8.3.4.1 Gain	8.3-11
8.3.4.2 Antenna Geometry Measurements	8.3-12
8.3.4.3 Boresight	8.3-13
8.3.5 Experiments	8.3-19
8.3.5.1 Listing of Experiments	8.3-19
8.3.5.2 Basic Electrical Measurements	8.3-25
8.3.5.3 Basic Geometric Measurements	8.3-33
8.3.5.4 Supporting Electrical Measurements	8.3-37
8.3.6 Derivation of Equipment Requirements.	8.3-40
8.3.6.1 Electrical Measurements Experiments Equipment	8.3-40
8.3.6.2 Geometric Measurement Experiment Equipment	8.3-54
8.3.6.3 Summary of Required Equipment.	8.3-55
8.4 Orientation Control System	8.4-1
8.4.1 General Discussion	8.4-1
8.4.2 Listing of Experiments	8.4-3
8.4.3 Basic Experiments	8.4-5
8.4.3.1 General	8.4-5
8.4.3.2 Pointing Performance	8.4-5
8.4.3.3 Tracking Performance	8.4-8
8.4.4 Equipment Requirements	8.4-10
8.5 Interferometer	8.5-1
8.5.1 General	8.5-1
8.5.2 Listing of Experiments	8.5-2

TABLE OF CONTENTS (Cont'd)

<u>Section</u>	<u>Page</u>
8.5.3 Basic Experiments	8.5-4
8.5.3.1 General	8.5-4
8.5.3.2 Experiment I-1 - Verification of Operation	8.5-5
8.5.3.3 Experiments I-2 and I-3 - Internal Parameter Measurements	8.5-7
8.5.3.4 Experiment I-4 - Angle Error Measurement - Medium Accuracy	8.5-10
8.5.3.5 Experiment I-5 - Angle Error Measurement - High Accuracy	8.5-12
8.5.3.6 Experiment I-6 - Field of View	8.5-14
8.5.3.7 Experiment I-8 - Angle Difference Measurement	8.5-16
8.5.3.8 Experiment I-11 - Spacecraft Pointing	8.5-18
8.5.3.9 Experiment I-13 - System Life Verification	8.5-19
8.5.3.10 Experiment I-18 - Thermal Cycle Monitoring	8.5-21
8.5.4 Derivation of Equipment Requirements	8.5-23
8.6 Phase-Steered Array Antenna	8.6-1
8.6.1 General	8.6-1
8.6.2 Technical Background of Measurements	8.6-1
8.6.2.1 General	8.6-1
8.6.2.2 Component Similarity	8.6-2
8.6.2.3 Impedance Match	8.6-2
8.6.2.4 Physical Geometry	8.6-3
8.6.2.5 Radiation Characteristics	8.6-3
8.6.3 Parameter Selection	8.6-4
8.6.3.1 General	8.6-4
8.6.3.2 Internal Parameters	8.6-5
8.6.3.3 Gain	8.6-5
8.6.3.4 Beam Pointing Direction	8.6-5
8.6.4 Experiments	8.6-6
8.6.4.1 List of Experiments	8.6-6
8.6.4.2 Basic Electrical Measurements	8.6-11
8.6.5 Derivation of Equipment Requirements	8.6-20
8.7 Supplementary Experiments	8.7-1
8.7.1 General	8.7-1
8.7.2 Prime Experiment Augmentation	8.7-1
8.7.2.1 Parabolic Antenna Geometric Instrumentation	8.7-1
8.7.2.2 Parabolic Antenna Ultra-Wide Band Communications	8.7-2
8.7.2.3 Parabolic Antenna Side Lobe Measurement	8.7-2
8.7.2.4 Polarization Measurements from the Parabolic Antenna	8.7-2
8.7.2.5 Monopulse Installation	8.7-3

TABLE OF CONTENTS (Cont'd)

<u>Section</u>	<u>Page</u>
8.7.2.6 Phase-Steered Array Monitoring	8.7-5
8.7.2.7 Interferometer Yaw Axis Stabilization	8.7-5
8.7.2.8 Synthetic Angle Generation.	8.7-6
8.7.2.9 Interferometer Transmit Mode	8.7-8
8.7.3 Prime Experiment Applications	8.7-9
8.7.3.1 High Data Rate Meteorological Sensor	8.7-9
8.7.3.2 FM and TV Direct Broadcast	8.7-13
8.7.3.3 Navigation and Air and Ship Traffic Control	8.7-21
8.7.3.4 Communications with Low-Orbit Spacecraft	8.7-22
8.7.3.5 Multiple Access Communications Satellite	8.7-25
8.7.4 Passenger Experiments.	8.7-26
8.7.4.1 Millimeter Communications and Transmission	8.7-27
8.7.4.2 Laser Communications and Transmission.	8.7-28
8.7.4.3 Earth Radiation Measurements	8.7-28
8.8 Operational System for Experiments	8.8-1
8.8.1 General	8.8-1
8.8.2 Experiment Operational System Requirements	8.8-2
8.8.2.1 Operational Flow	8.8-2
8.8.2.2 ATS-4 Ground Station Operational and Experi- mental Capability Requirements	8.8-5
8.8.3 Experiment Control	8.8-12
8.8.4 Data Acquisition, Processing and Display.	8.8-21
8.8.5 Contingency Planning.	8.8-24
8.8.6 Reporting	8.8-24
 9 SUPPORT OPERATIONS	 9-1
9.1 Introduction	9-1
9.2 Summary	9-1
9.3 Equipment Requirements.	9-1
9.4 Mechanical Support Equipment (MSE)	9-1
9.4.1 Scope	9-1
9.4.2 Study Approach.	9-5
9.4.3 Mechanical Support Concepts	9-5
9.4.3.1 Vehicle Assembly and Handling	9-5
9.4.3.2 Alignment Equipment and Deployed Antenna Measurements	9-7
9.4.3.3 Mass Properties, Spin Balance and Apogee Thrust Vector Alignment	9-7
9.4.3.4 Deployment.	9-9
9.4.3.5 Pneumatic and Fuel Servicing and Leak Testing.	9-10
9.4.3.6 Vibration	9-10

TABLE OF CONTENTS (Cont'd)

<u>Section</u>	<u>Page</u>
9.4.3.7 Structural Static Test	9-11
9.4.3.8 Spin Test	9-11
9.4.3.9 Acoustics Test	9-12
9.4.3.10 RF Compatibility Tests	9-12
9.4.3.11 Thermal-Vacuum Tests.	9-12
9.4.3.12 Attitude Control Demonstration	9-13
9.4.3.13 Transportation and Shipping	9-13
9.4.4 Equipment and Complexity Appraisal	9-14
9.5 Electrical Support Equipment (ESE)	9-16
9.5.1 Scope	9-16
9.5.2 Approach.	9-16
9.5.2.1 General	9-16
9.5.2.2 Fail Safe.	9-16
9.5.2.3 Human Factors	9-16
9.5.2.4 Isolation.	9-16
9.5.2.5 Accuracy.	9-16
9.5.2.6 Parts.	9-17
9.5.2.7 Use of Telemetry Subsystems for Testing	9-17
9.5.3 Electrical Support Concepts	9-17
9.5.3.1 General	9-17
9.5.3.2 Subsystem Tests	9-17
9.5.3.3 Earth Viewing Equipment Module Tests	9-18
9.5.3.4 Aft Equipment Module Testing	9-18
9.5.3.5 System Tests	9-18
9.5.3.6 Thermal Vacuum Tests.	9-19
9.5.3.7 RF.	9-19
9.5.3.8 Pad	9-19
9.5.4 Equipment List	9-19
9.6 Test Facilities	9-20
9.6.1 Test Facility Support.	9-20
9.6.2 Test Facility Problem Areas	9-20
9.6.2.1 Vibration, Deployed	9-20
9.6.2.2 Large Antenna RF Testing.	9-24
9.7 Launch Facilities	9-24
9.7.1 Mechanical Support Operations	9-24
9.7.2 Existing Launch Facilities	9-25
9.8 Orbital Support	9-28
9.9 Software	9-32

Appendix A.	Parabolic Reflector Feed Selection Charts	A-1
Appendix B.	Launch Window Restriction Due to Precession Control Sun Sensors	B-1
Appendix C.	Transfer Orbit Disturbance Torque Analysis	C-1
Appendix D.	On-Station Disturbance Torque Analysis	D-1
Appendix E.	Mathematical Model for Orientation Control Servo Analysis	E-1
Appendix F.	Stability Investigation and Pointing Error Analysis of the Three-Axis Star Tracker System	F-1
Appendix G.	Solar Array Computer Program	G-1
Appendix H.	Radiation Effects on Silicon Solar Cells	H-1
Appendix I.	Basic Design Data for Subsystem Comparison	I-1
Appendix J.	Coupling of Structural Flexibility with a Control System Feedback Loop	J-1
Appendix K.	Coning Control	K-1
Appendix L.	Elements of Monopulse	L-1
Appendix M.	Plume Calculations for Walter Kidde Two-Pound Thrust Nozzle and for a Resistance Jet Ammonia Nozzle	M-1

TABLE OF CONTENTS
VOLUME II
PRELIMINARY PROGRAM PLAN

Section		Page
1	INTRODUCTION	1-1
2	PROJECT SCHEDULE	2-1
2.1	Introduction	2-1
2.2	Phased Project Planning	2-1
2.3	Overall Schedule	2-12
2.4	Schedule of AGE Utilization	2-14
2.5	Long Lead Items	2-15
3	ENGINEERING DEVELOPMENT	3-1
3.1	Introduction	3-1
3.2	Development Problem Areas	3-1
3.2.1	Parabolic Antenna Development	3-2
3.2.2	Spacecraft Structure	3-3
3.2.2.1	Ascent Environment Design	3-3
3.2.2.2	Orbital Environment Design	3-4
3.2.3	Thermal Environment Control	3-4
3.2.3.1	The Earth Viewing Module	3-5
3.2.3.2	Aft Equipment Module	3-5
3.2.4	Electrical Power and Distribution	3-6
3.2.4.1	Batteries	3-6
3.2.4.2	Power Profile	3-7
3.2.5	Attitude Sensing and Control	3-7
3.2.5.1	IR Sensor and Star Tracker	3-7
3.2.5.2	Ground Station - Orientation Control Interface	3-8
3.2.5.3	Attitude Control During Initial Acquisition	3-9
3.2.5.4	Long Life Reliability	3-10
3.2.5.5	Orientation Control System Operational Ground Test	3-10
3.2.6	Telemetry Tracking and Command	3-10
3.2.7	Propulsion	3-10
3.2.7.1	Vernier Propulsion Unit	3-11
3.2.7.2	Stationkeeping System	3-11
3.2.8	Operational Experiments	3-12
3.2.8.1	Parabolic Antenna Experiment	3-12
3.2.8.2	Phased Steered Array Experiment	3-15
3.2.8.3	Interferometer Experiment	3-16
3.2.8.4	Orientation Control Experiment	3-18

TABLE OF CONTENTS (Cont'd)

Section	Page
3.2.9 Ground Station Operation and Data Analysis	3-20
3.2.9.1 Determination of Experiment Down Link Equipment and Functions to be Provided at Each ATS-4 Station	3-20
3.2.9.2 Data Acquisition, Logistics, Merging, Storage	3-20
3.2.9.3 Attitude Determination During Transfer Orbit, Apogee Burn and Achievement of Synchronous Orbit	3-21
3.2.9.4 Determination of Spacecraft and Experiment Axes Orientation During Flight	3-21
3.2.10 Ground Handling, Test and Checkout Equipment	3-22
3.3 Development Approach	3-22
3.3.1 Attitude Control Subsystem	3-23
3.3.2 Telemetry, Tracking and Command Subsystem	3-23
3.3.3 Propulsion Subsystem	3-23
3.3.4 Solar Arrays	3-24
3.3.5 Structure	3-24
3.3.6 Power Conditioning Equipment	3-25
3.3.7 Batteries	3-25
4 INTEGRATED TEST	4-1
4.1 Principal Features	4-1
4.2 Component Test	4-4
4.3 System Test	4-4
4.3.1 In-House System Tests	4-4
4.3.2 Field Tests	4-11
4.3.3 Development Test Hardware	4-11
4.3.3.1 Engineering Development Spacecraft	4-11
4.3.3.2 Structural Dynamic Model	4-12
4.3.3.3 Attitude Control Engineering Model	4-13
4.3.3.4 Parabolic Antenna Development Model	4-13
4.3.3.5 RF Antenna Models	4-13
4.3.3.6 Clearance Model	4-13
4.3.3.7 Harness Mockup	4-13
4.3.3.8 Vehicle Mockup	4-14
4.4 Summary	4-14
5 MANAGEMENT AND SUPPORT ASPECTS	5-1
5.1 Project Control	5-1

TABLE OF CONTENTS (Cont'd)

Section	Page
5.1.1	Uniform Project Control 5-2
5.1.2	Schedule Integration 5-4
5.1.3	Project Visibility 5-4
5.1.4	Interface Control 5-5
5.1.5	Approach 5-6
5.2	Configuration Management 5-7
5.2.1	Introduction 5-7
5.2.2	Guidelines 5-8
5.2.2.1	Configuration Identification 5-8
5.2.2.2	Configuration Control 5-9
5.2.2.3	Configuration Accounting 5-9
5.2.3	Requirements 5-10
5.2.4	Approach 5-10
5.2.5	Implementation 5-11
5.3	Data Management 5-12
5.3.1	Introduction 5-12
5.3.2	Approach 5-13
5.3.3	Requirements 5-13
5.3.4	Critical Areas 5-14
5.3.4.1	Data Identification 5-14
5.3.4.2	Acquisition, Storage and Retrieval 5-14
5.3.4.3	Timely and Accurate Input/Output 5-15
5.3.5	Implementation 5-15
5.4	Manufacturing/Facilities 5-16
5.4.1	Introduction 5-16
5.4.2	Manufacturing 5-16
5.4.2.1	In-Process Handling 5-17
5.4.2.2	Alignment of Critical Subsystems and Components 5-18
5.4.2.3	Solar Array Fabrication 5-20
5.4.3	Facilities 5-20
5.5	Procurement 5-20
5.5.1	Make or Buy 5-24
5.5.2	Source Selection 5-24
5.5.3	Subcontractor Management and Control 5-26
5.6	Product Assurance 5-26
5.6.1	Introduction 5-26
5.6.2	Problems 5-27
5.6.3	Approaches to Problem Solutions 5-27

TABLE OF CONTENTS (Cont'd)

Section	Page
5.6.3.1	Long Life System Requirements 5-27
5.6.3.2	Handling of Equipment 5-28
5.6.3.3	Traceability 5-29
5.6.3.4	Subcontractor and Associate Contractor Controls 5-30
5.7	Reliability 5-31
5.7.1	Introduction 5-31
5.7.1.1	Objective of the Program 5-31
5.7.1.2	Special Attention to the Long-Life Problem 5-32
5.7.2	Program Elements 5-32
5.7.3	Contractor/Customer Relationships 5-33
5.8	Safety 5-35
5.8.1	Introduction 5-35
5.8.2	Approach 5-36
5.8.3	Safety Plan Requirements 5-36
5.8.4	Associated Safety Program Requirements 5-37
5.8.5	Hazard Identification 5-38
5.9	Parts Program 5-39
5.9.1	Introduction 5-39
5.9.2	Parts Policy 5-39
5.9.3	Selection and Approval 5-40
5.9.3.1	Approved Lists 5-40
5.9.3.2	Standardization of Parts, Materials, and Processes 5-40
5.9.3.3	Qualification 5-41
5.9.3.4	Nonstandard Parts Approval 5-41
5.9.3.5	Use of Approved Lists 5-42
5.9.3.6	Parts and Materials Application Review 5-43
5.9.4	Parts Screening 5-43
5.9.4.1	Test Program 5-43
5.9.4.2	Typical Screening 5-44
5.9.5	Specifications 5-44
5.9.5.1	Standards 5-44
5.9.5.2	New Drawings 5-45
5.9.5.3	Document Approval 5-45
5.9.6	Product Engineering Standards 5-45
5.9.6.1	Design Standards 5-45
5.9.6.2	Process Standards 5-46
5.9.7	Failure Reporting and Analysis 5-46
5.9.8	Subcontractor Requirements and Controls 5-47
5.9.8.1	General 5-47
5.9.8.2	Parts Program 5-47
5.9.8.3	Subcontractor Parts Lists 5-47

TABLE OF CONTENTS (Cont'd)

Section		Page
6	COST	6-1
6.1	Cost Breakdown	6-1
6.2	Expenditure Rate	6-5
6.3	Phasing Alternatives	6-5
6.3.1	Four-Month Breakpoint	6-6
6.3.2	Six-Month Breakpoint	6-6
6.3.3	Eight-Month Breakpoint	6-6
6.3.4	Twelve-Month Breakpoint	6-7
6.3.5	Summary	6-8

LIST OF ILLUSTRATIONS

Figure		Page
5.2-1	ATS-4 Mission Sequence	5.2-4
5.3-1	Selected Configuration (Orbital View).	5.3-2
5.3-2	ATS-4 Selected Configuration, Inboard Profile and Orbital Configuration	5.3-5
5.3-3	ATS-4 System Block Diagram	5.3-11
5.3-4	ATS-4 Payload Growth.	5.3-30
5.4-1	Petaline Rigid Reflector Configuration	5.4-3
5.4-2	Deployment Drive Mechanism	5.4-5
5.4-3	Feed Configuration	5.4-7
5.4-4	Stowed Configuration	5.4-9
5.4-5	Reflector, Typical Sector	5.4-16
5.4-6	Panel Structure Composite	5.4-17
5.4-7	Deviation from True Contour	5.4-18
5.4-8	Configuration of Expanded Metal for RF Reflecting Material	5.4-19
5.4-9	Deployment Trusses	5.4-21
5.4-10	Interface Ring	5.4-25
5.4-11	Three-Foot Diameter Demonstration Model.	5.4-32
5.4-12	Composite Feed on Earth Viewing Equipment Module	5.4-34
5.4-13	Influence of Open Area on Antenna Design	5.4-37
5.4-14	ATS-4 Parabolic Antenna Temperature Distribution	5.4-38
5.4-15	Antenna Isotherms 39-90	5.4-39
5.5-1	ATS-4 Guidance and Control Subsystem Block Diagram.	5.5-4
5.5-2	Spacecraft Configuration -- Station Acquisition	5.5-11
5.5-3	Coning and Precession Control	5.5-12
5.5-4	Principle of Orientation Measurement	5.5-16
5.5-5	Sun Sensor	5.5-17
5.5-6	Rhumb Line Precession	5.5-19
5.5-7	ATS-4 Reference Design: Antenna Half-Beam Angle During Transfer Orbit	5.5-22
5.5-8	Impulse Requirement versus Spin Rate	5.5-24
5.5-9	Sun Acquisition	5.5-26
5.5-10	ATS-4 Configuration--Orientation Control	5.5-28
5.5-11	On-Station Orientation Control	5.5-32
5.5-12	Integrated Stationkeeping-Wheel Unloading Mass Expulsion System Control Logic	5.5-39
5.5-13	Thrust and Impulse Required for East-West Station Change	5.5-44
5.5-14	Spin Sun Sensor Output.	5.5-49
5.5-15	Polarized RF Antenna	5.5-50
5.5-16	Pulse Lengths for Various RPM's and θ 's	5.5-54
5.5-17	Effect on I_{sp} for Various Pulse Widths for Hydrazine	5.5-55
5.5-18	Radial Impulse Efficiency.	5.5-55
5.5-19	Station Acquisition System Schematic.	5.5-56

LIST OF ILLUSTRATIONS (Cont'd)

Figure		Page
5.5-20	RAPS Rate Mode Total Uncertainty Limits	5.5-59
5.5-21	Miniature Rate Integrating Gyro	5.5-61
5.5-22	Director, Cone Angle Sun Sensor, Coarse Eye Assembly	5.5-62
5.5-23	Control Axes Coarse Sun Sensor Set Relative Response Characteristic.	5.5-62
5.5-24	Single Eye Output versus Angle Characteristic.	5.5-63
5.5-25	Acquisition Scan Pattern	5.5-65
5.5-26	Possible Tracking Scan Patterns	5.5-65
5.5-27	OA0 Flywheel Cross Section.	5.5-71
5.5-28	General Electric Resistance Jet System	5.5-74
5.5-29	Liquid Ammonia, Zero-g Storage Tank Schematic	5.5-75
5.5-30	Polaris Sensor View Angles	5.5-83
5.5-31	Pitch and Roll Sun Sensors Fields of View	5.5-84
5.5-32	Station Acquisition and Yaw Sun Sensor Fields of View	5.5-85
5.6-1	Large Parabolic Antenna Experiment Subsystem	5.6-7
5.6-2	Typical Receiver.	5.6-9
5.6-3	Typical Transmitter	5.6-9
5.6-4	Relation of Incident Signal to Interferometer Antennas	5.6-17
5.6-5	Phase Comparison System	5.6-19
5.6-6	Phase Diagram for Σ - Δ System	5.6-19
5.6-7	Σ - Δ System	5.6-19
5.6-8	Pilot Tone Concept	5.6-21
5.6-9	Antenna Location on Cannister	5.6-22
5.6-10	ATS-4 Interferometer System, Block Diagram.	5.6-23
5.6-11	System Block Diagram.	5.6-30
5.7-1	TT&C Subsystem Block Diagram Reference Design	5.7-6
5.7-2	Goddard R&R S-Band Transponder.	5.7-7
5.7-3	Command Decoder, Functional Block Diagram.	5.7-8
5.7-4	Relay Logic	5.7-10
5.7-5	Typical Main Frame	5.7-14
5.7-6	ATS-4 Reference Design: Antenna Half-Beam Angle During Transfer Orbit	5.7-17
5.7-7	Half-Beam Angle Definition	5.7-17
5.7-8	ATS-4 Reference Design: Antenna Half-Beam Angle During Vernier Maneuvers While in Synchronous Orbit	5.7-18
5.7-9	Antenna Coverage	5.7-19
5.7-10	Antenna Switching Reference Configuration	5.7-20
5.7-11	Antenna Design	5.7-21
5.7-12	TT&C Block Diagram, Redundant Configuration	5.7-29
5.7-13	Antenna Switching, Redundant Configuration	5.7-31

LIST OF ILLUSTRATIONS (Cont'd)

Figure		Page
5.8-1	Load Power Requirements During Launch Transfer Orbit	5.8-2
5.8-2	Load Power Requirements During Near-Synchronous Orbit Vernier Maneuvers	5.8-2
5.8-3	ATS-4 Reference Design Load Requirements	5.8-4
5.8-4	Power Subsystem, Block Diagram	5.8-9
5.8-5	Solar Array Power	5.8-12
5.8-6	Daily Average Array Power versus Time in Orbit (For Equinox and Summer Solstice Orbits)	5.8-13
5.8-7	End-of-Life Array Power for Equinox Orbits	5.8-14
5.8-8	End-of-Life Array Power for Summer Solstice Orbit	5.8-15
5.8-9	Solar Array Power Capability of Loads for Equinox Orbits	5.8-16
5.8-10	Solar Array Power Capability of Loads for Summer Solstice Orbits	5.8-16
5.8-11	Solar Array V-I Curves	5.8-17
5.8-12	Solar Array Output During Stowed Launch Spin Mode	5.8-19
5.8-13	Solar Array Power Capability at Loads During Stowed Launch Spin Mode	5.8-20
5.8-14	Y-Axis Panels Area Growth Capability	5.8-22
5.8-15	ATS-4 Solar Cell Arrangements	5.8-25
5.9-1	Inboard Profile and Orbital Configuration	5.9-3
5.9-2	Static and Dynamic Envelope.	5.9-7
5.9-3	Launch Availability versus Limit Bending Moment	5.9-10
5.9-4	Nozzle Locations and Plume Details	5.9-11
5.9-5	Delta Motor (TE-364-3)	5.9-14
5.9-6	Maximum Expected Outside Surface Temperature versus Time for TE-M-364-4-3	5.9-15
5.9-7	TE-M-364-3 Altitude Thrust and Chamber Pressure versus Time	5.9-17
5.9-8	G-Loading Versus Time During Apogee Burn	5.9-17
5.9-9	Thrust and Chamber Pressure versus Time, Motor B	5.9-19
5.9-10	Relation of Major Structural Elements of Selected Configuration	5.9-25
5.9-11	Truss Tube End Design Concept	5.9-31
5.9-12	Solar Panel Latching	5.9-41
5.9-13	Separation Nut Operation	5.9-47
5.9-14	Response of Upper Mass (Mass 1) versus First Mode Shape	5.9-50
5.9-15	Typical Shutter Assembly.	5.9-59
5.9-16	Typical Shutter System Characteristics	5.9-60
5.9-17	Earth Viewing Equipment Module	5.9-64
5.9-18	EVM Panel Temperature Distribution (⁰ R) Based on Continuous Experiment Operation	5.9-66
5.9-19	EVM Panel 4 Transient Thermal Performance.	5.9-67
5.9-20	Aft Equipment Module Overall Component Installation	5.9-68
5.9-21	AFT Equipment Module	5.9-69
5.9-22	AEM Panel Temperature Distribution (⁰ R)	5.9-74
5.9-23	Truss Nodal Designation	5.9-75

LIST OF ILLUSTRATIONS (Cont'd)

Figure		Page
5.9-24	Transient Strut Temperature Profile ($^{\circ}\text{R}$), $\alpha/\epsilon = 1$	5.9-75
5.9-25	Transient Strut Temperature Profile ($^{\circ}\text{R}$), $\alpha/\epsilon = 1$	5.9-76
5.9-26	Transient Strut Temperature Profile ($^{\circ}\text{R}$), $\alpha/\epsilon = 2$	5.9-76
5.9-27	Transient Strut Temperature Profile ($^{\circ}\text{R}$), $\alpha/\epsilon = 2$	5.9-77
5.9-28	Transient Strut Temperature Profile ($^{\circ}\text{R}$), $\alpha/\epsilon = 3$	5.9-77
5.9-29	Transient Strut Temperature Profile ($^{\circ}\text{R}$), $\alpha/\epsilon = 3$	5.9-78
5.9-30	Maximum Solar Flux Distribution During Equinox	5.9-80
5.9-31	Maximum Solar Flux Distribution During Summer Solstice	5.9-81
5.9-32	Maximum Solar Flux Distribution for Inclined Paddles	5.9-82
5.9-33	Average Solar Paddle Temperature for the Antenna-Mounted Four-Paddle Spacecraft	5.9-83
5.9-34	Absorbed Free Molecule Heat Flux for Parking Orbit of 80 Nautical Miles	5.9-85
5.9-35	Absorbed Free Molecule Heat Flux for Parking Orbit of 90 Nautical Miles	5.9-85
5.9-36	Absorbed Free Molecule Heat Flux for Parking Orbit of 100 Nautical Miles	5.9-85
6.2-1	Basic Spacecraft Arrangements Used in Configuration Tradeoff Studies	6.2-3
6.2-2	Candidate Launch Vehicles and Early Conceptual Approaches	6.2-7
6.2-3	Launch Availability versus Limit Bending Moment	6.2-15
6.2-4	Launch Availability versus Engine Deflection	6.2-16
6.2-5	Static and Dynamic Envelope.	6.2-17
6.2-6	First Stage Design, Split Module Concept	6.2-23
6.2-7	First Stage Design, Single Module Concept	6.2-25
6.2-8	First Stage Design, Deployed Phased Array Concept	6.2-29
6.2-9	Star Tracker System for Orientation Control, View Angles	6.2-32
6.2-10	Polaris Tracker System for Orientation Control, View Angles	6.2-33
6.2-11	Second Stage Design, Phased Array Concept	6.2-37
6.2-12	Second Stage Design, Deployed Feed Concept	6.2-38
6.2-13	Third Stage Design, Tandem Concept.	6.2-43
6.2-14	Third Stage Design, Deployed Phased Array Concept	6.2-45
6.2-15	Deployed Configuration	6.2-49
6.2-16	Structural Load Paths	6.2-55
6.2-17	Electrically Powered Deployment System	6.2-57
6.2-18	Mechanically Powered Deployment System	6.2-59
6.2-19	Alternate Fixed Feed Design, Extended Surveyor Apogee Motor.	6.2-69
6.2-20	Alternate Fixed Feed Design, Antares I Apogee Motor	6.2-71
6.3-1	Wire-Grid Structure	6.3-4
6.3-2	Wire-Grid Structural Member	6.3-5
6.3-3	Tolerance Limitation of Mesh Attachment Method	6.3-5
6.3-4	Solar Collector Orbital Sequence	6.3-8

LIST OF ILLUSTRATIONS (Cont'd)

Figure		Page
6.3-5	Chemically Rigidized Reflector (Two-Foot Model)	6.3-9
6.3-6	Mirror-Supported by Rigid Foam (44.5-Foot Model)	6.3-9
6.3-7	Cross Section of Rigidized Solar Concentrator	6.3-10
6.3-8	Solar Concentrator (Initial and Final Fabrication Phases)	6.3-11
6.3-9	Stretched-Screen Reflector Surface Contour Accuracy	6.3-12
6.3-10	Thermal Deflection Comparison	6.3-13
6.3-11	Design with Cables Behind Reflector Surface	6.3-14
6.3-12	Swirlabola Antenna	6.3-15
6.3-13	Deployment of a Petal Antenna	6.3-19
6.3-14	Aluminum-Sandwich Frame Member	6.3-20
6.3-15	Typical Sector of Petal Lattice Pattern	6.3-27
6.3-16	Ultimate Tensile Strength versus Temperature for Aluminum and Titanium	6.3-32
6.3-17	Yield Strength versus Temperature for Aluminum and Titanium	6.3-32
6.3-18	Modulus of Elasticity versus Temperature for Aluminum and Titanium	6.3-33
6.3-19	Coefficient of Thermal Expansion versus Temperature for Aluminum and Titanium	6.3-33
6.3-20	Possible Configuration of Expanded Metal for RF Reflecting Material	6.3-35
6.3-21	Reverse Folding Pattern, Triangular Petals Folded Outward	6.3-41
6.3-22	Deployment Scheme	6.3-41
6.3-23	Reverse Folding Pattern, Triangular Petals Folded Radially Outward	6.3-51
6.3-24	Reverse Folding Pattern, Triangular Petals Folded Towards Center	6.3-51
6.3-25	Causes of Thermal Deflections	6.3-52
6.3-26	Heat Inputs	6.3-54
6.3-27	Internal Geometry Effects - Antenna Blockage	6.3-54
6.3-28	Two-Node Thermal Model	6.3-56
6.3-29	One-Dimensional Heat Transfer	6.3-59
6.3-30	Analytical Model.	6.3-59
6.3-31	Average Antenna Temperature	6.3-60
6.3-32	Temperature Differentials Through the Thickness	6.3-61
6.3-33	Temperature Differentials Tip-to-Tip	6.3-62
6.3-34	Isotherms for Solid-Rod Antenna	6.3-63
6.3-35	Isotherms for Solid and Open Antenna at 90-Degree Orbital Position	6.3-64
6.3-36	Folded Reflector Load Distribution and Geometry.	6.3-69
6.3-37	Radial Petal Member, Typical Section	6.3-70
6.3-38	Approximate Loading of a Beam	6.3-75
6.3-39	Computer Loads Printout, Stress Analysis and Margin of Safety Calculation	6.3-77
6.3-40	Computer Loads Printout, Stress Analysis, and Margin of Safety for One of Six Members Common to Truss Point 89	6.3-79

LIST OF ILLUSTRATIONS (Cont'd)

Figure		Page
6.3-41	Computer Loads Printout, Stress Analysis, and Margin of Safety for One of Six Members Common to Truss Point 89	6.3-80
6.3-42	Computer Loads Printout, Stress Analysis, and Margin of Safety for One of Six Members Common to Truss Point 89	6.3-81
6.3-43	Computer Loads Printout, Stress Analysis, and Margin of Safety for One of Six Members Common to Truss Point 89	6.3-82
6.3-44	Computer Loads Printout, Stress Analysis, and Margin of Safety for One of Six Members Common to Truss Point 89	6.3-83
6.3-45	Computer Loads Printout, Stress Analysis, and Margin of Safety for One of Six Members Common to Truss Point 89	6.3-84
6.3-46	Member Loads at Joint 89	6.3-85
6.3-47	Model Used for Face Sheet - Core Thermal Compatibility Analysis	6.3-85
6.3-48	Truss Members	6.3-92
6.3-49	Two-Node Diameter Mode of Vibration	6.3-100
6.3-50	45-Degree Sector of Antenna Representing Overhanging Beam on Two Supports.	6.3-100
6.3-51	Antenna Isotherms 39-90	6.3-106
6.3-52	Antenna Isotherms 39-0	6.3-106
6.3-53	Antenna Isotherms 39-45	6.3-106
6.3-54	Antenna Isotherms 39-135	6.3-106
6.3-55	Antenna Isotherms 39-180	6.3-106
6.3-56	Deformed Shape at Below Ambient Temperatures (Free Hub, No Deployment Trusses)	6.3-111
6.3-57	Deformed Shape at Below Ambient Temperature (Fixed Hub, No Deployment Trusses)	6.3-111
6.3-58	Structural Simulation for Digital Computer Program.	6.3-114
6.3-59	Computer-Drawn Schematic (or a Structural Antenna Simulation)	6.3-115
6.3-60	Contour Deflection for Fixed Hub	6.3-118
6.3-61	Contour Deflection for Free Hub	6.3-118
6.3-62	Antenna Deflections Due to Temperature Gradients, Displacements of Radial Members $\theta = 180$ Degrees	6.3-119
6.3-63	Antenna Deflections Due to Temperature Gradients, Displacements of Radial Members $\theta = 160$ Degrees	6.3-119
6.3-64	Antenna Deflections Due to Temperature Gradients, Displacements of Radial Members $\theta = 140$ Degrees	6.3-120
6.3-65	Antenna Deflections Due to Temperature Gradients, Displacements of Radial Members $\theta = 120$ Degrees	6.3-120
6.3-66	Antenna Deflections Due to Temperature Gradients, Displacements of Radial Members $\theta = 100$ Degrees	6.3-121
6.3-67	Case 39-90, Deviation Plot (Symmetrical about Centerline)	6.3-122
6.3-68	Truss Geometry and Nomenclature used for Feed Distortion Analysis	6.3-130
6.3-69	0.3 f/D Geometry	6.3-132
6.3-70	0.4 f/D Geometry	6.3-133

LIST OF ILLUSTRATIONS (Cont'd)

Figure		Page
6.3-71	0.5 f/D Geometry	6.3-133
6.3-72	Cassegrain Antenna Nomenclature	6.3-135
6.3-73	Subreflector Blocking Gain Loss	6.3-136
6.3-74	Subreflector Included Angle versus $2f/d$ for 30-Foot Diameter Parabola	6.3-136
6.3-75	Horn Aperture and Length versus Secondary Focus H, $F/D = 0.3$	6.3-137
6.3-76	Horn Aperture and Length versus Secondary Focus H, $F/D = 0.4$	6.3-137
6.3-77	Horn Aperture and Length versus Secondary Focus H, $F/D = 0.5$	6.3-138
6.3-78	Syncom SHF Feed Patterns	6.3-148
6.3-79	Feed Configuration	6.3-148
6.3-80	Gain Degradation versus Scan Angle	6.3-149
6.3-81	Gain Performance for Scanning Scheme	6.3-150
6.3-82	Loci of Best Azimuth Focus for Various Elevation Angles θ	6.3-151
6.3-83	Comparison of Point Source and Line Source E-Plane Patterns, 15-Degree Steering	6.3-151
6.3-84	Coma Coefficient versus Scan Angle	6.3-153
6.3-85	Subreflector Grid Sizes	6.3-158
6.3-86	Strut Model Configuration	6.3-159
6.3-87	Three-V Strut Model Configuration	6.3-159
6.3-88	Four-Strut Model	6.3-160
6.3-89	Three V Struts on 2-Foot Diameter Circle	6.3-160
6.3-90	Three V Struts on 54-Inch Diameter Feed Circle	6.3-161
6.3-91	450-Foot Test Range, From Source	6.3-161
6.3-92	Measured Patterns	6.3-163
6.3-93	Case 39-90, Deviation Plot (Symmetrical About Centerline)	6.3-171
6.4-1	Star Tracker Field of View Requirements	6.4-7
6.4-2	Antenna Half-Beam Angle During Vernier Maneuvers During Synchronous Orbit	6.4-17
6.4-3	Data for GE Resistance Jet	6.4-21
6.4-4	Resistance Jet Stationkeeping/Orientation Control Subsystem (GE)	6.4-22
6.4-5	Propellant Weight versus Total Impulse at 1800°F (GE System)	6.4-23
6.4-6	Total System Weight versus Total Impulse (GE System)	6.4-23
6.4-7	Mollier Chart of Properties of Ammonia	6.4-25
6.4-8	AVCO Resistance Jet Subsystem	6.4-27
6.4-9	Propellant Weight versus Total Impulse ($I_{sp} = 150$ sec), AVCO System	6.4-28
6.4-10	Total System Weight versus Total Impulse (AVCO System).	6.4-28
6.4-11	GE Resistance Jet and AVCO Resistance Jet Operating Temperatures	6.4-30
6.4-12	Coning Control Sensor Location.	6.4-33
6.4-13	Regulated and Blowdown Monopropellant System	6.4-37
6.4-14	Bipropellant System Schematic	6.4-40
6.4-15	Total Impulse for Various Spin Rates and I_r/r	6.4-43

LIST OF ILLUSTRATIONS (Cont'd)

Figure		Page
6.4-16	Candidate Spinup Motors	6.4-45
6.4-17	ATS-4 Spacecraft Configuration.	6.4-48
6.4-18	X_B and Y_B Components of Aerodynamic Torque	6.4-50
6.4-19	X_B and Y_B Components of Magnetic Torque.	6.4-51
6.4-20	X_B and Y_B Components of Gravity Gradient Torque	6.4-53
6.4-21	Assumed Configuration for Disturbance Torques	6.4-56
6.4-22	Disturbance Torque Profile (Yaw Axis Pointed to Local Vertical)	6.4-57
6.4-23	Disturbance Torque Profile (Yaw Axis Pointed to 0° Pitch, 8.7° Roll).	6.4-58
6.4-24	Disturbance Torque Profile (Yaw Axis Pointed to Rosman Station)	6.4-59
6.4-25	Disturbance Torque Profile (Yaw Axis Pointed to Mojave Station)	6.4-60
6.4-26	Flywheel Momentum Profile (Yaw Axis Pointed to Local Vertical)	6.4-62
6.4-27	Flywheel Momentum Profile (Yaw Axis Pointed to 0° Pitch, 8.7° Roll).	6.4-63
6.4-28	Flywheel Momentum Profile, Autumnal Equinox, (Yaw Axis Pointed to Rosman Station)	6.4-65
6.4-29	Flywheel Momentum Profile (Yaw Axis Pointed to Mojave Station)	6.4-67
6.4-30	Locus of Spin Axis After Booster Separation	6.4-71
6.4-31	Coning Damper	6.4-72
6.4-32	Thruster Efficiency versus Pulse Width	6.4-77
6.4-33	Apogee Motor Burn	6.4-81
6.4-34	Initial Stabilization Pitch Axis	6.4-84
6.4-35	Sun Stabilization System, Block Diagram	6.4-85
6.4-36	Gyroscopic Torques	6.4-86
6.4-37	Attitude and Sun Sensor Geometry	6.4-87
6.4-38	Phase Plane Diagram	6.4-90
6.4-39	Earth Stabilization Roll Axis, E1	6.4-93
6.4-40	Earth Stabilization Pitch Axis, E2	6.4-93
6.4-41	Earth Stabilization Roll Axis, E3	6.4-93
6.4-42	Earth Stabilization Pitch Axis, E4.	6.4-93
6.4-43	Earth and Star Stabilization System	6.4-94
6.4-44	Nonlinear Flywheel.	6.4-95
6.4-45	Velocity-Momentum Transfer Function for Rigid Vehicles with Flexible Appendages.	6.4-95
6.4-46	Attitude Geometry	6.4-97
6.4-47	Earth Scanner Geometry	6.4-98
6.4-48	Flywheel Unloading Jet Controller	6.4-99
6.4-49	Signal Processing Null.	6.4-100
6.4-50	Open Loop Frequency Response.	6.4-100
6.4-51	Sun Sensor Geometry for Star Stabilization	6.4-102
6.4-52	Primary Pointing System, Block Diagram	6.4-103
6.4-53	Roll Axis Pointing, P2.	6.4-105
6.4-54	Pitch Axis Pointing, P5	6.4-105
6.4-55	Yaw Axis Pointing, P8.	6.4-105

LIST OF ILLUSTRATIONS (Cont'd)

Figure		Page
6.4-56	Roll Axis Pointing, P1.	6.4-106
6.4-57	Pitch Axis Pointing, P4	6.4-106
6.4-58	Yaw Axis Pointing, P7.	6.4-106
6.4-59	Roll Axis Pointing, P3.	6.4-107
6.4-60	Pitch Axis Pointing, P6	6.4-107
6.4-61	Roll Axis Slew, S1	6.4-108
6.4-62	Roll Axis Slew, S2	6.4-108
6.4-63	Roll Axis Slew, S3	6.4-108
6.4-64	Pitch Axis Slew, S4.	6.4-108
6.4-65	Roll/Pitch Axis Slew, Yaw Axis, S5	6.4-109
6.4-66	Gravity Gradient Rod, Roll Axis Slew, S6	6.4-109
6.4-67	Roll Axis Track, T6	6.4-111
6.4-68	Roll Axis Track, T1	6.4-111
6.4-69	Roll Axis Track, T2	6.4-111
6.4-70	Roll Axis Track, T3	6.4-112
6.4-71	Pitch Axis Track, T4	6.4-112
6.4-72	Roll Axis Track, T5	6.4-112
6.5-1	Results of Tracking Analysis	6.5-4
6.5-2	Minimum Δt for Memory	6.5-11
6.5-3	Maximum Δt for Memory	6.5-13
6.6-1	Trapped Electron Environment	6.6-2
6.6-2	Solar Flare Environment	6.6-3
6.6-3	Segment of 30-Foot Diameter Petal Antenna Reflector	6.6-11
6.6-4	Segment of 30-Foot Diameter Petal Antenna Reflector	6.6-11
6.6-5	Sun Shadow Distribution	6.6-13
6.6-6	Bypass Diode Functional Arrangement	6.6-14
6.6-7	Comparison of V-I Curves for a Partially Shaded Array Series String, With and Without Bypass Diodes	6.6-15
6.6-8	Illustration of Effects of a Number of Elements Shaded on Degradation of an Array Series String Operating at String Peak Power Voltage	6.6-16
6.6-9	Illustration of Effects of a Number of Elements Shaded on Degradation of an Array Series String When Operating Voltage is Off Peak Power Point of Array	6.6-16
6.6-10	Array Located in Shadow of Antenna Reflector Structure	6.6-18
6.6-11	Dependence of Solar Cell Output on Angle of Incidence	6.6-22
6.6-12	Orbital Variations of Geometry Factor $K_G/\cos \psi$	6.6-25
6.6-13	Comparison of Four-Panel and Two-Panel Solar Array Power Capability at Loads	6.6-32
6.6-14	Efficiencies of 1-Ohm Centimeter and 10-Ohm Centimeter Cells Subjected to Radiation Degradation	6.6-34
6.6-15	Solar Cell Degradation After Two Years	6.6-38

LIST OF ILLUSTRATIONS (Cont'd)

Figure		Page
6.6-16	One Ohm-Centimeter Solar Cell Degradation versus Orbit Time	6.6-39
6.6-17	Maximum Power Degradation versus Orbit Time	6.6-40
6.6-18	Ten Ohm-Centimeter Solar Cell Degradation versus Orbit Time	6.6-41
6.6-19	Solar Cell Cover Thickness Optimization	6.6-42
6.6-20	Power Distribution Comparison.	6.6-51
6.6-21	Power System Block Diagram, Series Regulator	6.6-53
6.6-22	Power System Block Diagram, Series Regulator with Voltage Limiter	6.6-54
6.6-23	Power System Block Diagram, Shunt Regulator	6.6-54
6.6-24	Load Sharing Problems	6.6-55
6.7-1	Coordinate and Normalized Sign Conventions	6.7-5
6.7-2	Primary Structure Model.	6.7-6
6.7-3	Results of Feed Support Truss Tradeoff Study	6.7-8
6.7-4	Geometry of the Aft Structure	6.7-10
6.7-5	Tape Drive Deployment System	6.7-50
6.7-6	Solar Panel Latching and Deployment Design	6.7-53
6.7-7	Coordinate Convention and Locations, Deployed Configuration	6.7-58
6.7-8	Coordinate Convention and Locations, Selected Configuration.	6.7-59
6.7-9	Coordinate Conventions and Locations, Antenna-Mounted Solar Array Configuration.	6.7-70
6.7-10	Response Coordinate Locations, Selected Configuration.	6.7-76
6.7-11	Launch Response Coordinate Locations, Deployed Configuration.	6.7-77
6.7-12	Typical Electronic Panel, Alternate Approach.	6.7-93
6.7-13	Voyager Standard Panel	6.7-95
6.8-1	Antares I (X254A1)	6.8-8
6.8-2	Antares II (X259A2).	6.8-9
6.8-3	Delta Motor (TE-364-3)	6.8-9
6.8-4	Extended Surveyor Motor.	6.8-10
7.2-1	ATS-4 Reference Design Ascent Trajectory Ground Trace.	7-4
7.2-2	Perigee Burn Description and Orientations	7-5
7.2-3	Apogee Burn-Circularizing and Plane Change Maneuver	7-6
7.4-1	Variation of Injection Longitude with Launch Azimuth, Perigee Burn Crossing, Apogee Burn Opportunity.	7-12
7.4-2	Effect of Launch Azimuth on:(1) Apogee Longitude at Injection, ϵ_I , (2) Additional Apogee Inclination Change, Δi , (3) Corresponding Apogee Velocity Penalty, ΔV	7-12
7.5-1	Perigee Velocity Impulse versus Inclination Change at Perigee	7-19
7.5-2	Apogee Velocity Impulse versus Inclination Change at Apogee.	7-19
7.5-3	Variation of Total Velocity Impulse (from 100 nm Circular Parking Orbit to Synchronous Circular Equatorial Orbit) versus Inclination Change at Perigee	7-19
7.5-4	Variation of Perigee Burn Thrust Direction with Inclination Change at Perigee	7-19

LIST OF ILLUSTRATIONS (Cont'd)

Figure		Page
7.5-5	Variation of Apogee Burn Thrust Direction with Inclination Change at Apogee.	7-21
7.5-6	Variation of Required Transfer Orbit Payload with Apogee Burn Velocity Impulse	7-21
7.5-7	Payload Loss, and Inclination Change, of Transfer Orbit as Function of Excess Perigee Velocity	7-22
7.5-8	Payload Determination (Non-Optimum Apogee Motors)	7-23
7.5-9	Determination of Payload Capabilities for Modified Surveyor and Antares I Apogee Motors as a Function of Maximum Centaur P/L Capability.	7-24
7.5-10	Variation of Useful Payload into Synchronous Orbit with Maximum Centaur Capability	7-26
7.5-11	Growth Capability as a Function of Maximum Centaur Capability and Various Retro Motors	7-26
7.5-12	Description of Orbit Injection Error Sources and Vernier Engine Thrust Directions	7-28
7.5-13	Variation of Vernier Velocity Requirements with Apogee Burn Orientation Error	7-38
7.5-14	Variation of Total Payload Weight Cost with Launch Azimuth (or Injection Longitude) and Orientation Errors at Apogee Burn	7-43
7.5-15	Variation of Total Payload Weight Cost with Apogee Motor Orientation Errors	7-43
7.7-1	Variation of Maximum Longitude Excursion with Synchronous Orbit Inclination	7-59
7.7-2	Variation in Maximum Longitude Excursion with Eccentricity or Apogee-Perigee Distance	7-60
7.7-3	Variation of Individual Velocity Impulse Magnitude with Time Duration Between Thrusting	7-62
7.7-4	ΔV Requirement per Year as a Function of Synchronous Position.	7-62
7.7-5	ΔV Required to Zero Out Inclination (Impulse Applied at Nodal Crossing)	7-64
7.7-6	Thrust Inefficiency versus Error in Longitude of Nodal Crossing	7-64
7.7-7	Determination of Uncertainty in Nodal Location	7-67
7.8-1	ATS Ground Station Activity During Vernier Maneuvers.	7-75
8.3-1	Spillover Efficiency and Illumination Efficiency	8.3-4
8.3-2	Composite Patterns Measured on 30-Foot Paraboloid at 1700, 1820 and 1900 MHz	8.3-5
8.3-3	Sidelobe Level Versus Edge Illumination.	8.3-7
8.3-4	Large Aperture Antenna Equal Power Contours at 8.0 GHz Frequency.	8.3-14
8.3-5	Large Aperture Antenna Main Lobe Patterns	8.3-16
8.3-6	Graphic Representation of RF Boresight Measurement Technique	8.3-16
8.3-7	Curve Fitting Angle Data	8.3-17

LIST OF ILLUSTRATIONS (Cont'd)

Figure		Page
8.3-8	Boresight Error Combination Illustration	8.3-18
8.3-9	Thirty-Foot Antenna Gain Measurement Test Set-Up, ATS-4 Experiments	8.3-27
8.3-10	Alternate 30-Foot Antenna Gain Measurement Test Set Up, ATS-4 Experiments	8.3-27
8.3-11	Large Parabolic Antenna Experiment.	8.3-34
8.3-12	Typical Receiver	8.3-53
8.3-13	Typical Transmitter	8.3-53
8.7-1	Yaw Axis Stabilization Geometry	8.7-7
8.7-2	Spacecraft Transmit System	8.7-8
8.7-3	Ground Station Circuitry for Transmit Experiment	8.7-9
8.8-1	Operational System Simplified Functional Flow Diagram	8.8-3
8.8-2	Experiment Analysis Reporting Schedule.	8.8-26
9.3-1	ATS-4 Major Article Test Flow.	9-3
9.7-1	Cape Kennedy Launch Sites	9-26
9.7-2	Launch Complex 36B Gantry Service Tower	9-29

LIST OF TABLES

<u>Tables</u>	<u>Page</u>
4.1-1 Value of ATS-4 Experiments to Operational Missions	4-2
5.2-1 Launch Vehicle Capability	5.2-6
5.3-1 Parabolic Antenna Performance	5.3-19
5.3-2 Orientation Control System Three-Sigma Error Budget	5.3-20
5.3-3 Orientation Control Subsystem Performance Summary.	5.3-21
5.3-4 Performance Requirements Summary - Phase-Steered Array Antenna .	5.3-22
5.3-5 Interferometer Performance Summary	5.3-23
5.3-6 Interferometer Error Budget	5.3-23
5.3-7 Command and Telemetry Subsystem Capability	5.3-24
5.3-8 Power Subsystem Capability	5.3-26
5.3-9 Detail Weight Summary of Selected Design.	5.3-27
5.3-10 Inertia and Center-of-Mass Summary	5.3-28
5.4-1 Parabolic Antenna Experiment Loss Budget	5.4-13
5.4-2 Comparison of Feed System Requirements.	5.4-35
5.5-1 Error Budget	5.5-7
5.5-2 Weight and Power Summary for Initial Acquisition and Orientation Control Subsystems	5.5-8
5.5-3 Station Acquisition Impulse Requirements	5.5-10
5.5-4 Mass Expulsion Subsystem Requirements for Orientation Control and Stationkeeping	5.5-37
5.5-5 Component Description	5.5-46
5.5-6 Impulse Requirements for Station Acquisition and Despin Mass Expulsion Subsystem	5.5-52
5.5-7 Station Acquisition System Weight	5.5-58
5.5-8 Resistance Jet System Weight	5.5-76
5.5-9 Command Requirements	5.5-78
5.5-10 ATS-4 Telemetry Requirements	5.5-79
5.5-11 O/C Component Mounting, Alignment and Field of View Requirements .	5.5-86
5.6-1 Large Parabolic Antenna Experiment Equipment Characteristics . . .	5.6-5
5.6-2 Geometric Instrumentation	5.6-12
5.6-3 Weight and Power Estimates for the Interferometer System	5.6-26
5.6-4 Major Characteristics of Phase-Steered Array Antenna System. . . .	5.6-31
5.7-1 Telemetry Requirements.	5.7-3
5.7-2 Significant Reference Configuration Parameters	5.7-5
5.7-3 Margin Calculations-Telemetry Data.	5.7-23
5.7-4 Margin Calculations-Tracking	5.7-24
5.7-5 Margin Calculations-Command Link.	5.7-25
5.7-6 Summary of Component Power, Weight and Size	5.7-26
5.7-7 Summary of Design Status	5.7-32
5.8-1 Summary of Array Power and Energy Capability.	5.8-12
5.8-2 Battery Depths of Discharge for New and Old Arrays	5.8-21
5.8-3 Summary of Power Conditioning Equipment Operating Efficiencies. . . .	5.8-33
5.8-4 Summary of Power Subsystem Weights and Sizes.	5.8-34
5.8-5 Summary of Power Conditioning Equipment Thermal Dissipations . . .	5.8-34
5.9-1 Atlas/Centaur Qualification Test Specifications	5.9-9

LIST OF TABLES (Cont'd)

<u>Tables</u>	<u>Page</u>
5.9-2 Payload Capability Using TE-364-3 Improved Delta Motor	5.9-16
5.9-3 Performance and Physical Data on the Improved Delta Motor (TE-364-3)	5.9-18
5.9-4 Performance Parameters for Optimum Motor Extended Surveyor	5.9-19
5.9-5 Summary of Spacecraft Design Constraints and Significance to Selected Design	5.9-22
5.9-6 Major Structural Elements	5.9-27
5.9-7 Structure Weight Summary	5.9-39
5.9-8 Response Accelerations to Base Excitation.	5.9-52
5.9-9 Comparison of Analog Simulation Transfer Functions with Transfer Functions used for Selected Configuration	5.9-55
6.2-1 Launch Vehicles Comparison	6.2-9
6.2-2 Titan III C-Flight Loads Environment	6.2-12
6.2-3 Summary of Maximum Measured Flight Loads (Atlas/Centaur Flight AC-2 to AC-6)	6.2-21
6.2-4 Deployed Antenna Frequency Comparison	6.2-31
6.2-5 Performance of Deployed Configuration.	6.2-52
6.2-6 Deployed Configuration Weight Summary	6.2-53
6.2-7 Deployment System Comparison	6.2-67
6.3-1 Comparison of Space Deployable Antennas	6.2-23
6.3-2 ATS-4 Structural Parameters	6.3-29
6.3-3 Mechanical Properties of Aluminum and Titanium	6.3-34
6.3-4 Effect of Temperature on the Tensile Strength of FM-1000 Adhesive Bonded Aluminum Honeycomb Panels.	6.3-37
6.3-5 Effect of Temperature and Vacuum on the Tensile Strength of FM-1000 Adhesive Bonded Aluminum Honeycomb Panels.	6.3-38
6.3-6 Estimate of Mass Properties	6.3-49
6.3-7 Maximum Compression Load Launch Condition	6.3-68
6.3-8 Truss Member Loads.	6.3-94
6.3-9 Directional Displacements for Structural Joints (1 of 6) thru (6 of 6)	6.3-123
6.3-10 Feed Thermal Displacements	6.3-131
6.3-11 Antenna Loss Budget No. 1	6.3-154
6.3-12 Antenna Loss Budget No. 2	6.3-155
6.3-13 Antenna Loss Budget No. 3	6.3-156
6.3-14 Final Configuration Loss Budget	6.3-171
6.4-1 Body Rate and Acceleration Amplitude for Practical Sensor Locations	6.4-35
6.4-2 Atlantic Research Corporation Spinup Motor Data	6.4-42
6.4-3 Atlantic Research Corporation Motor Data	6.4-44
6.4-4 Spacecraft Parameters Associated with On-Station Disturbance Torque Computation.	6.4-55
6.4-5 Sun Stabilization System Nomenclature	6.4-88
6.4-6 Sun Stabilization System Parameter Values	6.4-89

LIST OF TABLES (Cont'd)

<u>Tables</u>	<u>Page</u>
6.4-7 Three-Sigma Error Budget Data	6.4-114
6.5-1 136 HMZ TLM (Carrier and Data).	6.5-2
6.5-2 Position and Velocity Error.	6.5-5
6.5-3 Antenna Configuration Tradeoff For Alternate Design Configuration	6.5-8
6.6-1 Yearly Integrated Intensities of Solar Cosmic Rays	6.6-4
6.6-2 Abundancy of Cosmic Rays	6.6-5
6.6-3 Power Equation Factors for Various Array Configurations $P = K(A_T) (K_G) F_T F_S$	6.6-26
6.6-4 Array Area Requirements for Various Configuration (300 watt maximum array).	6.6-29
6.6-5 Maximum Power Required from Battery-Watt Hours	6.6-44
6.6-6 Battery Sizing and Performance	6.6-46
6.6-7 Time and Power Required to Recharge Batteries (33 A-HRS).	6.6-49
6.6-8 Power Distribution Weight Comparison	6.6-52
6.6-9 Power Conditioning Equipment Weight Summary	6.6-56
6.6-10 Power Systems Comparison Summary	6.6-60
6.7-1 Ultimate Launch Loads (g)	6.7-2
6.7-2 Separation Device Tradeoff Chart.	6.7-56
6.7-3 Sinusoidal Vibration Testing Specifications.	6.7-59
6.7-4 Transfer Functions for ATS-4 Configuration with Antenna-Mounted Solar Arrays	6.7-72
6.7-5 Maximum Acceleration Due to Unit Load or Moment Impulse at Point One on Deployment Column	6.7-72
6.7-6 Antenna with $f/D = 0.4$	6.7-75
6.7-7 Frequency Shift with f/D Variation	6.7-75
6.7-8 Launch Accelerations for the Selected and Deployed Configuration Due to $A1\text{ g}$ or RAD/sec^2 Input	6.7-77
6.7-9 Mass Distributions.	6.7-78
6.7-10 Frequency Comparison Selected and Deployed Feed Configuration	6.7-81
6.7-11 Dirac Delta Response Comparison	6.7-82
6.7-12 Control Transfer Functions.	6.7-84
6.7-13 Transfer Functions for Gravity Gradient Rods	6.7-86
6.8-1 Payload Capability Using TE-364-3 Delta Motor	6.8-3
6.8-2 Apogee Motor Tradeoff Matrix.	6.8-4
6.8-3 Physical and Performance Data of Six Motors Considered	6.8-7
6.8-4 Data on Candidate Apogee Motors.	6.8-7
6.8-5 Apogee Motor Puff Chart.	6.8-12
7.2-1 Sequence of Events.	7-3
7.4-1 Perigee of Transfer Orbit at First Equatorial Crossing of Parking Orbit	7-11
7.4-2 Perigee of Transfer Orbit at Second Equatorial Crossing of Parking Orbit	7-11

LIST OF TABLES (Cont'd)

<u>Tables</u>	<u>Page</u>
7.5-1 Summary of Total Vernier Maneuver Impulse Requirements	7-27
7.5-2 Vernier Weight Tradeoff Summary	7-42
7.5-3 Injection Bias Summary ($\theta_{\epsilon} = 1$ degree)	7-52
7.7-1 In-Orbit Stationkeeping Velocity Requirements	7-66
7.7-2 Orbit Determination Summary	7-69
8.3-1 Individual Experiments - Parabolic Antenna	8.3-20
8.3-2 Required Signal Characteristics - Parabolic Antenna Measurements . .	8.3-42
8.3-3 Gains and Beamwidths - Perfect 30-Foot Parabolic Antenna	8.3-43
8.3-4 System Performance Parabolic Antenna Transmission Measurements. .	8.3-45
8.3-5 System Performance Gain Standard Antenna Transmission Measurements	8.3-45
8.3-6 System Performance Parabolic Antenna Receiving Measurements . . .	8.3-45
8.3-7 Limiting Power and Bandwidth Requirements Parabolic Antenna . . .	8.3-48
8.3-8 On-Board Equipment Characteristics Parabolic Antenna Measurements.	8.3-49
8.3-9 Experiment Equipment Summary	8.3-55
8.4-1 Individual Experiments - Orientation Control System	8.4-3
8.5-1 Individual Experiments - Interferometer	8.5-2
8.5-2 Interferometer Telemetry Monitoring Signals.	8.5-6
8.6-1 Individual Experiments - Phased Array Antenna	8.6-6
8.6-2 System Performance Steered Phase Array Antenna-Transmission and Reception Measurements (RF Bandwidth: 30 MHz)	8.6-21
8.7-1 System Performance High Data Rate Meteorological Sensors - Satellite to Surface (10 GHz; TV Data Rates).	8.7-11
8.7-2 Weight and Power Requirements of Sensors and Optics.	8.7-13
8.7-3 Transmission Link Characteristics Audio FM Broadcast to Home TV Receiving Sets	8.7-15
8.7-4 User Accessibility Versus Field Strength	8.7-17
8.7-5 Field Strength Versus On-Board Radiated Power.	8.7-17
8.7-6 Limited Area Audience Experiment	8.7-18
8.7-7 TV Broadcast Configurations Link Calculations	8.7-19
8.7-8 System Performance MOL Relay - MOL to Satellite - TV Bandwidths. .	8.7-24
8.8-1 Experiment and Ground Station Capability Tradeoffs	8.8-6
8.8-2 Required and Recommended Transmitting/Receiving Frequencies for Ground Stations	8.8-8
8.8-3 ATS-4 Operational Ground Station Configuration Matrix Assuming Additional ATS-4 Antenna at Rosman	8.8-10
8.8-4 ATS-4 Operational Ground Station Configuration Matrix Assuming One Antenna Per Station with Interchangeable Feeds	8.8-13
8.8-5 Operational Integration of Experimental Tasks, Facilities and Schedule.	8.8-15

LIST OF TABLES (Cont'd)

<u>Tables</u>	<u>Page</u>
8.8-6 Experiment Combinations	8.8-18
8.8-7 Contingency Matrix	8.8-25
9.2-1 Ground Support Summary Matrix	9-2
9.4-1 Equipment List (MSE).	9-15
9.5-1 Equipment List (ESE).	9-21
9.8-1 Ground Station Equipment Requirements Summary	9-30
9.9-1 ATS-4 Computer Program Requirements	9-33

SECTION 7 FLIGHT DYNAMICS

7.1 INTRODUCTION

The ultimate requirement of the ATS-4 mission is to place the ATS-4 spacecraft into an earth synchronous equatorial orbit at a longitude that will permit the most favorable conditions for conducting and verifying the proper operation of all the on-board experiments. For the purpose of analysis, the initial operating longitude has been selected as 90°W , with the provision for repositioning further west (about 150°W longitude) later in the mission.

WTR launch azimuth restrictions produce orbits that require prohibitively large plane change maneuvers in achieving an equatorial orbit. For this reason, only ETR launch facilities are considered in this discussion. The launch vehicles under consideration are the Atlas SLV-3A/Agena D, the Atlas SLV-3C/Centaur, and the Titan IIC. Each booster and upper stage vehicle has its own limitations and imposes various constraints on the boost phase and transfer orbit trajectories.

The final constraint placed on the orbit selection process is the decision to use an available motor (rather than design an optimum one) for the apogee burn maneuver. The selected motor cannot put the full Atlas/Centaur payload potential into a synchronous equatorial orbit. Rather than off-load the Centaur's fuel tanks, the "excess" Centaur capability is used to make a plane change during the perigee burn maneuver. Thus, maximum use is made of the Centaur/Apogee Motor combination. The payload capability of the Atlas/Agena launch vehicle with an available apogee motor was not sized in detail, since its payload capability was not sufficient for the ATS-4 design requirements. The Titan IIC transtage performs the apogee burn maneuvers, thus separate apogee motor considerations are not applicable to this booster.

Each of the major operational events from launch vehicle liftoff to stabilization in the synchronous orbit are discussed in this section together with the rationale for the selected launch trajectory.

7.2 REFERENCE DESIGN SEQUENCE OF EVENTS - SUMMARY

7.2.1 LAUNCH TRAJECTORY - GENERAL

The ATS-4 reference design launch vehicle is comprised of the Atlas (SLV-3C) booster with the Centaur upper stage and the improved Delta apogee motor. The Centaur establishes the parking orbit during the launch boost phase and provides the total velocity impulse for initiating the orbit transfer. A maximum coast time of 25 minutes between Centaur burns has been established as an operational limit. Therefore, the transfer orbit velocity impulse must be applied at the first crossing of the Centaur over the equator. The synchronous equatorial orbit is obtained by establishing perigee of the transfer ellipse at this first equatorial crossing. A plane change maneuver is included in the perigee burn to reduce the inclination of the transfer orbit by 8.05 degrees. The apogee motor is used to both circularize the orbit at synchronous altitude, and rotate the orbit plane into coincidence with the equatorial plane. Table 7.2-1 presents a summary of each of the major elements of the launch trajectory. Figure 7.2-1 shows the ascent trajectory ground trace during the boost, parking orbit, and orbit transfer phases of the mission.

7.2.2 BOOSTER/LAUNCH PHASE

7.2.2.1 Booster Phase

The SLV-3C/Centaur is launched from ETR (28.5°N latitude) at an azimuthal heading of 90° clockwise from due north. The SLV-3C (Atlas) is separated from the Centaur after burnout. The Centaur first burn is used for final insertion into the park orbit, at approximately 500 seconds after liftoff.

7.2.2.2 Parking Orbit

The Centaur/ATS-4 payload combination is placed in a 100 nm altitude circular orbit and after 20 minutes it crosses the equator heading from north to south at a longitude of 4°E. The orbital velocity is 25,567 ft/sec and the orbit inclination is 28.5 degrees.

Table 7.2-1. Sequence of Events

<p>1. Launch: SLV-3C/Centaur ETR (28.5°N) (279.5°E) 90° Launch Azimuth</p> <p>2. Parking Orbit: 100 nm Altitude 28.5° Inclined Orbit Velocity 25,567 ft/sec</p> <p>3. Perigee Burn: (Initiate Transfer Maneuver to Synch. Orbit Altitude) Centaur orientation: 2.8° up from equator Burn at equatorial crossing: 4° E Long. Velocity Impulse 9051 ft/sec; Δi -8.05°</p> <p>4. Transfer Orbit: Alt Perigee: Velocity 33,631 ft/sec (Perigee alt. 100 nm) Incl. 20.45° Reorient Centaur through 163.5°, separate ATS-4, spin up to 71.7 rpm Longitude of second perigee 154°W</p> <p>Transfer Coast: Coast time 15.75 hr Spin Stabilized - Coming and precession controlled</p> <p>Spin Orientation at Apogee: Horizontal & 19.4° down from equatorial plane when at perigee or apogee. Altitude 19,324 nm Velocity 5236 ft/sec Longitude of first apogee 105°E Longitude of 2nd Apogee 53°W</p>	<p>5. Apogee Burn: (Circularize orbit at synchronous altitude and rotate orbit plane into coincidence with the earth's equatorial plane) Apogee Motor: Modified Surveyor retro motor for improved Delta Longitude: 53°W Velocity Impulse - 5498 ft/sec Orientation: Horizontal - down 19.4° from equatorial plane</p> <p>6. Vernier Maneuvers System: Hydrazine vernier propulsion system Orbit: Equatorial synchronous (nominally) Altitude 19,324 ± 165 nm Velocity: 10,087 ± 100 to 120 ft/sec Inclination: 0 ± 0.5° Orientation: same as Apogee Motor Burn</p> <p>Velocity Requirements Basic: 210 ft/sec Total: 255 ft/sec (orientation and thrusting inefficiency included) Residual - 10 ft/sec excess (1.0° drift/day westward)</p> <p>Despin: Use rate gyros - Hydrazine Propellant System Vent Hydrazine tanks with Despin System closing loop After venting, lock out vernier system</p> <p>7. Deployment: Stabilize to sun (resistance jets, stationkeeping system) Initiate deployment command</p> <p>8. Initial Stabilization Acquire Earth Acquire Polaris</p>
--	---

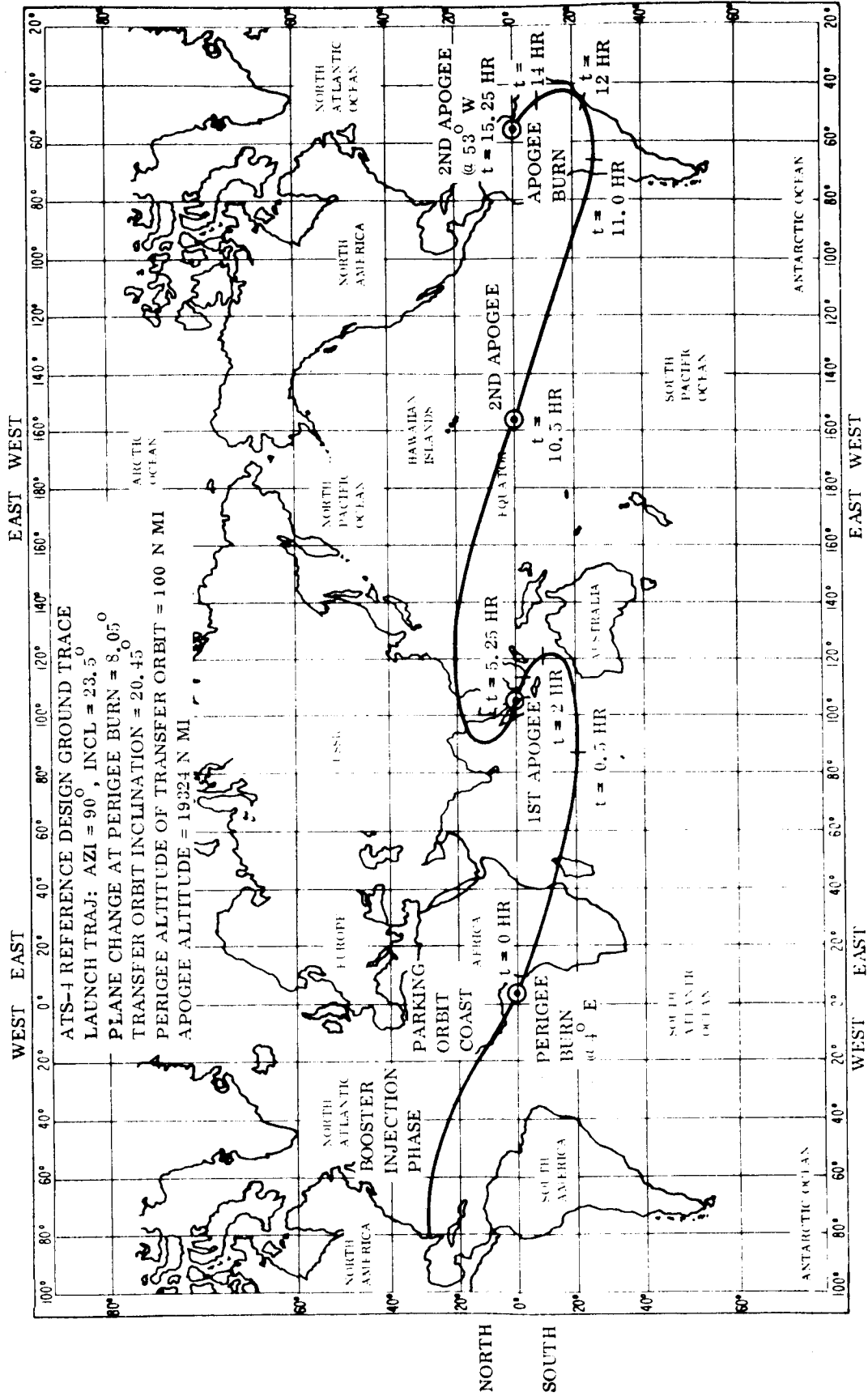


Figure 7.2-1. ATS-4 Reference Design Ascent Trajectory Ground Trace

7.2.2.3 Perigee Burn

Prior to perigee burn, the Centaur is rotated through 31.3° counterclockwise about the local vertical (as viewed from above). It will now be pointing 2.8° upward from the equator (see Figure 7.2-2). When crossing the equator, the Centaur engines are turned on. Thrusting is continued until a velocity increment of 9051 ft/sec has been added. The total orbital velocity is now 33,634 ft/sec. This results in an inclination reduction from 28.50 to 20.45 degrees. The 100-nm altitude perigee and the synchronous apogee altitude of 19,324 nm are the altitude extremes of the transfer orbit.

7.2.3 INITIAL ACQUISITION PHASE

7.2.3.1 Transfer Orbit

Immediately after perigee burn, the Centaur is rotated through 163.5° clockwise about the yaw (local vertical) axis, the ATS-4 payload is separated from the Centaur vehicle and spun-up, using two solid motors. This Centaur reorientation-separation-spin-up maneuver

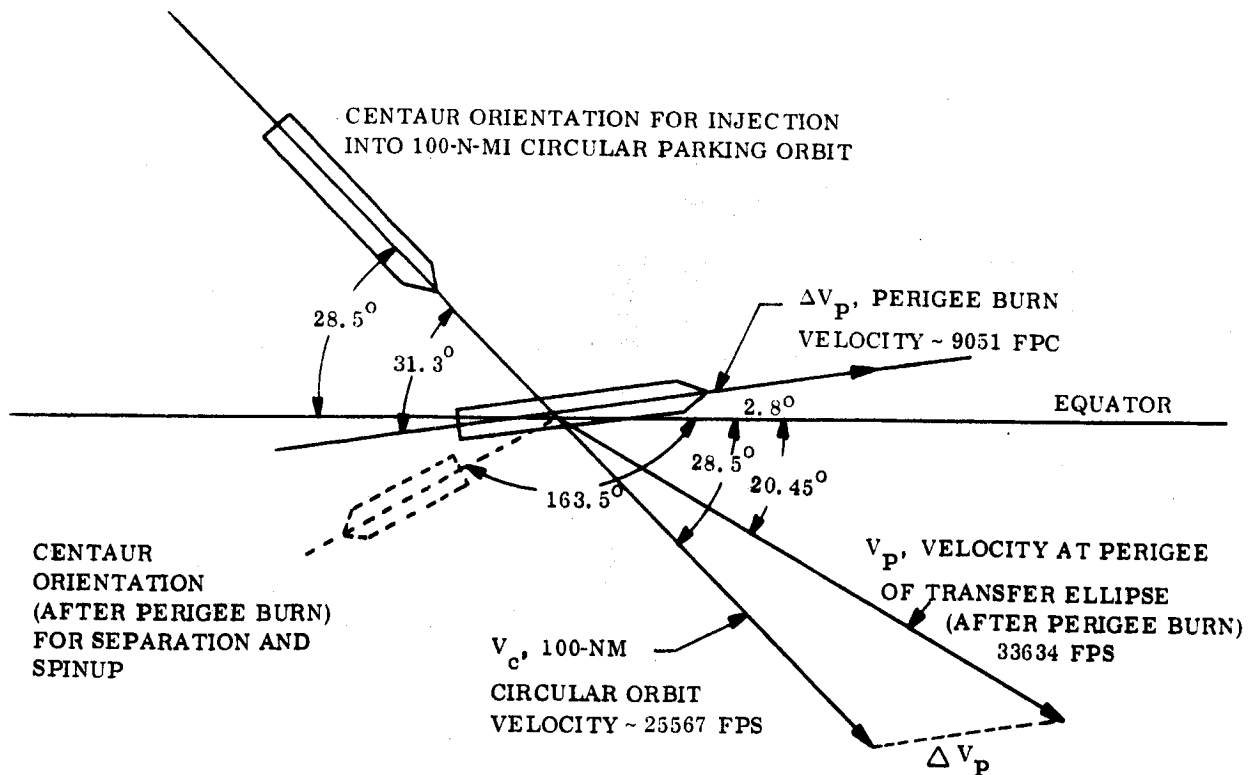


Figure 7.2-2. Perigee Burn Description and Orientations

is designed to provide the spinning spacecraft the orientation for apogee burn. During the course of the transfer orbit, coning suppression control is required. Shortly before the second apogee is reached, the angular momentum vector is precessed to remove orientation errors induced by separation dynamics and disturbance torques. The time duration of the transfer orbit is 15.75 hours.

7.2.3.2 Apogee Motor Burn

The solid fueled apogee motor (Improved Delta motor) is ignited at the second apogee, over the equator, at a longitude of 53° W heading from south to north. The orbital velocity at apogee is 5236 ft/sec. The total velocity impulse imparted by the apogee motor is 5498 ft/sec at an angle of 19.4° to the equator southward; i. e., the azimuth direction of apogee motor impulse is 109.4° clockwise from due north (see Figure 7.2-3). Engine ignition would be controlled from the ground; the timing of the ignition being based on ground tracking and orbit computations.

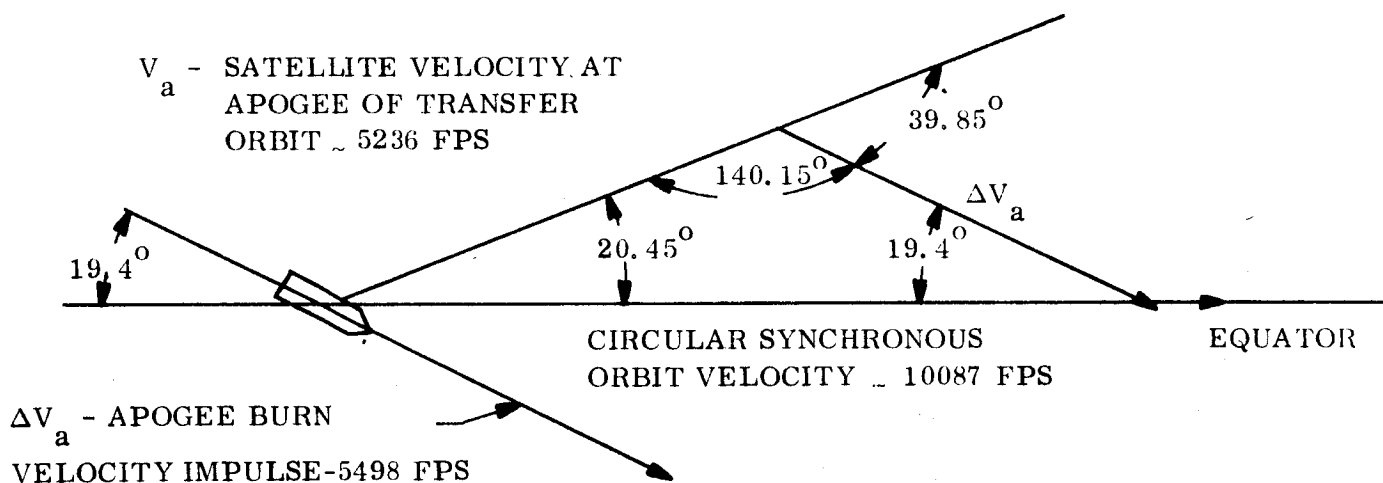


Figure 7.2-3. Apogee Burn - Circularizing and Plane Change Maneuver

7.2.3.3 Vernier Maneuvers

Ideally, the spacecraft would be in a synchronous, circular, equatorial orbit, at a longitude of 53° W; however, due to errors in the perigee burn and in the solid motor burn, the ideal orbit is not attained. The actual orbit is determined from ground tracking, and the vernier

propulsion system is used to remove the injection errors. This is expected to take no more than two days.

A residual velocity of 10 ft/sec, in excess of the synchronous orbit velocity, is desired to induce spacecraft drift toward the operating longitude of 90°W . The orientation of the spinning vehicle is held to apogee burn attitude during the vernier maneuver. Precession of the vehicle to produce spinning perpendicular to the orbit (equatorial) plane is not planned.

7.2.3.4 Despin

The vernier propulsion system is used for despinning the spacecraft at the termination of the vernier maneuvers. Rate gyros are used to monitor the despin.

7.2.3.5 Initial Stabilization Phase

Upon completion of the despin and vernier propulsion venting sequence, the low thrust orientation control/stationkeeping propulsion system, made up of nine resistance jet thrusters, is used to orient and stabilize the spacecraft yaw axis to the sun. In this attitude and at low rates, the parabolic antenna and solar array are deployed. Following this, and maintaining yaw axis sun orientation, the earth will come into view of the earth sensors, at which time the earth is acquired. The star tracker is then directed to lock onto Polaris.

The deployed spacecraft is checked out while it slowly drifts to the west. The resistance jets are used to gradually slow the drift; i.e., the orbit's period is gradually being synchronized with the earth spin rate and at the same time the orbit is being circularized. Up to 50 days of drift may be required from the time of vernier despin until the 90°W longitude station is acquired.

7.3 OPERATING LONGITUDE EVALUATION

The selection of the operating longitude for the ATS-4 spacecraft in a synchronous equatorial orbit has been considered from several standpoints: communications, experiment calibration and launch trajectories. For the purpose of this study, it is assumed that the spacecraft will

be initially located at 90° W longitude and that later in the mission, it will be repositioned further West (tentatively 150° W longitude) for possible use with the Australian ATS ground station. Some of the rationale for this selection is presented in the following discussion.

Ground control of spacecraft position and attitude in realtime or near realtime will be required during the initial phases of the mission for evaluating the performance of the prime experiments and in calibrating these subsystems. This will necessitate the high speed transmission of telemetry data from the receiving station to a central processing facility where a digital computer would be used for the determination of spacecraft attitude from telemetry data and the selection and formatting of orientation control commands. It is assumed that the mission control center and associated data processing facilities will be located at the Goddard Space Flight Center (GSFC). A wide band (1MHz) data link between GSFC and the data acquisition station at Rosman, North Carolina, is currently in operation. This link will be more than adequate for realtime transmission of telemetry data from Rosman to a data processing facility at GSFC. Realtime command of the spacecraft from GSFC via the Rosman station can also be accomplished with existing communication facilities. It is recommended that Rosman be used as the prime station for command transmission and telemetry data acquisition during the ATS-4 mission. One of the primary considerations in the selection of the ATS-4 operational longitude is that the spacecraft should be in view of the Rosman acquisition station. The STADAN stations at Ft. Meyers, Florida, Mojave, California, and Blossom Point, Maryland can be used as alternate or backup stations for command and control purposes if Rosman is not available. The transmission of data between these stations and GSFC is limited to teletype and voice quality circuits. The STADAN stations outside the North American continent are considered undesirable for command and control purposes because of the limited, and in some cases unreliable, communications facilities between these stations and GSFC. Locating the spacecraft between 70° to 100° W longitude would place the spacecraft within continuous view of Rosman, Ft. Meyers, Blossom Point and Mojave stations.

The selection of 90° W longitude out of the 70° to 100° W longitude range was made because it represented realistic requirements from launch trajectory, vernier thrusting and station-

keeping standpoints. Additionally, all of the STADAN stations in the United States, South America, and Newfoundland would see the spacecraft with a minimum antenna elevation angle of 20 degrees with the exception of the Alaskan stations (these would have a minimum elevation angle of 2 to 3 degrees).

7.4 ASCENT TRAJECTORY SELECTION

7.4.1 TRAJECTORY INFLUENCING PARAMETERS

In this section the flight dynamics aspects of attaining ascent trajectories which allow variations in the longitudes of injection into synchronous orbit will be considered first. Then the manner in which the launch vehicle constraints dictate which range of the possible injection longitudes can actually be achieved will be shown. For the ATS-4 mission, the ascent trajectory includes: (1) powered flight from ground to insertion into a low altitude circular orbit, (2) coast in this orbit until the desired equatorial crossing is reached, (3) establishment of a transfer ellipse with perigee at an equatorial crossing and apogee altitude equal to synchronous orbit altitude, and (4) the velocity impulse (apogee burn) which simultaneously plane-changes and circularizes the orbit at the longitude of the apogee of the transfer ellipse. It can be seen, therefore, that the operational longitude is obtained by varying the longitude of the transfer ellipse apogee.

There are three methods that may be employed to shift the longitude of the apogee of the transfer ellipse:

- a. Vary launch azimuth
- b. Vary stay time in low altitude earth parking orbit
- c. Vary stay time in elliptical transfer orbit

Combinations of all three methods will be shown parametrically. As mentioned above, all launches originate from Cape Kennedy (28.5°N latitude, 279.5° longitude).

The most predominate influence on longitude selection is the launch azimuth. Variation in launch azimuth produces continuous variations in injection longitude, whereas stay times in the orbits will produce discrete variations in the injection longitude. However, a variation in launch azimuth from due east results in a payload loss due to the loss of the earth's rotational velocity and to the increased orbital inclination which must be nulled by the plane change maneuver at apogee of the transfer ellipse.

The loss of payload into the transfer orbit due to launch azimuth variations is 2.5 pounds per degree for the Atlas/Agena launch vehicle and 12 pounds per degree for the Atlas/Centaur. The Titan III C incurs no penalty since its capability is in excess of that which it is permitted to put into orbit. The velocity penalty at apogee burn is included in Figure 7.4-2 as a function of launch azimuth. The nominal apogee burn velocity impulse is 6030 ft/sec for a due east (90°) launch azimuth.

Varying time spent in the low altitude (100 nm) circular parking orbit results in an earth longitude shift of 167.5 degrees to the east between equatorial crossing. Since the transfer orbit which is initiated by the perigee burn can occur only when over the equator, only discrete 167.5-degree variations in injection longitude are permitted; 158-degree shifts to the west (202° to the east) result for each transfer ellipse orbital revolution. Note that in going from perigee burn to the first apogee, a shift of only one-half this amount (101° to the east) results.

The injection longitude capability is summarized in Tables 7.4-1 and 7.4-2, and Figures 7.4-1 and 7.4-2. Table 7.4-1 applies to transfer orbits that are initiated (via the perigee burn) at the first crossing of the equator by the upper stage of the launch vehicle for the perigee burn. Note that a launch azimuth of about 92° and a perigee burn at second equatorial crossing produces the first apogee longitude at 90° W. Barring all other constraints, this would produce the most desirable launch trajectory. Figure 7.4-2 shows only those perigee/apogee burn combinations that produce injections near the selected operational longitude.

Table 7.4-1. Perigee of Transfer Orbit at First Equatorial Crossing Of Parking Orbit

Launch Azimuth (deg)	75	80	85	90	95	100	105	110
Longitude of Perigee (deg)	32.5E	24.0E	14.0E	4.0E	5.5W	15.0W	23.5W	31.0W
Longitude of 1st Apogee (deg)	133.5E	125.0E	115.0E	105.0E	95.5E	86.0E	77.5E	70.0E
Longitude of 2nd Apogee (deg)	24.5W	33.0W	43.0W	53.0W	62.5W	72.0W	80.5W	88.0W
Longitude of 3rd Apogee (deg)	177.5E	169.0E	159.0E	149.0E	139.5E	130.0E	121.5E	114.0E
Orbital Inclination (deg)	31.9	30.1	28.9	28.5	28.9	30.1	31.9	34.4
Plane Change Velocity Penalty (ft/sec)	252	120	40	0	40	120	252	440

Table 7.4-2. Perigee of Transfer Orbit at Second Equatorial Crossing Of Parking Orbit

Launch Azimuth (deg)	75	80	85	90	95	100	105	110
Longitude of Period (deg)	159.0W	167.5W	177.0W	173.0E	163.0E	154.0E	145.0E	137.5E
Longitude of 1st Apogee (deg)	58.0W	66.5W	75.5W	85.5W	96.0W	105.0W	113.5W	121.5W
Longitude of 2nd Apogee (deg)	144.0E	135.5E	126.5E	116.5E	106.0E	97.0E	88.5E	80.5E
Longitude of 3rd Apogee (deg)	14.0W	22.5W	31.5W	41.5W	52.0W	61.0W	69.5W	77.5W
Orbital Inclination (deg)	31.9	30.1	28.9	28.5	28.9	30.1	31.9	34.4
Plane Change Velocity Penalty (ft/sec)	252	120	40	0	40	120	252	440

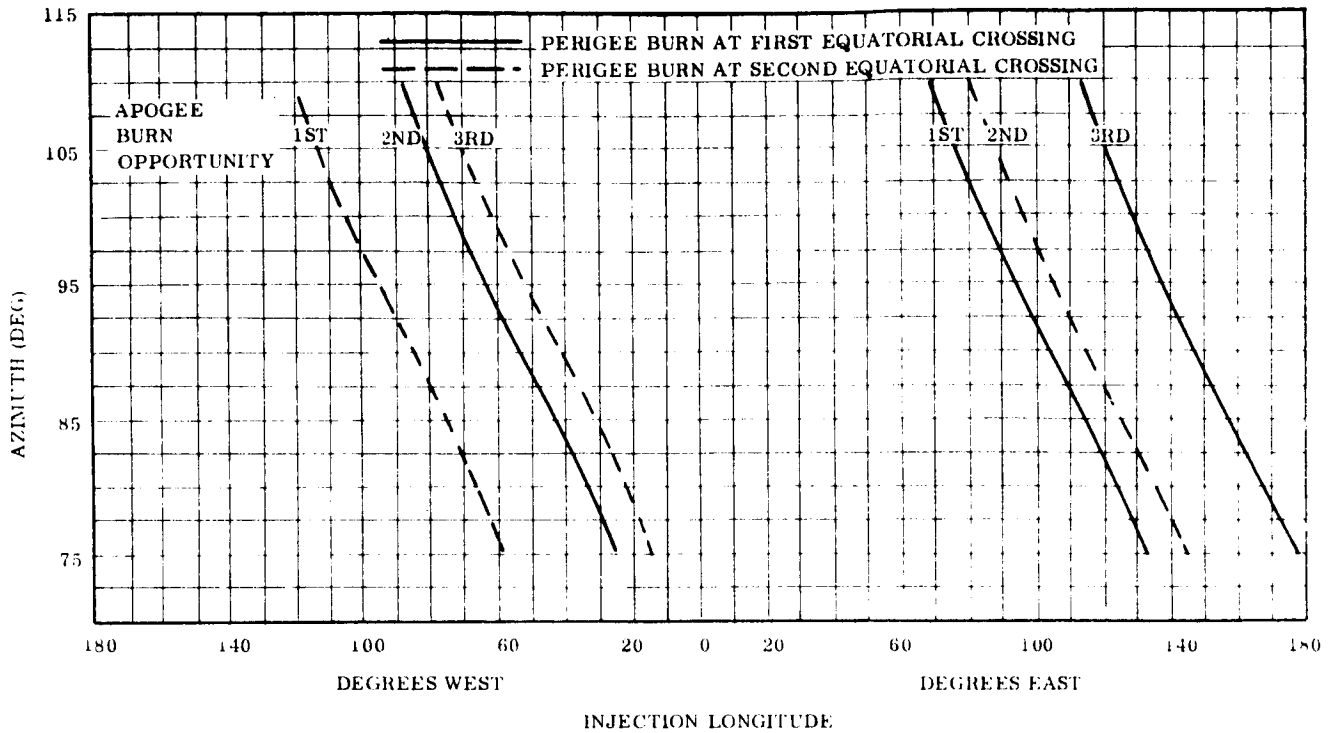


Figure 7.4-1. Variation of Injection Longitude with Launch Azimuth, Perigee Burn Crossing, Apogee Burn Opportunity

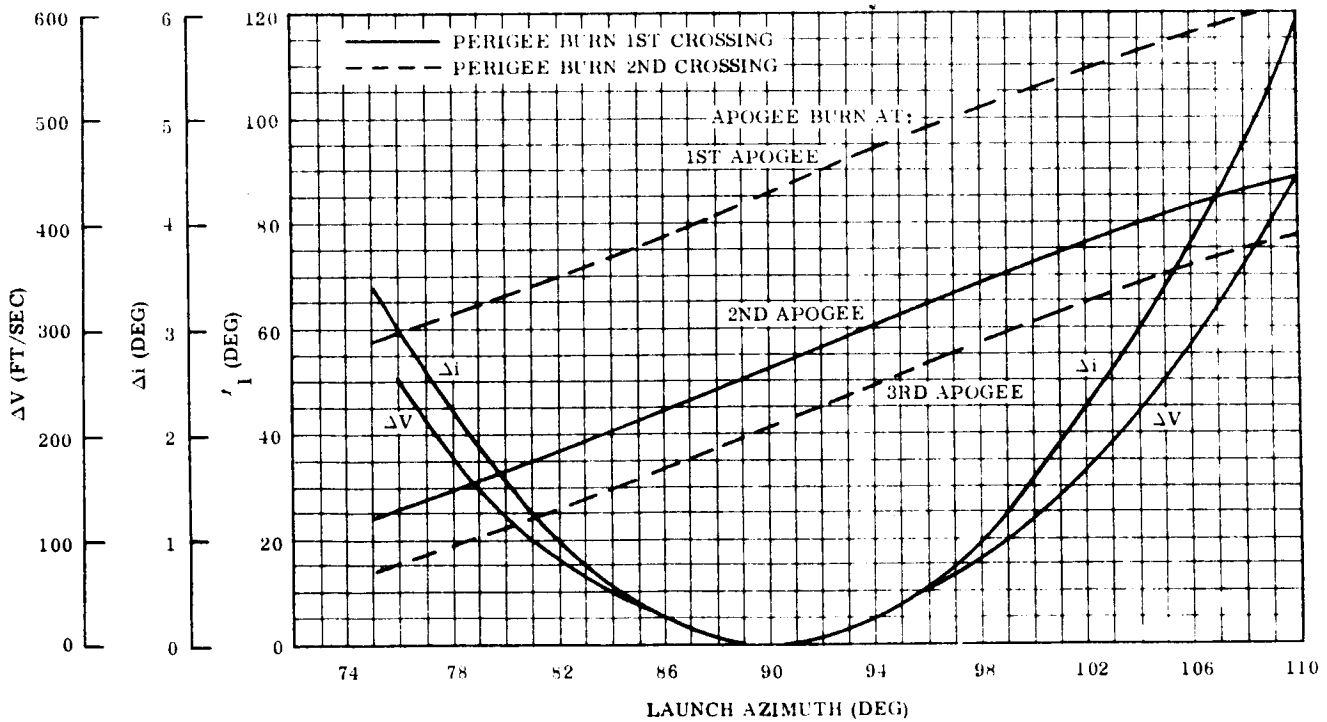


Figure 7.4-2. Effect of Launch Azimuth on: (1) Apogee Longitude at Injection, l_1 , (2) Additional Apogee Inclination Change, Δi , (3) Corresponding Apogee Velocity Penalty, ΔV .

7.4.2 LAUNCH VEHICLE CONSTRAINTS

The three launch vehicles will be considered separately. The limitations the constraint imposes on the ascent trajectory parameters will also be shown. The principal deficiency of the Atlas/Centaur is in the very limited coast time permitted between the first and second burns of the Centaur, approximately 25 minutes. The time between equatorial crossings while in the 100-nm parking orbit is nearly 44 minutes. Thus, the Atlas/Centaur configuration must initiate the transfer orbit at the first equatorial crossing (Table 7-2). There is no particular constraint on the choice for apogee burn.

The Titan IIC principal deficiency lies in the relatively short lifetime of the transtage. Synchronous orbit injection (apogee burn) must take place 6.5 to 7 hours after launch from Cape Kennedy. With a 5.25-hour coast from perigee to first apogee in the transfer ellipse, perigee burn can occur at either of the first two equatorial crossings while in the 100-nm parking orbit. Thus, either Table 7.4-1 or 7.4-2 is applicable, but only for the longitudes of the first apogee for injection into synchronous orbit. An additional Titan IIC restriction is that the launch azimuth must be 93 degrees or greater. (Note that launch azimuth is measured clockwise from due north.)

The Atlas/Agena possesses no overriding constraints that limit its ascent trajectory. Thus, any of the perigee burn/apogee burn combinations shown in Tables 7.4-1 and 7.4-2 are acceptable for this launch vehicle.

7.4.3 TRAJECTORY SELECTION

As discussed in the preceding section, the Atlas/Centaur launch vehicle combination must use the first equatorial crossing as the point for making the perigee burn. Thus, only Table 7.4-1 is applicable. The second apogee is the only one which produces longitudes near the desired 90° W operating longitude. Therefore, the Atlas/Centaur selected orbit initiates transfer at first equatorial crossing and injects to synchronous orbit at the second apogee. The particular launch azimuth chosen is dependent upon the technique for removing injection errors, and upon the time allowed to remove these errors, deploy the parabolic antenna, and synchronize to the proper longitude.

The Titan IIC can initiate the transfer orbit at either the first or second equatorial crossing, but must inject into the synchronous orbit only at the first apogee. Examining the two tables reveals that only the second equatorial crossing yields first apogee longitude near 90°W ; thus, if the Titan IIC is used, second equatorial crossing for perigee burn, and first apogee for injection is the selected orbit. The 93-degree launch azimuth results in injections at about 92°W longitude.

Since the Atlas/Agena is essentially unrestricted in its launch parameters, it will also perigee burn at the second equatorial crossing and apogee burn at the first apogee. At launch, azimuth will be approximately 92 degrees, with the resultant injection longitude being 90°W longitude.

The rationale for selecting the Atlas/Centaur was discussed in Section 5. Briefly, the Atlas/Agena was rejected because of its insufficient payload capability.

The Titan IIC is not used as the reference design launch vehicle because its cost effectiveness is not competitive with the Atlas/Centaur. However, the reference design could be readily made acceptable to this booster, in which case its trajectory, described above, becomes the reference trajectory. A slight plane change of between 2 and 3 degrees might be performed at perigee with this booster.

The Atlas/Centaur trajectory includes a 8.05-degree plane change at perigee to accommodate the nonoptimum apogee retromotor while still utilizing the full Centaur capability. Thus, after the perigee burn, the orbit inclination is 20.45 degrees. This orbit inclination change does not alter the longitude at each apogee. The launch azimuth is selected to be 90° (due east) since this will maximize the payload capability of the launch vehicle. As will be brought out more fully in the vernier maneuver tradeoff analyses (Section 7.5.3), the decision has been made to drift toward the operating point over a period of 30 to 50 days while the antenna-deployed spacecraft is being checked out. In this case, it is better that injection not take place at or very near the operating longitude, since the low thrust in-orbit stationkeeping system will require many days to gradually reduce the drift rate to zero. An alternate

approach analyzed was to synchronize at the operating longitude before deploying the parabolic antenna. Five days was the maximum allowable time to reduce injection errors, drift to and synchronize at the operating longitude, and deploy. The best injection longitude in this case was 62.5°W using a 95° -degree launch azimuth. However, the payload penalty (see Figure 7.5-14, $\theta_E = 1.0^{\circ}$, 90° azimuth, constant ΔV_d , versus 95° azimuth constant drift time) is nearly 70 pounds for drifting on station within 5 days. Thus, the obvious decision is to employ the vernier propulsion system only to eliminate the synchronous orbit injection errors and to induce a 10-ft/sec (1 deg/day) drift toward the 90°W longitude. The station-keeping system, using low thrust resistance jets, monitors and controls the final station acquisition velocity maneuvers.

7.5 INITIAL ACQUISITION PHASE ANALYSES

This section will deal primarily with the velocity impulse required for each of the events making up the initial acquisition phase. The bulk of the vernier velocity requirements are generated by the necessity for removing the synchronous orbit velocity and altitude injection errors. These velocity requirements are dependent upon the magnitude of the apogee burn velocity impulse which is, in turn, dependent upon transfer orbit inclination. Therefore, the analysis will include the perigee burn inclination changes which are made by the Centaur to be compatible with the payload capability of nonoptimum apogee kick motors.

Two separate studies were performed for determining vernier velocity requirements. The preliminary study considered point-mass dynamics only. It did not consider the effects, as such, of the orientation control and stabilization system, nor its sensors. The primary purpose of the study was to pinpoint the major error sources and the manner in which they influence the vernier velocity requirements.

The second study, the reference design analysis, took into account the spin stabilized orientation, the earth sensor, the sun sensors, the changing inertias and center of mass locations before and after apogee burn, and the inertial orientation maintained during the vernier propulsion maneuvers. Also considered in the design analysis is the determination

of the optimum spin rate (between 70 rpm and 80), coning and precession controls, and the despin maneuver. The detailed tradeoff analysis and system description are given in Sections 6.4.3.3 and 5.5.2.1, respectively.

7.5.1 SPIN-UP MOTORS

As discussed in Section 5.5.3.1, the Atlantic Research Corporation Marc 7E1 solid fueled motor is selected for spinning up the transfer orbit payload immediately following payload separation from the Centaur. The exhaust end of the motor is canted away from the vehicle body by 20 degrees, to prevent serious plume impingement on the surface of the spacecraft. The spin rate is 71.7 rpm.

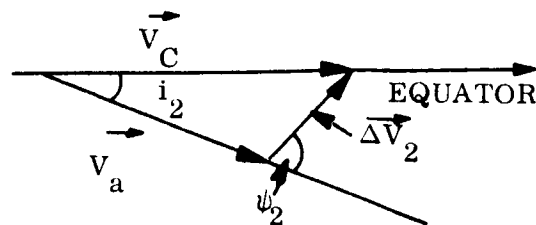
7.5.2 TRANSFER TRAJECTORY ANALYSIS

7.5.2.1 Plane Change Velocity Requirements

To obtain an equatorial orbit, a plane-change maneuver is required since the smallest orbital inclination for launches from Cape Kennedy is 28.5 degrees. For the straightforward orbit transfer mission, this plane change is performed simultaneously with the circularizing maneuver at apogee of the transfer ellipse. The magnitude of the impulse, ΔV_2 , can be determined from the inclination, i_2 ; the apogee velocity, V_a ; and the circular velocity, V_c ; at synchronous altitude.

$$\Delta V_2 = \left[V_a^2 + V_c^2 - 2V_a V_c \cos i_2 \right]^{1/2}$$

The direction in which the velocity impulse is applied can also be found from the following vector diagram.



where $\sin \psi_2 = \frac{V_c}{\Delta V_2} \sin i_2$.

For the minimum inclination of 28.5 degrees and a transfer ellipse with a perigee altitude of 100 nautical miles and apogee altitude equal to synchronous altitude, ΔV_2 equals 6030 ft/sec and $\psi_2 = 53$ degrees.

One method of reducing ΔV_2 is to decrease i_2 by performing a plane change at perigee of the transfer ellipse. The velocity impulse, ΔV_1 , required at perigee is:

$$\Delta V_1 = \left[V_p^2 + V_{c_1}^2 - 2V_p V_{c_1} \cos \alpha \right]^{1/2}$$

where:

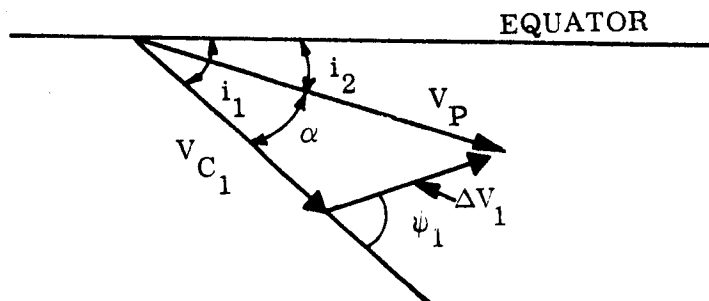
V_p = perigee velocity after impulse ΔV_1 is applied

V_{c_1} = circular velocity at perigee altitude

α = inclination change at perigee

This ΔV_1 is applied at an angle ψ_1 relative to the perigee velocity vector where:

$$\sin \psi_1 = \frac{V_p}{\Delta V_1} \sin \alpha$$



If the entire inclination is removed at apogee, the total velocity, ΔV_t , required to establish and to circularize and plane change at apogee is:

$$\Delta V_t = (V_p - V_{c_1}) + \Delta V_2$$

If inclination changes are performed at apogee and at perigee, the total velocity required is:

$$\Delta V_t = \Delta V_1 + \Delta V_2$$

where:

$$\Delta V_2 = \left[V_a^2 + V_c^2 - 2V_a V_c \cos(i_1 - \alpha) \right]^{1/2}$$

Note that $i_1 - \alpha = i_2$.

Figure 7.5-1 shows ΔV_1 as a function of perigee inclination change, α , while Figure 7.5-2 shows ΔV_2 as a function of apogee inclination change, $i_1 - \alpha$, where i_1 is the original orbital inclination. The total velocity requirement, ΔV_t , is plotted in Figure 7.5-3 with i_1 as a parameter. It can be seen that ΔV_t has a minimum value for α which is approximately equal to 2.5 degrees. For example, consider an orbital inclination of 28.5 degrees with $\alpha = 2.5$. The total velocity is seen to be reduced by 80 ft/sec which is due to an increase of 100 ft/sec at perigee to plane-change 2.5 degrees, and to a decrease of 180 ft/sec at apogee to plane-change 26 degrees. The important consideration here, however, is the ultimate payload capability. For a Titan IIC launch vehicle whose transtage is used for both perigee and apogee burns, a definite saving is realized. However, the Atlas/Centaur launch vehicle requires a separate apogee kick motor whose I_{sp} is different from the I_{sp} of the Centaur. Therefore, additional analysis is often required to maximize the payload into orbit.

Figures 7.5-4 and 7.5-5 present the yaw angles ψ_1 and ψ_2 as a function of α and $i_1 - \alpha$, respectively.

7.5.2.2 Apogee Motor Payload Analysis

Maximum in-orbit payload can be obtained by designing, fabricating, and qualifying an apogee kick motor to meet the very specific requirements imposed by the launch vehicle payload capability, the final orbit altitude, and the apogee burn velocity impulse. This is obviously more expensive than using a readily available flight qualified kick motor. If, however, the total impulse of the available kick motor is not exactly that required for apogee burn, then

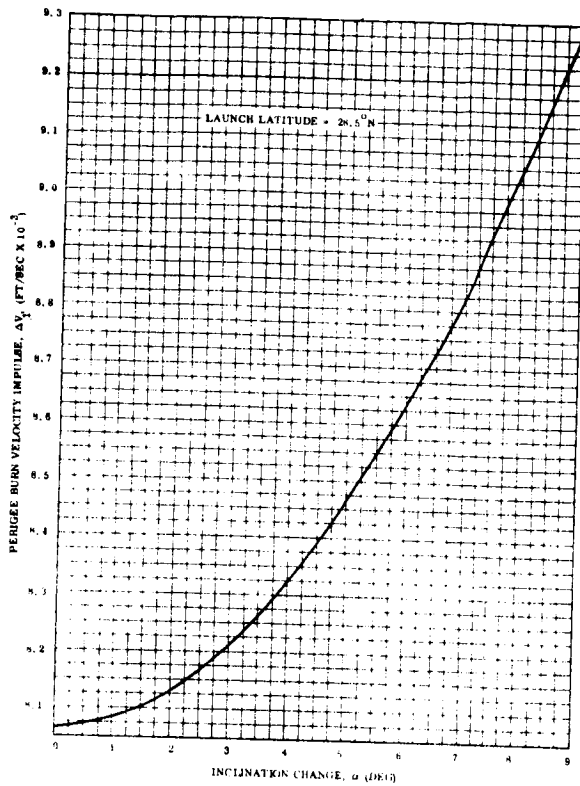


Figure 7.5-1. Perigee Velocity Impulse vs Inclination Change at Perigee

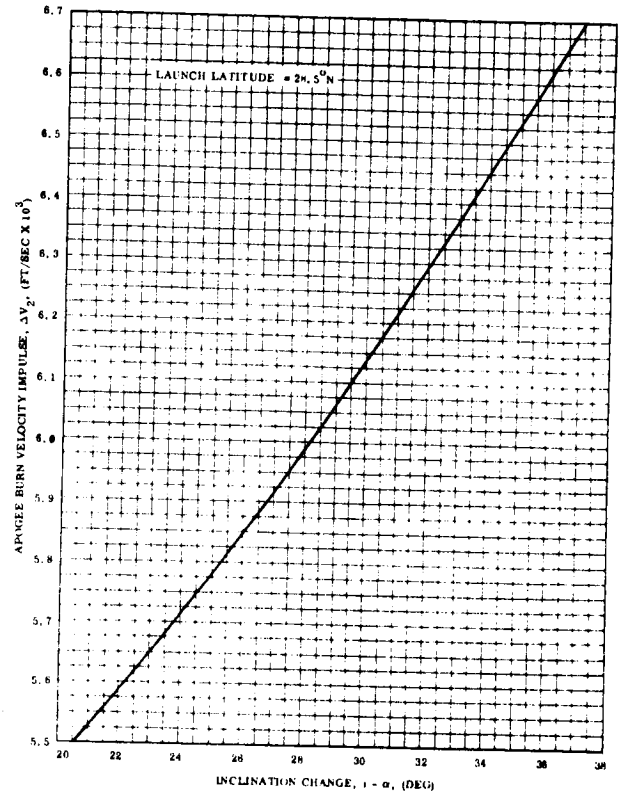


Figure 7.5.2. Apogee Velocity Impulse vs Inclination Change at Apogee

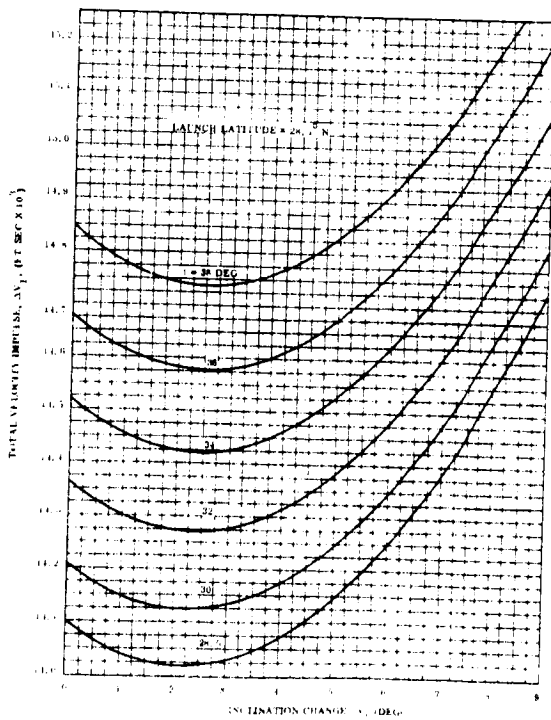


Figure 7.5-3. Variation of Total Velocity Impulse (from 100 nm Circular Parking Orbit to Synchronous Circular Equatorial Orbit) vs Inclination Change at Perigee

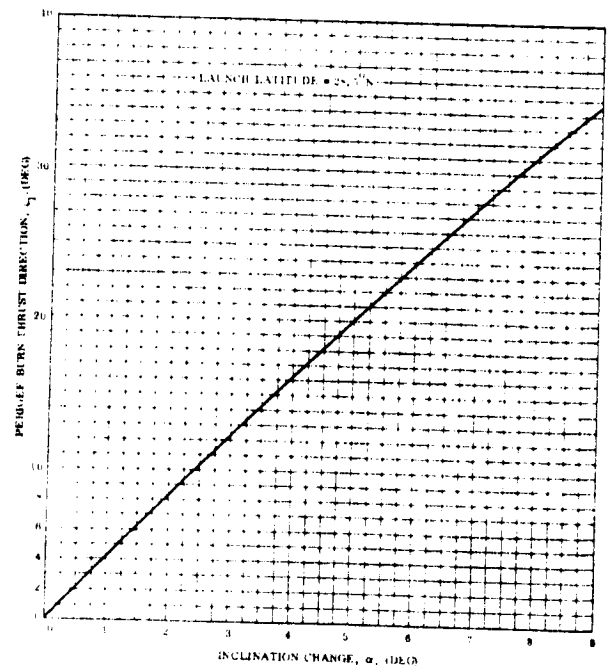


Figure 7.5-4. Variation of Perigee Burn Thrust Direction with Inclination Change at Perigee

compromises must be made. The amount of payload that can be put into the synchronous orbit becomes a function of the total velocity impulse required by the motor. With a given propellant weight, the relationships between weight before and after apogee burn, as a function of apogee burn velocity impulse, are:

$$W_f = W_o e^{-\Delta V_a / g I_{sp}}$$

$$W_f = W_o - \Delta W_p$$

where W_f , the final weight, is the weight after burn.

This weight includes inert apogee motor (dry weight). W_o is the total weight at initiation of apogee burn; ΔW_p is the total propellant weight of the apogee motor; ΔV_a is the apogee burn velocity impulse, and I_{sp} is specific impulse.

From the two expressions, we obtain:

$$W_o = \Delta W_p / \left[1 - e^{-\Delta V_a / g I_{sp}} \right]$$

then:

$$W_f = \Delta W_p \left[\frac{e^{-\Delta V_a / g I_{sp}}}{1 - e^{-\Delta V_a / g I_{sp}}} \right]$$

The net payload weight W_N is $W_N = W_f - W_M$ where W_M is the dry motor weight.

The principal result of this analysis is the determination of the weight the spacecraft in transfer orbit must have if it is to be placed into a synchronous orbit by an apogee motor having specified values for W_p , W_M , and I_{sp} . This weight is a function of the apogee burn velocity impulse, ΔV_a . Figure 7.5-6 shows the W_o versus ΔV_a for both the Antares I motor and the modified Surveyor retrorotor.

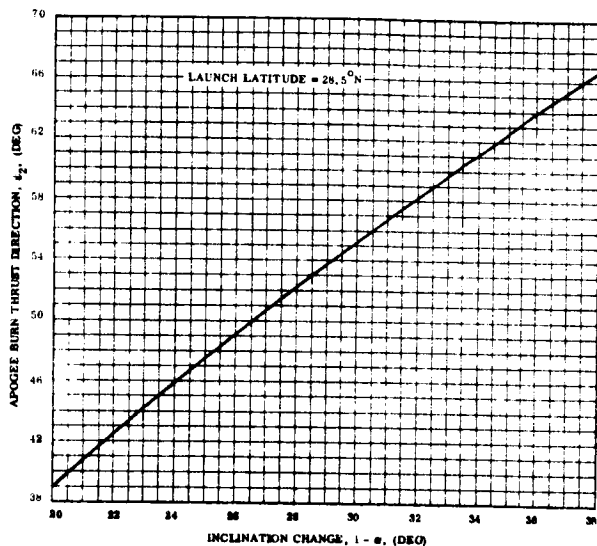


Figure 7.5-5. Variation of Apogee Burn Thrust Direction with Inclination Change at Apogee

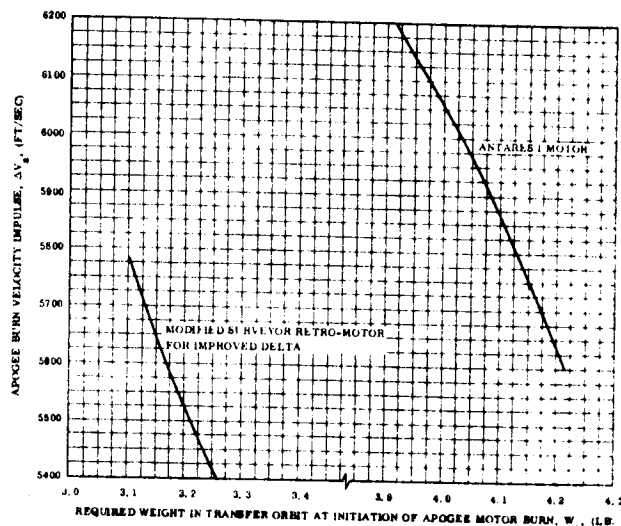


Figure 7.5-6. Variation of Required Transfer Orbit Payload with Apogee Burn Velocity Impulse

It is now necessary to determine the amount of weight the Centaur can put into the transfer orbit as a function of inclination change at perigee. The inclination change at perigee then determines the ΔV_a required of the apogee motor. Before this can be done, however, additional information is required. This includes the payload loss into the transfer orbit as a function of excess velocity impulse at perigee, payload degradation due to Surveyor fairing extension, the weight of the Centaur payload adapter, mass expended during transfer orbit, and the variation of ΔV_a with perigee burn inclination changes.

Payload loss into transfer orbit as a function of excess perigee burn is shown in Figure 7.5-7. This information was obtained from General Dynamics-Convair Division, San Diego, California. The data is applicable specifically to a 4400-pound payload atop the Centaur vehicle. Payloads weighing less than 4400 pounds should result in less payload loss per ft/sec

of perigee burn velocity impulse excess, ΔV_{pE} , since the initial weight is less and the ΔV_{pE} more efficient. Conservatism, however, dictates the decision to use the information obtained from General Dynamics as is.

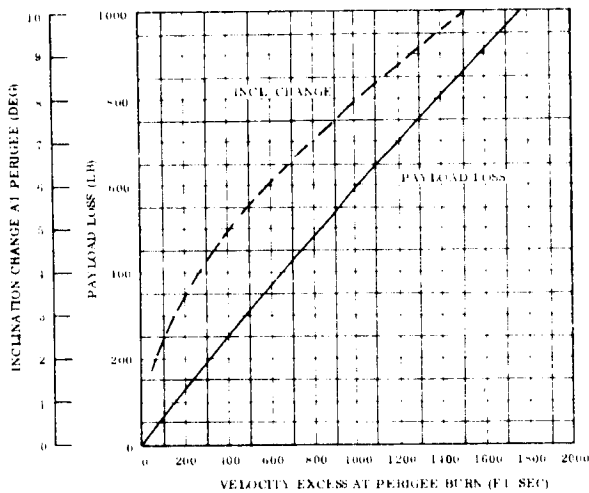


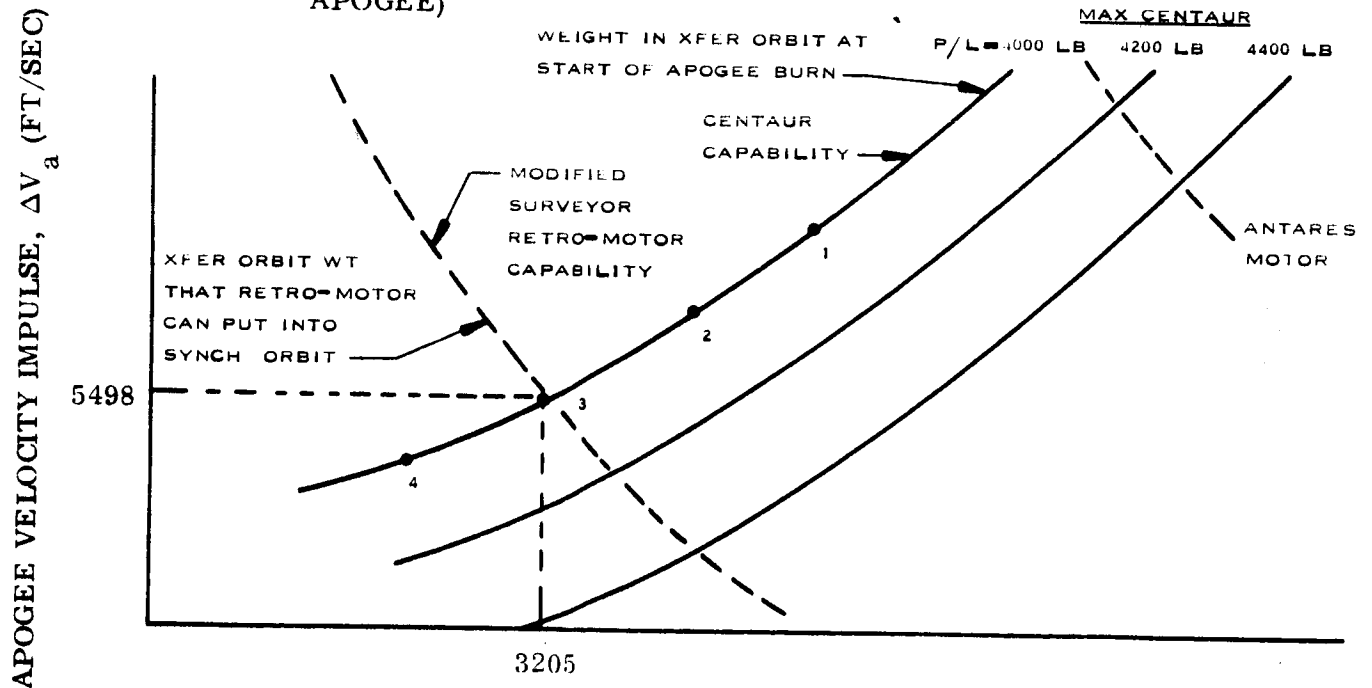
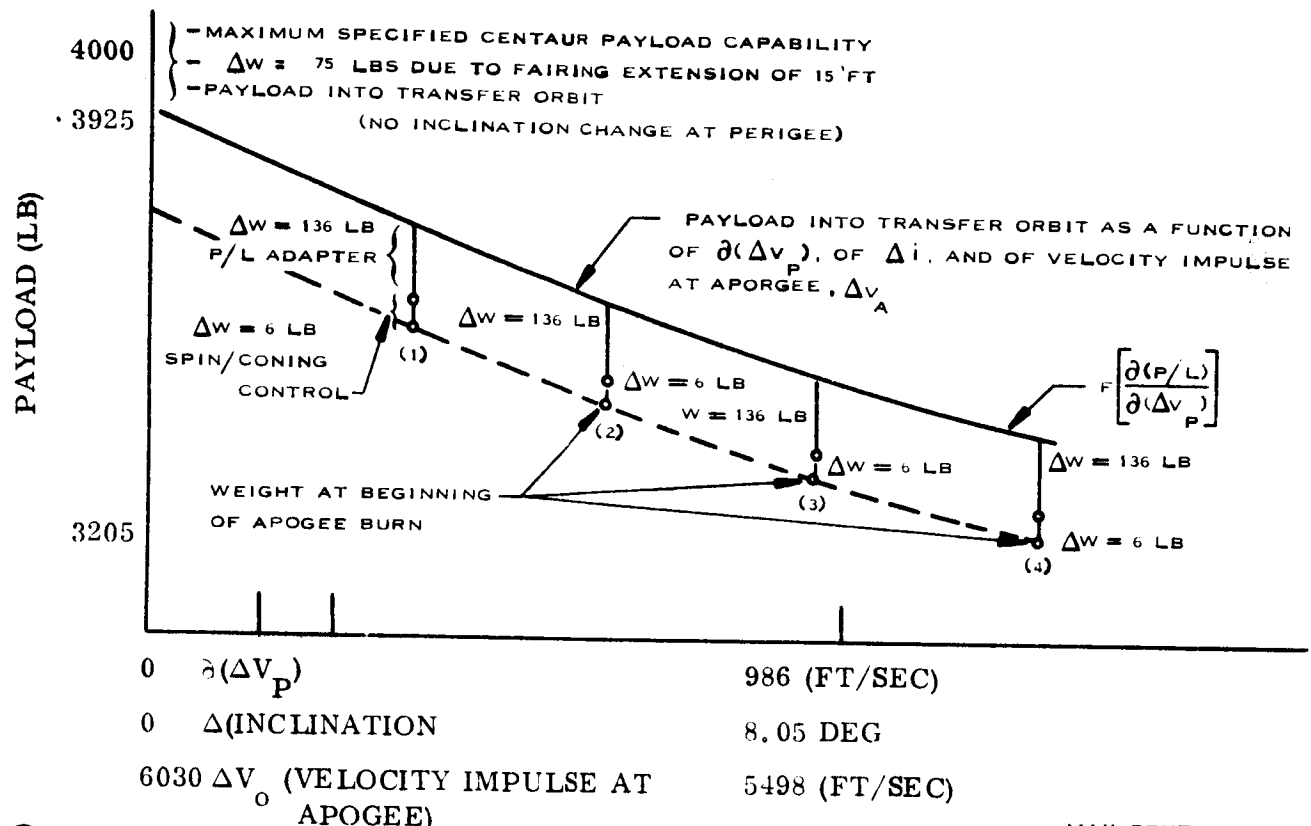
Figure 7.5-7. Payload Loss, and Inclination Change, of Transfer Orbit as Function of Excess Perigee Velocity

The 15-foot Surveyor fairing extension required for the ATS-4 design produces a 75.5-pound payload reduction into the transfer orbit. Thus, for our purposes, the Centaur can inject 3975 pounds into the transfer orbit when the velocity impulse at perigee burn is 8065 ft/sec. This is the nominal ΔV_1 for zero inclination change at perigee burn (see Figure 7.5-1).

There is now information available to determine the payload into transfer orbit. The technique for tying this in with the apogee motor capability is shown functionally in Figure 7.5-8A and B. Figure 7.5-8A shows the 75.5-pound reduction, and the loss in payload with perigee burn velocity excess (reference Figure 7.5-7). Also shown along the abscissa is the corresponding inclination

change and apogee burn velocity impulse. Some of the structural weight, used to absorb booster thrusting induced loads, remains with the Centaur. This is the payload adapter weight ΔW_c . Additional weight (ΔW_E) in terms of fuel expended by the spin-up rockets and in the coning and precession control system, results in additional reduction of weight at initiation of apogee burn. The dotted line shows the net weight at initiation of apogee burn.

The dotted line curve of Figure 7.5-8A is replotted in Figure 7.5-8B. This curve applies only to the 15-foot fairing extension and the specific values of ΔW_c and ΔW_E shown. Since



RETRO MOTOR: ALLOWABLE WEIGHT AT START OF APOGEE BURN
 CENTAUR: ACTUAL WEIGHT IN TRANSFER ORBIT AT START OF APOGEE BURN

Figure 7.5-8. Payload Determination (Nonoptimum Apogee Motors)

the slope of the curve of payload loss with excess perigee burn velocity is constant, the slopes of the curves of Figure 7.5-8A and B are constant. Thus, changes in any of the weights, results in a simple horizontal translation of the solid curve in Figure 7.5-8B. The dotted line curves of Figure 7.5-8B are a replot of the curves of Figure 7.5-6. The intersection of the dotted and solid line curves gives both the necessary weight at initiation of apogee burn and the apogee burn velocity impulse. The rest of the orbit information is obtained from Figures 7.5-1 through 7.5-5. The in-orbit payload is simply $W_o - \Delta W_p$ and the net payload is $W_o - \Delta W_p - W_M$.

7.5.2.3 Reference Design Orbit Characteristics

For the ATS-4 analysis, the information analogous to that shown in Figure 7.5-8B is given in Figure 7.5-9 for both the modified Surveyor retromotor and the Antares I. Centaur payloads of 4000, 4200, and 4400 pounds and two values of ΔW are also shown. Note that $\Delta W = \Delta W_c + \Delta W_E$.

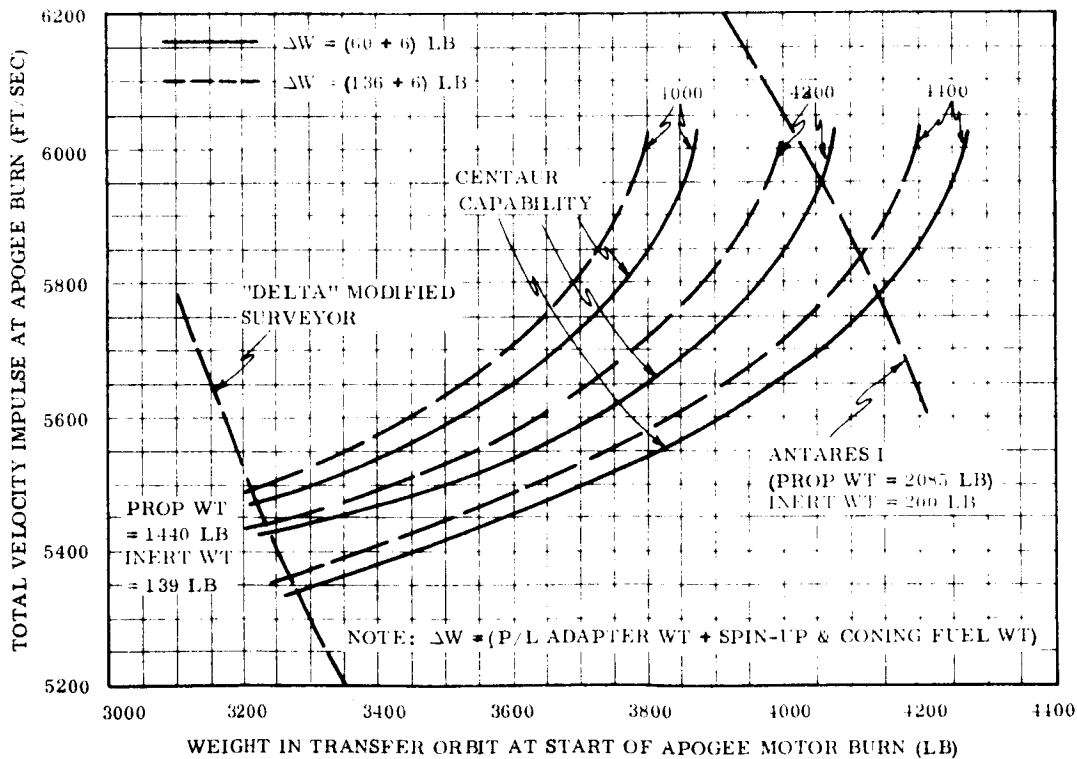


Figure 7.5-9. Determination of Payload Capabilities for Modified Surveyor and Antares I Apogee Motors as a Function of Maximum Centaur P/L Capability

The total payload capability using the modified Surveyor, the Antares I and the extended Surveyor (optimum motor) is shown as a function of maximum Centaur capability in Figure 7.5-10. Figure 7.5-11 shows the growth capability for the same three retromotors as a function of Centaur growth capability. The growth capability is measured with respect to the modified Surveyor retromotor capability using the 4000-pound Centaur payload.

The applicable motor parameters in going from Figures 7.5-9 and 7.5-10 are:

	Antares I	Modified Surveyor	Extended Surveyor
Propellant Weight (lb)	2085	1440	1885 to 2080 (Variable with initial Centaur weight)
Inert Motor Weight (lb)	200	139	126

The selected operating point for the ATS-4 reference design, utilizing the modified Surveyor retromotor as shown in Figure 7.5-9 is:

$$W_o = 3205 \text{ lb}$$

$$\Delta V_a = 5498 \text{ lb}$$

$$W_f = 1765 \text{ lb}$$

$$W_N = 1626 \text{ lb}$$

From the plane change velocity requirements curves (Figures 7.5-1 through 7.5-5) the following information is obtained:

$$\Delta V_p = 9051 \text{ ft/sec}$$

$$\psi_1 = 31.3$$

$$\psi_2 = 39.85$$

$$i_2 = 20.45^\circ (i_1 = 28.5^\circ)$$

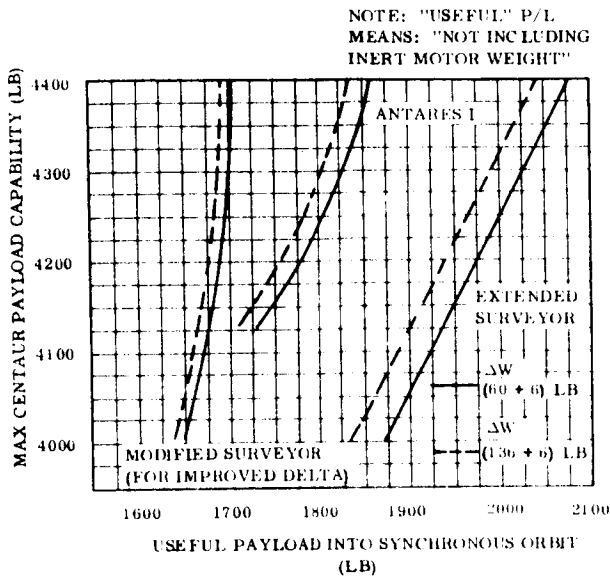


Figure 7.5-10. Variation of Useful Payload Into Synchronous Orbit with Maximum Centaur Capability

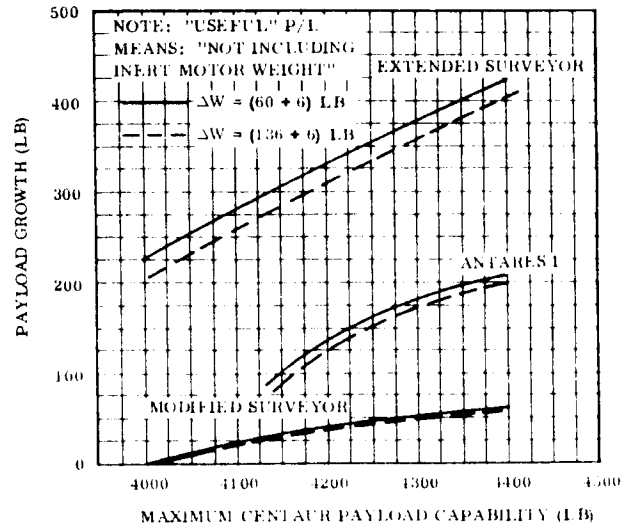


Figure 7.5-11. Growth Capability as a Function of Maximum Centaur Capability and Various Retro Motors

7.5.3 VERNIER VELOCITY REQUIREMENTS

7.5.3.1 Reference Design Vernier Velocity Requirements

This section presents a summary of reference design requirements and an analysis relating to a comparison between vernier maneuver when oriented perpendicular to the orbit plane and when spinning at the orientation of apogee motor burn.

The complete analysis for vernier velocity requirements is described in Sections 6.4 and 5.3. The final results are listed in Table 7.5-1. The source of perigee burn errors is given in Section 7.5.3.2.

The selection of a spinning spacecraft instead of three-axis stabilization is discussed in Section 6.4.2.1. Basically the reason is that spacecraft stabilization during apogee motor

Table 7.5-1. Summary of Total Vernier Maneuver Impulse Requirements

A. VERNIER VELOCITY MANEUVERS		
<u>Error Source 3σ</u>	<u>ΔV - Radial Engine</u>	<u>ΔV - Axial Engine</u>
Apogee Motor		
Total Impulse (1.5%)		± 82 ft/sec
Sun Sensor ($\pm 0.5\%$)	± 48 ft/sec	
Earth Sensor (RF Polang $\pm 1.0^\circ$)	± 96 ft/sec	-1.0 ft/sec
Apogee Motor Angular		
Momentum Vector (0.55°)	± 52.8 ft/sec	-0.3 ft/sec
Apogee Motor Coning (0.55°)	-	-0.3 ft/sec
Perigee Burn (± 8.0 nm ± 60 ft/sec)	<u>± 12.5 ft/sec</u>	<u>± 34.5 ft/sec</u>
RSS ΔV Requirements	123 ft/sec	89 ft/sec
Pulsed Thrusting Inefficiency (71.7 rpm, 175 sec pulse width)	14 ft/sec	
10% Orientation Errors	12.3 ft/sec	9.0 ft/sec
Initiate Drift to 1° /Day	<u>3.4 ft/sec</u>	<u>9.0 ft/sec</u>
Total ΔV Requirements:	152.7 ft/sec	107 ft/sec
Total Impulse (55.5 slug S/C)	8474.9 lb-sec	5933.5 lb-sec
B. CONING, PRECESSION, AND DESPIN TOTAL IMPULSE REQUIREMENTS		
Coning	245 lb-sec	
Precession	264 lb-sec	
Despin	617 lb-sec	
Total Orientation Impulse Requirements	1126 lb-sec	
C. TOTAL VERNIER IMPULSE REQUIREMENTS		
	15539.4 lb-sec	

is mandatory. A three axis stabilized spacecraft will require two sets of thrust levels; a high thrust level system during apogee motor burn, and a low level system for the fine vernier corrections. An alternate set of attitude sensors would also be necessary. In short, a spinning spacecraft does not require active stabilization during apogee motor burn.

For the reference design, the injection errors are referenced to a coordinate system aligned along the vernier velocity propulsion system thruster axes. Thus, the errors will be specified as those which must be removed via the axial engine and those by the radial engine. The axial engine will provide thrusting in a direction parallel to the apogee motor thrust direction. The radial engine can be pulsed in any direction in a plane perpendicular to the spin axis (axial thrust direction, see Figure 7.5-12). This engine must be pulsed since it is aligned perpendicular to the spin axis. There is an approximate 10 percent inefficiency due to the engine pulse width on-time (approximately 175 milliseconds), and the rotation through an angle of 75 degrees (± 37.5 degrees about the desired direction) during each thrusting pulse.

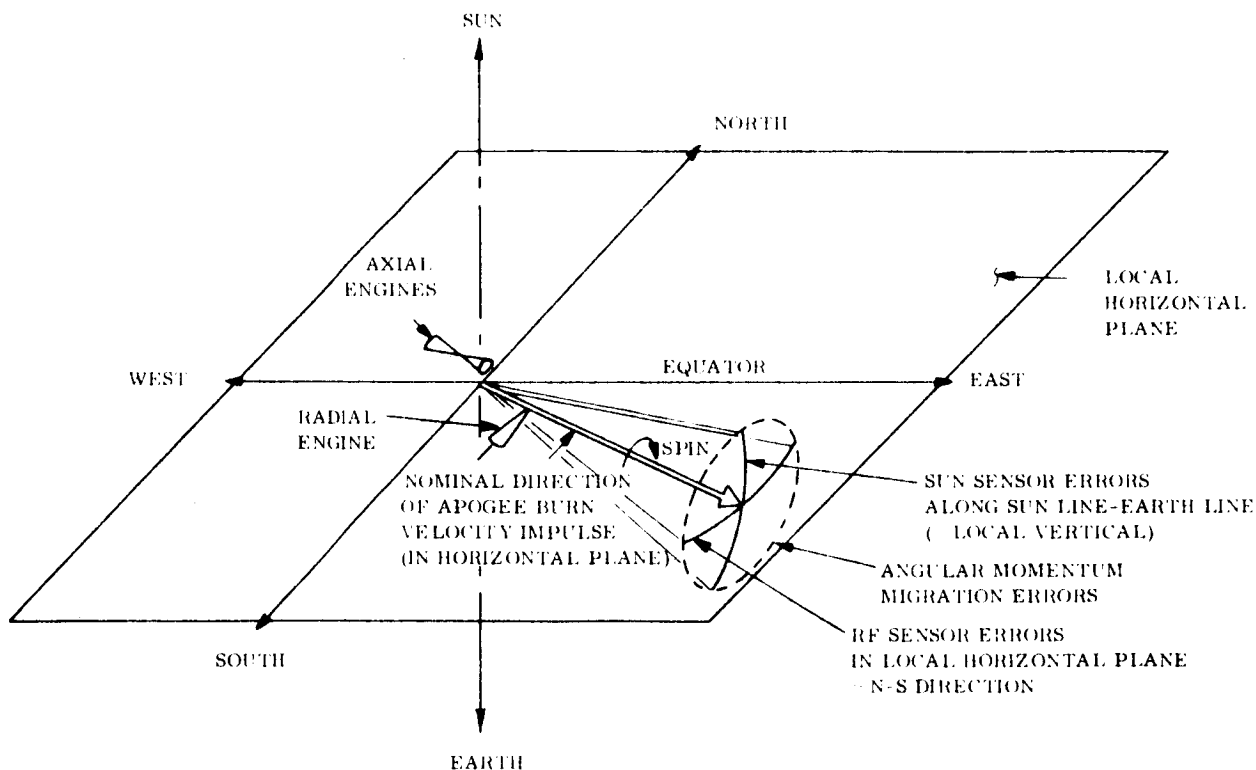
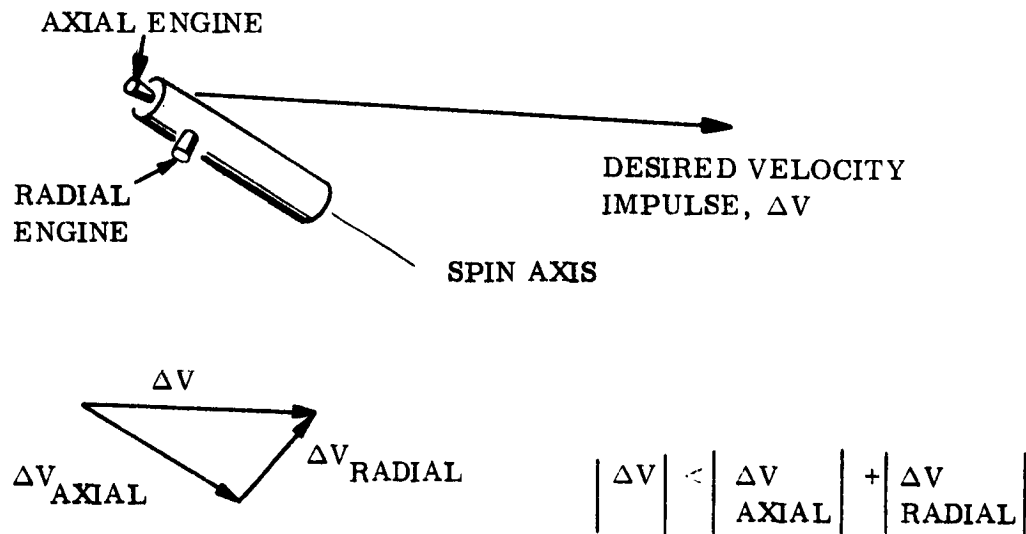


Figure 7.5-12. Description of Orbit Injection Error Sources and Vernier Engine Thrust Directions

The vernier errors will be removed at the apogee motor burn point in the orbit, and perhaps 180 degrees from this point if there are altitude errors at injection. Limited analyses have not shown a more optimum point at which to make the vernier maneuvers. If the vehicle were spinning perpendicular to the orbit plane, then the optimum point for removing the errors is at the apogee and perigee points of the orbit. However, with the orientation held to the apogee burn orientation, neither engine alone is likely to be in the proper direction, therefore, some inefficiency results (see sketch below).



The method for removing altitude errors is to obtain a horizontal component of velocity when making the first vernier velocity correction. Thus, 180 degrees away is perigee, and the second correction is made there. Assuming perigee burn errors only, it will be shown in a later section that the 3σ normalized altitude error, $\delta r_a / r_c$, is 0.0073 and the normalized injection velocity error, $\delta V_c / V_c$, is -0.0036. It is also shown later, that the first velocity correction, ΔV_a , should be:

$$\Delta V_a \left| \frac{\delta V_c}{V_c} + \frac{3}{4} \frac{\delta r_a}{r_c} \right| V_c = 18.5 \text{ ft/sec for } V_c \approx 10^4 \text{ ft/sec}$$

where V_c is the synchronous orbit velocity.

This is in a horizontal direction.

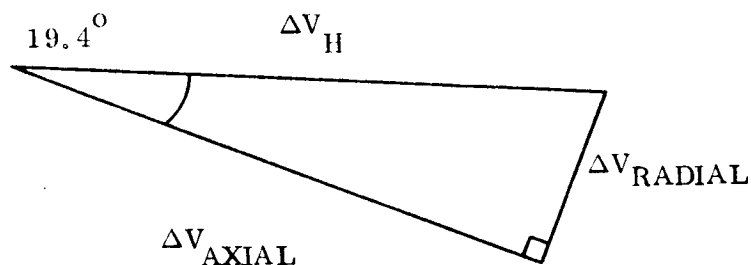
The second correction, ΔV_p , applied at perigee, should be

$$\Delta V_p = \left| \frac{1}{4} \frac{\delta r_a}{r_c} \right| v_c = 18.5 \text{ ft/sec}$$

or the total is

$$\Delta V_H = \Delta V_A + \Delta V_p.$$

The following vector diagram indicates the penalty. The orientation angle is 19.4 degrees.



$$\Delta V_{\text{AXIAL}} = \Delta V \cos 19.4$$

$$\Delta V_{\text{RADIAL}} = \Delta V \sin 19.4$$

$$\Delta V_H = \Delta V_{\text{AX}} + \Delta V_{\text{RAD}} = \Delta V \{ \sin 19.4^\circ + \cos 19.4^\circ \}$$

Thus, the 18.5 ft/sec impulses require 17.5 ft/sec and 6.2 ft/sec of axial and radial velocity impulse, respectively, for each burn. Also, the 10 ft/sec vernier impulse maneuver components are 3.4 and 9 ft/sec for the radial and axial engines, respectively.

The apogee burn errors produce injection velocity errors only. They can be removed at the apogee burn point without suffering the penalties described above for the perigee burn

errors. This is the principal reason for recommending that the vernier thrusting take place at the apogee motor burn point. The relationship of sensor errors to vernier thrust engine is shown in Figure 7.5-12. The sun sensors and earth sensor produce errors along axes which are perpendicular to each other. Since they are both in a plane perpendicular to the spin axis, they are both removed by the radial engine. The angular momentum migration error also produces its major component perpendicular to the spin vector; therefore, it is also removed via the radial engine. The total impulse error is the only apogee burn error that contributes significantly to the axial velocity impulse requirements.

In Table 7.5-1, the 10 percent efficiency loss is estimated on the 71.7 rpm, 175-millisecond thrust duration. Actually the propulsion subsystem was sized on only the basic velocity requirements; i. e., on the total RSS velocity due to injection errors plus the 10 percent orientation and 10-ft/sec drift maneuver (see Section 5.5.3.6). There the precise effect of finite thrust duration was included in determining the total propellant requirements. All the coning, precession, and despun requirements shown in Table 7.5-1 are detailed in Section 5.5.2.1.

7.5.3.2 Preliminary Velocity Requirements Analysis

The preliminary analysis is given here because many of the basic tradeoffs were a result of the conclusions obtained herein. Namely, orientation errors at time of apogee burn should be no greater than one degree; and injection biases provided no payload or operational advantages. Also the slow drift to station, requiring 10 ft/sec and 30 to 50 days, is much more reasonable than the 100 ft/sec (or more) required for fast (5 day) reposition to operating longitude.

The ground rules upon which this analysis is based are somewhat different from those ultimately chosen. No sensors, orientation restrictions, or propulsion system limitations are assumed. For purposes of total impulse and propellant calculations, the spacecraft weight is 2000 pounds. Comparisons will be made on the basis of vernier system weight differences. Transfer orbit inclination is 28.5 degrees.

7.5.3.2.1 Analysis

The two sources of orbit injection errors are perigee and apogee burns. Perigee burn errors result in altitude and velocity errors at apogee of the transfer ellipse. Apogee burn errors produce additional velocity errors at injection, but no additional altitude errors.

The two principal sources of perigee error are the altitude and velocity error at end of perigee burn. This is due to pitch attitude errors. Yaw attitude errors produce comparatively small injection errors not considered in this analysis.

The perigee burn errors are:

$$\text{Altitude, } \delta h_p = \pm 8 \text{ nm}$$

$$\text{Velocity, } \delta V_p = \pm 60 \text{ ft/sec}$$

Note that the two error sources are correlated by -1.

These errors will propagate to apogee injection errors according to the following partial derivatives:

$$\partial r_a / \partial (\Delta V_p) = 10.11 \text{ nm/ft/sec}$$

$$\partial r_a / \partial (r_p) = 54.2 \text{ nm/nm}$$

$$\partial V_a / \partial (\Delta V_p) = -2.2 \text{ ft/sec/ft/sec}$$

$$\partial V_a / \partial r_p = 11.0 \text{ ft/sec/nm}$$

$$\partial V_c / \partial V_a = 0.8788 \text{ ft/sec/ft/sec}$$

$$\partial V_l / \partial (\Delta V_p) = 0.336 \text{ ft/sec/ft/sec}$$

Normalizing these errors yields:

$$\delta r_a / r_c = 0.44 \times 10^{-3} \delta (\Delta V_p) + 2.38 \times 10^{-3} \delta r_p$$

$$\delta V_c / V_c = -0.19 \times 10^{-3} \delta (\Delta V_p) - 0.962 \times 10^{-3} \delta r_p$$

$$\delta V_l = 0.336 \delta (\Delta V_p)$$

where r is distance from center of earth, V is velocity, Δ is impulse change, δ denotes error. The subscripts are: p = perigee, a = apogee, c = circular orbit conditions, \perp = perpendicular to orbit plane.

The in-plane errors, (subscript IN) are measured in the equatorial plane, which is the local vertical plane; the out-of-plane errors (subscript OUT) are measured in local horizontal plane.

For the purposes of worst combinations of errors, all in-plane velocity errors are in the east-west direction, that is, there is no radial component of velocity error in the orbit plane. All out-of-plane errors are in the north-south direction, perpendicular to the nominal orbit (equatorial) plane.

The apogee burn errors are due to apogee motor total impulse uncertainties, $\delta(\Delta V_b)$, and spacecraft orientation errors, θ_ϵ . For this analysis, $\delta(\Delta V_b)/\Delta V_b$ is 1.5 percent, a conservative estimate of retromotor capability. θ_ϵ will be investigated parametrically; values of θ_ϵ , the orientation error, being 0, 1, and 2 degrees. The following partial derivative expressions describe the orbit injection errors for $\delta(\Delta V_b)$ and θ_ϵ :

$$\left. \begin{aligned} \partial V_c / \partial \Delta V_b &= 0.91 \text{ ft/sec} \\ \partial V_\theta / \partial \theta_\epsilon &= -44.5 \text{ ft/sec/deg} \end{aligned} \right\} \text{ in-plane}$$

$$\delta V_\perp = 0.42 \delta(\Delta V_b) \text{ ft/sec/ft/sec} + 93.32 \theta_\epsilon \text{ ft/sec/deg (Out-of-plane)}$$

Normalizing the in-plane errors yields:

$$\delta V_c / V_c = 0.91 \times 10^{-4} \delta(\Delta V_b)$$

$$\delta V_\theta / V_c = -0.445 \times 10^{-2} \theta_\epsilon$$

The final injection errors, using the error source magnitudes and partial derivative expressions above, are tabulated as follows:

<u>Error Source</u>	$\frac{\Delta V_{IN}}{}$	$\frac{\Delta V_{OUT}}{}$	$\frac{\delta a}{a}$	
Perigee burn ($\delta(\Delta V_p) = 60$ ft/sec; $\delta h_p = \pm 80$ nm) $\delta r_a = 165$ nm	37 ft/sec	15 ft/sec	0.0072	
Apogee burn $\delta(\Delta V_b) = 92$ ft/sec	84 ft/sec	38.5 ft/sec	0.0168	
δV_θ				RSS: $(\frac{\delta a}{a})_T$
$\theta_\epsilon = 0^\circ$	0	0	0	0.0182
$\theta_\epsilon = 1^\circ$	44.7 ft/sec	97.8 ft/sec	0.00894	0.0204
$\theta_\epsilon = 2^\circ$	89.4 ft/sec	195.6 ft/sec	0.01788	0.0256

To consider the method by which these errors are to be removed by the vernier propulsion system, it is first necessary to convert the errors into orbital energy or semimajor axis errors, $\frac{\delta a}{a}$. This is done by obtaining the root-sum-square (RSS) of all the randomly occurring independent sources of error:

$$(\delta a)^2 = \sqrt{(\delta a)_p^2 + (\delta a)_a^2}$$

where:

$(\delta a)_p$ is the energy error due to perigee burn,

$(\delta a)_a$ is the energy error due to apogee burn errors, and

$(\delta a)_i$ is energy error in general.

For small deviations from circular orbits, the perigee burn energy error can be expressed as follows:

$$\left(\frac{\delta a}{a}\right)_p = \frac{2\delta r_a}{r_c} + \frac{2\delta V_c}{V_c}$$

For apogee burn:

$$\left(\frac{\delta a}{a}\right)_a^2 = (2\delta V_b/V_c)^2 + (2\delta V_\theta/V_c)^2$$

Note that $\delta r_a = 0$ due to apogee burn errors; also δV_θ is the velocity error induced by θ_ϵ .

For $\left(\frac{\delta a}{a}\right)^2$:

$$\left(\frac{\delta a}{a}\right)^2 = \left(2\frac{\delta r_a}{r_c} + 2\frac{\delta V_c}{V_c}\right)^2 + \left(\frac{2\delta V_b}{V_c}\right)^2 + \left(2\frac{\delta V_\theta}{V_c}\right)^2$$

Only in-plane errors contribute to energy errors.

Since the altitude errors and semimajor axis at injection are known, the total velocity injection error, δV_{ct} , with respect to the nominal circular orbit velocity, V_c , can be computed from the expression:

$$2\frac{\delta V_{ct}}{V_c} = 2\frac{\delta r_c}{r_c} - \frac{\delta a}{a}$$

The total orbit injection error, and, therefore, the actual injection orbit, is known. Assume now the injection errors are to be removed via the two-impulse Hohmann transfer. For the first impulse, applied at the apogee burn point in the orbit, it is required that the perigee distance, $r_{pc} = (R_e + h_c)$, 180 degrees around the orbit, must equal the synchronous orbit altitude, h_c . For discussion purposes the injection errors are assumed to be high, that is, altitude and energy is greater than synchronous orbit energy.

The velocity at apogee necessary to produce the desired perigee altitude is a function of the apogee altitude error itself. The expression is derived as follows:

$$\text{At apogee we have } V_{a_o} = V_c + \delta V_{c_t}$$

The desired velocity at apogee, is, from the vis viva integral:

$$V_{a_1} = \sqrt{\frac{2\mu}{r_a} \cdot \frac{r_{pc}}{r_a + r_p}}$$

where μ is the universal gravitation constant and V_{a_1} is the desired velocity at apogee.

Letting $r_a = r_c + \delta r_a$, V_{a_1} becomes, to a first order or accuracy:

$$V_{a_1} = \frac{\mu}{r_c} \left(1 - \frac{3}{4} \frac{\delta r_a}{r_c} \right).$$

The difference, ΔV_1 , is

$$\Delta V_1 = V_{a_1} - V_{a_0} = -\delta V_{c_t} - \frac{3}{4} \frac{\delta r_a}{r_c} V_c.$$

The second impulse magnitude applied at this perigee in such a manner as to produce apogee altitude also equal to synchronous altitude (and thereby circularize the orbit) is derived as follows:

Velocity when at perigee, V_{p_1} , is from angular momentum conservations:

$$V_{p_1} = V_c + \frac{1}{4} \frac{\delta r_a}{r_c} V_c$$

We want this to be the circular orbit velocity, V_c :

$$V_c = \sqrt{\frac{\mu}{r_c}}$$

The differences, ΔV_2 , is:

$$\Delta V_2 = V_{p_1} - V_{pc} = -\frac{1}{4} \frac{\delta r_a}{r_c} V_c.$$

The total impulse, ΔV_H , is:

$$\Delta V_H = -\delta V_{c_t} - (\delta r_a / r_c) V_c$$

The total absolute impulse is:

$$\Delta V_H = \left| \Delta V_1 \right| + \left| \Delta V_2 \right| = \left| \delta V_{c_t} + \frac{\delta r_c}{r_c} V_c \right|$$

Rearranging this expression:

$$\Delta V_H / V_c = \delta V_{c_t} / V_c + \frac{\delta r_a}{r_a} = \frac{1}{2} \frac{\delta a}{a}$$

therefore,

$$\Delta V_H = \frac{1}{2} \frac{\delta a}{a} V_c$$

Now the vernier velocity requirements for removing the injection error will be computed using either ΔV_H expression above.

The vernier velocity requirements are as follows: where $\Delta V_t = \Delta V_H + \Delta V_{out}$, and where ΔV_{out} is based on RSS values as given in the previous table:

$\frac{\theta}{\epsilon}$	$\frac{\Delta V_H}{V_c}$	$\frac{\Delta V_{out}}{V_c}$	$\frac{\Delta V_t}{V_c}$
0°	91	44	135
1°	102	107	209
2°	128	200	328

The results are plotted in Figure 7.5-13. These are simply the requirements to remove the injection errors, not those required to get back either to the injection longitude or some other longitude.

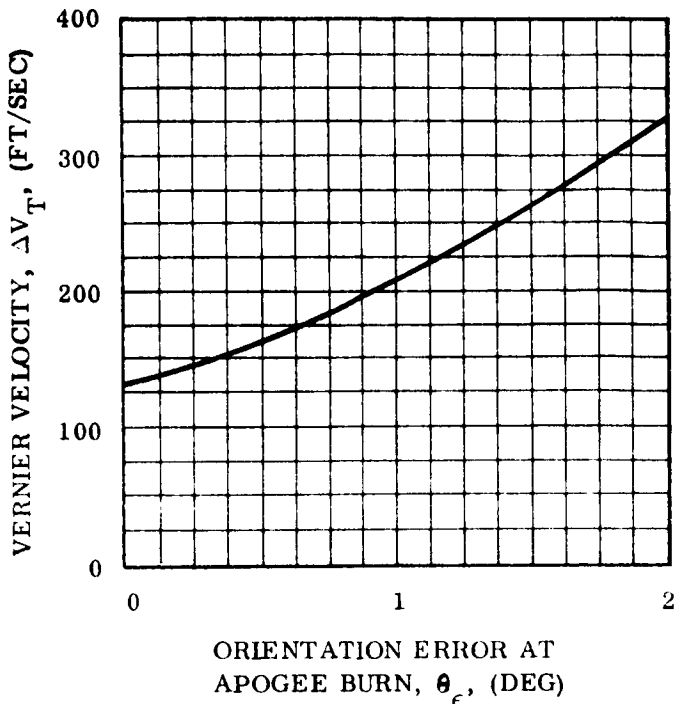


Figure 7.5-13. Variation of Vernier Velocity Requirements with Apogee Burn Orientation Error

One result of injection errors is to cause the spacecraft to slowly drift with respect to an earth ground point. Thus, it is usually necessary to reposition the spacecraft to some desired longitude, after injection errors are removed. The cost of this in terms of time and velocity impulse, ΔV_d , is determined as follows: required longitude drift rate, $\dot{\phi}$, is

$$\dot{\phi} = \Delta\phi_o / t_d$$

where t_d is drift time in days, and $\Delta\phi_o$ is the longitude change desired, in degrees. A rule-of-thumb coefficient relating drift rate to velocity difference is for each 10 feet per second of velocity difference between actual orbit velocity and synchronous orbit velocity, the longitudinal drift rate is one degree per

day. Thus, the velocity, ΔV_d , required to accomplish this maneuver is:

$$\Delta V_d = 2 (10 \dot{\phi}).$$

The 2 in this equation results because $(10 \times \dot{\phi})$ ft/sec are required to first speed up the spacecraft, and then another $(10 \dot{\phi})$ ft/sec are required to stop it again upon reaching the desired longitude.

Consider first the velocity required to simply return to the injection longitude. This is a function of the total energy error at injection and the time required before the first corrective impulse is made. The drift rate as a function of δa is:

$$\begin{aligned}\dot{\phi}_o &= 5.4 \times 10^2 \delta a/a && \text{(deg/day)} \\ &= 2.37 \times 10^{-2} \delta a && \text{(deg/day)}.\end{aligned}$$

Assuming vernier velocity corrections are made at the first apse (1/2 day after apogee burn) and at the first return to the injection point (one day after apogee motor burn, the total drift distance will be between $1/2 \dot{\phi}_o$ and $1 \dot{\phi}_o$. Therefore, let us use $3/4 \dot{\phi}_o$ as the initial drift distance. Then

$$\begin{aligned}\Delta\phi_o &= \frac{3}{4} \dot{\phi}_o = 4.05 \times 10^2 \delta a/a && \text{(deg)} \\ &= 1.78 \times 10^{-2} \delta a && \text{(deg)}.\end{aligned}$$

The rate $\dot{\phi}_o$ is nulled when the velocity injection errors are removed. In order to return to the injection longitude, the additional velocity, ΔV_d , is:

$$\Delta V_d = 15 \dot{\phi}_o / t_d.$$

Now consider the problem of moving from the injection longitude, L_1 , to the operating longitude, L_o . Since the operating longitude is fixed, ΔV_d comparisons become a function of injection longitude only. Then ΔV_d for this is:

$$\Delta V_d = 20 \left[L_1 - L_o \right] / t_d = 20 \Delta L_o / t_d.$$

The combined ΔV_d for the two parts, $\Delta\dot{\phi}_o$ and ΔL_o , is:

$$\Delta V_d = 20 \left[\frac{3}{4} \dot{\phi}_o + \Delta L_o \right] / t_d.$$

The variation of launch azimuth and injection longitude must be considered when determining ΔL_o . A due east launch, 90° , produces $53^\circ W$ longitude injections. $\Delta L_o = 37$ degrees for this case. A 100-degree launch azimuth produces a $72^\circ W$ longitude injection and $\Delta L_o = 18$ degrees. Therefore, ΔV_d is less for the latter case. However, there is a double payload penalty associated with launch azimuth variations.

The first penalty is a 1.2-pound payload loss into transfer orbit per degree of launch azimuth variation, which yields a 0.6-pound payload loss per degree into synchronous orbit. The second penalty, shown in Table 7.4-1 or Figure 7.4-2, is the inclination plane-change penalty at apogee. This penalty can be converted to payload loss via the equation:

$$W_f = W_o e^{-\Delta V_a / g I_{sp}}$$

$$\partial W_f = -W_f \frac{\partial (\Delta V_a)}{g I_{sp}}$$

For a typical apogee motor with an I_{sp} of 280 lb-sec/lb and for a nominal injection weight, W_f , of 2000 pounds, the payload loss per foot per second of ΔV_a is:

$$\partial W_f = \Delta V_a / 9016 = 1.1 \times 10^{-4} W_f$$

or

$$\text{(for } W_f = 2000 \text{ lb)}$$

$$\partial W_f = 0.22 \text{ lb/ft/sec}$$

The total vernier velocity can be related to vernier system propellant weight by computing the total impulse, $\Delta V_t \cdot (W_f / 32.2)$ and then dividing by the specific impulse, I_{sp} . Assume the I_{sp} of the vernier propellant to be 225 lb-sec/lb. Then, fuel weight, W_E , is

$$W_E = \Delta V_t W_f / g I_{sp} = \Delta V_t W_f / 7.23 \times 10^3.$$

Again with $W_f = 2000$ lb, W_E is, per foot per second of ΔV_t

$$W_E = 0.275 \text{ lb/ft/sec}$$

Tankage weight is about 15 percent of fuel weight, therefore, the total vernier weight, W_V , is:

$$W_V = 0.316 \text{ lb/ft/sec}$$

Detailed tradeoffs between launch azimuth, injection longitude and orientation errors can now be made.

Summarizing, we have:

1. Figure 7.5-13 which gives $\Delta V_H + \Delta V_O$ as a function of θ_ϵ .
2. ΔV_d , as a function of injection longitude and, therefore, launch azimuth, let $t_d = 4$ days.
3. Payload penalty due to launch azimuth
 $\partial (P/L) = 0.6 \text{ lb/deg} + 0.22 \text{ lb/ft/sec}$
 (Figure 7.4-2 gives the velocity penalty as a function of launch azimuth for the second term on the righthand side.)
4. Vernier propulsion weight penalty: 0.316 lb/ft/sec of additional vernier velocity. The total vernier velocity, V_t , is computed from:

$$V_t = \Delta V_H + \Delta V_{out} + \Delta V_d$$

Figures 7.5-14 and 7.5-15, along with Table 7.5-2 summarize the results of the study. Figure 7.5-14 presents vernier weight requirements as a function of launch azimuth. Then for the minimum weight launch azimuth (95°) the vernier weight is plotted as a function of θ_ϵ , the orientation errors at apogee burn. An additional parameter is to be noted in these summary illustrations and table. It was decided to investigate the possible weight advantage by letting the spacecraft slowly drift to the operating longitude, at a rate of 1 deg/day. As shown, up to 66 pounds of vernier weight reduction is possible at $\theta_\epsilon = 1$ degree. Therefore, if we let $\Delta V_d = 10 \text{ ft/sec}$, the drift rate will be a constant 1 deg/day and the total drift time will be variable. With $t_d = 4$ days, the drift rate is variable and the drift time constant.

7.5.3.2.2 Discussion of Results

In Table 7.5-2 all the payload penalty contributions to the total vernier reference payload are shown. Particularly interesting is the decrease in ΔV_d as the injection longitude approaches $90^\circ W$. Meanwhile launch azimuth and inclination change payload penalties

Table 7.5-2. Vernier Weight Tradeoff Summary

Launch Azimuth, θ_c (deg)	Inj. Long L_o (deg)	Drift Dist. ΔL_o (deg)	Payload Penalty Lau Azi (lb)	Payload Penalty Δ (incl) (lb)	$3/4 \phi_o$ (deg)	$3/4 \phi_o + \Delta L_o$ (deg)	ΔV_d (fps)	$\Delta(P.L.)$ Due to ΔV_d (lb)	Total P.L. Penalties (lb)	P.L. - Inj. Errors $\Delta V_T = \Delta V_H + V_C$ (lb)	Total Reference Weight Cost (Constant drift rate = $1^\circ/\text{day}$)	P/L ΔV_d 10 ft. sec (lb)	Total Reference Weight Cost (lb)
90, 0	53.0	37.0	0.0	0.0	7.4	41.4	222.0	70.0	70.0	42.7	112.7	3.2	45.4
90, 1	53.0	37.0	0.0	0.0	8.2	43.2	226.0	71.5	71.5	66.1	137.7	3.2	69.3
90, 2	53.0	37.0	0.0	0.0	10.4	47.4	237.0	75.0	75.0	102.0	177.0	3.2	105.2
95, 0	62.5	27.5	3.0	8.5	7.4	35.0	175.0	55.2	67.0	42.7	109.7	3.2	57.7
95, 1	62.5	27.5	3.0	8.4	8.2	35.7	178.5	56.5	68.3	66.1	134.4	3.2	81.1
95, 2	62.5	27.5	3.0	8.5	10.4	38.0	190.0	60.0	71.8	102.0	173.8	3.2	117.0
100, 0	72.0	18.0	6.0	26.5	7.4	25.4	127.0	40.2	72.7	42.7	115.4	3.2	78.2
100, 1	72.0	18.0	6.0	26.3	8.2	26.2	131.0	41.5	74.0	66.1	140.1	3.2	101.6
100, 2	72.0	18.0	6.0	26.5	10.4	28.4	142.0	45.0	77.5	102.0	179.5	3.2	137.5
105, 0	80.5	9.5	9.0	55.6	7.4	16.9	84.5	26.7	91.3	42.7	134.0	3.2	107.5
105, 1	80.5	9.5	9.0	55.6	8.2	17.7	88.5	28.1	92.7	66.1	158.8	3.2	130.9
105, 2	80.5	9.5	9.0	55.6	10.4	19.9	99.5	31.5	96.1	102.0	198.1	3.2	166.8
110, 0	88.0	2.0	12.0	97.0	7.4	9.4	47.0	14.9	123.9	427.0	166.6	3.2	115.0
110, 1	88.0	2.0	12.0	97.0	8.2	10.2	51.0	16.2	125.2	66.1	191.3	3.2	178.4
110, 2	88.0	2.0	12.0	97.0	10.4	12.4	62.0	19.6	128.6	102.0	230.6	3.2	214.3

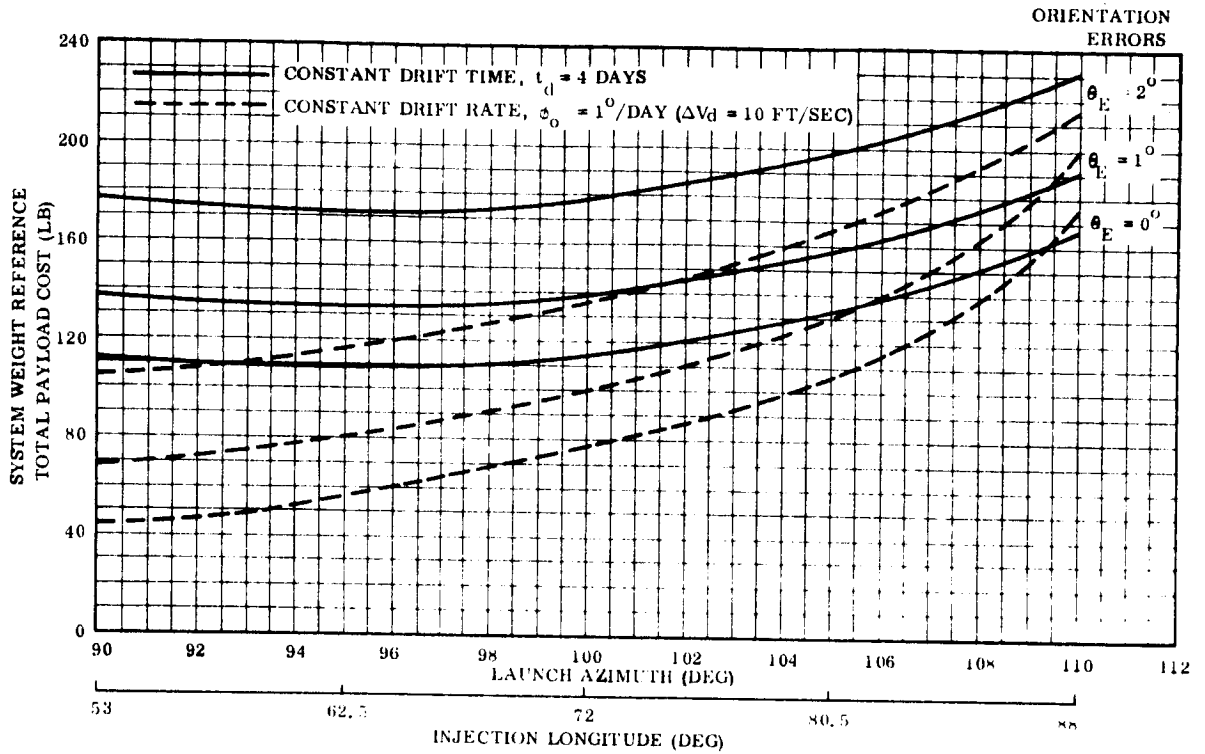


Figure 7.5-14. Variation of Total Payload Weight Cost with Launch Azimuth (or Injection Longitude) and Orientation Errors at Apogee Burn

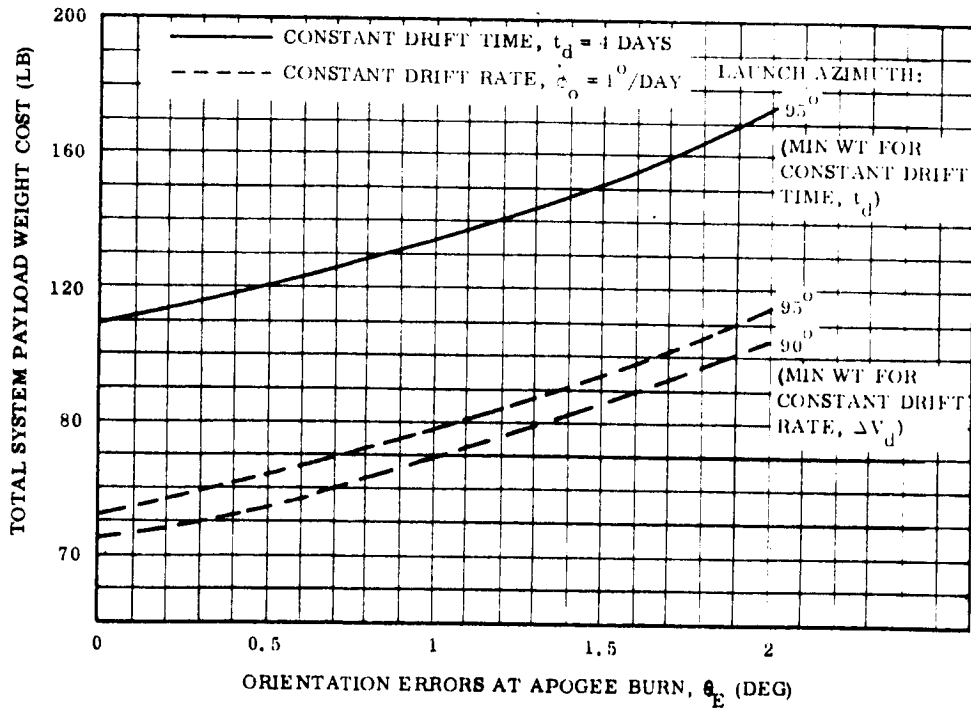


Figure 7.5-15. Variation of Total Payload Weight Cost with Apogee Motor Orientation Errors

increase even more rapidly, thus, a minimum is reached at about 95° launch azimuth as shown in Figure 7.5-14 (see third column in from right, "Total Ref Weight Cost"). The two columns on the extreme right show the payload cost when the drift rate is held constant. The graph of Figure 7.5-15 shows the payload savings much more dramatically. Approximately 66 pounds is saved by going at a 90° launch azimuth and 1 deg/day residual drift rate.

Two additional modifications to the injection sequence are available for reducing vernier propulsion requirements. They are based on ground tracking and modification of the apogee motor burn velocity. Assume that $\theta_\epsilon = 1$ degree. Perigee burn errors could be reduced by tracking, orbit determination, and a fine correction to the apogee burn thrust correction. If the total perigee error is eliminated, the 3σ RSS $\delta a/a$ is

$$\left(\frac{\delta a}{a}\right)^2 = 4\left(\frac{\delta V_b}{V_c}\right)^2 + 4\left(\frac{\delta V_\theta}{V_c}\right)^2$$

which for $\theta_\epsilon = 1$ degree is

$$\approx 4 \left[\left(\frac{4}{10^4}\right)^2 + \left(\frac{44.7}{10^4}\right)^2 \right]$$

and

$$\frac{\delta a}{a} = 0.0180$$

Now the drift rate error due to injection errors is

$$\dot{\phi}_p = 9.75 \text{ deg/day}$$

instead of 11 deg/day with perigee burn errors included.

The drift distance is $3/4 \dot{\phi}_p$, or 7.3 degrees, instead of the 8.2 deg/day shown in Table 7.5-2. Now ΔV_d is reduced by $20/4 (0.9) = 4.5$ ft/sec, which in terms of vernier weight is 1.42 pounds.

The second modification assumes an accelerometer can be aligned parallel to apogee burn direction. If the apogee burn total impulse is low, the axial thrusters are immediately turned on to make up this difference. Assume the perigee errors are also being eliminated as above. Now the energy error is

$$\frac{\delta a}{a} = 2 \frac{\delta V}{V_c} \theta$$

and the drift rate error is

$$\phi'_{\theta_\epsilon} = 4.85 \text{ deg}$$

and the initial drift distance is

$$\frac{3}{4} \phi'_{\theta_\epsilon} = 3.65 \text{ deg}$$

Compared with 8.2 degrees, this is a reduction of 4.55 degrees. Now the ΔV_d reduction is 22.75 ft/sec and the weight saving is 7.2 pounds. An additional saving is realized by a reduction in the ΔV_{out} . It goes from 107 to 97.8 ft/sec, a decrease of 9.8 ft/sec which is 3.1 pounds. Note that the 107 ft/sec is equivalent to 33.8 pounds; therefore, over 30 pounds of vernier weight is attributable to the out-of-plane component of θ_ϵ (orientation) injection errors. This is the principal reason for requiring θ_ϵ to be not more than one degree.

7.5.3.2.3 Summary of Results

- a. For constant drift times (5 days, 4 days after injection errors removed) the minimum vernier weight is realized when launch azimuth is 95° , injection longitude $62.5^\circ W$.
- b. Constant drift rate (1 deg/day) produces minimum vernier propulsion requirements when the launch azimuth is 90° , launch injection is $53^\circ W$. Up to 50 days drift time is required. The vernier weight is approximately 66 pounds less than that required for the best constant drift time injection parameters.

- c. Modifying the apogee burn can result in a saving of up to 10.3 pounds. However, the on-board equipment required to monitor and control the modified burn, may well exceed 10.3 pounds, and may introduce additional spacecraft system operations. This result does not apply to the constant drift rate maneuver.
- d. The principle contribution to injection error magnitudes is the out-of-plane contribution due to orientation errors. The vernier weight penalty is approximately 30 lb/deg.

7.5.3.2.4 Conclusions

The obvious conclusions are:

- a. Permit a constant drift rate of approximately 1 deg/day to get on station.
- b. Minimize orientation errors at apogee burn.
- c. Modification of apogee burn does not seem to produce any significant weight savings.

7.5.3.3 Injection Bias Analysis

An orbit injection bias analysis was performed. The purpose was to determine if it is more economical, in terms of net useful payload, to induce a drift rate by altering the perigee or apogee burn magnitudes, and thereby alter the energy of the spacecraft in orbit. For injections to the east of the operating longitude, an energy excess at injection will produce a drift in the westward direction. Alternately, injections to the west of the operating longitude require an energy deficit to induce drift toward the operating longitude. Both cases are examined.

In the analysis, two payload factors are compared; the additional (or decrease in) energy expended at perigee, or apogee, burn results in a loss (or gain) in in-orbit payload capability, but the decrease in initial drift rate velocity, ΔV_d , results in a decreased vernier propulsion system weight and, therefore, a gain in payload weight. Again the launch azimuth will be varied and the consequent loss in payload included. However, only one value of orientation error, θ_ϵ , is considered; that is $\theta_\epsilon = 1$ degree.

The injection will be biased by an amount that allows the spacecraft to arrive on station 5 days after orbit injection if the injection were perfect. It is assumed, however, that one day will be required to remove injection errors. Therefore, t_d still equals 4 days.

The desired drift rate at injection, $\dot{\phi}_B$, is $\dot{\phi}_B = \Delta L_o / (t_d + 1)$
 where ΔL_o is the difference between the injection and operating longitudes.

From the expression given above for $\frac{3}{4} \dot{\phi}_o$ the required injection bias is:

$$(\delta a/a)_B = 1.85 \times 10^{-3} \dot{\phi}_B$$

Assume first an energy excess bias; launch is to the east of the operating longitude. The worst case in terms of ΔV_d occurs when the biased injection itself is 3σ energy deficient. Now the drift rate may be very low or even in the wrong direction. In this case, the energy at injection $(\delta a/a)_I$ is

$$\left(\frac{\delta a}{a}\right)_I = \left(\frac{\delta a}{a}\right)_B - \left(\frac{\delta a}{a}\right)_{\theta_\epsilon = 1^\circ}$$

The total distance ΔL to the operating longitude, after one day is spent reducing the injection errors, is

$$\Delta L = \Delta L_o + \left[\frac{3}{4} \dot{\phi}_o - \frac{\Delta L_o}{(t_d + 1)} \right]$$

which, in terms of $\delta a/a$ is

$$\Delta L = \Delta L_o + \left[405 \left(\frac{\delta a}{a}\right) - \left(\frac{\delta a}{a}\right) / 3.7 \times 10^4 (t_d + 1) \right].$$

The bracketed terms represents the change in longitude during the one day required to remove the injection errors. The quantity $\frac{3}{4} \dot{\phi}_o = 405 \frac{\delta a}{a}$ equals 9.2 degrees when $\theta_\epsilon = 1$ degree. Therefore, using the former expression above, ΔL becomes

$$\begin{aligned} \Delta L &= 9.2 + \Delta L_o \left[1 - \frac{1}{t_d + 1} \right] \\ &= 9.2 + \Delta L_o \left[t_d / (t_d + 1) \right] \end{aligned}$$

With the injection errors removed, the drift rate is equal to the biased drift rate, $\Delta L_o / (t_d + 1)$.

The required drift rate to get on station in 4 days is

$$\Delta L / t_d = 9.2 / t_d + \frac{\Delta L_o}{t_d + 1}$$

but this is simply $(\frac{3}{4} \phi_o' / t_d + \phi_B')$. The actual drift rate is ϕ_B' , therefore, the desired increase in drift rate is $(3/4) (\phi_o' / t_d)$. The drift rate velocity required to produce this rate is

$$\Delta V_{d1} = 7.5 \phi_o' / t_d.$$

The velocity required to remove the drift rate when on station is

$$\begin{aligned} \Delta V_{d2} &= 10 \left| \Delta L / t_d \right| \\ &= 7.5 \phi_o' / t_d + 10 \Delta L_o / (t_d + 1). \end{aligned}$$

For nominal injections, the velocity required to induce, or remove, the drift rate, $1/2 \Delta V_d$, was shown to be

$$1/2 \Delta V_d = 7.5 \phi_o' / t_d + 10 \Delta L_o / t_d$$

$$\frac{\Delta V_d}{2} - \Delta V_{d1} = 10 \frac{\Delta L_o}{t_d}$$

The velocity reduction to remove the drift rate is

$$\frac{\Delta V_d}{2} - \Delta V_{d2} = \frac{10 \Delta L_o}{t_d(t_d + 1)}$$

The total velocity saving, ΔV_s , is

$$\begin{aligned} \Delta V_s &= \frac{10 \Delta L_o}{t_d} \left(1 + \frac{1}{t_d + 1} \right) \\ &= \frac{10 \Delta L_o}{t_d} \left(\frac{t_d + 2}{t_d + 1} \right) \end{aligned}$$

with $t_d = 4$ days $\Delta V_s = 3\Delta L_o$ where ΔV_s is in feet per second, and ΔL_o in degrees. The vernier weight saving, $(P/L)_s$ is 0.316 lb/ft/sec.

$$\therefore (P/L)_s = 0.948 \Delta L_o \text{ lb}$$

Although the preceding analysis was based on an energy excess biased injection, exactly the same equation applies when the energy deficit biased injection is employed for injection longitudes west of the operating longitude. The worst case now occurs when the injection errors produce a 3σ excess of energy.

To complete the analysis, it is necessary to determine the payload penalty for attaining the excess energy at injection. For the energy deficit cases, this is actually an additional payload saving. However, the applicable launch azimuths for injections west of $90^\circ W$ incur extremely large apogee burn inclination change payload penalties.

The required energy excess (or deficit) is a function of ΔL_o since this dictates the rate at which initial drifting is to take place. It was shown previously that $(\delta a/a)_B = 3.7 \times 10^4 \Delta L_o$. If the perigee burn is to provide the energy excess (or deficit), then the normalized error equations derived at the beginning of Section 7.5.3.2 are

$$\frac{\delta r_a}{rc} = 0.44 \times 10^{-3} \delta(\Delta V_p)$$

$$\frac{\delta V_c}{V_c} = 0.19 \times 10^{-3} \delta(\Delta V_p)$$

The total energy was also shown to be $(\delta a/a)_i = 2 \delta V_c/V_c + 2 \delta r_a/rc$, thus, we obtain for $\delta(\Delta V_p)$

$$\frac{\delta a}{a}_i = 0.5 \times 10^{-3} \delta(\Delta V_p)$$

$$\text{or } \delta(\Delta V_p) = (3.7 \times 10^{-4} \Delta L_o / 5 \times 10^{-4}) = 0.74 \Delta L_o$$

From Figure 7.5-7, the transfer orbit payload penalty, as a function of perigee burn velocity excess is 0.70 lb/ft/sec. The loss in in-orbit payload is $\delta(\omega_f) = \delta(\omega_o) e^{-\Delta V_a/gI_{sp}}$, which, for $\Delta V_a \approx 6100$ ft/sec and $I_{sp} = 280$ sec, $e^{-\Delta V_a/gI_{sp}} = 0.51$. Therefore, the net loss in payload is $(p/L)_{loss} = (0.7) (0.51) \delta(\Delta V_p) = 0.264 \Delta L_o$

It is seen that the perigee burn induces a relatively small payload penalty in terms of in-orbit energy requirements. Unfortunately, however, there is an out-of-plane induced velocity component that must be removed. The normalized error component here is:

$$\begin{aligned} \Delta V_{\perp} &= 0.33 (\Delta V_p) \\ &= (0.336) (0.74 \Delta L_o) \\ &= 0.249 \Delta L_o \end{aligned}$$

with the payload loss becoming, for 0.316 lb/ft/sec

$$(p/L)_{loss} = 0.079 \Delta L_o \text{ lb}$$

with the payload loss becoming, for 0.316 lb/ft/sec

$$(p/L)_{loss} = 0.079 \Delta L_o \text{ lb}$$

It is possible that this loss could be made up by proper compensation of the direction of apogee burn, which itself would produce a small penalty. However, the penalty is still small even assuming that this additional velocity error is to be removed by the vernier system.

Should the apogee burn be used to produce the energy bias, the following normalized error equation results:

$$\frac{\delta V_c}{V_c} = 0.91 \times 10^{-4} \delta(\Delta V_b)$$

and

$$\left(\frac{\delta a}{a_i}\right) = \frac{2 \delta V_c}{V_c}$$

Also out-of-plane:

$$\delta V_{\perp} = 0.42 (\delta V_b)$$

As a function of ΔL_o , we obtain:

$$\delta a/a = 1.8 \times 10^{-4} \delta(\Delta V_b)$$

or

$$\begin{aligned} \delta(\Delta V_b) &= (3.7 \times 10^{-4} \Delta L_o) / 1.8 \times 10^{-4} \\ &= 2.05 \Delta L_o \end{aligned}$$

The apogee burn penalty was shown to be

$$\delta_{\omega_f} = \left\{ 1.1 \times 10^{-4} \delta(\Delta V_b) \right\} \omega_f$$

$$\text{With } \omega_f = 2000 \text{ lb (p/L)}_{\text{loss}} = 0.451 \Delta L_o$$

The out-of-plane contribution is

$$\delta V_{\perp} = 0.86 \Delta L_o$$

and the payload loss, based on 0.316 lb/ft/sec of vernier velocity is

$$(p/L)_{\text{loss}} = 0.272 \Delta L_o \text{ lb}$$

Comparing the payload coefficients, energy bias application at the perigee burn point is much more efficient than at apogee burn. Therefore, further attention will be given only to the perigee burn energy bias.

The total payload loss (or gain) for perigee burn from the two individual contributions is

$$(p/L)_{\text{loss}} = 0.343 \Delta L_o$$

Now Table 7.5-3 can be completed. Much of the data will be taken directly from Table 7.5-2. The payload due to injection errors, based on ΔV_t will not be included since it is the same in all cases ($\theta_\epsilon = 1$ degree only).

Table 7.5-3. Injection Bias Summary ($\theta_\epsilon = 1$ degree)

Launch Azimuth (deg)	ΔL_o (deg)	Total (P/L) Loss Launch Azimuth (lb)	(P/L) Loss Inj. Bias (lb)	P/L Gain Via Less ΔV_d (lb)	Net P/L Difference (lb)	Net P/L W/O Launch Azimuth (lb)
80	57.0	32.5	19.6	51.0	1.9	34.4
85	47.0	11.8	16.1	44.5	16.6	28.4
90	37.0	0.0	12.7	35.0	22.3	22.3
95	27.5	11.8	9.5	26.2	4.9	16.7
100	18.0	32.5	6.2	17.1	-21.6	10.9
105	9.5	64.6	3.3	9.0	-58.9	5.7
110	2.0	109.0	0.7	1.9	-107.8	1.2
115	4.5	176.0	-1.5	4.3	-170.2	5.8

The extreme right column of Table 7.5-3 shows the net payload gain as compared with the weight contribution to $\Delta (P/L)$ due to ΔV_d shown in Table 7.5-2. This shows the advantage of the injection bias over that of the nonbiased injection upon which Table 7.5-2 is based.

The second column from the right, Net P/L Difference, considers the total payload penalty azimuth (Total $(P/L)_{\text{loss}}$ Launch Azimuth) plus the payload loss due to perigee burn energy excess. It also considers the difference in payload for ΔV_d between the biased and nonbiased cases, but does not include the ΔV_t due to injection errors since $\theta_\epsilon = 1$ degree only. The purpose of this column is to show launch azimuth penalties eventually exceed the gains attained through biased injections.

7.5.3.3.1 Conclusion

The biased injection shows a significant payload advantage over nonbiased injections if constant drift time requirements of 4 days are imposed. For the constant 1 deg/day drift rate maneuver, the biased injection could reduce the vernier weight by only 3.16 pounds (assuming no perigee payload penalty). Therefore, injection biases are not considered for the constant drift rate maneuver.

7.5.3.4 Despin

Upon elimination of injection errors and initiation of the drift toward the operating longitude, the spacecraft is despun. The vernier propulsion system is used for this maneuver. The rate gyro package monitors the despin and provides control commands to the despin thrusters. Following despin, the vernier propulsion tanks are vented of their hydrazine propellant. Torques induced by the venting process will be sensed by the rate gyros and controlled by vernier thrusters. Thus, when venting is completed, the spacecraft body angular velocities are still below the 0.01 deg/sec threshold. A complete description of the despin operation can be found in Section 5.5.2.2

7.6 INITIAL STABILIZATION AND DEPLOYMENT

The initial stabilization and deployment system operation is described in detail in Section 5.5.2.2.

The negative yaw axis (apogee motor end of the longitudinal axis) is locked on the sun prior to deployment. Eight sun sensors provide complete spherical coverage, thus, the sun can be located. The orientation control is provided by a low thrust resistance jet system. This is the same propulsion system used for in-orbit stationkeeping and flywheel unloading. The sun acquisition maneuver is initiated at about 1:00 AM local time.

Any time after the negative yaw axis locks on the sun the parabolic antenna is deployed. The deployment sequence is initiated via ground commands. The solar cells, extended from the antenna, are unfolded. They will be in position to obtain near maximum power from the sun. The deployment maneuver should occur no later than about 11:00 AM local time. At 11:30 AM, the earth stabilization sequence begins. The earth will move slowly into view of the earth sensors field-of-view point which is along the positive yaw axis. The low thrust levels of the resistance jet are capable of providing orientation control during earth capture and stabilization. The positive yaw axis stays locked on the earth, but the yaw rates are not nulled. Pitch and roll rates are nulled. Therefore, the sun is used as a yaw reference and the yaw rates can be nulled. Now the negative pitch axis can be aligned perpendicular to the orbit plane, pointing north. Stabilization is completed when the star tracker, pointing along the negative pitch axis, acquires and locks on Polaris.

7.7 SYNCHRONOUS ORBIT STATIONKEEPING REQUIREMENTS

The orbital dynamic aspects of the synchronous satellite orbit will be discussed briefly. A description of the orbit perturbations, and their effects on the motion of the spacecraft will follow. Application of the results of the perturbation analysis will then be made to the ATS-4 mission, including the total velocity requirements which must be included in the stationkeeping propulsion system. The effect of orbit determination uncertainties due to ground tracking inaccuracies, on both the spacecraft motion and the velocity requirements, will also be shown.

7.7.1 DYNAMICS

7.7.1.1 Nominal Orbit

The nominal orbit parameters are defined, for use in this study, as the following:

Orbit inclination, $i = 0$ deg

Orbit eccentricity, $e = 0$

Orbit altitude, $h_c = 19,324$ nm

Orbit velocity, $V_c = 10,087$ ft/sec

Orbit period, $T_c = 23.935$ hr (1 sidereal day)

Orbit angular velocity, $n_c = 15.041$ deg/hr

Additional information, relevant to the synchronous spacecraft motion will be presented in the analyses below. This information will include the effects of variations in orbit velocity on the angular velocity and position of the spacecraft, and also the effects of nonzero orbit inclination and eccentricity on the daily longitudinal excursions of the ATS-4 spacecraft.

7.7.1.1.1 Orbit Period

Let the spacecraft orbit period, t_c , be given by

$$t_c = 2\pi \sqrt{a^3/\mu}$$

where

$$a = \frac{\mu r_p}{2\mu - V_p^2}$$

and where r_p and V_p are perigee conditions, a is the semimajor axis, and μ is the universal gravitational constant ($=1.40752 \times 10^{16}$ ft³/sec²).

For the circular orbit, $r_p = r_c$ and $V_p = V_c$, assume now a small velocity impulse, ΔV , is applied. At the point of application, r_p still equals r_c , but $V_p = V_c + \Delta V$. To a first order, a becomes

$$\frac{\Delta a}{a} = 2 \frac{\Delta V_p}{V_p}$$

and for Δt

$$\frac{\Delta t}{t_c} = \frac{3}{2} \cdot \frac{\Delta a}{a} = 3 \frac{\Delta V_p}{V_p}$$

The variation in angular velocity, using $\eta_c = 2\pi/t_c$, is

$$\Delta \eta = \frac{2\pi}{t_c} \cdot \frac{\Delta t}{t_c}$$

or

$$\Delta \eta = -3\eta_c \frac{\Delta V_p}{V_c}$$

and

$$\eta = \eta_c + \Delta \eta$$

Assume now that $\Delta V_p = 10$ ft/sec. Then $\Delta \eta$ becomes -0.045 deg/hr, and in one sidereal day, the spacecraft will have rotated through $(360 - 23.935 \Delta \eta)$ degrees. During this same time the earth will have rotated through 360 degrees. The total difference in angular travel, $\Delta \theta$, is

$$\Delta \theta = 23.935 \Delta \eta = 1.07 \text{ degrees.}$$

Thus, the spacecraft appears to have drifted 1.07 degrees to the west.

In estimating drift times, and in sizing propulsion systems, the rule-of-thumb calculations used is: one degree of drift per day for each 10 feet per second of velocity deviation from the synchronous orbit velocity.

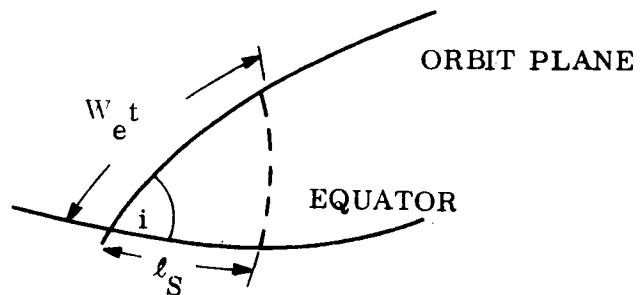
7.7.1.1.2 Inclination

Inclination induced longitude excursions arise because the component of velocity parallel to the equatorial plane of the inclined orbit varies as the spacecraft traverses its orbit. At the ascending node, the equatorial component of spacecraft velocity is less than the equatorial velocity of the earth. Thus, the spacecraft ground point moves to the west of the longitude of the ascending node. However, at the maximum latitude, both the earth and the spacecraft have moved through 90 degrees of angular travel, and the longitudes line up again. Carrying this out through 360 degrees of travel results in the familiar "figure-8" ground trace as viewed on a Mercator Projection of the Earth. The equations describing this motion follow. From the spherical trigonometry, the inertial longitude change of the spacecraft l_s is (see sketch below):

$$l_s = \tan^{-1} [\cos i \tan \omega_e t]$$

The inertial longitude change of the earth, l_e , is simply the earth's rate, ω_e , times time, t .

$$l_e = \omega_e t$$



The difference in longitude, Δl , is

$$\begin{aligned}\Delta l &= l_s - l_e \\ &= \tan^{-1} \left\{ \cos i \tan \omega_e t \right\} - \omega_e t\end{aligned}$$

Letting the differential of Δl with respect to $\omega_e t$, equal zero yields the time of occurrence (t_{\max}) of maximum longitude difference, Δl_{\max}

$$\frac{d(\Delta l)}{d(\omega_e t)} = \frac{\cos i \sec^2 \omega_e t}{1 + \cos^2 i \tan^2 \omega_e t} - 1 = 0$$

which is satisfied by:

$$\sin^2(\omega_e t) = \frac{1}{\cos i + 1}$$

and

$$t_{\max} = \frac{1}{\omega_e} \sin^{-1} \left[\frac{1}{\cos i + 1} \right]^{1/2}$$

Now, Δl_{\max} becomes

$$\Delta l_{\max} = \tan^{-1} \left\{ \cos i \tan \left[\sin^{-1} \sqrt{\frac{1}{\cos i + 1}} \right] \right\} - \sin^{-1} \left(\frac{1}{\cos i + 1} \right)$$

The latitude, λ_{\max} , at which the maximum longitude excursion occurs is given as

$$\lambda_{\max} = \sin^{-1} \left[\sin i \sin \omega_e t \right]$$

Figure 7.7-1 shows the maximum longitude excursion, as a function of the orbit inclination.

$\omega_e^t = 45$ degrees for all inclinations shown, therefore $t_{\max} \approx 3, 9, 15,$ and 21 hours. The maximum longitude excursion can be expressed, to a high degree of accuracy, as $\Delta \ell_{\max} = k i^2$ where i is in degrees, and $k = 4.4 \times 10^{-3}$ /degrees.

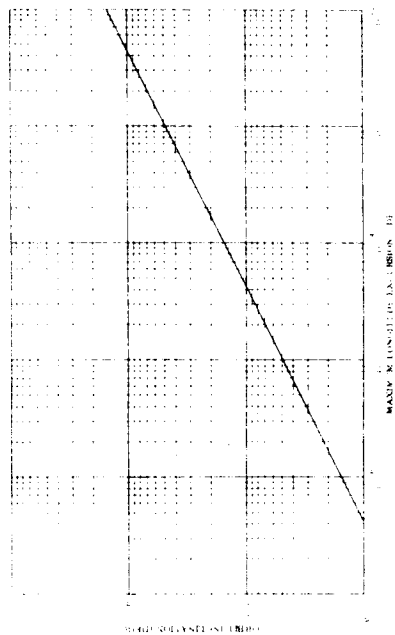


Figure 7.7-1. Variation of Maximum Longitude Excursion with Synchronous Orbit Inclination

The ATS-4 stationkeeping system together with ground tracking and orbit determination, will attempt to maintain the inclination at 0.1 degree. Approximately 0.0004 degree of longitude excursion would then occur. As much as 0.5 degree of inclination would still produce only 0.001 degree of longitude excursion.

7.7.1.1.3 Ellipticity

A spacecraft in an elliptic orbit does not move with constant angular velocity. At, and near, the perigee of an elliptic synchronous orbit, the spacecraft will move ahead of the operating longitude (to the east) as seen from earth, but near apogee, its angular rate is less than nominal, and it drifts to the west. After one orbital revolution, the spacecraft is back to the longitude from which it started. The

angular position of a circular synchronous spacecraft is equal to the mean anomaly, M , expressed as $M = E - e \sin(E)$, where E is eccentric anomaly and e is eccentricity.

The true angular position of the satellite in a slightly elliptic orbit is given by the true anomaly, η , expressed as

$$\eta = 2 \tan^{-1} \left| \sqrt{\frac{1+e}{1-e}} \tan \frac{E}{2} \right|$$

The difference $\Delta \ell_{\max}$ gives the maximum longitude excursion.

Figure 7.7.2 shows the longitude excursion with eccentricity. This maximum difference is approximately equal to two times the eccentricity in radians. Thus, the longitude excursion

of a satellite in an orbit with an eccentricity of 0.001, is 0.114 degree. Also shown in Figure 7.7-2 is the altitude difference required to produce the eccentricity. Tracking over half an orbit should result in altitude determination errors of no more than one nautical mile (see tracking discussion in Section 7.7.3 below). Thus, it should be possible to reduce the eccentricity to 0.45×10^{-4} and the corresponding longitude excursion to 0.0052 degree. Even a 10-nautical mile total apogee-perigee altitude difference results in only 0.026 degree of longitude excursion.

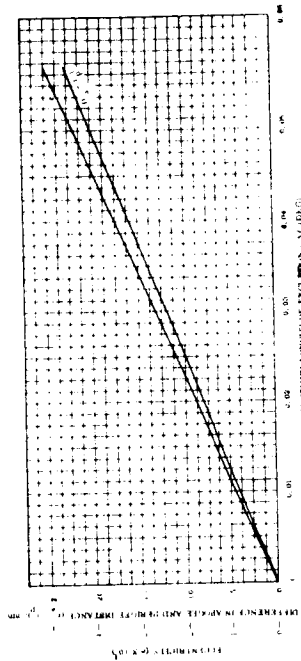


Figure 7.7-2. Variation in Maximum Longitude Excursion with Eccentricity or Apogee-Perigee Distance

7.7.1.2 Perturbations

The two major perturbations to a synchronous spacecraft orbit are the eccentricity of the

equator and the gravitational attraction on the spacecraft produced by the sun and moon. The former perturbation affects the east-west (in-orbit) motion while the latter affects the north-south (out-of-plane) motion. The effects produced by the forces will be emphasized without an analytical derivation of the perturbations themselves.

7.7.1.2.1 East-West Perturbations

The ellipticity of the equator causes a long term, periodic longitude drift of spacecraft in a synchronous orbit of small eccentricity and small inclination. The period of this longitude drift is dependent upon the nominal longitude of the spacecraft relative to the semiminor axis of the equator. The periodic motion is a longitudinal oscillation of the spacecraft about the semiminor axis, assumed for this analysis to pass through the 107°W longitude, and the 73°E longitude meridians. Thus, starting at 90°W longitude, the uncontrolled motion would see the spacecraft drift past 107°W by 17° to 124°W then reverse its direction and return to the 90°W longitude. The period of the oscillation would be in excess of two years. The velocity impulse required to constrain the spacecraft to lie within a very narrow longitude band, or limit cycle, is relatively low, being on the order of from 2 to 6 ft/sec/yr. The velocity impulse varies significantly with longitude, but only slightly with the longitude limit cycle width, when this width is on the order of a degree or less. Two figures are used to summarize the velocity requirements. The first, Figure 7.7-3 shows the velocity impulse, ΔV , per correction versus the frequency of thrusting as a function of the nominal longitude distance from the nearest semiminor axis and the maximum longitude excursion (limit cycle) from the nominal longitude. Figure 7.7-4 shows the yearly velocity impulse requirements as a function operating longitude, as seen on the Mercator Earth Projection. This is a visual aid in relating the velocity requirement to the land masses over which it might be desired to place a synchronous spacecraft.

7.7.1.2.2 North-South Perturbations

Solar-lunar gravitational perturbations will cause the inclination of a synchronous orbit to increase at a rate of between approximately 0.86 degree per year to almost 0.95 degree per year, depending upon the inclination of the moon's orbits to the earth's equatorial plane. In early 1969, the moon will be at its maximum inclination of 28 degrees. The normal way of eliminating orbit inclination, when desired, is by applying a velocity impulse perpendicular to the equatorial plane as the spacecraft crosses the equator; i. e., at the orbit's line of nodes. Figure 7.7-5 shows the ideal velocity impulse, ΔV_I , as a function of inclination change, for a synchronous orbit. The coefficient is 176 ft/sec/degree.

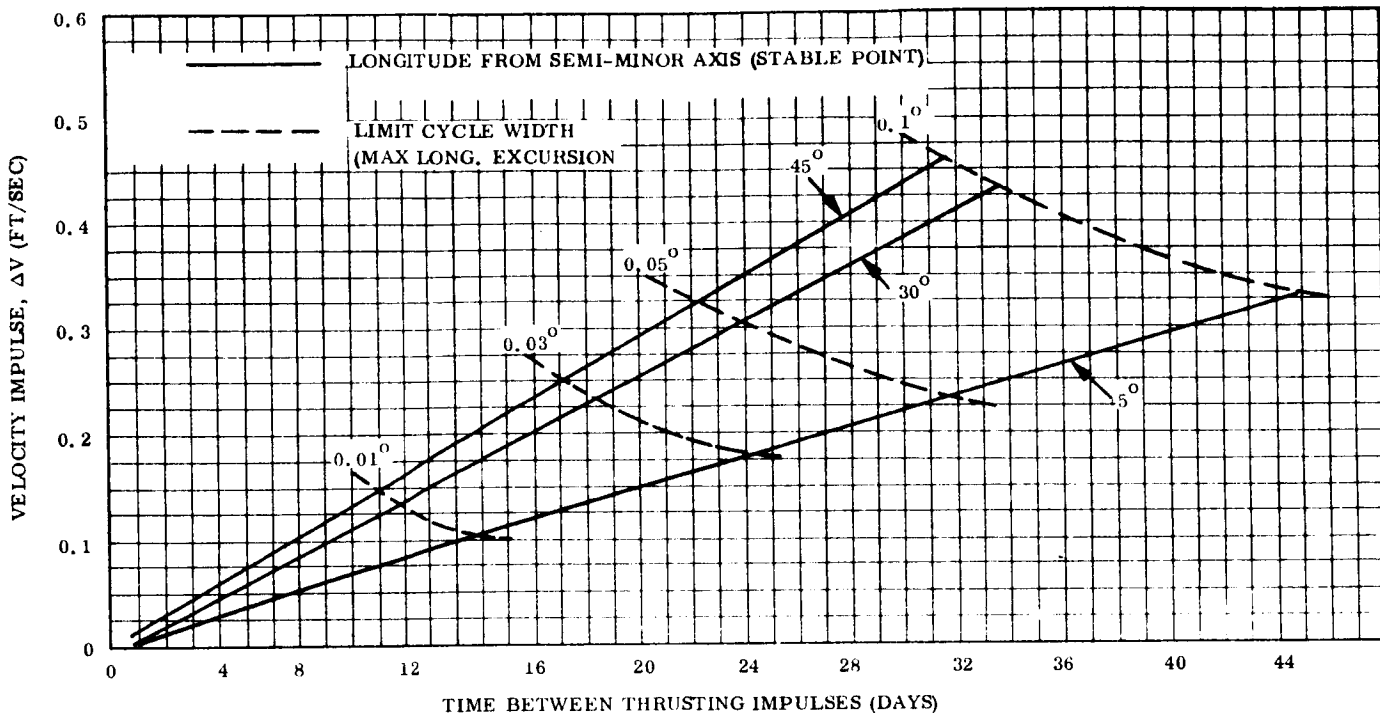


Figure 7.7-3. Variation of Individual Velocity Impulse Magnitude with Time Duration Between Thrusting

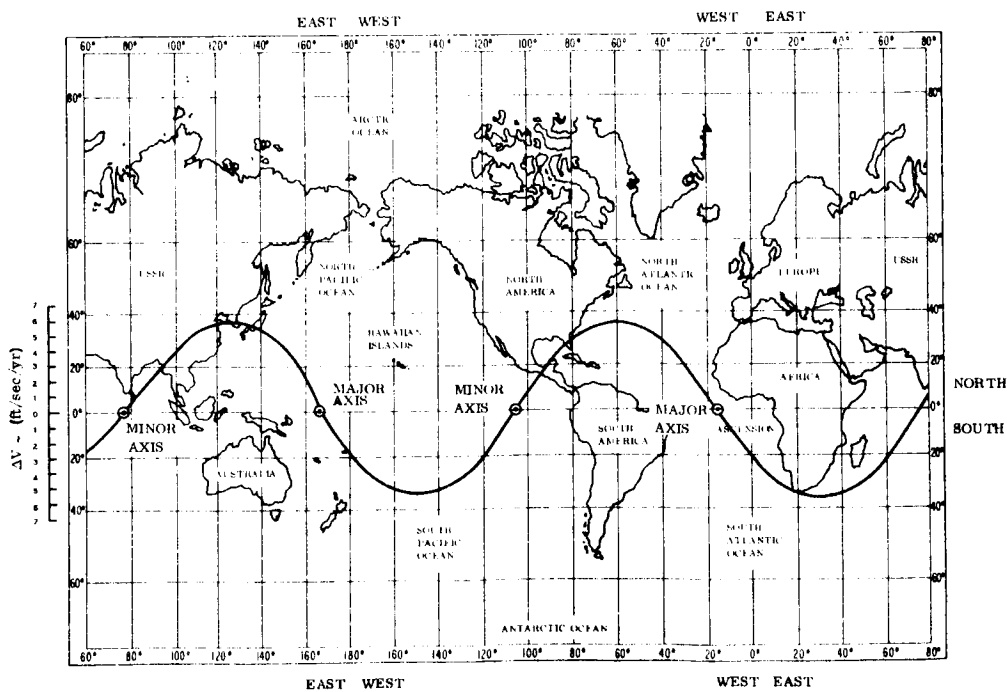


Figure 7.7-4. ΔV Requirement Per Year as a Function of Synchronous Position

The ΔV_I shown in Figure 7.7-5 assumes the impulse is applied right at the node. If, however, it is not, there is a residual inclination and a shift in location of the line of nodes. Based on a 1-degree initial inclination, the resulting inclination after applying the ideal ΔV_I is a function of the error (or uncertainty) in the location of node; the inefficiency is shown in Figure 7.7-6. The resulting inclination is also interpreted as a measure of the additional velocity impulse required to completely remove the residual inclination. Curves are shown for three values of thrusting duration, 8 minutes (2 degrees of angular travel during thrusting), 2-2/3 hours (40 degrees), and 5-1/3 hours (80 degrees). Note that beyond 15 degrees of nodal errors, the residual inclination is virtually independent of thrusting durations of up to at least 5-1/3 hours.

7.7.2 VELOCITY REQUIREMENTS

7.7.2.1 East-West

For the purpose of east-west stationkeeping and facilitating the accuracy of pointing the parabolic antenna, the east-west limit cycle has been set at between 0.01 and 0.03 degree centered about the 90°W longitude. From the curves of Figure 7.7-3, the velocity impulse requirement is about 2.68, or perhaps 2.7 ft/sec/yr for the first year. The thrusting duration is 28 or 48 minutes at a frequency of 13.8 or 24.5 days for the 0.01- and 0.03-degree limit cycle longitude widths, respectively. Thrusting on a daily basis results in a 0.005-degree limit cycle with a thrusting duration of 1.97 minutes. Similar data can be extracted from the figures for the second year of operation when the spacecraft is positioned at 150°W. Table 7.7-1 summarizes all this information for both years of east-west stationkeeping.

In addition to the equatorial eccentricity, there are other contributions to east-west stationkeeping velocity requirements. First is the 10 ft/sec required to reduce the drift rate residual from vernier propulsion maneuvers, second is the 100 ft/sec required for the reposition maneuver, and last, there should be some additional east-west capability to handle such contingencies as uncertainty in the location of the semiminor axis, and cross coupling effects from the north-south stationkeeping velocity impulses due to orientation control errors. This contingency ΔV will be 2.2 ft/sec. A summary of all the east-west stationkeeping velocity requirements are included in Table 7.7-1.

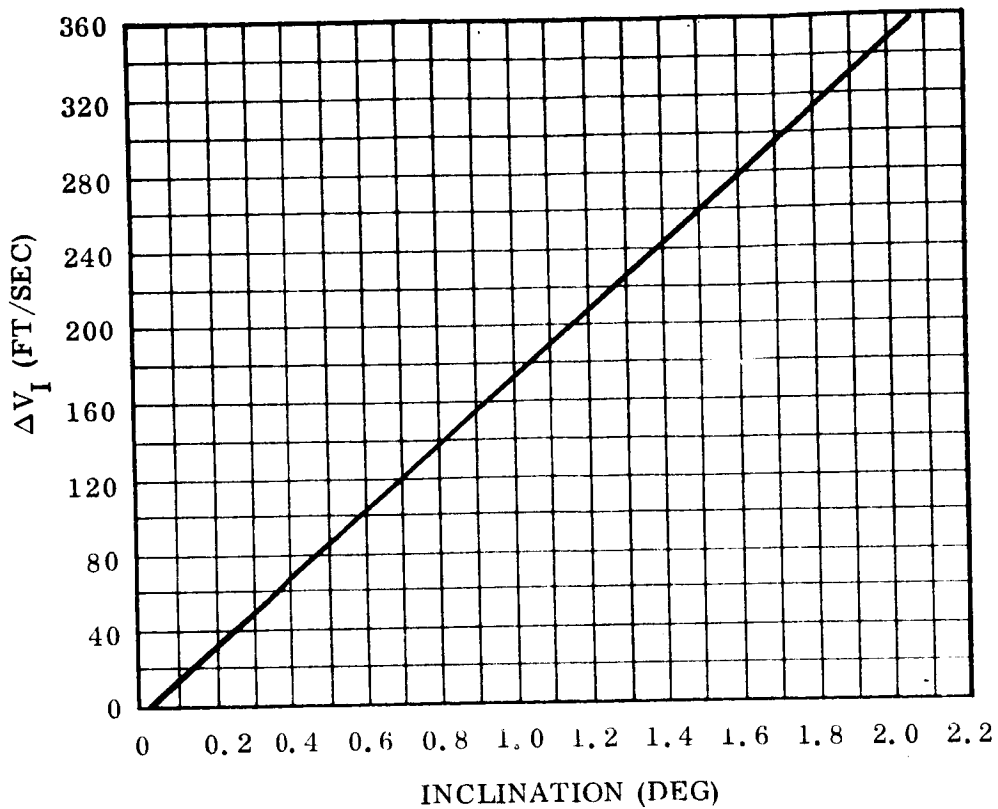


Figure 7.7-5. ΔV Required to Zero Out Inclination (Impulse Applied at Nodal Crossing)

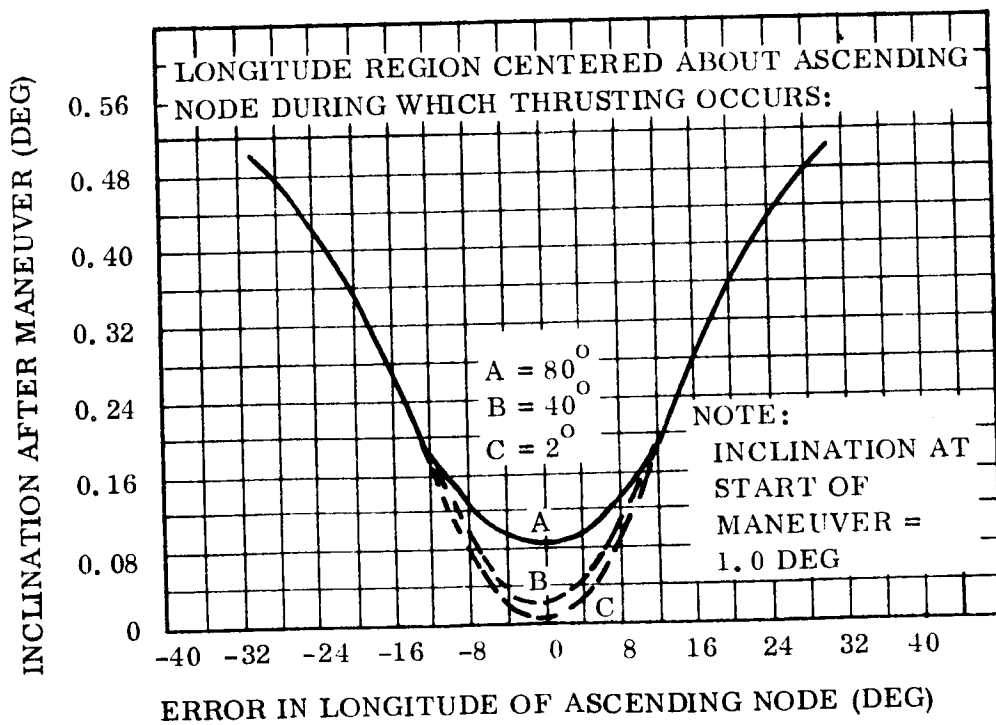


Figure 7.7-6. Thrust Inefficiency vs Error in Longitude of Nodal Crossing

7.7.2.2 North-South

The north-south stationkeeping velocity requirements are based simply upon maintaining the orbit inclination near zero. As will be shown in the following Section (7.7.3) an inclination of 0.1 degree is permitted. This will result in a maximum nodal uncertainty of 15 degrees between tracking periods. Figure 7.7-6 therefore, shows a thrusting inefficiency of 25 percent. Assuming the inclination increase is 0.94 degree per year for 1969-1970 time period, Figure 7.7-5 shows that 166 ft/sec ideally are required. The 25 percent inefficiency is an additional 41 ft/sec bringing the total to 207 ft/sec/yr. Since north-south stationkeeping is required for only one year, 207 ft/sec is the total requirement. The north-south and east-west stationkeeping velocity requirements are summarized in Table 7.7-1.

7.7.3 TRACKING FOR ORBIT DETERMINATION

The rf tracking characteristics (tracking frequencies, antenna gain, lb loss, etc.) have been discussed in Section 6.5.2. The information for use here, as relates to the stationkeeping requirements and orbit determination capability, is included in the summary in Table 7.7-2. Of particular interest is the Goddard Range and Range Rate System tracking capability which is given in Table 7.7-2. This information shows that orbit determination uncertainties are approximately 0.008 degree out of plane and 0.00064 degree in plane, 1 σ . The propagation rate is fairly large, thus, an attempt is made to use separate position fixes spread over half an orbit (twelve hours) then essentially curve-fit the orbit to this data. The reason for doing this lies in the difficulty in determining the nodal crossing for near zero inclinations. Thus, rather than use tracking position and velocity information, position and time, and a number of points are used (see Figure 7.7-7A as an example). It is important to have a position determination when near a nodal crossing, otherwise the uncertainties of the node become prohibitively large. Position determination at the maximum latitude results in maximum nodal crossing uncertainty, although it provides the best measure of inclination. By enlarging the orbit trace of Figure 7.7-7A in Figure 7.7-7B, at the nodal crossing point, the method for calculating the uncertainty is seen. For small angular distances, the uncertainty in nodal crossing, δN , is given as

$$\delta N = \delta \ell / \sin i \approx \frac{\delta \ell}{i \text{ radians}}$$

Table 7.7-1. In-Orbit Stationkeeping Velocity Requirements

EAST - WEST

1. Drift onto Station	10 ft/sec
2. Triaxiality	
1st Year	2.68 ft/sec
2nd Year	5.12 ft/sec
Contingencies:	2.20 ft/sec
(N-S cross coupling, uncertainty in long of semiminor axis, E-W thrusting inefficiencies)	
3. Reposition Maneuver	100 ft/sec
Total velocity requirements	120 ft/sec

Conditions: 0.03° limit cycle

1st Year: $\Delta V = 0.18$ ft/sec once every 24.5 days-thrust for 48 minutes

2nd Year: $\Delta V = 0.225$ ft/sec once every 18.2 days-thrust for 60 minutes

Note: If thrust on a daily basis: $\Delta V = 0.0074$ ft/sec; 0.005° limit cycle, thrust for 1.97 minutes

NORTH - SOUTH

1. 0.94 deg inclination	166 ft/sec
growth due to solar-lunar perturbations	
2. 25% inefficiency due to 15 deg uncertainty in nodes	41 ft/sec
Total velocity requirements	207 ft/sec

Conditions: 1 yr duration only

Thrust for 2.9 hr/days; $\Delta V = 0.57$ ft/sec (includes inefficiencies)

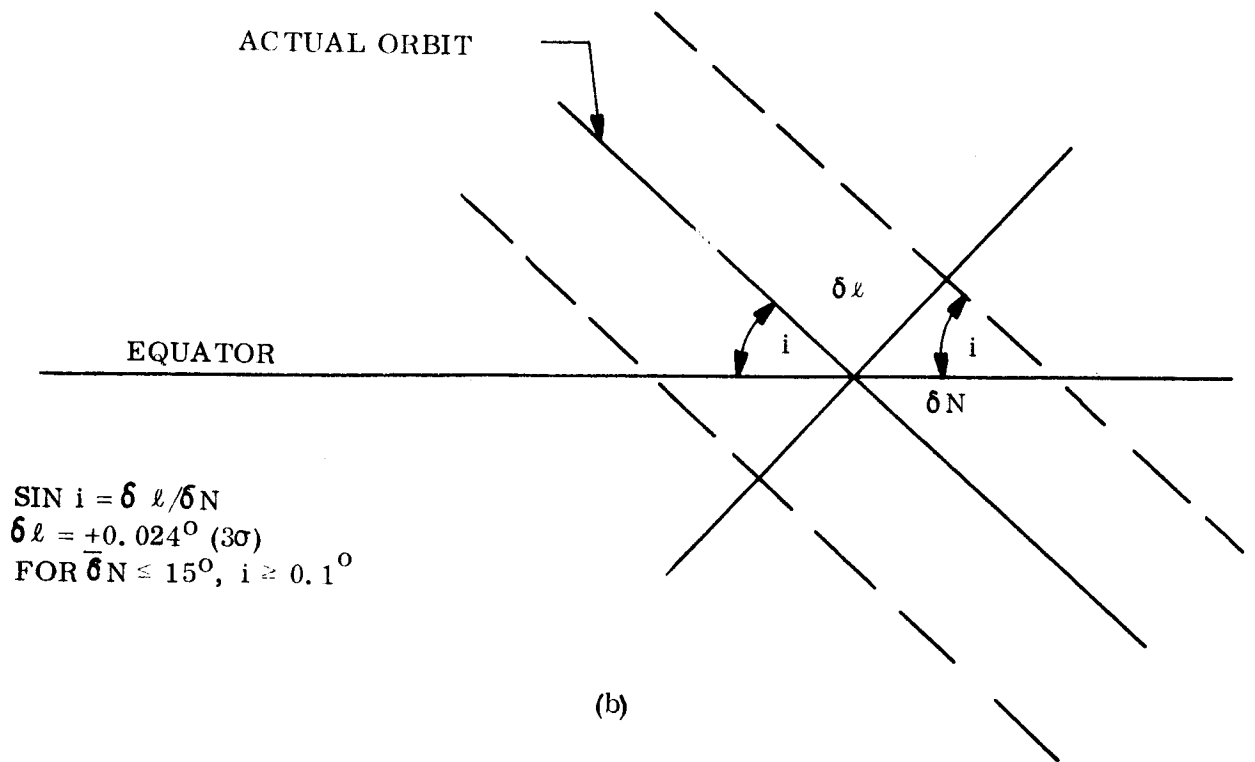
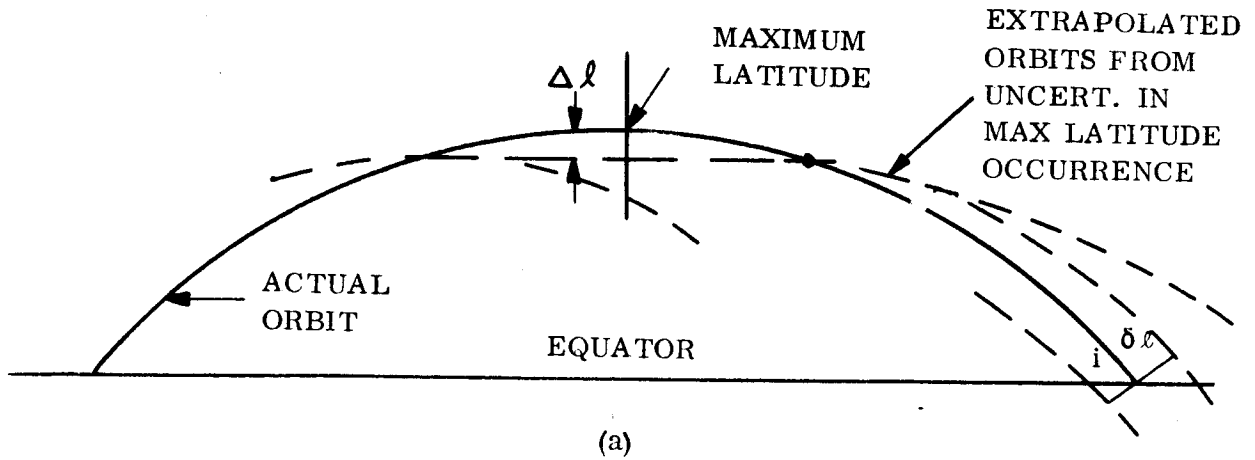


Figure 7.7-7. Determination of Uncertainty in Nodal Location

where δl is the out-of-plane position uncertainty. An inclination of 0.1 degree (0.001745 rad) results in a δN of 13.80 degrees when $\delta l = 0.024$ degree, (3σ). The small shift in the node itself due to nodal location uncertainties will result in the final node being no greater than 15 to 16 degrees, 10 days to 2 weeks after tracking.

Errors in orbital period can be determined by noticing the longitude position of the spacecraft on successive days. This might be done during the drift on to operating longitude. After this time, the one week to ten days tracking frequency will also indicate period errors, after allowing for the drift due to triaxiality.

Orbit eccentricity can be determined from the variation in altitude over a half-an-orbit of tracking data. During the drift on to station, the stationkeeping propulsion system velocity impulses will be applied in such a manner so as to reduce the altitude errors, thereby reducing eccentricity.

A modestly conservative approach selected for the ATS-4 mission is to provide tracking and orbit determinations once every 7 to 10 days. The orbit determination is obtained by tracking for one-hour durations, starting every other hour, for a half day. Thus, six determinations are made and one of the determinations will occur near a node. The maximum of 15 degrees of nodal uncertainty is, therefore, felt to be within the capability of the ATS-4 tracking/orbit determination system.

The inclination selection of 0.1 degree is based on a brief analysis that showed that when inclinations are reduced below this value, the shift in the node itself begins to become appreciable. After a few days the nodal uncertainty without additional tracking and orbit determinations, is larger than 15 degrees, and thrusting inefficiencies become prohibitively large.

Table 7.7-2. Orbit Determination Summary

Tracking Duration = 1 hr Goddard Range - Range Rate System		Range Bias = 55 ft Range Rate Bias = 0.06 ft/sec Angle Bias = 5 arc minutes			Random Measurement Errors Range = 50 ft Range Rate = 0.33 ft/sec Azimuth and Elevation = 0.1 deg		
		Position Uncertainty σ ft x 10^5 σ (deg) x 10^4			Velocity Uncertainty σ (ft/sec) (deg/sec) x 10^{-7}		
Time After Start of Tracking (hr)	Along Track	Cross Track	Radial	Along Track	Cross Track	Radial	
1	0.0167	0.191	0.0195	0.120	4.140	0.476	
	6.9100	79.100	8.0700	0.497	17.140	1.970	
2	0.0248	0.328	0.0329	0.222	3.656	0.528	
	10.3000	135.800	13.6000	0.919	15.110	2.190	
3	0.0421	0.445	0.0452	0.312	2.920	0.607	
	17.4000	134.300	18.7000	1.290	12.090	2.510	
4	0.0666	0.532	0.0548	0.383	2.010	0.706	
	27.6000	220.300	22.7000	1.590	8.320	2.920	

7.8 OPERATIONAL SYSTEM

7.8.1 LAUNCH AND PARKING ORBIT

7.8.1.1 Atlas Flight Phase

After completion of prelaunch preparations and final countdown, the Atlas booster, sustainer, and vernier engines are ignited seconds before liftoff and the umbilical connections are severed as the launch vehicle rises from the pad. The vehicle will follow a programmed trajectory. During the latter portions of the boost phase and after booster staging, programming will be assisted by radio-guidance commands. At a predetermined staging point, the booster engines are shut down and jettisoned. The sustainer engine will continue to operate until the desired altitude, attitude, and velocity have been attained, after which it is cut off. The vernier engines will then provide fine corrections to the Centaur attitude and velocity, and will be cut off within seconds after sustainer cutoff. Should a malfunction occur before separation from the Atlas, the flight will be aborted by means of destruct commands transmitted from the ground to both the Atlas and Centaur destruct systems.

7.8.1.2 Centaur Separation

Separation of the Centaur from the Atlas booster is controlled by a programmer in the Centaur, and begins upon command signal from the booster guidance. Upon separation and post-separation coast phase, the Centaur engine is ignited and continues to burn until the Centaur/ATS-4 payload combination is placed into a 100 nautical mile altitude circular orbit at approximately 500 seconds after liftoff.

7.8.1.3 Launch-to-Injection Operations

Full launch-vehicle tracking and telemetry coverage is required from liftoff through parking orbit injection and operations should be consistent with standard launch requirements.

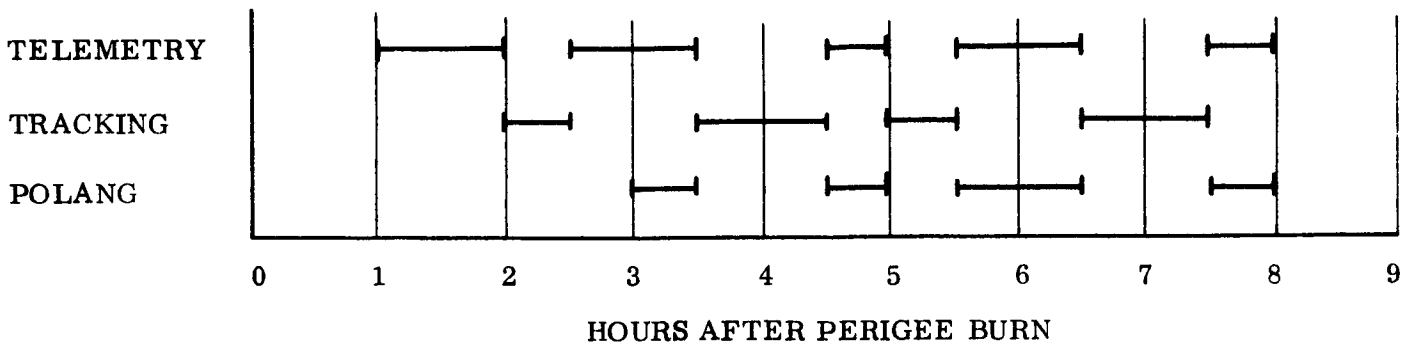
7.8.1.4 Perigee Burn

The Centaur/ATS-4 payload combination will coast in the 100 nautical mile parking orbit until it crosses the equator at a longitude of 4°E. Shortly before the combination crosses the equator, the Centaur is rotated through 32.8 degrees counterclockwise about the local vertical. As the payload combination crosses the equator, the Centaur engines are turned on. Thrusting is continued until a sufficient velocity increment is added to place the Centaur/ATS-4 payload combination into the desired transfer orbit.

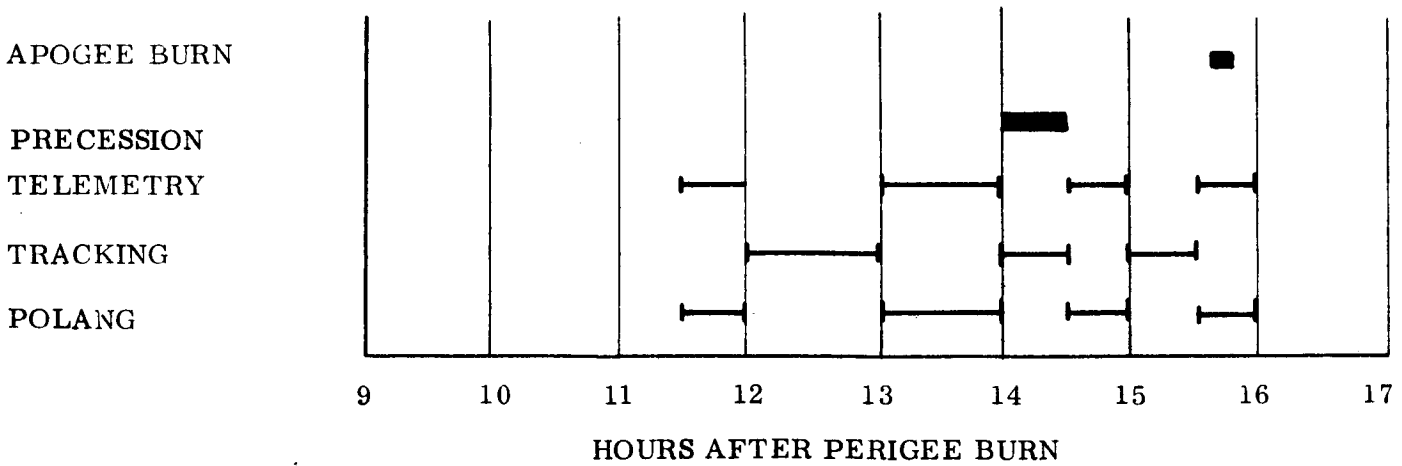
7.8.2 TRANSFER ORBIT

All command activity from perigee burn through spacecraft separation and spin-up is expected to be generated from within the Centaur or the spacecraft. Ground operational activity during this period of flight will be concentrated on tracking and telemetry data collection.

Approximately one hour after perigee burn, the spinning spacecraft will come into view of the Toowoomba Tracking Station and will remain in view for approximately seven hours as the spacecraft passes through the first apogee. During this period of flight, the Toowoomba Tracking Station will obtain range and range rate measurements which will be displayed on a Sanborn type recorder and punched on teletype tape for transmission to Goddard Space Flight Center (GSFC). At GSFC, these measurements will be utilized to calculate transfer orbit characteristics. In addition to range and range rate data, Toowoomba will receive telemetered sun sensor data and will measure a polarized rf signal, called POLANG, transmitted from the spacecraft. This information will also be transmitted to GSFC for calculation of the spacecraft spin axis orientation. A schedule of activity for Toowoomba for this period is shown below:



Between 8 and 11 hours after perigee burn, the spacecraft will not be in view of any ATS tracking station. The spacecraft will come into view of Rosman at approximately 11-1/2 hours after perigee burn. The Rosman tracking station will become an integral part of the Precession Control "Loop" as the spacecraft approaches the second apogee. By receiving telemetered sun sensor data and by measuring POLANG, the spacecraft spin axis orientation will be calculated. Based on these calculations, the spacecraft will be commanded by Rosman to the desired second apogee orientation about two hours prior to second apogee. Another spin axis orientation determination will be made to confirm proper reorientation of the spin axis via the precession maneuver. In addition to spacecraft attitude determination, Rosman will make range and range rate measurements to determine the exact time of apogee. When the spacecraft reaches the second apogee (approximately 15.75 hours after perigee burn), Rosman will command the apogee motor to fire. A schedule of activities for Rosman during this period of time is shown below.



7.8.3 VERNIER MANEUVERS

Due to errors in perigee and apogee burns, the desired orbit will most likely not be attained. During the two days following apogee burn, a series of vernier maneuvers will be performed to remove the injection errors and produce a near-synchronous orbit in which the spacecraft will be drifting slowly to the west.

The spin-stabilized spacecraft will be in full view of both the Rosman and Mojave Tracking Stations throughout the two days, however, due to the rotation of the spacecraft with respect to ATS ground stations and the physical location of spacecraft antennas, communications with the spacecraft will most likely be deteriorated between the times shown below:

- a. 1 hr and 2.5 hr after apogee
- b. 8.6 hr and 10.4 hr after apogee
- c. 25 hr and 26.5 hr after apogee
- d. 32.6 hr and 34.4 hr after apogee

The range and range rate systems of Rosman and Mojave Tracking Stations will be utilized to obtain data for determination of orbit characteristics. These data will be transmitted to GSFC where the orbit injection errors will be calculated and the required vernier thrusting command sequence established. After each vernier thrusting (at approximately 12, 24, 36, and 48 hours after apogee) the orbit errors will be calculated and a new vernier thrusting command sequence will be generated until the desired orbit is achieved.

In addition to tracking and vernier propulsion commanding, the Rosman and Mojave Tracking Stations will be receiving telemetry data and measuring the antenna polarization angle.

The orientation of the spacecraft spin axis will be determined and if required, a command sequence will be generated to precess the spin axis to the desired orientation for vernier thrusting.

The anticipated ATS operation ground station activity during the two day vernier maneuvers is shown in Figure 7.8-1.

7.8.4 DESPIN, DEPLOYMENT, AND INITIAL STABILIZATION

Once the desired orbit is achieved, the spacecraft will be despun and the residual vernier propellants vented by means of 1-pound vernier thrusters, the rate gyro package, and the appropriate ground command.

Ground commands and telemetry monitoring will be necessary during the following initial stabilization maneuvers:

- a. At approximately 1:00 AM local sun time, the "Initiate Sun Stabilization" command will be ground-commanded.
- b. Once the negative yaw axis is stabilized to the sun line, the parabolic antenna deployment can be commanded.
- c. By approximately 11:30 AM spacecraft positive yaw axis will be oriented along the local vertical with the earth in the field of view of the earth sensors. Yaw axis orientation control is switched from the sun to the earth by the generation of an "Initiate Earth Stabilization" ground command.
- d. At approximately 4:00 PM, local time, the "Initiate Yaw Sun Stabilization" ground command is generated which directs a pitch axis orientation that will permit inclusion of the star Polaris in the star sensor field-of-view.
- e. Periodically update the on-board memory and clock which provides star sensor command corrections to account for the apparent motion of Polaris as the spacecraft traverses the earth.

The ground station activity during this portion of flight will be concentrated on commanding the spacecraft throughout the initial stabilization modes and monitoring telemetry attitude performance data. It is anticipated that 12 minutes of telemetry data at 1 hour intervals will be required for adequate evaluation of spacecraft performance through this phase of flight. In addition, tracking data bursts at 2 hour intervals will be required for subsequent spacecraft drift corrections.

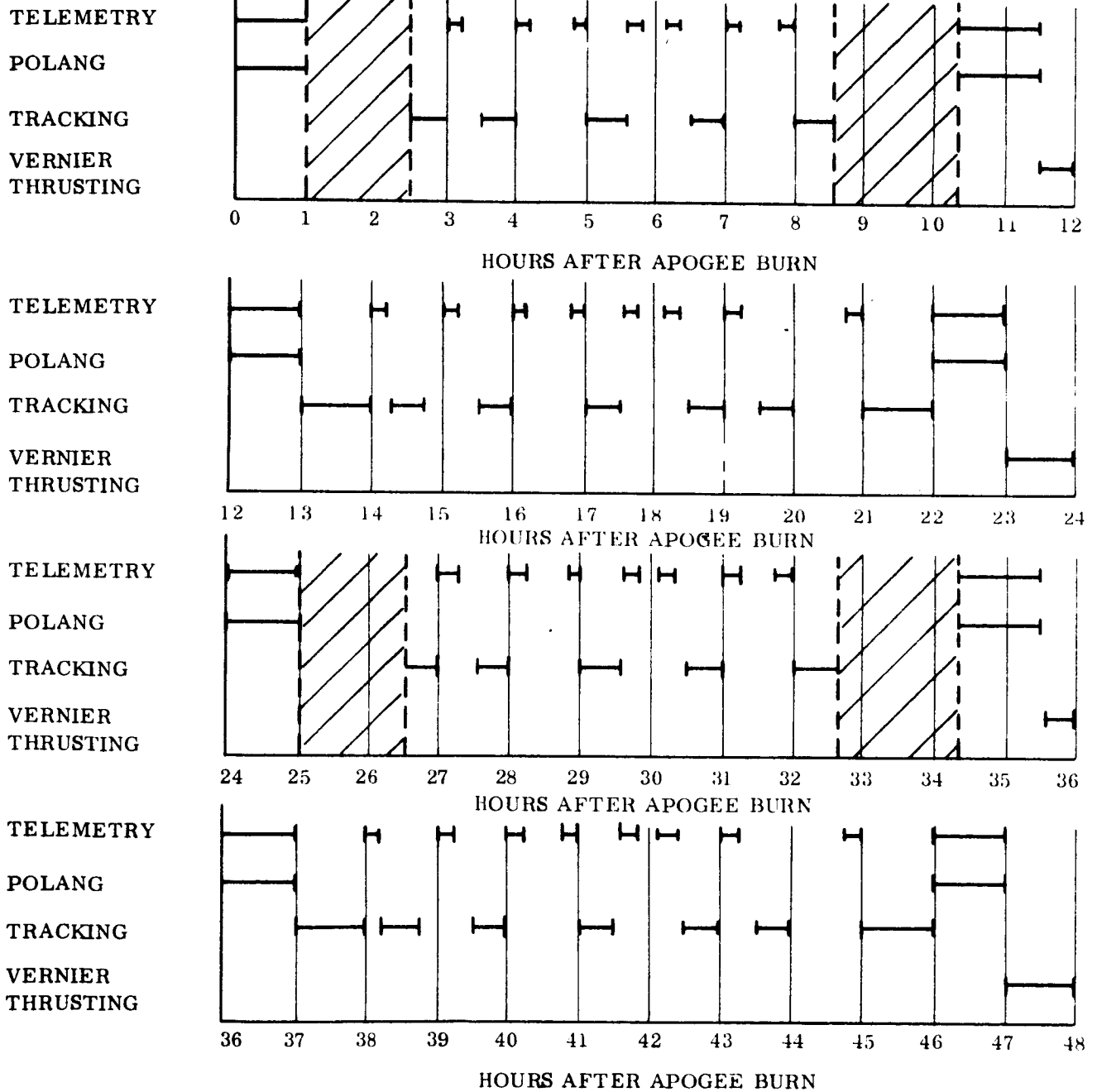


Figure 7.8-1. ATS Ground Station Activity During Vernier Maneuvers

7.8.5 FINAL STATION ACQUISITION

The orbit established at the termination of vernier maneuvers will produce approximately one degree per day of drift to the west toward the operating longitude at 90°W.

Throughout this period of drift (30 to 50 days) the spacecraft position is monitored by the Rosman and Mojave Tracking Stations and based on this tracking data, a sequence of "Resistance" jet thruster firings will be developed at GSFC to gradually synchronize the orbit period with the earth spin rate.

As the spacecraft slowly drifts to the west, the spacecraft will be "checked out" according to an orbit systems checkout plan to verify that all spacecraft systems are operating properly.

7.8.6 OPERATIONAL SYSTEMS CONTINGENCY PLANNING

All orbit operations from launch to final station acquisition will follow procedures prescribed in the Orbit Operations Plan. All operations will be under the control of ATS Operations Control Center (ATSOCC) at NASA GSFC. Each ATS ground station will follow a series of standing instructions for all nominal orbit operations. In the event of spacecraft system or orbit anomalies, contingency plans will be developed at NASA-GSFC and the required corrective procedures will be transmitted to the appropriate ATS ground stations by teletype for implementation.

SECTION 8

EXPERIMENT OPERATIONAL PHASE SEQUENCE

8.1 GENERAL

This section will discuss the experiments and measurements programs: the derivation of measurement requirements from mission objectives, formulation of measurement procedures, integration of these procedures into the overall operational program, and the derivation of experiment equipment requirements. Technical and operational problems and recommended solutions and procedures will be discussed within each of the above areas.

The purposes and objectives of the ATS-4 mission center around the deployment, pointing and utilization of large aperture antennas in space. In support of these purposes, four prime experiments were specified: Parabolic Antenna, Orientation Control System, Radio Interferometer, and Phase-steered Array Antenna. An additional benefit sought is a better understanding of the problems of deploying and pointing any large aperture instrument in space.

In each of the prime experiments, the major objectives are to verify the basic feasibility and verify that it is possible to meet the performance requirements specified for the corresponding system. While meeting these objectives, it is desired to obtain as complete an understanding as possible of the design and performance problems of the system in order to support specification and design of similar systems for future experimental and operational space missions.

In formulating an effective program to meet the requirements of the ATS-4 mission, it is necessary to provide means for exercising the prime experiments and deriving the information required from the results of these exercises. These results will be in the form of measurements of the characteristics and performance of the prime experiments before, during, and after the exercises.

In the discussion of the experiments program in this section, each prime experiment is considered more or less independently. Every effort was made to arrange experiment and experiment equipments so that if necessary, the experiments can be performed, at least to some extent, independently. This is desirable in the interest of system reliability so that a deficiency in one experiment will not grossly handicap the others. However, in the interests of an efficient and effective program, the primary modes of most experiments are intended to take full advantage of the capabilities of the others; e. g. , the pointing accuracy of the interferometer, and the high gain of the parabolic antenna.

It was necessary to apply a limited cost-effectiveness criterion to the program; i. e. , to evaluate each proposed measurement in terms of its contribution to the mission objectives and of its anticipated costs (mainly in terms of system time, on-board weight, power, and form factor and ground support requirements). Otherwise, the costs of some measurements would have been excessive.

The objectives in formulation of individual experiments/measurements was to formulate experiments in the scientific sense; i. e. , to measure sets of parameters in the system in such a fashion that the procedure and requirements would be well defined, and the important characteristics of the results - accuracy, precision, level of confidence, etc. would be known. After such formulations were complete, these individual experiments were then integrated into an overall program; e. g. , scheduled to be performed separately or together, and in any combination which would make most effective use of the overall system while preserving the integrity of the experiment results.

A number of measurements beyond the scope of the present study present points of considerable interest; among them, more comprehensive investigation of the static and dynamic characteristics of the deployed spacecraft/antenna system in space, measurement of various facets of the parabolic antenna communications performance, and augmentation of the capabilities of the parabolic antenna and the interferometer. Some of these measurements, notably the instrumentation for the spacecraft characteristics, would require development programs to instrument. A number of the more interesting possibilities are discussed at the end of this section.

8.2 EXPERIMENT AXES REFERENCE

One somewhat troublesome problem which is common to all the experiments is the determination of pointing direction; i. e., how one verifies that the parabolic antenna electrical and mechanical axes, the radio interferometer axes, the orientation control axes, and the phased array beams are correctly oriented. This problem really breaks down into two problems:

- a. Boresight Problem - All pointing sensors measure angles with respect to their own set of de facto coordinates. The antenna mechanical axes do not coincide with any particular sensor, but must be derived from measurements of the antenna-feed system geometric configuration. Since these sensors are located at different positions about the structure, considerable difficulty may be anticipated in keeping various sensors and their accompanying coordinate systems properly aligned. Fortunately, this problem is somewhat simplified by the fact that absolute alignment is not required, so long as the relative misalignments can be detected and measured. For example, if the interferometer should by some structural or equipment shift be misaligned with the earth trackers, it will be quite feasible to compensate by the insertion of appropriate offsets into one system or the other. Similar measures can be taken with each of the other pointing systems. Even without this capability, calibration of the pointing-systems axes relative to one another would allow the ground command system to provide the compensation.
- b. Calibration Problem - In approaching the problem of in-space calibration, fine boresight alignment and small angle measurements comparisons can be made by commanding the Orientation Control (OC) system to point directly toward a station, then statistically comparing the angle readouts. Assuming that all systems are operating normally, the OC system will produce an error which is normally distributed about the real direction of the ground station (in earth sensor coordinates) with a zero mean and a 3σ value of 0.1 degree). The signal can be read out at the OC system. The interferometer output will produce an error signal which should have the same deviations, but (unless the interferometer and earth sensor coordinate systems are precisely aligned), a nonzero mean in both angles. The same will also be true of any other precision pointing sensors. Given enough data for a good statistical evaluation including complete ground calibration, a comparison of the mean values will give the boresight alignments, while a comparison of the distributions will indicate the comparative small angle readouts.

This measurement can be made more complete and reliable by switching one after another of the precision pointing sensors into the OC loop and repeating the measurement process.

Since variation in boresight alignment with thermal disturbance must be anticipated, it will be necessary to continue and/or repeat these measurements over at least one and probably a number of 24-hour cycles. Mathematical analysis will readily identify and determine the magnitude of any significant 24-hour or other cyclic effects.

Comparisons of the angle measurement outputs of the precision pointing sensors, as described in the preceding paragraph, will indicate the extent of agreement for small angles and will permit calibration of the sensors against one another along boresight.

In addition to the above relative calibration, along boresight, off-axis pointing requires complete calibration of at least one sensor. The most appropriate technique appears to be to calibrate the interferometer by measuring the angle subtended by two ground stations a known distance apart. Since the ranges from the ground stations to the satellite can be determined very accurately, the actual angle they subtend as seen from the satellite can also be very accurately determined. Comparing the real angle with that measured by the interferometer provides an absolute calibration of this value.

Calibrations across a range of values can be obtained by use of multiple stations or, in principle, by mounting beacons on aircraft or other vehicles. However, some difficulty may be anticipated with vehicle-mounted stations because of the ERP problem.

Two ground stations spaced about 2500 miles apart will provide an angle of about 5 to 6 degrees. For very small angles, of the order of 0.01 degree, station spacings of about 5 miles will be required; representative intermediate values include 50 miles or so for 0.1 degree, 250 miles for 0.5 to 0.6 degree, etc. These values assume that the line between the stations is orthogonal to the direction of the ATS-4 satellite.

A fairly complete calibration would require using some 10 fixed-station beacons. However, a reasonably good estimate could be obtained with about 3; say, one each at Rosman and Mojave and a third at one of these sites, removed from the other beacon on the site by not less than 5 miles nor more than 250 miles.

8.3 PARABOLIC ANTENNA

8.3.1 GENERAL DISCUSSION

The major objectives of the parabolic antenna experiment, and to a great extent the ATS-4 program, are to verify the basic feasibility of deploying and using the large antenna and to verify that it is possible to meet the specified performance requirements.

The large parabolic antenna experiment shall have a minimum aperture diameter of 30 feet with an objective of achieving the largest feasible aperture and shall be capable of both transmit and receive operation at frequencies up to 10 GHz. Specifically, the antenna feed system shall be capable of transmitting at 100, 800, 2300, and 7300 MHz and shall also be capable of receiving at 1700, 2100, and 8000 MHz. It is not necessary that either transmission or reception be simultaneous on all of the above frequencies. Bandwidth capability of the system at the specified frequencies shall be 10 percent. System antenna efficiency shall be at least 50 percent.

In approaching the antenna experiment problem, it should be pointed out that a large, deployable parabolic antenna in space must do two things simultaneously in the space environment - meet electrical performance requirements, and match the structure and attitude control system so that it can be pointed and controlled.

The measurements for evaluating the antenna design in terms of these basic requirements will overlap somewhat; i. e., mechanical measurements will to some extent indicate electrical performance, and conversely.

The electrical performance of a directional antenna is expressed by its gain as a function of direction and frequency, and by such parameters as phase relationships, polarization, etc. In a paraboloidal antenna, these parameters are controlled by the geometric configuration of the paraboloid, the location, orientation and structure of the feeds, and the design and structural integrity of the supporting rf structure.

The mechanical behavior includes the behavior during deployment, the static structural configuration, temperature distribution and thermal effects on the structure, and dynamic behavior, i. e., vibration amplitudes, frequencies, and damping characteristics. Deploy-

ment behavior is a matter of how all the moving parts behave and interact (hinge lines, joints, torque tube, motor, etc.) during deployment, and the characteristics of any excessive dynamic disturbances (modes, amplitudes, frequencies, and damping characteristics) caused by the deployment impulse. Thermal effects are those deformations caused by thermal expansions and contractions; these will be mostly if not entirely caused by the sun, and hence will have a strong 24-hour cycle component as the satellite rotates with the earth. Dynamic effects are vibrations induced by any mechanical disturbances, presumably for the most part attitude control and stationkeeping impulses.

8.3.2 TECHNICAL BACKGROUND OF MEASUREMENTS

8.3.2.1 Introduction

Before formulating specific measurement techniques to obtain the required performance data, the interrelationships of the antenna parameters and their relative influence on performance must be examined. This section will define the parameters which must be measured and will derive the required measurement accuracies.

8.3.2.2 Direction and Gain

In this section, the physical parameters controlling the gain of an antenna and its variation with direction are discussed. As will be pointed out, these parameters and their effects can be separated and measured on the ground, but in a normal antenna, usually not in space.

Directivity - Directivity is defined as the ratio of maximum radiated power to the average radiated power. Alternately, directivity is the comparison of a lossless test antenna with a fictitious lossless isotrope. Theoretically, calculation of directivity requires that the entire three dimensional radiation pattern be known. In practice, a limited number of planar patterns can be used to accurately calculate directivity.

Being essentially a measure of dispersion, directivity is affected by and hence is a measure of all parameters which contribute to the relative radiation pattern. These parameters include all structural parameters but do not include internal feed parameters such as loss and VSWR effects.

Directivity is seldom used as an evaluation of high gain antennas because it does not reference the performance to accessible terminals.

Gain - Gain is defined as the ratio of the radiated power per unit solid angle in a given direction in the antenna beam that is formed to the same power radiated isotropically (i. e., radiated in all directions equally). A plane aperture which is uniformly illuminated with equiphased energy radiates a gain pattern of the form:

$$G(\theta) = \left(\frac{\sin u}{u} \right)^2$$

where u is a function of the directional angle θ . It can be demonstrated that the maximum gain of such an aperture is:

$$G = 10 \log \frac{4\pi A}{\lambda^2}$$

Where G = gain (dB above isotrope)

A = aperture area

λ = wavelength.

A paraboloidal reflector can be analyzed as a plane aperture with certain departures from the ideal. Departure from either the uniform illumination or the equiphased wave front cause the gain to be less than the theoretical.

Real antenna feeds cannot radiate the unusual pattern which would be required to uniformly illuminate the reflector and to have the total energy from the feed intercepted by the reflector. The loss of gain due to nonuniform illumination (illumination efficiency) must be compromised with the loss of gain due to energy radiated by the feed but not intercepted by the reflector (spillover efficiency). A typical set of curves is shown in Figure 8.3-1.

Additional perturbation of the illumination is caused by blockage effects of the Earth Viewing Module and feed supports. The loss of gain due to feed blockage, is given by:

$$L_f = 20 \log (1 - 2 B^2)$$

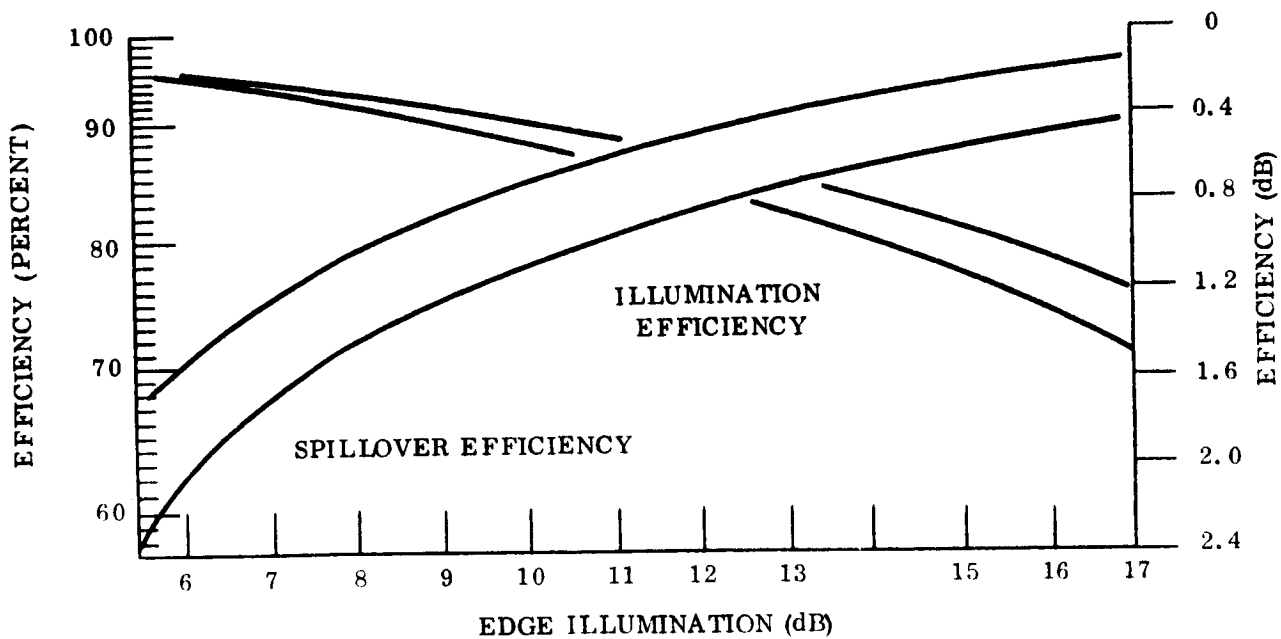


Figure 8.3-1. Spillover Efficiency and Illumination Efficiency

where $B = \text{Blocking ratio} = \frac{\text{Earth Viewing Module diameter}}{\text{reflector diameter}}$

The loss of gain due to strut blockage, L_s , is given by*

$$L_s = 20 \log \left(1 - \frac{1.55 n s}{D} \right)$$

where:

- n = number of pairs of struts
- s = diameter of the struts
- D = diameter of the parabola

*Gray, C. L., "Estimating the Effect of Feed Support Member Blocking on Antenna Gain and Sidelobe Level," Microwave Journal, pp. 88-91, March 1964.

The effects of strut blockage will be investigated in detail in ground measurements. In space, separate measurement of these effects is impractical, except in the event of gross deformations of the strut/Earth-Viewing Module configuration. In such a case, gross changes in gain, boresight and main lobe configuration would be encountered, and it would be important to determine the cause.

Phase errors arise from three main sources:

- a. Imperfections in the reflecting surface
- b. Defocusing
- c. Feed phase center errors or movement

Since the best gain measurement accuracy that could be expected is in the order of ± 0.5 dB, a change in rms surface accuracy of 0.25 in. would be required before a change of gain could be detected. The feed displacement causing defocusing can be separated into two components:

- a. Axial displacement, which causes gain loss, but little pattern distortion. The anticipated displacement of about 0.14 inch causes a negligible loss, of the order of 2 percent, at 8 GHz. At the same frequency, a displacement of 0.22 inch is required to cause a loss of 0.1 dB and more than half an inch to lose 0.5 dB.
- b. Off-axis displacement, which causes both gain loss and change of beam pointing direction. In the configuration given (with $F/D = 0.4$), at 8 GHz, a loss of 0.5 dB is equivalent to a beam displacement of approximately 0.06 degree or about 0.15 inch. The anticipated thermally induced displacement is slightly less than this.

Thus, it is doubtful that the expected values of these motions could be detected by gain measurements made on the ground, of the antenna deployed in space.

Additional phase-front perturbations arise because conventional feeds do not radiate perfectly spherical waves. However, this cannot be directly measured in space.

8.3.2.2.1 Principal Plane Patterns

The radiation pattern of an antenna is the angular variation of the gain function. An envelope of patterns measured on a 30-foot paraboloid is shown in Figure 8.3-2.

The main beam is usually described by giving the angular width at the half-power and tenth-power points. This beamwidth is primarily controlled by the illumination and is affected to a lesser degree by feed displacement and other geometrical factors.

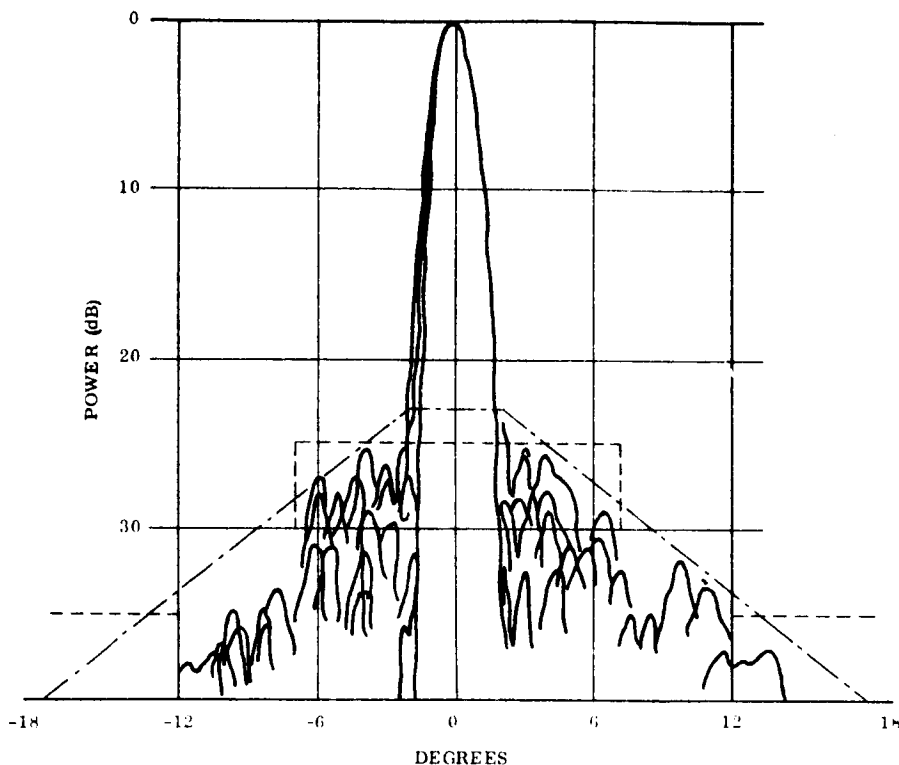


Figure 8.3-2. Composite Patterns Measured on 30-Foot Paraboloid at 1700, 1820 and 1900 MHz

Dispersive effects are qualitatively described by giving the maximum sidelobe level, average sidelobe level, and front-to-back ratio.

The maximum sidelobe level in general is controlled by the illumination, as indicated in Figure 8.3-3. Degradation of the design sidelobe level is caused by energy dispersed by the feed (or subreflector) and the struts.

Dispersions in directions far from the main beam are primarily controlled by the amount of spillover energy.

Measurement of sidelobe structure at the S-band and X-band frequencies is feasible. Derivation of the contributions of the individual causes in general is not.

8.3.2.2.2 Boresight

Boresight is the relationship of the pointing direction of the main beam to some mechanical reference, usually the axes of the paraboloid. The electrical pointing direction and the mechanical axes of the reflector are aligned very closely during check-out of the antenna. A deviation from this alignment indicates a systematic phase taper, such as would be caused by off-axis feed displacement or an equivalent reflector distortion.

The misalignment anticipated is of the order of 1 milliradian; about 0.05 to 0.06 degree. This quantity can probably be measured, but correct assignment of the causes of misalignment to feed displacement and reflector distortion is not amenable to direct measurement.

8.3.3 SELECTION OF PARAMETERS

8.3.3.1 General

In order to permit evaluation of the parabolic antenna and provide guidance for the design of future large-aperture antennas, a limited set of parameters must be selected for in-space measurement such that having an extensive matrix of data generated during ground testing it will be possible to correlate the two types of measurement to yield the most efficient acquisition of knowledge of the antenna performance.

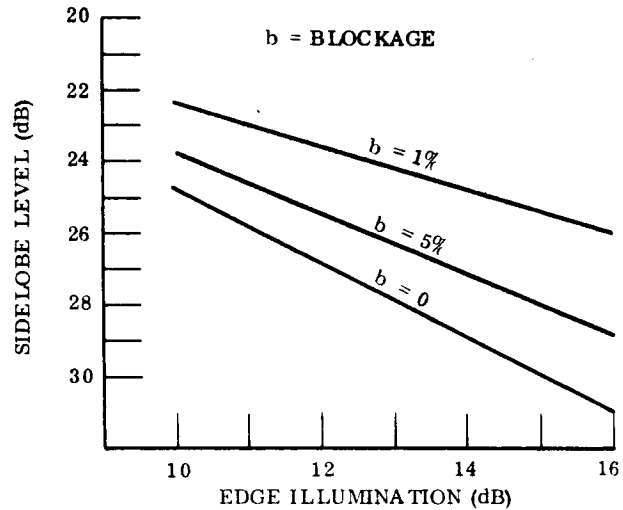


Figure 8.3-3. Sidelobe Level Versus Edge Illumination

8.3.3.2 In-Space Measurements

The parameters recommended for measurement in space are based on past experience and knowledge of interrelations of antenna characteristics. The discussion of the antenna geometry and its effects on the rf performance has demonstrated that certain electrical parameters are affected by virtually every type of error in the antenna. Other parameters are affected for the most part by particular types of errors.

Of prime interest in the parabolic antenna tests is the evaluation of the antenna for high gain communication applications. Thus from an operational standpoint we wish to first measure the gain of the antenna versus frequency and time, and then the boresight accuracy and stability with respect to a suitable reference (i. e., the spacecraft mechanical axis or an accurate attitude sensor axis) versus frequency and time. These two factors will permit the evaluation of this particular antenna in an operational communication system.

Further, it is planned that any additional parameters, which will allow more detailed identification of the performance of elements (i. e., reflector, feed, rf components) of the antenna system will be measured so that design improvements may be made, and new concepts evaluated with a high degree of assurance in the results. Of major importance here is a measurement of the surface tolerance of the main reflector. Gain and boresight will both be affected by reflector surface errors, as discussed earlier. Thus, it would seem essential to make at least enough additional measurements to independently determine the parabola surface variations and to at least 0.25 inch.

It will further be highly desirable to make VSWR measurements to assure that significant gain losses do not result from failure or mismatch in rf components.

Antenna patterns can be deduced from the above set of data. However, measuring these patterns would provide additional confidence to the other measurements by providing redundancy. With a limited accuracy in the OC system it will be difficult to take precise patterns. However, in evaluating ways to make gain and boresight measurements a great deal of the principle plane patterns are found to be essentially free. Thus, as much pattern data will be taken as possible without setting up special tests for this purpose.

Thus the antenna parameters to be measured in space are boresight accuracy and stability, gain, VSWR, reflector contour, and to a limited degree antenna patterns.

8.3.3.3 Ground Testing

In order to correlate the in-space measurements with detailed quantitative evaluation of the antenna parameters, an extensive ground test program should be conducted. This program would have the following objectives:

- a. To determine that the design goals have been met.
- b. To obtain additional information about the antenna performance which would be used for comparison with measurements of the antenna when deployed in space.
- c. To determine the effect of predicted deformations, possible failure modes, etc., on the antenna performance.

Radiation performance measurements of the antenna are meaningful only if the antenna geometry on the ground is representative of the geometry expected when the antenna is deployed in space. Assurance of such geometry requires compensation for gravitational effects, stiffness scaling to compensate for accelerations, and protection against and/or compensation for wind loads. The following description of ground measurements assumes these compensations have been made and the antenna geometry conforms to the design.

The radiation performance should be described by a contour plot of field strength versus angle. The contour plot should be generated from many planar patterns. These patterns would be taken at the center and edges of each frequency band. All angular regions into which the antenna radiates with a level within 25 dB of the peak gain would be plotted. A mathematical model of the main beam would be synthesized from the measured data.

The polarization, as indicated by the orthogonal linear components, should be measured over the angular region of the contour plot and indicated on a common angular scale. These rf maps would be used as a basis for comparison with the space measurements which require statistical correlation with ground measurements.

The absolute gain of the antenna should be measured at three frequencies in each of the specified frequency bands. Where possible, the gain should be referenced to more than one gain standard. This procedure yields essentially independent measurements which allows reduction of systematic errors due to range effects, gain standard and equipment calibration, etc., and thus a more accurate measurement. These gain measurements would be used to demonstrate compliance of the design with the aperture efficiency specification and to normalize the pattern measurements to an absolute reference.

The boresight of the antenna will be adjusted during preliminary testing to align the electrical and mechanical axes as closely as possible. The feed adjustment will be selected which produces the best alignment at S- and X-bands, where the beam widths are narrowest, requiring the best pointing accuracy.

After this alignment has been optimized, the boresight relationships will be measured. These data will be used as a reference to angularly normalize the radiation patterns and as a reference for the determination of the effects of antenna perturbations which may be caused by thermal gradients and accelerations.

The input VSWR of the antenna system should be measured at five frequencies in each frequency band. These measurements constitute primarily a verification of feed design and construction. Additional VSWR measurements should be made in the 7.3 to 8.0 GHz band during antenna deployment. Should the VSWR exhibit, during the deployment cycle, regular and suitably sensitive variations, this parameter would warrant consideration for use as a gross deployment indicator.

In addition to the measurements of the antenna in its design configuration, performance data should be obtained for certain configurations which deviate from design. These deviations should as closely as possible, duplicate the effects of thermal gradients and stationkeeping and pointing and tracking accelerations. Deviation due to definable probable failure modes and age should also be simulated. Simulation of predicted deformations would of course be limited to those which can be simulated without permanent damage to the antenna.

The effects of these deviate geometries on gain, boresight and main beam shape should be measured. These data, in combination with the data matrix on the design geometry, constitute a basis for antenna evaluation at any orbital position throughout the life of the mission.

8.3.4 IN SPACE MEASUREMENT TECHNIQUES

8.3.4.1 Gain

Measurement of the absolute gain of the large parabolic antenna at a particular frequency consists of the comparison of the power radiated from (or received by) the test antenna with the power radiated from (or received by) a reference antenna both having the same input power. Three techniques suggest themselves: 1) direct substitution of a reference antenna in space, 2) measurement of absolute field strength and adjustment for propagation effects, and 3) calculation of antenna gain from radar cross-section measurements.

Direct substitution of a reference antenna most closely parallels the technique commonly used in ground tests. The large parabola and the reference antenna are pointed at the ground station and the signal path is switched between them and the difference is noted. Since the exact directions of the peak gains may not be known, repetitive measurements may be required. These data sets would then be correlated with the mathematical model of the beam shape derived from ground tests and the peak gain would be deduced even though the exact peak might never have been reached. The gain of the reference antenna should be as close as possible to the gain of the test antenna. However, the requirement of a reference antenna for each frequency band makes the use of a single, broadband antenna attractive. Such broadband antennas are limited to about 10-12 dB maximum gain. Ideally, the reference antenna should be deployed away from the test antenna to minimize interaction. Interactions could be somewhat compensated for during ground test, however.

The substitution method has been selected as the approach to be implemented for gain measurements, since it appears to provide the best measurement accuracy. For purposes of evaluating reflector surface contour errors it would be desirable to measure gain to a

few tenths of a dB. It may be possible to implement the measurement so that a resolution of a few tenths of a dB is possible but it is highly doubtful if the gain standard antenna and rf loss will be accurate or stable enough to obtain absolute accuracies that good. It is expected that with well designed gain standard antennas and careful measurement techniques an absolute gain accuracy of ± 1 dB could be achieved at the higher frequencies.

Measurement of absolute field strength is simple in principal but in practice is complicated by requirements of system stability, and calibration. The gain measurement accuracy is directly dependent on these factors and knowledge of atmospheric effects. This technique could yield very precise measurements through repetitive sampling. However, the sources of the largest and most probable errors are systematic in nature and are not easily compensated for. This technique requires probably less system time per sample than the alternate techniques. This technique is probably best suited to the down link, i. e., transmit from space, where only approximate gain measurements will be made, anyway.

The feasibility of determining antenna parameters by measurements of the scattering cross section has been established. * Theoretical accuracy of this technique is commensurate with the objectives of this experiment, and it could be done entirely from the ground. However, the theoretical accuracies appear very difficult to achieve, and use of the technique may impose limitations on the antenna design.

8.3.4.2 Antenna Geometry Measurements

Measurement of the antenna geometry includes: 1) verification of grossly proper deployment, 2) measurement of antenna-feed geometry and distortions caused by mechanical and thermal disturbances, and 3) surface contour.

*Skarote, S. J., "An Investigation of a Method of Determining Antenna Parameters by Scattering Cross Section Measurements," Ohio State University, 15 May 1965, N 65-27474.

Gross geometry verification will be required only during deployment. Many simple schemes for this verification are evident and final evaluation of techniques and devices will be dependent upon the details of the antenna design. Possible schemes include the following: 1) monitoring the locking mechanisms with make-or-break electrical sensors; 2) monitoring the overall deployment sequence through a television camera; 3) monitoring some gross rf parameter, such as VSWR, whose variation during deployment check would indicate the proper completion of the sequence, determine the advisability of continuing, and provide diagnostic information to guide possible corrective action. At this time schemes 1) and 3) are recommended.

Antenna geometry measurements should be made to describe the deployed geometry, and to detail the nature of any deviations from the design and provide guidance for possible corrective action and/or reduction of mission objectives. Geometry measurements would be made throughout the life of the mission, to determine that the distortions caused by thermal and mechanical disturbances and the variations therein due to aging do not exceed the detectable level of about 0.25 inch.

Conformity of the reflector contour to the prescribed values can be determined through measurement of stresses by strain gauges, pressure transducers, etc. Such measurements would be referenced to the equivalent measurements made during ground testing. These comparisons would be complicated by the differences in gravitational fields. Measurement devices must be calibrated over the entire temperature range which the antenna is likely to encounter, and the temperature of each sensor must be known over the measurement period.

8.3.4.3 Boresight

At 8 GHz, the antenna half-power beamwidth is approximately 0.3 degree. Figure 8.3-4 shows a plot of equal power contours for this antenna beam. From this figure we see that a pointing error of ± 0.1 degree (estimated 3σ error for the orientation control system) would produce a gain change of approximately 1.5 dB. This may be acceptable as a system error for a communication link. However, to evaluate the antenna itself we would like

our measurement error significantly less than this. Again referring to Figure 8.3-4, it is seen that a boresight error of 0.03 degree would produce approximately 0.1 dB gain loss, and would also be a fairly small error term in a 0.1 degree pointing system. Thus we will proceed here with a nominal specification for boresight measurement accuracy of 0.03 degree rms. Accuracies better than this (down to about 0.01 degree) would be desirable but not essential. The following is a proposed technique for measuring the antenna boresight axis without a monopulse feed available.

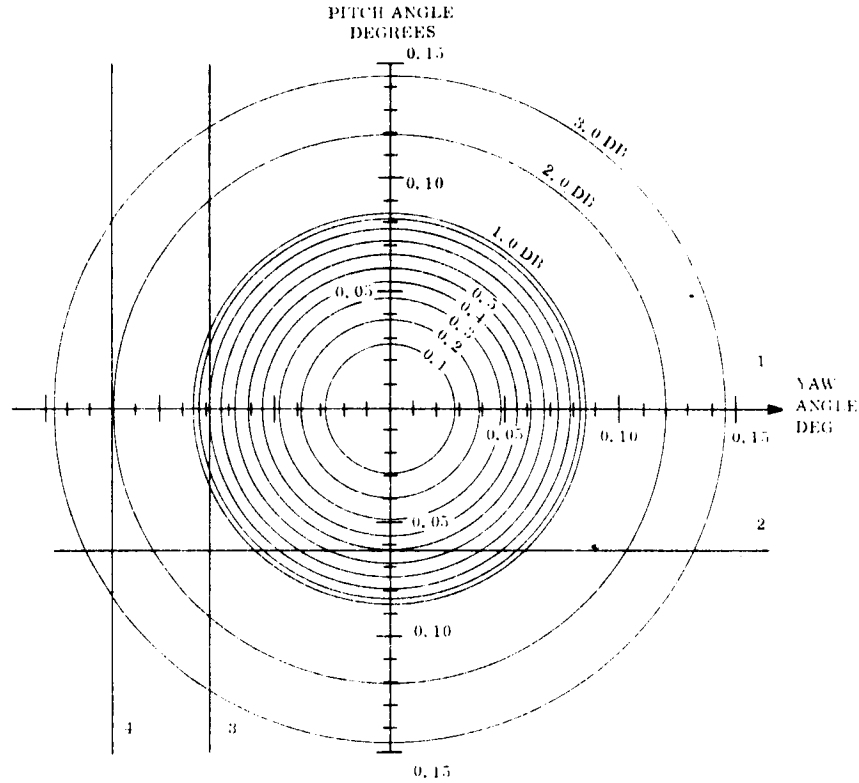


Figure 8.3-4. Large Aperture Antenna Equal Power Contours at 8.0 GHz Frequency

An error analysis is presented which indicates an accuracy of 0.03 to 0.05 degree could be achieved. (To improve this measurement accuracy a monopulse feed would be required. The monopulse approach would improve the measurement accuracy (± 0.01 degree rms), plus simplifying the measurement procedures and reducing the measurement time).

Basically it is desired to measure the position of the large antenna beam rf axis (defined here as a line drawn from the phase center of the dish through the maximum gain point in

the antenna for field pattern), with respect to the spacecraft axis (as measured by either the interferometer or OC sensor). To do this the spacecraft can be rotated so as to move the antenna rf axis away from the main ground station in one axis only. The beam can then be moved so as to slowly swing the antenna beam across the ground station. It will be assumed for this analysis that this pass may be made to cut through at least the 3 dB points on the pattern (± 0.12 degree off boresight at 8 GHz). As the main lobe of the antenna is approaching the station, the spacecraft orientation control will be set so as to maintain constant angular velocity on the pass. The angular rate will be kept to 0.01 deg/sec or less which, with an interferometer measurement rate of 1/sec, will provide spacecraft angular position data at intervals of 0.01 degree or less.

Figure 8.3-4 shows equal power contours of the antenna main beam, and Figure 8.3-5 shows the beam pattern for off boresight slices. Inspection of Figures 8.3-4 and 8.3-5 show that for any slice through the main beam, a line constructed perpendicular to the line of the slice, and passing through the point on this line where the maximum signal is observed, will pass through the beam center (Figure 8.3-6). Thus, by making two perpendicular slices through the beam, the beam center can be found from the intersection of the constructed perpendiculars (Figure 8.3-6).

It may also be seen from inspection of Figure 8.3-6 that the two pattern slices need not be exactly perpendicular although the measurement accuracy degrades somewhat if the slices are not approximately so.

There will be two error sources in our location at the rf boresight using this technique. First will be the errors in location of the point along the slice where the maximum signal power was received. This will be a function of our signal level measurement resolution, and equipment power drifts over the measurement interval. The former (resolution) will depend primarily on signal-to-noise ratio in the measurement channel. A S/N of 20 dB would provide a resolution capability of about 0.1 dB or an angular error of less than 0.03 degree rms. A more complete analysis of equipment errors would be required, but there appears to be no reason a measurement of 0.03 degree rms cannot be made.

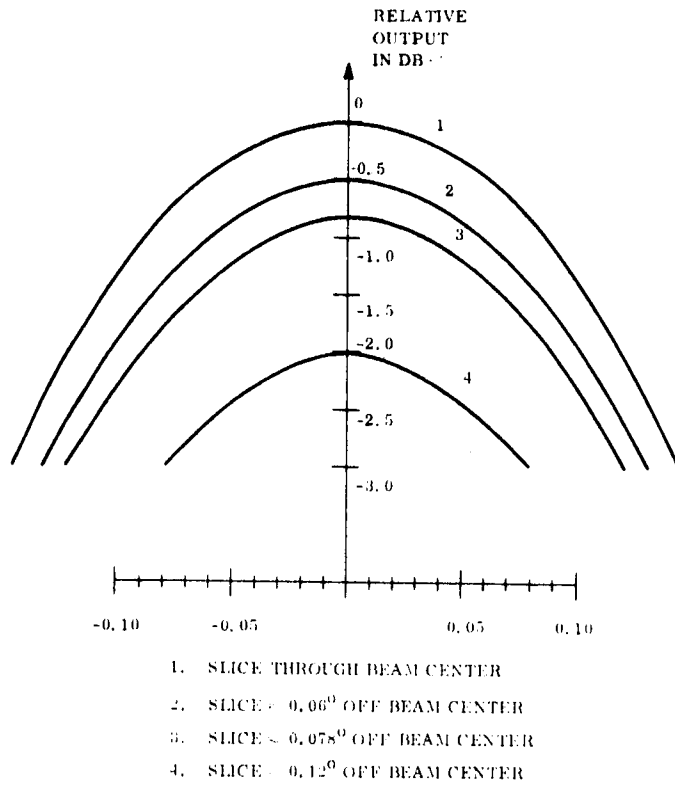


Figure 8.3-5. Large Aperture Antenna Main Lobe Patterns

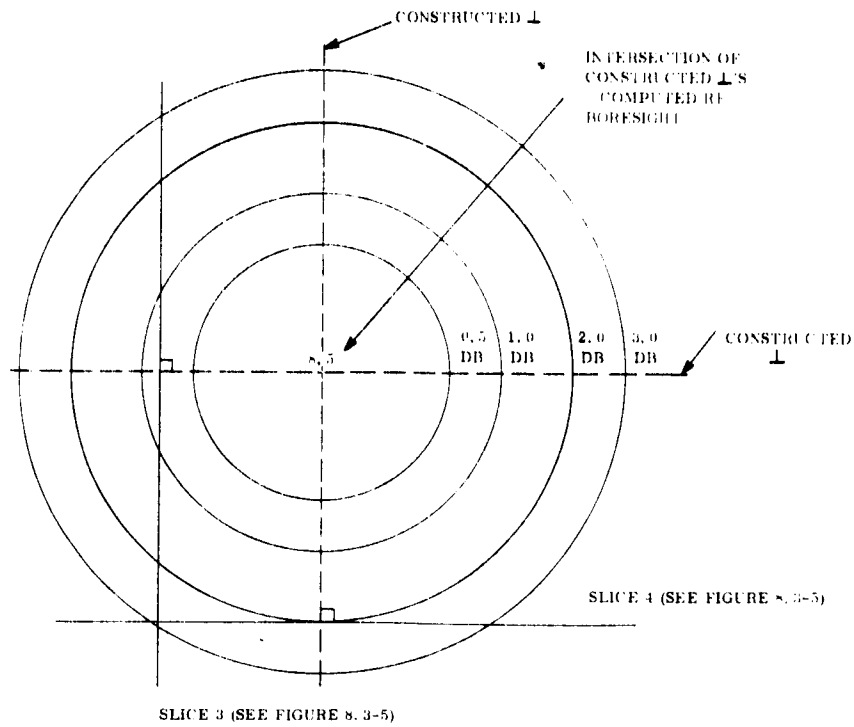


Figure 8.3-6. Graphic Representation of RF Boresight Measurement Technique

The second source of error is an uncertainty of the slope of the slice taken through the beam, resulting in a slope uncertainty of the constructed perpendicular. This slope uncertainty results from the errors in our attitude sensing system (± 0.01 degree rms for the interferometer). As shown in Figure 8.3-7 our measured data will be a set of angle data points spaced approximately 0.01 degree apart, with a one σ error of 0.01 degree ($1\sigma = 0.01$). The problem then is to curve fit a straight line to this set of data points so as to minimize the mean square errors. We would here like to know what the error is in the slope of the fitted straight line as a function of the errors in the measured data points.

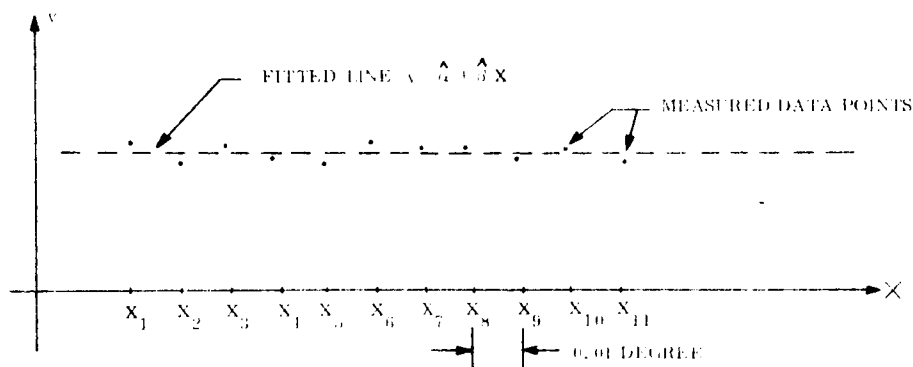


Figure 8.3-7. Curve Fitting Angle Data

For the case shown here with 11 data points, X_6 is the mean (i. e., $\bar{X} = X_6$)

$$\begin{aligned} \sum (X_i - \bar{X})^2 &= 2(5 \Delta X^2 + 4 \Delta X^2 + 3 \Delta X^2 + 2 \Delta X^2 + \Delta X^2) \\ &= (0.01)^2 (2) (55) = 0.011 \text{ (for } \Delta X = 0.01 \text{ deg)} \end{aligned}$$

$$\sigma_\beta^2 = \frac{(0.01)^2}{(0.011)} \cong 0.01$$

$$\sigma_\beta \cong 0.1 \text{ deg/deg}$$

Thus, if the slice is θ degrees off boresight, the boresight measurement error resulting from the slope error will be:

$$\sigma_S \cong (\sigma_\beta) (\theta) = 0.1 (\theta) \text{ degree}$$

Thus, if our slice is always within the 2 dB point ($0.12^\circ = \theta$) the maximum boresight error due to slope errors will be:

$$\sigma_{S_{\max}} = (0.1) (0.12) = 0.012 \text{ degree}$$

Thus, if the slope and displacement errors are combined as shown in Figure 8.3-8, our approximate rms boresight measurement error becomes:

$$\begin{aligned} \sigma_{BS}^2 &= \sigma_D^2 + \sigma_{S_{\max}}^2 = (0.03)^2 + (0.012)^2 \\ &= (0.032)^2 \end{aligned}$$

$$\sigma_{BS} \cong 0.032 \text{ degree}$$

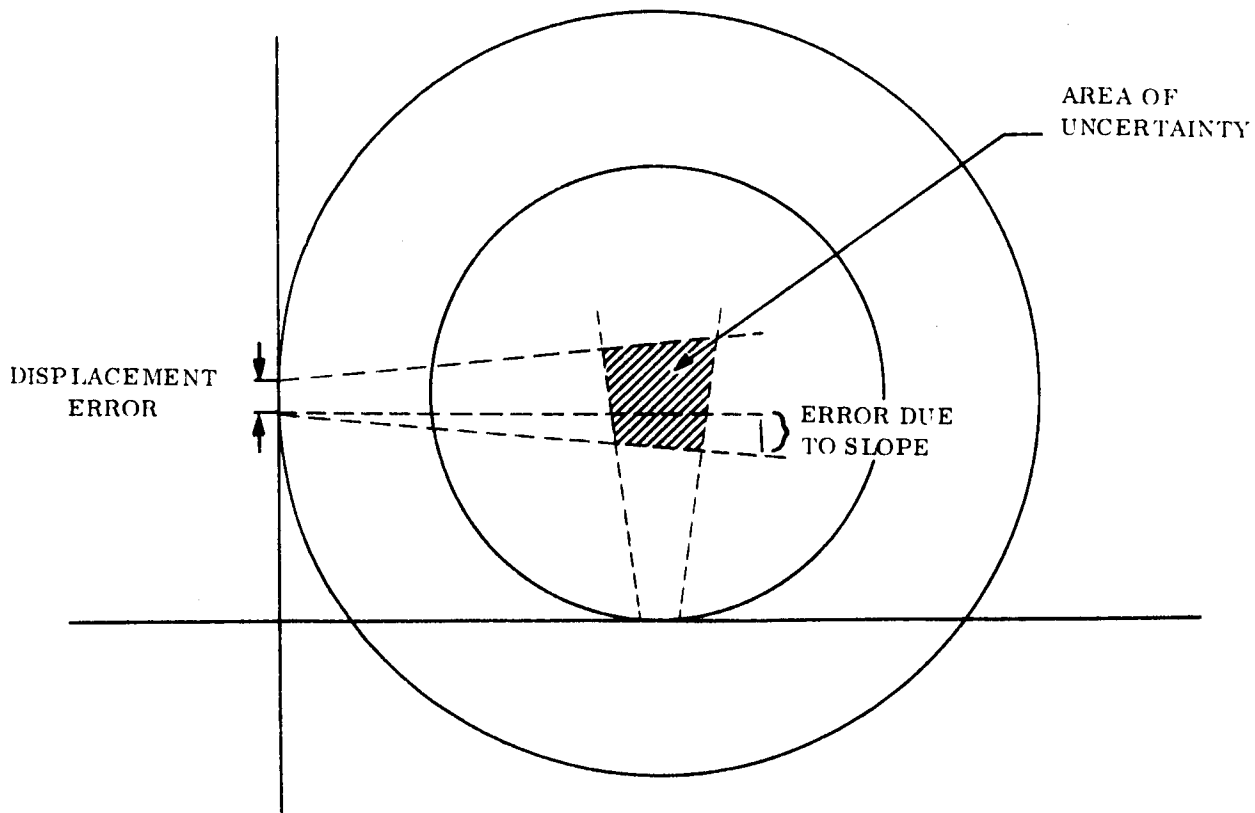


Figure 8.3-8. Boresight Error Combination Illustration

This has been worked out in the literature ("Introduction to the Theory of Statistics," Mood & Graybill, pp. 329-333) and gives:

$$\sigma_{\beta}^2 = \frac{\sigma^2}{\sum (X_i - \bar{X})^2}$$

The analysis and description presented here describes a graphical technique for reduction of data. In the actual experiment it is expected that the data would be reduced by a computer program, which could perform the optimum curve fitting, and compute the rf boresight from the raw data. It would also be possible to make gain measurements on each pattern slice (at the peaks) using the gain standard horn. By feeding this maximum gain figure to the computer it would be possible to compensate for the fact that the slice was not through the true beam peak and compute the maximum lobe gain. Thus, if properly instrumented, it appears that one set of data would permit the antenna gain and boresight to be accurately computed. Also resulting from the data is a set of patterns for the main lobe in the major planes.

8.3.5 EXPERIMENTS

8.3.5.1 Listing of Experiments

Table 8.3-1 is a list of experiments which is recommended for evaluation of the parabolic antenna. These experiments range in importance from crucial (e. g., gain, basic geometric configuration) to merely convenient or "nice to have," such as very wideband transmission experiments. The more important of these are described in some detail in the remainder of this section.

Where additional technical discussion is necessary to make the physical and electrical basis of a measurement clear, this discussion is either included or referenced in the experiment description.

The experiments in Table 8.3-1 are divided into the following types:

- a. Crucial - Necessary to attainment of mission objectives, Type 1.
- b. Important - Contributes substantially to fulfillment of mission objectives, Type 2.
- c. Useful - Contributes in a minor way to fulfillment of mission objectives, Type 3.
- d. Process - Not useful or only incidentally useful in itself, but necessary or desirable in preparing for the performance of useful experiments, Type 4.

The type of each experiment is indicated in Table 8.3-1 by the number after the title; i. e.,

A-1 Verification of Deployment - 1

Table 8.3-1. Individual Experiments - Parabolic Antenna

PARABOLIC ANTENNA

A-1 Verification of Deployment - 1

To verify that deployment occurred and that there is no major malfunction.

A-2 Verification of Equipment Operation - 4

To verify that the equipment associated with the antenna (transmitters, receivers, switching, etc.) is working.

A-3 Measurement of Internal Parameters - 4

To verify that the internal system parameters (transmitter power, receiver sensitivity, frequency stability, etc.) are within design tolerances.

A-4 Verification of Operational Characteristics - 4

To verify that the operational characteristics of the parabolic antenna system (ability to transmit and receive high-quality signals, and antenna performance characteristics) are qualitatively correct.

Table 8.3-1. Individual Experiments - Parabolic Antenna (Cont)

A-5 Gain Measurement Experiments

A-5-1 Gain Measurement Experiments without High Accuracy Pointing Devices - 1

A-5-1-a To measure, with the highest accuracy attainable, the absolute gain of the parabolic antenna, using the technique of comparison with standard gain horns, and assuming that the interferometer or other high-accuracy pointing sensor is not available.

A-5-1-b Gain Measurement - High Accuracy - 2

To measure, with the highest accuracy attainable, the absolute gain of the parabolic antenna, using the technique of measuring transmitted and received power, and assuming that a high-accuracy pointing sensor (e. g., the interferometer) is not available.

A-5-1-c Gain Measurement - High Accuracy - 3

To measure, with the highest accuracy attainable, the absolute gain of the parabolic antenna, using the technique of passive reflectivity measurement, without a high-accuracy pointing sensor.

A-5-2 Gain Measurement Experiments with High Accuracy Pointing Devices

A-5-2-a Gain Measurement - High Accuracy - 1

To measure, with the highest accuracy attainable, the absolute gain of the parabolic antenna, using the technique of comparison with standard gain horns, and assuming that the interferometer or other high-accuracy pointing sensor is available.

A-5-2-b Gain Measurement - High Accuracy - 2

To measure, with the highest accuracy attainable, the absolute gain of the parabolic antenna, using the technique of measuring transmitted and received power, and assuming that a high-accuracy pointing sensor (e. g. the interferometer) is available.

A-5-2-c Gain Measurement - High Accuracy - 3

To measure, with the highest accuracy attainable, the absolute gain of the parabolic antenna, using the technique of passive reflectivity measurement, with a high-accuracy pointing sensor.

Table 8.3-1. Individual Experiments - Parabolic Antenna (Cont)

A-6 Boresight Measurement

A-6-1 Boresight Measurement - High Accuracy - 1

To measure, with the highest accuracy attainable, the electrical/mechanical boresight of the parabolic antenna, without a high-accuracy pointing sensor.

A-6-2 Boresight Measurement - High Accuracy - 1

To measure, with the highest accuracy attainable, the electrical/mechanical boresight of the parabolic antenna, using a high-accuracy pointing sensor.

A-7 Pattern Measurement

A-7-1 Pattern Measurement - 2

To measure, to the highest accuracy attainable, the main lobe pattern and the accessible side lobes of the parabolic antenna, without a high-accuracy pointing sensor.

A-7-2 Pattern Measurement - 2

To measure, to the highest accuracy attainable, the main lobe pattern and the accessible side lobes of the parabolic antenna, using a high-accuracy pointing sensor.

A-8 Verification of Signal Transmission - 4

To verify that transmission of intelligible signals through the parabolic antenna can be performed.

A-9 Verification of Signal Reception - 4

To verify that reception of intelligible signals through the parabolic antenna can be performed.

A-10 Verification of Signal Switching Operation - 4

To verify that the designed signal switching operations of the parabolic antenna system can be performed.

Table 8.3-1. Individual Experiments - Parabolic Antenna (Cont)

A-11 Measurement of Low Data Rate Performance - 4

To measure as accurately as possible the performance of the parabolic antenna in transmitting and receiving digital data at low (10 to 10^3 bps) data rates.

A-12 Measurement of Medium Data Rate Performance - 4

To measure as accurately as possible the performance of the parabolic antenna in transmitting and receiving digital data at medium (10^3 to 10^5 bps) data rates.

A-13 Measurement of High Data Rate Performance - 2

To measure as accurately as possible the performance of the parabolic antenna in transmitting and receiving digital data at high (10^5 to 10^7 bps) data rates.

A-14 Measurement of Audio AM Performance - 3

To measure as accurately as possible the performance of the parabolic antenna in transmitting and receiving audio signals, AM.

A-15 Measurement of Audio FM Performance - 3

To measure as accurately as possible the performance of the parabolic antenna in transmitting and receiving audio signals, wide band FM.

A-16 Measurement of Video SSB AM Performance - 3

To measure as accurately as possible the performance of the parabolic antenna in transmitting and receiving video signals, vestigial sideband (commercial standards) AM.

A-17 Measurement of Video Wideband FM Performance - 2

To measure as accurately as possible the performance of the parabolic antenna in transmitting and receiving video signals, wideband FM.

A-18 Measurement of Signal Amplitude Fluctuations - 3

To measure to the highest accuracy attainable the fluctuations in signal amplitude (1 cps to 10^7 cps) caused by atmospheric propagation and/or antenna vibration effects.

A-19 Measurement of Signal Phase Fluctuations - 3

To measure to the highest accuracy attainable the fluctuations in signal phase caused by atmospheric propagation and/or antenna vibration effects.

Table 8.3-1. Individual Experiments - Parabolic Antenna (Cont)

A-20 Measurement of Signal Phase Distortions - 3

To measure to the highest accuracy attainable the distortion in signal phase caused by atmospheric propagation and/or antenna vibration effects.

A-21 Measurement of Polarization Effects - 3

To measure to the highest accuracy attainable the fluctuations and bias in polarization caused by atmospheric propagation and/or antenna vibration effects and to investigate the use of polarization in measuring spacecraft attitudes.

A-22 Measurement of Surface Contours - Medium Accuracy - 4

To determine to a reasonable approximation the contours which the parabolic antenna has assumed upon deployment.

A-23 Measurement of Surface Contours - High Accuracy - 1

To measure to the highest accuracy attainable the contours which the parabolic antenna has assumed.

A-24 Measurement of Mechanical Vibration Effects - High Accuracy - 1

To measure to the highest accuracy attainable the distortions of the antenna basic contours caused by mechanical disturbances.

A-25 Measurement of Thermal Contours - 1

To measure the thermal patterns of the antenna at all sun angles.

A-26 Measurement of Tracking Performance - 1

To measure to the highest accuracy attainable the performance of the parabolic antenna system while tracking.

A-27 Measurement of Slew Performance - 1

To measure to the highest accuracy attainable the performance of the parabolic antenna system during slew.

A-28 Incremental Angle Measurement - 3

To measure to the highest accuracy attainable the relative electrical performance and antenna system performance of the parabolic antenna with respect to two ground stations at known locations.

Table 8.3-1. Individual Experiments - Parabolic Antenna (Cont)

A-29 Band Limitation Measurements - 1

To measure to the highest accuracy attainable the performance of the parabolic antenna system in transmitting and receiving signals at the edges of the prescribed frequency bands.

A-30 Thermal Cycle Electrical Effects - 1

To measure to the highest accuracy attainable the effects of thermal distortion upon the electrical characteristics of the antenna.

A-31 Mechanical Disturbance Electrical Effects - 1

To measure to the highest accuracy attainable the effects of mechanical disturbances upon the electrical characteristics of the antenna.

A-32 System Life Characteristics - 1

To measure to the highest accuracy attainable the degradations in the electrical, thermal, and mechanical characteristics of the parabolic antenna with time.

8.3.5.2 Basic Electrical Measurements

8.3.5.2.1 Experiment Formulation

The crucial electrical measurements for evaluation of the parabolic antenna are absolute gain, electrical/mechanical borewidth, and VSWR. Of very great importance in support of these is a pattern analysis of the main lobe and the first few side lobes of the high end of the frequency spectrum.

The procedures for making these measurements overlap a great deal, and a considerable portion of the measurement data obtained in each measurement can be used in each of the others. However, there are important differences also, and each measurement is conceptually distinct. For these reasons it is necessary to consider each of them as a separate experiment.

The remaining important electrical experiments are, the communications experiments, and the antenna life experiments.

8.3.5.2.2 Experiment A-5 - Absolute Gain

a. Purpose

To measure the gain of the 30-foot-parabolic antenna at all specified frequencies.

b. Technical Description

In order to insure a good measurement accuracy, gain will be checked using a standard gain reference antenna. Two modes will be used; transmission from the spacecraft for the transmission frequencies and transmission from the ground for the reception frequencies. Configurations for use of these techniques are illustrated in Figures 8.3-9 and 8.3-10, respectively.

Gain measurements will be made in all frequency bands, but since the upper (7-8 GHz) ranges are most critical, measurements of that frequency will be described in this section.

The transmission mode technique is to radiate from the satellite through a standard antenna of known gain, establishing a signal level at the ground receiver. The spacecraft transmitter is then switched to the 30-foot antenna, and a precision attenuator on the ground is changed until the same signal level is indicated by the ground receiver. The 30-foot antenna gain is thus equal to the standard antenna gain plus the change in attenuation inserted in the ground equipment. The accuracy of this measurement will depend upon the accuracy of the precision variable attenuator, the accuracy of the gain figure for the standard horn, and the changes in line rf losses between the transmitter output and input to the antennas.

Provision is made for the insertion of a calibrate signal at the ground receiver. This calibrate signal has two purposes. First, using a calibrated power source to establish the same detector output as obtained in the gain measurement, the actual signal power

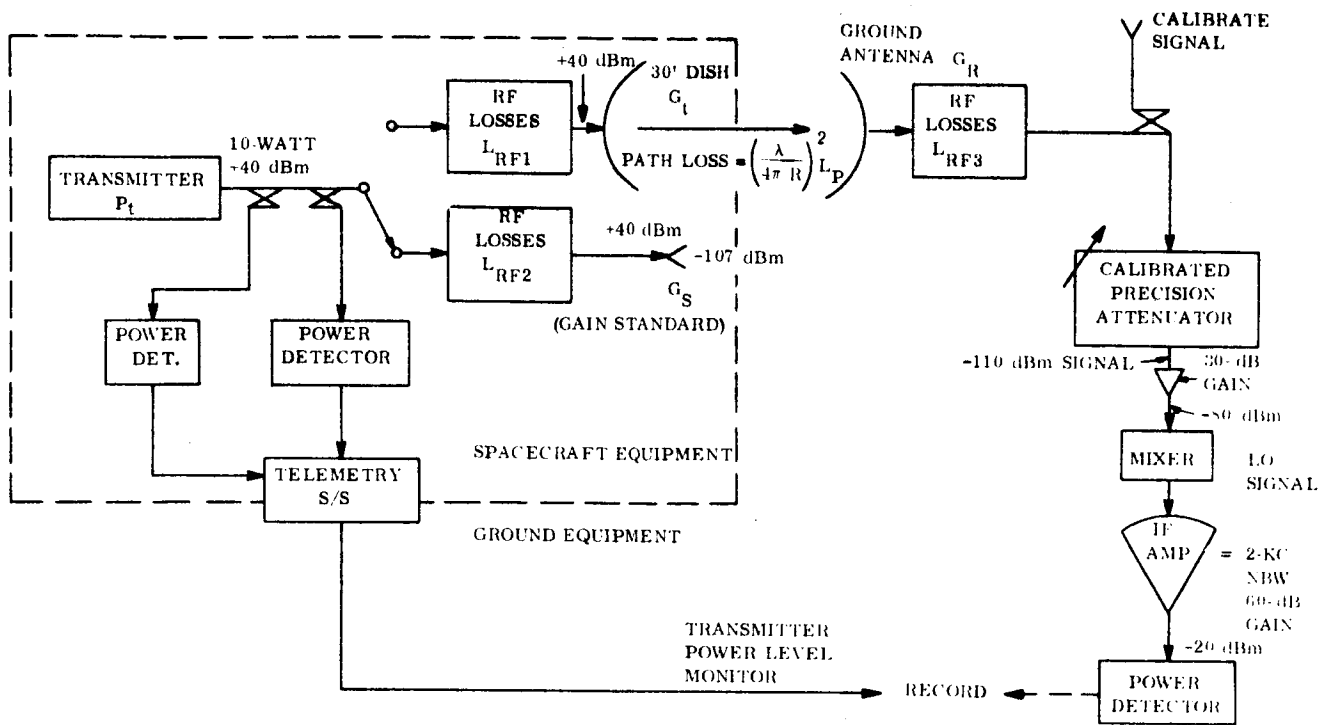


Figure 8.3-9. Thirty-Foot Antenna Gain Measurement Test Set-up, ATS-4 Experiments

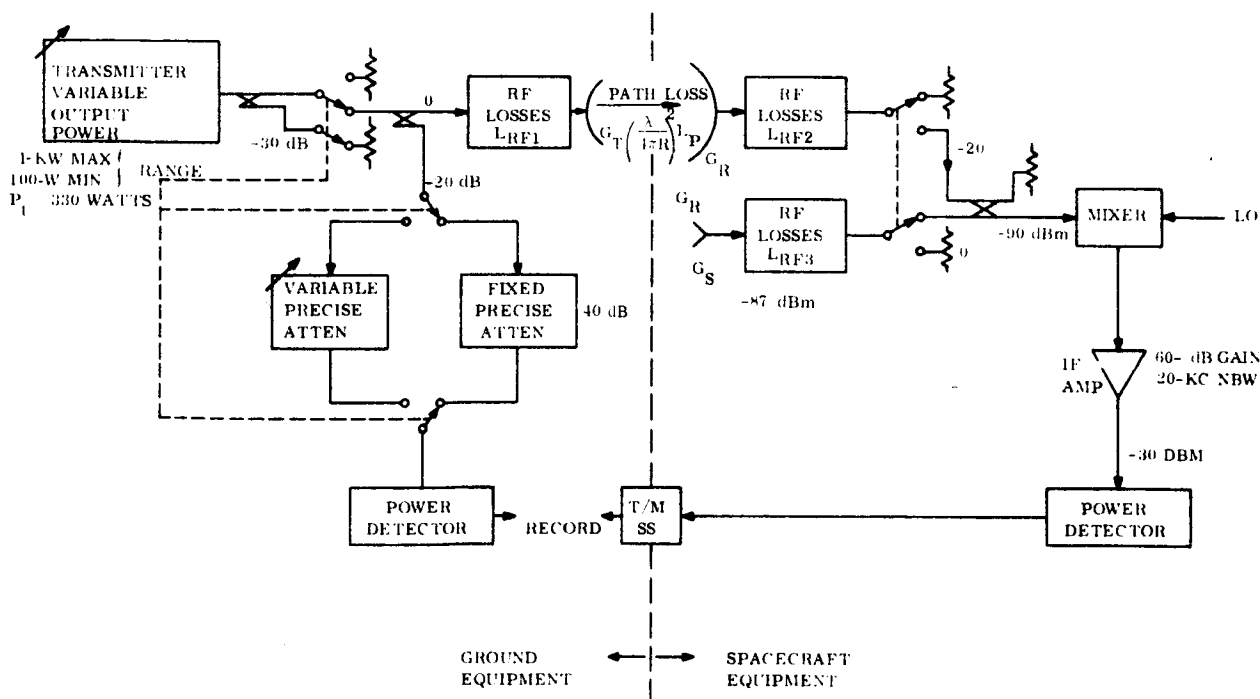


Figure 8.3-10. Alternate 30-Foot Antenna Gain Measurement Test Set-up, ATS-4 Experiments

level received can be determined, providing all the data necessary to accurately check the link loss calculation. Second, by varying the calibrate signal a known amount, the sensitivity of the detector circuit can be checked, to assure adequate sensitivity for the measurements.

The reception mode, using transmission from the ground as shown in Figure 8.3-10, involves varying the transmitted power in precisely controlled fashion, so that the signal level at the spacecraft on-board receiver does not change when the standard gain horn is substituted for the 30-foot paraboloid. Gain at the 30-foot paraboloid is then derived from the change in radiated power level required.

c. Background Information Required

Large antenna design specification.
Results of antenna ground testing.

d. Position in Operational Sequence

After deployment and preliminary evaluation.

e. Procedures

Satellite Transmission Mode

1. Command the satellite to point the large antenna at the ground station.
2. Command the 30-foot antenna into a configuration for X-band gain checks, transmit mode (see Figure 8.3-9) and turn on the spacecraft X-band transmitters. Set the transmitter for a frequency of 7300 MHz.
3. Calibrate the ground receiver equipment to assure that adequate detector sensitivity is available at the designed operating level.
4. Manually dither the 30-foot antenna pointing to find maximum received signal. By recording received signal level and spacecraft angular position (from OC sensor or interferometer) the position of this maximum can be located to better than 0.1 degree.
5. Set the precision variable attenuator for a suitable reading at the receiver detector output. Record several minutes of data (i. e., detector output, spacecraft power level, pitch and yaw angles, and time).

6. Switch the spacecraft transmitter to the X-band gain standard horn. Remove attenuation from the precision variable attenuator until the detector output is the same as the maximum values in Step 5.
7. Compute the 30-foot-antenna gain.

$$G_r = G_s + L_{att} + L_{RF_1} - L_{RF_2}$$

where

G_r is the gain at the 30-foot paraboloidal antenna.

G_s is the gain of the standard gain antenna.

L_{att} is the change in setting of the calibrated precision attenuator in Figure 8.3-9.

L_{RF_1} is the loss in the RF link between the on-board transmitter and the parabolic antenna.

L_{RF_2} is the loss in the RF link between the on-board transmitter and the standard gain antenna.

8. Use the calibrate signal to determine accurately the received power level. Using this and the measured spacecraft antenna gain and power level, check the path loss calculation.
9. Repeat Step 4 to assure that the antenna boresight has not shifted.
10. Repeat for all other transmission frequencies: 2300, 800, and 100 MHz.
11. Gain measurements will be repeated sufficiently often to evaluate long term (daily and longer) gain variation.

Satellite Reception Mode

1. Command the satellite to point the large antenna to the ground station.
2. Command the parabolic antenna into the configuration for X-band gain checks, receive mode (Figure 8.3-10) and turn on the spacecraft X-band receiver.
3. Turn on and calibrate the ground transmitter, and establish that adequate signal levels are available at the spacecraft receiver.

4. Manually dither the 30-foot antenna pointing to find maximum received signal.
5. Switch the spacecraft on-board receiver to the X-band standard gain horn, set the transmitter power level for a suitable reading of the on-board receiver output and record several minutes of data.
6. Switch the spacecraft on-board receiver to the 30-foot antenna. Turn off the transmitter, switch in the coupler and turn the transmitter back on. Adjust the transmitter power until the reading of the on-board receiver output is the same as with the X-band standard gain horn.
7. Compute the gain of the 30-foot antenna.
8. Repeat Step 4 to verify that the antenna boresight has not shifted.
9. Repeat for all other reception frequencies.

f. Data Produced

Antenna gain factor

Received power level

Transmitted power level

g. On-Board Equipment

Reference transmitters

Forward and reverse power monitors

T/M sensors

TT&C systems

Interferometer (or OC sensor) for attitude data

OC Subsystem.

h. Special Ground Facilities

Receiving configuration as shown in Figure 8.3-9

Transmitting configuration.

i. Time Required

One-half to 1 hour

8.3.5.2.3 Experiment A-6 and A-7 - Boresight and Pattern

a. Purpose

To measure the bias and long term variation of the large antenna rf axis with respect to the interferometer rf axis or attenuation control.

b. Technical Description

The boresight accuracy test described here assumes the following conditions:

1. The interferometer is on board, has been checked out, and performs to specification.
2. The antenna system has been gain tested at X-band and performs within expected design range.
3. All deployment and contour checks have been made and are within tolerance.

Since the angular accuracy with which the 30-foot antenna rf axes can be located is a function of the beam width, this test will be performed at X-band to provide the narrowest beamwidth, thus the greatest measurement accuracy.

The technique to be employed is to make two mutually perpendicular slices through the main lobe (within 2 dB points). The interferometer data will be used to locate these slices accurately with respect to the spacecraft axes. By correlating this angle data with the recorded signal level vs. time an accurate (± 0.05 degree RMS) estimate of rf boresight axis location can be made. A description of this approach along with a preliminary error analysis was described in Section 8.3.4.3.

c. Background Information Required

Large Antenna Design Specification

Results of Antenna ground testing

Results of interferometer accuracy tests.

d. Position in Operational Sequence

After deployment and contour evaluation

After interferometer evaluation.

e. Procedures

1. Set up equipment as shown in Figure 8.3-10. Using a known calibration reference signal calibrate the detector and recorder circuits.
2. Command the spacecraft attitude to point the large antenna rf axis at the ground station.
3. Manually dither the 30-foot antenna pointing to locate the approximate rf boresight.
4. Offset pitch axis by approximately one degree.
5. Command pitch axis back to the approximate boresight. As antenna main lobe approaches ground site, open OC loops to allow constant angular rates as pattern slice is taken. If care is taken, the pattern slice should come within 0.1 to 0.15 degree of a beam center slice.
6. Record angle data (from interferometer) and received signal amplitude versus time.
7. Repeat steps 4, 5, and 6 with a roll axis offset.
8. Reduce data with computer program to find antenna rf boresight with respect to the interferometer axis. If first slices were not within 0.15 degree of boresight repeat experiment.

f. Data Produced

Measured: Antenna main lobe patterns, transmitted and received power.

Computed: Antenna rf boresight.

g. On-Board Equipment

Large Antenna and Feed System	T/M Sensors
Reference Transmitter	TT&C System
Forward & Reverse Power Monitors	OC Subsystem
Interferometer Subsystem	

h. Special Ground Facilities

Equipment

Receiving and recording equipment as shown in Figure 8.3-11.

Software

Computer programming to process measured data to obtain boresight angles.

i. Time Required

One-half to 1 Hour

8.3.5.3 Basic Geometric Measurements

8.3.5.3.1 Experiment Formulation

The crucial geometric measurements for evaluation of the parabolic antenna are, verification of deployment, measurement of significant static deformations, verification that thermal deformation is below the allowable threshold, and verification that no mechanical vibrations occur which significantly affect performance.

8.3.5.3.2 Experiment A-1 - Deployment Monitoring and Verification

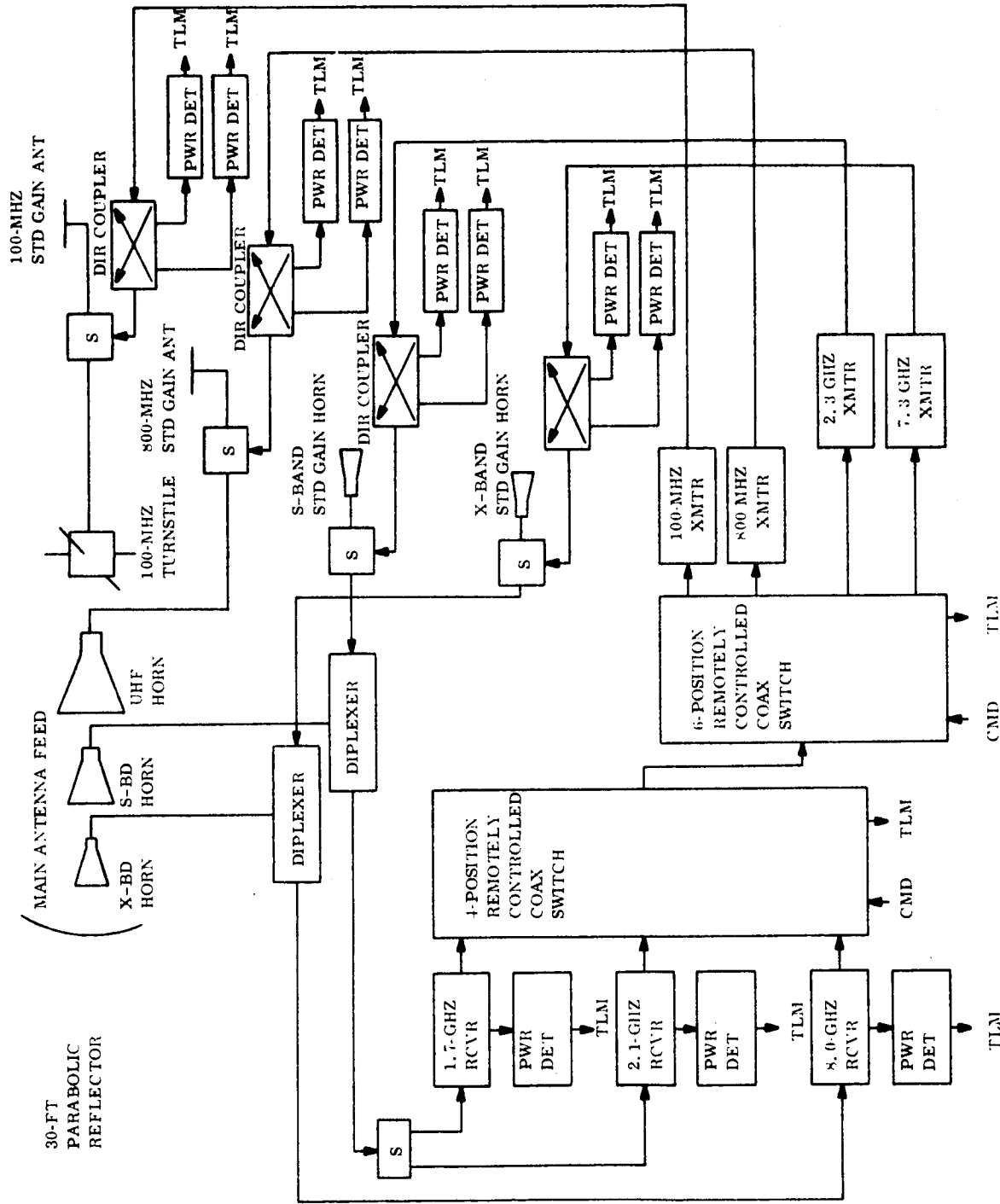
a. Purpose

To verify that deployment has occurred without major malfunction.

b. Technical Description

Deployment can be assumed to have occurred when all members of the deployment mechanism and all movable parts of the antenna have reached and remained in their final positions. It will be defined as successful if no major deformation in any member is present, and if stresses, etc. go through a normal sequence as the deployment process occurs.

Deployment is to some extent unique. It cannot be scheduled as an experiment, but must be monitored as it occurs, and the timing may be forced by overall system considerations rather than being chosen for its experimental convenience. It may or may not be possible to make more than one attempt at deployment in the event of a failure on a first attempt.



NOTE: S = REMOTELY CONTROLLED COAX SWITCHES

Figure 8.3-11. Large Parabolic Antenna Experiment

The final achievement of deployment will be monitored by microswitches or their functional equivalents to verify that relative positions of structural members is correct, and by strain gauges that verify that no abnormal stresses exist. Normality of deployment during the process will be indicated by measurements of stress versus time in the key structural members of the antenna, and by the fact that no abnormal mechanical vibrations occur as a result of the deployment impulses.

c. Background Information Required

Extensive evaluation of characteristics of instrumentation -- strain gauges, microswitches, voltage and current measuring devices, and temperature indicators for both normal and abnormal deployment possibilities.

d. Position in Operational Sequence

Deployment

e. Procedures

Verify that instrumentation is operating and that temperatures are recorded. Monitor microswitches, strain gauges, temperature readings, and voltage and current reading devices during deployment.

Analyze results to determine that proper deployment has occurred.

f. Data Produced

Verification that deployment has occurred, or any gross malfunction.

Monitoring of stresses, and accelerometers during deployment to verify that sequence was not grossly wrong.

g. On-Board Equipment

Strain gauges

TT&C System

Microswitches

Accelerometers

Voltage and current measuring devices

h. Special Ground Facilities

Software - Subroutine for reconstructing structural configuration from microswitch readings.

Subroutine for analyzing strain gauge readings as functions of time and reconstructing dynamic structural behavior from these readings.

Personnel - Experts in the spacecraft and antenna structure to verify deployment.

i. Time Required

Two minutes

8.3.5.3.3 Experiment A-2 - Thermal Contours

Monitoring of the temperature contours will be continuous, and the temperature data will be a part of the inputs of boresight measurements, antenna gain and pattern measurements and other crucial measurement experiments.

In addition, experiments will be performed to verify the behavior of the temperature contours as a function of the solar aspect. These will take the form of deliberately rotating the satellite to control within the limits of feasibility the direction and rate of change of the sun angle. They will include:

1. Holding the sun at selected definite angles with respect to the antenna (possibly for a matter of two hours or so). This will be repeated for a number of selected solar aspect angles.
2. Holding the sun angle at a definite rate of change.
3. Rotating the satellite to approximate a uniform illumination.

8.3.5.3.4 Experiment A-22 and A-23: Static and Thermal Deformations

These will be measured by configurations of temperature-compensated strain gauges. These gauges will verify that the static deformations from deployment are below the allowable threshold which would seriously degrade the electrical performance of the antenna, and that thermally induced deformations are not significantly greater than predicted.

8.3.5.3.5 Experiments A-24, A-26 and A-27 - Dynamic Analysis

The dynamic behavior of the antenna structure will be monitored by accelerometers which will verify that no mechanical vibrations exist of such amplitude as to degrade the performance of the antenna or the Orientation Control system.

8.3.5.4 Supporting Electrical Measurements

8.3.5.4.1 Nature of Measurements

A set of measurements is desirable to verify the quality of communications required of the system, i. e., that the system be able to transmit and receive in specified frequency ranges over a 10% bandwidth. These include in particular two classes of experiments; communications quality measurements and tuning range performance measurements.

8.3.5.4.2 Experiments A-8 through A-22 - Communications Quality Measurements

a. Purpose

To verify that the system can effectively transmit and receive at the frequencies specified and to measure the performance while so doing.

b. Technical Description

It is required that the capability of the parabolic antenna system to transmit and receive at the specified frequencies be established. As a strong corollary to this requirement, it is appropriate to verify the quality of such transmissions. In addition, properly selected signals, especially video signals, constitute one of the most sensitive diagnostic tools in determining whether the amplitude and phase behavior of the system, including the antenna/feed complex, is correct. By varying the bandwidths, power levels, and types of modulation as well as the constitution of the test signals, and by permitting the interconnections of on-board receivers and transmitters in the transmission links, it is possible to establish quite a good diagnosis of antenna system behavior.

The types of test signals used would include simple sine waves, audio and video test messages, PCM and special waveforms, all of varying information bandwidths. These signals would be transmitted via amplitude, frequency and phase modulation as appropriate.

c. Background Information Required

Antenna system design specifications and the results of ground performance tests. Results of approximate measurements of antenna gain.

d. Position in Operating Sequence

After initial checkout of parabolic antenna system and preliminary gain measurements.

e. Procedures

1. Command the Orientation Control system to point the antenna at the ground station.
2. Establish communications on one complete link from ground to satellite to ground, via the parabolic antenna system, and transmit a simple test message, for 2 minutes.
3. Methodically substitute on-board receivers and transmitters until all usable combinations have been exercised, repeating the same test message each time.
4. Repeat Steps 2 and 3 for each test message in the set.

f. Data Produced

Transmission quality of all possible transmit-receive links in the parabolic antenna system.

g. On-Board Equipment

Parabolic antenna system

Orientation Control system

TT&C system

h. Special Ground Facilities

Transmitting and receiving equipment for all frequencies and bandwidths

Test message transmission devices

Signal analysis software

i. Time Required

Four hours

8.3.5.4.3 Experiment A-29 - Tuning Range Performance Measurements

a. Purpose

To verify the performance of the antenna system across the required 10 percent bandwidths.

b. Technical Description

This experiment is essentially a measurement of communications quality across the required 10 percent bandwidths; of necessity with particular attention to performance near the edges of the bands. It consists of repeating selected portions of the performance measurements near the band edges, in sufficient detail to verify that significant degradation does not begin within the prescribed regions. The performance measurements will include gain, boresight, and communications quality measurements.

c. Background Information Required

Results of gain, boresight, and communications quality measurements near the band centers.

d. Position in Operating Sequence

After band-center performance of the antenna system has been established.

e. Procedures

This experiment will not be performed as a separate measurement entity. Rather, after each major measurement of gain, boresight and communications quality, the frequencies

will be shifted in steps to the edges of the bands and the frequencies at which significant degradations begin will be monitored. The degradations as functions of frequency will be measured, out to the point at which performance becomes unacceptable.

f. Data Produced

Parabolic antenna system operation as a function of frequency near the edges of the 10 percent frequency bands.

g. On-Board Equipment

Parabolic antenna system
Orientation Control system
TT&C system

h. Special Ground Facilities

All facilities required for gain, boresight, and communications performance experiments.

i. Time Required

Slight additions to experiment times of each experiment involved.

8.3.6 DERIVATION OF EQUIPMENT REQUIREMENTS

8.3.6.1 Electrical Measurements Experiments Equipment

The parabolic antenna/feed combination is considered as a separate major system, and its electrical characteristics are discussed in detail in Sections 5 and 6. The experiment equipment discussed in this section will be that necessary to the parabolic antenna measurements, e. g., ground-satellite transmission links, on-board interconnections and on-board measurements equipment.

The prime requirement of the transmission links will be to provide for the flow of signals between the ATS-4 spacecraft and other (mostly ground) stations, with appropriate bandwidths, data rates and signal-to-noise (S/N) ratios to make the necessary measurements.

For most of the experiment configurations, a major consideration will be to obtain a large enough signal-to-noise ratio and bandwidth at minimum cost in on-board weight and power.

In general, once it has been established that certain values of signal-to-noise ratio and bandwidth will be required for a given measurement sequence, certain key parameters must be manipulated to obtain them at minimum cost. Usually these parameters will be: antenna gains, frequencies, transmitter powers, link sensitivities (commonly in terms of noise figures or noise temperatures), modulation techniques, and rf bandwidths. In the ATS-4 experiments, however, a number of these parameters will be constrained, e.g., the gain of the standard gain antennas and the large parabolic antenna, and the frequencies required. The results required must then be achieved by appropriate selections of the remaining parameters.

The measurements required for evaluation of the parabolic antenna will include, as discussed in previous sections:

Gain	Antenna Patterns
Boresight	Communications analyses

These measurements must cover the frequencies listed in the work statement, i.e.,

<u>Transmission</u> (MHz)	<u>Reception</u> (MHz)
100	1700
800	2100
2300	8000
7300	

The link must be so constructed as to provide signals appropriate for the measurements listed above.

The key signal parameters from the link viewpoint will be bandwidth and signal-to-noise ratio. These describe the "payload" of the link and other parameters being equal, the power required will vary directly with each of them.

Some of the measurements, such as gain and boresight, will require quite high signal-to-noise ratios. Bandwidths required will vary widely; from very low (about 1 kHz assumed) values in measuring to perhaps 30 MHz for communications measurements.

A tentative list of bandwidth and S/N ratio requirements for the limiting measurements is shown in Table 8.3-2.

Table 8.3-2. Required Signal Characteristics - Parabolic Antenna Measurements

Measurement	Signal-to-Noise (dB)	Bandwidth (MHz)	Comments
Gain, boresight and Pattern	40	0.001	BW limited by equipment stabilization
Video, SSB, AM	32	4 - 6	Commercial standards
Video, wideboard FM	16	30	Modulation index 2.5 - 3.0

The highest signal-to-noise ratio, for precision measurements, will be about 40 dB; however, the bandwidth for these measurements can be very small. The larger bandwidths, for video transmitted using wideband FM, will be about 30 MHz, but the signal-to-noise ratio can be as low as 16 dB. (Actually, 12 dB could be used, but some margin is desirable.)

The characteristics of the on-board antenna will, of course, be fixed; the aperture will be 30 feet, and the gain at all frequencies up to and including 10 GHz will be that dictated by the aperture, less system efficiency. These values are readily available from tables, or calculated from standard formulas. They are reproduced for convenience in Table 8.3-3.

The ground antenna can be assumed to have a gain of at least 17 dB at the lowest frequency and to have at least a 30-foot aperture at the higher frequencies. Larger apertures can be obtained if required; as a rule of thumb, gains of 46 to 60 dB can be obtained without undue difficulty at any frequency in the 1.5 GHz to 10 GHz range. However, small mobile terminals may be more limited.

Table 8.3-3. Gains and Beamwidths - Perfect 30-Foot Parabolic Antenna

Frequency (MHz)	Gain (db)	Beamwidth (deg)
100	17	23
800	35	2.85
1700	41.6	1.35
2100	43.3	1.1
2300	44.2	1.0
7300	54.2	0.31
8000	55	0.29
10,000	57	0.23

The receivers in the spacecraft will have noise figures somewhere between 4.5 and 8.5 dB. In the Operational Control Center (OCC) or any other large ground station considerably higher performance levels can be obtained. ATS stations have system noise temperatures of the order of 60⁰K at frequencies up to 6 GHz. Small mobile terminals will have somewhat lower performance capability, but should be able to maintain noise figures of 4 to 7 dB.

The 100 MHz frequency will be a special case. Background noise levels at this frequency can be quite high (equivalent noise temperatures may be as great as 4000⁰K). This is shown in the Link Calculations, Table 8.3-4.

Transmitters in large ground stations can be very large if desired. In the ATS installations, radiated powers of about a kilowatt are available at some frequencies. In small mobile terminals, powers available will be somewhat lower, as will also be the case for aircraft and spacecraft.

Modulations required will depend upon the tests being made. For transmitting and receiving tests, a number of different modulations will probably be used; AM, PM and FM, at various bandwidths, special test waveforms and pulse trains. Various messages, audio, video, digital, etc., may be transmitted by any of the above modulation techniques which are appropriate.

The basic system performance is shown in Tables 8.3-4, 8.3-5 and 8.3-6. The Tables illustrate operation with a highly equipped ground station, so the on-board and ground transmission powers required will be small. They also ignore the degradations in on-board antenna gain caused by aperture blockage. These are discussed in Sections 5 and 6. From Tables 8.3-4 through 8.3-6 it is possible by scaling to obtain some idea of the requirements of the limiting measurements listed in Table 8.3-2.

From Table 8.3-5 it can be seen that gain measurement using the gain standard antennas require by far the most transmitter power on the spacecraft. This is a result of requiring a good signal-to-noise ratio ($\approx +40$ dB) for measurement accuracy while using the low gain standard antenna. From these calculations it appears that if a transmitter is provided which will permit accurate gain measurements there is more than enough power for any necessary wide band communication test using the large antenna.

For video SSB AM tests, the bandwidths are increased by approximately $(4 \times 10^3 = 36$ dB). However, the signal-to-noise ratio can be permitted to decrease by $(41 - 32 = 9)$ dB, leaving a net increase of 27 dB. For the two higher frequencies (2.3 GHz and 7.3 GHz) the resulting power requirements are manageable. For 800 MHz, the power requirements will be difficult (8 watts without margin and 32 watts with a reasonable margin) for 100 MHz, power requirements will be prohibitive. If the video measurements are required at these frequencies, it will be necessary to use special ground equipment. For example, an additional 10 dB on the ground antenna-receiver system would place the 800 MHz region within easy reach (3.2 watts radiated, with margin).

The video measurements with wideband FM will require an increase in rf bandwidth of about $(4 \times 10^4 = 46$ dB) but the signal-to-noise ratio can be permitted to decrease by $(41 - 16 = 25$ dB) leaving a net increase of 21 dB. In this measurement, the powers at 2.3 and 7.3 GHz will be easily manageable. That at 800 MHz will also be comparatively modest - a nominal 3 dBw, or 2 watts without margin and about 9 dBw (8 watts) with 6 dB margin.

Table 8.3-4. System Performance Parabolic Antenna Transmission Measurements

	<u>100 MHz</u>	<u>0.8 GHz</u>	<u>2.3 GHz</u>	<u>7.3 GHz</u>
P out	-8 dBw (160 mw)	-18 dBw (16 mw)	-28 dBw (1.6 mw)	-38 dBw (.16 mw)
Transmitter Antenna Gain (dB)	+ 17	+35	+45	+55
ERP (dBw)	+ 9	+17	+17	+17
Pattern Factor (dB)	- 3	- 1	- 1	- 1
Net ERP (dBw)	+ 6	+16	+16	+16
Path Loss (dB)	164	181	190	200
Power Density at Receiving Antenna (dBw)	-158	-165	-174	-184
Receiving Antenna Gain (dB)	+ 20	+37	+46	+56
Power At Receiver Terminal (dBw)	-138	-128	-128	-128
Line Losses (dB)	1	1.5	2	4
Converter Input (dBw)	-139	-129.5	-130	-132
Receiver Noise Figure (dB)	3	3	3	3
Reference (dBw)	-142	-132.5	-133	-135
KTB (dBw)	-162	-174	-174	-174
C/N (dB)	+ 20	+41.5	+41	+39
Modulation Gain (dB)	0	0	0	0
S/N (dB)	20	41.5	41	39

8.3-45

Table 8.3-5. System Performance Gain Standard Antenna Transmission Measurement.

	<u>100 MHz</u>	<u>0.8 GHz</u>	<u>2.3 GHz</u>	<u>7.3 GHz</u>
P out (dBw)	+ 10	+10	+10	+10
Transmitter Antenna Gain (dB)	5	10	10	10
ERP (dBw)	15	20	20	20
Transmitter rf Loss (dB)	- 3	- 1	- 1	- 1
Net ERP (dBw)	12	19	19	+19
Path Loss (dB)	-164	-181	-190	-200
Power Density at Receiving Antenna (dBw)	-152	-162	-171	-181
Receiving Antenna Gain	+ 20	+37	46	56
Power at Receiving Terminal (dBw)	-132	-125	-125	-125
Line Losses (dB)	- 1	1.5	- 2	- 4
Converter Input (dBw)	-133	-126.5	-127	-129
Receiver Noise Figure (dB)	3	3	3	3
Reference (dB)	-136	-129.5	-130	-132
KTb (2KCBW) (dBw)	-162	-171	-171	-171
C/N (dB)	+ 26	41.5	+41	+39
Modulation Gain	0	0	0	0
S/N (dB)	+ 26	41.5	+41	+39

8.3-46-1

Table 8.3-6. System Performance Parabolic Antenna Receiving Measurements

	<u>1.7 GHz</u>	<u>2.1 GHz</u>	<u>8 GHz</u>
P out	-17 dBw (20 mw)	-19 dBw (12.6 mw)	-30 dBw (1mw)
Transmitter Antenna Gain (dB)	+42	+44	+55
ERP (dBw)	+25	+25	+25
Pattern Factor (dB)	- 1	- 1	- 1
Net ERP (dBw)	+24	+24	+24
Path Loss (dB)	187	189	200
Power Density at Receiving Antenna (dBw)	-163	-165	-176
Receiving Antenna Gain (dBw)	+42	+44	+55
Power at Receiving Terminal (dBw)	-121	-121	-121
Line Losses (dB)	4	4	4
Converter Input	-125	-125	-125
Receiver Noise Figure (dB)	10	10	10
Reference (dBw)	-135	-135	-135
KTB (dBw)	-176	-176	-176
C/N (dB)	+41	+39	+39
Modulation Gain	0	0	0
S/N (dB)	+41	39	39

A list of limiting requirements for the various transmitting measurements is shown in Table 8.3-7. These are the measurements for each frequency, requiring the highest power level recommended, and also those requiring the highest bandwidth. Thus for 2300 and 7300 MHz the limiting measurement with regard to power will be the video SSB AM, while at 100 MHz, it will be the high-speed data transmission. In each case, all other experiments recommended using the parabolic antenna will require less radiated power and/or bandwidth.

Going through an identical procedure for the receiving measurements the ground transmitters power requirements are shown in the lower half of Table 8.3-7. As shown, no serious difficulties are anticipated. Receiver noise figures on-board are assumed to be 10 dB, as shown in Table 8.3-6.

Maximum bandwidths are also shown in Table 8.3-7. These are instantaneous signal bandwidths. For measurement purposes, a 10 percent bandwidth capability will be required at each frequency; these are also listed in Table 8.3-7.

From the above analysis, it is now possible to abstract certain basic requirements for the on-board equipment for the parabolic antenna measurements. These are summarized in Table 8.3-8.

On the basis of the above calculations and the system power considerations, it was decided to standardize on 10 watts radiated power for all transmitters.

To monitor the signal performance of the receivers and transmitters and verify that effective communications have been achieved, it was considered necessary to transmit test signals from the ground, receive them in the satellite through one of the receivers, then retransmit to the ground by one of the transmitters. The received signal can then be quantitatively compared with the signal originally transmitted, to determine the behavior of the link. In order to facilitate isolation of possible deficiencies, i. e., whether a transmitter or receiver was less than adequate in operation, it was decided

Table 8.3-7. Limiting Power and Bandwidth Requirements Parabolic Antenna

Frequency (MHz)	Limiting Measurement (1) Power, (2) Bandwidth	Nominal Radiated Power Required (Watts)	Margin (dB)	Actual Radiated Power, Req. Watts (Nominal x Margin)	Greatest Bandwidth Required (MHz) Inst.	Greatest Bandwidth Required (MHz) Total*
100	(1) High-speed Data (15 Kbps) (2) High-speed Data (15 Kbps)	2.16	6	8.64	0.1	10
800	(1) Wideband FM Video (2) Wideband FM Video	2.0	6	8.0	30.0	80
2300	(1) SSB Video (2) Wideband FM Video	1.0	6	16.0	30.0	230
7300	(1) SSB Video	1.0	10	10.0	30.0	730
RECEIVER MEASUREMENTS**						
(Ground Equipment)						
1700	(1) SSB Video (2) Wideband FM Video	10.0	6.0	40.0	40.0	170
2100	(1) SSB Video (2) Wideband FM Video	6.0	6.0	24.0	40.0	210
8000	(1) SSB Video (2) Wideband FM Video	1.0	10.0	40.0	40.0	800
* By contractual requirement, a total rf bandwidth of 10 percent shall be available at every frequency.						
** Not including power levels for use with standard gain antenna.						

Table 8.3-8. On-Board Equipment Characteristics Parabolic Antenna Measurements

Frequency (MHz)	Radiated Power (Watts)	Inst. Meas. Bandwidth (MHz)	Tuning Range (MHz)
100	10.0	6	10
800	10.0	30	80
2300	10.0	30	230
7300	0	30	730
Noise Figure (dB)			
1700	10	30	170
2100	10	30	210
8000	10	30	800
RECEIVERS			

to provide for switching the output of each receiver to any of the transmitters. By successive permutations, the performances of the various electronic components can be fairly well isolated and compensated for, thus arriving at the performance of the antenna system.

8.3.6.1.1 Communication Subsystem

The communication subsystem required for the Large Parabolic Antenna Experiment is illustrated in Figure 8.3-11. It depicts the satellite-located equipment.

The subsystem employs three receivers and four transmitters capable of receiving and/or transmitting at the specified frequencies tunable over a 10 percent frequency range and at a minimum bandwidth of 6 to 30 MHz from VHF through X-band, respectively. Any one of the receivers may either operate by itself with its output telemetered to ground or may feed any one of the transmitters for transmission to ground (over a wider bandwidth). Any one of the transmitters may also operate separately or in combination with a receiver.

The connections between receivers and transmitters are accomplished by two multi-position, command-controlled coaxial switches. Each switch position will be telemetered for command verification.

In order to provide verification of a received signal each receiver will be associated with a power detector that will pick up a signal from one of the front-end stages of the receiver.

To measure forward and reflected power in the transmit channels, a directional coupler in combination with two power detectors will be placed in the transmission line between transmitter and antenna feed. Also in series with the directional couplers will be remotely controlled coaxial switches that will connect the transmitters either to the parabolic antenna feeds or to the standard gain antennas in order to measure antenna gain. One standard gain horn will handle L - or S-band frequencies and one will operate on X-band frequencies. A standard gain dipole will be utilized for 800 MHz, and one

of the solar panels will be excited as a standard gain antenna at 100 MHz. The power detectors will be utilized in the gain measurements for measuring power flow either to the large antenna or to the standard gain antennas. The power detector outputs will be telemetered to ground.

All switching functions required during the measurements will be initiated by command signals from ground. The TT&C subsystem operates independently of the communications subsystem for the large antenna experiment and is not shown in Figure 8.3-11. However, a transponder combination of the communication subsystem may be used as a back up for ranging information.

All significant functions in the subsystem components will be telemetered as diagnostic data for evaluation on the ground.

The objectives of receiver design are to obtain the best available noise figures and other performance parameters at the lowest weight and power cost. This indicates a tunnel diode amplifier (TDA) input stage, and solid-state components.

Since it is desired to be able to retransmit the signals receiver, it is necessary to provide for this; but also to provide a method of at least crudely verifying that the receiver is operating properly. It is also necessary, of course, to provide tuning across the 10-percent tuning range required.

It was decided for retransmission to convert down only to the intermediate frequency (IF). Demodulation on-board is used only to measure received signal levels to verify receiver operation.

Figure 8.3-12 illustrates in detail a typical receiver for L-, S-, or X-band. The received signal from the horn feed is pre-amplified in a TDA after it has passed a diode limiter to prevent diode burnout of the TDA. Since the TDA is a wideband amplifier that covers the whole 10 percent tuning range, a tunable YIG filter acts as a preselector filter that

is tuned by the tuning control unit. A preselected number of receive frequencies may be tuned by command. The signal is then down-converted to an intermediate frequency (IF) by a mixer-preamplifier associated with a voltage-tuned oscillator, which in turn is tuned by a tuning control unit that is actuated by commands. The coax isolator prevents spurious frequencies from entering the YIG filter. The IF signal is further amplified in the IF amplifier, whose output is either coupled out to the multiposition coax switch, to enter a transmitter, or applied to a signal demodulator. The demodulator consists of a limiter and discriminator-amplifier. The demodulated signal is then telemetered to ground.

The objectives in transmitter design are to obtain the required power outputs, tuning ranges, bandwidths and other parameters with the minimum weight and power requirements. Reliability will also be an important consideration. It is possible to provide the required performance at 100 and 800 MHz using all solid-state circuitry; but at the S-band and X-band frequencies, traveling wave tubes must be used. These tubes have excellent performance and reliability records.

The details of a typical transmitter are illustrated in Figure 8.3-13. The 100-MHz and 800-MHz transmitters will provide approximately 100-watt output; they will consist completely of solid-state circuits. Their circuitry and especially the packaging will deviate somewhat from the L-, S-, and X-band transmitters; however, their building blocks will essentially be identical with the exception of the power amplifier, containing a traveling wave tube (TWT) of approximately 10-watt output. The transmitter may operate in either of two modes. Either an IF signal from a receiver will be up-converted in frequency by a mixer and VTO, which is tuned by a remotely controlled tuning control, or a fixed frequency from a local oscillator will substitute for the IF signal. The signal from the up-converter will then be filtered by an electronically controlled YIG filter, similar to the one used in the receiver, and will then be preamplified after passing through a coupler, and amplified to its proper power level in a power amplifier. The output signal of the power amplifier will pass a bandpass filter and isolator before it feeds the large antenna for transmission to ground. Provision will be made to couple a second signal with a

Table 8.3-8. On-Board Equipment Characteristics Parabolic Antenna Measurements

Frequency (MHz)	Radiated Power (Watts)	Inst. Meas. Bandwidth (MHz)	Tuning Range (MHz)
100	10.0	6	10
800	10.0	30	80
2300	10.0	30	230
7300	0	30	730
Noise Figure (dB)			
RECEIVERS			
1700	10	30	170
2100	10	30	210
8000	10	30	800

to provide for switching the output of each receiver to any of the transmitters. By successive permutations, the performances of the various electronic components can be fairly well isolated and compensated for, thus arriving at the performance of the antenna system.

8.3.6.1.1 Communication Subsystem

The communication subsystem required for the Large Parabolic Antenna Experiment is illustrated in Figure 8.3-11. It depicts the satellite-located equipment.

The subsystem employs three receivers and four transmitters capable of receiving and/or transmitting at the specified frequencies tunable over a 10 percent frequency range and at a minimum bandwidth of 6 to 30 MHz from VHF through X-band, respectively. Any one of the receivers may either operate by itself with its output telemetered to ground or may feed any one of the transmitters for transmission to ground (over a wider bandwidth). Any one of the transmitters may also operate separately or in combination with a receiver.

The connections between receivers and transmitters are accomplished by two multi-position, command-controlled coaxial switches. Each switch position will be telemetered for command verification.

In order to provide verification of a received signal each receiver will be associated with a power detector that will pick up a signal from one of the front-end stages of the receiver.

To measure forward and reflected power in the transmit channels, a directional coupler in combination with two power detectors will be placed in the transmission line between transmitter and antenna feed. Also in series with the directional couplers will be remotely controlled coaxial switches that will connect the transmitters either to the parabolic antenna feeds or to the standard gain antennas in order to measure antenna gain. One standard gain horn will handle L - or S-band frequencies and one will operate on X-band frequencies. A standard gain dipole will be utilized for 800 MHz, and one

8.3.6.3 Summary of Required Equipment

The equipment required for the parabolic antenna experiment is shown in summary form in Table 8.3-9.

Table 8.3-9. Experiment Equipment Summary

Prime Experiment	Experiment Equipment	Weight (lb)	Power (Watts)
Parabolic Antenna	Instrumentation to measure geometric configuration and dynamic behavior. RF equipment for measurements Electronics - transmitters receivers, electronic switches, etc. - for measurements, std. gain antennas	86.6	80
Orientation Control System	Incorporated in orientation control system	NA	NA
Interferometer	Interferometer antennas and electronics. Instrumentation to measure geometric distortion. Instrumentation to monitor dynamic behavior	35	39.2
Phase-Steered Array Antenna	Antenna elements and electronics. Internal monitoring equipment for measuring	100	420

8.4 ORIENTATION CONTROL SYSTEM

8.4.1 GENERAL DISCUSSION

The purpose of the Orientation Control experiment is to verify that the Orientation Control system fulfills the requirements of the Work Statement; the relevant paragraph is reproduced below for reference:

The Orientation Control system shall be capable of directing the main beam of the parabolic antenna to any point on the visible earth's surface to an accuracy consistent with the antenna beamwidth for the frequencies of interest (when used at 10 GHz, the Orientation Control system must be capable of a pointing accuracy of 0.1 degree). The time required to change the direction of the main beam from a terminal on one horizon to a terminal on the opposite horizon and stabilize within the required accuracy (i. e., plus or minus 0.1 degree) for a worst case maneuver will be no longer than thirty minutes. At a rate of 10 milliradians per minute, it shall be capable of tracking in response to ground commands with a pointing error not exceeding 0.5 degrees. The Orientation Control system shall demonstrate the specified performance during station-keeping operations.

The conceptual design of this system was a major task in the present study and is described in detail in Section 5 and 6 of this report.

The most troublesome technical problem in the Orientation Control experiment is the validation of the pointing accuracy; i. e., the question of how one verifies that the Orientation Control system has pointed the parabolic antenna, or any other system on board the satellite, where it has been commanded to point within the required 0.1 degree error.

This problem is somewhat complicated by the fact that the Orientation Control system is required not only to point the antenna to within 0.1 degree, but also to maintain a pointing error within 0.5 degree during tracking; and this accuracy too must be verified.

The problem divides, then, into boresight or pointing accuracy, and angle measurement accuracy. Operationally one wishes to be able to command the OC system to point the antenna to a station and maintain the direction, and to repeat this as many times as desired; and also to command the satellite to swing along some required arc within the required accuracy.

The boresight problem is somewhat simplified by the fact that absolute alignment is not required, so long as the relative misalignments can be detected and measured. Thus, if it is determined that in order to point the parabolic antenna at a station, the OC system must be commanded to point to a slightly different angle because of misalignments between the OC sensors and the antenna; this difference can be subtracted and the desired pointing accuracy achieved.

The measurement of angles of the OC system can be calibrated by commanding the OC system to swing between two stations at known locations, and measuring the error.

The standards by which the boresight alignment and angular measurement accuracy can be calibrated are the parabolic antenna and the radio interferometer. The parabolic antenna would of course be ideal, since the major accuracy requirement is in pointing the main beam of the parabolic antenna. However, the beamwidth of the parabolic antenna is only barely small enough (about 0.3 degree) to permit verification of the required accuracy. This problem was discussed in Section 8.3.4.3 in connection with the parabolic antenna boresight problem. A lobe comparison (monopulse) installation on the parabolic antenna would provide more than ample measurement of pointing accuracy (of the order of 0.01 degree estimated) but the feasibility of the incorporation of monopulse within the constraints of the present satellite has not yet been established. Therefore, the pointing accuracy must be established by a combination of the OC sensors, the radio interferometer, and the parabolic antenna beam in the 7-8 GHz region.

The accuracy of the OC measurement of angle can be verified by commanding the OC system to swing between two stations of known locations as described above, and checking the error by the same comparisons with the radio interferometer and the parabolic antenna. In particular, the readings of the earth tracking sensors would be compared with those of the interferometer and the parabolic antenna beam. Once the reliability of these sensors has been established, they can be used if desired in monitoring the tracking experiments.

8.4.2 LISTING OF EXPERIMENTS

Table 8.4-1 lists individual experiments which should be performed in the evaluation of the OC system. It is intended to include nearly all measurements which might be useful. The measurements which are considered crucial are described in the following sections.

Table 8.4-1. Individual Experiments - Orientation Control System

0-1 Verification of Equipment Operation -4

To verify that the equipment associated with the Orientation Control (OC) system (wheels, mass-expulsion devices, etc.) is working.

0-2 Measurement of Internal Parameters -4

To verify that the internal system parameters (sensor outputs, processing transfer functions, and component characteristics) are within design tolerances.

0-3 Verification of Operational Characteristics -4

To verify that the operational characteristics of the OC system (station acquisition and pointing characteristics, slew capability, etc.) are qualitatively correct.

0-4 Pointing Performance -1

To measure to the highest attainable accuracy and completeness of the performance of the OC system in pointing the spacecraft and/or antenna toward a selected ground station.

0-5 Slew Capability -1

To measure to the highest attainable accuracy and completeness of the performance of the OC system in accomplishing the required slew maneuvers.

0-6 Tracking

0-6-1 Tracking -3

To measure the performance of the OC system while tracking at the maximum rate, using a low-orbit satellite.

0-6-2 Tracking -1

To measure the performance of the OC system in tracking with a simulated low-orbit satellite.

Table 8.4-1. Individual Experiments - Orientation Control System (Cont'd)

0-7 Use of Interferometer

0-7-1 Use of Interferometer -2

To measure the performance of the OC system while using the interferometer as a pointing sensor.

0-7-2 Use of Interferometer -2

To measure the performance of the OC system while using the interferometer as a tracking sensor.

0-8 Station Keeping

0-8-1 Station Keeping -1

To measure the pointing performance of the OC system during station keeping maneuvers, real and simulated.

0-8-2 Station Keeping -1

To measure the tracking performance of the OC system during station keeping maneuvers, real and simulated.

0-9 System Life Characteristics

0-9-1 System Life Characteristics -1

To measure the pointing performance of the OC system as a function of system life.

0-9-2 System Life Characteristics -1

To measure the slew performance of the OC system as a function of system life.

0-9-3 System Life Characteristics -1

To measure the tracking performance of the OC system as a function of system life.

0-9-4 System Life Characteristics -4

To measure the internal system parameters as a function of system life.

Table 8.4-1. Individual Experiments - Orientation Control System (Cont'd)

0-10 Thermal Cycle Characteristics

0-10-1 Thermal Cycle Characteristics -1

To measure the pointing performance of the OC system as a function of the thermal cycle.

0-10-2 Thermal Cycle Characteristics -1

To measure the slew performance of the OC system as a function of the thermal cycle.

0-10-3 Thermal Cycle Characteristics -1

To measure the tracking performance of the OC system as a function of the thermal cycle.

0-10-4 Thermal Cycle Characteristics -4

To measure the internal system parameters as a function of the thermal cycle.

8.4.3 BASIC EXPERIMENTS

8.4.3.1 General

The crucial measurements for evaluation of the OC system are, station pointing-accuracy, tracking accuracy, and slewing performance. The most important supporting experiment is the use of other sensors.

8.4.3.2 Pointing Performance

a. Purpose

To verify the capability of the OC system to point the antenna to a station within the required accuracy.

b. Technical Description

The capability of the OC system to point to a station within the required accuracy will be verified by the parabolic antenna and by the radio interferometer. The procedure would be, to command the point, then to command limited swings across the station to find the peak of the parabolic antenna beam, while at the same time taking readings with both the earth tracking sensors and the radio interferometer. By comparing the nulls of these instruments, the boresight alignments can be determined, while a comparison of their distributions will compare the angle measurement output characteristics of the three instruments. (These comparisons involve relatively elementary statistical processing.)

It will be necessary to repeat these measurements at intervals to determine the effects of thermal environment (especially the 24-hour cycle) upon boresight alignment. Because of the spacecraft structure, it may be anticipated that the relative alignment of the interferometer, and the earth tracking sensors will remain relatively constant with the thermal cycle, but the boresight of the antenna could vary somewhat due to thermal distortions.

The accuracy with which the OC system can maintain its direction will be measured by attempting to hold a given direction for a relatively prolonged period and measuring the error continuously with the interferometer, the earth tracking sensors, and the parabolic antenna. The distribution of error signals will directly verify the accuracy of the OC system in this mode.

c. Background Information Required

OC system ground performance test results.

Interferometer performance verification.

Verification that the parabolic antenna system is operating correctly, and an approximate verification of the main lobe pattern.

d. Position in Operational Sequence

After initial interferometer calibration.

e. Procedure

1. Command the satellite to point to the ground station.
2. Obtain initial interferometer and OC (earth tracker) sensor comparison.
3. Command small-angle sweeps across the station, monitoring relative parabolic antenna gain, to find boresight, continuing to monitor interferometer and earth tracker error signals.
4. Command pointing to parabolic antenna boresight and record all sensor outputs.
5. Repeat Step 4 for commanded pointing to OC system null and interferometer null.

f. Data Produced

Boresight alignments among the OC system, the interferometer, and the parabolic antenna.
Accuracy of the OC system in holding a direction.
Accuracy of the OC system in repeating a commanded direction.

g. On-Board Equipment

OC system
Parabolic antenna
Interferometer
TT&C system

h. Special Ground Facilities

1. Equipment

Interferometer beacon

2. Software

Programs for statistical processing of pointing sensor outputs.

i. Time Required

Two hours

8.4.3.3 Tracking Performance

a. Purpose

To verify the capability of the OC system to point the antenna in response to tracking commands at the required rates within the required accuracies (not greater than a 0.5-degree error at rates of 10 milliradians per minute).

b. Technical Description

The two parameters which must be measured in this experiment are the tracking rate and error, i. e., the error between commanded angle and actual angle as a function of time, within the constraint of the maximum required tracking rate (i. e., a lag would not be an error if due entirely to the fact that commanded maneuvers would have required tracking rates greater than 10 milliradians per minute).

The procedure would be to use one ground station as a reference, commanding the OC system to rotate the satellite across it. Angles and rates will be measured and compared with commanded angles and rates. Measurement techniques will include:

1. Angles - Direct measurements with the interferometer, the OC sensors and the parabolic antenna (relative antenna gain). Integration of the rate gyro readings, measurements of wheel speeds.
2. Rates - Direct measurements with the rate gyros. Derivation of rates from the interferometer and OC sensors, by finding the slopes of the curves of angle versus time.

c. Background Information Required

OC system results of ground tests and the results of pointing performance measurements. Interferometer performance verification.

Parabolic antenna main lobe pattern.

d. Position in Operational Sequence

After OC pointing accuracy initial measurements.

e. Procedures

1. Command the satellite to point to the ground station and verify proper operation of all systems.
2. Command rotation at maximum rate of 10 milliradians per minute about one axis to the horizon. Reverse direction and sweep to other horizon. Monitor angles and rates with OC sensors, interferometer, rate gyros, and momentum wheel rates.
3. Sweep from horizon to horizon across the station at maximum slew rate. Stop at the horizon and settle to within 0.1 degree.
4. Repeat Steps 2 and 3 with both axes.

f. Data Produced

Tracking performance in rate and angular error as monitored by all available sensors.
Slewing performance from horizon to horizon, and settling time.

g. On-Board Equipment

OC system

Parabolic antenna

Interferometer

TT&C system

h. Special Ground Facilities

Equipment

Interferometer beacon

Software

Programs for statistical processing of sensor outputs

i. Time Required

Three hours.

8.4.4 EQUIPMENT REQUIREMENTS

No equipment requirements other than telemetry signal processors are required on board the spacecraft for these experiments. The telemetered signals are discussed in Section 5.5.4.

8.5 INTERFEROMETER

8.5.1 GENERAL

The radio interferometer is a system intended to provide high-accuracy determination of spacecraft attitude with respect to a specific point on the ground by tracking a radio beacon at that point. The interferometer is the most accurate pointing sensor specified in the present ATS-4 configuration.

The design of the interferometer is described in some detail in GE TIS R66ELS-89, "ATS-4 Satellite Interferometer Design Study", August, 1966. A summary of the interferometer design is given in Section 5.6.5.

The purpose of the interferometer experiment is to verify that the interferometer fulfills the requirements of the Work Statement; the relevant paragraph is reproduced below for reference.

An interferometer system configuration, geometry and electrical/mechanical design will be selected so as to fully demonstrate the capabilities and limitations of an on-board interferometer, as a spacecraft attitude determination device.

The interferometer antenna system will operate in a frequency range consistent with the attainment of the maximum resolution and accuracy performance characteristics required for the spacecraft attitude control system.

The most troublesome technical problem in the interferometer experiment is in the validation of the interferometer angle measurement accuracy; i. e. , the question of how the basic accuracy of the interferometer is verified. This problem is especially difficult because the interferometer is the most accurate pointing sensor specified.

There are two general problems; the boresight measurement and the angle measurement accuracy.

The boresight of the interferometer is of primary importance only in relation to other systems, i. e. , the OC system and the parabolic antenna. The major problem is to verify that any

interferometer null shifts with time are small by comparison with OC system errors and other measurement accuracy requirements. This is done by comparison of boresight alignments among the interferometer, the OC system, and the parabolic antenna.

The angle measurement accuracy must be confirmed directly by measurement of the angles subtended by a number of ground stations whose locations are accurately known. These can consist of the two ATS stations at Rosman and Mojave, and placing beacons at a number of other stations, with locations ranging from about 5 miles from the reference station to about 250 miles. This would establish the accuracy of the interferometer in making off-axis angle measurements.

8.5.2 LISTING OF EXPERIMENTS

The following Table 8.5-1 is a tabulation of individual experiments which can be performed in the evaluation of the interferometer system. The measurements which are considered crucial are described in the following sections.

Table 8.5-1. Individual Experiments-Interferometer

I-1 Verification of Operation - 4

To verify that the interferometer is working.

I-2 Internal Parameter Measurements - 4

To verify that the internal system parameters are within design tolerances, e. g. , gain, receiver noise figures, and frequency stability.

I-3 Verification of Operational Characteristics - 4

To verify that the interferometer qualitatively responds to errors and performs its designed functions.

I-4 Angle Error Measurement - Medium Accuracy - 4

To verify that the interferometer angle measurement is accurate within the limits of the orientation control system.

Table 8.5-1. Individual Experiments - Interferometer (Cont'd)

I-5 Angle Error Measurement - High Accuracy - 1

To determine with maximum precision the angle measurement accuracy of the interferometer.

I-6 Field of View Verification - 1

To measure the performance of the interferometer in working with stations of considerable angular displacements.

I-7 Small Angle Signal Characteristics - 1

To measure the output signal characteristics of the interferometer when nominally pointed at a beacon.

I-8 Angle Difference Measurement - 1

To compare the interferometer-measured angle between two stations with the known angle, as a verification of accuracy.

I-9 Low Signal-to-Noise Ratio Performance Measurement - 3

To measure the interferometer performance as a function of signal-to-noise ratio.

I-10 Atmospheric Propagation Monitoring - 3

To measure the effects of atmospheric propagation characteristics upon interferometer performance.

I-11 Spacecraft Pointing - 2

To measure the performance of the interferometer in a closed-loop with Orientation Control system, the interferometer being used in place of the earth sensor.

I-12 Antenna Pointing - 2

To measure the performance of the interferometer in pointing and holding the parabolic and phased array antenna.

I-13 System Life Verification - 1

To measure the degradation of performance, if any, with time.

Table 8.5-1. Individual Experiments - Interferometer (Cont'd)

I-14 Yaw Axis Stabilization - 3

To establish the feasibility of using the interferometer for this purpose, and measure the performance.

I-15 Tracking - 3

To verify the feasibility and measure the performance of the interferometer in tracking mobile stations.

I-16 Position Location - 3

To investigate the feasibility of interferometer navigation schemes.

I-17 Thermal Cycle Monitoring - 1

To measure the effects of the thermal environment upon interferometer performance.

I-18 Station Keeping Effects - 1

To measure the effects of station keeping impulses upon interferometer performance.

I-19 Small Terminal Operation - 3

To measure the performance of the interferometer in working with small mobile terminals.

8.5.3 BASIC EXPERIMENTS

8.5.3.1 General

The crucial measurements for evaluation of the interferometer system are pointing bore-sight accuracy and repeatability, angle measurement accuracy, field of view, and target acquisition performance. The most important supporting experiment is the attitude control experiment, in which the interferometer functions as the pointing sensor in the OC loop.

8.5.3.2 Experiment I-1 - Verification of Operation

a. Purpose

To verify that the interferometer is working.

b. Technical Description

Before measurements of interferometer performance can begin, it will be necessary to verify that the interferometer is working properly. This experiment is designed to be the first step in this verification. In this experiment, the interferometer will be turned on, its internal voltages and currents will be checked and the interferometer will be "exercised." The objective will be to verify that the interferometer does qualitatively what it is supposed to do.

The present experiment is described on the assumption that the initial exercise will be successful, i. e., that the interferometer will prove to be in operating condition. In case of significant malfunction, the experiment will be completed if possible, and the data subjected to analysis in an attempt at a diagnosis.

c. Background Information Required

Interferometer design and performance specifications.

Results of interferometer preflight testing.

d. Position in Operational Sequence

After deployment evaluation.

e. Procedures

1. Verify power is available.
2. Point interferometer toward OCC, and command interferometer on.
3. Check T/M monitors (see Table 8.5-2) to see that all supply voltages are within predetermined limits.

Table 8.5-2. Interferometer Telemetry Monitoring Signals

Measurement	Signal Description	Number of Measurement Points	
AGC Voltage	0 to 10V, 10 Hz Bandwidth	1 to 8	
Phase Detector Output	2V, 1 KHz Bandwidth	1 output	
Lock Detector Output	2V, 10 Hz Bandwidth	1 output	
VCO Control Voltage	10V, 10 Hz Bandwidth	1 output	
Input Signal Level	2V, 10 Hz Bandwidth	8	After first mixer? Before Pilot Tone Reject?
Pilot Tone Level	2V, 10 Hz Bandwidth	1	
1st IF Output Level	2V, 10 Hz Bandwidth	8	Measure 1st IF Gain
2nd IF Output Level	2V, 10 Hz Bandwidth	8	Measure 2nd IF Gain
Analog Error Signals	2V, 100 Hz Bandwidth	2 (to 4)	
Power Supply Monitors	28V, 1 Hz Bandwidth	6	
Temperature Monitors	2V, 1 Hz Bandwidth	8	
Digital Counter Readout	8 bit parallel binary number	2 to 4	(data rate 20Kbps), 200 bps with on board data smoothing
1st and 2nd LO Levels	2V, 10 Hz Bandwidth	2	

4. Activate ground transmitter. Check for proper acquisition of interferometer phase lock loop via T/M monitors.
5. Check interferometer output signals (digital data).
6. Calibrate interferometer and check accuracy of angle read outs. (Should be accurate to within OC system pointing accuracy; ± 0.1 degree)

f. Data Produced

Internal voltages, currents and temperatures

Receiver outputs

Angle Readouts

These data, if in the normal range, cumulatively demonstrate that the interferometer is operating and indicate that there is no gross malfunction.

g. On-Board Equipment

Interferometer

Telemetry Sensors

Support from TT&C and OC Systems

h. Special Ground Facilities

Equipment

Interferometer beacon

Software

Processing subroutine

i. Time Required

8 hours

8.5.3.3 Experiments I-2 and I-3 - Internal Parameter Measurement

a. Purpose

To measure the significant internal characteristics of the interferometer.

b. Technical Description

Once the interferometer has been demonstrated to be working, the next logical step is to verify that it is operating correctly. This can be accomplished by determining that its internal response to signals is correct, then by determining that its angle measurement outputs are correct.

The measurement of internal parameters is necessary because, since the interferometer is to a certain extent self-compensating, significant deviations in for example, antenna gain, could not be detected by merely monitoring the interferometer output signals. However, such deviations would be important in indicating the ability of the instrument to survive launch environments and hence the probability of failure in future operational missions.

c. Background Information Required

Interferometer design and performance specifications.

Verification that the interferometer is operating.

Results of interferometer pre-flight testing.

d. Position in Operational Sequence

After verification that the interferometer is operating.

After verification that the OC System is qualitatively correct.

e. Procedures

Activate the interferometer link and point toward the OCC.

Make gain measurements as outlined below:

1. Calibrate ground transmitted signal.
2. Lock interferometer receiver.
3. Compute receiver input signal power. Using data from interferometer final testing, determine AGC voltage corresponding to computed input signal power.

4. Compare computed and monitored AGC voltages. Compare computed and monitored input signal powers.
5. Repeat for several signal levels.
6. Determine difference between measured and computed system gain. See if this is within measurement tolerances (± 1.5 to 2.0 db).

Pattern Measurement - Rotate the spacecraft slowly about the pitch and yaw axes (one at a time), over the entire field of view. Record the signal level in all eight receiver channels (normal T/M monitored functions) and the fine and coarse error signals in both channels. This data will provide the following information:

- a. Pattern checks on all eight antennas.
- b. Linearity checks on the fine and coarse error signals over the field of view.
- c. By comparing the number of fine ambiguities in one cycle of the coarse system, the relative antenna spacing may be checked.

Doppler Checks - Offset the ground transmitter frequency in increments providing at least 10 frequency steps over the doppler range. At each of these frequencies do the following:

- a. By repeated trials determine the average lock time at each frequency.
- b. Record the phase and lock detector outputs, and the VCO input voltage for each acquisition. Compare this data with calculated Phase Lock Loop response curves to determine Phase Lock Loop performance.

Threshold Checks - Starting at maximum signal level (on frequency) reduce the transmitter power in increments until the Phase Lock Loop shows unlock approximately 50 percent of the time. Using data from fine counters, the phase detector and lock detector outputs, compare the threshold performance with system test data from interferometer acceptance tests.

f. Data Produced

Antenna gains

Antenna patterns

Error signal linearity

Receiver acquisition, threshold performance, and Doppler capability.

g. On-board Equipment

Interferometer

Signal monitor and conditioner circuits

T/M and command links

h. Special Ground Facilities

Equipment

Interferometer beacon (with Doppler offset capability)

Support from TT&C and display

Software

Processing subroutine

Personnel

Interferometer engineers (data analysis)

i. Time Required

Three hours

8.5.3.4 Experiment I-4 - Angle Error Measurement - Medium Accuracy

a. Purpose

To verify that the interferometer angle measurement is accurate within the limits of the orientation control system.

b. Technical Description

This will be a preliminary angular accuracy determination, intended to verify that the accuracy and precision of the interferometer are at least as good as that of the OC System. This will be accomplished by comparing in detail the interferometer output signals with those of the attitude control sensors, for at least two ground station locations. Long data runs will be recorded to provide both short term accuracy comparison and long term variations. A run of at least 24 hours on one station is planned without recalibration of the interferometer subsystem. This will provide a check on long term thermal cyclic effects.

c. Background Information Required

Verification that the interferometer internal operation is correct.

Results from interferometer preflight testing.

Results from OC subsystem preflight testing.

d. Position in Operating Sequence

OC subsystem operation tests successfully completed.

e. Procedures

1. Activate interferometer and point toward Ground Station. Use strong signal level.
2. Calibrate interferometer subsystem.
3. Record interferometer tracking data, and OC sensor error signals for a period of 24 hours. Record Power Supply voltages, and temperature. Continuous data will not be taken over this interval but a suitable sampling time and frequency will be determined.
4. Compute and plot the average and RMS value of the above data sets. Compare these values between the interferometer and OC sensor data to establish any long term or cyclic errors between the two systems.
5. After 24 hours, recalibrate the interferometer and record the change in calibration.
6. Repeat (for shorter time - 8 hours) on second station offset in angle by several degrees from the first.

f. Data Produced

Long and short term variations between the OC sensor and the interferometer subsystems.

g. On-Board Equipment

Interferometer and OC subsystems

Regular T/M and command equipment

h. Special Ground Facilities

Software computer equipment and data analysis subroutines.

i. Time Required

Forty-eight hours

8.5.3.5 Experiment I-5 - Angle Error Measurement - High Accuracy

a. Purpose

To determine the accuracy of the interferometer with the most precise measurement available.

b. Technical Description

The accuracy of the interferometer, as discussed before in this section, is composed of alignment accuracy and angle measurement accuracy, i. e. , the accuracy with which angles off boresight are measured.

The absolute geometric boresight accuracy is the accuracy with which it can be confirmed that a signal whose direction angles are read as zero, really comes from a direction orthogonally respective to the lines connecting the two antennas of each pair. This parameter is carefully measured on the ground before launch, but cannot be directly verified in space. The related quantities which can be measured are the relative boresight alignments of the interferometer and the other precision pointing sensors (earth trackers and the parabolic antenna X-band electrical axes) the variation of these alignments with time, and isolation of

any interferometer errors to actual geometric distortion of the rf section. The latter procedure makes it highly unlikely that any significant interferometer absolute boresight errors will occur, because significant thermal deformations of a type to affect the boresight are unlikely.

The angle measurement accuracy will be obtained in I-8, repeated as appropriate.

c. Background Information Required

Verification that interferometer measurements are roughly correct.

Verification that operations of the OC and parabolic systems are roughly correct.

d. Position in Operating Sequence

After rough evaluation of interferometer, OC system and parabolic antenna system.

e. Procedures

1. Activate interferometer, and point toward ground station. Use maximum feasible signal levels.
2. Calibrate interferometer system.
3. Activate parabolic antenna 7300 MHz transmitter.
4. Dither antenna as in boresight measurements to locate approximate center of antenna beam. Repeat at intervals over 48 hours.
5. In intervals between dither measurement, point to ground station.
6. Record interferometer tracking data, parabolic antenna relative gain, OC pointing and earth sensor data, and relevant diagnostic data.
7. Re-calibrate the interferometer at intervals not greater than 24 hours.
8. Repeat using two other ground stations.
9. Repeat I-8 is required to obtain angle measurements accuracy.

f. Data Produced

Precise long and short term variations in axes alignments between the interferometer, the OC sensors and the large parabolic antenna.

Absolute boresight alignment of the interferometer up to the antenna waveguide sections.

Absolute calibration of interferometer angle measurement accuracy.

g. On-Board Equipment

Interferometer	Parabolic antenna system
OC system	TT&C system

h. Special Ground Facilities

Software
Data analysis subroutines

i. Time Required

One hundred and forty-four hours

8.5.3.6 Experiment I-6 - Field of View

a. Purpose

To verify that the interferometer will resolve all ambiguities within a ± 11.5 degree field of view.

b. Technical Description

The OC system will be used to point the interferometer about 11 degrees away from the activated ground station. The angular displacement of the ground station will be measured by the interferometer to see that ambiguities are properly accounted for. The spacecraft will be allowed to slowly drift (or be commanded) toward the ground station. The interferometer output will be recorded to assure all ambiguities are properly resolved.

c. Background Information Required

Verification of correct operation of interferometer and OC

Preflight test results

d. Position in Operating Sequence

OC subsystem tests successfully completed

e. Procedures

1. Energize the central ground station and interferometer subsystem.
2. Using the OC system offset the interferometer from the ground site by 11 degrees.
3. Record the interferometer angle output readings as the interferometer axis is allowed to slowly swing through the ground station and off 11 degrees in the opposite direction.
4. Plot the recorded angle data versus time to assure smooth angle data readout without discontinuities due to ambiguity errors.
5. Repeat for the other interferometer axis.

f. Data Produced

Angle readings over entire field of view. Verifies ambiguity resolution capability of system.

g. On-Board Equipment

Interferometer and OC subsystem

Regular T/M monitor and command equipment

h. Special Ground Equipment

No special equipment

i. Time Required

Approximately 3 hours

8.5.3.7 Experiment I-8 - Angle Difference Measurement

a. Purpose

To verify that the interferometer can determine relative station location over the field of view to within the specification accuracies. This verifies interferometer measurement accuracy or discrete angular difference values, independent of other pointing sensors.

b. Technical Description

Keeping the spacecraft orientation as constant as possible the interferometer will be used to measure the angular position of several stations (sequentially). These stations will be selected to exercise the interferometer over the field of view (to the greatest extent practical). By computing angular differences of these stations from the measured data and comparing with accurately computed angle differences based on known locations of the sites and spacecraft, a relative measuring accuracy of the interferometer can be determined over the field of view. It is estimated that computed angle differences will be at least one order of magnitude more accurate than the interferometer measurements.

c. Background Information Required

Verification that the interferometer internal operation is correct
Results of interferometer preflight testing
Precise location of ground stations
Precise location of spacecraft

d. Position In Operating Sequence

Requires operational OC system
Requires operational interferometer

e. Procedures

1. Activate and calibrate the interferometer link and point toward OCC.

2. With the spacecraft orientation held as constant as possible, record short periods of tracking data from all available ground sites (sequentially). Also record all regular interferometer T/M data plus the Orientation Control system sensor error voltages.
3. Using the collected data, compute the angles to each site. Using angle data as close together in time as possible (to eliminate variations in spacecraft attitude) compute station separations.
4. Compare station separations computed above with known station location to determine relative accuracy of the interferometer system. Station location accuracies should be good enough to evaluate interferometer relative errors in the order of 0.001 degree.

f. Data Produced

Angle measurement data over interferometer field of view

T/M data for all tracks

Orientation Control system error voltages

g. On-Board Equipment

Interferometer

Support from TT&C and OC systems

h. Special Ground Facilities

Interferometer beacons and antennas located at several widely scattered locations (over the field of view)

TT&C equipment, monitor and display equipment

Computer facilities for data reduction

i. Time Required

Two to 4 hours

8.5.3.8 Experiment I-11 - Spacecraft Pointing

a. Purpose

To measure the performance of the interferometer in a closed-loop situation, and of the Orientation Control system with the interferometer as a pointer.

b. Technical Description

The analysis of the interferometer performance in previous experiments (I-1 through I-10) will provide the basis for an evaluation of the interferometer transfer characteristics.

In turn, this evaluation will (in principle) permit a theoretical prediction of the performance of the Orientation Control system with the interferometer substituted for the earth sensors.

This experiment is designed to verify the predicted performance. The interferometer will be placed in the loop and caused to point the spacecraft toward selected ground stations, slew from one station to another and maintain commanded angular offsets with respect to stations.

The performance of the Orientation Control system in the interferometer mode will be monitored by the standard internal checks of the Orientation Control system, the earth sensors in an open loop mode and the interferometer error signals in the closed loop mode. These signals will be analyzed to verify performance characteristics.

c. Background Information Required

Verification that interferometer open loop operation is within tolerances

d. Position in Operating Sequence

After OC subsystem and interferometer open loop tests successfully completed.

e. Procedures

1. Activate interferometer, point toward OCC and verify that the interferometer is operating properly.

2. Switch the interferometer into the OC system of the pointing sensor.
3. Verify gross system stability.
4. Monitor the system performance over a 24-hour period.
5. Command slewing from one station to another, both with the command link and by the interferometer.
6. Command tracking of hypothetical moving target and verification of errors.

f. Data Produced

Performance of the OC system with the interferometer as the pointing system.

g. On-Board Equipment

Interferometer, OC subsystem

T/M and command equipment

h. Special Ground Facilities

Ground beacons for interferometer

Data recording equipment

Computer and data analysis subroutines

On-Line displays of system performance

i. Time Required

Thirty-six hours

8.5.3.9 Experiment I-13 - System Life Verification

a. Purpose

To measure the degradation of performance with time.

b. Technical Description

This experiment consists of repeating the performance evaluation experiments I-1 through I-11 at intervals of a few days over the life of the system, and comparing results over this interval. Most of these repetitions would be necessary in any event in the course of using the interferometer to support antenna tests, accumulating statistical data on performance, etc. However, additional replications may be necessary to obtain data at appropriate intervals.

c. Background Information Required

Initial performance data on the OC system and all precision pointing systems.

Data on degradation, if any, of the OC system and the other precision pointing systems.

d. Position In Operating Sequence

Begins with initial performance evaluation tests, continues through the life of the satellite.

e. Procedures

1. Repeat performance tests, especially I-5, I-6 and I-8, at intervals of not more than one week.
2. Compute the major performance parameters as functions of time, and maintain a cumulative plot.

f. Data Produced

Performance data - error signals, AGC voltages, etc., over the life of the satellite.

g. On-Board Equipment

Interferometer	TT&C system
Pointing System	OC system

h. Special Ground Facilities

Ground beacons for interferometer
Data recording equipment
Computer and data analysis subroutines

i. Time Required

At appropriate intervals, over the life of the satellite.

8.5.3.10 Experiment I-18 - Thermal Cycle Monitoring

a. Purpose

To measure the effects of the thermal environment upon interferometer performance.

b. Technical Description

Most of the data for determining the effects of the thermal environment will be obtained in other interferometer experiments, especially those connected with basic performance evaluation, since these experiments will be scheduled so as to operate across the thermal cycle. However, it will be necessary to take additional measurements at points in the thermal cycle which may not be covered by other experiments.

The major thermal effects which must be investigated are, dimensional stability of the interferometer antenna system, variations in antenna path length, and thermally induced electronic processing errors.

Antenna system deformations can cause bias errors and orthogonality errors from changes in base line orientation, and angle errors due to changes in base line length. Bias errors can be detected by checking the agreement between the interferometer, the earth sensors and other precision pointing sensors across the thermal cycle. Negligible changes indicate negligible bias errors. *

*Disagreements in boresighting (i. e., variation in angle reading differences) across the thermal cycle will require complex comparison techniques to determine which pointing sensors have been affected in what manner.

Orthogonality errors can be checked by use of the Polaris sensor and by the yaw axis stabilization experiment (I-14).

Angle errors can be measured by performing the angle difference measurement (I-8).

c. Background Information Required

Basic performance evaluation of interferometer and other precision pointing sensors.

d. Position in Operational Sequence

After initial evaluation experiments have provided material to begin evaluation. Continue experiment until thermal effects are satisfactorily determined; repeat at intervals over the life of the satellite.

e. Procedures

1. Repeat error measurement, angle difference measurement, spacecraft pointing, and yaw axis stabilization experiments as required to provide adequate data.
2. Process on the ground to derive thermal effects.

f. Data Produced

Data appropriate to experiments listed in e.

g. On-Board Equipment

Interferometer

TT&C system

OC system

h. Special Ground Facilities

Ground station having standard interferometer beacon

Data analysis subroutines

i. Time Required

Experiments listed at intervals over the life of the satellite

8.5.4 DERIVATION OF EXPERIMENT EQUIPMENT

The interferometer experiment equipment is essentially self-contained and consists of the interferometer itself. Derivation of interferometer equipment requirements was discussed in detail in General Electric Technical Information Series (TIS) Report R66ELS-89, August 1966: "The ATS-4 Satellite Interferometer Design Study". The only special feature required is a shaping and matching network to insure that the electrical characteristics of the interferometer output signal meet the requirements of the Orientation Control system. Whether this should take the form of a separate network or should be designed into the output circuits of the interferometer is a designer's choice.

8.6 PHASE-STEERED ARRAY ANTENNA

8.6.1 GENERAL

One of the major objectives of the ATS-4 program will be to demonstrate pointing and utilization of the phase-steered array antenna. The requirements for the antenna evaluation experiments for this antenna are reproduced below for reference.

The phase-steered array experiment shall be capable of simultaneous transmit and receive, multibeam operation in the 7-8 GHz frequency band. Phase steering of this array may be accomplished either by means of a phasing network and discrete command or by means of pilot signals from the surface stations or some equivalent capability. The array shall be capable of providing four beams (two for transmitting, and two for receiving) each with a minimum gain, including antenna network losses, of 30 dB with an objective goal of 45 dB. Each beam shall be pointed with an accuracy consistent with the beam width at 7 and 8 GHz.

The purpose of the phase-steered array antenna evaluation experiment will be to demonstrate adequate performance of the phase-steered array antenna in meeting the above requirements. This will require measurement of the major antenna performance parameters while transmitting and receiving as specified, and of performance in acquiring and steering the beam to a station.

The phase-steered array antenna is assumed to be the redirective array designed by the Hughes Aircraft Company on NASA GFSC Contract No: NAS5-10101, and described in their Report No. P66-68, released in March, 1966.

8.6.2 TECHNICAL BACKGROUND OF MEASUREMENTS

8.6.2.1 General

The problem of evaluating the phase-steered array is considerably different from that of the parabolic antenna. This section will discuss parameters which could be measured as a part of the evaluation experiment and the technical bases for parameter selection.

8.6.2.2 Component Similarity

Proper operation of both the transmit and receive modes is predicated on proper maintenance of the radiating phases and amplitude of a large number of elements. The phasing must be maintained throughout the signal processing system. This requires that a large number of components (the 128 high-level mixers, for example) have the same characteristics throughout the life of the mission.

Provision of the proper amplitude relationships is a less severe problem because it is easier to design and fabricate components with small amplitude errors; also because amplitude errors will cause less degradation in antenna performance.

Changes in component performance caused by the space environment or by aging could be essentially random (as might be caused by differential changes in the individual mixers) or essentially systematic (which might be caused by changes in the power dividers or summers). Small random phase errors would cause pattern distortion. Systematic phase errors would cause boresight error and, when in combination with random errors, would amplify their effect.

Measurement of the phase performance of such a large number of components appears unreasonable. The selection of critical stages at which to measure component performance should be based on a detailed failure mode analysis of the flight hardware.

In summary, proper operation of the electronic components may be verified by measurement of the radiating characteristics of the antenna systems. Measurement of the performance of individual components in space appears very costly in terms of weight and volume of test equipment.

8.6.2.3 Impedance Match

Proper impedance matching of all components and especially the radiating elements must be maintained for all operating conditions. The problematical conditions include environment effects such as thermal gradients which might cause differential impedance changes

in the elements, and operational effects such as impedance changes due to mutual coupling changes with varying scan angles. Impedance irregularities and the attendant reflections can cause generation of false error signals and hence formation of spurious beams.

Measurement of impedance match throughout the system circuitry appears far beyond the scope of the in-space evaluation experiment. Ground testing and failure mode analysis may identify selected impedance measurements which may be valuable as diagnostic aids and these measurements can be made in a straightforward manner. Large-scale impedance measurements, however, appear to have little value as evaluation aids.

8.6.2.4 Physical Geometry

The transmit and receive apertures are to be flat and coplanar. Maintenance of the proper geometry should pose no problem and measurement of the geometry would be trivial.

8.6.2.5 Radiation Characteristics

Receipt of a pilot signal at the array causes a beam to be formed in the direction from which the pilot was received. This process is most easily discussed in terms of the transmit mode. The receive mode is analogous.

Proper beam formation is the result of correct operation of all component parts, and the measurement of the radiation pattern stimulated by a pilot signal from a given direction is a measurement, in varying degrees, of the performance of all component parts.

Measurement of null depths would be an excellent measure of small phase errors in the system. Comparison of measured beamwidths and sidelobe levels with ground test data would further verify proper operation.

As mentioned previously, a beam is formed in the direction from which the pilot was received. To measure radiation pattern of the antenna with the beam in that orientation requires either a moving receiver or many stationary receivers which have been cross-calibrated. Even at that, earth-based or low-orbit stations could measure only a small

portion of the pattern. The alternative of using a moving pilot source and fixed receiver requires less ground support but, since the array is continuously changing beam-pointing directions, would not yield a true pattern measurement. The moving pilot technique would detect gross deviations such as grating lobe formation or spurious beam generation. Patterns could be reconstructed by correlation with extensive ground test data taken in a similar manner.

The main beam of the array will be in a direction such that the individual elements are in phase. Proper operation of the baseline design array includes the formation of a beam in the direction of the pilot signal. Measurement of the beam-pointing direction for an array with predominantly random phase errors could be performed with a single ground station. If appreciable correlated phase errors are expected, multiple or moving stations would be required to determine the beam peak, but the search area would be smaller (probably less than 50-mile radius) than that required for pattern measurements.

The gain of the array when responding to a given pilot signal is a function of the operation of the entire antenna system. At broadside, the gain of the array is simply the sum of the element gains. The amplitude and phase errors which affect the array gain represent an accumulation of errors in components and processing in the system. The measurement of absolute gain is thus one of the most powerful evaluation parameters.

8.6.3 PARAMETER SELECTION

8.6.3.1 General

Parameters must be measured which permit evaluation of the self-steering phased array and provide guidance for the selection and design of future phased array antennas for specific operational missions. Due to the high cost (in terms of dollars, on-board weight, volume and power, mission time, and ground support) of any measurement in space, heavy reliance will be placed upon correlation of space measurement with extensive ground test data.

The attitude of the array should be known before operational functional measurements are started. Proper operation of the attitude measurement system should be determined and the indicated attitude should agree with indications from other attitude sensors. This gross check requires measurement accuracies on the order of a few degrees.

8.6.3.2 Internal Parameters

The first operational test should include verification that all active components are properly enabled or operating. Proper operation of the components will be verified by measuring selected critical parameters (i.e., local oscillator frequencies, amplifier gains, etc.). Other parameters such as effective transmitter power and receiver sensitivity may be measured for other purposes (such as gain measurement) and will corroborate the critical component tests.

8.6.3.3 Gain

The measurement of the gain of the array will constitute one of the principal evaluation experiments. The ability to deduce system operational parameters from the gain is dependent, to some extent, on the accuracy of the gain measurement. Absolute gain measurement accuracies of ± 0.5 dB can be expected.

8.6.3.4 Beam-Pointing Direction

Grossly proper beam direction will be determined by comparison of measured gain with anticipated gain. Measurement of pointing direction independent of the absolute gain measurement would require multiple or moving sensing or pilot stations. Measurement accuracies of about 0.5 degrees are probably sufficient for operational evaluation of the array. Higher accuracies might be required if beam direction is to be used for other purposes, such as attitude cross check.

8.6.4 EXPERIMENTS

8.6.4.1 List of Experiments

Table 8.6-1 is a tabulation of individual experiments which can be performed in the evaluation of the phase-steered array antenna.

The measurements which are considered crucial are described in the following section.

Table 8.6-1. Individual Experiments - Phased Array Antenna

ø -1	<u>Verification of Equipment Operation - 4</u>
	To verify that the equipment associated with the antenna (transmitters, receivers, switching, etc.) is working.
ø -2	<u>Measurement of Internal Parameters - 4</u>
	To verify that the internal system parameters (transmitter power, receiver sensitivity, frequency stability, etc.) are within design tolerances.
ø -3	<u>Verification of Operational Characteristics - 4</u>
	To verify that the operational characteristics of the phased array antenna system (ability to transmit and receive high-quality signals, and antenna performance characteristics) are qualitatively correct.
ø -4	<u>Gain Measurements - Medium Accuracy - 4</u>
	To measure the approximate gain characteristics of the phased array.
ø -5	<u>Gain Measurement Experiment</u>
ø -5-1	<u>Gain Measurement Experiments Without High Accuracy Pointing Devices - 1</u>
ø -5-1-a	The measure, with the highest accuracy attainable, the absolute gain of the phased array antenna, using the technique of comparison with standard gain horns, and assuming that the interferometer or other high-accuracy pointing sensor is <u>not</u> available.

Table 8.6-1. Individual Experiments - Phased Array Antenna (Cont'd)

ϕ-5-1-b Gain Measurement - High Accuracy - 1

To measure, with the highest accuracy attainable, the absolute gain of the phased array antenna, using the technique of measuring transmitted and received power, and assuming that a high-accuracy pointing sensor (e.g., the interferometer) is not available.

ϕ-5-2 Gain Measurement Experiments with High Accuracy Pointing Devices

ϕ-5-2-a Gain Measurement - High Accuracy - 1

To measure, with the highest accuracy attainable, the absolute gain of the phased array antenna, using the technique of comparison with standard gain horns, and assuming that the interferometer or other high-accuracy pointing sensor is available.

ϕ-5-2-b Gain Measurement - High Accuracy

To measure, with the highest accuracy attainable, the absolute gain of the phased array antenna, using the technique of measuring transmitted and received power, and assuming that a high-accuracy pointing sensor (e.g., the interferometer) is available.

ϕ-6 Pattern Measurement

ϕ-6-1 Pattern Measurement - 1

To measure, to the highest accuracy attainable, the main lobe pattern and the accessible side lobes of the phased array antenna.

ϕ-6-2 Gain vs Attitude - 1

To measure as accurately as possible the gain of the antenna as a function of its geometric attitude.

ϕ-7 Verification of Signal Transmission - 4

To verify that transmission of intelligible signals through the phased array antenna can be performed.

ϕ-8 Verification of Signal Reception - 4

To verify that reception of intelligible signals through the phased array antenna can be performed.

Table 8.6-1. Individual Experiments - Phased Array Antenna (Cont'd)

ø-9 Verification of Signal Switching Operation - 4

To verify that the designed signal switching operations of the phased array antenna system can be performed.

ø-10 Measurement of Low Data Rate Performance - 4

To measure as accurately as possible the performance of the phased array antenna in transmitting and receiving digital data at low (10 to 10^3 bps) data rates.

ø-11 Measurement of Medium Data Rate Performance - 4

To measure as accurately as possible the performance of the phased array antenna in transmitting and receiving digital data at medium (10^3 to 10^5 bps) data rates.

ø-12 Measurement of High Data Rate Performance - 2

To measure as accurately as possible the performance of the phased array antenna in transmitting and receiving digital data at high (10^5 to 10^7 bps) data rates.

ø-13 Measurement of Audio AM Performance - 4

To measure as accurately as possible the performance of the phased array antenna in transmitting and receiving audio signals, AM.

ø-14 Measurement of Audio FM Performance - 4

To measure as accurately as possible the performance of the phased array antenna in transmitting and receiving audio signals, wide band FM.

ø-15 Measurement of Video SSB AM Performance - 2

To measure as accurately as possible the performance of the phased array antenna in transmitting and receiving video signals, vestigial sideband (commercial standards) AM.

ø-16 Measurement of Video Wideband FM Performance - 1

To measure as accurately as possible the performance of the phased array antenna in transmitting and receiving video signals, wideband FM.

ø-17 Measurement of Extreme Bandwidth Performance - 2

To measure as accurately as possible the performance of the phased array antenna in transmitting and receiving selected signals at very large rf bandwidths.

Table 8.6-1. Individual Experiments - Phased Array Antenna (Cont'd)

ø-18 Measurement of Signal Amplitude Fluctuations - 3

To measure to the highest accuracy attainable the fluctuations in signal amplitude (1 Hz to 10^7 Hz) caused by atmospheric propagation and/or antenna vibration effects.

ø-19 Measurement of Signal Phase Fluctuations - 3

To measure to the highest accuracy attainable the fluctuations in signal phase caused by atmospheric propagation and/or antenna vibration effects.

ø-20 Measurement of Signal Phase Distortions - 3

To measure to the highest accuracy attainable the distortion in signal phase caused by atmospheric propagation and/or antenna vibration effects.

ø-21 Measurement of Polarization Effects - 3

To measure to the highest accuracy attainable the fluctuations and bias in polarization caused by atmospheric propagation and/or antenna vibration effects and to investigate the use of polarization in measuring spacecraft attitudes.

ø-22 Two-Beam Performance - 1

To measure to the highest attainable accuracy the performance of the antenna system in the complete single-channel operation.

ø-23 Four-Beam Performance - 1

To measure to the highest attainable accuracy the performance of the antenna system in a complete two-channel operation.

ø-24 Measurement of Tracking Performance - 3

To measure to the highest accuracy attainable the performance of the phased array antenna system while tracking.

ø-25 Measurement of Slew Performance - 3

To measure to the highest accuracy attainable the performance of the phased array antenna system during slew.

ø-26 Incremental Angle Measurement - 2

To measure to the highest accuracy attainable the relative electrical performance and antenna system performance of the phased array antenna with respect to two ground stations at known locations.

Table 8.6-1. Individual Experiments - Phased Array Antenna (Cont'd)

ø-27 Band Limitation Measurements - 2

To measure to the highest accuracy attainable the performance of the phased array antenna system in transmitting and receiving signals at the edges of the prescribed frequency bands.

ø-28 Thermal Cycle Electrical Effects

ø-28-1 Thermal Cycle Electrical Effects - 2

To measure to the highest accuracy attainable the effects of thermal distortion upon the electrical characteristics of the antenna.

ø-28-2 Thermal Cycle Electrical Effects - 2

To measure to the highest accuracy attainable the effects of thermal distortion upon the transmission and reception performance of the antenna system.

ø-29 Mechanical Disturbance Electrical Effects

ø-29-1 Mechanical Disturbance Electrical Effects - 2

To measure to the highest accuracy attainable the effects of mechanical disturbances upon the electrical characteristics of the antenna.

ø-29-2 Mechanical Disturbance Electrical Effects - 2

To measure to the highest accuracy attainable the effects of mechanical disturbances upon the transmission and reception performance of the antenna system.

ø-30 System Life Characteristics - 1

To measure to the highest accuracy attainable the degradation of system performance with time.

8.6.4.2 Basic Electrical Measurements

8.6.4.2.1 Experiment Formulation

The crucial electrical measurements for evaluation of the phase-steered array antenna are, absolute gain, gain as a function of antenna attitude, and verification of bandwidth and multibeam operation. The more important supporting measurements include the analysis of the primary lobe pattern.

All in-space measurements will rely heavily upon the fact that thorough and extensive ground evaluation will have been performed upon the phase-steered array, both during the development and testing of the array and upon flight hardware before launch.

8.6.4.2.2 Experiments ϕ -4 and ϕ -5 - Gain

a. Purpose

To measure the gain of the phase-steered array antenna system and the gains of the transmitting and receiving arrays.

b. Technical Description

The antenna gain of the phase-steered array should be approximately 30 dB each for the transmitting and receiving array. Measurement of the gain is by two methods; substitution and power level measurements.

In the substitution technique, the overall gain of the phase-steered array receiving system is compared with that of a receiving system involving the standard gain antenna or the large parabolic antenna, after the gain of the latter has been evaluated. Gain of the receiving array is determined by comparing the signal-to-noise ratios, and adjusting the power changes in the ground transmitter until there is no change in signal-to-noise ratios when the power is changed as the systems are substituted. The gain of the transmitting array is measured by changing the attenuation in the ground receiver so that the power levels do not change when the attenuation is switched in synchronization with substitution of the standard system with the phase-steered array system.

If the design of the phase-steered array in its space-rated configuration permits, this measurement will be supplemented by substitution of major elements of the systems; feeding the output of the phase-steered array receiving system to a standard transmitter, feeding the output of the phase-steered array TWT alternately to the phase-steered array transmitting array and a standard gain antenna.

The backup mode is simply to measure the power transmitted from the ground and the power and signal-to-noise ratio of the signals received. Since the space losses will be known fairly well, the total antenna gain can be determined to a moderate accuracy.

c. Background Information Required

Results of phase-steered array ground tests

Verification that phase-steered array is functioning

Verification that standard gain and parabolic antenna equipments are operating correctly.

Verification that the Orientation Control and TT&C systems are operating correctly.

d. Position in Operational Sequence

After initial gain measurements of parabolic antenna system have been completed.

e. Procedures

1. Command the satellite to point directly toward the ground station.
2. Establish contact with the phase-steered array, on one channel.
3. Transmit a test signal; verify that it is received and measure received power and signal-to-noise ratio.
4. Substitute standard reference system on board, and adjust transmitter power and receiver attenuator setting on the ground until there are no changes in received power or signal-to-noise ratio when the substitution is made.
5. Repeat, substituting transmitting and receiving arrays with their standard counterparts on board, if design of the phase-steered array permits.
6. Repeat for a period of approximately one hour, continually monitoring transmitted and received power both on board and on the ground.

f. Data Produced

Measurements of phase-steered transmitter and receiver array gains and overall system gains by two independent methods.

g. On-Board Equipment

Phase-steered array	Standard gain antennas
TT&C System	Parabolic antenna system
Orientation control system	Power measuring sensors

h. Special Ground Facilities

1. Equipment

Transmitter and receiver equipment at specified frequencies in the 8 GHz band.

Precision control of ground transmitter radiated power and ground receiver attenuation.

Power measurement equipment for transmitter and receiver.

Signal-to-noise ratio measuring equipment.

Display and plotting equipment.

2. Software

Subroutines for computing gains and statistical analyses of data.

3. Personnel

Analyst to evaluate system behavior to guide experiment.

i. Time Required

Two hours

8.6.4.2.3 Experiment 6.6-2 Gain Versus Array Attitude

a. Purpose

To measure the effect of array attitude upon the system gain. Secondly, to measure the effect of array attitude upon the gains of each array: transmitter and receiver.

b. Technical Description

The overall system gain, as well as the gain of each array, transmitter and receiver, will vary with system attitude, being of course greatest at boresight if the system is operating properly.

The measurement is made by pointing both arrays at the same ground station and swinging the satellite across the ground station by command, measuring the changes in gains as a function of angle. A convenient test signal is transmitted from the ground and returned. In order to cover the beamwidth, the satellite will be scanned in a raster fashion. Because of the relatively large beamwidth, the 0.1 degree accuracy of the Orientation Control system will be quite adequate for the scan.

The measurement procedure is to vary the setting of an attenuator in a ground-based receiver in such a fashion as to keep the output from the receiver constant with change in angle as the satellite swings. Since the IF amplifiers will keep the receiver output and hence the input to the transmitter in the phase-steered array constant for small changes in input signal, the output of the transmitter will be nearly constant, and the variations in attenuation with angle will measure the changes in the gain of the transmitter array. The measurement will then be repeated, varying the power output of the ground-based transmitter to keep the signal-to-noise ratio of the signal received on the ground constant. Since the transmitted power from the satellite is essentially constant, the signal-to-noise ratio with angle will measure directly the changes in gain of the receiver antenna. The scan can then be repeated, performing both measurements at once.

These measurements should be accurate within 1 to 2 dB. Since the results of each scan are essentially statistically independent, a considerable improvement can be obtained if desired by repeating the measurements a number of times.

c. Background Information Required

Results of ground tests on phase-steered array

Verification that phase-steered array equipment is functioning

Verification that the Orientation Control system and/or other precision pointing sensors will provide pointing data to at least 0.1 degree.

d. Position in Operational Sequence

After deployment and initial checkout of all major systems.

e. Procedures

1. Command the satellite to point directly toward the ground station.
2. Establish contact with the phase-steered array, using the test signal, and verify that the array parameters are approximately correct.
3. Command a raster-type scan of the satellite, maintaining the output of the ground receiver constant by operation of the attenuator; record continuously the setting of the attenuator.
4. Repeat, varying the output of the ground-based transmitter to keep the signal-to-noise ratio constant at the ground receiver input.
5. Repeat, performing both measurements at the same time.

f. Data Produced

Gain changes of transmitter array with array attitude.

Gain changes of receiver array with array attitude.

g. On-Board Equipment

Phase-steered array antenna

Orientation Control system

TT&C system

h. Special Ground Facilities

1. Equipment

Precision control of transmitter radiated power (e. g., by attenuator)

Precision attenuator at receiver input

Signal-to-noise ratio measurement equipment

2. Software

Subroutines for statistical analyses of measured data.

i. Time Required

Two hours.

8.6.4.2.4 Experiments ϕ -13, ϕ -15, ϕ -16, ϕ -22, and ϕ -23 Bandwidth and Multibeam Operation

a. Purpose

To verify that both two-beam and four-beam operations are feasible and measure the performance of the antenna system in these modes.

b. Technical Description

The phase-steered array is designed to operate using four beams in a configuration generating two complete channels. It is necessary to verify that these channels can indeed operate successfully, without undue interference, by transmitting signals from the ground to the satellite and back again in these modes. It is useful to operate first with two-beam, one-channel operation, then with two channels, to verify that mutual interference is not a problem. In order to verify that beam steering is as specified, it is desirable during the latter stages of the measurement to use two separated ground stations.

c. Background Information Required

Results of ground tests on phase-steered array

Verification that the phase-steered array has roughly the correct gain and beam characteristics.

Verification that orientation system operation is approximately correct.

d. Position in Operational Sequence

After deployment and initial checkout of all major systems.

e. Procedures

1. Command the satellite to point toward the ground station.
2. Establish contact with the phase-steered array, by sending a simple signal up and back.
3. Transmit the test signals; this will include at least video pictures and test charts, high-speed data, multiplexed data special test waveforms.
4. Switch to the other channel and repeat Step 3.
5. Switch on both channels and repeat Steps 3 and 4.
6. Command the satellite to point to a point halfway between two ground stations, e.g., Rosman and Mojave.
7. Repeat Step 5 from each of the ground stations in turn.
8. Repeat Step 5 using Rosman and Mojave as terminals of the two channels.
9. Command the satellite to point to each station in turn and repeat Step 8.
10. Command the satellite to rotate slowly and repeat Step 8.

f. Data Produced

Verification that the phased array can perform two-channel, four-beam operation, with a single ground station and between two ground stations, in any reasonable attitude and with moderate rotation rates.

g. On-Board Equipment

Phase-steered array antenna

Orientation Control system

TT&C system

h. Special Ground Facilities

1. Software

Subroutines for signal phase and amplitude analysis.

Subroutines to facilitate analysis of video waveforms and special test waveforms.

2. Personnel

Analyst at each station to perform on-line analyses sufficient to guide procedures during measurement operations.

i. Time Required

Three and one-half to 4 hours.

8.6.4.2.5 Primary Lobe Pattern Analysis

a. Purpose

To measure the structure of the phase-steered array main lobe.

b. Technical Description

The analysis of the primary lobe of the phase-steered array is complicated by the fact that the beam is designed to point directly at the station with which it is communicating, regardless of the geometric attitude of the array.

One procedure for circumventing this problem is to place the necessary test equipment in an aircraft which works with the ground station. While the ground station and aircraft alternately cause the beams to be pointed, the aircraft flies a course which takes it

across the beam, measuring signal strength as a function of distance, for both the transmit and receive beams. The total flight path of the aircraft is approximately 2500-3000 miles in order to cross the 3 dB points of the beam. Signal strength changes at both the aircraft and ground station are measured for each switch. In this way, a fairly detailed measurement of the main lobe structure of all four beams can be obtained.

This is a fairly prolonged and expensive measurement, involving a 2500 to 3000-mile flight for each measurement run, and requires a number of runs per experiment.

c. Background Information Required

Results of ground tests on phase-steered array.

Verification that phase-steered array equipment is functioning.

Verification that the Orientation Control system will provide pointing data to at least 0.1 degree.

d. Position in Operational Sequence

After deployment and initial checkout of all systems.

e. Procedures

Get the aircraft into position to begin measurements, orbiting over the ground station.

Command the satellite to point directly to the ground station.

Verify that link operates correctly with both ground and airborne stations and that all airborne instrumentation operates correctly.

Fly the aircraft radially from station, measuring relative gains in both channels, alternating between the ground station and the aircraft. Continue until the aircraft reaches a geographic location which is at the 3 dB point when the beam is pointing at the ground station.

Repeat with a return flight across the beam to the opposite 3 dB location.

f. Data Produced

Detailed measurement of main lobe pattern.

g. On-Board Equipment

Phase-steered array antenna

Orientation Control system

TT&C system

h. Special Ground Facilities

1. Equipment

Instrument aircraft

Equipment for relative gain measurement

2. Software

Subroutines for statistical analyses of measurement data

i. Time Required

Eighteen hours.

8.6.5 EQUIPMENT REQUIRED

No additional spacecraft equipment is required other than standard telemetry signal processors.

Link calculations indicating ground transmitter and receiver requirements are shown in Table 8.6-2.

Table 8.6-2. System Performance Steered Phase Array Antenna - Transmission and Reception Measurements (rf Bandwidth: 30 MHz)

	<u>Transmission</u>	<u>Reception</u>
P_{out}	-6 dBw 1/4 watt*	+15.3 dBw 20 watt
Transmitter Antenna Gain (dB)	+30	+60
ERP (dBw)	+24	+75.3
Pattern Factor (dB)	-1	-0
Net ERP (dBw)	+23	+75.3
Path Loss (dB)	201	201
Power Density at Receiver Antenna (dBw)	-178	-125.8
Receiver Antenna Gain (dB)	+60	+30
Power at Receiver Terminal (dBw)	-118	-95.8
Line Losses (dB)	0	2
Converter Input (dBw)	-118	-97.8
Receiver Noise Figure (dB)	3	15.2
Reference (dBw)	-121	-113
KTb (dBw)	-133	-133
S/N	+12	+20

* Power available is -5 dBw

8.7 SUPPLEMENTARY EXPERIMENTS

8.7.1 GENERAL

It is of interest to consider experiments which might be performed in the ATS-4 program or immediate outgrowths, beyond those required for evaluation of the prime experiments. Some of these experiments would require additional equipment on-board, or modifications to existing on-board experiment equipment.

These experiments are discussed in the following categories:

- a. Augmentations of prime experiments, to provide additional information which might be of interest.
- b. Applications of prime experiments; e. g. , experiments which would take advantage of the high data rate capability or the precision pointing capability.
- c. Passenger experiments, which merely take advantage of the existence of a synchronous satellite.

8.7.2 PRIME EXPERIMENT AUGMENTATION

8.7.2.1 Parabolic Antenna Geometric Instrumentation

Vibration - Detailed analysis of the dynamic behavior of the parabolic antenna/satellite structure system would be of considerable value in the design of future large structures in space. It would be interesting to measure amplitudes, frequencies, damping factors, coupling coefficients, etc. Instrumentation to make such measurements in space would require a fairly substantial development program. A number of approaches have been suggested, including the use of phase and/or doppler shift measurements at millimeter and optical wavelengths, sensitive crystal pickups, accelerometers, etc. The initial step in a proper development program would be consideration of all promising approaches in order to select one or more for further investigation.

Static Configuration - The static configuration of the paraboloidal antenna is quite complex, i. e. , the paraboloid can deform in a number of ways, the feed structure can displace or

rotate about any axis with respect to the focus, and the internal configuration of the feed structure can be distorted in each of a number of ways. Investigation of very small changes would begin with consideration of appropriate reference points and/or planes for measurements and would consider ways of measuring the very small deflections. Approaches which have been suggested include use of phase comparisons at millimeter and optical frequencies to measure distances, measuring distortions of geometric designs as seen by a television camera, optical measurements of angular deflections, and improved strain gauges.

8.7.2.2 Parabolic Antenna Ultra Wide Band Communications

This experiment in principle would consist of transmitting and/or receiving through the parabolic antenna at each frequency the widest bandwidth signal which reasonable equipment limitations permit, up to the 10 percent bandwidth of the antenna system. This will verify performance of the antenna system in this mode, and also indicate whether any type of atmospheric interference is significant.

8.7.2.3 Parabolic Antenna Side Lobe Measurement

This experiment is an investigation of the side lobe structure of the parabolic antenna, probably in the X-band and S-band ranges. It would require permitting the spacecraft to rotate far enough to obtain a good idea of the side lobe structure in the S-band, and perhaps some idea of the structure in the 800 MHz region, and to provide sufficient power to investigate the nulls. This does not appear to impose any particular difficulty.

8.7.2.4 Polarization Measurements from the Parabolic Antenna

The availability of a high signal-to-noise ratio X-band signal from the parabolic antenna, together with the highly accurate Polaris tracker in the orientation control system, provide an excellent background for investigating the utility of polarization measurement for determining spacecraft attitude; in this case, yaw. The polarization presently used in the parabolic antenna is circular, but a very minor modification would permit generation of linear polarization at will.

8.7.2.5 Monopulse Installation

Analysis of experiment requirements indicates that incorporation of a simultaneous lobe comparison (monopulse) installation in the parabolic antenna at the upper end of its frequency range (about 8 GHz) would add considerably to the effectiveness and convenience of the pointing measurements.

This analysis was not carried to the point at which a definite recommendation is possible; however, it definitely merits further detailed consideration.

The more important advantages of the monopulse are:

- a. High-accuracy measurement of electrical boresight*
- b. High-accuracy measurement of antenna-interferometer boresight*
- c. Verification of interferometer accuracy*
- d. Supporting verification of orientation control system performance*
- e. Simplification of tracking problem*
- f. Reduction in small-station beacon ERP for some measurements
- g. Slight improvement in accuracy (pointing)
- h. Alternate pointing technique in case of interferometer malfunction
- i. Feasibility demonstration of both interferometer and monopulse
- j. Possible direct comparison of propagation effects on precision tracking systems at 8 GHz and 10 GHz.

As can be seen, the first four entries in the above list will contribute heavily to the solution of the precision pointing calibrating problem. The effect of the first entry is that the experimenters will know directly, unequivocally and to a very high accuracy, when the electrical boresight of the parabolic antenna is pointed at the ground station. This makes measurement

*Considered to be important

of gain, electrical boresight and main lobe pattern more simple, direct, accurate and reliable. The next three entries, as listed, indicate support for evaluation of the interferometer, the orientation control system, and the structural alignment measurements. The remaining entries are self-explanatory.

The costs of the monopulse installation are:

- a. Requirement for minor revision of feed system design
- b. Moderate increase in rf complexity
- c. Additional weight - about 12 pounds
- d. Additional power - about 10 watts during some experiments
- e. Moderate additional system complexity
- f. Slight additional ground processing requirements
- g. Additional ground beacons

Perhaps the most important cost is that first listed: the necessity for revising the feed system design of the parabolic antenna. This should not be excessively difficult.

It involves loading the X-band horn with a dielectric to permit excitation for multimode operation, which of necessity makes the horn slightly larger. Since the three horns are coaxial and carefully matched, the size of the other two horns, S-band and L-band, must be correspondingly increased, with the result that the entire installation becomes somewhat larger and more bulky.

It was decided that a complete design of a monopulse installation, including as it must, revision of feed system design, would absorb excessive amounts of man-hours if done within the scope of the present study. Therefore, work was limited to a preliminary study, sufficient to obtain a first estimate of the performance and cost factors involved. (See Appendix L) A small development program culminating in a detailed design is suggested for the next phase of the study. Such a program might well be included in the antenna development program.

8.7.2.6 Phase-Steered Array Monitoring

It would be of interest to measure the internal operation of the phase-steered array, to monitor the effects of individual channels, the various antenna, and electronic devices, etc. The major parameters which it would be interesting to measure include:

- a. Gain of each array, measured directly
- b. Gain of each element
- c. Gain of each channel
- d. Phase relationships in each channel

Gains of the arrays would involve comparing the arrays with standard gain horns. Gains of each element could be obtained by disabling all other channels and measuring the gain of a single channel. Phase relationships can be determined by using the attitude determination systems already incorporated in the phase-steered array system, together with switches to connect these systems to various combinations of channels.

The equipments required, even though consisting mostly of switching equipment, would require some redesign and re-packaging of the phase-steered array, and addition of considerable telemetry capability.

8.7.2.7 Interferometer Yaw Axis Stabilization

The ability to provide roll-axis stabilization may be added to the interferometer with a negligible increase in onboard weight and power. However, on the ground, it would be necessary to have two transmit stations. These stations would be required to have a separation of between 50 and 300 miles and to have facilities for switching between them at about a 3-kHz rate.

With the transmitted signal being switched at 3-kHz between two stations of about equal power, the error signal produced on the satellite-borne interferometer (which is essentially dc) will be modulated at this rate. Roll axis stabilization can now be accomplished in two steps.

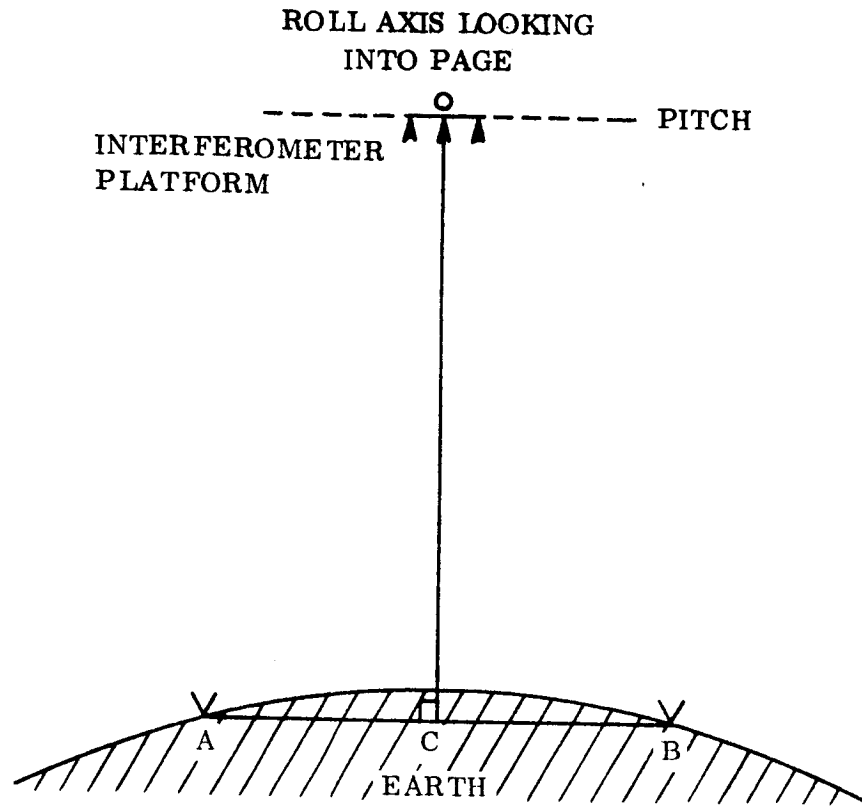
First the yaw-axis error signal is driven to a constant zero output. This places the yaw axis perpendicular to an imaginary line AB passing through the two transmit antennas and perpendicular to a line CD from the midpoint of AB. This situation is illustrated in Figure 8.7-1. The orientation of the pitch axis is still arbitrary at this point and may be at any angle in the plane on Figure 8.7-1 (a).

Now the pitch axis error signal is driven so that it switches between a positive value and an equal negative value. This is accomplished by integrating the pitch axis perpendicular to line CD. The satellite's attitude is now exactly as pictured in Figure 8.7-1 and is fixed with respect to the yaw, pitch, and roll axes. The accuracy attainable about the roll axis is comparable to that of the basic interferometer system.

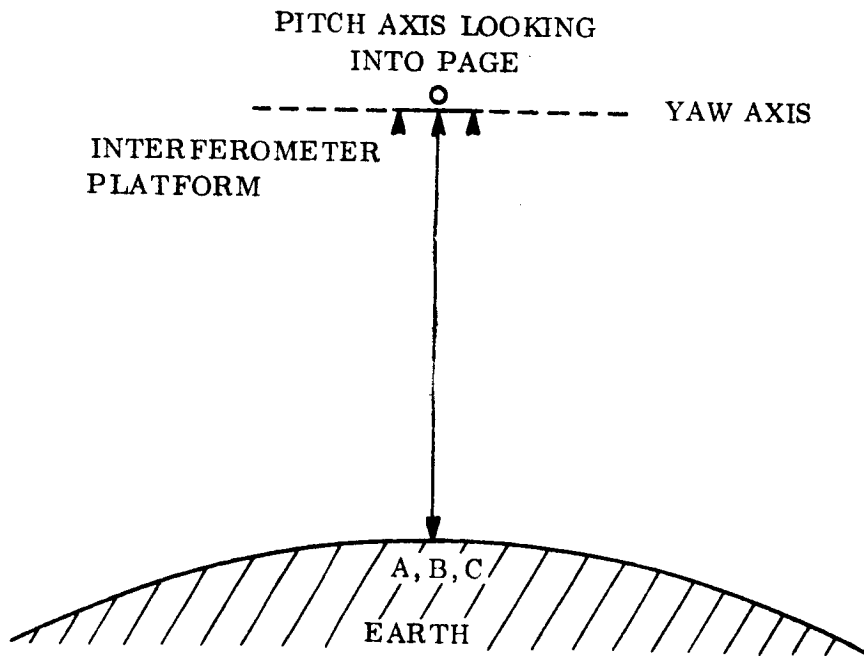
8.7.2.8 Synthetic Angle Generation

A possibility exists of using an angle synthetically generated on the ground to calibrate the interferometer over its entire field of view.

Synthetic angle generation requires the transmission of both a right and a left circularly polarized wave from the ground. One of the pair of interferometer channels to be calibrated would be switched to receive left circular polarization. The other channel will receive right circular, as usual. Thus, by accurately adjusting on the ground, the phase difference between the right and left circular waves, a synthetic angle may be generated to be measured by the interferometer. In this manner, the angle measurement made by the interferometer may be compared to a very accurate phase difference adjusted on the ground. It should be noted that propagation effects through the earth's atmosphere are different, in general, for right and left circularly polarized waves. However, at 10 GHz this effect is never more than a phase difference of 0.03 electrical degree, or about 10^{-4} degree in actual angle for a 39λ antenna spacing. At the ground station it is necessary to employ two feeds on the transmitting dish used for this experiment, one for each polarization. It is estimated that with some care the phase between the circularly polarized waves introduced at the two antenna feeds may be controlled to 0.5 electrical degree. This corresponds to an overall accuracy of 0.002 degree in actual angle for a 39λ antenna spacing.



(a) PLANE OF LINE A AND PITCH AXIS



(b) PLANE OF MIDPOINT OF LINE A AND YAW AXIS

Figure 8.7-1. Yaw Axis Stabilization Geometry

8.7.2.9 Interferometer Transmit Mode

It is possible to perform an experiment that tests the feasibility of transmitting from the satellite to a single ground station, for the purpose of attitude determination. This is equivalent to operating the interferometer in reverse, as a transmitter instead of a receiver. The onboard system necessary to do this is shown in Figure 8.7-2. It is necessary to time multiplex the transmitter between Σ , Δ_1 and Δ_2 transmissions. First, the coarse system operates until a minimum error signal is determined on the ground, and then the fine system is switched in to achieve full accuracy.

The ground station would require extra processing equipment, as shown in Figure 8.7-3. The signal-to-noise ratio of the system would be degraded by the duty factor of the time-multiplexing circuit, which would be about 5dB in this case. However, this might be easily compensated on the ground by using a better receiver than is possible on the spacecraft. Thus, for a 60-foot ground receiving antenna and a ground receiver with 5dB noise figure, the necessary power radiation from the satellite, for this experiment is 12 watts. This requires about 90 watts prime power aboard the spacecraft. However, by reducing the

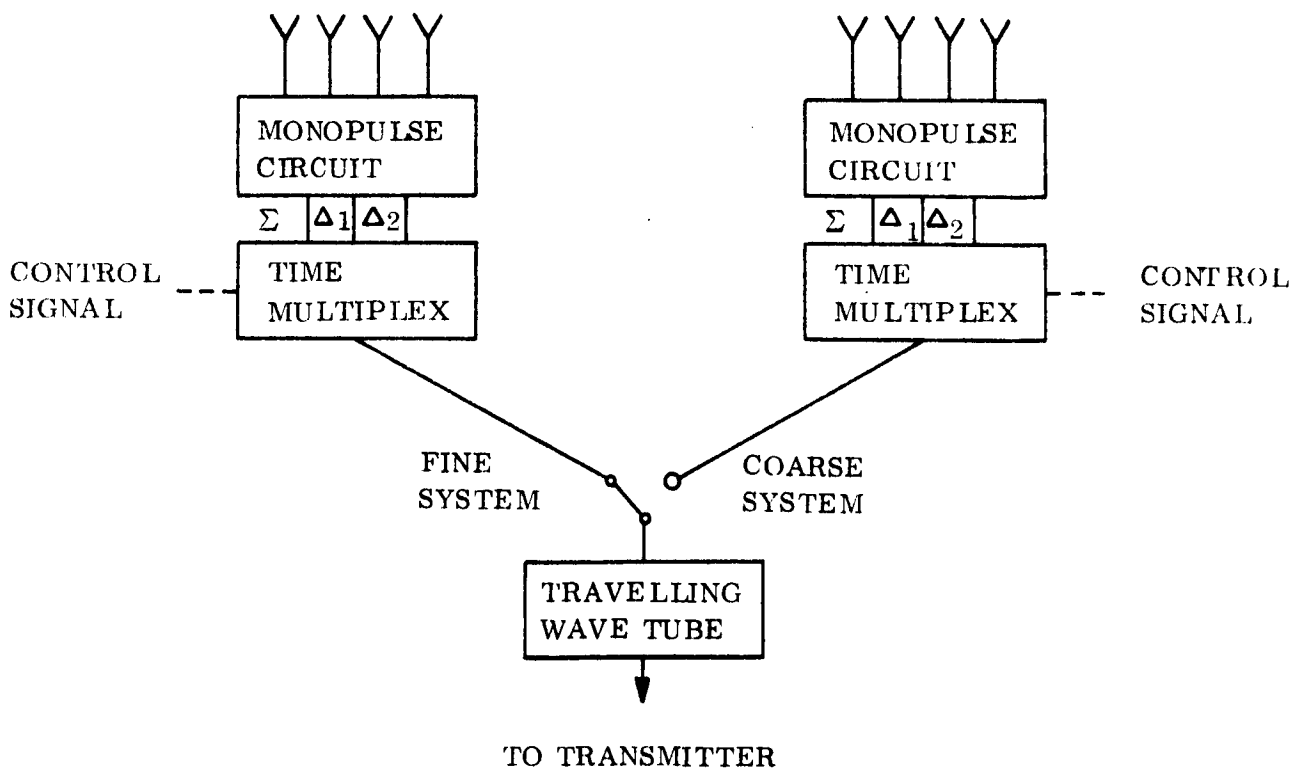


Figure 8.7-2. Spacecraft Transmit System

angular accuracy required for this mode of operation to 0.03 degree, the prime power required aboard the spacecraft may be reduced to 20 watts.

8.7.3 PRIME EXPERIMENT APPLICATIONS

A number of potential applications for the ATS-4 prime experiments are discussed here. All of these in one way or another are intended to take advantage of the data rate, precision pointing, or electronic beam steering capabilities of the ATS-4 system. The specific applications discussed are:

- a. Meteorology
- b. Satellite direct broadcast
- c. Navigation and air and ship traffic control
- d. Communications with low-orbit spacecraft
- e. Multiple access communications

8.7.3.1 High Data Rate Meteorological Sensor

8.7.3.1.1 Nature and Purpose

Ever since the first satellite meteorological pictures were obtained, the questions of the value of such pictures as a function of the various major parameters has existed. These parameters include:

- | | |
|---------------------------------|------------------|
| a. Coverage | c. Resolution |
| b. Continuity | d. Dynamic Range |
| e. Color (or spectral response) | |

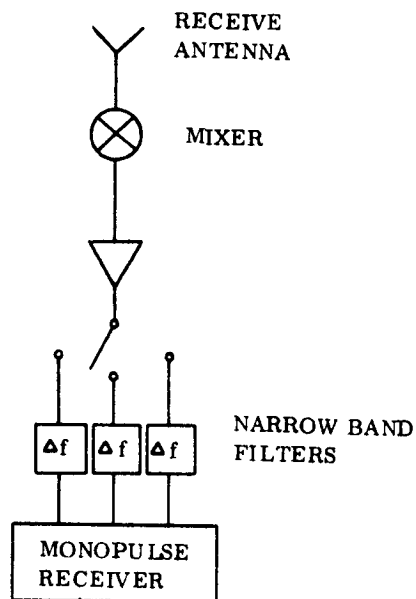


Figure 8.7-3. Ground Station Circuitry for Transmit Experiment

The synchronous satellite is ideally located for tests of coverage and continuity. In principle, it is possible for such a satellite to observe over one-quarter of the earth's surface with a television camera during the entire daylight hours, and to systematically vary:

- a. Frame
- b. Resolution
- c. Dynamic Range
- d. Spectral Response

Analysis of the data from such observations will permit determination of the relative value to meteorologists of the various observational parameters.

8.7.3.1.2 Value

It has been estimated that improvement of weather forecasting to permit highly reliable five-day forecasts would save several billion dollars per year in property damage. Intensive efforts to that effect have been recommended. It is also possible that within a few years a beginning may be made on weather modification, e. g. , in decreasing the intensity or influencing the course of hurricanes by cloud seeding and related techniques. Observations from weather satellites is a matter of extreme importance.

A corresponding need exists for weather forecasting and if possible control, in support of military operations. Air strikes, refueling, amphibious operations, ground combat, submarine and surface naval operations are crucially dependent on weather. It is of course obvious that if any influence could be exerted on hurricanes in a military theater, the tactical and strategic advantages could be enormous.

8.7.3.1.3 Equipment and Procedures

Adequate empirical investigations of high data rate sensors have previously been deterred mainly by the high costs of placing the necessary communications facilities in orbit. However, since the large antenna is already available, the prorated costs of using it for this experiment become more manageable.

As can be seen from the margin calculations of Table 8.7-1, it is quite feasible to transmit television bandwidth data from synchronous altitude. This data rate capability can be used to permit a number of different types of observations; one possibility is described below:

Table 8.7-1. System Performance (High Data Rate Meteorological Sensors - Satellite Surface, 10 GHz TV Data Rates)

P_{out}	+4 dBw 3 watts
Transmitter Antenna Gain (dB)	+54
ERP (dBw)	+58
Pattern Factor (dB)	-3
Net ERP (dBw)	+55
Path Loss (dB)	-204
Power Density at Receiver Antenna (dBw)	-149
Receiver Antenna Gain (dB)	+44
Power at Receiver Terminal (dBw)	-105
Line Losses (dB)	3
Converter Input (dBw)	-108
Receiver Noise Figure (dB)	3
Reference (dBw)	-111
KTb (dBw)	-127
C/N (dB)	+16
Modulation Gain (dB)	+25
Signal to Noise out	+41

Suppose that it is desired to scan the entire earth, in sunlight only, with a resolution of 1 statute mile at the subsatellite point. The projected area of the earth is approximated by a circle 8000 statute miles in diameter requiring at least 8000^2 or 64×10^6 TV resolution elements. This is equivalent to 64 frames at 1000 lines per frame. In order to make these same observations in color, $4 \times 64 = 256$ 1000-line frames will be required. A standard 4 to 5

MHz video channel will transmit $30/4 = 7.5$ frames/sec; therefore, under these conditions the earth can be observed once in $\frac{256}{7.5} = 34.133$ seconds.

The scanning can be accomplished by some combination of rotating mirrors, multiple lenses, moving camera, and "rocking" the satellites.

For these sunlight observations, the required camera apertures will be relatively modest. Also, the 1000-line vidicon weighing less than 10 pounds will be suitable.

If desired, scanning can be stopped and the entire 7.5 frames/sec devoted to one area. It is also feasible, as can be seen in Table 8.7-1, to transmit the 1000-line pictures at 30 frames/sec; however, such a requirement appears unlikely.

If very high resolutions are desired, say, down to 0.1 nautical mile or 600 feet, an aperture of about 20 cm (roughly 8 inches) will be required. For testing purposes, such a lens might be held stationary, pointing vertically downward. Detailed observations (to 0.1 nautical mile) would then be possible over an area at approximately 100 x 100 nautical miles directly beneath the satellite.

For observations at night, preliminary calculations indicate that an aperture of at least 6 inches and an image orthicon camera will be required.

Observations into part, but possibly not all, of the terminator can be made by using an extended image orthicon (EIO) and an occulting disc or other techniques to block out interference from the sunlit areas.

It is also possible to observe the earth with IR sensors, e. g., the Nimbus HRIR subsystem or an IR vidicon. However, from synchronous altitudes both resolution and signal strength will pose problems. The availability of these devices for the ATS Program has not yet been established.

8.7.3.1.4 Feasibility and Costs

The feasibility of daylight observations from space with vidicon cameras has been very well established. Color observations can be done with filters, either mechanically inserted or switched-in by opening and closing alternate shutters. Color transmission will be frame-sequential. Scanning appears to offer no serious technical problems, nor does incorporation of a large stationary aperture. The EIO suggested for night observations has not yet been space qualified, but should offer no serious difficulty.

The increasing cost of the experiment to the satellite is essentially the weight and power requirement of the sensors and optics. (The antennas, transmitter, and orientation control are not charged to the experiment.) These are summarized below in Table 8.7-2.

Table 8.7-2. Weight and Power Requirements of Sensors and Optics

Item	Weight (lb)	Power (watts)
Vidicon	10	10
Vidicon Optics*	10	5
EIO	30	40
EIO Optics	20	10
*Includes color filters		

8.7.3.2 FM and TV Direct Broadcast

General - A limited augmentation of the on-board equipment required in the parabolic antenna system is permissible to support design and development of a satellite system for direct broadcast of radio and television programs to the home by demonstration, by discovering and/or helping to solve technical problems, and by investigating audience reaction as a function of the quality of programs and any special expenses.

8.7.3.2.1 Specific Objectives

In support of the general purposes, the following specific objectives are sought:

- a. To transmit high-quality audio program material, e. g. , music - directly from the ATS-4 satellite to home television sets, audio sections only, without any requirement for the listeners to buy special equipment. Modulation is FM.
- b. To transmit the same type of material to home television sets whose owners have low-gain antennas (8 dB or so).
- c. To transmit the same type of material to home television sets whose owners have high-gain antennas (about 18 dB) and to properly equipped monitoring stations.
- d. To transmit high-quality television signals to educational and distribution stations on the ground.

8.7.3.2.2 Technical Discussion

Objective a, above, would be quite useful, because of the substantial audience participation. Objective b would be still fairly useful, while c would be merely incidental. Objective d will be discussed at the end of this paragraph. As will be seen, little additional onboard equipment will be required if Objective a is achieved.

The discussion in the present section will suggest that with a modest addition of on-board transmitter capability, involving an additional 15 pounds or so, Objective a can be achieved over selected areas.

The transmission link considered would involve UHF channels 70 to 83, in the frequency range of 806-890 MHz. Ordinary receivers having noise figures of the order of 10 dB are assumed. The parabolic antenna has a gain of about 35 to 36 dB in this range.

The transmission link considerations for such a link are shown in Table 8.7-3. As can be seen from this table, accomplishment of purpose No. 1 with 10 watts radiated power is quite marginal. Either the power must be increased by several dB, or the listeners must be asked to buy a more expensive antenna. Such an antenna would cost not less than \$10.00 nor

Table 8.7-3. Transmission Link Characteristics Audio FM Broadcast
to Home TV Receiving Sets

P_{out}	+ 17 dBw, 50 watts
Transmitter Antenna Gain (dB)	35
ERP (dBw)	+52
Path Loss (dB)	-184
Power Density at Receiver Antenna (dBw)	-132
Receiver Antenna Gain (dB)	3
Power at Receiver Terminals (dBw)	-129
Line Losses at Receiver (dB)	2
Converter Input (dBw)	-131
Receiver Noise Figure (dB)	10
Reference (dBw)	-141
KTB (dBw)	-153
C/N (dB)	12
S/N (dB)	50

more than \$35.00, including installation charges. This agrees approximately with available data, which estimates the field strength requirements for FM broadcasts for various receiver, antenna and location configurations as shown in Table 8.7-4.

The conversion between on-board transmitter power and field strength of the antenna is given by the following expression:

$$\frac{P_T G_T}{2 \pi d^2} = \frac{E^2}{120 \pi}$$

where

P_T = Transmitter power, in watts

G_T = Antenna power gain (about 35 dB)

d = Transmission distance, in meters

E = Field strength, in volts per meter

Field strength for various on-board transmitter powers are given in Table 8.7-5.

The field strength uses shown in Table 8.7-5 allow the station types specified to be spaced across the antenna beam between the 3 dB points. Since the beam is approximately 2.6 degrees wide, these points are about 1100 miles apart. By restricting the station locations to a small area near the center of the beam (say, a city and an adjacent rural area), the power requirements for a given performance level can be reduced by a factor of about two. This will permit reaching with 10 watts radiated power any listener, rural or urban, who is willing to buy a low-gain antenna (\leq \$35.00). At the other end of the power scale, a radiated power of 65 watts would permit the satellite to reach any station in this limited area without any special antenna. These options can be summarized, as shown in Table 8.7-6.

Table 8.7-4. User Accessibility versus Field Strength

Antenna	Location	Output S/N (db)	Preamplifier Noise Figure Gain		Field Strength, Microvolts/Meter
Loop	Urban	37.5	No		100
Loop	Urban	37.5	8	17	97
Loop	Rural	37.5	No		61
Low Gain	Urban	37.5	No		50
Loop	Rural	37.5	8	17	50
Low Gain	Rural	37.5	No		45
Low Gain	Urban	37.5	8	17	35
Low Gain	Rural	37.5	8	17	25
High Gain	Urban	37.5	No		15
High Gain	Rural	37.5	No		15
High Gain	Urban	37.5	8	17	10
High Gain	Rural	37.5	8	17	10

Table 8.7-5. Field Strength versus On-Board Radiated Power

Radiated Power (watts)	Field Strength Microvolts/Meter	Lowest Receiver Performance Level at Which Usable
10	28	Rural with low-gain antenna Any with high-gain (3) antenna
20	40	Any with low-gain (2) antenna
50	63	Rural with loop (1) antenna Urban with low-gain antenna
100	89	Rural with loop antenna Urban with low-gain antenna
126	100	Any
250	140	Any

(1) Loop antenna is the internal antenna furnished with a home television receiver.

(2) Low-gain antenna is the approximately 8 dB simple antenna, e.g., an 8 element Yagi, costing somewhere between \$10.00 and \$35.00 installed.

(3) High-gain is about an 18 dB gain installation, probably something like a 4 foot paraboloid or a helix about 6 feet long and 2 feet in diameter. Cost installed is estimated to be of the order of \$75.00 to \$125.00

Table 8.7-6. Limited Area Audience Experiment

Audience	Radiated Power (watts)	Prime Power (watts)	Modifications to On-Board Equipment Required
Any with low-gain antenna (\$35.00) in area	10	30	None
Any set in area	65	165	Larger 800 MHz power amplifier, about 15 pounds weight increase

It will be assumed in the present section that both types of experiments will be conducted at the higher power level (65-75 watts radiated) involving a relatively large audience participation in each of a number of major metropolitan areas. Longer term programs will be conducted at the low power level (10-20 watts radiated); these can be heard via any TV set having a low-gain antenna available.

The power levels discussed above include the requirements for transmitting the video carrier. This is required for demodulation (demodulators in use operate on the intercarrier frequency relationships rather than on the absolute frequency of the audio carrier).

Transmitting high-quality TV program material to a central ground station for re-broadcasting will demonstrate the capability of a broadcast satellite to broadcast to education stations, distribution stations, etc., and by scaling, will verify the power required to broadcast to home television sets.

Two alternate modulation techniques appear plausible: the conventional vestigial sideband AM and wideband FM. Both are shown in the link calculations of Table 8.7-7. The VSB transmission requires more satellite power, but the FM requires transformation from FM to VSB and is hence somewhat less realistic, as an investigation tool, for later direct broadcast.

Table 8.7-7. TV Broadcast Configurations Link Calculations

P_{out}	+16 dBw	40w	+8 dBw	6.3w
Transmitter Antenna Gain (dB)	+35		+35	
ERP (dBw)	+51		+43	
Path Loss (dB)	-184		-184	
Power Density at Receiver Antenna (dBw)	-133		-141	
Receiver Antenna Gain (dB)	+36		+36	
Power at Receiver Terminals (dBw)	-97		-105	
Line Losses at Receiver (dB)	2		2	
Converter Input (dBw)	-99		-107	
Receiver Noise Figure (dB)	6		6	
Reference (dB)	-105		-113	
KTB (dBw)	-137		-128	
S/N (dB)	32		32	
Modulation Gain	0		17	
C/N (dB)	32		15	

The ground system will be identical in each case; a 30-foot paraboloid to provide about 36 dB gain, and a 6 dB receiver.

It will be assumed in this paragraph that both types of experiments will be performed, and comparisons of quality made. The necessary transmitter power for the VSB AM mode will already be available if the FM broadcast experiment is performed. The material can be re-broadcast by local TV stations if station time is made available.

a. Background Information Required

Parabolic antenna system performance.

b. Position in Operational Sequence

After initial checkouts of all systems.

c. Procedures

1. Point parabolic antenna toward selected area.
2. Activate transmitter and selected receivers and verify operation and establishment of link.

FM Broadcasts

3. Transmit test message and verify quality
4. Transmit program at high power, monitoring continuously
5. Transmit program at low power, also monitoring
6. Gauge audience reaction as a function of technical quality

TV Broadcasts

7. Verify operation and establishment of link
8. Transmit test message and verify quality
9. Transmit program on VSB AM, monitoring continuously
10. Transmit program on FM, also monitoring continuously
11. Evaluate quality and gauge audience reaction if re-broadcast is available

d. Data Produced

FM

Audience reaction as a function of technical quality and signal levels

Verification that the technical performance with various power levels, antenna gains and receiver noise levels is as predicted

TV

Signal quality as a function of modulation, verification that technical relationships are as predicted

Limited audience reaction if re-broadcast is available.

e. On-Board Equipment

Parabolic antenna with 800 MHz transmitter augmented for 65 watts radiated power.

f. Special Ground Equipment

Monitoring station, incorporating various antennas, receivers and signal recording and monitoring equipment, at each test area, together with SSB AM and FM reception for TV.

Transmission facility, to transmit program material to satellite.

g. Time Required

Six hours.

8.7.3.3 Navigation and Air and Ship Traffic Control

8.7.3.3.1 Nature and Purpose

As intercontinental air use increases, the need for effective traffic control and efficient utilization of the air routes increases. Additionally, in emergency situations both ships at sea and aircraft need more effective and reliable techniques to determine their position in order to notify rescue services.

To assist in fulfilling these navigational and control needs, various navigational satellite systems have been proposed. These satellite systems consist of a number of satellites in orbit together with a control station and several reference stations. By measuring distances

from three reference stations the satellite position is determined. Measurement of the direction of several reference stations in relation to the satellite axes determines the satellite attitude. Similar measurements of distance and directions are made to the ship or aircraft. These measurements completely determine the ship or aircraft position.

8.7.3.3.2 Procedures and Equipment

In order to determine the ship or aircraft direction, an experiment to determine the performance of the interferometer is indicated. The interferometer is essentially two satellite antennas separated by a known distance. The ground transmitted wavefront exhibits a phase difference because of the difference in path lengths to the two antennas. This permits the calculations of the bearing angle.

8.7.3.4 Communications With Low-Orbit Spacecraft

8.7.3.4.1 Nature and Purpose

Use of a satellite link to the Manned Space Center bypassing the ground link network could be tested for further Apollo and MOL flights. Four equatorial synchronous satellites spaced at 90 degrees apart with one above the NASA Manned Space Center would permit direct communication from the Spacecraft to the Manned Space Center without the use of ground links. If successful, such an installation might reduce considerably the number of ground stations needed, and provide continuous high data rate communications between the spacecraft and Manned Space Center.

The problem of satellite-to-satellite transfer of information where large dishes and narrow beams are used implies sophisticated pointing capabilities. Systematic pointing experiments using mechanical steering, electronic steering and control of vehicle attitude are indicated.

8.7.3.4.2 Value

An operational synchronous communication relay and tracking system would provide continuous very high data rate communications with the Manned Space Center, as well as continuous, high-accuracy tracking. In addition, a military version, by using frequencies to which the atmosphere is virtually opaque, could provide near-complete immunity to intercept or jamming by enemy surface installations.

The same installations, either civilian or military, can provide range, range rate and angle data on the spacecraft, essentially continuously.

A successful installation may then provide:

- a. More reliable, continuous, higher data rate communication
- b. Better communications security
- c. More continuous tracking data
- d. Continuing, high data rate communications between widely separate surface range installations
- e. Removal of requirements for a number of surface range installations, including ships, thereby reducing the overall cost of the worldwide range installations.

8.7.3.4.3 Equipment and Procedures

The experiment objectives will be to demonstrate feasibility, estimate attainable performance and costs of an operating system and evaluate the major problems. As in most of the communications experiments, a major part of the experimental work will consist of measuring signal strength (or signal-to-noise ratios) antenna patterns, and scan rates, which can best be done at a properly equipped surface station. In addition, it will be useful, if scheduling problems can be solved, to actually relay data from a low-orbit spacecraft - Apollo, MOL, etc.

As can be seen from Table 8.7-8, to relay video information would require an antenna of considerable gain on the low-orbit spacecraft. However, for test purposes the data rate can be

reduced, say, to that of an audio channel, permitting voice communication, data to above 40,000 bits per second (bps), etc., so that the high gain antenna will not be necessary.

Tracking of the low-orbit spacecraft by the large antenna will be required. Normally, the spacecraft will move across the earth, crossing an angle of about 17 degrees in approximately 45 minutes, or at a rate of about $\frac{17}{45} = 0.38$ degree/min. This rate is highly predictable and requires no high accelerations.

Table 8.7-8. System Performance Spacecraft Relay - Spacecraft to Satellite - TV Bandwidths

P_{out}	+11 dbw 12.6 watts
Transmitter Antenna Gain (dB)	+34 (2-foot paraboloid)
ERP (dBw)	+45
Pattern Factor (dB)	-3
Net ERP (dBw)	+42
Path Loss (dB)	-204
Power Density on Receiving Antenna (dBw)	-162
Receiver Antenna Gain (dB)	+54
Power at Receiver Terminal (dBw)	-108
Line Losses	0
Converter Input (dBw)	-108
Receiver Noise Figure (dB)	3
Reference (dBw)	-111
KTB (dBw)	-127
C/N (dB)	+16
Modulation Gain (dB)	+25
S/N (dB)	+41

8.7.3.4.4 Costs

Costs, in terms of weights and power requirements, will be quite small.

8.7.3.5 Multiple Access Communications Satellite

Work is underway toward the development of a "multiple access" communications satellite, i. e. , a satellite which can accept signals simultaneously from a number of transmitting stations and relay each signal to its designated recipient. Such a satellite must of course allocate its frequency and power among its users and must respond in some acceptable fashion to overloads and interference (in the case of the enemy, purposeful interference).

Basically, the allocation of the satellite's resources may be made by:

- a. Frequency division multiplexing
- b. Time division multiplexing
- c. Spread spectrum techniques (noise modulation)
- d. Combinations and special cases of the above

The proposed experiment will, among other things, compare these techniques in terms of traffic handling capability, error rate, susceptibility to jamming, etc.

8.7.3.5.1 Value

The multiple access capability will provide the most flexible and useful general purpose communications relay satellite for either civilian or military use.

8.7.3.5.2 Equipment and Procedures

It should be pointed out that the proposed experiment will be only a small part of the process of developing an operational multiple access satellite. Most of the work will consist of theoretical analysis, ground-based experiments, etc.

The tests will consist essentially of transmitting data to the satellite and measuring performance while the major parameters are systematically varied over their ranges. These parameters will include:

- a. Total data rate
- b. Number of channels
- c. Noise
- d. Modulation techniques
- e. Acquisition techniques

The performance parameters will include:

- a. Achieved data rates
- b. Error rates or distortion
- c. Time to establish contact
- d. Reliability (i. e. , probability of completing a call or data transmission as a function of elapsed time)

Probably most the the experimental work will be done using a single ground station for both transmission and reception, as well as command and control, insertion of interference. etc.

It may also be advisable to make measurements of such physical parameters as time delay, differential phase delay, polarization, effects of weather, etc. , during the experiment.

8.7.3.5.3 Costs

The experiment will require, in addition to the antennas, approximately 50 pounds of electronics to investigate the various techniques, having a power drain of perhaps 25 watts. The duration of the experiment will be determined by the experiment design.

8.7.4 PASSENGER EXPERIMENTS

There is an extremely large number of possible experiments of scientific interest which might be flown as passengers aboard a stabilized satellite at synchronous altitude. Some of the more interesting ones are discussed briefly below.

8.7.4.1 Millimeter Communications and Transmission

It presently appears probable that millimeter waves will become increasingly important in communications in space, complementing the later development of laser communications. Millimeter waves may also be expected to be important in space in radiometry, radio astronomy, and active radar-type sensing.

A relatively small antenna operating at 35 GHz aboard the ATS-4 would permit interesting initial investigations, supplementing those proposed for the other ATS programs, into atmospheric transmission, pointing, radiometry, etc. If feasible, a small phase-steered array should be considered; however, the small sizes and severe tolerances impose difficult problems. A paraboloid, independently steered, would have to be only some 1 to 2 feet in diameter to achieve reasonable gain.

8.7.4.2 Laser Communications and Transmission

Development of a laser suitable for initial experiments from the ATS-4 system should be seriously considered. Initial studies would include atmospheric effects, acquisition problems, beam breakup problems, and overall link gain measurements. If both a laser and millimeter system can be afforded, direct comparisons should be most illuminating.

8.7.4.3 Earth Radiation Measurements

Measurements of the characteristics of radiation from the earth in the visual and IR are useful for scientific studies of the planet. These could be usefully performed from a stabilized satellite. Optical instrumentation could also be readily swept across the terminator, synchronized with it, etc., to observe the behavior of earth, clouds, atmosphere, etc., between day and night.

8.8 OPERATIONAL SYSTEM FOR EXPERIMENTS

8.8.1 GENERAL

In order to achieve maximum value from the four major experiments, an integrated operational system must be carefully designed and thoroughly tested prior to flight. The system would have the following objectives:

- a. Maximum experiment data collection
- b. Efficient coordination and control of experiments
- c. Coordination of facilities with other NASA programs
- d. Accurate measurements and efficient data processing
- e. Timely analysis of experiment results
- f. Meaningful documentation and adequate reporting procedures

The primary task required to assure the most efficient operational system is that of detailed planning. The priority of the experiments has been assumed to be Parabolic Antenna, Orientation Control, Interferometer, and Phased Array in sequence. Although this sequence will be generally followed in carrying out the experiment plan, it must be recognized that all experiments must be operationally interlaced, particularly during the first few months of flight, to assure the following:

- a. Maintenance of an optimum power profile
- b. Efficient utilization of ground stations
- c. Completion of the basic goals of all experiments during the early flight phase
- d. Attainment of the most accurate data possible through a deliberate, well-planned sequence of measurements
- e. Feedback of experimental data into planning throughout the flight

The recommended experiment plan, broadly outlined in this section, is therefore based on the following general sequence:

- a. Verification of spacecraft operational/functional status

- b. Verification of operational/functional status of each experiment
- c. Checkout and accurate calibration of the Orientation Control system functional characteristics
- d. Calibration of the high accuracy sensors
- e. Determination of the operational capability of high accuracy sensors for Orientation Control
- f. Accurate determination of boresights and reference axes of each system relative to a selected reference system
- g. Pattern measurements of each antenna
- h. Signal transmission and receiving characteristics of the communications experiments
- i. Thermal characteristics determination
- j. Determination of the effects of mechanical and electrical influences
- k. Reliability and long life characteristics

8.8.2 EXPERIMENT OPERATIONAL SYSTEM REQUIREMENTS

A simplified functional flow diagram of the total operational system is presented in Figure 8.8-1. This diagram is intended to demonstrate the operational and/or decision making control between each segment of the system.

8.8.2.1 Operational Flow

Detailed experiment procedures, adequately developed and tested prior to launch, would be implemented under direction of the ATS-4 OCC at GSFC throughout the flight. Command loads, generated at the center, would be transmitted to the designated tracking station via SCAMA lines along with operational instructions, experiment schedules, and information.

Each tracking station would be prescheduled for ATS-4 operations in a manner consistent with its overall scheduling of other programs, such as ATS and Nimbus. It is considered extremely important that a "fit" of ATS-4 activities and schedule with those of other programs be attempted very early in the program, and iterated frequently until all aspects of experiment design and nominal operational plans are resolved. ATS-4 spacecraft and experiment activity will be primarily dictated by power profile and by time of day. Some experimental measurements will require short durations of spacecraft/ground station operation with short

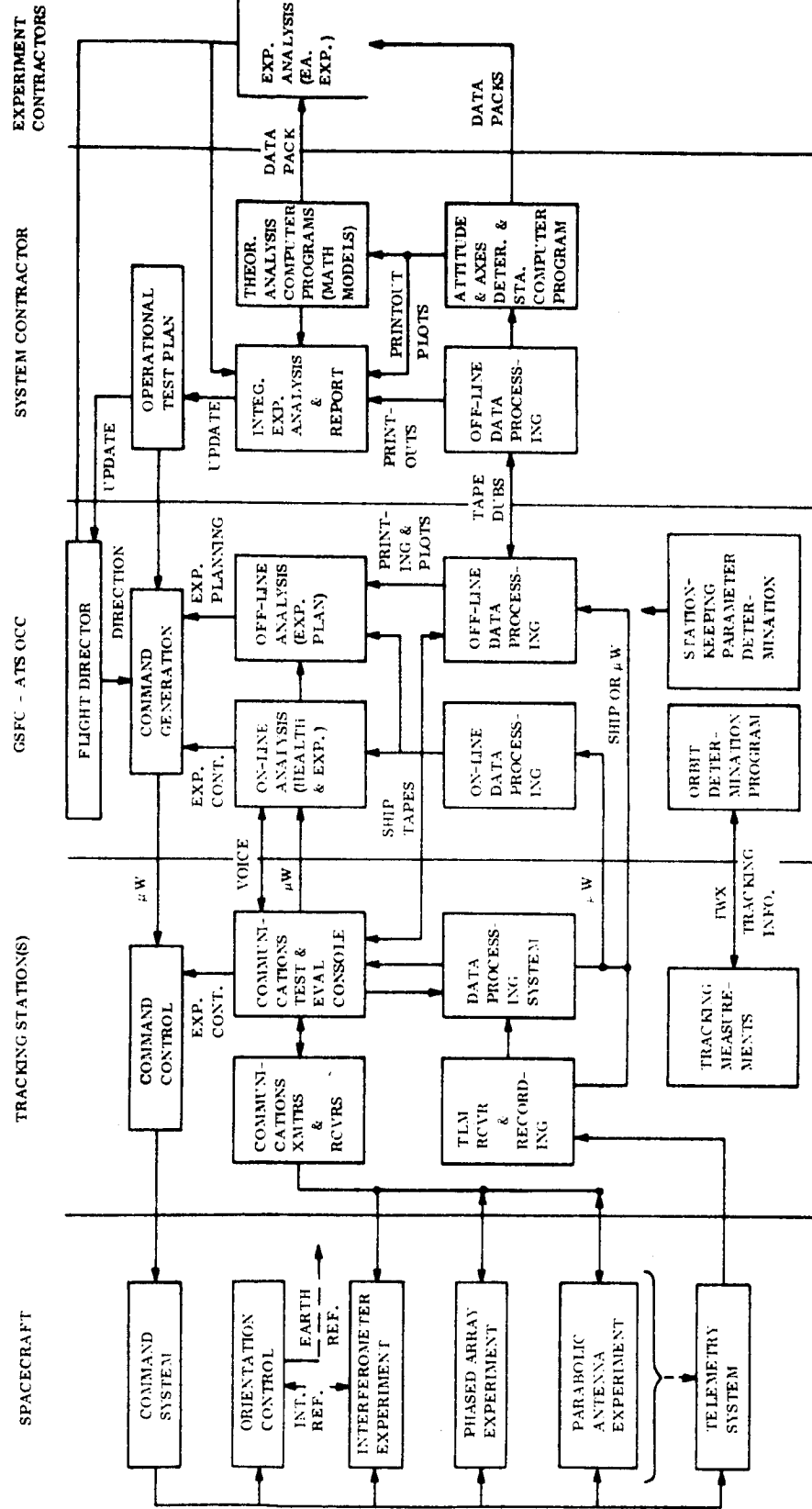


Figure 8.8-1. Operational System Simplified Functional Flow Diagram

intervals (e.g., 15 minutes of operation/hour for 24 hours). Other experiments will require a long, continuous operation at a pre-established time of day and/or year (i.e., for several hours). Still others can be implemented on a "when available" basis.

It is recognized that contingencies or the requirements for gaining increased experimental data may dictate a change in schedule for the ATS-4 satellite or for other programs. Therefore the same effective planning and control flexibility presently exhibited must remain available.

Data from both the spacecraft telemetry system and communications experiment evaluation consoles would be collected at the tracking stations, annotated with system time and pre-processed in the following ways:

a. **Telemetry Data**

1. Demodulation
2. Recording of total wavetrain on magnetic tapes and shipment to ATS-4 OCC
3. Selected data reduction conversion to engineering units
4. Selected data converted to compatible format for transmission to the ATS-4 OCC via microwave link and/or phone lines.

b. **Experiment Measurements**

1. Recording and display at communications test and evaluation console
2. Tape recording with time annotation and shipment to ATS-4 OCC of all data possible to record
3. Readout of selected critical measurements via voice net(s) and TWX
4. Transmittal of selected measurements by microwave link simultaneously with TLM data

Data arriving at GSFC would be processed in the following ways:

- a. On-line computer conversion printout, plot and display for near-real time integrated control by ATS-4 OCC flight director and his team
- b. Off-line computer conversion, printout plot and calculations necessary to verify experimental data and spacecraft operational performance as required to perform detailed planning of subsequent operations and experimentation.

Data received at the integrating contractor's facility would be processed through computers which would accomplish in part the following tasks:

- a. Conversion to engineering units
- b. Merging of telemetry, experiment and orbit data
- c. Calculations involving 2 or more measured (telemetry and/or experiment) parameters
- d. Mean value and deviation (statistical) calculations
- e. Printouts in data pack formats for experimenters
- f. Automated plots
- g. Geometrical transform calculations
- h. Math model correlations
- i. Antenna pattern mapping
- j. Best fit calculations

8.8.2.2 ATS-4 Ground Station Operational and Experiment Capability Requirements

NASA publication S2-0000 (Section 5.0) for the ATS (A through E) program contains a detailed summary and description of Ground Stations assigned to ATS program operations. The stations will require similar control and data equipment and operating procedures for the ATS-4 program. It is expected that some of the communications experiments test and evaluation consoles and equipment may serve both programs, providing the experiments are of similar design and utilize similar frequencies. However, the wide range of frequencies required for the ATS-4 experiments, particularly those for the parabolic antenna, require

unique antenna feed and receiving/transmitting equipment. To define and estimate cost of the equipment adequately requires resolution of the tradeoff criteria presented in Table 8.8-1.

Table 8.8-1. Experiment and Ground Station Capability Tradeoffs

Function or Experiment	Frequency	Alternatives and Stations	Recomm.	Remarks
Command and Telemetry	1.7-1.85	1. One station R,		
	2.2-2.3	2. Two stations R, T		
		3. Two stations R, M		
		4. Three stations R, M, T		
		5. Four stations R, M, T, O	X	R, M for experiments T, O, for launch orbits and contingencies
Parabolic Antenna Experiment Transmitting	1.7	1. All frequency R capability M	X	Requires feed channels
	2.1 8.0	(2 or more T feeds)		
Exp. Receiving	0.1	2. Frequencies R compatability M	X	Allows simultaneous parab. exp & CMD/TLM
	0.8	TLM & CMD T	X	
	2.3	only (single feed system 1.7-		
	7.3	1.85/2.1-2.3)		
Phased Array Transmitting and Receiving	3.0	1. One station R,		May require one station for TLM/CMD, or multiply Two fixed stations desired for full exp. value and aircraft transmitting and/or receiving to determine boresight and antenna patterns
		2. Two stations R, M		
		3. Three stations R, M, T		
		4. Two stations R, M, & A/C A	X	
		5. Three stations R, M, & A/C T, A		
		6. Use experiment stations (additional to others)	X	
Interferometer Transmit	10.0	1. One station R, 2. Two stations R, M 3. Three stations R, M, T	X	Combine with 7-8 GHz feeds to allow simultaneous phased array and/or highest frequency parabolic exp

The capability tradeoffs are based on the assumption that a) existing 40 and 85-foot dish antennas will be used, with different multi-feeds installed for various experimental phases or tasks, and b) a single multi-feed arrangement which can cover all ATS-4 frequencies with a single antenna is impractical from the standpoints of development cost and complexity.

Table 8.8-2 is a summary of recommended transmitting/receiving frequency capability with a breakdown of minimal feed arrangements considered practical from the experimental point of view.

The minimal system outlined results in the following criteria for experimental control:

- a. Command and telemetry capability can be maintained by any of the three ATS-4 stations while conducting parabolic antenna experiments involving 1.7, 2.1, or 2.3 GHz frequencies.
- b. One station can conduct phased array and/or parabolic antenna (8.0-7.3 GHz) simultaneously with interferometer control, but a second station would probably be required for command and telemetry when any of these experiments were in process.
- c. Interferometer control would not be available for pointing to a station experimenting with parabolic antenna experimental frequencies other than 7.3 and 8.0 GHz.
- d. Experiments involving large on-board step-down or step-up of frequencies (i. e., from 8.0 GHz received by the spacecraft to 0.8 transmitted by the spacecraft) could not be conducted except with one station on-boresight, and another off-boresight. Furthermore, for the special case presented, command and telemetry would either not be available or a third station would be required.
- e. Simultaneous coordinated experiments involving monopulse and interferometer control modes could be conducted (monopulse at 8.0 GHz). A second station is required for telemetry and command.

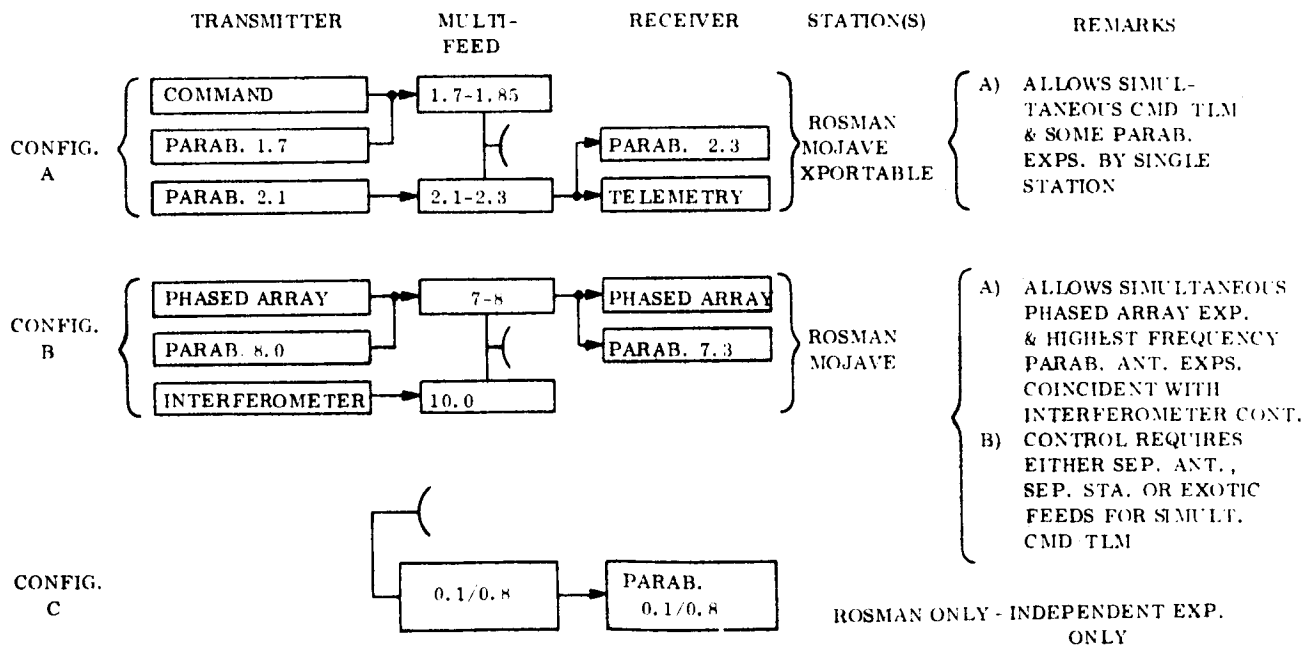
Table 8.8-2. Required and Recommended Transmitting/Receiving Frequencies for Ground Stations

	Transmitting Frequencies				Receiving Frequencies						
	CMD 1.7- 1.85	Parabolic Antenna 1.7 2.1 8.0			Phased Array 7	Interfero- meter 10.0	TLM 2.2- 2.3	Parabolic Antenna 0.1 0.8 2.3 7.3			Phased Array 8
Rosman	(X)	(X)	(X)	(X)	(X)	(X)	(X)	(X)	(X)	(X)	(X)
Mojave	(X)	X	X	X	(X)	X	(X)		X	X	(X)
XPortable	(X)	X	X				(X)		X		
Aircraft					(X)						X
Extra G/S	X						X				

LEGEND: (X) Required
X Desirable/Recommended

NOTES

1. Antenna feeds required are unique to ATS-4
2. Minimal feed arrangements are diagrammed below (Aircraft excluded)



It is evident that the experiment criteria presented above can be modified to produce far more flexibility in all experiments by either:

- a. Further combining feeds
- b. Installing an additional antenna at either Rosman or Mojave.

The second alternative is recommended (without having a detailed cost tradeoff comparison between the two approaches) for the following reasons:

- a. Use of the additional antenna continuously for ATS-4 with control of other satellite programs from the existing antenna.
- b. Use of both antennas at the chosen site when required for those experiments which involve a wide range of frequencies handled by a single ground station. This would make the other primary ground station independently available for other programs.
- c. The possibility exists that the use of a single feed for transmitting and receiving similar frequencies simultaneously may jeopardize quality of the experimental frequencies. For example, operating the phased array at 7-8 GHz and monopulsing through the parabolic antenna at 7.3 GHz simultaneously from the same feed and antenna dish could result in degradation of the transmitted signal which would bias the monopulse lobes. Two separate antennas at the same location would help assure against such supposed possibility of degradation should it become a problem.

The capabilities of an operational system based on an additional antenna available for ATS-4 (assumed at Rosman) are illustrated in Figure 8.8-3. Each antenna is assumed to have available feed configurations as previously shown in Table 8.8-2; these are shown in the column in Table 8.8-3 labeled "Feed Configurations".

The bases for selection of these configurations were:

- a. Feed configuration A (required for TLM, CMD capability) must be available at all times at one station.

**Table 8.8-3. ATS-4 Operational Ground Station Configuration Matrix
Assuming Additional ATS-4 Antenna at Rosman**

Station	Antenna No.	Feed** Configuration	System Configuration										
			1	2	3	4	5	6	7	8	9	10	11
Rosman	1	A,O	A	A	O	O	O	O	O	A	O	A	A
Rosman	2	B,C	B	C	B	B	C	C	C	B	B	-	C
Mojave	1	A,B,O	O	B	A	O	A	B	O	B	B	O	O
Transport	1	A,O	O	O	O	A	O	A	A	O	A	O	O
Aircraft	1	(ϕ T/R)	ϕ	ϕ	ϕ	ϕ	O	ϕ	O	O	O	O	O
Experiment Coverage	Command		R1	R1	M	T	M	T	T	R1	T	R1	R1
	Telemetry		R1	R1	M	T	M	T	T	R1	T	R1	R1
	A Transmitter 1.7		R1	R1	M	T	M	T	T	R1	T	R1	R1
	Transmitter 2.1		R1	R1	M	T	M	T	T	R1	T	R1	R1
	Transmitter 8.0		R2	M	R2	R2	-	M	-	R2/M	R2/M	-	-
	A RCV 0.1		-	R2	-	-	R2	R2	R2	-	-	-	R2
	RCV 0.8		-	R2	-	-	R2	R2	R2	-	-	-	R2
	RCV 2.3		R1	R1	M	T	M	T	T	R1	T	R1	R1
	RCV 7.3		R2	M	R2	R2	-	M	-	R2/M	R2/M	-	-
	ϕ Transmitter 7-8		R2	M	R2	R2	-	M	-	R2/M	R2/M	-	-
	*2 STA (EITHER) OR A		A	A	A	A	-	A	-	*	*	-	-
	ϕ RCV 7-8		R2	M	R2	R2	-	M	-	R2/M	R2/M	-	-
	Interferometer		R2	M	R2	R2	-	M	-	R2/M	R2/M	-	-
	G.S. Avail. Other Prog.		M/T	T	R1/T	R1/M	R1/T	R1	R1/M	T	R1	M/T	M/T

**See Configurations Diagrammed in Table 8.8-2.

LEGEND: A, B, C - Selected ATS-4 antenna feed configurations
O - Configurations required for other NASA programs
R1, R2 - Rosman antennas
M - Mojave
T - Transportable
A - Aircraft
 ϕ - Phased array experiment Transmitter/RCV

- b. System configurations which resulted in redundant A feed configurations were deleted because they merely represent combinations.
- c. Because Rosman was considered the primary station only those system configurations which included Rosman in some capacity were listed (e.g., configuration 9 could be used for single A & B feeds without Rosman B feed, but most likely configuration 1, 2 or 3 would be selected for this purpose).
- d. Aircraft utilization is shown only when operating with a single B feed configuration (primarily for use with phased array experiments). The aircraft is optional in each configuration listed and not necessarily required.

Eleven different ground system configurations are therefore considered available.

These ground system configurations are shown in Table 8.8-3, and represent stations which are used, and the feed configuration used at each station as the basis for operational planning.

In configuration 1 of Table 8.8-3, for example, both Rosman antennas (and if required the aircraft) are used, but Mojave and the Transportable Station are not. Rosman Antenna No. 1 will be in Feed Configuration A, No. 2 in Feed Configuration B, and the Aircraft in its sole available Configuration, ϕ . Mojave and the Transportable Station, not being used, will be in Configuration O, for "other," which merely means that they are available for other programs.

Below the line in Table 8.8-4, the remainder of the Configuration 1 Column 1 summarizes the allocations of the various functions in this particular ground system configuration. As can be seen, these are:

- Command - Rosman Antenna No. 1
- Telemetry - Rosman Antenna No. 1
- Transmission at 1.7 and 2.1 GHz -(Rosman Antenna No. 1)
- Transmission at 8.0 GHz - Rosman Antenna No. 2
- Reception at 0.1 and 0.8 GHz - No capability in this configuration
- Reception at 2.3 GHz - Rosman Antenna No. 2

- Reception at 7.3 GHz - Rosman Antenna No. 2
- Transmission and reception with the phase - steered array antenna - Rosman Antenna No. 2 and the Aircraft
- Available for other Programs - Mojave and the Transportable Station

As can be seen from the above explanation, the material below the line in Table 8.8-3 is redundant, i. e., it is merely an expansion of station assignments already indicated by the Feed Configurations shown above the line. This material is included here to reduce the necessity for referring to Table 8.8-2 and make Table 8.8-3 more nearly self contained.

This ground operational system will be flexible enough to conduct virtually every possible experiment without impeding other programs or requiring frequent antenna reconfiguration. This is partially confirmed in the last line of Table 8.8-3, in which it can be seen that for all ground operational system configurations at least one antenna is available for other programs, and for most configurations two antennas are available.

An operational system without the extra antenna at Rosman is shown in Table 8.8-4. As can be seen this is much less flexible. Some configurations are not available at all, and in others no antennas are available for other programs. In only one configuration are two antennas available for other programs.

In the discussion of experiment control in the next section, it will be assumed that the additional antenna is available.

8.8.3 EXPERIMENT CONTROL

In conducting the experiments planned for the ATS-4 satellite, it is necessary to utilize all the systems involved in ATS-4 operations in a manner which is efficient and which results in maximum experimental value. Therefore, it appears that for most efficient use of experimentation time, the experiments should be interlaced as much as possible and in a manner that would optimize data collection for all experiments involved.

**Table 8.8-4. ATS-4 Operational Ground Station Configuration Matrix
Assuming One Antenna Per Station with Interchangeable Feeds**

Station	Feed** Configuration	System Configuration (2)										
		1	2	3	4	5	6	7	8	9	10	11
Rosman	A, B, C, O	A	B	B		C	C	C		B	A	
Mojave	A, B, O	B	A	O	Not Available	A	B	O	Not Available	B	O	Not Available
Transport.	A, O	O	O	A	Not Available	O	A	A	Not Available	A	O	Not Available
Aircraft	∅ _{T/R}	∅	∅	∅	Not Available	O	∅	O	Not Available	O	O	Not Available
GS Avail. Other Prog.		T	T	M	Not Available	T	O	M	Not Available	O	M/T	Not Available

NOTE: (1) Configuration numbers and experiment coverage correspond to those presented in Table 8.8-3.

**See configurations diagrammed in Table 8.8-2.

LEGEND: A, B, C - Selected ATS-4 antenna feed configurations
 O - configurations required for other NASA programs
 R1, R2 - Rosman antennas
 M - Mojave
 T - Transportable
 A - Aircraft
 ∅ - Phased array experiment

To accomplish this, integrated tasks should be defined so that measurements and operational criteria allow efficient detailed and independent procedures to be written for each. This has been accomplished on a preliminary basis and is presented in Table 8.8-5.

Individual experimental measurements were defined and coded in Sections 8.3 5.1, 8.4.2, 8.5.2, and 8.6.4 1. These were studied and combined into the 35 integrated tasks presented in the table. These tasks, in the order shown in the table, were sequenced for the initial experiment phase, which is expected to last about 80 days and which would accomplish most of the ATS-4 experimental goals, except those involving long term trends or characteristics.

Table 8.8-5. Operational Integration of Experimental Tasks, Facilities and Schedule

COMBINED EXPERIMENTS*	PRIMARY OPERATIONAL CONFIGURATION (SEE NOTE 2)						GROUND STATIONS REQ'D (NOT NECESSARILY THROUGHOUT)					POINTING REQUIREMENTS			SCHED. CRITERIA (SEE NOTE 3)	SCHED. REQ'TS	OPERATING SCHEDULE
	1	2	3	4	8	10	R(1)	R(2)	M	T	A	LOCAL VERT	STATION	VARIABLE	X, Y, Z	DAYS	FLT. DAY
	✓					✓	✓					✓			Z	1	1
	✓						✓					✓			Z	1	1
	✓						✓					✓			Z	1	2
	✓						✓					✓			Z	1	3
	✓						✓					✓			X, Z	1	4
	✓						✓					✓			Z	1	5
	✓				✓		✓					✓			X, Z	2	6-7
	✓				✓		✓					✓			X, Z	2	8-9
	✓						✓					✓			X	4	10-13
	✓						✓					✓			X	4	14-17
	✓						✓					✓			X	4	18-21
	✓						✓					✓			X	2	22-23
	✓						✓					✓			Z	2	24-25
	✓						✓					✓			Y	1	26
	✓						✓					✓			Y	1	27
	✓						✓					✓			Y	3	28-30
	✓						✓					✓			Y	2	31-32
	✓						✓					✓			Y	2	33-34
	✓						✓					✓			Y	2	35-36
	✓						✓					✓			Y	1	37
	✓						✓					✓			Y	1	38
	✓						✓					✓			Y	4	39-42
	✓						✓					✓			X	3	43-45
	✓						✓					✓			Z	2	46-47
	✓						✓					✓			X	4	48-51
	✓						✓					✓			Y	2	52-53
	✓						✓					✓			Z	4	54-57
	✓						✓					✓			X	1	58
	✓						✓					✓			X	4	59-62
	✓						✓					✓			Y	2	63-64
	✓						✓					✓			Y	4	65-68
	✓						✓					✓			Y	2	69-70
	✓						✓					✓			Y	4	71-74
	✓						✓					✓			X	3	75-77
	✓						✓					✓			Y	3	78-80
	✓						✓					✓			Y	<1	-
	✓						✓					✓			Z	<1	-
	✓						✓					✓			Y	<1	-
	✓						✓					✓			Y	<1	-

e outlined
 8.6.4.1)
 ondry (backup)

8.8-16

Routine tasks, which will be performed when required (e. g., during stationkeeping) or to obtain survey information (e. g., yearly thermal cycle effects) are shown separately. These must be flexibly scheduled throughout the entire flight, and cannot be realistically pre-planned at this point.

It is recognized that many of the experimental tasks are of such a nature that they will require periodic repetition to gain maximum experimental value (e. g., to establish a yearly profile for solar effect on boresight). However, since the performance of the first cycle of experimentation will, to a large extent, act as a determinant with respect to which experiments will be chosen for repetition, it appears that broad flexible planning for this effort should be accomplished prior to flight. The detailed procedures for each task which will be developed for the initial experimental period would be made compatible for the long term repetitive experimentation schedules.

Experiments which involved combinations of various ATS-4 systems (primarily phased array and parabolic antenna systems) have not been previously discussed in detail within this study. The experimental value of these is questionable; however, the demonstration of their usefulness for military and commercial purposes can be important. They have therefore been included as optional tasks 30-34 in the table. Summary descriptions of the individual measurements and corresponding codes are presented for reference in Table 8.8-6.

Likewise, monopulse experiments (tasks 12, 13) are listed as options without having been previously considered in the study as a prime experimental objective.

Table 8.8-6. Experiment Combinations

C-1 Comparison of Performance Characteristics

C-1-1 Comparison of Low Data Rate Performance, Parabolic and Array Antennas

To compare the transmission and reception performance of the parabolic antenna with that of the phased array at low data rates, by receiving test messages with one antenna and transmitting them back to the ground with the other.

C-1-2 Comparison of Low Data Rate Performance, Parabolic and Array Antennas

To compare the transmission and reception performance of the parabolic antenna with that of the phased array at low data rates, by using test messages sent over the TT&C Link.

C-2 Comparison of Medium Data Rate Performance/Parabolic and Array Antennas

To compare the transmission and reception performance of the parabolic antenna with that of the phased array at medium data rates, by receiving test messages with one antenna and transmitting them back to the ground with the other.

C-3 Comparison of High Data Rate Performance, Parabolic and Array Antennas

To compare the transmission and reception performance of the parabolic antenna with that of the phased array at high data rates, by receiving test messages with one antenna and transmitting them back to the ground with the other.

C-4 Comparison of Audio AM Performance, Parabolic and Array Antennas

To compare the transmission and reception performance of the parabolic antenna with that of the phased array with Audio AM, by receiving test messages with one antenna and transmitting them back to the ground with the other.

C-5 Comparison of Audio FM Performance, Parabolic and Array Antenna

To compare the transmission and reception performance of the parabolic antenna with that of the phased array with Audio FM, by receiving test messages with one antenna and transmitting them back to the ground with the other.

Table 8.8-6. Experiment Combinations (Cont'd)

C-6 Comparison of Video SSB AM Performance/Parabolic and Array Antennas

To compare the transmission and reception performance of the parabolic antenna with that of the phased array with Video SSB AM, by receiving test messages with one antenna and transmitting them back to the ground with the other.

C-7 Comparison of Wideband FM Performance, Parabolic and Array Antennas

To compare the transmission and reception performance of the parabolic antenna with that of the phased array with Wideband FM, by receiving test messages with one antenna and transmitting them back to the ground with the other.

C-8 Verification of Point-to-Point Transmission Using Both Antennas

To verify that ATS-4 relay from one point to another on the ground is feasible using one antenna for reception and the other for transmission.

C-9 Measurement of Point-to-Point Relay Performance at Low Data Rates Using Both Antennas

To measure low data rate relay performance while relaying from one point to another on the ground using one antenna for reception and the other for transmission.

C-10 Measurement of Point-to-Point Relay Performance at Medium Data Rates Using Both Antennas

To measure medium data rate relay performance while relaying from one point to another on the ground using one antenna for reception and the other for transmission.

C-11 Measurement of Point-to-Point Relay Performance at High Data Rates Using Both Antennas

To measure high data rate relay performance while relaying from one point to another on the ground using one antenna for reception and the other for transmission.

Table 8.8-6. Experiment Combinations (Cont'd)

C-12 Measurement of Point-to-Point Relay Performance with Audio AM Using Both Antennas

To measure audio AM performance while relaying from one point to another on the ground using one antenna for reception and the other for transmission.

C-13 Measurement of Point-to-Point Relay Performance with Audio FM Using Both Antennas

To measure audio FM performance while relaying from one point to another on the ground using one antenna for reception and the other for transmission.

C-14 Measurement of Point-to-Point Relay Performance with Video SSB AM Using Both Antennas

To measure Video SSB AM performance while relaying from one point to another on the ground using one antenna for reception and the other for transmission.

C-15 Measurement of Point-to-Point Relay Performance with Wideband FM Using Both Antennas

To measure Wideband FM performance while relaying from one point to another on the ground using one antenna for reception and the other for transmission.

C-16 Pointing System Comparison

To compare the error angle outputs of all precision pointing systems.

C-17 Pointing System Boresight

To measure the boresight misalignments of all precision pointing systems.

C-18 Pointing System Thermal Effects

Repeat C-16 and C-17 across the thermal cycle.

C-19 Pointing System Vibration Effects

Repeat C-16 and C-17 during stationkeeping, real or simulated.

C-20 Gain Measurement Comparison

To compare the antenna gains by simultaneous measurements using all available techniques.

Table 8.8-5 is intended to provide an operational planning basis within the scope of program to definition now available. In addition, it shows the criteria by which the integrated tasks were initially selected these criteria are:

- a. Objectives - The basic experimental objectives of each integrated task.
- b. Operational Configuration - The best possible operational configurations required to handle the functions involved in the execution of a given task. That is, the number of antennas and the command/telemetry capability at a ground station or at several ground stations needed to perform each task. Obviously, other configurations could be substituted for the configurations used, but these configurations would be less efficient or not as desirable from the standpoint of operational control (See Section 8.8.2.2).
- c. Ground Stations Required - Identification of ground stations utilized at least part time during each task, consistent with the operational configuration selected. This assumes two antennas available at Rosman, as discussed in Section 8.8.3.
- d. Pointing Requirements - Whether or not the spacecraft will be pointing to: a) local vertical; b) a specific station or stations, or whether c) the pointing is variable in character, during task performance.
- e. Time Schedule Criteria - The schedule criteria required to perform each task are: a) Some tasks will require short durations of spacecraft/ground station operations with repeated short time intervals throughout the monitoring period labeled in the table (X); b) Other experimental tasks will be conducted on a "when available" basis (Y); c) Still other tasks will require long, continuous operations at preestablished times of the day or year, e. g., 4 hours a day at noon on Day 1 and Day 80, etc. (Z). A "fallout" of the table was a preliminary schedule for the initial experiment phase. Days required for each task were estimated and listed in the table. The accumulation of these resulted in definition of an 80 day period during which all the basic objectives (except those requiring a repetition to measure long term trends) would be completed.

8.8.4 DATA ACQUISITION, PROCESSING AND DISPLAY

Each experiment task (preliminarily defined in 8.8.3) will require a detailed procedure which involves not only experiment command and control tasks, but also those tasks which assure optimum spacecraft and experiment data acquisition.

Data Acquisition Ground Rules

The general ground rules for collecting telemetry data are:

- a. Collect a telemetry data burst of at least three main frames immediately prior to and immediately following all experiment tasks and if possible, at intervals between significant functions during each task.
- b. If practicable, consistent with power and ground station transmit/receive capability, collect telemetry data continuously during significant experimental measurements of 5 minutes or less or a burst of at least three telemetry main frames every 10 minutes during longer experiments.
- c. Conduct a routine health check during any day when experiments are not scheduled (reference Task A, 8.8-3) or at least once per week. The health check procedure will exercise all systems and collect basic measurements under controlled conditions. This will hopefully result in earliest possible identification of hardware trends and appropriate contingency planning and may affect experiment schedules.
- d. Collect telemetry data continuously throughout stationkeeping maneuvers.
- e. Collect data during initiation of all experiments, during turn-on of any spacecraft transmitter or receiver, during initiation and completion of slewing and throughout any re-acquisition of Polaris or earth horizon reference.

It is recognized that many experiment measurements will most efficiently be made and/or recorded manually. The format of this data must be designed to facilitate conversion for merging with telemetry data, with other experimental data, and with reference data, such as earth and solar ephemerides. Some data must be merged within computers both at the ATS-4 OCC for experiment control and in detailed experiment analysis at integration contractor or experiment contractor facilities. No computer merging is seen necessary at the tracking stations or for on-line processing and analysis at GSFC.

Telemetry data reduction at the ground stations and at GSFC should be routine and will involve computers and procedures very similar to those developed for Nimbus, Syncom and ATS (A-E). S-band receivers and demodulators at the various ground stations will convert the raw telemetry signal to a digital wave train which will be recorded on magnetic tape. Some data will be reduced to engineering unit reference and displayed ("quick look") at the tracking station to permit verification of spacecraft command and general health status. Selected reduced scientific and telemetry data will be sent via teletype and phone lines to the ATS-4 OCC and, when scheduled (Rosman only), wave trains will be transmitted via the microwave link to GSFC.

At GSFC, selected segments of the wave train data arriving via the microwave link will be fed directly (on-line) to computer facilities for additional near-real time analysis and display for purposes of experiment control and spacecraft housekeeping (e. g., power status, thermal control and control gas management).

All other data received, either via microwave or on magnetic tapes, will be available for additional (off-line) processing, merging with experiment data, printed and plotted as required to qualitatively analyze experiment results and to evaluate spacecraft performance. This wavetrain data must also be merged with ground station data, scientific data and orbit information (orbit and sun ephemerides) on magnetic tapes which would be sent to the experiment integration contractor where a detailed quantitative experiment data reduction and analysis will be centered. At the integration contractor's facility, computer programs (which will have been designed and checked out) would be utilized to perform the following tasks:

- a. Axes systems transforms
- b. Statistical determination of experimental means and deviations (e. g., mean boresight axes, etc.)
- c. Cross-plots of related performance and experiment parameters
- d. Correlation of experimental and spacecraft performance parameters with math models
- e. Prediction programs

Data requiring more detailed analysis by an experimenter at the experimenter's own facility would be provided by the integration contractor in the form of a "data pack", containing all experiment parameters and derived spacecraft and orbit performance parameters necessary to determine experiment results. These results would be submitted to both the NASA ATS-4 Program Director and the integration contractor for utilization in integration and comparison with other experimental and operational results.

8.8.5 CONTINGENCY PLANNING

Some possible flight anomalies which can result in either catastrophic or partial degradation of some experiments may have no effect on others. Table 8.8-7 is a matrix of some of the more significant of these anomalies, effect on the experiments, and contingency planning which can be implemented to gain maximum value.

8.8.6 REPORTING

Timely, efficient reporting is required throughout the flight in order to assure:

- a. Optimum feed-back into planning and implementation of follow-up experiments
- b. Earliest possible utilization of data in design of other NASA satellite programs
- c. Determination of any operational problem areas and implementation of corrective action

It is assumed that routine progress reporting of general spacecraft and experiment performance will be accomplished in a manner similar to other programs by NASA ATS-4 OCC with the assistance of experimenter and experiment integration contractor personnel comprising the OCC team. Reporting of detailed experiment analysis results and recommendations to NASA by the experiment integration contractor and by various individual experiment contractors must also be accomplished in an integrated manner which will result in a concise summary of total accomplishment. The following procedure is recommended:

In conjunction with the recommendations presented in Section 8.8.4, the integration contractor will supply processed correlated data-packs to each experimenter. The experimenters will thoroughly analyze their experiments, with additional support as required from the integrating contractor. The results of analyses will be published in draft form by the individual experimenters on a monthly basis with copies to the NASA ATS-4 Program Manager and to the integration contractor.

The integration contractor will study the individual reports, determine all significant experiment and spacecraft performance interfaces and inter-effects, and determine integrated

Table 8.8-7. Contingency Matrix

Single Anomaly Description	*Effects on Experiments					Basic Contingency Planning Elements
	A	∅	O	I	C	
Inclined Orbit (< 10°)	U	U	U	U	U	1A-Increased complexity in tracking, data processing, experiment planning (increased operational cost)
Nonsynchronous Orbit	P	U	U	U	U	2A-More tracking stations 2B-Same as 1A
Eccentric Orbit With 24 Hour Period - Near Nom. Asc./Dec. nodes	P	U	U	U	U	3A-Same as 1A 3B-If eccentricity is large, 2A also required; determination of solar effects of all experiments difficult
No Earth Sensors	U	U	P	U	P	4A-Use interferometer for station pointing
No Polaris Sensor	U	U	P	U	P	5A-Try interferometer for yaw control when yaw required
No Pitch or No Roll Momentum Control	P	P	L	P	P	6A-Same as 1A
No Parabolic Antenna Deployment (Solar Paddles also Affected)	L	P	U	U	L	7A-Revise experiments for power available 7B-Delete A experiment 7C-Checkout nozzle effects (planning) on stationkeeping and orientation control
Inoperative A Command	L	P	U	U	L	8A-Delete A experiments
Inoperative ∅ Command	U	L	U	U	L	9A-Delete ∅ experiments
Partial Solar Paddle Deployment	U	P	U	U	P	10A-Determine power profile 10B-Stretch out schedule accordingly
<p>LEGEND: L - Lost P - Partial Loss U - Essentially Unaffected A - Parabolic Antenna ∅ - Phased Array O - Orientation Control I - Interferometer C - Combined experiments</p> <p style="text-align: right;">} if contingency plan implemented*</p>						
<p>*It is assumed that if any experimental value can be gained, all efforts will be initiated regardless of cost or schedule to gain the maximum available.</p>						

experiment and operational planning criteria. The results of this effort will be published in a formal document to the NASA ATS-4 Program Manager monthly, 2 weeks after receipt of the individual experiment reports. Figure 8.8-2 diagrams the approximate schedule required to implement this procedure in a timely manner.

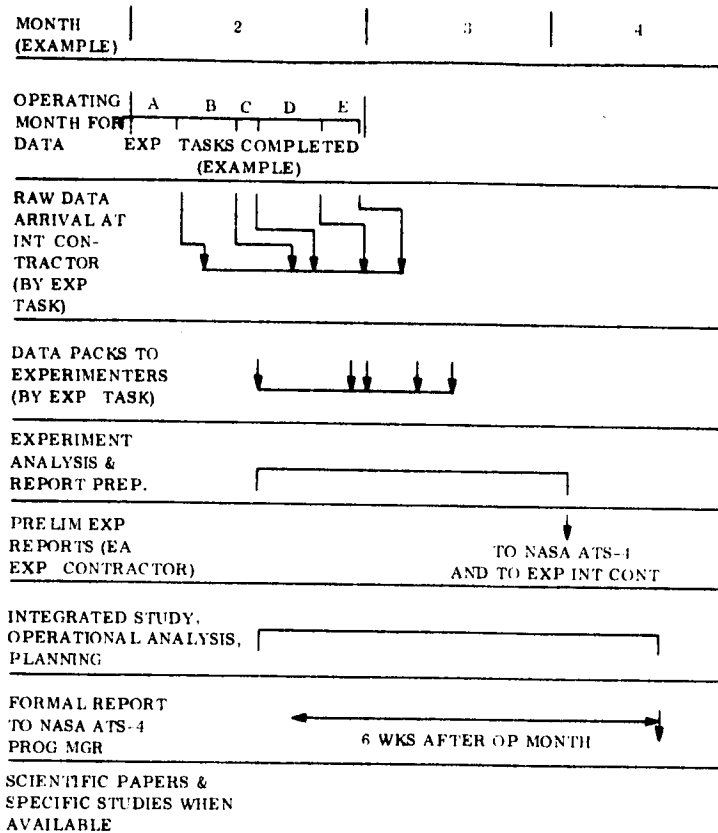


Figure 8.8-2. Experiment Analysis Reporting Schedule

SECTION 9

SUPPORT OPERATIONS

9.1 INTRODUCTION

This section presents the overall support equipment required for completion of the ATS-4 experimental mission. Both new and existing equipment and facilities for development, fabrication, launch and operation are identified. Unique ground support equipment is stressed.

9.2 SUMMARY

Based on the preliminary Integrated Test Plan and the Operational Plan, support equipment necessary for the ATS-4 mission has been identified. In general, equipment that must be procured is within the present state-of-the-art. Equipment support relating to the large antenna presents several problems, especially dynamic and rf testing. Facilities for testing and launch support operations are generally satisfactory. For orbital support, existing ground stations must be supplemented with auxiliary equipment to support the experiments. A Ground Support Summary Matrix is shown as Table 9.2-1.

9.3 EQUIPMENT REQUIREMENTS

The support equipment requirements for the ATS-4 Program up to launch were determined from the Integrated Test Plan. Figure 9.3-1 is repeated from the Program Plan and shows the significant steps in the test program.

Requirements for orbital support equipment were taken from the Operational Plan as described in Sections 7 and 8.

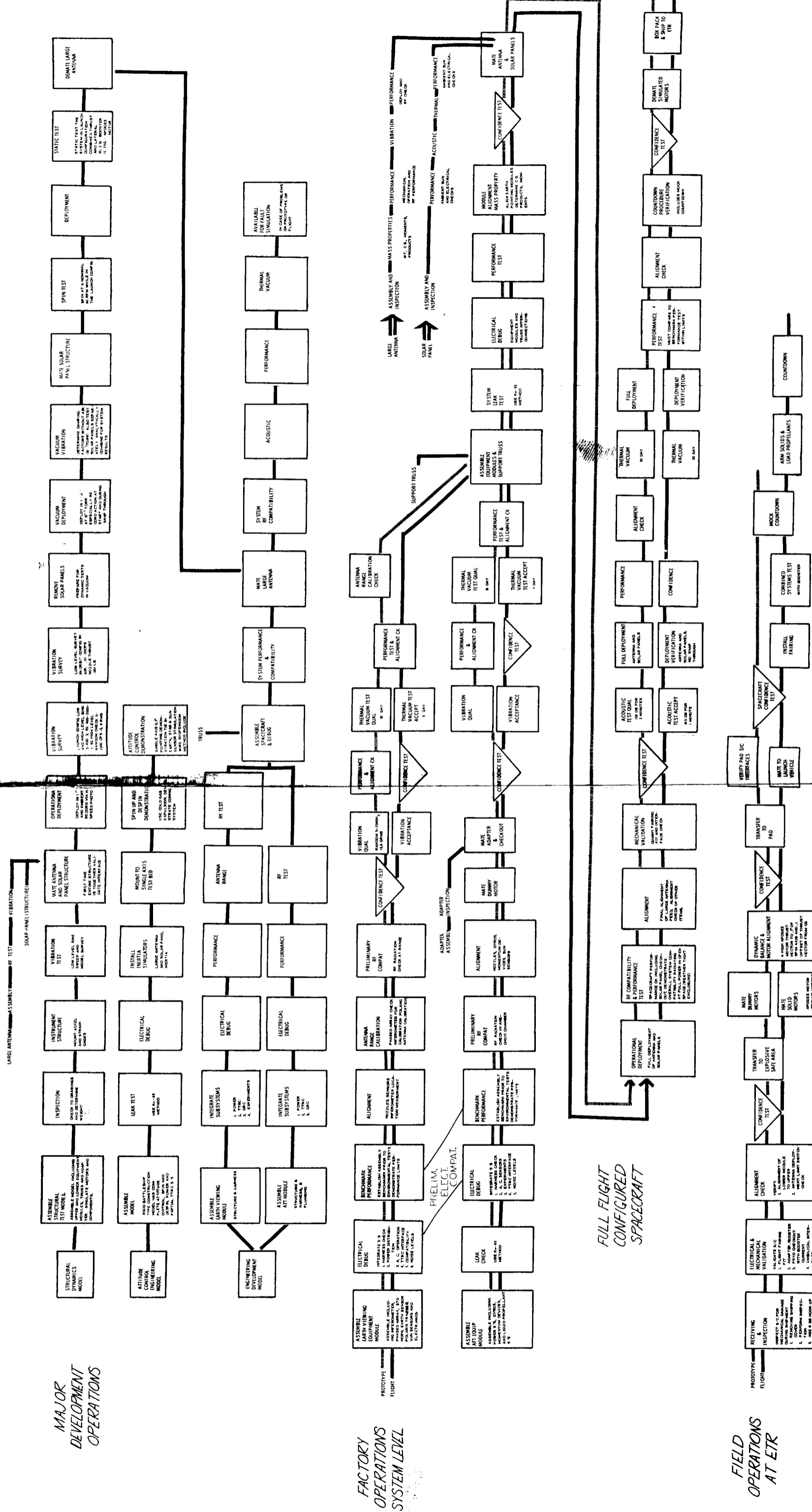
9.4 MECHANICAL SUPPORT EQUIPMENT (MSE)

9.4.1 SCOPE

The Mechanical Support Equipment encompasses all mechanical support equipment, except that which is facility oriented, necessary for engineering testing, handling, transportation,

Table 9.2-1. Ground Support Summary Matrix

Program Phase	SUPPORT EQUIPMENT			Facilities
	Mechanical	Electrical	Software	
Development	<p>Assembly Equipment Handling Equipment Spin Table Vibration Fixtures Deployment Equipment Antenna Support Fixture (Rf Evaluation)</p>	<p>Subsystem AGE Development System AGE Stimulators</p>		<p>Vibration Exciters Low Level 0.01-20 cps High Level 5-2000 cps Large (30-foot dia.) Low Pressure Chamber Large Antenna Range High Bay Area</p>
Fabrication and Test	<p>Assembly Equipment Handling Equipment Environmental Fixtures Shipping Containers Deployment Equipment Alignment Equipment Leak Test Equipment</p>	<p>Subsystem AGE Earth-viewing Module AGE Aft Module AGE System AGE Environmental Special Test Equipment TT&C Ground Station Stimulators (Sensors) Rf Dummy Loads</p>	<p>System Performance & Evaluation Commands</p>	<p>Vibration Exciters Med. Level 5-2000 cps Medium Size (11-foot dia.) Thermal-Vacuum Chamber Large Acoustic Chamber Large (30-foot dia.) Thermal- Vacuum Chamber Antenna Range Mass Property Facility High Bay Area</p>
Launch	<p>Handling Equipment Shipping Containers Spin Fixture Alignment Equipment Leak Test Equipment Propellant Servicing</p>	<p>System AGE TT&C Ground Station Stimulators (Sensors) Pad AGE Simulator Spacecraft/Adapter Simulator Rf Dummy Loads</p>	<p>System Performance & Evaluation Commands</p>	<p>Clean Area at ETR 40 x 40 x 40 feet Dynamic Balance Facility Explosive Safe Area Launch Pad with Environmental Control</p>
Orbit		<p>Transportable Equipment for Phased Array Experiment Supplemental Ground Station Equipment</p>	<p>Commands Precession Control Tracking Stationkeeping System Performance & Evaluation Experiment Support</p>	<p>Rosman II GS Mojave GS Towomba GS GSFC Command & Data Processing Computers</p>



MAJOR DEVELOPMENT OPERATIONS

FACTORY OPERATIONS SYSTEM LEVEL

FIELD OPERATIONS AT ETR

Figure 9.3-1. ATS-4 Major Article Test Flow

9-4

9-3

servicing, checkout, packaging and maintenance of the spacecraft during its complete ground mission profile including factory, remote test facility and field operations.

9.4.2 STUDY APPROACH

The MSE approach to this study is to adequately satisfy ground mission requirements with a minimum cost effort and within the constraints of accepted design practices. In pursuit of this objective, the following characteristics will be significant factors:

- a. Equipment concepts include time sharing from manufacturing through field support and adapting existing support and servicing equipment, existing inventory equipment and off-the-shelf and standard commercial equipment whenever applicable.
- b. Shipment of the complete spacecraft to the field or remote test sites will be based on a fully assembled configuration less explosive.

In order to ensure multiple use of support equipment, the requirements for the various tests included in the ground mission have been grouped into common operation for which identical or adapted support equipment may be used. Variations in instrumentation and vehicle model will in most cases account for differences in test scope, level of input and required results.

9.4.3 MECHANICAL SUPPORT CONCEPTS

9.4.3.1 Vehicle Assembly and Handling

An analysis of the preliminary integrated test flow indicates that the vehicle will generally be tested in a consistent yaw-axis-vertical attitude except for Mass Property determination and Shipping. The turnover capacity required for these operations will be incorporated into the Mass Property and Shipping Equipment. However, yaw-axis-horizontal attitude is feasible for much of the assembly and testing. A tradeoff study to identify the optimum approach is recommended for early in Phase C.

The assembly and handling equipment ranges from the Spacecraft Assembly Fixture, which is the central assembly and test station, through the fixtures required to support each removable subassembly, including the large antenna and solar panels.

The spacecraft will be assembled and aligned with the yaw axis vertical in the assembly fixture. Access platforms will be required for the convenience of servicing the test personnel. Spacecraft movement into and out of the assembly fixture will be by overhead crane.

Antenna handling will always be accomplished in the yaw-axis vertical attitude during factory operations. A handling ring will be applied to the baseplate and will remain on the baseplate during all handling and shipping operations. During lifting operations (by overhead crane) a girth ring will be utilized at the upper portion of the antenna to stabilize it.

The assembly procedure requires that the center portion of the antenna surface, which could either be an rf absorber or a reflector, be pre-installed. The antenna petals and hub assembly, partially opened but still restrained radially, is lowered over the spacecraft and bolted to the aft module flange. The petals are then fully cinched up against the stowage ring provided in the support trusses, and the outer band tensioned to the specified value.

The shipping container will also be coordinated to expedite handling by using the container to rotate the antenna from the horizontal to vertical position prior to removing it from the container. The apogee motor shipping container will be arranged to present its mounting interface with the nozzle facing down.

The Spacecraft Assembly Fixture will be the most complex item of the group. It is the heart of the assembly and handling group and the remaining items of assembly equipment will support its function. However, the assembly fixture will be well within the state-of-the-art and is not considered a program critical development item.

9.4.3.2 Alignment Equipment and Deployment Antenna Measurements

To the greatest extent possible, alignment of critical surfaces and orientation will be controlled by manufacturing tolerances and coordinate tooling. However, all critical alignments will be checked at the final assembly level and the Spacecraft Assembly Fixture will be utilized for alignment.

The basic design approach is to use gravity as the common reference between items being aligned and the optical tooling equipment being used. Since the spacecraft orientation for assembly purposes is with the yaw axis vertical, the first step in alignment will be to verticalize the yaw axis. This will be accomplished by leveling the separation plane between the Flight Spacecraft and the Adapter. Spacecraft manufacturing tooling will be used to establish the pitch axis. Through this axis a vertical reference plane will be erected by optical tooling. Individual component mounting surfaces will be checked for parallelism, perpendicularity and pointing relative to spacecraft axes by normal optical tooling procedures. Alignment equipment is not program critical and is within the state-of-the-art.

Apogee motor thrust vector alignment is discussed in the next subsection.

The support equipment required to check compliance of the deployed antenna with required parabolic configuration tolerances in its operational gravity field is undetermined at this phase and the concept development should be designated as a major study effort during the program development phase.

9.4.3.3 Mass Properties, Spin Balance and Apogee Thrust Vector Alignment

The following schedule of mass property measurement is planned in order to establish a base from which the Orientation Control subsystem requirements may be checked against analytics. These measurements as well as dynamic balancing can be conveniently accomplished, with a minimum of effort in the field.

<u>Configuration</u>	<u>Measurement</u>	<u>Equipment</u>
a. Spacecraft with Dummy Rocket less Antenna, Solar Panels, Adapter and fuel	Weight	Mechanical Scale
	Center of Gravity	Pelton Model 10A or equivalent
	Ip (ZY Plane-Null) (XZ Plane-Null) (XY Plane-Meas.)	Pelton Model 10A or equivalent
	Im (3 axes)	Bifilar Pendulum
b. Antenna (Folded)	Weight	Mechanical Scale
	Ip (ZY & XZ Planes) (Null)	Pelton Model 10 or equivalent
	Im (Yaw Axis Only)	Bifilar Pendulum
c. Complete Spacecraft, Launch Configuration less adapter	Dynamic Balance (Yaw Axis Only)	Gisholt Machine or equivalent

Remaining mass property information for the operational mode may be obtained by supplementing the above measurements by calculations. The measurements of configuration a, above, will require one fixture which will incorporate turnover capability. The measurements of configuration b will require a lightweight fixture with a central core to support the hub of the folded antenna. The same fixture may be used for all measurements and turnover capability will not be required.

Dynamic balancing will require an explosive safe facility at the launch site, which includes a spin balance machine identical (except for size) to the 80.5-inch Gisholt currently in use at the AMR NASA (Douglas) Project DELTA facility. The existing electronic readout equipment from the DELTA operation could be utilized without change for ATS-4 dynamic balancing. Apogee motor mate to the spacecraft and its thrust vector alignment with the spacecraft will also occur at this same explosive safe facility and adequate floor space for both operations is required.

Thrust vector alignment with the spacecraft principal spin axis will be accomplished as follows:

- a. The 0.1-inch allowable radial deviation will be controlled by use of matched and coordinated tooling during the manufacturing process. The apogee motor interface on the spacecraft will be match drilled to closely controlled concentricity tolerance with the separation interface of the spacecraft. The conical interface adapter for the Girth Ring on the apogee motor will be match drilled while mounted to the motor to closely controlled concentricity with the centerline of the motor thrust nozzle. Thus the total 0.1-inch allowable concentricity deviation is well within controlled tolerances when divided between the two coordinated drill jigs.
- b. The 0.1° allowable angular deviation will be controlled by orienting the centerline of the apogee motor thrust nozzle and the spacecraft separation interface normal to local gravity during the assembly of the apogee motor to the spacecraft. The apogee motor is transferred to the assembly stand, which is equipped with adjustable legs. The adjustable legs of the stand are used to level two sensitive bubble levels, at right angles to each other, mounted on a concentric plug in the thrust nozzle of the motor. When the thrust vector is vertical, the spacecraft, less adapter, is lowered over the apogee motor and interface bolts torqued.
- c. With the spacecraft mated to the apogee motor, whose thrust vector is vertical, the spacecraft separation interface is optically measured for deviation from the horizontal plane on two or more sightings. The spacecraft separation interface is then brought into horizontal by shimming at the apogee motor interface bolts.

With the spacecraft aligned to the apogee motor thrust vector, the complete spacecraft is transferred to the spin balance machine whose spin axis is also controlled concentric to the spacecraft separation interface. The spin balance operation then brings the CG to the superimposed thrust and spin axes. The balance operation at this point should be minimal because of the nulling of products inertia accomplished at the factory. The relative flexibility of the spacecraft is not expected to pose any major problems for the balancing operation. All operations and equipment indicated above are well within the state-of-the-art.

9.4.3.4 Deployment

The 30-foot antenna and the solar panels will be deployed in a 1g field. The antenna and solar panel designs are such that they can support their own weight in the 1g field, therefore

the deployment portion of the test will not require additional support equipment. However, after deployment the antenna must be folded back into the stowed position. It is anticipated that some type of external mechanical application will be required to perform this operation. This equipment will be developed in parallel with antenna detail design.

9.4.3.5 Pneumatic and Fuel Servicing and Leak Testing

9.4.3.5.1 Orbit Adjust and Precession Control

This is a hot gas propulsion system with a monopropellant (Hydrazine). The system requires servicing with 75 pounds of hydrazine and N_2 at 300 psi on the launch pad. Servicing equipment will be conventional and could utilize Martin Marietta's Propulsion Servicing Unit #40904, which can be placed next to the satellite in the gantry.

9.4.3.5.2 Attitude Control and Stationkeeping

This system will use vapor ammonia as a propellant and will require servicing with 95 pounds of ammonia. Servicing equipment will consist of a storage tank type loading unit which utilizes the vapor pressure of the ammonia for liquid transfer. A vacuum pump will also be included on the unit for evacuating the spacecraft system prior to loading.

9.4.3.5.3 Leak Test

Leak testing can be accomplished using a calibrated mass spectrometer and standard procedures. Accuracies of 60 scc/hr can be determined while the sensitivity is within 2 scc/hr. Another method of leak testing using Kr-85, should be investigated during Phase B. This method shows much promise for system leak tests and allows sensitive testing even when the propellant is loaded.

9.4.3.6 Vibration

The structural dynamics model, in the complete launch configuration, and the prototype and flight spacecraft earth viewing equipment module, aft equipment module and antenna assembly will be subjected to vibration testing.

In order to perform these tests satisfactorily, the testing should be accomplished in a vibration facility. The facility crane hook height must be approximately 35 feet in order to handle the Structural Dynamics Model on the vibration exciters. Also, the area of the facility must be large enough for antenna deployment during the low frequency torsional test.

Support equipment for thrust axis vibration will include fixtures, to adapt the vehicle interface to vibration heads, and load balancing equipment consisting of either elastic suspensions or pneumatic supports. For lateral and torsional vibration, hydraulic Teem bearings and adapting fixtures are required. Adaption for multiple use of fixtures will be included in design concepts. Support equipment for vibration testing will be conventional and within the state-of-the-art.

9.4.3.7 Structural Static Test

The structural dynamics model will be subjected to two static tests in which combined thrust and lateral loads of 10.2 g will be applied to the Booster Interface and 11.25 g to the apogee motor interface. The static test arrangement will support the model in a yaw axis vertical attitude on a rugged fixture representative of the booster or apogee motor interfaces, depending upon the specific test. The same fixture will be adapted for both interfaces and the fixture will be structurally anchored to react lateral loads.

9.4.3.8 Spin Test

The structural dynamics model will be subjected to a controlled spin test with yaw axis vertical to establish structural integrity relating to the applied centrifugal forces.

The support equipment required will comprise a stabilized spin table, series motor drive and remote control and a vehicle adapter fitting to adapt the spacecraft interface to the spin table.

The spin table, drive and control, and the fixture will be conventional equipment. However, facility and/or machine size limitations indicate that new equipment will probably be required. During test the spinning vehicle must be enclosed by protective curtains or walls to eliminate personnel hazards.

9.4.3.9 Acoustics Test

The support equipment required to accommodate this test will include transport equipment, erection and transfer equipment and an acoustic test dolly that will accept the vehicle in the yaw-axis-vertical attitude, roll it into the acoustic chamber and by-pass wheel contact with the floor of the chamber during the test. The dolly structure must also be capable of withstanding the acoustic test levels.

The large antenna and the solar panels will also be subjected to acoustic environments in the powered flight attitude. Support fixtures that simulate the vehicle interface will be required for these tests.

9.4.3.10 Rf Compatibility Tests

Rf compatibility tests will be performed on the assembled spacecraft in an area that provides no rf interference in the area of the radiation cone of the parabolic reflector. In order to accommodate this requirement it may be necessary to conduct the compatibility test outdoors. If such is the case, the spacecraft will be protected by an rf transparent enclosure large enough to accommodate the deployed antenna and solar panels.

The spacecraft will be supported on the acoustic test dolly at the booster interface to insure that no rf interference is present in the operational area of the spacecraft. Mechanical support equipment for this test will be within the scope of conventional equipment.

9.4.3.11 Thermal-Vacuum Tests

The prototype and flight vehicles will be subjected to the following thermal-vacuum environment:

Heat Flux	-	1 solar constant
Pressure	-	10^{-6}
Wall Temperature	-	liquid nitrogen cooled
Rotation Rate	-	1 revolution per day

The spacecraft will be placed in a vacuum chamber that will include a lamp array to provide the heat flux. The rotational rates may be achieved by either rotating the vehicle by means of a drive or preferably by rotating the heat flux relative to the spacecraft. This test seems to present no significant problems and could be performed in available facilities.

9.4.3.12 Orientation Control Demonstration

Tests will be conducted on the boiler plate Orientation Control Engineering Model to demonstrate the ability of the control system to correct for precession (coning) during the spin mode and the capability of the control system to point the vehicle about a single axis.

For both tests the mechanical support equipment envisioned will comprise a suspension wire connecting the orientation control model at its cg to an overhead thrust bearing end of the wire, a selsyn motor and drive will rotate the bearing at a near synchronous speed with the rotating orientation control to minimize the torsional effect of the wire. The selsyn motor speed will be controlled by a photoelectric cell that rotates with the wire and is sensitive to a beam of light from the rotating model.

9.4.3.13 Transportation and Shipping

The spacecraft shipping configuration will be without the solid rocket motors. These items will be installed in the SAB. For all major or over-the-road movements, the spacecraft will be shipped horizontally. It will be supported at each end: the booster interface ring and the earth viewing equipment module support structure. The spacecraft will be mounted on a Transportation Handling Dolly. This dolly will have limited mobility (Type I per Mil M 008090) and be provided with a tow bar. The dolly will be equipped with a lightweight cover that will provide weather protection, dirt control and condensation protection and it will also be equipped with frame-mounted trunnions to rotate the spacecraft to vertical for installation and removal. The dolly and spacecraft assembly will be transported to the nearest airport mounted on a commercial air-suspension flat bed trailer.

The above arrangement will present an oversize load since the width of the spacecraft with protective cover is approximately 10 feet. The overall height will be within legal limits. This movement will require coordination with the local authorities but no problems are anticipated.

Upon arrival at the airport, the dolly and spacecraft will be lifted off the flat bed trailer and shipped by an Air Force C133 aircraft or the NASA Pregnant Guppy or Super Guppy aircraft. It is doubtful that an Air Force C124 aircraft can be used but further detailed study will be necessary for confirmation.

Upon arrival at ETR, the dolly and spacecraft is unloaded from the aircraft and the same flat bed trailer transportation method will be utilized to transfer the spacecraft to the SAB.

9.4.4 EQUIPMENT AND COMPLEXITY APPRAISAL

The equipment required for mechanical support of the ground mission indicated in Sections 9.3 and 9.4.3 is categorically identified in Table 9.4-1 and appraised as to development complexity. Complexity ratings are assigned each category of equipment in accordance with the following key:

- A. Little or no development required - existing equipment can be modified or similar equipment designed, or off-the-shelf items provided from commercial stock.
- B. Conventional equipment but new custom design required - within the state-of-the-art.
- C. Complex and major custom design - still within the state-of-the-art.
- D. Complex and requires state-of-the-art development.

Table 9.4-1. Equipment List (MSE)

Equipment Identification	Complexity Rating			
	A	B	C	D
Spacecraft Assembly		X		
Spacecraft Handling		X		
Space Transportation			X	
Antenna Handling		X		
Adapter Handling		X		
Protective Covers	X			
Apogee Motor Handling		X		
Orientation Control and Spin-Up Demonstration			X	
High Pressure He/N ₂ Supply Unit	X			
Leak Test	X			
Ammonia Servicing Unit	X			
Propellant Servicing Unit	X			
Solar Array Handling		X		
Deployment Support		X		
Access Stands	X			
Alignment		X		
Mass Property and Spin Balance			X	
Antenna Configuration Checkout				X
Thermal-Vacuum Support			X	
Vibration Support			X	
Environmental Control (Cleanliness)	X			
Structural Spin Test Support		X		
Acoustic Test Support		X		
Separation Test Support		X		

9.5 ELECTRICAL SUPPORT EQUIPMENT (ESE)

9.5.1 SCOPE

This section describes all electrical support equipment required to checkout each subsystem of the vehicle, to support system testing of the vehicle, and to support prelaunch and launch activities at ETR.

9.5.2 APPROACH

9.5.2.1 General

In general, the approach to the Electrical Support Equipment should be to provide equipment to adequately satisfy ground mission requirements at a minimum cost, consistent with good design practice.

9.5.2.2 Fail Safe

The Electrical Support Equipment should be designed so that the failure of any part of the equipment will not cause damage to the spacecraft. Where the failure of any part of the Electrical Support Equipment would cause a critical delay to the mission, (e.g., launch), the equipment will use high reliability parts or redundancy.

9.5.2.3 Human Factors

The Electrical Support Equipment should be designed to minimize the chance of human error during testing.

9.5.2.4 Isolation

The Electrical Support Equipment should not introduce any ground loops into the test setup. All signals coming from the spacecraft should be isolated to prevent damage to the spacecraft and to minimize loading effects.

9.5.2.5 Accuracy

Equipment accuracies should be no greater than those required to adequately demonstrate system performance. Accuracies greater than ten times the flight equipment accuracies should be avoided in order to avoid excessive cost. A minimum of three times the flight accuracy would be acceptable.

9.5.2.6 Parts

Special circuits should be kept to a minimum, with extensive use of commercial test equipment preferred.

Where possible, commercial grade parts should be used in preference to MIL or space qualified parts, with the exception of connectors which mate to the spacecraft. These should be flight hardware where commercial equivalents differ in critical parameters, e. g., contact material.

9.5.2.7 Use of Telemetry Subsystems for Testing

Use of the on-board telemetry subsystems is the preferred measurement technique. This avoids duplication of measurement circuits and minimizes the number of breaks in the vehicle harness.

9.5.3 ELECTRICAL SUPPORT CONCEPTS

9.5.3.1 General

Electrical tests on the spacecraft, above the component level, fall into four categories: Subsystem Tests, Earth Viewing Equipment Module Tests, Aft Equipment Module Tests, and System Tests. In addition there are three special test areas affecting ESE design: thermal-vacuum, rf, and pad tests.

The equipment required for each of these seven areas is discussed below.

9.5.3.2 Subsystem Tests

Subsystems may be broken up into two categories: experiments, which are mainly in the Earth Viewing Equipment Module, and non-experiments, which are basically in the Aft Equipment Module. Each Experiment Subsystem should be serviced by a test set which is capable of supplying power, monitoring test points and exercising input and output functions. Non-experiment Subsystems (Guidance and Control, TT and C, and Power) should be serviced by one basic test set since these subsystems are, in general, tested together. The Test

Set should include the TT and C Ground Station and a console capable of supplying power, monitoring test points, exercising input and output functions, and controlling Guidance and Control sensor stimulators.

9.5.3.3 Earth Viewing Equipment Module Tests

The equipment required to run tests on the Earth Viewing Equipment Module would consist of the Input/Output sections of each Experiment Subsystem Test Set. In addition, a console would be required, which would be capable of supplying power to the module, stimulating and monitoring the Guidance and Control sensors, and in general simulating the interface with the Aft Equipment Module.

9.5.3.4 Aft Equipment Module Testing

The equipment required to run tests on the Aft Equipment Module would be essentially the same equipment used to test the three non-experiment subsystems. Additional equipment would be required to provide for those portions of the experiment subsystems that are housed in the Aft Equipment Module, to simulate the Guidance and Control sensors which are in the Earth Viewing Equipment Module, and in general simulate the interface with the Earth Viewing Equipment Module.

9.5.3.5 System Tests

System tests are actually a combination of the Earth Viewing and Aft Equipment Module Tests. The equipment required would consist of:

- a. TT and C Ground Station
- b. Input/Output Sections of Experiment Subsystem Test Sets
- c. Guidance and Control Sensor Stimulation Section of Earth Viewing Equipment Module Test Set
- d. Aft Equipment Module Test Set

9.5.3.6 Thermal-Vacuum Tests

These tests would require special equipment, in addition to the test sets discussed in Sections 9.5.3.2 through 9.5.3.5 (as applicable), to support the special environmental requirements. Guidance and Control Sensor stimulators would require changes to adapt them to the thermal-vacuum environment. Heaters for temperature control of the spacecraft would be needed, as well as temperature monitoring equipment.

9.5.3.7 Rf

Test equipment to conduct rf measurements on the spacecraft would be basically commercial rf test equipment.

9.5.3.8 Pad

The equipment required at ETR, to conduct prelaunch tests and to support launch, would consist of the System Test equipment, discussed in Section 9.5.3.5, plus special equipment needed to checkout the pad wiring. This last would consist of an AGE simulator and a Spacecraft and Adapter simulator, which would allow verification of cabling interface between the spacecraft and the AGE, (the only "new" link at launch), without tying up or endangering the actual units.

9.5.4 EQUIPMENT LIST

Table 9.5-1 is a list of the Electrical Support Equipment (ESE), by functional group. The Use heading refers to those areas discussed in Section 9.5.3 and the Complexity heading is based on the following key:

- A. Little or No Development Required - Existing equipment can be modified, similar equipment designed or off-the-shelf commercial items used.
- B. New Design - Within the State-of-the-Art - Equipment would require design, but no major development would be required.
- C. New Design - State-of-the-Art Development - Equipment would require a significant development program.

Table 9.5-1. Equipment List (ESE)

Name	Description	Use Area						Complexity		
		Sub-Sys.	Mod.	Sys.	T/V	RF	Pad	A	B	C
9.5.4.1 <u>Phased Array Test Set</u> 9.5.4.1.1 <u>Subsystem Console</u>	Supply power to subsystem, monitor test points, and provide troubleshooting capability.	X							X	
9.5.4.1.2 <u>Input/Output Console</u>	Capable of end-to-end check of subsystem, provide verification of input/output functions.	X	X	X	X		X		X	
9.5.4.2 <u>Interferometer Test Set</u> 9.5.4.2.1 <u>Subsystem Console</u>	Supply power to subsystem, monitor test points, and provide troubleshooting capability.	X							X	
9.5.4.2.2 <u>Input/Output Console</u>	Capable of end-to-end check of subsystem, provide verification of input/output functions.	X	X	X	X		X		X	
9.5.4.3 <u>Parabolic Antenna Test Set</u> 9.5.4.3.1 <u>Subsystem Console</u>	Supply power to subsystem, monitor test points, and provide troubleshooting capability.	X							X	
9.5.4.3.2 <u>Input/Output Console</u>	Capable of end-to-end check of subsystem, provide verification of input/output functions.	X	X	X	X		X		X	
9.5.4.4 <u>Earth Viewing Equipment Module Test Set</u> 9.5.4.4.1 <u>G&C Sensor Stimulators & Controls</u>	Provide controlled stimulation to G&C sensors.	1	X	X	2		X		X	
9.5.4.4.2 <u>Aft Equipment Module Simulator</u>	Provide power to the module, monitor test points, and simulate electrical interface with Aft Equipment Module.		X						X	
9.5.4.5 <u>Aft Equipment Module Test Set</u>	Provide power to the module, simulate G&C Sensors, monitor test points, and simulate Earth Viewing Equipment Module interface.		X	X	X		X		X	
9.5.4.6 <u>TT&C Ground Station</u>	Receive rf Telemetry signal, record, process and display information in usable form. Supply rf signal to enter commands into the spacecraft.	X	X	X	X		X		X	
9.5.4.7 <u>RF Test Set</u> 9.5.4.7.1 <u>RF Test Console</u>	Commercial equipment required to perform VSWR, power measurements, antenna tuning, etc. on the spacecraft.					X		X		
9.5.4.7.2 <u>RF Dummy Load Box</u>	Provide isolation to protect spacecraft transmitters against open circuits during hardware tests.		X	X	X		X	X		
9.5.4.8 <u>Spacecraft/Adapter Simulator</u>	Unit will contain spacecraft and adapter electrical loads and will be used to verify pad wiring prior to mating with spacecraft.						X		X	
9.5.4.9 <u>Pad AGE Simulator</u>	Unit will contain equipment to simulate the power supplied by the AGE & the loads presented by the AGE, to the pad wiring. Used in conjunction with 9.5.4.8.						X		X	
9.5.4.10 <u>Launch Cable Configuration Simulator</u>	Unit will contain components to simulate loading effects of cables used in the launch configuration, for mock count-down tests.			X				X		
9.5.4.11 <u>Thermal-Vacuum Test Equipment</u> 9.5.4.11.1 <u>Temperature Control & Readout</u>	Equipment required to control the spacecraft temperature and monitor this temperature while the spacecraft is in the thermal-vacuum environment.				X				X	
9.5.4.11.2 <u>G&C Sensor Stimulators</u>	Provide stimulation to G&C sensors in the thermal vacuum environment. Must be compatible with the controls of item 9.5.4.4.1.				X				X	

1 Used for testing of G&C Subsystem
2 Used to control item 9.5.4.11.2.

17-6

22-6

9.6 TEST FACILITIES

9.6.1 TEST FACILITY SUPPORT

A review of the Major Article Test Flow, Figure 9.3-1, shows major test facility requirements. In the main, presently available commercial or government facilities will meet the program needs. The Facility column in the Support Equipment Matrix, Table 9.2-1, presents an overall view of these facilities for subsystem and system requirements. Facilities for component testing have not been presented, since these are generally available to any large spacecraft contractor. The several problem areas are further discussed below.

9.6.2 TEST FACILITY PROBLEM AREAS

9.6.2.1 Vibration, Deployed

While vibration testing of the spacecraft in the launch configuration is possible at several existing locations, testing the deployed configuration is unique. The large area, lightweight construction and low resonant frequencies must be considered. Sine surveys at the required 0.01 to 20 cps range generally have not been necessary for spacecraft. This, coupled with the necessity to evaluate antenna and spacecraft with space simulated damping, dictates vibration testing in a large low pressure (10^{-1} torr) enclosure.

The present deployed configuration with solar panels would then require a facility with a 45 to 50 foot diameter. The solar panels could be simulated dynamically and the facility dimensions would then be constrained only by the antenna 30-foot diameter. This allows the use of several vacuum chambers throughout the country.

The low frequency requirement can be met by commercially available hydraulic exciters.

The remaining problem is then integrating the exciters and the chamber. Since the vacuum requirement is not severe, and the force level not high, this integration is not a state-of-the-art extension.

9.6.2.2 Large Antenna RF Testing

As far as can be determined, no present antenna range can adequately evaluate the large antenna. The high gain, narrow-beam antenna presents a pattern measurement and evaluation problem. This is further complicated by the antenna 1-g sag. Additional study is required before an adequate solution can be found.

9.7 LAUNCH FACILITIES

9.7.1 MECHANICAL SUPPORT OPERATIONS

The field operations are based on the least amount of assembly while establishing the maximum of confidence in the vehicle systems. The Mechanical Support Equipment (MSE) for the field operations utilizes the same equipment used during the factory operations and will be in most cases that equipment previously used for support of the Prototype Spacecraft.

The necessary field operations are:

- a. Transportation between remote facilities, e. g. , Missile Assemble Building and Explosive Safe Area and Launch Pad.
- b. Support the spacecraft during checkout system and validation tests. (9.4.3.1)*
- c. Alignment and Alignment checks of subsystem, components, and Apogee motor. (9.4.3.2)
- d. Mating operations of
 1. Apogee motor and spin motors to the spacecraft
 2. Spacecraft to the booster (9.4.3.1 and 9.4.3.3)
- e. Spin balancing of spacecraft with the Apogee motor. (9.4.3.3)
- f. Leak checking of the pneumatic systems. (9.4.3.5)
- g. Loading of consumables. (9.4.3.5)
- h. Arming

*Refer to previous sections describing the equipment and operations

This MSE will have been checked out during the dry run of the prototype vehicle, thus it will be ready for use when the flight vehicle arrives at ETR.

9.7.2 EXISTING LAUNCH FACILITIES

The facilities currently available at AFETR appear adequate to support the receiving inspection, checkout, test and launch of the ATS-4. Existing clean rooms, assembly areas and launch pad facilities and cranes can easily be adapted with a minimum amount of modification and expenditure for this program. NASA Merritt Island Launch Area (MILA) facilities were not considered in this study because of the Apollo Launch schedules planned.

If the clean room area in hanger AE proves to be too small in future evaluations, hanger AM could be utilized with a minimum amount of modifications.

Transportation of the spacecraft with its yaw-axis vertical, assuming a total height of 35 inches above the road surface, would not present a problem.

The current configuration of Launch Complex 36B Gantry Service Tower is satisfactory for installation of the payload. Some modification of the existing tower environmental enclosure may be required and any required access platforms must be provided.

Other services available should not present a problem. The proposed propellant, ammonia and gas servicing units can be lifted to the payload gantry level by crane or elevator, thus eliminating servicing units.

The launch facilities at the AFETR are shown in Figure 9.7-1. Indicated on the sketch is a 10,000 foot skid strip capable of handling lightly loaded turbine aircraft. The strip is currently used by NASA to receive C-130 and modified B-377 aircraft carrying Apollo capsular and S-IVB Saturn V stages. This strip is available to receive daylight landings of aircraft capable of operation from a 10,000 ft. runway length. An additional landing area is available at Patrick Air Force Base.

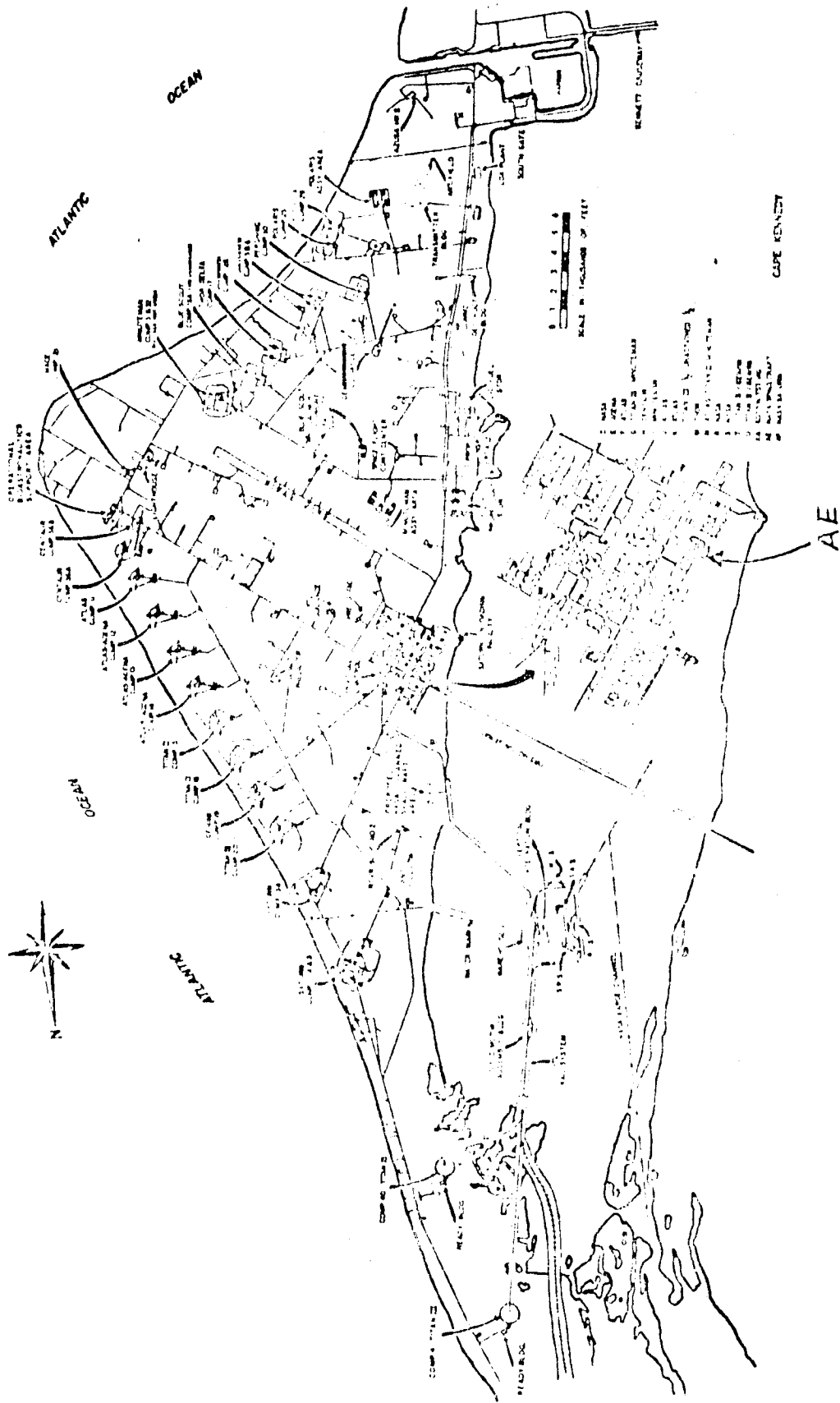


Figure 9.7-1. Cape Kennedy Launch Sites

Several hangers located in the industrial area at AFETR are of sufficient size for the receiving inspection, checkout and preassembly operations required to support an ATS program. Currently hangers AE and AM are assigned to the NASA Unmanned Launch Operations Group. Hanger AE indicated in Figure 9.7-1, is equipped with a 40 foot wide x 40 foot long x 40 foot high laminar flow clean room. Hanger AM is not equipped with a clean room but is environmently controlled. Humidity levels in this hanger can be maintained at 50 to 60% relative humidity. Operation of the air-conditioning system for 1 to 1 1/2 days after closing the hanger will provide 100,000 class clean room conditions. The high bay dimensions of hanger AM are approximately 70 feet wide x 120 feet long x 35 feet high.

The handling of the proposed apogee rocket motor, a Class III explosive, in the assembly area would be restricted by the AFETR range safety office. The rocket motor could be stored in the range solid propellant storage area. This facility is equipped with radiation equipment capable of checking the rocket motor grade. Installation of the rocket motor to the spacecraft can be accomplished at the Unmanned Spacecraft Spin Test Facility. This facility, currently under construction, will be available in 1967. Spin testing of the spacecraft can also be accomplished in this facility, which is approved for hazardous operations.

The launch area equipped to handle Atlas-Centaur launch vehicles is Launch Complex 36. Two pads, A and B, are located in this complex. Their positions are indicated in Figure 9.7-1. Two land roadways approximately 18 feet wide connect the launch complex with the industrial area. Suitable routing along these roadways can provide a route clear of overhead obstacles. Missile grade liquids available at the launch complex are:

- a. RF-1 (kerosene)
- b. Liquid Oxygen, LO_2
- c. Helium, H_2
- d. Nitrogen, N_2
- e. Liquid Nitrogen, LN_2
- f. Liquid Hydrogen, LH_2

A side elevator sketch of the Launch Complex 36B Gantry Service Tower is shown in Figure 9.7-2. This tower, equipped with a bridge crane, has a clearance from payload-Centaur mating plane to top hook height of approximately 48 feet. It is designed to allow a future height extension of 30 feet. The tower is divided into 22 levels of which the lower eight are 8 feet 6 inches high and upper 14 are 10 feet high. All levels from the launch vehicle base to the top of the tower may be enclosed by closing sliding panels and their respective windows. An environmental enclosure is currently installed in the tower. It is located approximately 90 feet 6 inches above the Atlas base, and it extends 30 feet. An elevator approximately 4 feet x 5 feet is included that extends to the level immediately below the bridge crane. A stair case of equal length is included on the opposite side of the structure.

9.8 ORBITAL SUPPORT

The facilities required to support the ATS-4 operational program during launch and during orbital experiments have been broadly discussed in Sections 7 and 8. The identification of exact facilities required involve a complex tradeoff of cost, experiment design, and operational considerations but assume a necessity for the following:

- a. Command Generation Computers (GSFC)
- b. On-line computers for Data Processing (GSFC) (7094 or equivalent)
- c. Off-line computers (GSFC and Initial Contractors) (7094 or equivalent)
- d. Rosman II, Mojave and Transportable (Towoomba) Ground Stations and all existing equipment and capability.
- e. Aircraft (or other transportable facility) equipped for Phased Array Experiments
- f. Supplemental Ground Station Equipment

Facilities listed in items a through e are assumed to exist and available for ATS-4 operations.

The Supplemental Ground Station Equipment (f) required to implement the desirable ATS-4 experiments as outlined and discussed in Section 8 are shown in Table 9.8-1.

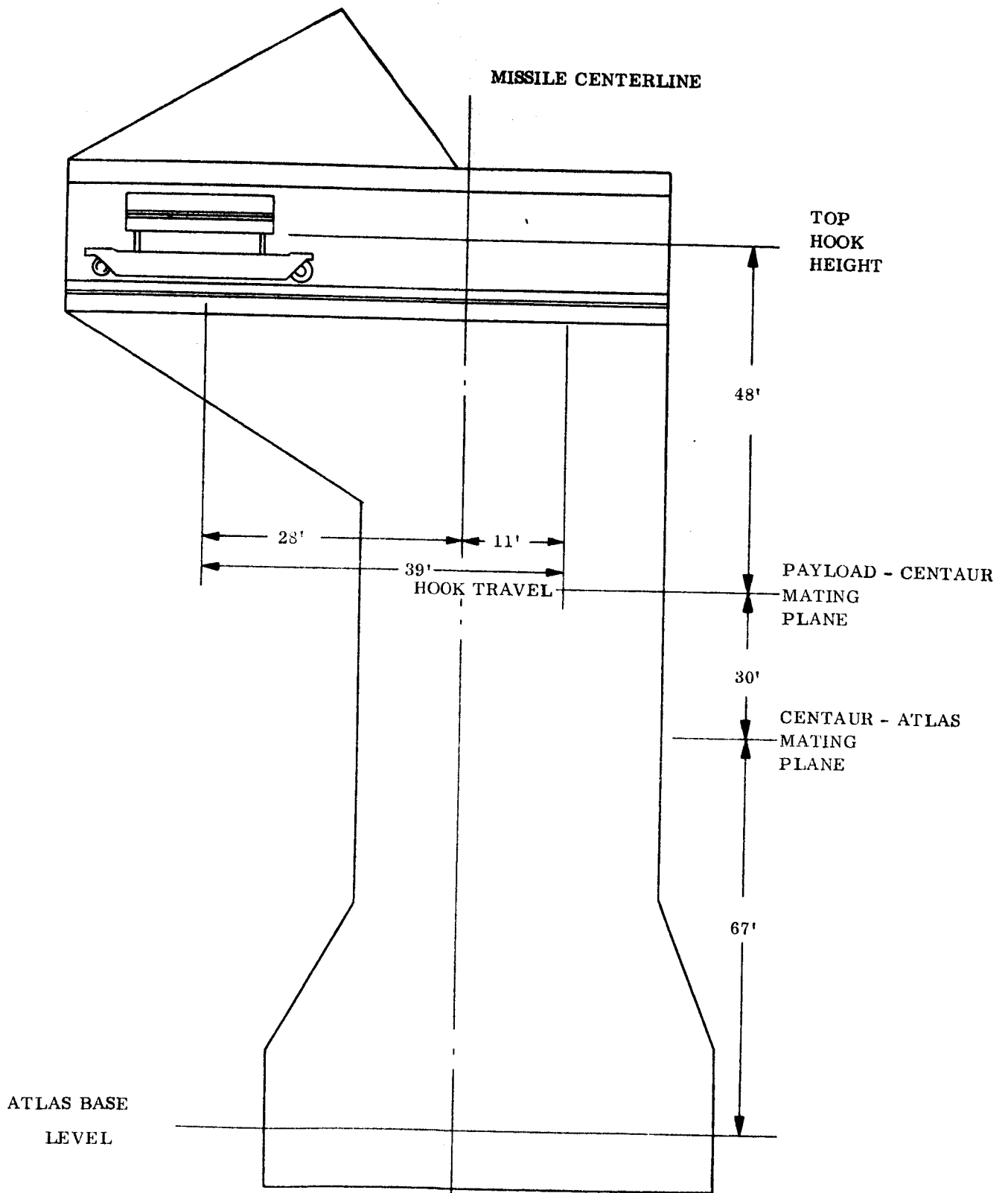


Figure 9.7-2. Launch Complex 36B Gantry Service Tower

Table 9.8-1. Ground Station Equipment Requirements Summary

Item No.	Description	Stations			Requirements
		R	M	T	(Total)
A1	Additional reflector (40 foot Dia. or larger, Parab, Casseg. feed)	X			1
A2	C _{C/X} band Cassegrain feed assy. 7-8 GHz Xmit/RCV; 2.2-2.3 RCV	X	X		2
A3	X _{C/f} band Cassegrain feed assy. 1.7-2.1 GHz Xmit/RCV; 2.2-2.3 RCV	X	X	X	3
A4	L _T band Cassegrain Assy. 0.8 and 0.1 GHz receive only	X			1
S1	AM transmitter modulator and control	X	X		2
S2	Video WB FM transmitter modulator and control	X	X		2
S3	AM power amplifier	X	X		2
S4	Video WB FM power amplifier	X	X		2
S5	Power supplies and heat exchangers, AM and video WB FM	X	X		2
S7	SSB receiver	X	X		2
S8	Video WB FM receiver	X	X		2
S9	AM receiver	X	X		2
S10	Spacecraft polarization E-vector sensing and orientation measurement console	(X)		X	2

Table 9.8-1. Ground Station Equipment Requirements Summary (Cont'd)

Item No.	Description	Stations			Requirements (Total)
		R	M	T	
S11	7-10 GHz frequency gen. osc. stage *(2 ea.)	X*	X		3
	Driver stage *(2 ea.)	X*	X		3
	Power amplifier *(2 ea.)	X*	X		3
E1	Comm. test & eval. consoles				
	a) Parabolic antenna	X	X	X	3
	b) Phased array	X	X		2
	c) Interferometer	X	X		2
E2	Ground station - comm. exp. interface and test consoles and equip- ment				
	a) All experiments	X	X		2
	b) Parabolic antenna only			X	1
T1	Test set AM Xmit/RCV	X	X		2
T2	Test set video WB FM Xmit/RCV	X	X		2
A1	Aircraft controlling communications net	X			1
A2	Aircraft (or other transportable ground station) Equipped with phased array challenge or receiving capability	X			1

9.9 SOFTWARE

The various computer programs necessary to implement ATS operations involve three general categories:

- a. Orbit
- b. Command and control
- c. Data handling and processing.

Of these, only the last will involve design, development and implementation problems significantly different from previous NASA programs.

The various computer programs, their design and development problems are outlined in Table 9.9-1.

Table 9.9-1. ATS-4 Computer Program Requirements

Item	Description	Similar Program Complexity	Location			Integration Contractor
			GSFC	G/S		
				R	M	
C1	Command generation software	Syncom II	X			
C2	Command initiation software	Syncom II		X	X	X
C3	Precession control S. W.	ATSB ATSC	X			
C4	Precession control initiation S. W.	ATSB ATSC		X		X
T1	Range/range rate system		X	X	X	X
T2	Synchronous orbit tracking system		X	X	X	X
E1	Orbit determination software		X			
E2	Stationkeeping parameter determ. prog.		X			
E3	Sun ephemeris det.		X			
E4	Sun-to-satellite oreintation prog.		X			
DS1	G/s on-line S/C status data display			X	X	X
DS2	G/s command verif. prog.			X	X	X
DS3	G/s off-line data reduction/display			X	X	X

Table 9.9-1. ATS-4 Computer Program Requirements (Cont'd)

Item	Description	Similar Program Complexity	Location				Integration Contractor
			GSFC	G/S			
				R	M	T	
DG1	GSFC on-line data red and status		X				
DG2	Experiment param. data red and display		X				
DG3	Data merging program (TLM, Exp. , Ephem)		X				
DG4	Off-line data reduction program		X				
DG5	Quick look attitude determination program		X				
DG6	Spin axis attitude determination program		X				
DI1	Attitude determination and geometrical transforms program						X
DI2	Data pack generation program						X
DI3	Math model correlation program						X
DI4	Statistical parameter program (S)						X
DI5	Antenna pattern mapping						X

TECHNICAL APPENDIXES

APPENDIX A

PARABOLIC REFLECTOR FEED SELECTION CHARTS

PARABOLIC REFLECTOR FEEDS

TYPE	FOCUS		FOCUS			
	PRIME	CASSE-GRAIN	LINEAR	CIRCULAR		
1. Conical spiral	X			X		
2. Conical spiral		X		X		
3. Dieguide	X			X		
4. Dieguide		X		X		
5. Dipole	X		X		59 in.	59 in.
6. Dipole	X			X	59 in.	59 in.
7. Dipole		X		X		
8. Helix	X			X	8 ft dia	
9. Helix		X		X	8 ft dia	
10. Horn	X			X	9 ft	9 ft
11. Horn		X		X	18 ft	18 ft
12. Log periodic	X			X		Excessive
13. Log periodic		X		X		Excessive
14. Planar spiral	X			X	60 in.	60 in.
15. Planar spiral		X		X		
16. Slot	X		X		59 in.	
17. Slot		X	X			59 in.

ART FREQUENCY 100 MHz (Transmit)

FEED						MECHANICAL COMPLEXITY						
LENGTH	WEIGHT	PRECISION	PACKAGING	DEPLOYMENT	THERMAL	TYPE	POLARIZERS			WT	AVAIL	
							SIZE					
							HT	WD	DF			
Approx. 70 ft											-	
30 in.	12 lb	Low	None req'd	None req'd	Almost open						-	
30 in.	12 lb	Low	None req'd	None req'd	Almost open	Coax cables					-	
10 ft											-	
23 ft											-	
4 ft											-	
20 ft											-	
35 in.	26 lb	Low	None req'd	None req'd	Half open	Not req'd					-	
30 in.	30 lb										-	

A-2-2

AUXILIARY EQUIPMENT

ELECTRICAL CIRCUITRY

FILTERS						HYBRIDS						INTERCONNECTING TRANS LINE					
TYPE	SIZE			WT	AVAIL.	TYPE	SIZE			WT	AVAIL.	TYPE	SIZE			WT	
	HT	WD	DP				HT	WD	DP				HT	WD	DP		
Not req req'd						Not req'd						Coax					
Not req'd																	

MECHANICAL EQUIPMENT															PERFORMANCE LIMITATIONS
TRANS LINE TO INTERFACE					DEPLOYMENT					FEED MOVEMENT					
TYPE	SIZE			WT	TYPE	SIZE			WT	TYPE	SIZE			WT	
	HT	WD	DP			HT	WD	PD			HT	WD	DP		
					None						None				Feeding problem
					None						None				Mechanically too large No suitable feed available for this frequency & 30 ft dish No suitable feed available for this frequency & 30 ft dish No advantage (with slot) over circ. dipole array Proper aperture illumination Insufficient gain Too much feed blockage Too much feed blockage Too much feed blockage Too much feed blockage Too much feed blockage Proper aperture illumination Insufficient gain Insufficient gain

DEVELOPMENT		FEED COMPATIBILITY WITH OTHER FEEDS AT OTHER FREQUENCIES (except 100 MHz)	REMARKS
REQUIREMENTS	RISK		
		Not compatible with other feeds.	Unsuitable
		No convenient feeding scheme available for feeding 100 MHz portion only	Unsuitable
		Not compatible with other feeds	Unsuitable
			Unsuitable
			Unsuitable
		Must be used with slot for circular polarization	Unsuitable
		Possibility of using sub-dish split into dipole sections	Conditional
		Too much feed blockage for other feeds	Unsuitable
		Too much feed blockage for other feeds	Unsuitable
		Too much feed blockage for other feeds	Unsuitable
		Too much feed blockage for other feeds	Unsuitable
		Possibility of winding spiral behind sub-dish of Cassegrain	Unsuitable Unsuitable Conditional
		Must be located in ground plane structure not compatible	Unsuitable Unsuitable Unsuitable

A-2-5

PARABOLIC REFLECTOR FEED SELECTION CHART

TYPE	FOCUS		POL		HEIGHT	WIDTH		
	PRIME	CASSE- GRAIN	LINEAR	CIRCULAR				
1. Conical spiral	X			X	5 in. dia			
2. Conical spiral		X		X	4 in. dia			
3. Dieguide	X			X		Horn		
4. Dieguide		X		X		Horn		
5. Dipole	X		X		8 in.	8 in.		
6. Dipole	X			X	8 in.	8 in.	4 in.	0.7
7. Dipole		X		X				
8. Helix	X			X	12 in. dia		14 in.	2 lb
9. Helix		X		X	12 in. dia		34 in.	3 lb
10. Horn	X			X	14 in.	14 in.	4 in.	1 lb
11. Horn		X		X	27 in.	27 in.	29 in.	4 lb
12. Log periodic	X			X	10 in.	10 in.	10 in.	1.2
13. Log periodic		X		X			Excessive	
14. Planar spiral	X			X	9 in. dia		5 in.	1 lb
15. Planar spiral		X		X				
16. Slot	X		X		8 in.	8 in.	4 in.	3 lb
17. Slot		X	X					

FREQUENCY 800 MHz (Transmit)

MECHANICAL COMPLEXITY											
WEIGHT	PRECISION	PACKAGING	DEPLOYMENT	THERMAL	TYPE	POLARIZERS				AVAIL.	TYPE
						SIZE			WT		
						HT	WD	DP			
	Some detail of winding	Not req'd	Fixed	Almost opaque	Not req'd						
More than 1 lb		Not package- able									
0 lb		Not package- able									
5 lb	Little	Not req'd	Fixed	Almost open	Phase (coax) net- work with slot				Yes	Not req'd	
5 lb	Little	Not req'd	Fixed	Almost open	Coax cables				Yes	Not req'd	
	Some detail of winding	Not req'd	Fixed	Almost open	Not req'd					Not req'd	
	Some detail of winding	Not req'd	Fixed	Almost open	Not req'd					Not req'd	
	Some detail	Not req'd	Fixed	Almost opaque	Probe coupled		In horn		Develop	Not req'd	
	Some detail	Not req'd	Fixed	Almost opaque	Probe coupled		In horn		Develop	Not req'd	
1 lb	Some layout detail	Not req'd	Fixed	Almost open	Not req'd						
	Some detail	Flat disc	Fixed	Half open	Not req'd					Space filters for cavity band- width	
	Some detail of cavity	Not req'd	Fixed	Almost opaque	Phase net- work with dipole				Yes	Not req'd	


AUXILIARY EQUIPMENT

ELECTRICAL CIRCUITRY

FILTERS					HYBRIDS					INTERCONNECTING TRANS LINE					TRANS LINE	
SIZE			WT	AVAIL.	TYPE	SIZE			WT	AVAIL.	TYPE	SIZE			WT	TYPE
HT	WD	DP				HT	WD	DP				HT	WD	DP		
					Not req'd						Balun-coax			8 in.		Coax
					Not req'd						Strip line power split & phase shifter					
											Strip line power split & phase shifters					

MECHANICAL EQUIPMENT														PERFORMANCE LIMITATIONS	IC
NE TO INTERFACE				DEPLOYMENT				FEED MOVEMENT							
SIZE			WT	TYPE	SIZE			WT	TYPE	SIZE			WT		
HT	WD	DP			HT	WD	PD			HT	WD	DP		WT	
				None					Axial					Efficiency, match at all frequencies	Balun
				None					None					Efficiency, match at all frequencies	high fr
				None					None					Gain questionable	Some
				None					None					Gain questionable	Some
				None					None					Insufficient gain	Some
				None					None					Circularity question-able	Some
				None					None					None noted	Some
				None					None					None noted	Phase
				None					None					None noted	trol w
				None					None					None noted	al cur
				None					None					None noted	Phase
				None					Axial					None noted	trol w
				None					Axial					Gain for antenna of practical length	Some.
				None					Axial					None noted	Mainta
				None					None					Insufficient gain	width
				None					None					Gain questionable	Some
				None					None					Insufficient gain	Some

DEVELOPMENT		FEED COMPATIBILITY WITH OTHER FEEDS AT OTHER FREQUENCIES (except 100 MHz)	REMARKS	
REQUIREMENTS	RISK			
Compatible with frequency end	Medium		Conditional	
		Too long to be compatible with other feeds	Unsuitable	
	High	Must be used for all feeds	Unsuitable	
	High	Must be used for all feeds	Unsuitable	
	Little	Must be used with slot for circular polarization	Conditional	
	Little	Coupling with external members	Conditional	
	Medium	Coupling with external members	Unsuitable Conditional	
	Little	Coupling with external members	Conditional	
	Amplitude control probe, external	Medium	External currents disturb small horn, coaxial modes possible with internal feeds	Conditional
		Little	External members have little effect. Coaxial modes possible with antenna feeds	Acceptable
Little			Not compatible with other feeds	Conditional
Constant beam-	Medium	External members have little effect	Unsuitable	
			Conditional	
	Little	Must be used with linear dipole for circular polarization	Unsuitable Conditional	
			Unsuitable	

A-4-4


PARABOLIC REFLECTOR FEED SELECTION CHART

TYPE	FOCUS		POL		HEIGHT	WIDTH
	PRIME	CASSE- GRAIN	LINEAR	CIRCULAR		
1. Conical Spiral	X			X	5 in. Dia.	
2. Conical Spiral		X		X	4 in. Dia.	
3. Dieguide	X			X		Horn
4. Dieguide		X		X		Horn
5. Dipole	X		X			
6. Dipole	X			X		
7. Dipole		X		X		
8. Helix	X			X	5 in. Dia.	
9. Helix		X		X	5 in. Dia.	
10. Horn	X			X	6 in.	6 in.
11. Horn		X		X	11 in.	11 in.
12. Log periodic	X			X	10 in.	10 in.
13. Log Periodic		X		X		Excessive
14. Planar Spiral	X			X	9 in. Dia.	
15. Planar Spiral		X		X		
16. Slot	X		X		3 in.	3 in.
17. Slot		X	X			

A-5

T FREQUENCY 1.7 and 2.1 GHz (Receive), 2.3 GHz (Transmit)													
FEED													
MECHANICAL COMPLEXITY													
DEPTH	WEIGHT	PRECISION	PACKAGING	DEPLOYMENT	THERMAL	TYPE	POLARIZERS				WT	AVAIL.	
							SIZE			WT			AVAIL.
							HT	WD	DP				
13 in.	1 lb.	Some detail of winding	None req'd	Fixed	Almost open	Not req'd							
9 in.	4 lb.	More than Cassegrain 500 lb. 3500 lb.	None req'd	Fixed	Almost open	Not req'd							
			Not packageable										
			Not packageable										
6 in.	0.2 lb.	Some detail of winding	None req'd	Fixed	Almost open	Not req'd							
14 in.	0.3 lb.	Some detail of winding	None req'd	Fixed	Almost open	Not req'd							
1.5 in.	0.5 lb.	Some detail	None req'd	Fixed	Almost opaque	Probe coupled		In Horn				Develop	
11 in.	1 lb.	Some detail	None req'd	Fixed	Almost opaque	Probe coupled		In Horn				Develop	
10 in.	1.25 lb.	Some layout detail	None req'd	Fixed	Almost open	Not req'd							
5 in.	1 lb.	Some detail	None req'd	Fixed	Half open	Not req'd							
1.5 in.	1.5 lb.												

AUXILIARY EQUIPMENT

ELECTRICAL CIRCUITRY

FILTERS						HYBRIDS						INTERCONNECTING TRANS LINE					
TYPE	SIZE			WT	AVAIL.	TYPE	SIZE			WT	AVAIL.	TYPE	SIZE			WT	
	HT	WD	DP				HT	WD	DP				HT	WD	DP		
												Balun-coax					

MECHANICAL EQUIPMENT															PERFORMANCE LIMITATIONS
TRANS LINE TO INTERFACE					DEPLOYMENT					FEED MOVEMENT					
TYPE	SIZE			WT	TYPE	SIZE			WT	TYPE	SIZE			WT	
	HT	WD	DP			HT	WD	PD			HT	WD	DP		
					None						Axial				Lossy conductors Efficiency, match all frequencies Efficiency, match all frequencies Dipole is bandwidth limited Dipole and C-P circuitry are bandwidth limited Insufficient gain Circularity questionable None noted None noted None noted Dish illumination v frequency Gain: for antenna practical length Lossy conductors Insufficient gain No dipole available for C. P. combination Insufficient gain
											Axial				
					None						None				
					None						None				
					None						None				
					None						None				
					None						None				
					None						None				

A-6-3

DEVELOPMENT		FEED COMPATIBILITY WITH OTHER FEED AT OTHER FREQUENCIES (except 100 MHz)	REMARKS
REQUIREMENTS	RISK		
Balun compatible with high frequency end	Medium	Not compatible with other feeds	Conditional
	High	Too long to be compatible with other feed	Unsuitable
		Must be used for all feeds	Unsuitable
		Must be used for all feeds	Unsuitable
			Unsuitable
		Unsuitable	
Some	Medium	Coupling with external members	Unsuitable Conditional
Some Phase 4 amplitude control with probes, external currents	Little	Coupling with external members	Acceptable
	Medium	External currents disturb small horn, coaxial modes possible with internal feeds	Conditional
Phase 4 amplitude control with probes	Little	No problems with external mem- bers, coaxial modes possible with internal feeds	Acceptable
Feed detail, suitable balun	Medium	Not compatible with other feeds	Conditional
			Unsuitable
Maintain constant beam- width	Medium	Not compatible with other feeds	Conditional
			Unsuitable
			Unsuitable

A-6-4


PARABOLIC REFLECTOR FEED SELECTION CHART

TYPE	FOCUS		POL		HEIGHT	WIDTH
	PRIME	CASSE-GRAIN	LINEAR	CIRCULAR		
1. Conical Spiral	X			X	5 in. Dia.	
2. Conical Spiral		X		X	4 in. Dia.	
3. Dieguide	X			X		Horn
4. Dieguide		X		X		Horn
5. Dipole	X		X			
6. Dipole	X			X		
7. Dipole		X		X		
8. Helix	X			X	1.5 in. Dia.	
9. Helix		X		X	1.5 in. Dia.	
10. Horn	X			X	1.5 in.	1.5 in.
11. Horn		X		X	3 in.	3 in.
12. Log Periodic	X			X	10 in.	10 in.
13. Log Periodic		X		X		Excessive
14. Planar Spiral	X			X	9 in. Dia.	
15. Planar Spiral		X		X		
16. Slot	X		X			
17. Slot		X	X			

FREQUENCY 7.3 GHz (Transmit), 8.0 GHz (Receive)

FEED

MECHANICAL COMPLEXITY

DEPTH	WEIGHT	PRECISION	PACKAGING	DEPLOYMENT	THERMAL	TYPE	POLARIZERS					
							SIZE			WT	AVAIL	
							4T	WD	DP			
13 in.	0.75 lb.	Detailed	None req'd	Fixed	Almost open	Not req'd						
9 ft.	More than Cassegrain 500 lb 3500 lb		Not packageable Not packageable									
2 in.	0.1 lb.	Detailed	Wire-mesh ground plane	Fixed structure radiator	Almost open	Not req'd						
4 in.	0.1 lb.	Detailed	Wire-mesh ground plane	Fixed structure radiator	Almost open	Not req'd						
0.5 in.	0.1 lb.	Detailed	Fixed structure	Fixed structure	Almost opaque	Probe coupled			In Horn			Develop
3 in.	0.5 lb.	Detailed	Fixed structure	Fixed structure	Almost opaque	Probe coupled			In Horn			Develop
10 in.	1.25 lb.	Detailed	None req'd	Fixed	Almost open	Not req'd						
5 in.	1 lb.	Detailed	None req'd	Fixed	Half open	Not req'd						

A-8-1

AUXILIARY EQUIPMENT


ELECTRICAL CIRCUITRY

FILTERS						HYBRIDS						INTERCONNECTING TRANS LINE				
TYPE	SIZE			WT	AVAIL.	TYPE	SIZE			WT	AVAIL.	TYPE	SIZE			WT
	HT	WD	DP				HT	WD	DP				HT	WD	DP	
												Balun-coax				

A-8-2

MECHANICAL EQUIPMENT															PERFORMANCE LIMITATIONS	
TRANS LINE TO INTERFACE					DEPLOYMENT					FEED MOVEMENT						
TYPE	SIZE			WT	TYPE	SIZE			WT	TYPE	SIZE			WT		
	HT	WD	DP			HT	WD	PD			HT	WD	DP			
WR-112					None						Axial					Lossy conductors High losses in spiral winding Efficiency, match all frequencies Efficiency, match
WR-112					None						None					Dipole is bandwidth limited Dipole and circuit bandwidth limited Insufficient gain High line losses, poor axial ratio
WR-112					None						None					High line losses
WR-112					None						None					None noted
WR-112					None						None					None noted
WR-112					None						Axial					Lossy conductors feed line, illumination change with frequency Gain: for antenna practical length
WR-112					None						None					Lossy conductors Insufficient gain No dipole available for C.P. combination Insufficient gain

DEVELOPMENT		FEED COMPATIBILITY WITH OTHER FEEDS AT OTHER FREQUENCIES (except 100 MHz)	REMARKS
REQUIREMENTS	RISK		
Feedpoint detail nonradiating balun	Medium	Not compatible with other feeds	Used only if conical spiral is used for lower frequencies --Conditional-- Unsuitable
	High	Too long to be compatible with other feeds	Unsuitable
	High	Must be used for all feeds	Unsuitable
	High	Must be used for all feeds	Unsuitable
Some	Medium	External and internal fields near the helix	Unsuitable
Some	Little	External and internal fields near the helix	Conditional
Phase & amplitude control with probes, external currents	Medium	External currents disturb small horn	Conditional
Phase & amplitude control with probes	Little	No problems	Acceptable
Feed point detail suitable balun	Medium	Not compatible with other feeds	Used only if log-periodic is used for lower frequencies --Conditional-- Unsuitable
Maintain constant beamwidth, feedpoint detail, suitable balun	Medium	Not compatible with other feeds	Used only if planar spiral is used for lower frequencies --Conditional-- Unsuitable
			Unsuitable
			Unsuitable

A-8-4


PARABOLIC REFLECTOR FEED SELECTION CHART

TYPE	FOCUS		POL		HEIGHT	WIDTH
	PRIME	CASSE- GRAIN	LINEAR	CIRCULAR		
1. Conical spiral	X			X	10 in.	10 in.
2. Conical spiral		X		X	12 in.	12 in.
3. Dieguide	X			X		Horn
4. Dieguide		X		X		Horn
5. Dipole	X		X			
6. Dipole	X			X		
7. Dipole		X		X		
8. Helix	X			X		
9. Helix		X		X	14 in.	14 in.
10. Horn	X			X	6 in.	6 in.
11. Horn		X		X	11 in.	11 in.
12. Log periodic	X			X	24 ft	24 in.
13. Log periodic		X		X	24 in.	24 in.
14. Planar spiral	X			X	18 in.	18 in.
15. Planar spiral		X		X	18 in.	18 in.
16. Slot	X		X		9 in.	9 in.
17. Slot		X	X		9 in.	9 in.

RT FREQUENCY 1.7 and 2.1 GHz (Receive) Monopulse

FEED						MECHANICAL COMPLEXITY					
DEPTH	WEIGHT	PRECISION	PACKAGING	DEPLOYMENT	THERMAL	TYPE	POLARIZERS				
							SIZE			WT	AVAIL.
							HT	WD	DP		
15 in.	3.5 lb	Some detail	None req'd	Fixed	Almost open	Not req'd				-	
15 in.	6 lb	Some detail	None req'd	Fixed	Almost open	Not req'd				-	
	More than Cassegrain 500 lb 3500 lb		Not package-able Not package-able			Not req'd				-	
						Not req'd				-	
6 in.	0.4 lb	Some detail	None req'd	Fixed	Almost open	Not req'd				-	
1 in.	2 lb	Reasonable	None req'd	Fixed	Almost opaque	Probe-coupled		In Horn		-	Devel
5 in.	3.5 lb	Reasonable	None req'd	Fixed	Almost opaque	Probe-coupled		In Horn		-	Devel
8 in.	8 lb	Some detail	None req'd	Fixed	Almost open	Not req'd				-	
10 in.	8 lb	Some detail	None req'd	Fixed	Almost open	Not req'd				-	
5 in.	1 lb	Some detail	None req'd	Fixed	Half open	Not req'd				-	
5 in.	4 lb	Some detail	None req'd	Fixed	Half open	Not req'd				-	
3 in.	4 lb					Not req'd				-	
3 in.	4 lb					Not req'd				-	

A-10-1

AUXILIARY EQUIPMENT

ELECTRICAL CIRCUITRY

FILTERS						HYBRIDS						INTERCONNECTING TRANS. LINE					
TYPE	SIZE			WT	AVAIL.	TYPE	SIZE			WT	AVAIL.	TYPE	SIZE			WT	
	HT	WD	DP				HT	WD	DP				HT	WD	DP		

A-10-2

MECHANICAL EQUIPMENT														PERFORMANCE LIMITATIONS		
TRANS LINE TO INTERFACE					DEPLOYMENT					FEED MOVEMENT						
TYPE	SIZE			WT	TYPE	SIZE			WT	TYPE	SIZE				WT	
	HT	WD	DP			HT	WD	PD			HT	WD	DP			
					None						Axial					Efficiency, poor illumination
					None						Axial					Efficiency
																Efficiency, match all frequencies
																Efficiency, match all frequencies
																Efficiency, Dipole bandwidth limited
																Efficiency, Dipole circuit is bandwidth limited
																Efficiency, Dipole circuit is bandwidth limited
																Efficiency poor illumination & ratio
					None						None					Efficiency
					None						None					Efficiency
					None						None					Efficiency
					None						Axial					Efficiency, poor illumination
					None						Axial					Efficiency
					None						None					Efficiency, poor illumination and spacing
					None						None					Efficiency, array spacing suitable, frequency limited
																Efficiency, poor illumination, no pole available for CP combination
																Efficiency, poor illumination, no pole available for CP combination

DEVELOPMENT		FEED COMPATIBILITY WITH OTHER FEED AT OTHER FREQUENCIES (except 100 MHz)	REMARKS
REQUIREMENTS	RISK		
Balun compatible with high frequency end.	Medium	Must be used for all frequencies (monopulse array not compatible)	Unsuitable
	Medium	Must be used for all frequencies (monopulse array not compatible)	Unsuitable
Balun compatible with high frequency end	High	Must be used for all feeds	Unsuitable
	High	Must be used for all feeds	Unsuitable
			Unsuitable
			Unsuitable
			Unsuitable
		Coupling with external members	Unsuitable due to performance limitations
Some Isolation between horns	Little	Coupling with external members	Unsuitable
	Medium	External currents distort small horns	Unsuitable
Phase & amplitude control with isolation	Medium	External members have little effect	Unsuitable
Feed detail, suitable balun	Medium	Must be used for all frequencies (monopulse array not compatible)	Unsuitable
Feed detail, suitable balun	Medium	Must be used for all frequencies (monopulse array not compatible)	Unsuitable
Maintain constant beamwidth	High	Must be used for all frequencies (monopulse array not compatible)	Unsuitable
Maintain constant beamwidth	High	Must be used for all frequencies (monopulse array not compatible)	Unsuitable
			Unsuitable
			Unsuitable

A-10-4



PARABOLIC REFLECTOR FEED SELECTION CHART

TYPE	FOCUS		POL.		HEIGHT	WIDTH	DEPTH
	PRIME	CASSE- GRAIN	LINEAR	CIRCULAR			
1. Conical spiral	X			X	12 in.	12 in.	15 in.
2. Conical spiral		X		X	10 in.	10 in.	15 in.
3. Dieguide	X			X		Horn	
4. Dieguide		X		X		Horn	
5. Dipole	X		X		2 in.	2 in.	1 in.
6. Dipole	X			X	2 in.	2 in.	1 in.
7. Dipole		X		X	2 in.	2 in.	1 in.
8. Helix	X			X			
9. Helix		X		X	1 in.	1 in.	1.5 in.
10. Horn	X			X	1.5 in.	1.5 in.	0.5 in.
11. Horn		X		X	3 in.	3 in.	1.5 in.
12. Log periodic	X			X	24 in.	24 in.	8 in.
13. Log periodic		X		X	24 in.	24 in.	10 in.
14. Planar spiral	X			X	18 in.	18 in.	5 in.
15. Planar spiral		X		X	18 in.	18 in.	5 in.
16. Slot	X		X		2 in.	2 in.	1 in.
17. Slot		X	X		2 in.	2 in.	1 in.

A-11

FREQUENCY 8.0 GHz (Receive) Monopulse

MECHANICAL COMPLEXITY						POLARIZERS					
WEIGHT	PRECISION	PACKAGING	DEPLOYMENT	THERMAL	TYPE	SIZE			WT	AVAIL.	TY
						HT	WD	DP			
6.0 lb	Detailed	None req'd	Fixed	Almost open	Not req'd						
3.5 lb	Detailed	None req'd	Fixed	Almost open	Not req'd						
More than Cassegrain 500 lb 3500 lb 0.5 lb		Not package-able Not package-able			Not req'd						
0.5 lb	Detailed	None req'd	Fixed structure	Almost open	Dipole lengths		In Dipole			Develop	Not req'd
0.5 lb	Detailed	None req'd	Fixed structure	Almost open	Dipole lengths		In Dipole			Develop	Not req'd
0.3 lb	Detailed	None req'd	Fixed structure	Almost open	Not req'd						
0.4 lb	Detailed	None req'd	Fixed structure	Almost opaque	Probe-coupled		In Horn			Develop	
0.8 lb	Detailed	None req'd	Fixed structure	Almost opaque	Probe-coupled		In Horn			Develop	
8 lb	Detailed	None req'd	Fixed	Almost open	Not req'd						
8 lb	Detailed	None req'd	Fixed	Almost open	Not req'd						
4 lb					Not req'd						
4 lb	Detailed	None req'd	Fixed	Half open	Not req'd						
0.7 lb					Not req'd						
0.7 lb					Not req'd						

AUXILIARY EQUIPMENT

ELECTRICAL CIRCUITRY

DE	FILTERS					HYBRIDS					INTERCONNECTING TRANS LINE					TH	
	SIZE			WT	AVAIL.	TYPE	SIZE			WT	AVAIL.	TYPE	SIZE				WT
	HT	WD	DP				HT	WD	DP				HT	WD	DP		

A-12-2

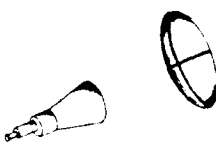
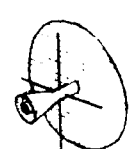
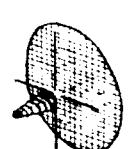
MECHANICAL EQUIPMENT															PERFORMANCE LIMITATIONS
TRANS LINE TO INTERFACE					DEPLOYMENT					FEED MOVEMENT					
TYPE	SIZE			WT	TYPE	SIZE			WT	TYPE	SIZE			WT	
	HT	WD	DP			HT	WD	PD			HT	WD	DP		
					None						Axial				Efficiency, poor Illumination, lossy circuit
					None						Axial				Efficiency, lossy circuit, lossy spiral winding Efficiency, match at all frequencies Efficiency, match at all frequencies Efficiency poor Illumination, lossy circuitry
					None						None				Efficiency poor Illumination, lossy circuitry
					None						None				Efficiency poor Illumination, lossy circuitry
					None						None				Efficiency poor Illumination & axial ratio, lossy circuitry
					None						None				Efficiency, lossy circuitry
					None						None				Efficiency
					None						Axial				Efficiency, poor Illumination
					None						Axial				Efficiency
					None						None				Efficiency, poor Illumination phase centers widely spaced Efficiency, phase centers widely spaced Efficiency, poor Illumination, lossy circuitry Efficiency, poor Illumination, lossy circuitry, insufficient gain

DEVELOPMENT		FEED COMPATIBILITY WITH OTHER FEED AT OTHER FREQUENCIES (except 100 MHz)	REMARKS
REQUIREMENTS	RISK		
Feedpoint detail, non-radiating balun	Medium	Must be used for all frequencies (monopulse array not compatible)	Used only if conical spiral is used for lower frequencies Unsuitable
Feedpoint detail, non-radiating balun	Medium	Must be used for all frequencies (monopulse array not compatible)	Unsuitable
	High	Must be used for all feeds	Unsuitable
	High	Must be used for all feeds	Unsuitable
		Must be used with slot, too complex for suitable monopulse	Unsuitable
Feed circuit	Medium	Coupling with external members	Unsuitable
Feed circuit	Medium	Coupling with external members	Unsuitable
		Coupling with external members	Unsuitable due to performance limitations
Some	Little	Coupling with external members	Unsuitable
Isolation between horns	Medium	External currents disturb small horn	Unsuitable
Phase & amplitude control with isolation	Medium	External members have little effect	Unsuitable
Feedpoint detail, suitable balun	Medium	Must be used for all frequencies (monopulse array not compatible)	Unsuitable
Feedpoint detail suitable balun	Medium	Must be used for all frequencies (monopulse array not compatible)	Unsuitable
Feedpoint detail suitable balun	High	Must be used for all frequencies	Unsuitable due to performance limitations
Feedpoint detail suitable balun	High	Must be used for all frequencies	Unsuitable
		Must be used with dipole, too complex for suitable monopulse	Unsuitable
			Unsuitable

A-12-4

PARABOLIC REFLECTOR COMPOSITE FEED SELECTION CHART

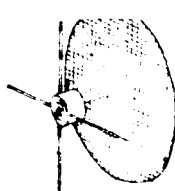





FEED	FREQUENCY (MHz)							FOCUS		POLARIZATION	POSSIBLE CONSTRUCTION	EST. WGT.	PKG. SIZE
	100	800	1700	2100	2300	7300	8000	PRIME	CASS.				
Dipole	X							X		CP	Split Sub-Reflector	—	—
Horn		X							X	CP	Fixed Horns	6 lb	50 in. DIA x 40 in. long
Horn			X						X	CP	Fixed Horns		
Horn				X					X	CP	Fixed Horns		
Horn					X				X	CP	Fixed Horns		
Horn						X			X	CP	Fixed Horns		
Horn							X		X	CP	Fixed Horns		
Horn								X	X	CP	Fixed Horns		
Dipole	X							X		CP	Wire Mesh Ground Plane	12 lb	—
Horn		X						X		CP	Fixed Horns	2 lb	14 in. DIA x 16 in. long
Horn			X					X		CP	Fixed Horns		
Horn				X				X		CP	Fixed Horns		
Horn					X			X		CP	Fixed Horns		
Horn						X		X		CP	Fixed Horns		
Horn							X	X		CP	Fixed Horns		
Horn								X	X	CP	Fixed Horns		
Dipole	X							X		CP	Wire Mesh Ground Plane	12 lb	—
Conical Spiral		X						X		CP	Fixed	1 lb	5 in. DIA x 13 in. long
Conical Spiral			X					X		CP	Fixed		
Conical Spiral				X				X		CP	Fixed		
Conical Spiral					X			X		CP	Fixed		
Conical Spiral						X		X		CP	Fixed		
Conical Spiral							X	X		CP	Fixed		
Conical Spiral								X	X	CP	Fixed		

SKETCH	DEPLOYMENT	TRANS LINE TO INTERFACE	COMPATIBILITY LIMITATIONS	
<u>SCHEME A</u> 	None Required ↓	COAX	Must be developed with other nearby structure in position	50% Effici
		COAX	Some development will be required to insure compatibility of coaxial horns	None
		COAX	Some development will be required to insure compatibility of coaxial horns	None
		COAX	Some development will be required to insure compatibility of coaxial horns	None
		COAX	Some development will be required to insure compatibility of coaxial horns	None
		WAVEGUIDE	Some development will be required to insure compatibility of coaxial horns	None
<u>SCHEME B</u> 	None Required ↓	COAX	Must be displaced from focal point in order not to interfere with horns	50% Effici
		COAX	Small horns and their external fields will require significant multihorn development	None
		COAX	Small horns and their external fields will require significant multihorn development	Efficiency require
		COAX	Small horns and their external fields will require significant multihorn development	Efficiency require
		COAX	Small horns and their external fields will require significant multihorn development	Efficiency require
		WAVEGUIDE	Small horns and their external fields will require significant multihorn development	None
<u>SCHEME C</u> 	None Required ↓	COAX	Must be displaced from focal point in order not to interfere with spiral	50% Effici
		COAX	No Significant Limitations	Cone mus frequency
		COAX	No Significant Limitations	Cone mus frequency
		COAX	No Significant Limitations	Cone mus frequency
		COAX	No Significant Limitations	Cone mus frequency
		COAX TO WAVEGUIDE	No Significant Limitations	Efficiency
COAX TO WAVEGUIDE	No Significant Limitations	Efficiency		

PERFORMANCE LIMITATIONS	ACCEPTABILITY	REASON	FEED
Efficiency Questionable	Marginal	Marginal Parabola Illumination	Dipole
Noted	Acceptable		Horn
Noted	Acceptable		Horn
Noted	Acceptable		Horn
Noted	Acceptable		Horn
Noted	Acceptable		Horn
Noted	Acceptable		Horn
Efficiency with Feed Off Focus	Marginal	Marginal Parabola Illumination	Dipole
Noted	Acceptable		Horn
may not be met for 1.7 to 2.3 GHz (external field of small horn)	Marginal	Bandwidth Limited	Horn
may not be met for 1.7 to 2.3 GHz (external field of small horn)	Marginal	Bandwidth Limited	Horn
may not be met for 1.7 to 2.3 GHz (external field of small horn)	Marginal	Bandwidth Limited	Horn
Noted	Acceptable		Horn
Noted	Acceptable		Horn
Efficiency with Feed Off Focus	Marginal	Marginal Parabola Illumination	Dipole
to be re-positioned for each to maintain efficiency	Unacceptable	Movement Req'd During Mission	Conical Spiral
to be re-positioned for each to maintain efficiency	Unacceptable	Movement Req'd During Mission	Conical Spiral
to be re-positioned for each to maintain efficiency	Unacceptable	Movement Req'd During Mission	Conical Spiral
to be re-positioned for each to maintain efficiency	Unacceptable	Movement Req'd During Mission	Conical Spiral
with Lossy Conductors	Unacceptable	Movement Req'd During Mission	Conical Spiral
with Lossy Conductors	Unacceptable	Movement Req'd During Mission	Conical Spiral

PARABOLIC REFLECTOR COMPOSITE FEED SELECTION CHART

FEED	FREQUENCY (MHz)							FOCUS		POLARIZATION	POSSIBLE CONSTRUCTION	EST. WGT.	PRG. SIZE
	100	800	1700	2100	2300	7500	8000	PRIME	CASS.				
Dipole	X							X		CP	Wire Mesh Ground Plane	12 LB	7 FT DIA. x 2.5 FT
Planar Spiral		X						X		CP	Printed Circuit	↑ ↓	↑ ↓
Planar Spiral			X					X		CP			
Planar Spiral				X				X		CP			
Planar Spiral					X			X		CP	1 LB		
Planar Spiral						X		X		CP			
Planar Spiral							X	X		CP			
Planar Spiral								X	X	CP			
Dipole	X							X		CP	Split Sub-Reflector	↑ ↓	↑ ↓
Helix		X							X	CP	Wire Mesh Ground Plane		
Helix			X						X	CP	Wire Mesh Ground Plane		
Helix				X					X	CP	Wire Mesh Ground Plane		
Helix					X				X	CP	Wire Mesh Ground Plane		
Helix						X			X	CP	Wire Mesh Ground Plane		
Helix							X		X	CP	Wire Mesh Ground Plane, Fixed Structure		
Planar Spiral	X							X		CP	Fixed	↑ ↓	↑ ↓
Planar Spiral		X						X		CP	Fixed		
Planar Spiral			X					X		CP	Fixed		
Planar Spiral				X				X		CP	Fixed		
Planar Spiral					X			X		CP	Fixed		
Planar Spiral						X		X		CP	Fixed		
Planar Spiral							X	X	X	CP	Fixed		
Planar Spiral								X	X	CP	Fixed		
Planar Spiral										CP	Fixed	26 lb	60 in. DIA. x 35 in.

SKETCH	DEPLOYMENT	TRANS LINE TO INTERFACE	COMPATIBILITY LIMITATIONS	PERFORMANCE
<p><u>SCHEME D</u></p> 	<p>None Required</p> 	<p>COAX</p> <p>COAX</p> <p>COAX</p> <p>COAX</p> <p>COAX</p> <p>COAX TO WAVEGUIDE</p> <p>COAX TO WAVEGUIDE</p>	<p>Center portion of dipole feed blocked by planar spiral</p> <p>10:1 bandwidth requirement, space filter for cavity requires significant development</p> <p>10:1 bandwidth requirement, space filter for cavity requires significant development</p> <p>10:1 bandwidth requirement, space filter for cavity requires significant development</p> <p>10:1 bandwidth requirement, space filter for cavity requires significant development</p> <p>10:1 bandwidth requirement, space filter for cavity requires significant development</p> <p>10:1 bandwidth requirement, space filter for cavity requires significant development</p>	<p>50% Efficiency</p> <p>Multiple elements</p> <p>Multiple elements</p> <p>Multiple elements</p> <p>Multiple elements</p> <p>Multiple elements</p> <p>Efficiency</p> <p>Efficiency</p>
<p><u>SCHEME E</u></p> 	<p>None Required</p> 	<p>COAX</p> <p>COAX</p> <p>COAX</p> <p>COAX</p> <p>COAX</p> <p>COAX TO WAVEGUIDE</p> <p>COAX TO WAVEGUIDE</p>	<p>Must be developed with other nearby structure in position</p> <p>Significant development req'd with multiple helices, pattern control difficult</p> <p>Significant development req'd with multiple helices, pattern control difficult</p> <p>Significant development req'd with multiple helices, pattern control difficult</p> <p>Significant development req'd with multiple helices, pattern control difficult</p> <p>Significant development req'd with multiple helices, pattern control difficult</p> <p>Significant development req'd with multiple helices, pattern control difficult</p>	<p>50% Efficiency</p> <p>Feed must be at frequency</p> <p>Feed must be at frequency</p> <p>Feed must be at frequency</p> <p>Feed must be at frequency</p> <p>Feed must be at frequency</p> <p>Feed must be at frequency</p>
<p><u>SCHEME F</u></p> 	<p>None Required</p> 	<p>COAX</p> <p>COAX</p> <p>COAX</p> <p>COAX</p> <p>COAX</p> <p>COAX TO WAVEGUIDE</p> <p>COAX TO WAVEGUIDE</p>	<p>80:1 bandwidth requirement, space filter for cavity requires significant development</p> <p>80:1 bandwidth requirement, space filter for cavity requires significant development</p> <p>80:1 bandwidth requirement, space filter for cavity requires significant development</p> <p>80:1 bandwidth requirement, space filter for cavity requires significant development</p> <p>80:1 bandwidth requirement, space filter for cavity requires significant development</p> <p>80:1 bandwidth requirement, space filter for cavity requires significant development</p>	<p>50% Efficiency</p> <p>Multiple elements</p> <p>Multiple elements</p> <p>Multiple elements</p> <p>Multiple elements</p> <p>Multiple elements</p> <p>Efficiency</p> <p>Efficiency</p>

PERFORMANCE SITUATIONS	ACCEPTABILITY	REASON	FEED
Feed with Feed Off Focus	Marginal	Marginal Parabola Illumination	Dipole
Multiple outputs may be lossy	Acceptable		Planar Spiral
Multiple outputs may be lossy	Acceptable		Planar Spiral
Multiple outputs may be lossy	Acceptable		Planar Spiral
Multiple outputs may be lossy	Acceptable		Planar Spiral
Multiple outputs with Lossy Conductor	Marginal	50% efficiency may not be met with lossy-feed and multiple outputs	Planar Spiral
Multiple outputs with Lossy Conductor	Marginal	50% efficiency may not be met with lossy-feed and multiple outputs	Planar Spiral
Feed Questionable	Marginal	Marginal Parabola Illumination	Dipole
Feed re-positioned for each output to maintain efficiency	Unacceptable	Movement Req'd During Mission	Helix
Feed re-positioned for each output to maintain efficiency	Unacceptable	Movement Req'd During Mission	Helix
Feed re-positioned for each output to maintain efficiency	Unacceptable	Movement Req'd During Mission	Helix
Feed re-positioned for each output to maintain efficiency	Unacceptable	Movement Req'd During Mission	Helix
Feed re-positioned for each output to maintain efficiency	Unacceptable	Movement Req'd During Mission	Helix
Feed re-positioned for each output to maintain efficiency	Unacceptable	Movement Req'd During Mission	Helix
Feed Questionable	Unacceptable	Loss should be too great for 80:1 bandwidth spiral	Planar Spiral
Multiple outputs may be lossy	Unacceptable	Loss should be too great for 80:1 bandwidth spiral	Planar Spiral
Multiple outputs may be lossy	Unacceptable	Loss should be too great for 80:1 bandwidth spiral	Planar Spiral
Multiple outputs may be lossy	Unacceptable	Loss should be too great for 80:1 bandwidth spiral	Planar Spiral
Multiple outputs may be lossy	Unacceptable	Loss should be too great for 80:1 bandwidth spiral	Planar Spiral
Multiple outputs with Lossy Conductors	Unacceptable	Loss should be too great for 80:1 bandwidth spiral	Planar Spiral
Multiple outputs with Lossy Conductors	Unacceptable	Loss should be too great for 80:1 bandwidth spiral	Planar Spiral

APPENDIX B

LAUNCH WINDOW RESTRICTION DUE TO PRECESSION CONTROL SUN SENSORS

In this appendix the launch window restriction due to the field of view of the precession control sun sensors is discussed.

The sun line is defined with respect to inertial frame $X_1 Y_1 Z_1$ by the Right Ascension, RA, and declination, δ_s . It is assumed that RA and δ_s do not change during the period of the launch window, so that the sun line is fixed in inertial space. The direction cosines of the sun line with respect to $X_1 Y_1 Z_1$ are

$$(\cos RA \cos \delta_s, -\sin \delta_s, \sin RA \sin \delta_s) \quad (1)$$

The spacecraft spin axis at apogee burn must be normal to the local vertical and rotated by an angle α_i out of the equatorial plane. If the injection point is at longitude $-\lambda$ ($\lambda^{\circ}W$) and the latitude 0° , the direction cosines of the local vertical with respect to $X_1 Y_1 Z_1$ are (Figure B-1)

$$(-\sin(W_e t - \lambda), 0, \cos(W_e t - \lambda)) \quad (2)$$

where W_e is the earth rate and t is Greenwich Mean Time. The correct apogee burn attitude is then given by the direction cosines:

$$\begin{aligned} &(-\sin(W_e t - \lambda) \cos \alpha_i, \sin \alpha_i, \\ &\cos(W_e t - \lambda) \cos \alpha_i) \end{aligned} \quad (3)$$

The assumption is now made that, prior to booster separation, the booster is oriented to the attitude indicated by direction cosines in Equation (3) above; that is, the booster

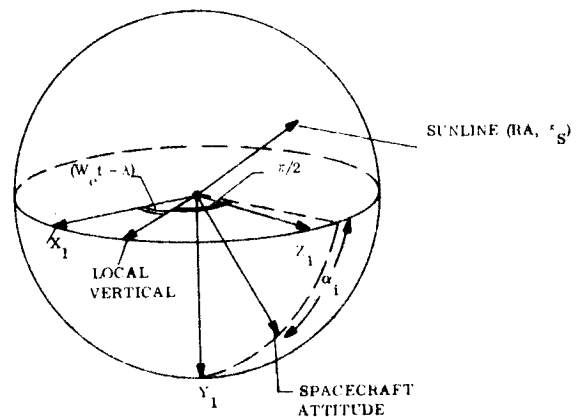


Figure B-1. Apogee Burn Coordinates

orientation is modified to take account of launch time variation. If errors Δ_1 and Δ_2 occur respectively out of, and in, the horizontal plane at apogee due to precession during the transfer orbit, the real spacecraft spin-axis direction cosines at the time when attitude correction is made will be

$$\left(-\sin (W_e t - \lambda + \Delta_1) \cos (\alpha_i + \Delta_2), \sin (\alpha_i + \Delta_2), \cos (W_e t - \lambda + \Delta_1) \cos (\alpha_i + \Delta_2) \right) \quad (4)$$

and the cosine of the angle ζ between the sun line and the spacecraft spin axis is given by the cross product of the sun line and the spin axis,

$$\begin{aligned} \cos \zeta = & -\sin (W_e t - \lambda + \Delta_1) \cos (\alpha_i + \Delta_2) \cos RA \cos \delta_s \\ & -\sin (\alpha_i + \Delta_2) \sin \delta_s + \cos (W_e t - \lambda + \Delta_1) \cos (\alpha_i + \Delta_2) \sin RA \cos \delta_s \end{aligned}$$

which reduces to

$$\cos \zeta = -\sin (W_e t - \lambda - RA + \Delta_1) \cos (\alpha_i + \Delta_2) \cos \delta_s - \sin (\alpha_i + \Delta_2) \sin \delta_s \quad (5)$$

It is further assumed that the center of the launch window is chosen at a time t_o such that ζ as defined by Equation (5) above, with $\Delta_1 = \Delta_2 = 0$, is equal to $\pi/2$. Thus ζ at a time Δt from the launch window center (Δt negative for early launch) is given by the relations

$$\begin{aligned} \cos \zeta = & -\sin (W_e t_o + W_e \Delta t - \lambda - RA + \Delta_1) \cos (\alpha_i + \Delta_2) \cos \delta_s \\ & -\sin (\alpha_i + \Delta_2) \sin \delta_s \end{aligned} \quad (6)$$

$$0 = -\sin (W_e t_o - \lambda - RA) \cos \alpha_i \cos \delta_s - \sin \alpha_i \sin \delta_s$$

Relations expressed in Equations (6) enable the field of view requirement for the sun sensors to be determined. The field of view for the ψ Sensor is given by

$$F_\psi = (\pi - 2\zeta)$$

The field of view for the ψ_2 sun sensor is given by

$$F_{\psi_2} = 2 \sin^{-1} (\cos \zeta / \cos 35^\circ) = 2 \sin^{-1} (1.220 \cos \zeta)$$

F_ψ and $F_{\psi_2} = 2$ may be calculated by the following process:

- a. Insert values of α_i , δ_s in the second relation of Equations (6) and determine $(W_e t_0 - \lambda - RA)$
- b. Insert α_i , δ_s , $(W_e t_0 - \lambda - RA)$ in the first relation of Equations (6), determine the worst case combination of Δ_1 and Δ_2 , insert values of Δt and calculate F_ψ and F_{ψ_2} .

In the case where Δ_1 and Δ_2 are circularly distributed, that is,

$$(\Delta_1^2 + \Delta_2^2)^{1/2} = \Delta$$

then Equations (6) may be rewritten

$$\begin{aligned} \cos (\zeta + \Delta) &= -\sin (W_e t_0 - \lambda - RA + W_e \Delta t) \cos \alpha_i \cos \delta_s + \sin \alpha_i \sin \delta_s \\ 0 &= -\sin (W_e t_0 - \lambda - RA) \cos \alpha_i \cos \delta_s - \sin \alpha_i \sin \delta_s \end{aligned} \quad (7)$$

which reduce to

$$\begin{aligned} \cos (\zeta + \Delta) &= -\sin \alpha_i \sin \delta_s (1 - \cos (W_e \Delta t)) \\ &+ \sin (W_e \Delta t) (\cos (\alpha_i + \delta_s) \cos (\alpha_i - \delta_s))^{1/2} \end{aligned} \quad (8)$$

For the ATS-4, the precession error distribution is nearly circular ($\Delta_1 = 9.6$ degrees, $\Delta_2 = 9.3$ degrees) and a circular distribution with $\Delta = 13.4$ degrees has been assumed for the calculation of F_ψ and F_{ψ_2} . Inserting $\alpha_i = 19.4$ degrees and $\delta_s = \pm 23.5$ degrees (solstice) or 0 degree (equinox) in Equation (8) the following relations are obtained.

$$\text{Solstice: } \zeta = -13.4 \text{ degrees} + \cos^{-1} \left\{ 0.1324 + 0.7425 \sin (W_e \Delta t - 10.2 \text{ degrees}) \right\}$$

$$\text{Equinox: } \zeta = -13.4 \text{ degrees} + \cos^{-1} \left\{ 0.9432 \sin (W_e \Delta t) \right\}$$

The variation of F_ψ and F_{ψ_2} with launch window duration ($2\Delta t$) is shown in Figure B-2. For instance, for a launch window of four hours, $F_\psi = 84$ degrees, $F_{\psi_2} = 110$ degrees. Note that the ideal launch time is approximately at the center of the launch window. Providing that the spacecraft is not in the earth shadow, two launch windows occur each day.

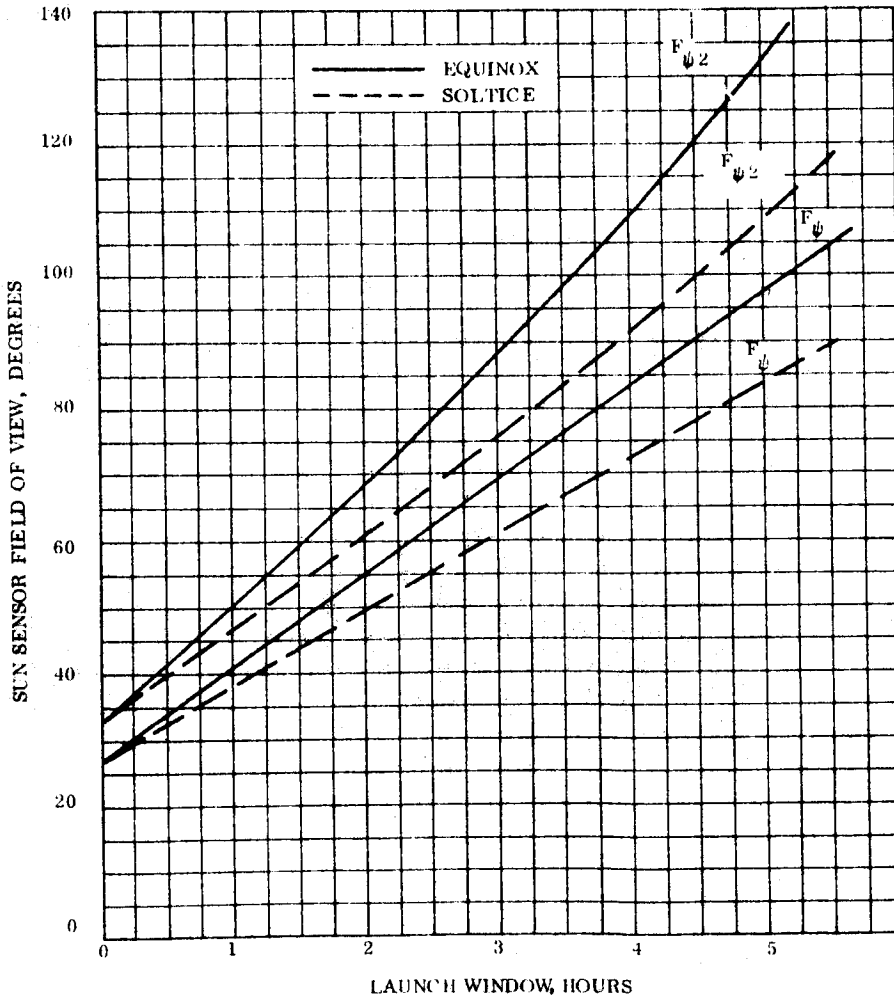


Figure B-2. Variation of Launch Window With Sun Sensor Field of View

APPENDIX C

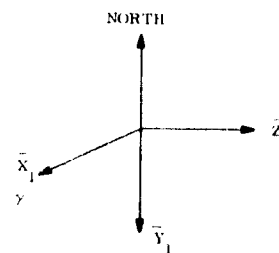
TRANSFER ORBIT DISTURBANCE TORQUES

Presented here is the analysis of the disturbance torques acting on the ATS-4 spacecraft during its transfer orbit. The disturbances include gravity gradient, solar radiation pressure, aerodynamic pressure, and magnetic torques.

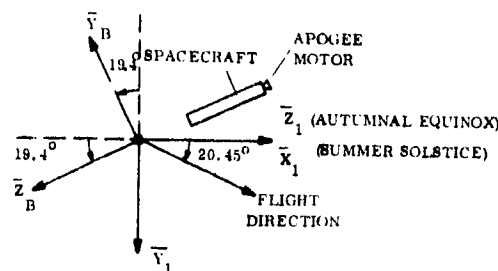
The analysis of disturbance torques assumes that the orientation of the spin axis is inertially fixed. As a consequence of this assumption, the use of an inertial reference frame, with one axis aligned with the spacecraft spin axis, is convenient for the torque computations. The transfer orbit consists of one and one-half revolutions about the earth, from booster separation at perigee to injection at apogee.

Near perigee, certain of the orbital variables change rapidly. These include altitude, orbit angle, latitude, and longitude. Other variables such as the flight path angle and the magnitude of the velocity, vary more slowly. Values near perigee were obtained from a computer run with closely spaced time intervals.

Two inertial reference frames and an orbital reference frame were used. One inertial frame is $\bar{X}_1 \bar{Y}_1 \bar{Z}_1$ (ref. NASA-GSFC Drawing GC1183111) shown in Figure C-1a. The second inertial reference frame (body inertial frame $\bar{X}_B \bar{Y}_B \bar{Z}_B$) is determined by the spacecraft orientation at perigee. This frame is illustrated in Figure C-1b. \bar{Z}_B lies along the longitudinal axis at perigee and is negative toward the apogee motor. The \bar{X}_B axis coincides with the local vertical at perigee, and is positive upward. \bar{Y}_B forms a right-handed



(a) Geographic Inertial Frame



(b) Body Inertial Frame

Figure C-1. Reference Frames

system. At the autumnal equinox, \bar{X}_B coincides with \bar{X}_1 , and at the summer solstice, \bar{X}_B coincides with $-\bar{Z}_1$.

At the autumnal equinox, the body inertial frame is produced from the geographic inertial frame by a single rotation of 199.4 degrees about the \bar{X}_1 axis. At the summer solstice, two rotations are required. The first is a rotation of 90 degrees about the \bar{Y}_1 axis, and the second is a rotation of 199.4 degrees about the \bar{X}_B axis.

The orbital reference frame is described by the triad $\bar{R} \bar{P} \bar{Q}$. \bar{R} is along the local vertical and positive upward. \bar{Q} is along the orbital angular velocity vector. \bar{P} forms a right-handed system and lies along the flight direction at perigee and at apogee. The orbital reference frame is produced from the inertial reference frame by three rotations: (1) Ω_N about the \bar{Z}_1 axis, (2) ι about the line of nodes, and (3) η about the \bar{Q} axis. Ω_N is the right ascension of the ascending node, ι is the orbital inclination, and η is the orbital position angle, relative to the ascending node. The inclination is 20.45 degrees. At the fall equinox, Ω_N is 180 degrees, and at the summer solstice, Ω_N is 90 degrees. In both cases the initial value of η is 180 degrees.

It should be noted that an observer stationed in space above the perigee point would see the same profile of events at any time of year. However, the orientation of the earth-spacecraft-observer system, relative to inertial space, would vary with the time of year. The four primary sources of disturbance torque are discussed below.

C.1 SOLAR RADIATION PRESSURE TORQUE

The solar radiation pressure torque is a constant, during any transfer orbit, because of the assumption of the fixed inertial attitude of the spin axis and because of the symmetry of the spacecraft about the axis. The magnitude of the torque, on a cylindrical surface, aligned as the spacecraft, is

$$T_S = P_S A L (2C_Z - L) \left(1 + \frac{1}{3} \rho_s + \frac{\pi}{6} \rho_d \right) \quad (1)$$

where P_s is the solar constant, 9.537×10^{-8} pounds per square foot, A is the radius of the cylinder, L is its length, ρ_s is the specular reflectance of the surface, ρ_d is its diffuse reflectance, and C_Z is the center of mass coordinate relative to the $-\bar{Z}_B$ end of the cylinder.

At the autumnal equinox, the solar unit vector, \bar{S} , along the direction of the solar flux at the spacecraft, lies along \bar{X}_B and the solar torque is

$$\vec{T}_S = \bar{S} \times \bar{Z}_B T_S = -\bar{Y}_B T_S \quad (2a)$$

At the summer solstice, the solar unit vector is

$$\bar{S} = \bar{X}_B \cos 23.45^\circ + \sin 23.45^\circ (-\bar{Y}_B \cos 19.4^\circ + \bar{Z}_B \sin 19.4^\circ) \quad (2b)$$

and the solar torque is

$$\vec{T}_S = T_S (-\bar{X}_B \sin 23.45^\circ \cos 19.4^\circ - \bar{Y}_B \cos 23.45^\circ) \quad (2c)$$

When the spacecraft consists of a number of cylindrical sections, the value of T_S to be used in the above equations is the algebraic sum of the values for each section.

C.2 AERODYNAMIC PRESSURE TORQUES

The aerodynamic pressure torques acting on the spacecraft are assumed to be due to free molecular flow. It is further assumed that the molecules are diffusely reflected in accordance with the Lambert Law, that all of the momentum of the incident particles is imparted to the spacecraft and that the momentum imparted by the reflected particles corresponds to a velocity which is a fraction, A_{VC} , of the velocity of the incident particles.

For the purpose of computing aerodynamic torques, the ATS-4 spacecraft is taken as a cylinder with A_{VC} equal to 0.5.

The aerodynamic torque on such a cylinder, about axes passing through a center of mass on the axis, may be expressed as

$$\vec{T}_A = 2P_A (\vec{V} \times \vec{Z}_B) \left\{ AL \left[(2C_Z - L) \left(\frac{\pi}{6} A_{VC} + (V_{XB}^2 + V_{YB}^2)^{1/2} \right) - \frac{\pi}{2} AV_{ZB} \right] \right\} \quad (3)$$

where A is the radius and L is the length of the cylinder, C_Z is the coordinate of the center of mass, relative to the $-\vec{Z}_B$ end of the cylinder, \vec{V} is a unit vector in the direction of the relative wind, having direction cosines in the body inertial frame defined by

$$\vec{V} = \vec{X} V_{XB} + \vec{Y}_B V_{YB} + \vec{Z}_B V_{ZB}, \quad (4)$$

P_A is the aerodynamic pressure,

$$P_A = \frac{\rho_A V_{REL}^2}{2}, \quad (5)$$

and V_{REL} is the magnitude of the relative wind velocity. This velocity is computed under the assumption that the earth's atmosphere rotates with the earth. This assumption yields

$$\vec{V}_{REL} = \vec{R} V_{RELR} + \vec{P} V_{RELP} + \vec{Q} V_{RELQ}, \quad (6)$$

where

$$V_{RELR} = -\dot{R}_C$$

$$V_{RELP} = -R_C (\cos \iota \omega_{ES} \dot{\eta})$$

$$V_{RELQ} = -R_C \sin \iota \cos \eta \omega_{ES}$$

R_C is the geocentric altitude, and ω_{ES} is the earth's spin rate. The direction cosines of \vec{V} in the orbital frame are

$$V_R = \frac{V_{RELR}}{V_{REL}} \quad (7)$$

$$V_P = \frac{V_{RELP}}{V_{REL}}$$

and

$$V_Q = \frac{V_{RELQ}}{V_{REL}}$$

where

$$V_{REL} = \left(\dot{R}_C^2 + R_C^2 \left| \dot{\eta}^2 - 2 \cos \epsilon \dot{\eta} \omega_{ES} + \omega_{ES}^2 (1 - \sin^2 \epsilon \sin^2 \eta) \right| \right)^{1/2}$$

The direction cosines of \bar{V} , in the body inertial reference frame are given by

$$\begin{bmatrix} V_{XB} \\ V_{YB} \\ V_{ZB} \end{bmatrix} = \begin{bmatrix} C \\ A \end{bmatrix}^T \begin{bmatrix} V_R \\ V_P \\ V \end{bmatrix} \quad (8)$$

where $|C|$ and $|A|$ are the matrices relating the body and the orbital reference frames respectively to the inertial (X_1, Y_1, Z_1) frame. It can be shown that V_{YB} at the summer solstice is equal to $-V_{XB}$ at the autumnal equinox, that V_{XB} at the summer solstice is equal to V_{YB} at the autumnal equinox, and that V_{ZB} at the summer solstice is the same as at the autumnal equinox. Therefore, the function in braces in Equation (3) has the same time profile at both seasons. This is designated $f(t)$.

Then, at the autumnal equinox, the components of the aerodynamic torque, in the body inertial frame, are

$$T_{AX} = V_{YB} P_A f(t) \quad (9)$$

$$T_{AY} = -V_{XB} P_A f(t)$$

The components at the summer solstice are easily found from those at the autumnal equinox,

$$T_{AX} = -V_{XBE} P_A f(t) \quad (10)$$

$$T_{AY} = -V_{YBE} P_A f(t)$$

where the additional subscript E designates the value at the autumnal equinox.

C.3 MAGNETIC TORQUES

The magnetic disturbances may include the effects of hysteretic material in the spacecraft, eddy currents induced by the spin motion of the spacecraft in the geomagnetic field, and interaction of the residual magnetic dipole of the spacecraft with the earth's magnetic field. The magnetic hysteresis torque depends upon the amount of ferromagnetic or other hysteretic material present and upon its characteristics. It is best to avoid the use of such material as much as possible. If such material is used, the hysteresis torque may be evaluated by empirical methods. If only small quantities of hysteretic material are present, the hysteresis torque is usually small in comparison with other disturbances.

The eddy-current torque on a thin-walled cylinder spinning about its axis is (ref. G. L. Smith "A Theoretical Study of the Torques Induced by a Magnetic Field on Rotating Cylinders," NASA Technical Report R-129, 1962).

$$\vec{T}_{EC} = \pi \sigma C^{-2} h^2 \omega r^3 L t \left(1 - \frac{2r}{L} \tanh \frac{L}{2r} \right) \left(\bar{i} \sin \lambda \cos \lambda - \bar{k} \sin^2 \lambda \right) \quad (11)$$

where σ is the conductivity of the shell, C is the velocity of light, h is the magnitude of the ambient magnetic field, ω is the spin rate, r is the radius of the cylinder, L is its length, t is the thickness of the shell, and λ is the angle between the magnetic field and the cylinder axis. \bar{k} is a unit vector along the cylinder axis and \bar{i} is the transverse unit vector in the plane containing the magnetic field vector and the cylinder axis.

The magnetic dipole torque is

$$\vec{T}_{MD} = \vec{M}_S \times \vec{H}_E \quad (12)$$

where \vec{M}_S is the magnetic moment of the spacecraft and \vec{H}_E is the geomagnetic field. The M_X and M_Y torque components contribute only a sinusoidal ripple, which has no secular effect, and whose torque impulse during any half-cycle is negligibly small. Therefore, the only appreciable torque impulse arises from the M_Z component. The resulting torque components in the body inertial frame are

$$T_{MX} = -H_{CZ} H_Y \quad (13)$$

$$T_{MY} = +H_{CZ} H_X$$

where H_X and H_Y are the components of the geomagnetic field in the body inertial frame.

C.4 GRAVITY GRADIENT TORQUE

The gravity gradient torques, about principal axes of inertia, are

$$T_{GX} = \frac{3K}{R_c^3} R_Y R_Z (I_Z - I_Y) \quad (14)$$

$$T_{GY} = \frac{3K}{R_c^3} R_X R_Z (I_X - I_Z)$$

$$T_{GZ} = \frac{3K}{R_c^3} R_X R_Y (I_Y - I_X)$$

where K is the product of the earth's mass and the universal gravitational constant, R_c is the geocentric altitude, I_X , I_Y , I_Z are the principal moments of inertia, and R_X , R_Y , R_Z are the direction cosines of the local vertical unit vector in the body reference frame.

For the ATS transfer orbit, the local vertical unit vector is

$$\bar{R} = -\bar{X}_B \cos \eta + \bar{Y}_B \cos \phi \sin \eta + \bar{Z}_B \sin \phi \sin \eta \quad (15)$$

where η is the orbital position angle, measured from the ascending node (apogee) and ϕ is the complement of the angle between the \bar{Z}_B axis and the orbit plane.

The axial moment of inertia of the ATS-4 spacecraft was assumed to be 533 slug-feet², and the average transverse moment of inertia 4523 slug-feet². The spacecraft was assumed to have cylindrical mass symmetry, and so the \bar{Z}_B component of the torque is zero. The other two components are

$$T_{GX} = \frac{3K}{R_c^3} \sin \phi \cos \phi \sin^2 \eta (I_Z - I_X) \quad (16)$$

$$T_{GY} = \frac{3K}{R_c^3} \sin \phi \sin \eta \cos \eta (I_Z - I_X)$$

APPENDIX D

ON-STATION DISTURBANCE TORQUES

D. 1 INTRODUCTION

The on-station disturbance torques are primarily determined by solar pressure and gravity gradient effects. Discussed herein is the analysis of the gravity gradient and solar radiation pressure torques on the ATS-4 spacecraft. The equations were programmed for the IBM 7094 computer, and the results are disturbance torque profiles. These profiles provide design information for the momentum wheels and pneumatic system, as well as inputs for the analog computer simulation of the spacecraft orientation dynamics.

The analysis assumes constant pointing orientation of the spacecraft, relative to the local vertical reference frame, throughout an orbit. The deviations from such an orientation allowed by the active control system are too small to have any appreciable effect on the disturbance torques. The computations are performed at equally spaced time intervals for a 24-hour period. The desired spacecraft pointing orientation is included in the initial conditions for the computer run.

Because the final configuration was not chosen before the analysis was begun, considerable flexibility was provided. This takes the form of optional inclusion of various geometrical components, such as cylinders, spheres, cones, flat plates, etc. The details are given in the discussion of solar radiation pressure torques. Because of the complexity which would have been involved, the effects of parts of the spacecraft shading other parts were neglected, as well as reflections between parts. The program included the simplified earth shadow effects.

D. 2 PHYSICAL PARAMETERS REQUIRED FOR COMPUTATION OF DISTURBANCE TORQUES

D. 2. 1 ORBIT COMPUTATIONS

The earth's orbit about the sun is assumed to be circular, and the orbital angular rate is considered constant. This affects only the apparent sun angle, and only one-orbit computer

runs were anticipated, so that errors arising from this assumption are negligible. A run may be started at any time of year. The spacecraft's orbit is also assumed to be circular, but precession of right ascension of the ascending node may be included, if desired. Any altitude, inclination, initial orbital position of the spacecraft, and initial position of the right ascension of the ascending node may be chosen. For an orbit which is equatorial, the equinox line is used as a reference in lieu of the line of nodes.

The orbital and related inputs required for the program are

- a. F_{KK} , the product of the earth's mass and the universal gravity constant.
- b. $\dot{\mu}_E$, the earth's average orbital angular rate.
- c. P_O , the solar radiation pressure constant.
- d. R_E , the earth's radius.
- e. μ_{EO} , the initial value of the earth's celestial longitude, measured from the autumnal equinox.
- f. Δt , the time interval between torque computations.
- g. Ω_{NO} , the initial value of the right ascension of the ascending node.
- h. $\dot{\Omega}_N$, the nodal precession rate.
- i. i , the orbital inclination.
- j. τ_O , the initial orbital position angle.
- k. τ , the orbital period.
- l. R_C , the orbit geocentric altitude.

The local vertical reference frame is described by the $\bar{R} \bar{P} \bar{Q}$ triad of unit vectors. \bar{R} is in the direction from the geocenter to the spacecraft. \bar{P} is in the direction of the spacecraft

velocity. \bar{Q} is in the direction of the orbital angular velocity vector.

The inertial reference frame is described by the $\bar{X}_I \bar{Y}_I \bar{Z}_I$ triad of unit vectors. \bar{X}_I points to the first point of Aries, and \bar{Z}_I points to the north geographic pole. \bar{Y}_I forms a right-handed system.

D. 2. 2 SPACECRAFT ORIENTATION

The spacecraft orientation is expressed in terms of three Euler rotations: (1) θ_P about the positive \bar{Y}_I axis, (2) θ_R about the positive \bar{X}_I axis, and (3) θ_Y about the positive Z_I axis. The subscripts stand for pitch, roll, and yaw, respectively.

D. 2. 3 MASS MOMENTS

Flexibility is provided in the computation of the spacecraft center of mass and its moments and products of inertia. The moments and products of inertia of the entire spacecraft are computed about the prescribed spacecraft geometrical axes, translated without rotation to the overall center of mass. The inputs include the following mass characteristics of the main (rodless) body:

- a. M_{RS} , the mass of the rodless body.
- b. X_{MC} , Y_{MC} , and Z_{MC} , the coordinates of the rodless body center of mass, relative to a prescribed reference point on the longitudinal axis.
- c. V_{XXM} , V_{YYM} , V_{ZZM} , V_{XYM} , V_{XZM} , and V_{YZM} , the moments and products of inertia of the rodless body, about geometric axes translated without rotation to the rodless body center of mass.

A gravity gradient rod and its tip weight may be included in the simulation or not. If they are not included, an input indicator, N_{ROD} , is set equal to zero, and the inputs listed above are used as the spacecraft mass characteristics. The computed coordinates of the spacecraft center of mass are X_{CM} , Y_{CM} , and Z_{CM} . The moments and products of inertia are I_{XX} , etc.

D.3 DERIVATION OF RELATIONS FOR COMPUTATION OF DISTURBANCE TORQUES

D.3.1 GRAVITY GRADIENT TORQUES

The gravity gradient torques on the spacecraft are computed for a perfectly spherical gravity field. The torque then depends upon the geocentric altitude, R_C , the spacecraft moments and products of inertia, and the direction cosines of the local vertical in the spacecraft reference frame.

The inertia matrix is

$$[I] = \begin{bmatrix} I_{XX} & -I_{XY} & -I_{XZ} \\ -I_{XY} & I_{YY} & -I_{YZ} \\ -I_{XZ} & -I_{YZ} & I_{ZZ} \end{bmatrix} \quad (1)$$

The direction cosines relate the local vertical unit vector, \bar{R} , to unit vectors along the spacecraft reference axes.

$$\bar{R} = \bar{X}_1 E_{11} + \bar{Y}_1 E_{21} + \bar{Z}_1 E_{31} \quad (2)$$

Where the E's are elements of the rotational transformation matrix from the $\bar{P} \bar{Q} \bar{R}$ frame to the $\bar{X}_1 \bar{Y}_1 \bar{Z}_1$ frame. The gravity gradient torques are computed from the matrix equation.

$$\begin{bmatrix} T_{GX} \\ T_{GY} \\ T_{GZ} \end{bmatrix} = \frac{3F}{R_C^3} \begin{bmatrix} 0 & -E_{31} & E_{21} \\ E_{31} & 0 & -E_{11} \\ -E_{21} & E_{11} & 0 \end{bmatrix} [I] \begin{bmatrix} E_{11} \\ E_{21} \\ E_{31} \end{bmatrix} \quad (3)$$

D.3.2 SOLAR RADIATION PRESSURE TORQUES

The differential force on a differential element, dA , of the spacecraft surface area may be expressed as

$$\vec{d^2F} = P_0 dA \left[\bar{S} (1 - \rho_s) (\bar{S} \cdot \bar{N}) + 2\bar{N} \rho_s (\bar{S} \cdot \bar{N})^2 + \frac{2}{3} \bar{N} \rho_d (\bar{S} \cdot \bar{N}) \right] \quad (4)$$

where \bar{S} is the unit vector along the sun's rays, \bar{N} is the unit vector perpendicular to and positive toward the surface element, ρ_s is the specular reflectance of the surface, and ρ_d is the diffuse reflectance. These are related to the absorptance, α , by

$$\alpha + \rho_s + \rho_d = 1 \quad (5)$$

Equation (4) is based on the assumption that the absorptance and reflectance characteristics are constant with angle of incidence, and on the assumption that all of the solar rays at the spacecraft are parallel.

The solar radiation pressure torque on the area element is the vector cross-product of the moment arm and the force. The torque is to be computed about axes through the spacecraft center of mass, and so the moment arm is the vector from the center of mass to the area element. The torque is the integral of the elementary expression over the illuminated portion of the surface area. The torque on individual components of the spacecraft is computed, as explained in the following subsections. These contributions are added, to obtain the total solar torque on the spacecraft. By the inclusion or omission of components, any of the required spacecraft configurations may be simulated.

D.3.2.1 Solar Cell Panels

Any number of solar panels from one to four may be accommodated. The number is specified as an input index, N_{SP} . The analysis for the J th panel is presented. The equations for any panel are obtained by changing the subscript J .

The following inputs are prescribed for each panel:

- a. X_{SPJ} , Y_{SPJ} , and Z_{SPJ} , the coordinates of the centroid of the Jth panel, relative to the prescribed reference point.
- b. P_{SPXJ} , P_{SPYJ} , and P_{SPZJ} , the direction cosines, in the $\bar{X}_1 \bar{Y}_1 \bar{Z}_1$ spacecraft reference frame, of the unit vector perpendicular to and pointing toward the front surface of the Jth panel.
- c. R_{SPJ} , and R_{DPJ} , the specular and diffuse reflectances of the front surface of the Jth panel.
- d. R_{SRJ} and R_{DRJ} , the specular and diffuse reflectances of the reverse side of the Jth panel.
- e. A_{SPJ} , the area of the Jth panel.

The cosine of the angle of incidence of radiation of the front surface of the Jth panel is

$$\bar{S} \cdot \bar{N} = S_{DNJ} = S_{X1} P_{SPXJ} + S_{Y1} P_{SPYJ} + S_{Z1} P_{SPZJ} \quad (6)$$

where S_{X1} , S_{Y1} , and S_{Z1} are the direction cosines of \bar{S} in the spacecraft reference frame.

If S_{DNJ} is positive, the front surface is illuminated, and the components of the solar force on this surface are.

$$\begin{aligned} F_{SPXJ} &= S_{DNJ} P_O A_{SPJ} \left| S_{X1} (1-R_{SPJ}) + P_{SPXJ} (2 R_{SPJ} S_{DNJ} + 2/3 R_{DPJ}) \right| , \\ F_{SPYJ} &= S_{DNJ} P_O A_{SPJ} \left| S_{Y1} (1-R_{SPJ}) + P_{SPYJ} (2 R_{SPJ} S_{DNJ} + 2/3 R_{DPJ}) \right| , \\ F_{SPZJ} &= S_{DNJ} P_O A_{SPJ} \left| S_{Z1} (1-R_{SPJ}) + P_{SPZJ} (2 R_{SPJ} S_{DNJ} + 2/3 R_{DPJ}) \right| . \end{aligned} \quad (7)$$

The components of the moment arm, from the spacecraft center of mass to the panel centroid, are

$$\begin{aligned}
R_{SPXJ} &= X_{SPJ} - X_{CM} \\
R_{SPYJ} &= Y_{SPJ} - Y_{CM} \\
R_{SPZJ} &= Z_{SPJ} - Z_{CM}
\end{aligned}
\tag{8}$$

The solar torque components are

$$\begin{bmatrix} T_{SPXJ} \\ T_{SPYJ} \\ T_{SPZJ} \end{bmatrix} = \begin{bmatrix} 0 & -R_{SPZJ} & R_{SPYJ} \\ R_{SPZJ} & 0 & -R_{SPXJ} \\ -R_{SPYJ} & R_{SPXJ} & 0 \end{bmatrix} \begin{bmatrix} F_{SPXJ} \\ F_{SPYJ} \\ F_{SPZJ} \end{bmatrix}
\tag{9}$$

If S_{DNJ} is negative, the reverse surface is illuminated, and the components of the solar force on this surface are

$$\begin{aligned}
F_{SPXJ} &= S_{DNJ} P_O A_{SPJ} \left| S_{X1} (R_{SRJ} - 1) + P_{SPXJ} (-2 R_{SRJ} S_{DNJ} + 2/3 R_{DRJ}) \right| \\
F_{SPYJ} &= S_{DNJ} P_O A_{SPJ} \left| S_{Y1} (R_{SRJ} - 1) + P_{SPYJ} (-2 R_{SRJ} S_{DNJ} + 2/3 R_{DRJ}) \right| \\
F_{SPZJ} &= S_{DNJ} P_O A_{SPJ} \left| S_{Z1} (R_{SRJ} - 1) + P_{SPZJ} (-2 R_{SRJ} S_{DNJ} + 2/3 R_{DRJ}) \right|
\end{aligned}
\tag{10}$$

The equations for the components of the moment arm and for those of the torques are the same as before. If S_{DNJ} is zero, the torques are zero. The components of the sum of the solar torques on all of the paddles are

$$\begin{aligned}
T_{SPX} &= \sum_{J=1}^{N_{SP}} T_{SPXJ} \\
T_{SPY} &= \sum_{J=1}^{N_{SP}} T_{SPYJ} \\
T_{SPZ} &= \sum_{J=1}^{N_{SP}} T_{SPZJ}
\end{aligned}
\tag{11}$$

D.3.2.2 Box-Shaped Phased Array

The solar radiation pressure torques on the box-shaped phased array may be included as an option. If included, the input index N_{BA} is set equal to one. If not included, the index is set equal to zero. If the array is included, the following inputs are specified:

- a. X_{BAC} , Y_{BAC} , and Z_{BAC} , the coordinates of the geometric center of the array.
- b. X_{BAD} , Y_{BAD} , and Z_{BAD} , the dimension of the array, parallel to the respective satellite axes.
- c. R_{SBA} and R_{DBA} , the specular and diffuse reflectances of the surface which nominally faces the earth.
- d. R_{SBB} and R_{DBB} , the specular and diffuse reflectances of the other surfaces.

If S_{Z1} is negative, the surface which nominally faces downward is illuminated. The components of the solar force on this surface are

$$\begin{aligned}
 F_{BZX} &= -S_{Z1} S_{X1} P_O X_{BAD} Y_{BAD} (1 - R_{SBA}) \\
 F_{BZY} &= -S_{Z1} S_{Y1} P_O X_{BAD} Y_{BAD} (1 - R_{SBA}) \\
 F_{BZZ} &= -S_{Z1} P_O X_{BAD} Y_{BAD} \left[S_{Z1} (1 + R_{SBA}) - \frac{2}{3} R_{DBA} \right]
 \end{aligned} \tag{12}$$

The components of the moment arm from the spacecraft center of mass to the centroid of the surface are

$$\begin{aligned}
 R_{BZX} &= X_{BAC} - X_{CM} \\
 R_{BZY} &= Y_{BAC} - Y_{CM} \\
 R_{BZZ} &= Z_{BAC} - Z_{CM} + \frac{1}{2} Z_{BAD}
 \end{aligned} \tag{13}$$

The components of the solar torque on the surface are computed from

$$\begin{bmatrix} T_{SBZX} \\ T_{SBZY} \\ T_{SBZZ} \end{bmatrix} = \begin{bmatrix} 0 & -R_{BZZ} & R_{BZY} \\ R_{BZZ} & 0 & -R_{BZX} \\ -R_{BZY} & R_{BZX} & 0 \end{bmatrix} \begin{bmatrix} F_{BZX} \\ F_{BZY} \\ F_{BZZ} \end{bmatrix} \quad (14)$$

If S_{Z1} is positive, the surface which nominally faces upward is illuminated. The components of the solar force on this surface are

$$\begin{aligned} F_{BZX} &= S_{Z1} S_{X1} P_O X_{BAD} Y_{BAD} (1 - R_{SBB}) \\ F_{BZY} &= S_{Z1} S_{Y1} P_O X_{BAD} Y_{BAD} (1 - R_{SBB}) \\ F_{BZZ} &= S_{Z1} P_O X_{BAD} Y_{BAD} \left[S_{Z1} (1 + R_{SBB}) + \frac{2}{3} R_{SBB} \right] \end{aligned} \quad (15)$$

Equations (13) and (14) hold, but the sign of the Z_{BAD} term in equation (13) is minus.

If S_{Z1} is zero, neither of these two surfaces is illuminated, and so the solar torques on them are zero.

The other pairs of surfaces are similarly treated. The torques on the surfaces normal to the \bar{X}_1 axis are designated T_{SBXX} , T_{SBXY} , and T_{SBXZ} . The torques on the surfaces normal to the \bar{Y}_1 axis are designated T_{SBYX} , T_{SBYY} , and T_{SBYZ} .

The total solar torques on the box-shaped phased array are

$$\begin{aligned} T_{SBX} &= T_{SBXX} + T_{SBYX} + T_{SBZX} \\ T_{SBY} &= T_{SBXY} + T_{SBYY} + T_{SBZY} \\ T_{SBZ} &= T_{SBXZ} + T_{SBYZ} + T_{SBZZ} \end{aligned} \quad (16)$$

D. 3.2.3 Cone Frustum

The inclusion of a cone-shaped component in the simulation is optional. If it is included, the input index N_{CFO} is set equal to one. If not, the index is set equal to zero.

D. 3.2.4 Rod and Tip Weight

The computation of the solar radiation pressure torques on the rod and tip weight may be included as an option. If included, the input index N_{ROD} is set equal to one. If not included, the index is set equal to zero.

D. 3.2.5 Cylindrical Body Sections

The solar radiation pressure torque on one or more cylindrical body sections is included. The input index N_{CYL} indicates the number of such sections which have both flat ends exposed. In the present program, N_{CYL} is limited to two. If one cylinder with one flat end exposed is included, another index, N_{CZ} , is set equal to one. If no such cylinder is included, N_{CZ} is set equal to zero. In the present program the exposed end must be the one which nominally faces downward.

The analysis of only one cylinder is included here, because they are all similar. The inputs required for the Kth cylinder are

- a. X_{CYK} , Y_{CYK} , and Z_{CYK} , the coordinates of the center of the end facing the $-\bar{Z}_1$ direction.
- b. L_{CYK} , the length of the cylinder.
- c. R_{CYK} , the radius of the cylinder.
- d. R_{SCYK} and R_{DCYK} , the specular and diffuse reflectances of the cylindrical surface.
- e. R_{SAK} and R_{DAK} , the specular and diffuse reflectances of the flat end facing the $-\bar{Z}_1$ direction.
- f. R_{SBK} and R_{DBK} , the specular and diffuse reflectances of the flat end facing the $+\bar{Z}_1$ direction.

$$\text{If } C_{SSA} = S_{X1}^2 + S_{Y1}^2 \quad (17)$$

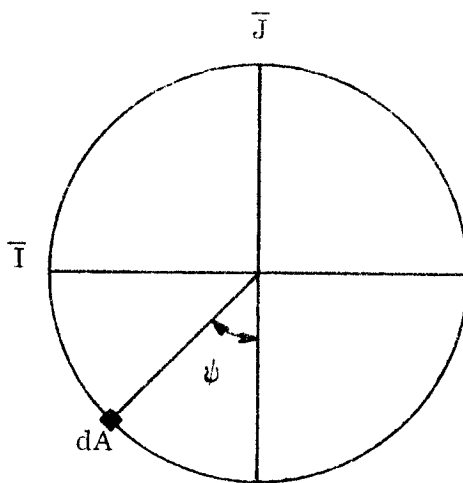
is very small, the sun is nearly parallel to the axis of the cylinder and the solar torque on the cylindrical surface is zero. Otherwise, the torque is computed.

It is convenient to use the sun-spacecraft reference frame for the analysis. This frame is defined by the triad $\bar{I} \bar{J} \bar{K}$, with \bar{K} coinciding with \bar{Z}_1 , and \bar{I} and \bar{J} oriented such that \bar{S} has a positive \bar{J} component and no \bar{I} component. The matrix of the rotational transformation from the spacecraft frame to the sun-spacecraft frame is the $[S]$ matrix,

$$\begin{bmatrix} \bar{I} \\ \bar{J} \\ \bar{K} \end{bmatrix} = [S] \begin{bmatrix} \bar{X}_1 \\ \bar{Y}_1 \\ \bar{Z}_1 \end{bmatrix} \quad (18)$$

The elements of the $[S]$ matrix are computed from

$$\begin{aligned} C_{SA} &= (C_{SSA})^{1/2} \\ S_{11} &= S_{Y1} / C_{SA} \\ S_{12} &= -S_{X1} / C_{SA} \\ S_{21} &= -S_{12} \\ S_{22} &= S_{11} \\ S_{33} &= 1 \\ S_{13} &= S_{23} = S_{31} = S_{32} = 0 \end{aligned} \quad (19)$$



An angular coordinate, ψ , is defined as illustrated in Figure D-1. The components in

Figure D-1. Spacecraft Cross Section

the sun-spacecraft frame of the vector from the spacecraft center of mass to the center of the base (at the $-\bar{Z}_1$ end) are computed from

$$\begin{bmatrix} C_{DI} \\ C_{DJ} \\ C_{DK} \end{bmatrix} = \begin{bmatrix} S \\ \end{bmatrix} \begin{bmatrix} (X_{CYK} - X_{CM}) \\ (Y_{CYK} - Y_{CM}) \\ (Z_{CYK} - Z_{CM}) \end{bmatrix} \quad (20)$$

The moment arm from the spacecraft center of mass to an element of area on the cylindrical surface is

$$\vec{R} = \bar{I} (C_{DI} + R_{CYK} \sin \psi) + \bar{J} (C_{DJ} - R_{CYK} \cos \psi) + \bar{K} (C_{DK} + l) \quad (21)$$

where l is the length coordinate.

The unit vector perpendicular to and positive toward the surface is given by

$$\bar{N} = -\bar{I} \sin \psi + \bar{J} \cos \psi \quad (22)$$

The solar unit vector is

$$\bar{S} = \bar{J} \bar{C}_{SA} + \bar{K} S_{Z1} \quad (23)$$

The cosine of the angle of incidence is

$$\bar{S} \cdot \bar{N} = C_{SA} \cos \psi \quad (24)$$

The element of area is

$$dA = R_{CYK} dl d\psi \quad (25)$$

The element of solar force on the element of area is

$$\begin{aligned} d^2 \vec{F} = & \bar{P}_O \bar{R}_{CYK} d\ell d\psi \left\{ \bar{I} (-C_{SA} F_C \sin \psi \cos \psi) \right. \\ & + \bar{J} \left(C_{SA} F_C \cos^2 \psi + C_{SSA} \cos \psi (1 - R_{SCYK}) \right) \\ & \left. + \bar{K} C_{SA} S_{Z1} \cos \psi (1 - R_{SCYK}) \right\} \end{aligned} \quad (26)$$

$$\text{where } F_C = 2R_{SCYK} C_{SA} \cos \psi + 2/3 R_{DCYK} \quad (27)$$

The element of torque is given by $d^2 \vec{T} = \bar{R} \times d^2 \vec{F}$. This is integrated with respect to ψ between the limits of $-\pi/2$ and $+\pi/2$, corresponding to the illuminated half of the cylinder. The result is then integrated with respect to ℓ between the limits of zero and L_{CYK} . It is convenient to use two intermediate variables,

$$\begin{aligned} V_{SDA} &= P_O R_{CYK} L_{CYK} S_{Z1} C_{SA} (1 - R_{SCYK}) \\ V_{SDB} &= P_O R_{CYK} L_{CYK} \left[C_{SSA} (1 - 1/3 R_{SCYK}) + \pi/6 C_{SA} R_{DCYK} \right] \end{aligned} \quad (28)$$

The components of the solar torque on the Kth cylindrical surface in the sun-spacecraft frame are

$$\begin{aligned} T_{SDIK} &= V_{SDA} (2 C_{DJ} - \pi/2 R_{CYK}) \\ &\quad - V_{SDB} (2 C_{DK} + L_{CYK}) \\ T_{SDJK} &= -2 V_{SDA} C_{DI} \\ T_{SDKK} &= 2 V_{SDB} C_{DI} \end{aligned} \quad (29)$$

The corresponding components in the spacecraft reference frame are

$$\begin{bmatrix} T_{SCXK} \\ T_{SCYK} \\ T_{SCZK} \end{bmatrix} = [S]^T \begin{bmatrix} T_{SDIK} \\ T_{SDJK} \\ T_{SDKK} \end{bmatrix} \quad (30)$$

If S_{Z1} is positive, the flat end facing the $-\bar{Z}_1$ direction is illuminated. Then the solar forces on this surface are

$$\begin{aligned} F_{SEXK} &= \pi P_O R_{CYK}^2 S_{X1} S_{Z1} (1 - R_{SAK}) \\ F_{SEYK} &= \pi P_O R_{CYK}^2 S_{Y1} S_{Z1} (1 - R_{SAK}) \\ F_{SEZK} &= \pi P_O R_{CYK}^2 S_{Z1} \left\{ S_{Z1} (1 + R_{SAK}) + \frac{2}{3} R_{DAK} \right\} \end{aligned} \quad (31)$$

The components of the moment arm from the spacecraft center of mass to the center of the flat end are

$$\begin{aligned} R_{SEXK} &= X_{CYK} - X_{CM} \\ R_{SEYK} &= Y_{CYK} - Y_{CM} \\ R_{SEZK} &= Z_{CYK} - Z_{CM} \end{aligned} \quad (32)$$

If S_{Z1} is negative, the flat end facing the $+\bar{Z}_1$ direction is illuminated. Then the solar forces on this surface are

$$\begin{aligned} F_{SEXK} &= -\pi P_O R_{CYK}^2 S_{X1} S_{Z1} (1 - R_{SBK}) \\ F_{SEYK} &= -\pi P_O R_{CYK}^2 S_{Y1} S_{Z1} (1 - R_{SBK}) \\ F_{SEZK} &= \pi P_O R_{CYK}^2 S_{Z1} \left| -S_{Z1} (1 + R_{SBK}) + \frac{2}{3} R_{DBK} \right| \end{aligned} \quad (33)$$

In either case, the torque components are computed from

$$\begin{bmatrix} T_{SEXK} \\ T_{SEYK} \\ T_{SEZK} \end{bmatrix} = \begin{bmatrix} 0 & -R_{SEZK} & R_{SEYK} \\ R_{SEZK} & 0 & -R_{SEXK} \\ -R_{SEYK} & R_{SEXK} & 0 \end{bmatrix} \begin{bmatrix} F_{SEXK} \\ F_{SEYK} \\ F_{SEZK} \end{bmatrix} \quad (34)$$

If S_{Z1} is zero, neither of the flat end surfaces is illuminated, and the torques are zero. The total solar torques on the Kth cylinder are

$$\begin{aligned} T_{SDXK} &= T_{SCXK} + T_{SEXK} \\ T_{SDYK} &= T_{SCYK} + T_{SEYK} \\ T_{SDZK} &= T_{SCZK} + T_{SEZK} \end{aligned} \quad (35)$$

D.3.2.6 Parabolic Antenna

The solar radiation pressure torques on the antenna are always included in the program.

The following inputs are specified:

- a. R_{RIM} , the radius of the antenna rim.
- b. R_{DEP} , the depth of the antenna.
- c. X_{SAN} , Y_{SAN} , and Z_{SAN} , the coordinates of the center of the dish surface, relative to the specified reference point.
- d. R_{SOA} and R_{DOA} , the specular and diffuse reflectances of the convex surface of the antenna.
- e. R_{SIA} and R_{DIA} , the specular and diffuse reflectances of the concave surface of the antenna.
- f. R_{CAN} , the fraction of the antenna surface area which is closed (fractional area effective).

The parabolic antenna is approximated as a spherical cap. The geometric relations are illustrated in Figure D-2. From this figure,

$$R_{DEP} = R_{SPH} (1 - \cos \lambda_m) \quad (36)$$

$$R_{RIM} = R_{SPH} \sin \lambda_m$$

Then

$$\frac{R_{DEP}}{R_{RIM}} = \frac{1 - \cos \lambda_m}{\sin \lambda_m} \tan \left(\frac{\lambda_m}{2} \right) \quad (37)$$

or

$$\lambda_m = 2 \tan^{-1} \left(\frac{R_{DEP}}{R_{RIM}} \right) \quad (38)$$

$$R_{SPH} = \frac{R_{RIM}}{\sin \lambda_m}$$

$$\cos \lambda_m = \frac{\sin \lambda_m}{\tan \frac{\lambda_m}{2}} - 1$$

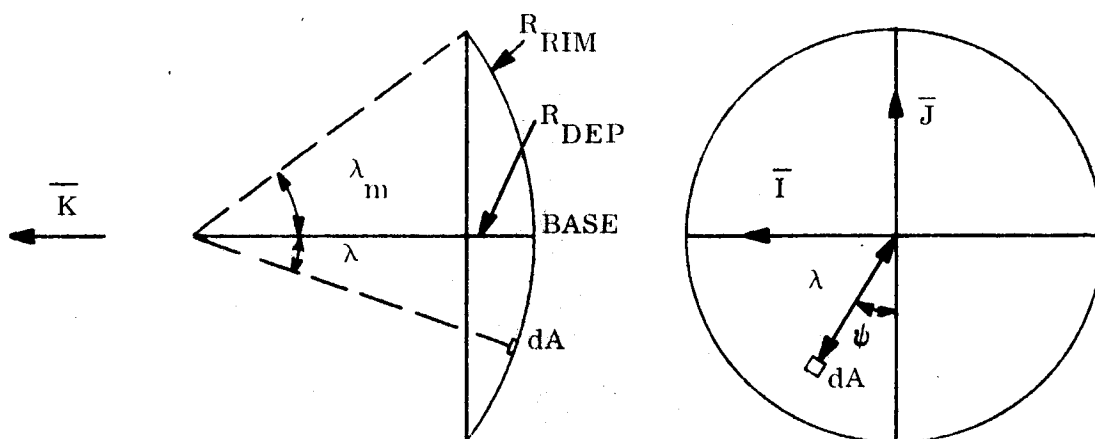


Figure D-2. Geometry of Spherical Cap

Thus, all of the geometric parameters of the sphere are determined. Both spherical and rectangular coordinates are used, as illustrated in Figure D-2. The rectangular system is the same as that used for the cylinders. The element of area is

$$dA = R_{SPH}^2 \sin \lambda d\lambda d\psi \quad (39)$$

The unit vector perpendicular to and positive toward the convex surface is

$$\bar{N}_O = -\bar{I} \sin \lambda \sin \psi + \bar{J} \sin \lambda \cos \psi + \bar{K} \cos \lambda \quad (40)$$

The unit vector positive toward the concave surface is

$$\bar{N}_i = -\bar{N}_O \quad (41)$$

The solar unit vector is

$$\bar{S} = \bar{J} \cos \sigma + \bar{K} \sin \sigma \quad (42)$$

where $\sin \sigma = S_{Z1}$

and $\cos \sigma = \left(X1^2 + S_{Y1}^2 \right)^{1/2}$

The cosine of the angle of incidence is

$$\bar{S} \cdot \bar{N} = \cos \sigma \sin \lambda \cos \psi + \sin \sigma \cos \lambda \quad (43)$$

The element of force on the element of area on the concave or convex surface can be expressed by a single equation, by using an index, N_{OI} . This is equal to plus one for the convex surface and minus one for the concave surface. Then the element of force is

$$\begin{aligned}
\vec{d}^2 F = & P_O R_{SPH}^2 d\lambda d\psi \left\{ \bar{I} (-F_A \sin^2 \lambda \sin \psi) \right. \\
& + \bar{J} (N_{OI} (\bar{S} \cdot \bar{N}_O) (1 - \rho_s) \sin \lambda \cos \sigma + F_A \sin^2 \lambda \cos \psi) \\
& \left. + \bar{K} (N_{OI} (\bar{S} \cdot \bar{N}_O) (1 - \rho_s) \sin \lambda \sin \sigma + F_A \sin \lambda \cos \lambda) \right\}
\end{aligned} \quad (44)$$

where $F_A = \frac{2}{3} \rho_d (\bar{S} \cdot \bar{N}_O) + 2 N_{OI} \rho_s (\bar{S} \cdot \bar{N}_O)^2$

ρ_s is the specular reflectance, and ρ_d is the diffuse reflectance of the surface under consideration. In addition, the factors for the fractions of closed and open areas of the mesh must be used, as described later.

The components of the moment arm from the satellite center of mass to the base of the antenna are computed from

$$\begin{bmatrix} C_{ANI} \\ C_{ANJ} \\ C_{ANK} \end{bmatrix} = [S] \begin{bmatrix} (X_{SAN} - X_{CM}) \\ (Y_{SAN} - Y_{CM}) \\ (Z_{SAN} - Z_{CM}) \end{bmatrix} \quad (45)$$

The moment arm from the satellite center of mass to the base of the antenna is

$$\begin{aligned}
\vec{R} = & \bar{I} (C_{ANI} + R_{SPH} \sin \lambda \sin \psi) + \bar{J} (C_{ANJ} - R_{SPH} \sin \lambda \cos \psi) \\
& + \bar{K} (C_{ANK} + R_{SPH} - R_{SPH} \cos \lambda).
\end{aligned} \quad (46)$$

The element of torque is given by equation (27). Because of the symmetry about the $\bar{J} \bar{K}$ plane, the terms involving $\sin \psi$ contribute nothing to the final result, and will be dropped. The results are expressed in terms of the differentials of intermediate variables,

$$\begin{aligned}
\vec{d}^2 T = & \bar{I} \left\{ C_{ANJ} d^2 T_{SAA} - (C_{ANK} + R_{SPH}) d^2 T_{SAB} + R_{SPH} d^2 T_{SAC} \right\} \\
& - \bar{J} C_{ANI} d^2 T_{SAA} + \bar{K} C_{ANI} d^2 T_{SAB}
\end{aligned} \quad (47)$$

where

$$d^2 T_{SAA} = 2P_O R_{SPH}^2 d\lambda d\psi \left\{ N_{OI} (1 - \rho_s) (\sin^2 \sigma \sin \lambda \cos \lambda \right. \\ \left. + \sin \sigma \cos \sigma \sin^2 \lambda \cos \psi) + 2N_{OI} \rho_s (\cos^2 \sigma \sin^3 \lambda \cos \lambda \cos^2 \psi \right. \\ \left. + \sin^2 \sigma \sin \lambda \cos^3 \lambda + 2\sin \sigma \cos \sigma \sin^2 \lambda \cos^2 \lambda \cos \psi) \right. \\ \left. + 2/3 \rho_d (\cos \sigma \sin^2 \lambda \cos \lambda \cos \psi + \sin \sigma \sin \lambda \cos^2 \lambda) \right\}$$

$$d^2 T_{SAB} = 2P_O R_{SPH}^2 d\lambda d\psi \left\{ N_{OI} (1 - \rho_s) (\cos^2 \sigma \sin^2 \lambda \cos \psi \right. \\ \left. + \sin \sigma \cos \sigma \sin \lambda \cos \lambda) + 2N_{OI} \rho_s (\cos^2 \sigma \sin^4 \lambda \cos^3 \psi \right. \\ \left. + \sin^2 \sigma \sin^2 \lambda \cos^2 \lambda \cos \psi + 2\sin \sigma \cos \sigma \sin^3 \lambda \cos \lambda \cos^2 \psi) \right. \\ \left. + 2/3 \rho_d (\cos \sigma \sin^3 \lambda \cos^2 \psi + \sin \sigma \sin^2 \lambda \cos \lambda \cos \psi) \right\}$$

$$d^2 T_{SAC} = 2P_O R_{SPH}^2 d\lambda d\psi N_{OI} (1 - \rho_s) \left\{ \cos^2 \sigma \sin^2 \lambda \cos \lambda \cos \psi \right. \\ \left. + \sin \sigma \cos \sigma \sin \lambda \cos^2 \lambda - \sin \sigma \cos \sigma \sin^3 \lambda \cos^2 \lambda \right. \\ \left. - \sin^2 \sigma \sin^2 \lambda \cos \lambda \cos \psi \right\}$$

These expressions have been multiplied by two, because of the symmetry about the $\bar{J}\bar{K}$ plane, and all integrations need be performed on only one side of this plane.

The expressions are integrated with respect to ψ and with respect to λ . The limits of integration depend upon the sun angle, σ . Six cases are distinguished.

- a. Case I. The sun's rays make an angle with the $+\bar{Z}_1$ axis which is equal to or less than λ_m , or

$$S_{Z1} \geq \sin \lambda_m \quad (48)$$

In this case the convex surface is completely illuminated and the concave surface is completely shaded. The reflectances of the convex surfaces are used in equations (47) and all the expressions are multiplied by R_{CAN} , the fraction of the antenna surface area which is closed. The integration with respect to ψ is between the limits of zero and π , and that with respect to λ is between the limits of zero and λ_m .

- b. Case II. The sun's rays make an angle with the $+\bar{Z}_1$ axis which is greater than in Case I, but equal to or less than 90 degrees,

$$0 \leq S_{Z1} < \sin \lambda_m \quad (49)$$

This case is illustrated in Figure D-3. The shadow line shown is the locus of points where the surface is tangent to the sun's rays. These points lie on an arc which is a portion of a great circle of the sphere. Along this arc, the angle of incidence is 90 degrees. The value of ψ at which this occurs depends upon λ , and the relation is obtained by setting Equation (43) equal to zero, and solving for

$$\psi_S = \cos^{-1} (-\tan \sigma \cot \lambda) \quad (50)$$

On one side of this shadow line, the convex surface is directly illuminated. On the other side, the concave surface is illuminated through the mesh. The integrations are most easily carried out over three separate regions. The first region is directly below the shadow line in Figure D-3. The limits for ψ are zero and ψ_S , and those for λ are σ and λ_m . The arc for which λ is equal to σ is shown by the dashed line in the figure, and the second region of integration is to the right of the dashed line. The limits for ψ are zero and π , and those for λ are zero and σ . For both of these regions, the reflectances for the convex surface are used, and the expressions are multiplied by R_{CAN} . The third region lies above the shadow line in Figure D-3. The limits for ψ are ψ_S and π , and those for λ are σ and λ_m . The reflectances of the concave surface are used, and the expressions are multiplied by $(1 - R_{CAN})$, the fraction of open area of the mesh, and also multiplied by R_{CAN} , the fraction of the closed area. The first factor accounts for the reduced intensity of the solar flux coming through the mesh, and the second factor accounts for the effective area of the concave surface.

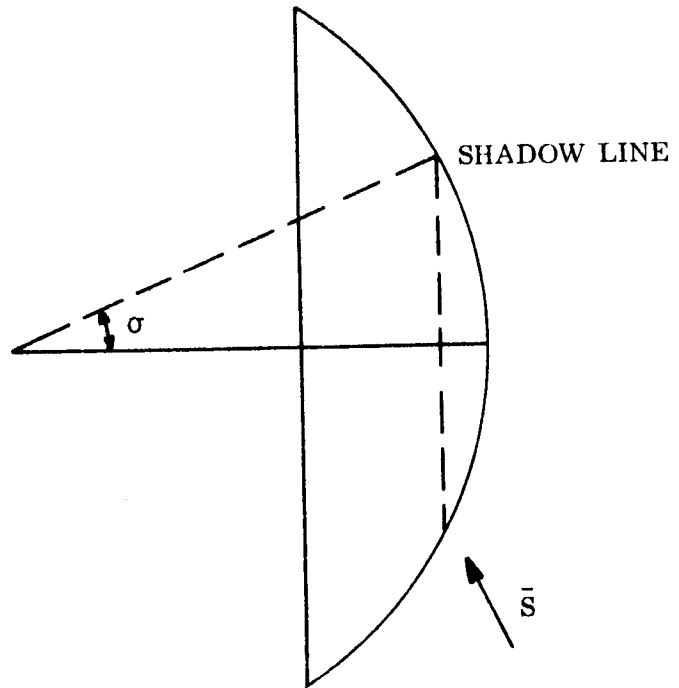


Figure D-3. Case II

The equations for Case I are obtained from those for Case II by setting ψ_S equal to π . Therefore, separate equations for Case I were not programmed.

- c. **Case III.** The sun's rays make an angle with the $+Z_1$ axis which is greater than 90 degrees, but less than $(90 \text{ degrees} + 1/3 \lambda_m)$

$$-\sin \frac{\lambda_m}{3} < S_{Z1} < 0 \quad (51)$$

This case is illustrated in Figure D-4.

The shadow line now appears in the lower portion of the figure. The rim shadow line is an arc which is the shadow cast by the antenna rim.

The relation between the ψ -coordinate, ψ_{RS} , and λ on this arc is derived as follows. For any point along the arc, the vector from the center of the sphere to the point is equal to the sum of two other vectors: (1) a vector from the center of the sphere to that point on the rim which casts the shadow, such point being located at an unknown value of ψ , designated ψ_R , and (2) a vector along the shadow-casting solar ray, of unknown magnitude, A . Setting the respective rectangular components of the one vector equal to the sum of the components of the other two yields

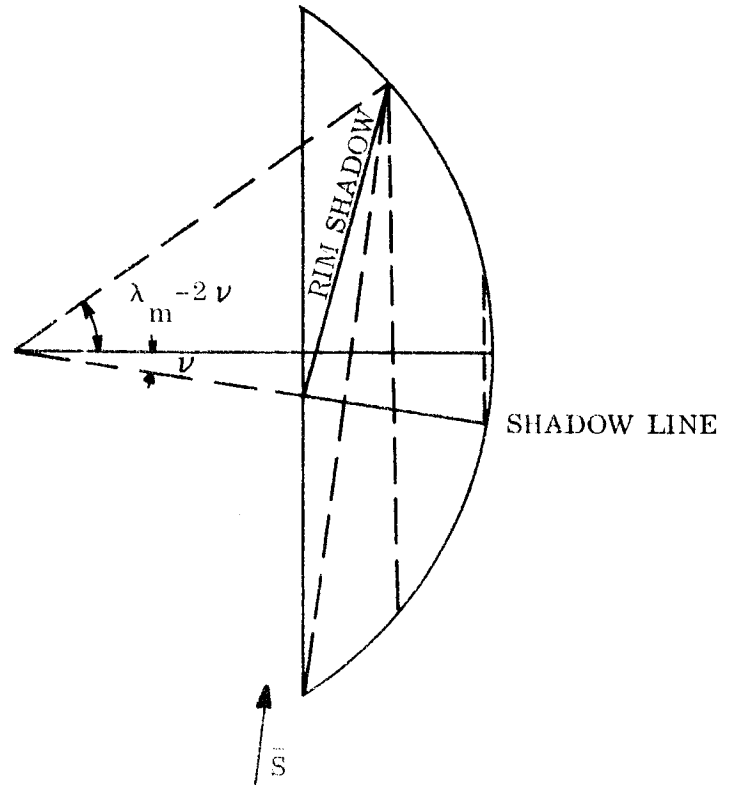


Figure D-4. Case III

$$\begin{aligned} R_{SPH} \sin \lambda_m \sin \psi_R &= R_{SPH} \sin \lambda \sin \psi \\ -R_{SPH} \sin \lambda_m \cos \psi_R + A \cos \sigma &= -R_{SPH} \sin \lambda \cos \psi \\ -R_{SPH} \cos \lambda_m + A \sin \sigma &= -R_{SPH} \cos \lambda \end{aligned} \quad (52)$$

R_{SPH} , A and ψ_R are eliminated from these equations, and the result is

$$\psi_{RS} = \cos^{-1} \left\{ \frac{\cos^2 \sigma (\cos \lambda - \cos \lambda_m)^2 - \sin^2 \sigma (\sin^2 \lambda_m - \sin^2 \lambda)}{2 \sin \sigma \cos \sigma \sin \lambda (\cos \lambda - \cos \lambda_m)} \right\} \quad (53)$$

The angle υ , shown in Figure D-4, is equal to the magnitude of the angle between the solar unit vector \bar{S} and the \bar{J} axis, which is parallel to the vertical in the figure. This angle was introduced in order to clarify the diagrams by using a positive acute angle.

Below the shadow line, the convex surface is directly illuminated. For this region, the factor R_{CAN} is used, the limits for ψ are 0 and ψ_S , and those for λ are υ and λ_m . Between the shadow line and the rim shadow line, the concave surface is illuminated through the mesh. Therefore, the factors R_{CAN} and $(1 - R_{CAN})$ are used. This region is divided into three subregions by the vertical dashed lines in Figure D-4. For the right-hand region, the limits for ψ are zero and π , and those for λ are zero and υ . For the middle region, the limits for ψ and ψ_S and π , and those for λ are υ and $(\lambda_m - 2\upsilon)$. For the left-hand region, the limits for ψ are ψ_S and ψ_{RS} , and those for λ are $(\lambda_m - 2\upsilon)$ and λ_m .

Above the rim shadow line, the concave surface is directly illuminated. Therefore, in this region, the reflectances of the concave surface and the factor R_{CAN} are used. The limits for ψ are ψ_{RS} and π , and those for λ are $(\lambda_m - 2\upsilon)$ and λ_m .

- d. Case IV. The sun's rays make an angle with the $+\bar{Z}_1$ axis which is equal to or greater than $(90 \text{ degrees} + 1/3 \lambda_m)$, but less than $(90 \text{ degrees} + 1/2 \lambda_m)$.

$$-\sin \frac{\lambda_m}{2} < S_{Z1} \leq -\sin \frac{\lambda_m}{3} \quad (54)$$

This case is illustrated in Figure D-5. The shadow line and the rim shadow line appear much the same as in Figure D-4, but the distinction between Cases III and IV is that, in the latter case, the minimum λ -coordinate of the shadow line is greater than that of the rim shadow line. Below the shadow line, the convex surface is directly illuminated, and this region is treated the same as in Case III.

Between the shadow line and the rim shadow line, the concave surface is illuminated through the mesh. The general treatment is the same as in Case III, but the three regions have limits of integration different from those of Case III. For the right-hand region, the limits for ψ are

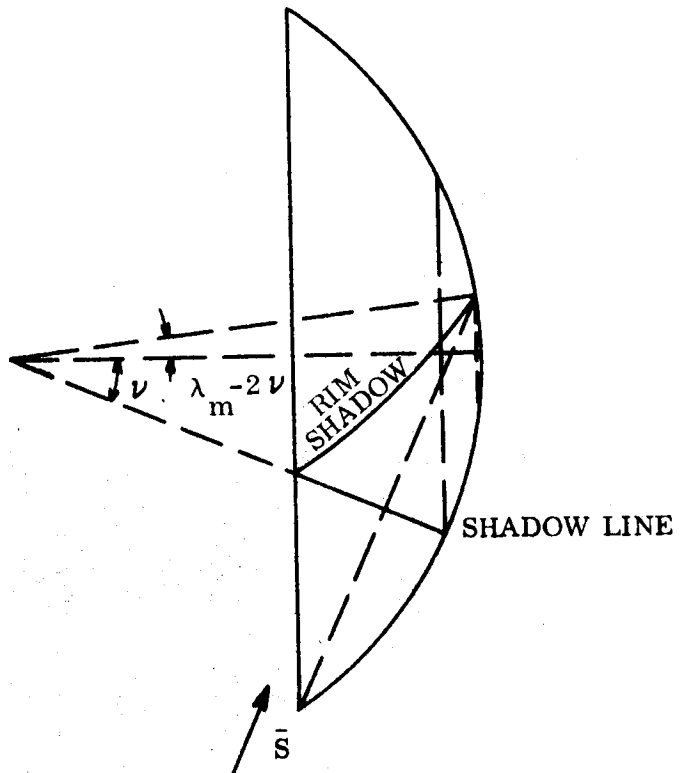


Figure D-5. Case IV

zero and π , and those for λ are zero and $(\lambda_m - 2\nu)$. For the middle region, the limits for ψ are zero and ψ_{RS} , and those for λ are ν and λ_m .

Above the rim shadow line, the concave surface is directly illuminated. This region is treated the same as in Case III, and the limits of integration are the same.

- e. Case V. The sun's rays make an angle with the $+\bar{Z}_1$ axis which is equal to or greater than $(90 \text{ degrees} + 1/2 \lambda_m)$, but less than $(90 \text{ degrees} + \lambda_m)$.

$$-\sin \lambda_m < S_{Z1} \leq -\sin \frac{\lambda_m}{2} \quad (55)$$

This case is illustrated in Figure D-6. The distinction between Cases IV and V is that, in the latter case, the apex of the rim shadow falls on the $-\bar{J}$ side of the $\bar{I}\bar{K}$ plane. Below the shadow line, the convex surface is directly illuminated, and this region is treated the same as in Case III. Between the shadow line and the rim shadow line, the concave surface is illuminated through the mesh. The general treatment is the same as in Case III, but there are only two regions, and the limits of integration are different.

For the right-hand region, the limits for ψ are zero and ψ_{RS} , and those for λ are $(2\nu - \lambda_m)$ and ν . For the left-hand region, the limits are the same as for Case IV. Above the rim shadow line, the concave surface is directly illuminated. While the general treatment is the same as in Case III, there are now two regions, and the limits of integration are different. For the right-hand region, the limits for ψ are zero and π , and those for λ are zero and $(2\nu - \lambda_m)$. For the left-hand region, the limits for ψ and ψ_{RS} are π , and those for λ are $(2\nu - \lambda_m)$ and λ_m .

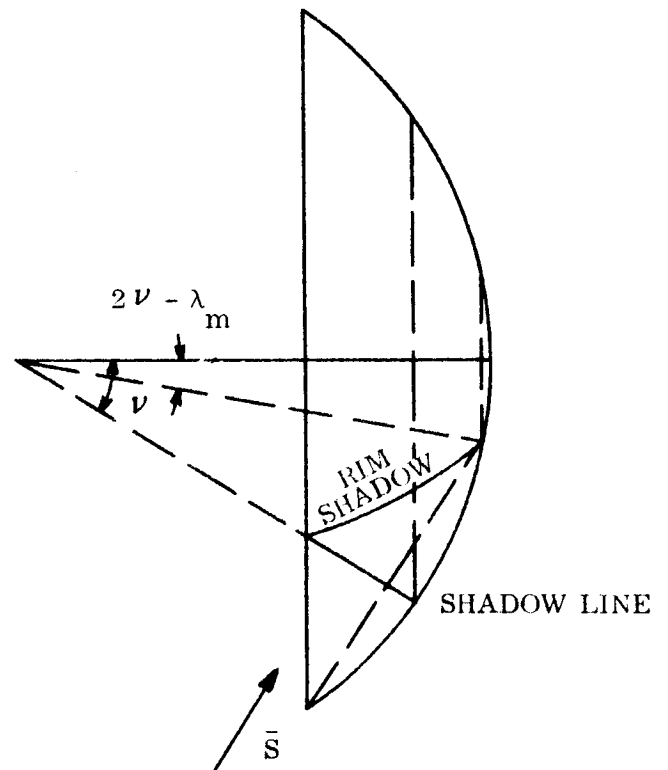


Figure D-6. Case V

In Cases III, IV, and V, the first integration, with respect to ψ , was always done in closed form. Some of the resulting expressions can be integrated with respect to λ in closed form, while others can not. They were all integrated numerically by the digital computer program.

- f. Case VI. The sun's rays make an angle with the $+\bar{Z}_1$ axis which is equal to or greater than $(90 \text{ degrees} + \lambda_m)$,

$$S_{Z1} \leq -\sin \lambda_m \quad (56)$$

In this case, the convex surface is completely shaded, and the entire concave surface is directly illuminated. The limits of integration are the same as for Case I. The equations are also the same, except that the reflectances of the concave surface are used, and N_{OI} is equal to minus one.

In all cases, the components of the solar torque in the spacecraft-sun frame are computed first, and then transformed into the spacecraft frame by

$$\begin{bmatrix} T_{SAX} \\ T_{SAY} \\ T_{SAZ} \end{bmatrix} = [S]^T \begin{bmatrix} T_{SAI} \\ T_{SAJ} \\ T_{SAK} \end{bmatrix} \quad (57)$$

APPENDIX E
MATHEMATICAL MODEL FOR ORIENTATION CONTROL SERVO ANALYSIS

Mathematical models of those components constituting the sun stabilization, earth stabilization, star acquisition, and primary pointing systems are described in this appendix in Sections E.1 through E.7 as follows: (1) Introduction, (2) Vehicle Dynamics, (3) Vehicle Orientation, (4) Torquers, (5) Controllers, (6) Sensors, and (7) Sensor Signal Processing.

E.1 INTRODUCTION

The block diagram of Figure E-1 applies to each of the above systems. The nomenclature used throughout this appendix is described in Section 6.4.3.3.1.

E.2 VEHICLE DYNAMICS

The equations describing the angular velocity of a rigid vehicle with nonrigid appendages are listed in this section. The derivation of these equations is outlined very briefly.

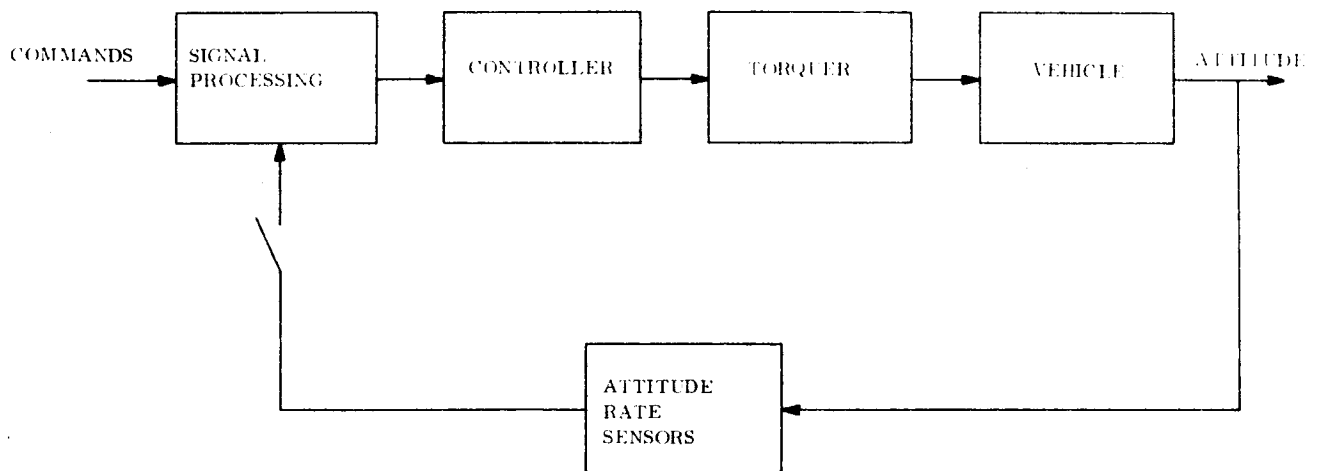


Figure E-1. Control System Block Diagram

E. 2. 1 DEFINITIONS

- a. Spacecraft - The spacecraft is the complete ATS-4 structure consisting of a rigid vehicle and deployed, flexible appendages.
- b. Vehicle - The vehicle is the rigid portion of the ATS-4 spacecraft and includes, principally, the basic satellite and the subsatellite.
- c. Flexible Appendages - The flexible appendages are those structures having sufficient flexibility to significantly affect, at least potentially, the performance of the Orientation Control system.
- d. Structural Admittance Matrix - The structural admittance matrix is a matrix of transfer functions describing the mechanical admittance of the vehicle. For a vehicle with rigid appendages the structural admittance matrix becomes the inverse of the matrix of moments and products of inertia.

E. 2. 2 COORDINATE SYSTEM

The ATS-4 vehicle dynamics are described in terms of the right hand body axis coordinate system illustrated in Reference E. 8. 1 and Figure E-2. The body axes are translated as necessary to maintain coincidence of the spacecraft center of mass and the origin of the coordinate system. The body axes coincide with the spacecraft principal axes only when the spacecraft instantaneous center of mass coincides with the spacecraft nominal center of mass (flexible appendages at rest).

E. 2. 3 SIGN CONVENTION

Positive angular displacements, velocities, and accelerations are counterclockwise when viewed from the positive end of an axis.

E. 2. 4 NOMENCLATURE

The nomenclature is described in Section 6. 4. 3. 3. 1.

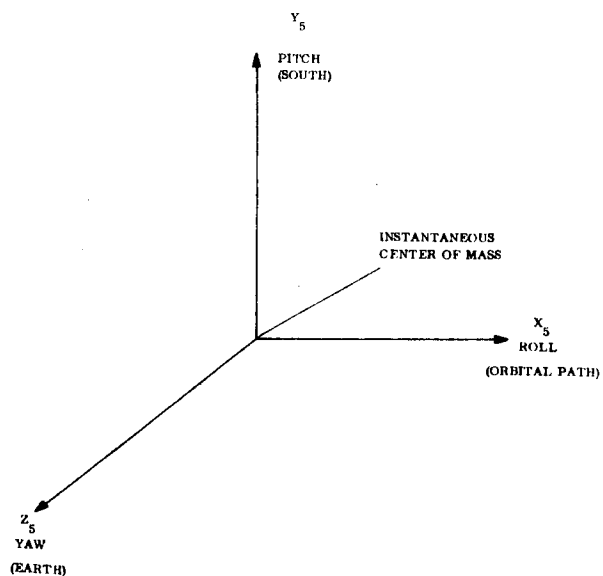


Figure E-2. Body Axis Coordinate System

E. 2. 5 EQUATIONS

Two equations are required: one of these describes the relationship between the external torques applied to the vehicle and the resultant vehicle momentum; the other, describes the relationship between the vehicle angular momentum and the vehicle angular velocity. The effect of flexible appendages is factored into the latter of these relationships.

The torque/momentum equation for each axis is:

$$h_{vx} = H_x(0) + \int_0^t (T_{Jx} + T_{Dx} - T_{Gx}) dt - h_{Wx} \quad (1a)$$

$$h_{vy} = H_y(0) + \int_0^t (T_{Jy} + T_{Dy} - T_{Gy}) dt - h_{Wy} \quad (1b)$$

$$h_{vz} = H_z(0) + \int_0^t (T_{Jz} + T_{Dz} - T_{Gz}) dt - h_{Wz} \quad (1c)$$

The momentum/velocity equation for each axis is expressed in terms of Laplace Transforms:

$$W_x = Y_{xx} h_{vx} + Y_{xy} h_{vy} + Y_{xz} h_{vz} \quad (2a)$$

$$W_y = Y_{yx} h_{vx} + Y_{yy} h_{vy} + Y_{yz} h_{vz} \quad (2b)$$

$$W_z = Y_{zx} h_{vx} + Y_{zy} h_{vy} + Y_{zz} h_{vz} \quad (2c)$$

The transfer functions $Y_{ij}(s)$ have the form,

$$Y_{ij} = A_{ij} + \sum_{K=1}^N \frac{S^2 A_{ijk}}{S^2 + 2jk\omega_{jk} S + \omega_{jk}^2} \quad (3)$$

and constitute the elements of the structural admittance matrix. The transfer function description of flexible structure effects is dictated by the methods currently used to derive numerical data for some given structure. In the absence of flexible appendages, the transfer functions reduce to a constant

$$Y_{ij} = A_{ij} \quad (4)$$

Where the A_{ij} are the elements of the inverse inertia tensor ; that is,

$$\|A_{ij}\| = \begin{bmatrix} I_{xx} & -I_{xy} & -I_{xz} \\ -I_{yx} & I_{yy} & -I_{yz} \\ -I_{zx} & -I_{zy} & I_{zz} \end{bmatrix}^{-1} \quad (5)$$

The components of total angular momentum (H_x, H_y, H_z) and the components of the gyroscopic torque (T_{Gx}, T_{Gy}, T_{Gz}) shown in equation (1) are as follows:

$$H_x = h_{vx} + h_{Wx} \quad (6a)$$

$$H_y = h_{vy} + h_{Wy} \quad (6b)$$

$$H_z = h_{vz} + h_{Wz} \quad (6c)$$

$$T_{Gx} = -\omega_z H_y + \omega_y H_z \quad (7a)$$

$$T_{Gy} = \omega_z H_x - \omega_x H_z \quad (7b)$$

$$T_{Gz} = -\omega_y H_x + \omega_x H_y \quad (7c)$$

E. 2. 6 DERIVATION

Equation (1), the relationship between torque and momentum, follows from an expansion of the equation of motion:

$$T_E = \dot{\bar{H}} = \bar{\dot{H}} + \bar{\omega} \times \bar{H} \quad (8)$$

Substituting into equation (8) the expressions:

$$\bar{T}_E = \bar{T}_D + \bar{T}_J \quad (9)$$

$$\bar{T}_G = \bar{\omega} \times \bar{H} \quad (10)$$

$$\dot{\bar{H}} = \dot{\bar{h}}_v + \dot{\bar{h}}_w \quad (11)$$

and solving for $\dot{\bar{h}}_v$ yields:

$$\dot{\bar{h}}_v = \bar{T}_J + \bar{T}_D - \bar{T}_G - \dot{\bar{h}}_w \quad (12)$$

or for each axis,

$$\dot{h}_{vj} = T_{Jj} + T_{Dj} - T_{Gj} - \dot{h}_{wj} \quad (13)$$

$$j = x, y, z$$

Integrating equation (13) from $t = 0$ to $t=t$ yields equation (1). Note that

$$\int_0^t \dot{h} dt = h - h(0) \quad (14)$$

The derivation of equations (2) and (3) for flexible structures has been described in Reference E. 8. 2 and discussed in Reference E. 8. 3.

E. 2. 7 NUMERICAL VALUES

The coefficients (A_{ijk}), natural frequencies (ω_{jk}), and damping factors (ξ_{ijk}) for the ATS-4 vehicle with and without deployed appendages are listed in Section 6. 4. 3. 3. 1.

E. 3 VEHICLE ORIENTATION

The equations describing the orientation of the ATS-4 body axes with respect to the sun, the earth, and a star are described in this section. References detailing the derivation of these equations are listed.

E. 3. 1 DEFINITIONS

- a. Orientation Reference - An orientation reference is the line of sight between the spacecraft center of mass and the sun, a star, or some point on the earth.
- b. Vehicle Orientation - The orientation of the vehicle is the relationship between the vehicle body axes and an orientation reference. This relationship is described by direction cosines, Euler Angles or Euler Parameters.
- c. Sunline - The sunline is the line of sight between the vehicle and the sun. The sunline is always assumed to be fixed in inertial space.
- d. Local Vertical - The local vertical is the line of sight between the vehicle and the center of the earth.
- e. Star Line - A star line is the line of sight between the vehicle and a star.

E. 3. 2 COORDINATE SYSTEMS

Two coordinate systems are required to describe the orientation of the vehicle: (1) the body axis coordinate system; and (2) the geocentric coordinate system. The body axis coordinate system has been described in Section E. 2 above. The geocentric coordinate system has been illustrated in Reference E. 8. 1.

The origin is attached to the vehicle instantaneous center of mass. The x axis coincides with the orbital velocity vector; the z axis coincides with the local vertical. The y axis is oriented as necessary to form a right-handed coordinate system.

E. 3. 3 SIGN CONVENTION

As in Section E. 2, positive angular displacements are counter-clockwise when the origin of a coordinate system is observed from the positive end of an axis.

E. 3. 4 NOMENCLATURE

The nomenclature is described in Section 6. 4. 3. 1. 1.

E. 3. 5 DIRECTION COSINES

Direction cosines are used to describe the orientation of the vehicle body axes relative to some orientation reference as illustrated in Figure E-3. A matrix of nine direction cosines is used to describe the transformation from one coordinate system to another; that is,

$$\begin{bmatrix} \bar{X}_B \\ \bar{Y}_B \\ \bar{Z}_B \end{bmatrix} = \begin{bmatrix} A_{11} & A_{12} & A_{13} \\ A_{21} & A_{22} & A_{23} \\ A_{31} & A_{32} & A_{33} \end{bmatrix} \begin{bmatrix} \bar{X}_A \\ \bar{Y}_A \\ \bar{Z}_A \end{bmatrix} \quad (15)$$

or

$$\begin{bmatrix} \bar{X}_A \\ \bar{Y}_A \\ \bar{Z}_A \end{bmatrix} = \begin{bmatrix} A_{11} & A_{21} & A_{31} \\ A_{12} & A_{22} & A_{32} \\ A_{13} & A_{23} & A_{33} \end{bmatrix} \begin{bmatrix} \bar{X}_B \\ \bar{Y}_B \\ \bar{Z}_B \end{bmatrix} \quad (16)$$

In general both of the coordinate systems are rotating and the direction cosines A_{ij} are described by a system of ordinary linear differential equations with time varying coefficients and several constraints. The differential equations, derived in Reference E. 8. 4, have been written in matrix form for convenience:

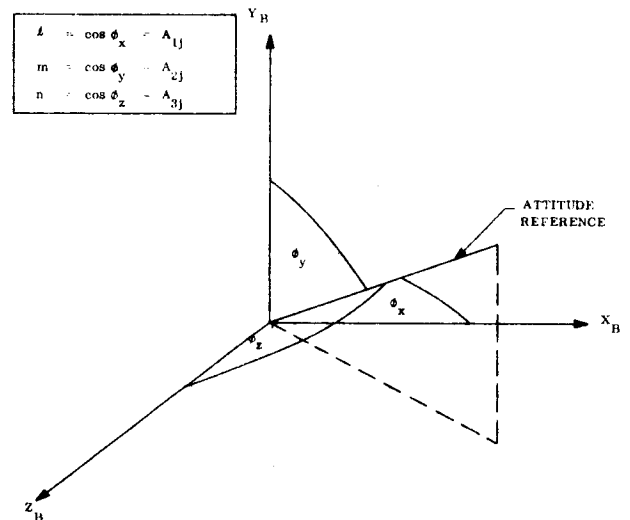


Figure E-3. Direction Cosines

$$\| \dot{A}_{ij} \| = \begin{bmatrix} 0 & \omega_z & -\omega_y \\ -\omega_z & 0 & \omega_x \\ \omega_y & -\omega_x & 0 \end{bmatrix} \| A_{ij} \| - \| A_{ij} \| \begin{bmatrix} 0 & \Omega_z & -\Omega_y \\ -\Omega_z & 0 & \Omega_x \\ \Omega_y & -\Omega_x & 0 \end{bmatrix} \quad (17)$$

where $\bar{\Omega}$ is the angular velocity of coordinate system A and $\bar{\omega}$ is the angular velocity of coordinate system B:

$$\bar{\Omega} = \Omega_x \bar{X}_A + \Omega_y \bar{Y}_A + \Omega_z \bar{Z}_A \quad (18)$$

$$\bar{\omega} = \omega_x \bar{X}_B + \omega_y \bar{Y}_B + \omega_z \bar{Z}_B \quad (19)$$

The constraint equations are those applicable to a transformation matrix between orthogonal coordinate systems:

$$A_{11}^2 + A_{12}^2 + A_{13}^2 = 1 \quad (20a)$$

$$A_{21}^2 + A_{22}^2 + A_{23}^2 = 1 \quad (20b)$$

$$A_{31}^2 + A_{32}^2 + A_{33}^2 = 1 \quad (20c)$$

$$A_{11} A_{21} + A_{12} A_{22} + A_{13} A_{23} = 0 \quad (21a)$$

$$A_{11} A_{31} + A_{12} A_{32} + A_{13} A_{33} = 0 \quad (21b)$$

$$A_{21} A_{31} + A_{22} A_{32} + A_{23} A_{33} = 0 \quad (21c)$$

E. 3.6 EULER PARAMETERS

Euler Parameters have been described in Reference E. 8. 4. These four quantities (e_1, e_2, e_3, e_4) describe the axis of rotation of coordinate system B and angular displacement about this axis as shown in Figure E-4, specifically,

$$e_1 = b_1 \sin \frac{u}{z} \quad (22a)$$

$$e_2 = b_2 \sin \frac{u}{z} \quad (22b)$$

$$e_3 = b_3 \sin \frac{u}{z} \quad (22c)$$

$$e_4 = \cos \frac{u}{z} \quad (22d)$$

where the direction cosines b_1, b_2 and b_3 , illustrated in Figure E-4 represent the angular displacements between the axis

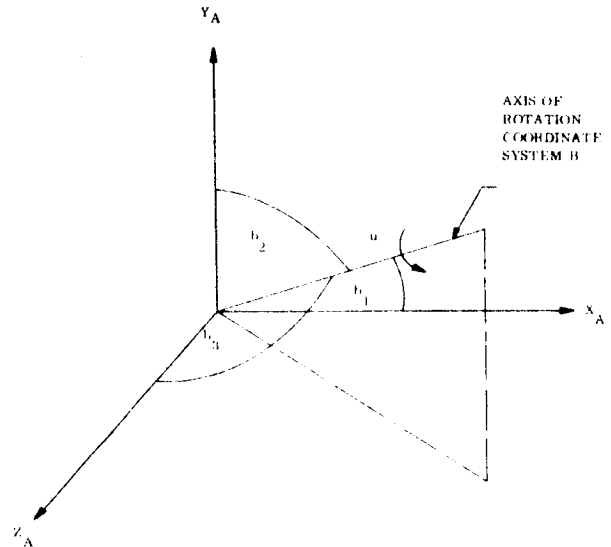


Figure E-4. Euler Parameters

of rotation of coordinate system B and the axes of coordinate system A. The Euler parameters are solutions to a system of ordinary linear differential equations with time varying coefficients and a single constraint:

$$\dot{e}_1 = \frac{1}{2} (\omega_z + \Omega_z) e_2 - \frac{1}{2} (\omega_y + \Omega_y) e_3 + \frac{1}{2} (\omega_x - \Omega_x) e_4 \quad (23a)$$

$$\dot{e}_2 = -\frac{1}{2} (\omega_z + \Omega_z) e_1 + \frac{1}{2} (\omega_x + \Omega_x) e_3 + \frac{1}{2} (\omega_y - \Omega_y) e_4 \quad (23b)$$

$$\dot{e}_3 = \frac{1}{2} (\omega_y + \Omega_y) e_1 - \frac{1}{2} (\omega_x + \Omega_x) e_2 + \frac{1}{2} (\omega_z - \Omega_z) e_4 \quad (23c)$$

$$\dot{e}_4 = -\frac{1}{2} (\omega_x - \Omega_x) e_1 - \frac{1}{2} (\omega_y - \Omega_y) e_2 - \frac{1}{2} (\omega_z - \Omega_z) e_3 \quad (23d)$$

$$e_1^2 + e_2^2 + e_3^2 + e_4^2 = 1 \quad (24)$$

As shown in Reference E. 8. 4, the direction cosines are related to the Euler Parameters as follows:

$$A_{11} = e_4^2 + e_1^2 - e_2^2 - e_3^2 \quad (25a)$$

$$A_{12} = 2 (e_1 e_2 + e_3 e_4) \quad (25b)$$

$$A_{13} = 2 (e_1 e_3 - e_2 e_4) \quad (25c)$$

$$A_{21} = 2 (e_1 e_2 - e_3 e_4) \quad (25d)$$

$$A_{22} = e_4^2 - e_1^2 + e_2^2 - e_3^2 \quad (25e)$$

$$A_{23} = 2 (e_2 e_3 + e_1 e_4) \quad (25f)$$

$$A_{31} = 2 (e_1 e_3 + e_2 e_4) \quad (25g)$$

$$A_{32} = 2 (e_2 e_3 - e_1 e_4) \quad (25h)$$

$$A_{33} = e_4^2 - e_1^2 - e_2^2 + e_3^2 \quad (25i)$$

E. 3. 7 EULER ANGLES

If coordinate system B is subjected to sequential angular rotations about its axes, the ultimate orientation of the coordinate system is a function of not only the magnitude of the rotations, but also the sequence in which the rotations are carried out. Classical Euler angles are distinguished from nonclassical Euler angles by the sequence in which the rotations are completed. Classical Euler angles are generated whenever the first rotation is about the z axis; the second, about the y axis; and the third, about the z axis once again. This constitutes a z-y-z sequence. Nonclassical Euler angles result whenever some sequence other than z-y-z is used.

If, as shown in Figure E-5, coordinate system B is rotated first through an angle Ψ about the z axis; secondly, through an angle θ about the y axis; and finally, through an angle ϕ about the x axis, the direction cosines for the orientation of the vehicle are determined from the following:

$$\|A_{ij}\| = \begin{bmatrix} 1 & 0 & 0 \\ 0 & \cos \phi & \sin \phi \\ 0 & -\sin \phi & \cos \phi \end{bmatrix} \begin{bmatrix} \cos \theta & 0 & -\sin \theta \\ 0 & 1 & 0 \\ \sin \theta & 0 & \cos \theta \end{bmatrix} \begin{bmatrix} \cos \Psi & \sin \Psi & 0 \\ -\sin \Psi & \cos \Psi & 0 \\ 0 & 0 & 1 \end{bmatrix} \quad (26)$$

Carrying out the indicated matrix multiplication:

$$A_{11} = \cos \Psi \cos \theta \quad (27a)$$

$$A_{12} = \sin \Psi \cos \theta \quad (27b)$$

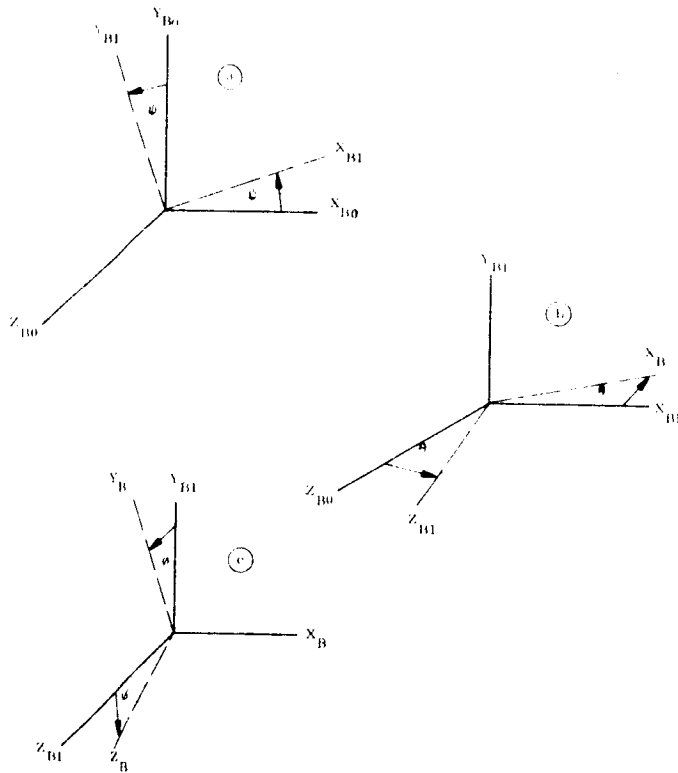


Figure E-5. Nonclassical Euler Angles

$$A_{13} = -\sin \theta \quad (27c)$$

$$A_{21} = -\sin \Psi \cos \vartheta + \cos \Psi \sin \theta \sin \vartheta \quad (27d)$$

$$A_{22} = \cos \Psi \cos \vartheta + \sin \Psi \sin \theta \sin \vartheta \quad (27e)$$

$$A_{23} = \cos \theta \sin \vartheta \quad (27e)$$

$$A_{31} = \sin \Psi \sin \vartheta + \cos \Psi \sin \theta \cos \vartheta \quad (27g)$$

$$A_{32} = -\cos \Psi \sin \vartheta + \sin \Psi \sin \theta \cos \vartheta \quad (27h)$$

$$A_{33} = \cos \theta \cos \vartheta \quad (27i)$$

E. 3. 8 ORIENTATION REFERENCED TO THE SUNLINE

Let the sunline be coincident with the z axis of coordinate system A and the body axes coincident with the axes of coordinate system B. Vehicle orientation relative to the sunline is then described by the three direction cosines A_{13} , A_{23} and A_{33} representing the angular displacements between the sunline and each of the body axes.

Since the sunline is assumed fixed in inertial space, the A coordinate system must have zero angular velocity about the x and y axes; that is,

$$\Omega_x = \Omega_y = 0 \quad (28)$$

From equation (17), the differential equations for the direction cosines A_{13} , A_{23} and A_{33} become:

$$\dot{A}_{13} = \dot{l} = \omega_z m - \omega_y n \quad (29a)$$

$$\dot{A}_{23} = \dot{m} = -\omega_z l + \omega_x n \quad (29b)$$

$$\dot{A}_{33} = \dot{n} = \omega_y l - \omega_x m \quad (29c)$$

The single applicable constraint is

$$l^2 + m^2 + n^2 = 1 \quad (30)$$

E. 3. 9 ORIENTATION REFERENCED TO THE LOCAL VERTICAL

Let the A coordinate system coincide with the geocentric coordinate system and the B coordinate system coincide with the body axes. Vehicle orientation relative to the local vertical (the z axis in the geocentric coordinate system) is then described by the three direction cosines A_{13} , A_{23} , and A_{33} representing the angular displacement between the local vertical and each of the body axes. The required direction cosines are most conveniently generated by first generating the Euler parameters per equations (23) and (24) and then calculating the direction cosines per equations (25e), (25f) and (25i). Since the xz plane of the geocentric coordinate system coincides, by definition, with the orbital plane, the angular velocity of the geocentric coordinate system is simply,

$$\bar{\Omega} = \Omega \bar{y}_3 \quad (31)$$

If the orbit is synchronous, the angular velocity, Ω , is equal to that of the earth about its axis; that is,

$$\Omega = 7.27 \cdot 10^{-5} \text{ radians/second}$$

E. 3. 10 ORIENTATION REFERENCED TO A STARLINE

Let the starline be coincident with the y axis of coordinate system A and the body axes coincident with the axes of coordinate system B. Vehicle orientation relative to the starline is then described by the three direction cosines A_{12} , A_{22} and A_{32} representing the angular displacements between the starline and each of the body axes.

Since the starline is fixed in inertial space, the A coordinate system must have zero angular velocity about the x and z axes, that is

$$\Omega_x = \Omega_z = 0 \quad (32)$$

From equation (17), the differential equations for the direction cosines A_{12} , A_{22} and A_{32} become:

$$\dot{A}_{12} = \dot{\ell}_s = \omega_z m_s - \omega_y n_s \quad (33a)$$

$$\dot{A}_{22} = \dot{m}_s = -\omega_z \ell_s + \omega_x n_s \quad (33b)$$

$$\dot{A}_{32} = \dot{n}_s = \omega_y \ell_s - \omega_x m_s \quad (33c)$$

The applicable constraint is

$$\ell_s^2 + m_s^2 + n_s^2 = 1 \quad (34)$$

E.3.11 ORIENTATION FOR SMALL ERRORS

If the body axes are very nearly aligned with the axes of some reference coordinate system, the relationships between direction cosines and some set of nonclassical Euler Angles reduces to:

$$\|A_{ij}\| = \begin{bmatrix} 1 & \Psi & -\theta \\ -\Psi & 1 & \emptyset \\ \theta & -\emptyset & 1 \end{bmatrix} \quad (35)$$

This relation is valid if Ψ , θ , and \emptyset are small (less than five degrees). Substituting equation (28) into equation (17), the differential equations for direction cosines, yields

$$\dot{\emptyset} = \omega_x - \Omega_x = \dot{\theta}_x \quad (36a)$$

$$\dot{\theta} = \omega_y - \Omega_y = \dot{\theta}_y \quad (36b)$$

$$\dot{\Psi} = \omega_z - \Omega_z = \dot{\theta}_z \quad (36c)$$

E.4 VEHICLE TORQUERS

E.4.1 JETS

The low thrust jets providing torque for rate stabilization and solar orientation as well as flywheel unloading have been modeled simply as on-off torques of 1.5, 1.5, and 0.8 inch-ounces for the vehicle roll, pitch, and yaw (X_5, Y_5, Z_5) axes, respectively.

E.4.2 MECHANICAL FLYWHEEL

The behavior of the flywheel providing control torque to the body axes can be described by the nonlinear differential equation:

$$\dot{h} = -a_1 h + a_2 V - hV (a_3 h + a_4 V) \quad (37)$$

The coefficients A_i can be derived from torque speed curves in several ways. One of these utilizes the maximum wheel momentum h_m , the rated voltage V_R , the stall torque at rated voltage T_s , the ratio of momentum at rated voltage to momentum at one-half rated voltage q_w , and the ratio of peak torque to stall torque at rated voltage q_t . In terms of these quantities,

$$a_1 = \frac{T_s}{h_m} \left(\frac{2}{3} q_w - \frac{2 - q_t}{3 q_w} - \frac{1}{6} q_t \right) \quad (38a)$$

$$a_2 = T_s / V_R \quad (38b)$$

$$a_3 = \frac{T_s}{h_m^2 V_R} \left(\frac{2 - q_t}{2} \right) \quad (38c)$$

$$a_4 = \frac{2 T_s}{3 h_m V_R^2} \left(q_t - q_w + \frac{2 - q_t}{2 q_w} \right) \quad (38d)$$

For some momentum and voltage, a wheel gain and time constant can be calculated:

$$k_m = \left(\frac{a_2}{a_1} \right) \frac{1 - 2 \frac{a_4}{a_2} hV - \frac{a_3}{a_2} h^2}{1 + 2 \frac{a_3}{a_1} hV + \frac{a_4}{a_1} V^2} \quad (39a)$$

$$T_m = \left(\frac{1}{a_1} \right) \cdot \frac{1}{1 + 2 \frac{a_3}{a_1} hV + \frac{a_4}{a_1} V^2} \quad (39b)$$

The ATS-4 wheels are to be the same as the flywheels used on the Orbiting Astronomical Observatory. For these wheels the following apply:

$$V_R = 32 \text{ volts}$$

$$h_m = 2.02 \text{ foot-pound-seconds}$$

$$T_s = 2.46 \text{ inch-ounces}$$

$$q_W = 1.15$$

$$q_t = 1.9$$

yielding coefficients of:

$$a_1 = 2.69 (10)^{-3} (\text{sec})^{-1}$$

$$a_2 = 0.077 \text{ inch-ounces/volt}$$

$$a_3 = 2.55 (10)^{-8} (\text{inch-ounce-sec}^2 \text{-volt})^{-1}$$

$$a_4 = 3.26 (10)^{-6} (\text{sec-volt}^2)^{-1}$$

E. 5 CONTROLLERS

E. 5. 1 STABILIZATION JET CONTROLLER

The threshold detector, valves and other hardware constituting the stabilization jet controller have been modeled simply as a level detector as shown in the block diagram of Figure 6. 4-35. Equipment characteristics such as threshold detector hysteresis and solenoid valve time delay have been neglected. The level detector and associated logic actuate the jet required to apply a negative torque to the vehicle whenever the detector input signal is greater than two degrees. The positive jet is fired whenever the detector input signal is greater than two degrees in the negative direction. In equation form:

$$T_{Jx} = -1.5 \text{ inch-ounces} \quad \epsilon_x \geq 2^0 \quad (40a)$$

$$T_{Jx} = 0 \text{ inch-ounces} \quad -2^0 < \epsilon_x < 2^0 \quad (40b)$$

$$T_{Jx} = 1.5 \text{ inch-ounces} \quad \epsilon_x \leq -2^0 \quad (40c)$$

$$T_{Jy} = -1.5 \text{ inch-ounces} \quad \epsilon_y \geq 2^0 \quad (41a)$$

$$T_{Jy} = 0 \text{ inch-ounces} \quad -2^0 < \epsilon_y < 2^0 \quad (41b)$$

$$T_{Jy} = 1.5 \text{ inch-ounces} \quad \epsilon_y \leq -2^0 \quad (41c)$$

$$T_{Jz} = -0.8 \text{ inch-ounces} \quad \epsilon_z \geq 2^0 \quad (42a)$$

$$T_{Jz} = 0 \text{ inch-ounces} \quad -2^0 < \epsilon_z < 2^0 \quad (42b)$$

$$T_{Jz} = 0.8 \text{ inch-ounces} \quad \epsilon_z \leq -2^0 \quad (42c)$$

The solenoid valve time delay can be neglected so long as the jet on-time exceeds the delay by a factor of one hundred as is frequently the case for sun stabilization of the ATS-4 vehicle with the relatively low control torques of 1.5, 1.5 and 0.8 inch-ounces. The approximation is less satisfactory during sun pointing, since no more than short bursts of thrust are required to maintain the rate and attitude deadband accuracy. Elimination of the time delay during an examination of pointing accuracy results in an optimistic picture of the system's capability.

The hysteresis of the threshold detector is of considerably greater significance during sun pointing than during sun stabilization; again, because the jet on-time is so great during stabilization using low thrust jets. The period of time during which the hysteresis is effective is much less than the time required for stabilization.

E. 5. 2 FLYWHEEL UNLOADING JET CONTROLLER

The jet unloading controller is shown in Figure 6.4-48. The jet firings take place independently on each axis whenever the wheel speed on the axis reaches 75 percent of its maximum value. The jet is turned off as soon as the wheel speed drops to 5 percent of its maximum value.

E. 5. 3 FLYWHEEL CONTROLLER

The flywheel controller consists of a lead/lag network, amplifier, and an amplifier saturation level as shown in Figure 6.4-43. The transfer function between error signal and wheel voltage in the linear range of the controller is:

$$\frac{V(s)}{\epsilon(s)} = A \frac{1 + sT_1}{1 + sT_2} \quad (43)$$

$$T_1 = 10 T_2 \quad (44)$$

The gain of 15 volts per arc-minute has been made as large as possible consistent with the amplitude of sensor noise and the amplifier saturation level. As a rule of thumb, the gain is adjusted such that the amplifier saturation level is at least three times the rms noise level. The sensor rms noise level of 0.42 arc-minute for the earth sensor permits a gain of approximately 20 volts per arc-minute. With the addition of a noise filter, it was subsequently desirable to reduce the gain to 15 volts per arc-minute to achieve greater phase margin. This gain was also satisfactory for the star sensor channel where the sensor noise is 0.60 arc-minute rms. The lead and lag time constants were selected, of course, to provide a maximum of phase margin. The open loop frequency response is shown in Figure 6.4-50.

E.6 RATE AND ATTITUDE SENSORS

E.6.1 RATE GYRO

The rate gyro used on all three axes has been modeled as a rate gain of 100 seconds. The gyro uncertainty, estimated to be 0.003 degree/second, was neglected. The gyro saturation has been assumed greater than the rates experienced by the vehicle during sun stabilization. The gyro bandwidth has been assumed sufficient to eliminate any significant dynamic error. The gyro uncertainty cannot be neglected when its important to accurately determine the rate deadband of the stabilization system during sun pointing. The stability and settling time of the sun stabilization system are not significantly affected by a gyro uncertainty of 0.003 degree per second, however, since the vehicle rates are typically much greater than this value.

E.6.2 SUN SENSORS - SUN STABILIZATION

Eight sun sensors with 180-degree field of view are to be mounted on the ATS-4 vehicle as shown in Figure E-6 to provide spherical coverage and a suitable signal gradient when the negative yaw axis is pointed to the sun(orientation null). Each sensor generates a signal proportional to the cosine of the angle θ between the sensor axis and the sunline whenever the sun is within the ± 90 degree field of view of the sensor; that is,

$$\epsilon = K \cos \theta \quad \frac{-\pi}{2} < \theta < \frac{\pi}{2} \quad (45)$$

If \bar{n}_k is a unit vector along the axis of the kth sensor then

$$\epsilon_k = k \bar{s} \cdot \bar{n}_k = k \cos \theta \quad \frac{-\pi}{2} < \theta < \frac{\pi}{2} \quad (46a)$$

$$\epsilon_k = 0 \quad \frac{-3\pi}{2} \leq \theta \leq \frac{-\pi}{2} \quad (46b)$$

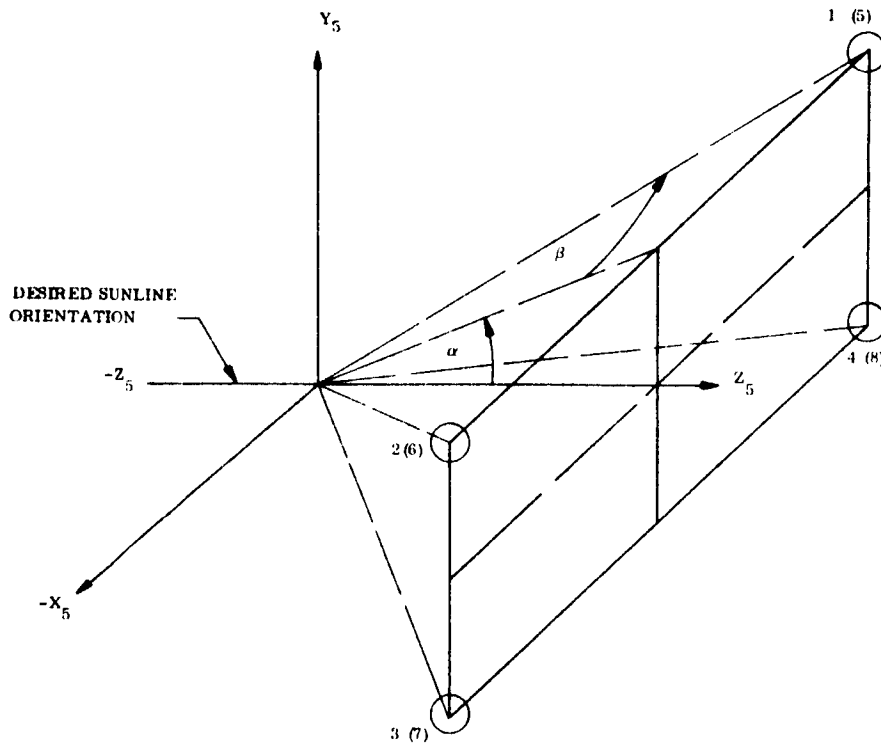


Figure E-6. Sun Sensor Mounting - Sun Stabilization

From Figure E-6,

$$\bar{n}_k = \sin \beta_k \bar{x}_5 + \cos \beta_k \sin \alpha_k \bar{y}_5 + \cos \beta_k \cos \alpha_k \bar{z}_5 \quad (47)$$

If sun sensors 1, 2, 3, and 4 are mounted at angles of $\pm\beta_1$ and $\pm\alpha_1$, and sensors 5, 6, 7, and 8, at angles of $\pm\beta_2$ ($\frac{\pi}{2} < \beta_2 < \frac{3\pi}{2}$) and $\pm\alpha_2$ then \bar{n}_k for each sensor becomes:

$$\bar{n}_1 = \sin \beta_1 \bar{x}_5 + \cos \beta_1 \sin \alpha_1 \bar{y}_5 + \cos \beta_1 \cos \alpha_1 \bar{z}_5 \quad (48a)$$

$$\bar{n}_2 = -\sin \beta_1 \bar{x}_5 + \cos \beta_1 \sin \alpha_1 \bar{y}_5 + \cos \beta_1 \cos \alpha_1 \bar{z}_5 \quad (48b)$$

$$\bar{n}_3 = -\sin \beta_1 \bar{x}_5 - \cos \beta_1 \sin \alpha_1 \bar{y}_5 + \cos \beta_1 \cos \alpha_1 \bar{z}_5 \quad (48c)$$

$$\bar{n}_4 = \sin \beta_1 \bar{x}_5 - \cos \beta_1 \sin \alpha_1 \bar{y}_5 + \cos \beta_1 \cos \alpha_1 \bar{z}_5 \quad (48d)$$

$$\bar{n}_5 = \sin \beta_2 \bar{x}_5 - \cos \beta_2 \sin \alpha_2 \bar{y}_5 + \cos \beta_2 \cos \alpha_2 \bar{z}_5 \quad (48e)$$

$$\bar{n}_6 = -\sin \beta_2 \bar{x}_5 - \cos \beta_2 \sin \alpha_2 \bar{y}_5 + \cos \beta_2 \cos \alpha_2 \bar{z}_5 \quad (48f)$$

$$\bar{n}_7 = -\sin \beta_2 \bar{x}_5 + \cos \beta_2 \sin \alpha_2 \bar{y}_5 + \cos \beta_2 \cos \alpha_2 \bar{z}_5 \quad (48g)$$

$$\bar{n}_8 = \sin \beta_2 \bar{x}_5 + \cos \beta_2 \sin \alpha_2 \bar{y}_5 + \cos \beta_2 \cos \alpha_2 \bar{z}_5 \quad (48h)$$

Evaluating the vector dot product $\bar{s} \cdot \bar{n}_k$ for each sensor yields the signals:

$$\epsilon_1 = k (\ell \sin \beta_1 + m \cos \beta_1 \sin \alpha_1 + n \cos \beta_1 \cos \alpha_1) \quad \epsilon_1 > 0 \quad (49a)$$

$$\epsilon_2 = k (-\ell \sin \beta_1 + m \cos \beta_1 \sin \alpha_1 + n \cos \beta_1 \cos \alpha_1) \quad \epsilon_2 > 0 \quad (49b)$$

$$\epsilon_3 = k (-\ell \sin \beta_1 - m \cos \beta_1 \sin \alpha_1 + n \cos \beta_1 \cos \alpha_1) \quad \epsilon_3 > 0 \quad (49c)$$

$$\epsilon_4 = k (\ell \sin \beta_1 - m \cos \beta_1 \sin \alpha_1 + n \cos \beta_1 \cos \alpha_1) \quad \epsilon_4 > 0 \quad (49d)$$

$$\epsilon_5 = k (\ell \sin \beta_2 - m \cos \beta_2 \sin \alpha_2 + n \cos \beta_2 \cos \alpha_2) \quad \epsilon_5 > 0 \quad (49e)$$

$$\epsilon_6 = k (-\ell \sin \beta_2 - m \cos \beta_2 \sin \alpha_2 + n \cos \beta_2 \cos \alpha_2) \quad \epsilon_6 > 0 \quad (49f)$$

$$\epsilon_7 = k (-\ell \sin \beta_2 + m \cos \beta_2 \sin \alpha_2 + n \cos \beta_2 \cos \alpha_2) \quad \epsilon_7 > 0 \quad (49g)$$

$$\epsilon_8 = k (\ell \sin \beta_2 + m \cos \beta_2 \sin \alpha_2 + n \cos \beta_2 \cos \alpha_2) \quad \epsilon_8 > 0 \quad (49h)$$

where

$$\ell = \bar{s} \cdot \bar{x}_5 \quad (50a)$$

$$m = \bar{s} \cdot \bar{y}_5 \quad (50b)$$

$$n = \bar{s} \cdot \bar{z}_5 \quad (50c)$$

Errors resulting from mechanical misalignment and sensor noise have been assumed to be negligible.

E. 6.3 SUN SENSORS - POLARIS STAR ACQUISITION

Four sun sensors with 180-degree field of view are to be mounted on the ATS-4 vehicle as shown in Figure E-7 to provide a hemispherical field of view of the sun and a suitable signal gradient when the x'_5 axis shown is pointed to the sun (attitude null). Note the relationship between the x'_5 and x_5 axes. Each sensor generates a signal proportional to the cosine of the angle θ between the sensor axis and the sunline whenever the sun is within the ± 90 -degree field of view of the sensor; that is,

$$\epsilon = k \cos \theta \quad \frac{-\pi}{2} < \theta < \frac{\pi}{2} \quad (51)$$

If \bar{n}_k is a unit vector along the axis of the kth sensor then

$$\epsilon_k = k \bar{s} \cdot \bar{n}_k = k \cos \theta \quad \frac{-\pi}{2} < \theta < \frac{\pi}{2} \quad (52a)$$

$$\epsilon_k = 0 \quad \frac{-3\pi}{2} < \theta < \frac{-\pi}{2} \quad (52b)$$

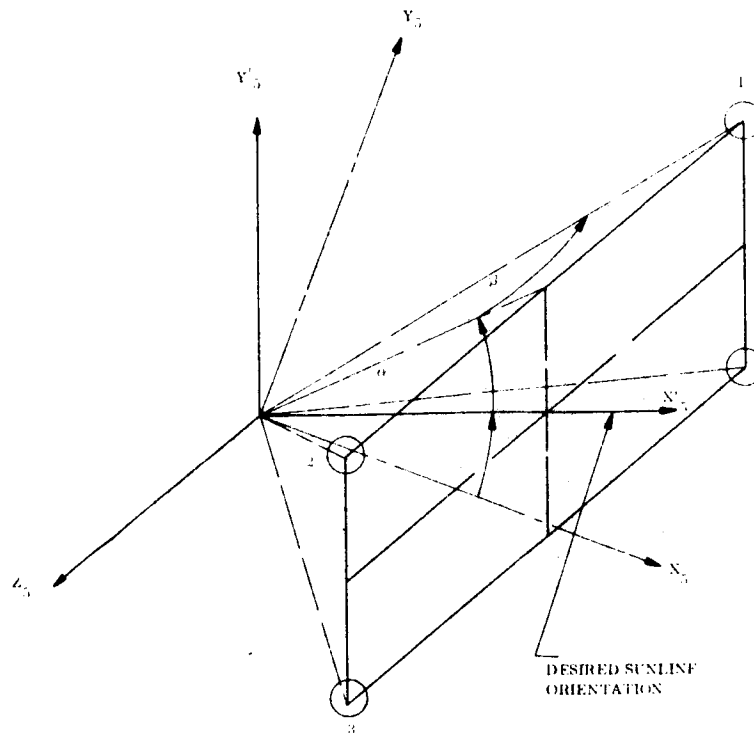


Figure E-7. Sun Sensor Mounting - Star Stabilization

From Figure E-7

$$\bar{n}_k = \sin \beta_k x'_5 + \cos \beta_k \sin \alpha_k y'_5 + \cos \beta_k \cos \alpha_k \bar{z}_5 \quad (53)$$

Further,

$$x'_5 = \cos \mu \bar{x}_5 + \sin \mu \bar{y}_5 \quad (54a)$$

$$y'_5 = -\sin \mu \bar{x}_5 + \cos \mu \bar{y}_5$$

Therefore,

$$\begin{aligned} \bar{n}_k &= (\sin \beta_k \cos \mu - \cos \beta_k \sin \alpha_k \sin \mu) \bar{x}_5 \\ &+ (\sin \beta_k \sin \mu + \cos \beta_k \sin \alpha_k \cos \mu) \bar{y}_5 \\ &+ \cos \beta_k \cos \alpha_k \bar{z}_5 \end{aligned} \quad (55)$$

Evaluating the vector dot product $\bar{s} \cdot \bar{n}_k$ for each sensor yields the signals:

$$\begin{aligned} \epsilon_1 &= k (\sin \beta \cos \mu - \cos \beta \sin \alpha \sin \mu) (\ell) \\ &+ k (\sin \beta \sin \mu + \cos \beta \sin \alpha \cos \mu) (m) \\ &+ k (\cos \beta \cos \alpha) (n) \end{aligned} \quad (56a)$$

$$\begin{aligned} \epsilon_2 &= k (\sin \beta \cos \mu + \cos \beta \sin \alpha \sin \mu) (-\ell) \\ &+ k (\sin \beta \sin \mu - \cos \beta \sin \alpha \cos \mu) (-m) \\ &+ k (\cos \beta \cos \alpha) (n) \end{aligned} \quad (56b)$$

$$\begin{aligned} \epsilon_3 &= k (\sin \beta \cos \mu - \cos \beta \sin \alpha \sin \mu) (-\ell) \\ &+ k (\sin \beta \sin \mu + \cos \beta \sin \alpha \cos \mu) (-m) \\ &+ k (\cos \beta \cos \alpha) (n) \end{aligned} \quad (56c)$$

$$\begin{aligned} \epsilon_4 = & k (\sin \beta \cos \mu + \cos \beta \sin \alpha \sin \mu)(l) \\ & + k (\sin \beta \sin \mu - \cos \beta \sin \alpha \cos \mu)(m) \\ & + k (\cos \beta \cos \alpha)(n) \end{aligned} \quad (56d)$$

Where

$$l = \bar{s} \cdot \bar{x}_5 \quad (57a)$$

$$m = \bar{s} \cdot \bar{y}_5 \quad (57b)$$

$$n = \bar{s} \cdot \bar{z}_5 \quad (57c)$$

Errors resulting from mechanical misalignment and sensor noise have been assumed to be negligible.

E. 6. 4 EARTH SENSORS

The earth sensor measures the angles γ_R and γ_P shown in Figure E-8. In terms of the direction cosines l_E , m_E and n_E describing displacements between the body axes and the local vertical,

$$\gamma_R = \tan^{-1} \left(\frac{m_E}{n_E} \right) \quad (58a)$$

$$\gamma_P = \tan^{-1} \left(-\frac{l_E}{n_E} \right) \quad (58b)$$

These equations are valid as long as the displacement between the yaw body axis and the local vertical does not exceed +10 degrees, the sensor saturation level; that is,

$$n_E > \cos 31^\circ \quad (59a)$$

$$n_E > 0.855 \quad (59b)$$

$$\gamma_R = +10^\circ \quad \tan^{-1} \left(\frac{m_E}{n_E} \right) \geq 10^\circ \quad (60a)$$

$$\gamma_R = -10^\circ \quad \tan^{-1} \left(\frac{m_E}{n_E} \right) \leq -10^\circ \quad (60b)$$

The sensor field of view is ± 20 degrees.

$$\gamma_P = 10^\circ \quad \tan^{-1} \left(\frac{l_E}{n_E} \right) \geq 10^\circ \quad (61a)$$

$$\gamma_P = -10^\circ \quad \tan^{-1} \left(\frac{l_E}{n_E} \right) \leq -10^\circ \quad (61b)$$

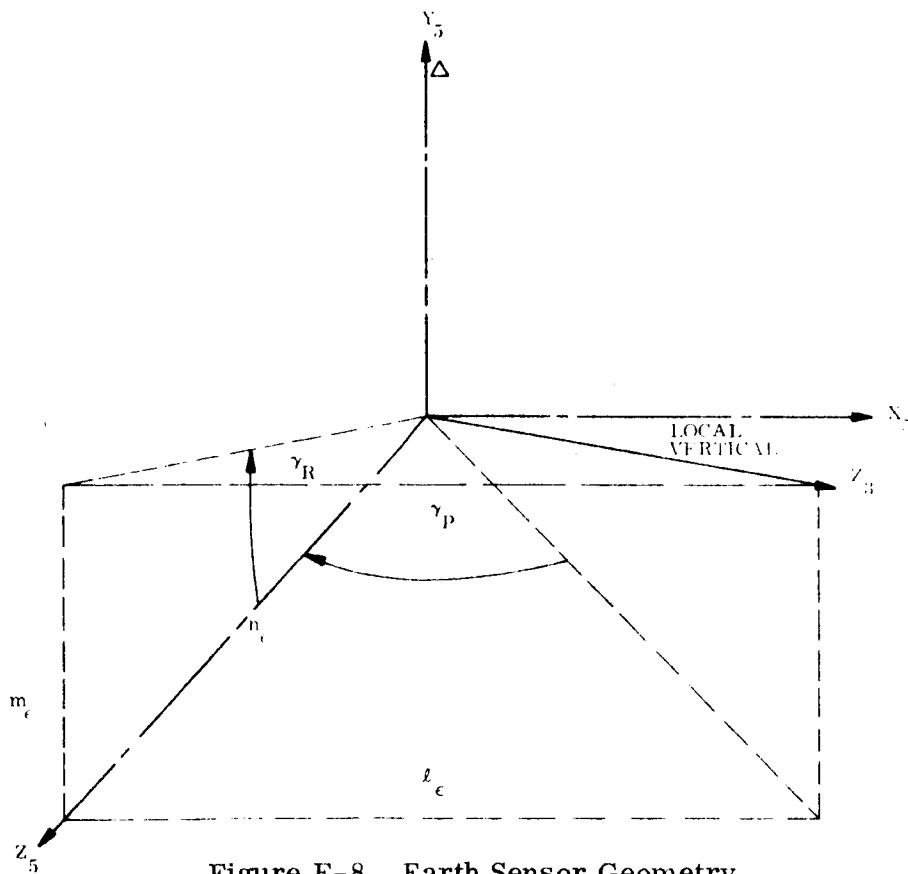


Figure E-8. Earth Sensor Geometry

Sensor amplitude degradation and phase shift have been assumed negligible in the vicinity of the principal control system frequencies. Sensor noise has been specified as 0.42 arc-minute rms. No information is yet available describing the spectral distribution of this noise. For the purposes of an analog computer simulation the noise was modeled as white noise bandlimited to 3.8 radians per second - the characteristics of the available noise generator. The sensor supplier, ATD, specified the noise amplitude.

E. 6.5 POLARIS STAR SENSOR

The Polaris star sensor points to the star Polaris along the negative pitch axis. The single electronic gimbal records angular displacement about the yaw axis as long as the negative pitch axis is pointed to within the ± 2 -degree square field of view of the sensor. The sensor output is simply

$$\epsilon_{sz} = -K\Psi \quad (62)$$

where Ψ is the angular displacement error about the yaw axis. The sensor break frequency at two radians per second has been ignored, since it is an order of magnitude above the yaw axis control loop crossover frequency. The sensor noise level has been specified as 0.01 degree rms. The spectral distribution of this noise has not been described. For the purpose of an analog computer simulation, the noise was modeled as white noise bandlimited to 3.8 radians per second.

E. 7 SENSOR SIGNAL PROCESSING

E. 7.1 RATE GYRO

In terms of the model the rate gyro signals are added to the sun sensor signals. The amplified yaw axis gyro signal is applied directly to the threshold detector of the jet controller.

E. 7. 2 SUN SENSOR - SUN STABILIZATION

The signals from the eight sun sensors are added as follows to generate roll (x) and pitch (y) axis error signals:

$$\epsilon''_{sx} = - \left[(\epsilon_1 + \epsilon_2) - (\epsilon_3 + \epsilon_4) + \epsilon_5 + \epsilon_6 - (\epsilon_7 + \epsilon_8) \right] \quad (63a)$$

$$\epsilon''_{sy} = - \left[(\epsilon_2 + 2\epsilon_3) - (\epsilon_1 + \epsilon_4) + (\epsilon_6 + \epsilon_7) - (\epsilon_5 + \epsilon_8) \right] \quad (63b)$$

Substituting equation (49) into equation (63) yields:

$$\epsilon''_{sx} = - m^4 (\cos \beta_1 \sin \alpha_1 - \cos \beta_2 \sin \alpha_2) k \quad (64a)$$

$$\epsilon''_{sy} = \ell^4 (\sin \beta_1 + \sin \beta_2) k \quad (64b)$$

The signs of the error signals are as required to point the negative yaw axis to the sun.

To point the positive yaw axis to the sun, the required error signals are:

$$\epsilon''_{sx} = m^4 (\cos \beta_1 \sin \alpha_1 - \cos \beta_2 \sin \alpha_2) k \quad (65a)$$

$$\epsilon''_{sy} = -\ell^4 (\sin \beta_1 + \sin \beta_2) k \quad (65b)$$

When the pointing error is less than ten degrees,

$$\epsilon''_{sx} = \theta'_x{}^4 (-\cos \beta_2 \sin \alpha_2) k \quad (66a)$$

$$\epsilon''_{sy} = \theta'_y{}^4 (\sin \beta_2) k \quad (66b)$$

Where θ'_x and θ'_y are angular displacements about the roll and pitch axes, respectively, in radians. The error signals are amplified and then limited. In terms of the model,

$$\theta_x = \epsilon'_{sx} = \left(\frac{57.3}{-4k \cos \beta_2 \sin \alpha_2} \right) \theta'_x (-4 \cos \beta_2 \sin \alpha_2) k \quad (67a)$$

$$\theta_y = \epsilon'_{sy} = \frac{57.3}{4k \sin \beta_2} \theta'_y 4 (\sin \beta_2) k \quad (67b)$$

Where θ_x and θ_y are now expressed in degrees. The approximations, again, are valid for

$$\sqrt{\theta_x^2 + \theta_y^2} < 10 \text{ DEGREES} \quad (68)$$

The signals θ_x and θ_y are limited at 7 degrees before being added to the rate gyro signal; that is,

$$\epsilon_{sx} = \theta_x \quad -7^\circ < \theta_x < 7^\circ \quad (69a)$$

$$\epsilon_{sy} = \theta_y \quad -7^\circ < \theta_y < 7^\circ \quad (69b)$$

$$\epsilon_{sx} = 7^\circ \quad \theta_x > 7^\circ \quad (70a)$$

$$\epsilon_{sy} = 7^\circ \quad \theta_y > 7^\circ \quad (71b)$$

$$\epsilon_{sx} = -7^\circ \quad \theta_x < -7^\circ \quad (72a)$$

$$\epsilon_{sy} = -7^\circ \quad \theta_y < -7^\circ \quad (72b)$$

The total error signal is the sum of the rate gyro and sensor signals; that is,

$$\epsilon_x = \epsilon_{gx} + \epsilon_{sx} \quad (73a)$$

$$\epsilon_y = \epsilon_{gy} + \epsilon_{sy} \quad (73b)$$

When the pointing error is less than 7 degrees on each axis,

$$\epsilon_x = 100 \omega_x + \theta_x \quad (74a)$$

$$\epsilon_y = 100 \omega_y + \theta_y \quad (74b)$$

Note that

$$\omega_x = \dot{\theta}_x \quad (75a)$$

$$\omega_y = \dot{\theta}_y \quad (75b)$$

E. 7.3 SUN SENSORS - POLARIS STAR ACQUISITION

The signals from the four sun sensors are added as follows to generate a yaw axis error signal:

$$\epsilon''_{sz} = - (\epsilon_1 + \epsilon_2 - \epsilon_3 - \epsilon_4) \quad (76)$$

Substituting equation (56) into equation (76) yields:

$$\epsilon''_{sz} = 4 \cos \beta \sin \alpha (\sin \mu \ell - \cos \mu m) k \quad (77)$$

When the x_5 axis points in the required direction,

$$\ell = \cos \mu \quad (78a)$$

$$m = \sin \mu \quad (78b)$$

and

$$\epsilon''_{sz} = 0 \quad (78c)$$

In the vicinity (less than 5 degrees) of the attitude null, let

$$l = \cos (\mu + d\Psi) \quad (79a)$$

$$m = \sin (\mu + d\Psi) \quad (79b)$$

Expanding the trigonometric functions above:

$$l = \cos \mu - d\Psi \sin \mu \quad (80a)$$

$$m = \sin \mu + d\Psi \cos \mu \quad (80b)$$

Substituting Equations (80) into (77) yields

$$\epsilon_{SZ} = -d\Psi \quad (81)$$

where $d\Psi$ is the attitude error about the yaw axis. In terms of the model,

ϵ_{SZ}'' is amplified by the gain

$$\epsilon_{SZ} = \frac{57.3 \epsilon_{SZ}''}{4k \cos \beta \sin \alpha}$$

In the vicinity of the null, the error signal is therefore measured in degrees when added to the rate gyro signal. The complete error signal applied to the jet controller is

$$\epsilon_Z = \epsilon_{SZ} + \epsilon_{gZ} \quad (82)$$

E. 7. 4 EARTH SENSOR

The earth sensor signals, γ_R and γ_P are applied directly, in terms of the model, to the flywheel controller input.

E. 7. 5 POLARIS STAR SENSOR

The Polaris star sensor signals, in degrees, are applied directly, in terms of the model, to the flywheel controller input.

E. 8 REFERENCES

- E. 8. 1 NASA Drawing No. GC1183111, COORDINATE SYSTEM ATS-4, July 12, 1966
- E. 8. 2 PIR 4145-GEN-143, COUPLING OF STRUCTURAL FLEXIBILITY WITH A CONTROL SYSTEM FEEDBACK LOOP, R. E. Roach, June 14, 1965
- E. 8. 3 PIR 4425-100, A SIMPLE ELECTRICAL ANALOG OF THE METHOD OUTLINED IN PIR 4145d-GEN-143, P. D. Holthenrichs, April 1, 1966
- E. 8. 4 TIS 65-SD-225, THE MOMENTUM APPROACH TO VEHICLE DYNAMICS AND THE USE OF EULER PARAMETERS FOR COORDINATE TRANSFORMATION, K. R. Folgate, March 8, 1965

APPENDIX F

STABILITY INVESTIGATION AND POINTING ERROR ANALYSIS OF THE THREE AXIS STAR TRACKER SYSTEM

F. 1 INTRODUCTION

Several approaches are possible for achieving three-axis orientation control with star trackers. The system utilizing two star trackers is investigated here. Once earth orientation has been acquired, it is maintained by continuously updating star tracker gimbal angles by an onboard programmer updated by ground command signals. The star tracker approach presents a condition where the accuracy is a function of earth pointing longitude and latitude and spacecraft location in orbit. Selection of guide stars is critical to system stability and accuracy. Several guide star combinations compatible with the gimbal travel of ± 43 degrees for the OAO star trackers were studied. The most promising star combination was $\alpha' Cru$ with ϵUma . The analysis indicates errors as large as 0.098 degrees; however, it is expected that by proper signal processing and gain selection an accuracy of 0.07 degree could be realized. The nomenclature used in this analysis is defined in Table F-1.

Table F-1. Nomenclature

$A_{1,2}$	Outer gimbal angle	$i_{S,1,2}$	Optical axis
$\alpha_{1,2}$	Star right ascension	i_I, j_I, k_I	Initial coordinates
$d\alpha_{1,2}$	Infinitesimal optical axis rotation	$OA_{1,2}$	Optical axis
$d\beta_{1,2}$	Infinitesimal inner gimbal rotation	$OG_{1,2}$	Outer gimbal
$d\gamma_{1,2}$	Infinitesimal outer gimbal rotation	θ_c	Rotation about vehicle pitch axis
$d\theta$	Infinitesimal roll axis rotation	θ'_c	Rotation about resolved vehicle roll axis
$d\theta$	Infinitesimal pitch axis rotation	θ_s	Satellite longitude
$d\psi$	Infinitesimal yaw axis rotation	θ_T	Target longitude
$E_{1,2}$	Inner gimbal angle	θ'_T	Target latitude
$\delta_{1,2}$	Star declination	r_T	Distance from earth center to target
$e_{X,1,2}$	Attitude error for roll axis	r_S	Distance from earth center to satellite
$e_{Y,1,2}$	Attitude error for pitch axis	R_{ST}	Distance from target to satellite
$e_{Z,1,2}$	Attitude error for yaw axis	X_E, Y_E, Z_E	Earth equatorial reference system
GHA_r	Greenwich hour angle	X_V, Y_V, Z_V	Satellite vehicle coordinate system
$IG_{1,2}$	Inner gimbal		

Note: 1, 2 subscripts refer to tracker numbers

F. 2 STABILITY INVESTIGATION

F. 2.1 STABILITY CRITERION

The stability of the ATS-4 orientation control system will be determined by using the criterion developed for the OAO system.

For a given system configuration, the roots of the system characteristic equations are functions of two parameters A and B which are dependent only on the star tracker gimbal (as many as six trackers can be operative in the OAO system). Stability of the linear system is assured if none of the characteristic equations have positive real parts. System performance may not be satisfactory even though stability is apparent since pairs of complex zeros might be characterized by low damping ratios. Loci of constant minimum damping ratio were thus derived as a function of the parameters A and B and plotted in the AB plane as shown in Figure F-1. For any AB point there will be one pair of complex zeros that has the minimum damping ratio indicated by the locus passing through the point.

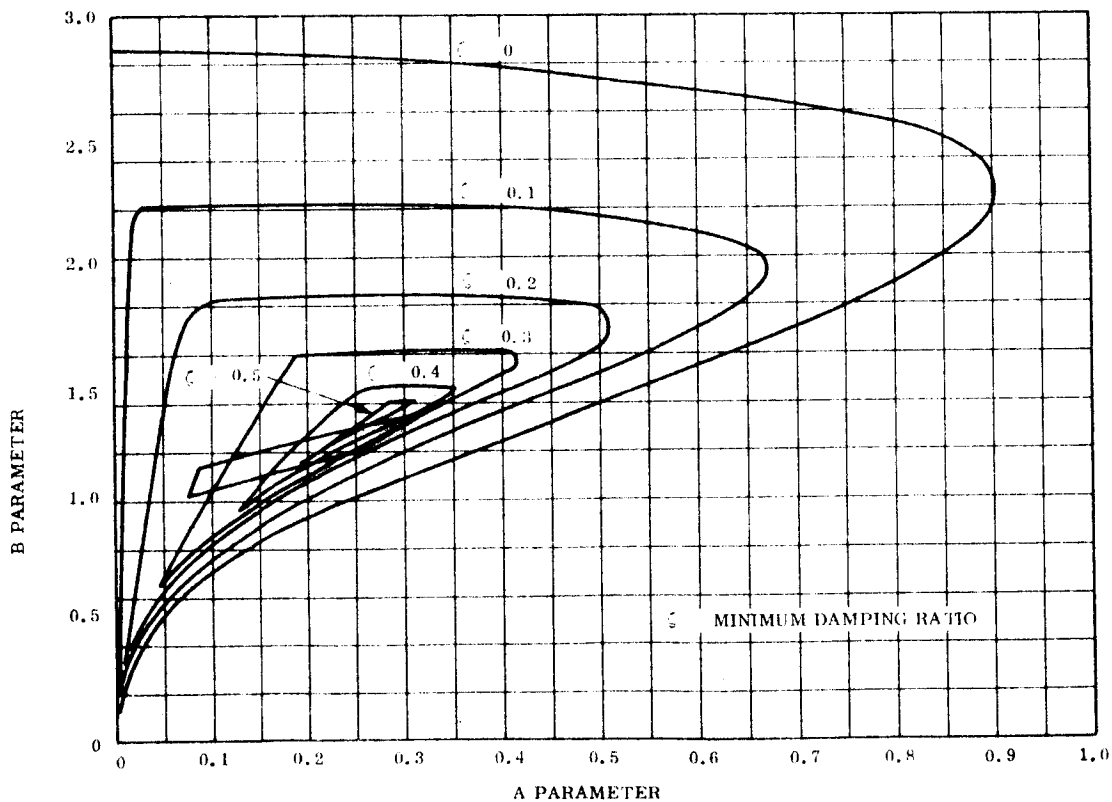


Figure F-1. Curves of Minimum Damping Ratio in AB Plane

This linear criterion was found to be not entirely satisfactory as a result of the nonlinearities in the control system. A new criterion was developed empirically from computer data and can be stated as follows: The system is stable if all AB points lie within the trapezoidal region in Figure F-1.

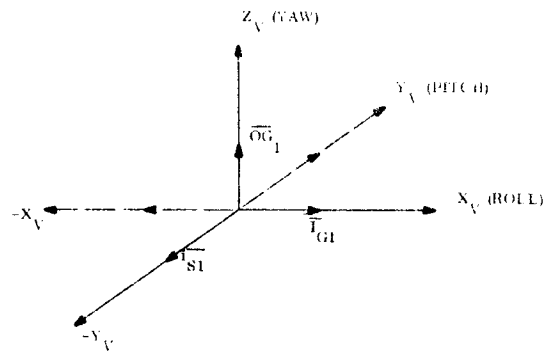
F. 2. 2 DERIVATION OF AB PARAMETERS

The AB parameters are defined as functions of the components of an error matrix. These components, in turn, are transcendental functions of the star tracker gimbal angles.

A system of two-pitch star trackers was selected to provide three-axis orientation control of the satellite. Pitch trackers were selected so as to avoid large gimbal angle excursions due to relative motion of star lines during the orbit. Tracker orientation relative to the vehicle is defined in Figure F-2.

Roll, pitch and yaw errors are generated by each tracker as a function of attitude errors. The errors generated by tracker 1 may be calculated with the aid of Figure F-3.

$$\begin{bmatrix} \overline{i_{S1}} \\ \overline{IG_1} \\ \overline{OG_1} \end{bmatrix} = [A] \begin{bmatrix} \overline{X_V} \\ \overline{Y_V} \\ \overline{Z_V} \end{bmatrix} \quad (1)$$



where,

$$A = \begin{bmatrix} \cos E_1 \sin A_1 & -\cos E_1 \cos A_1 & -\sin E_1 \\ \cos A_1 & \sin A_1 & 0 \\ 0 & 0 & 1 \end{bmatrix} \quad (2)$$

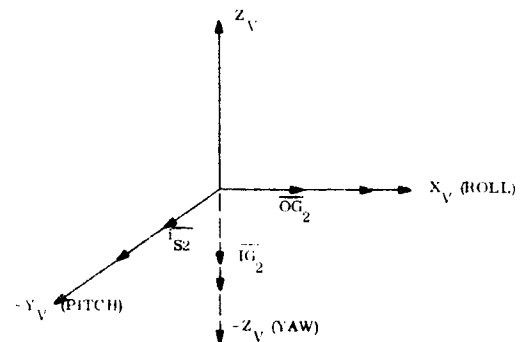


Figure F-2. Gimbal Orientation

Small gimbale errors occur due to small attitude errors. The defining relationship is related to matrix A as follows,

$$\begin{bmatrix} d\alpha_1 \\ d\beta_1 \\ d\gamma_1 \end{bmatrix} = \begin{bmatrix} A^T \end{bmatrix}^{-1} \begin{bmatrix} d\phi \\ d\theta \\ d\psi \end{bmatrix} \quad (3)$$

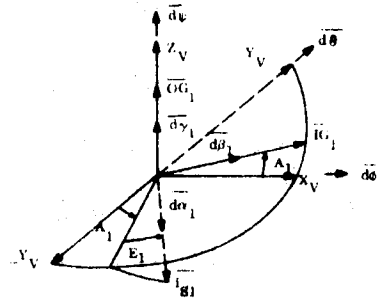


Figure F-3. Gimbal-Vehicle Orientation for Tracker No. 1

The inverse of the transpose of A is not equal to A since the system defined by i_{S1} , IG_1 , and OG_1 is nonorthogonal.

Instead,

$$\begin{bmatrix} A^T \end{bmatrix}^{-1} = \begin{bmatrix} \sin A_1 \sec E_1 & -\sec E_1 \cos A_1 & 0 \\ \cos A_1 & \sin A_1 & 0 \\ \tan E_1 \sin A_1 & -\tan E_1 \cos A_1 & 1 \end{bmatrix} \quad (4)$$

Also,

$$\begin{bmatrix} e_{1X} \\ e_{1Y} \\ e_{1Z} \end{bmatrix} = \begin{bmatrix} 0 & \cos A_1 & 0 \\ 0 & \sin A_1 & 0 \\ 0 & 0 & 1 \end{bmatrix} \begin{bmatrix} d\alpha_1 \\ d\beta_1 \\ d\gamma_1 \end{bmatrix} \quad (5)$$

since the inner gimbale error signal is resolved about the outer gimbale and lies in the pitch-roll plane and the outer gimbale error lies along the yaw axis. The three error signals in terms of attitude errors are readily obtained by combining these two matrices. They are:

$$\begin{bmatrix} e_{1X} \\ e_{1Y} \\ e_{1Z} \end{bmatrix} = \begin{bmatrix} \cos^2 A_1 & \cos A_1 \sin A_1 & 0 \\ \sin A_1 \cos A_1 & \sin^2 A_1 & 0 \\ \tan E_1 \sin A_1 & -\tan E_1 \cos A_1 & 1 \end{bmatrix} \begin{bmatrix} d\phi \\ d\theta \\ d\psi \end{bmatrix} \quad (6)$$

The errors generated by tracker No. 2 may be calculated with the aid of Figure F-4.

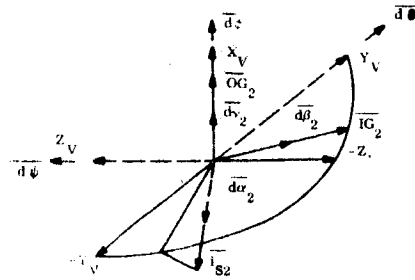


Figure F-4. Gimbal-Vehicle Orientation for Tracker No. 2

The following expressions can be derived for tracker 2.

$$\begin{bmatrix} \overline{iS_2} \\ \overline{IG_2} \\ \overline{OG_2} \end{bmatrix} = \begin{bmatrix} -\sin E_2 & -\cos E_2 \cos A_2 & -\cos E_2 \sin A_2 \\ 0 & \sin A_2 & -\cos A_2 \\ 1 & 0 & 0 \end{bmatrix} \begin{bmatrix} \overline{X_V} \\ \overline{Y_V} \\ \overline{Z_V} \end{bmatrix} \quad (7)$$

$$\begin{bmatrix} d\alpha_2 \\ d\beta_2 \\ d\gamma_2 \end{bmatrix} = \begin{bmatrix} 0 & -\sec E_2 \cos A_2 & -\sec E_2 \sin A_2 \\ 0 & \sin A_2 & -\cos A_2 \\ 1 & -\tan E_2 \cos A_2 & -\tan E_2 \sin A_2 \end{bmatrix} \begin{bmatrix} d\phi \\ d\theta \\ d\psi \end{bmatrix} \quad (8)$$

$$\begin{bmatrix} e_{2X} \\ e_{2Y} \\ e_{2Z} \end{bmatrix} = \begin{bmatrix} 0 & 0 & 1 \\ 0 & \sin A_2 & 0 \\ 0 & -\cos A_2 & 0 \end{bmatrix} \begin{bmatrix} d\alpha_2 \\ d\beta_2 \\ d\gamma_2 \end{bmatrix} \quad (9)$$

Combining the last two matrices,

$$\begin{bmatrix} e_{2X} \\ e_{2Y} \\ e_{2Z} \end{bmatrix} = \begin{bmatrix} 1 & -\tan E_2 \cos A_2 & -\tan E_2 \sin A_2 \\ 0 & -\sin^2 A_2 & -\sin A_2 \cos A_2 \\ 0 & -\sin A_2 \cos A_2 & \cos^2 A_2 \end{bmatrix} \begin{bmatrix} d\phi \\ d\theta \\ d\psi \end{bmatrix} \quad (10)$$

The total error matrix is obtained by summing and averaging the error matrices defined by Equation 6 and 9. Thus,

$$\begin{bmatrix} e_X \\ e_Y \\ e_Z \end{bmatrix} = \begin{bmatrix} e_{11} & e_{12} & e_{13} \\ e_{21} & e_{22} & e_{23} \\ e_{31} & e_{32} & e_{33} \end{bmatrix} \begin{bmatrix} d\phi \\ d\theta \\ d\psi \end{bmatrix} \quad (11)$$

where,

$$e_{11} = 1/2 (1 + \cos^2 A_1) \quad (12)$$

$$e_{12} = 1/2 (\cos A_1 \sin A_1 - \tan E_2 \cos A_2) \quad (13)$$

$$e_{13} = -1/2 \tan E_2 \sin A_2 \quad (14)$$

$$e_{21} = 1/2 \sin A_1 \cos A_1 \quad (15)$$

$$e_{22} = 1/2 (\sin^2 A_1 + \sin^2 A_2) \quad (16)$$

$$e_{23} = -1/2 \sin A_2 \cos A_2 \quad (17)$$

$$e_{31} = 1/2 \tan E_1 \sin A_1 \quad (18)$$

$$e_{32} = -1/2 (\tan E_1 \cos A_1 + \sin A_2 \cos A_2) \quad (19)$$

$$e_{33} = 1/2 (1 + \cos^2 A_2) \quad (20)$$

The A and B parameters are the following functions of the error parameters

$$\begin{aligned} A = & e_{11} e_{22} e_{33} + e_{13} e_{21} e_{32} + e_{12} e_{23} e_{31} - e_{13} e_{22} e_{31} \\ & - e_{11} e_{23} e_{32} - e_{12} e_{21} e_{33} \end{aligned} \quad (21)$$

$$B = e_{11} e_{22} + e_{22} e_{33} + e_{11} e_{33} - e_{12} e_{21} - e_{23} e_{32} - e_{13} e_{31} \quad (22)$$

In terms of gimbal angles,

$$A = 1/4 \left[1 - (\cos A_1 \cos A_2 - \tan E_2 \sin A_1)(\cos A_1 \cos A_2 + \tan E_1 \sin A_2) \right] \quad (23)$$

$$B = A + 1 \quad (24)$$

Rewriting this expression,

$$A = 1/4 \left[1 - \frac{(\bar{\xi}_1 \cdot \bar{X}_2) (\bar{\xi}_2 \cdot \bar{X}_1)}{(\bar{\xi}_2 \cdot \bar{X}_2) (\bar{\xi}_1 \cdot \bar{X}_1)} \right] \quad (25)$$

where, $\bar{\xi}$ is a unit vector defined by the relation.

$$\bar{\xi} = \bar{\zeta} \times \bar{\eta} \quad (26)$$

and \bar{X} is a unit vector along the tracker optical axis. The vectors $\bar{\zeta}$ and $\bar{\eta}$ are, respectively, unit vectors along the tracker outer gimbal and inner gimbal axes.

Using Equations 1 and 2 and the fact that there is a 1:1 relationship between vectors \bar{X}_1 , $\bar{\eta}_1$, $\bar{\zeta}_1$ and i_{S1} , IG_1 , OG_1 ,

$$\bar{X}_1 = \cos E_1 \sin A_1 \bar{X}_V - \cos E_1 \cos A_1 \bar{Y}_V - \sin E_1 \bar{Z}_V$$

$$\bar{\eta}_1 = \cos A_1 \bar{X}_V + \sin A_1 \bar{Y}_V$$

$$\bar{\zeta}_1 = \bar{Z}_V \quad (27)$$

From the definition of $\overline{\xi}_1$,

$$\overline{\xi}_1 = \overline{\zeta}_1 \times \overline{\eta}_1 = \overline{Z}_V \times (\cos A_1 \overline{X}_V + \sin A_1 \overline{Y}_V) = \cos A_1 \overline{Y}_V - \sin A_1 \overline{X}_V$$

so that,

$$\overline{\xi}_1 \cdot \overline{X}_1 = -\cos E_1 \quad (28)$$

Similarly, since,

$$\overline{X}_2 = -\sin E_2 \overline{X}_V - \cos E_2 \cos A_2 \overline{Y}_V - \cos E_2 \sin A_2 \overline{Z}_V$$

$$\overline{\eta}_2 = \sin A_2 \overline{Y}_V - \cos A_2 \overline{Z}_V$$

$$\overline{\zeta}_2 = \overline{X}_V \quad (29)$$

we have,

$$\overline{\xi}_2 = \overline{\zeta}_2 \times \overline{\eta}_2 = \sin A_2 \overline{Z}_V + \cos A_2 \overline{Y}_V$$

and,

$$\overline{\xi}_2 \cdot \overline{X}_2 = -\cos E_2 \quad (30)$$

Also,

$$\overline{\xi}_1 \cdot \overline{X}_2 = -\cos A_1 \cos E_2 \cos A_2 + \sin A_1 \sin E_2 \quad (31)$$

$$\overline{\xi}_2 \cdot \overline{X}_1 = -\sin E_1 \sin A_2 - \cos E_1 \cos A_1 \cos A_2 \quad (32)$$

Substituting Equations 28, 30, 31, and 32 in Equation 25, the parameter A becomes,

$A = 1/4 [1 - (\cos A_1 \cos A_2 - \tan E_2 \sin A_1)(\tan E_1 \sin A_2 + \cos A_1 \cos A_2)]$ which is in agreement with Equation 23.

F. 2. 3 DERIVATION OF GIMBAL ANGLES

Star tracker gimbal angles are a function of the following:

- a. The star position on the celestial sphere
- b. The target pointing location on earth
- c. The location-in-orbit of the satellite relative to inertial space.

They are:

$$\sin E_1 = \cos \delta_1 \cos \phi_c \cos (\theta_1 - \theta_s + \theta_c) - \sin \delta_1 \sin \phi_c \quad (33)$$

$$\tan A_1 = \frac{\cos \delta_1 \sin (\theta_1 - \theta_s + \theta_c)}{\cos \delta_1 \sin \phi_c \cos (\theta_2 - \theta_s + \theta_c) + \sin \delta_1 \cos \phi_c} \quad (34)$$

$$\sin E_2 = -\cos \delta_2 \sin (\theta_2 - \theta_s + \theta_c) \quad (35)$$

$$\tan A_2 = \frac{\cos \delta_2 \cos \phi_c \cos (\theta_2 - \theta_s + \theta_c) - \sin \delta_2 \sin \phi_c}{\cos \delta_2 \sin \phi_c \cos (\theta_2 - \theta_s + \theta_c) + \sin \delta_2 \cos \phi_c} \quad (36)$$

where,

$$\theta_1 = \alpha_1 - \text{GHA}_{\mathbf{r}} \quad (37)$$

$$\theta_2 = \alpha_2 - \text{GHA}_{\mathbf{r}} \quad (38)$$

$$\theta_2 = \theta_s = (\alpha_2 - \alpha_1) + (\theta_1 - \theta_s) \quad (39)$$

The angles are defined in the nomenclature included with this appendix. Figure F-5 is applicable for a synchronous orbit.

The angles θ_c and ϕ_c are pitch and roll rotations required to point the vehicle yaw axis to any target location from the local vertical. The sequence is illustrated in Figure F-6.

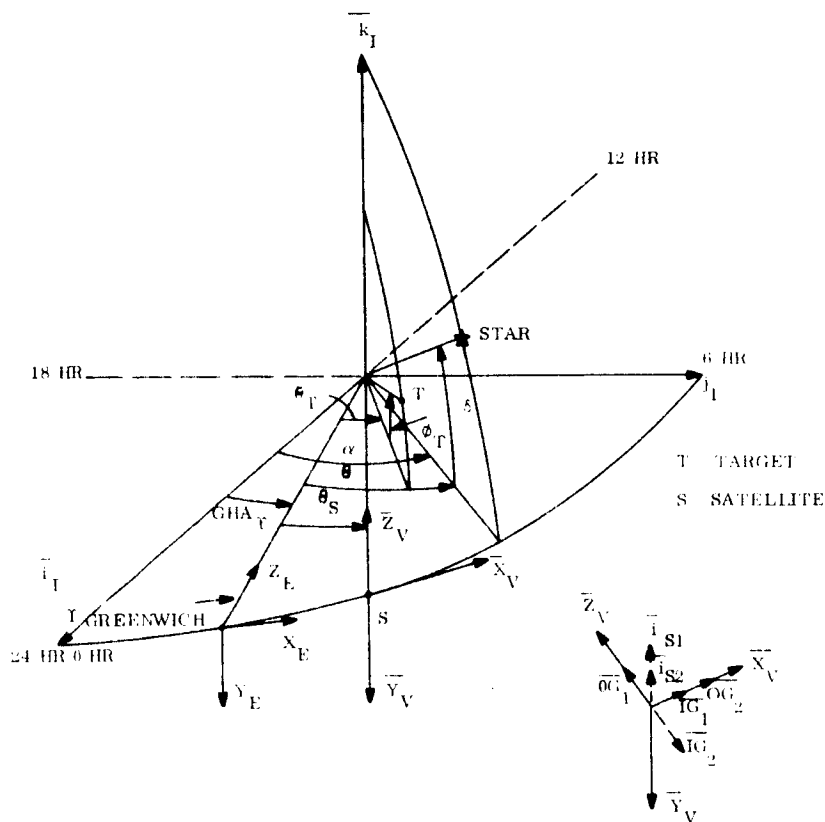


Figure F-5. Relative Position of Satellite, Target, and Star

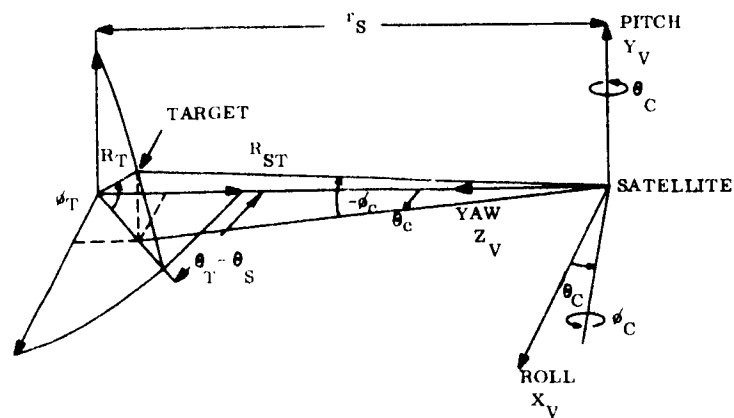


Figure F-6. Rotation of Vehicle Axes for Any Target Location

Maximum angular rotations of 8.68 degrees are required to point the yaw axis at a target on the horizon line. Target points may be defined in terms of $(\theta_T - \theta_S)$ and ϕ_T . Pairs of these two angles may lie anywhere within the region in Figure F-7. The outer boundary corresponds to the horizon line.

Two star combinations were selected for this study:

- a. The α' Cru and ϵ UMa stars
- b. The α' Cru and α UMi (Polaris) stars

The position of these stars on the celestial sphere is given in terms of their right ascension (α) and declination (δ).

Table F-2 gives these figures and the trackers which are used to track each star.

Table F-2. Magnitude and Equatorial Coordinates of Tracking Stars

Star Name	Magnitude	Right Ascension (Deg)	Declination (Deg)	Tracker No.
α' Cru	1.0	186.0	-62.895	1
ϵ UMa	1.7	192.8	56.16	2
α UMi (Polaris)	2.1	29.5	89.093	2

F. 2. 4 STABILITY OF ATS-4 ORIENTATION CONTROL SYSTEM

F. 2. 4. 1 α' Cru - ϵ UMa Star Combination

A digital program was set up to compute parameters A and B for all target points on the grid in Figure F-7. These include points on the horizon line and those whose latitude is 0 degree.

After data reduction, it was found that all pairs of AB points lie within the shaded rectangle on the AB plane in Figure F-8. The system is stable since the rectangle lies within the trapezoidal area which as mentioned earlier was empirically determined from a computer study on the similar OAO system.

The approximate effect of target location on the magnitude of the gimbal angles can be determined by simplifying equations (33) through (36) with the aid of the assumption that $\cos \phi_c \cong 1$ and $\sin \phi_c \cong \phi_c$ since the range of ϕ_c is $-8.68 \text{ degrees} \leq \phi_c \leq + 8.68 \text{ degrees}$.

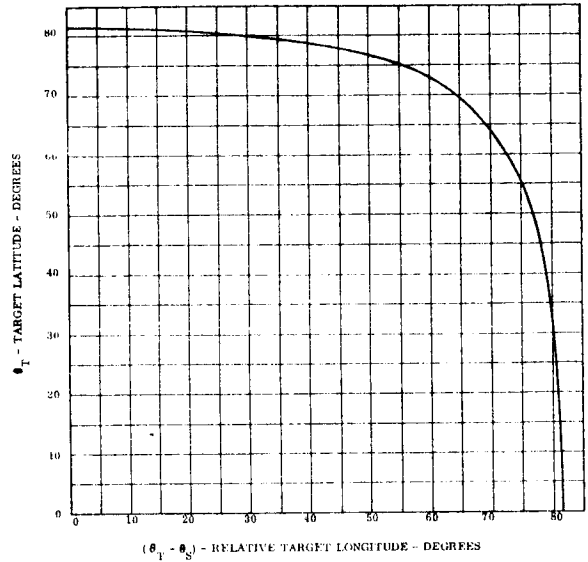


Figure F-7. Target Area in Terms of Meridional Coordinates

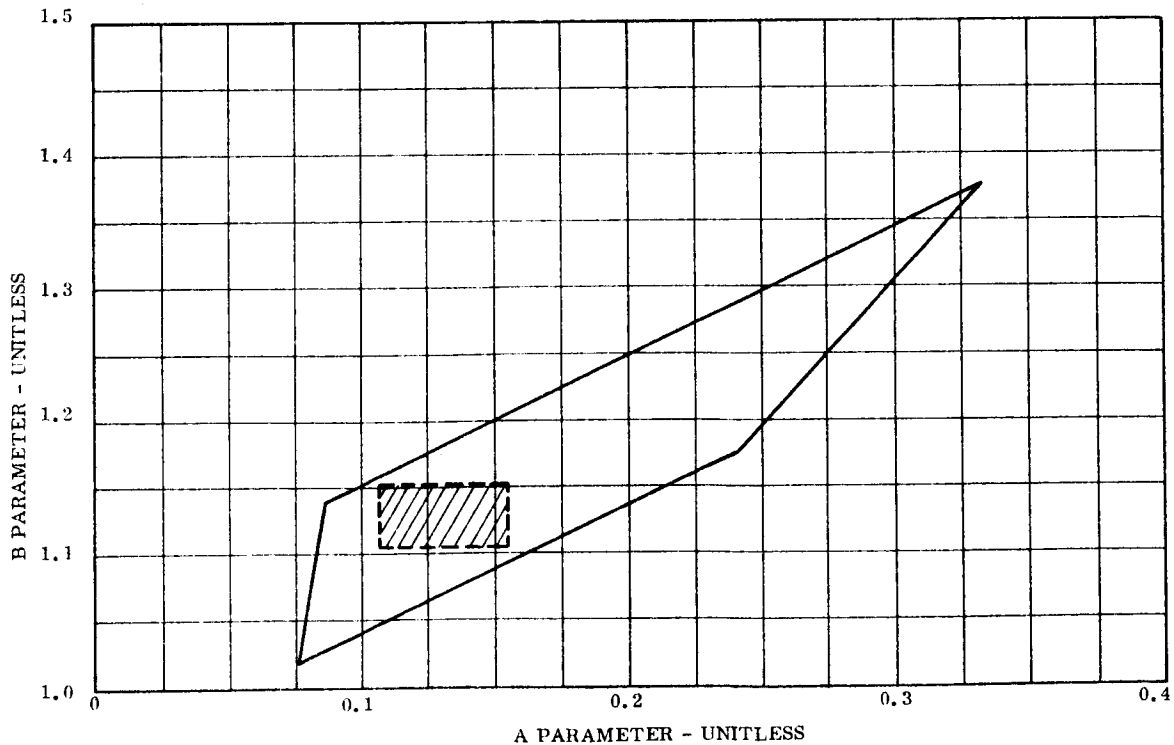


Figure F-8. Range of Variation for Parameter A and B, α' Cru - α UMa Star Combination

Then,

$$\sin E_1 \cong \cos \delta_1 [\cos (\theta_1 - \theta_s + \theta_c) - \phi_c \tan \delta_1] \quad (40)$$

$$\tan A_1 \cong \frac{\sin (\theta_1 - \theta_s + \theta_c)}{\phi_c \cos (\theta_1 - \theta_s + \theta_c) + \tan \delta_1} \quad (41)$$

$$\sin E_2 = -\cos \delta_2 \sin (\theta_2 - \theta_s + \theta_c) \quad (42)$$

$$\tan A_2 \cong \frac{\cos (\theta_2 - \theta_s + \theta_c) - \phi_c \tan \delta_2}{\phi_c \cos (\theta_2 - \theta_s + \theta_c) + \tan \delta_2} \quad (43)$$

Also,

$$\left. \begin{array}{l} \phi_c \cos (\theta_1 - \theta_s + \theta_c) \\ \phi_c \cos (\theta_2 - \theta_s + \theta_c) \end{array} \right\} \leq 0.152 \quad (44)$$

and from Table F-2,

$$\left| \tan \delta_2 \right| = \begin{cases} 1.49 & \text{for } \epsilon \text{ UMa star} \\ 63.2 & \text{for Polaris star} \end{cases}$$

$$\left| \tan \delta_1 \right| = 1.952 \quad (45)$$

so that the expressions for $\tan A_1$, and $\tan A_2$ may be further simplified to the following:

$$\tan A_1 \cong \cot \delta_1 \sin (\theta_1 - \theta_s + \theta_c) \quad (46)$$

$$\tan A_2 = \cot \delta_2 \cos (\theta_2 - \theta_s + \theta_c) - \phi_c \quad (47)$$

Equations (40), (42), (46), and (47) reveal the following facts pertaining to the effect of the target location on the gimbal angle variation:

- a. Gimbal angles A_1 and E_2 are essentially independent of target latitude.
- b. The effect of changing the target latitude, on the gimbal angles A_2 and E_1 , is to add a bias to each angle that varies proportionally with the latitude.
- c. The effect of target longitude is to shift each gimbal angle, with respect to the reference selected as per the sketch in Figure F-5, an equal amount and with the same polarity.

Gimbal angle variations are plotted on Figures F-9, F-10, and F-11 for three target locations selected to illustrate the above conclusions.

F.2.4.2 α' Cru - α UMi Star Combination

The parameters A and B were computed for the same target points used with the other star combination. The shaded rectangular region on Figure F-12 illustrates the range over which AB points may lie. Unsatisfactory operation is indicated since the entire region lies outside the trapezoidal area. Negative values for A parameter indicate an unstable linear system for certain target locations based on the linear data presented in Figure F-1.

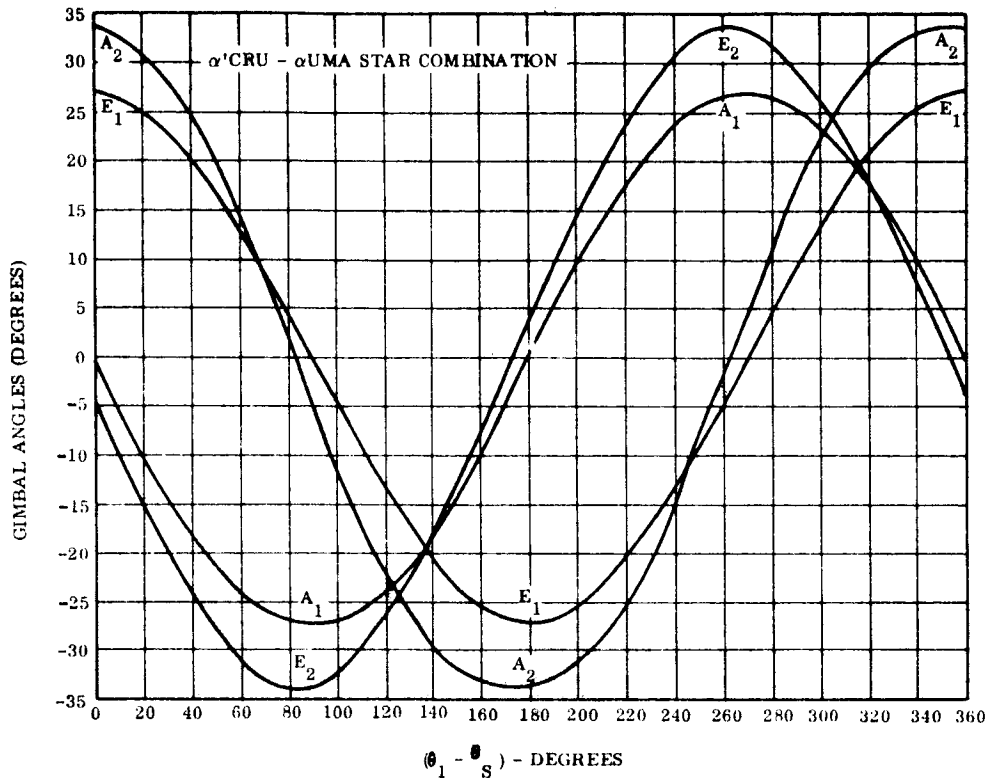


Figure F-9. Gimbal Angle Variation - $\phi_T = 0$, $(\theta_r - \theta_s) = 0$

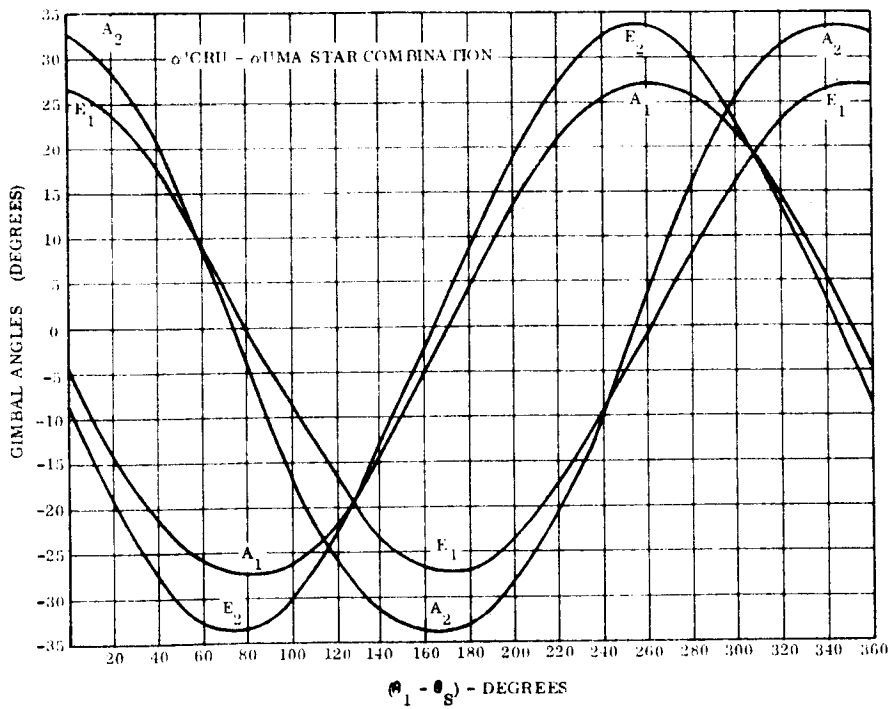


Figure F-10. Gimbal Angle Variation - $\phi_r = 0$, $(\theta_r - \theta_s) = 81.5$

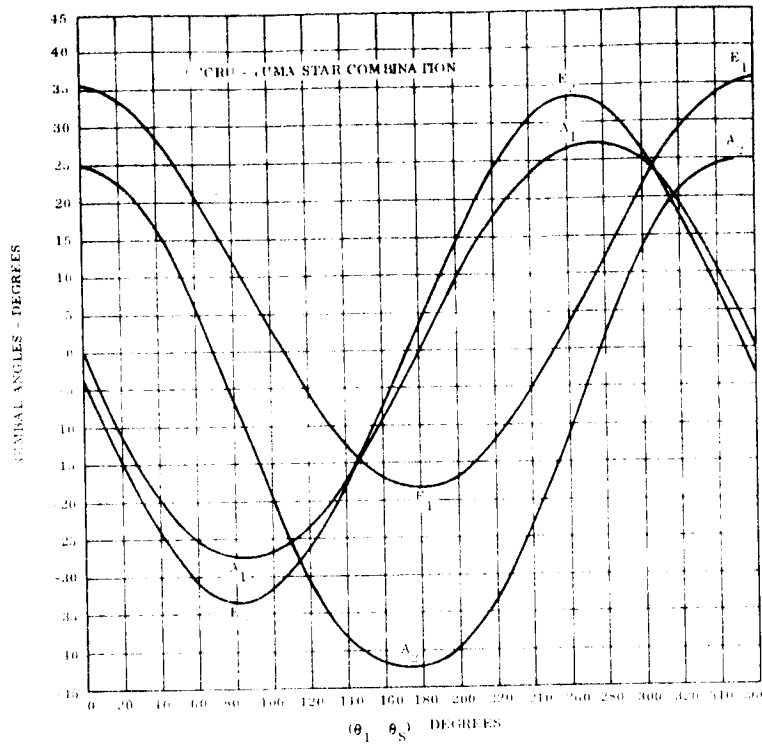


Figure F-11. Gimbal Angle Variation - $\phi_T = 81.5$, $(\alpha_T - \theta_S) = 0$

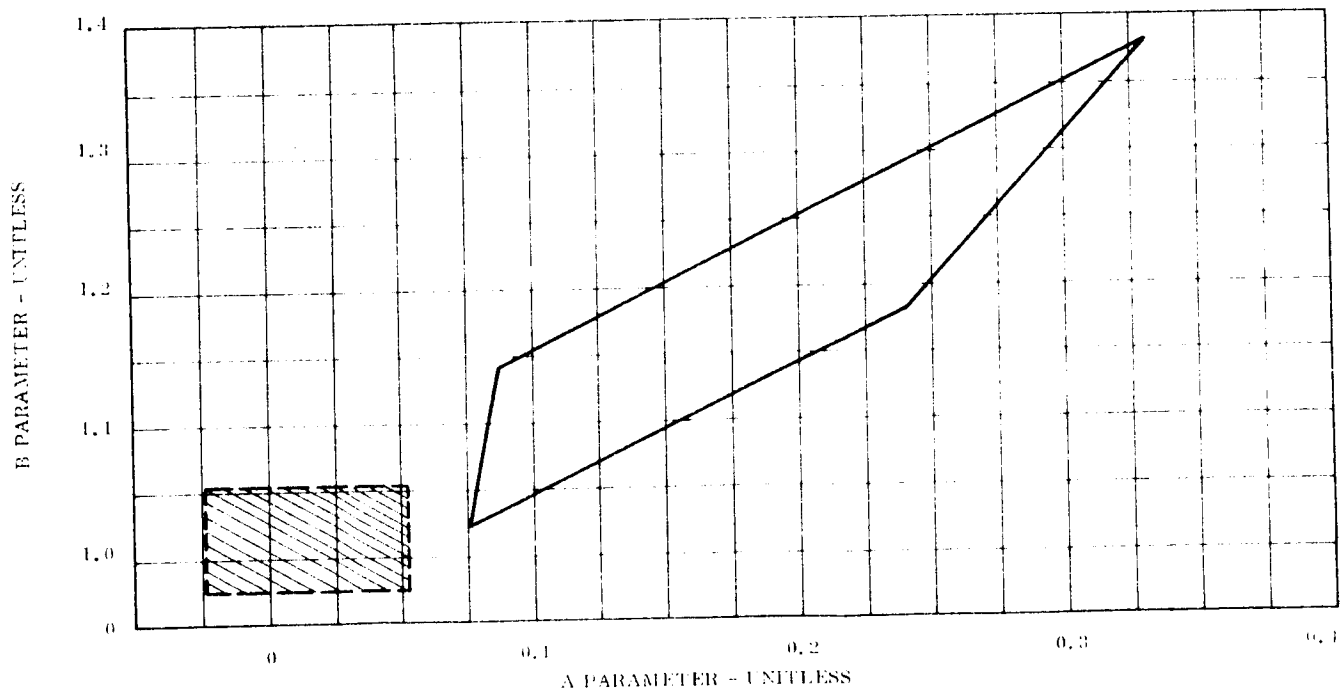


Figure F-12. Range of Variation for Parameters A and B α' Cru - α UMi Star Combination

Gimbal angle variations for the same target locations used in the previous section are plotted on Figures F-13, F-14, and F-15. Again it is noticed that target latitude changes affects only gimbal angles A_2 and E_1 .

Gimbal angle E_2 varies through small amplitude excursions because of the high declination of the Polaris star. Gimbal angle A_2 behaves in a similar manner for small target latitudes. However, its magnitude increases and becomes essentially equal to the target latitude for large latitudes as is evident from equation (47). This fact is significant in explaining why maximum control system errors become less as the target latitude increases. (Control system errors are discussed in Section F. 3. 3.)

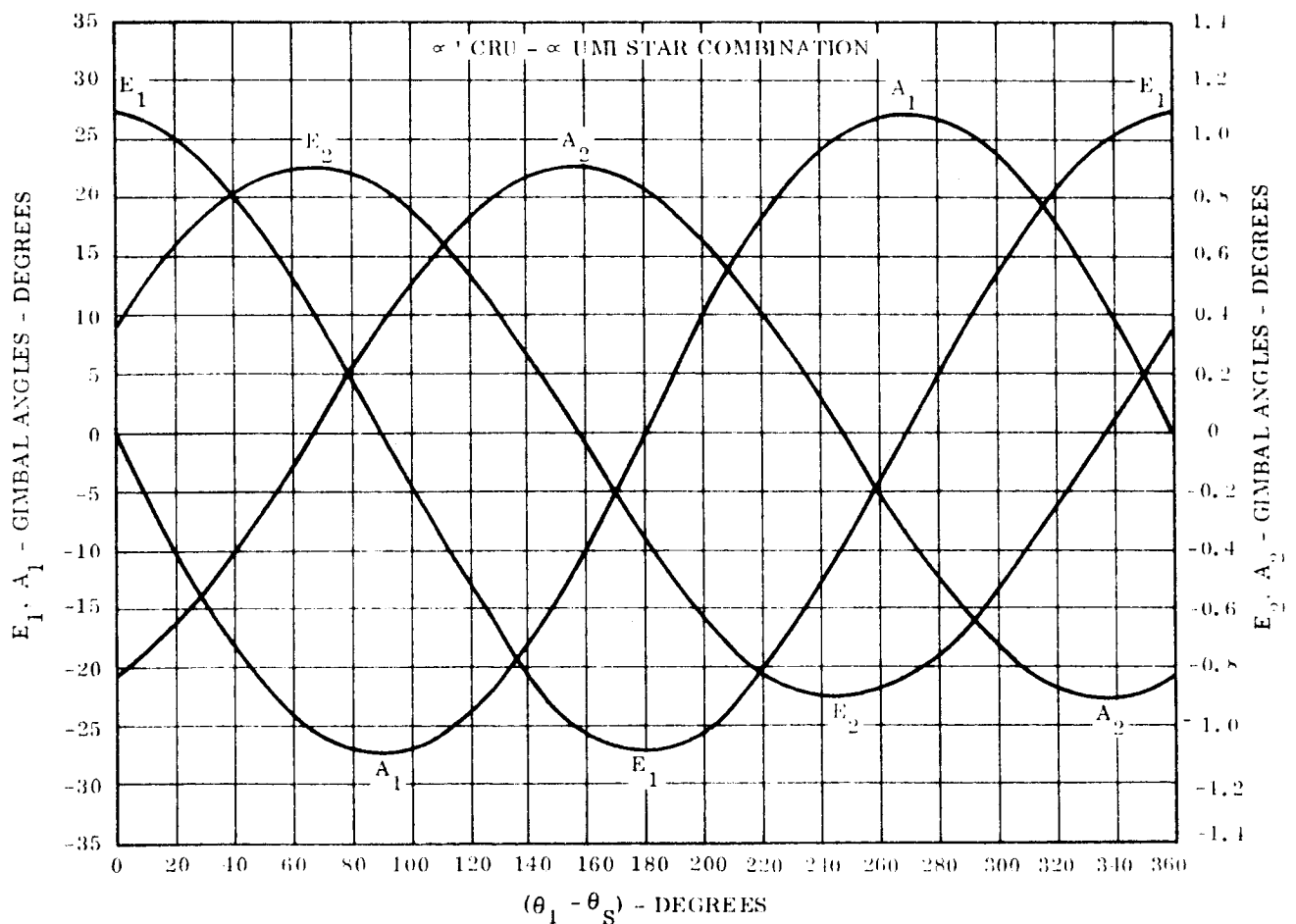


Figure F-13. Gimbal Angle Variation - $\phi_T = 0$, $(\theta_T - \theta_S) = 0$

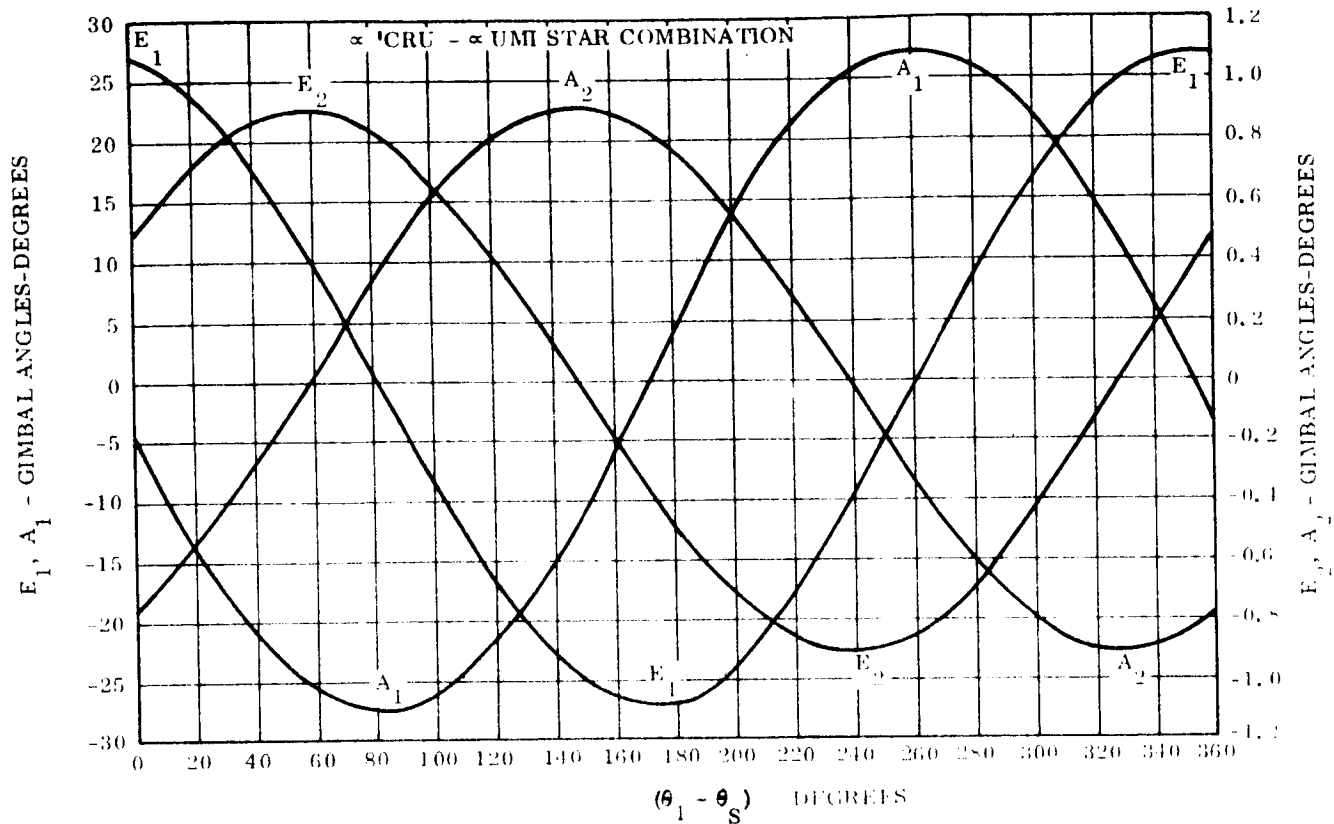


Figure F-14. Gimbal Range Variation - $\phi_T = 0$, $(\theta_T - \theta_S) = 81.5$

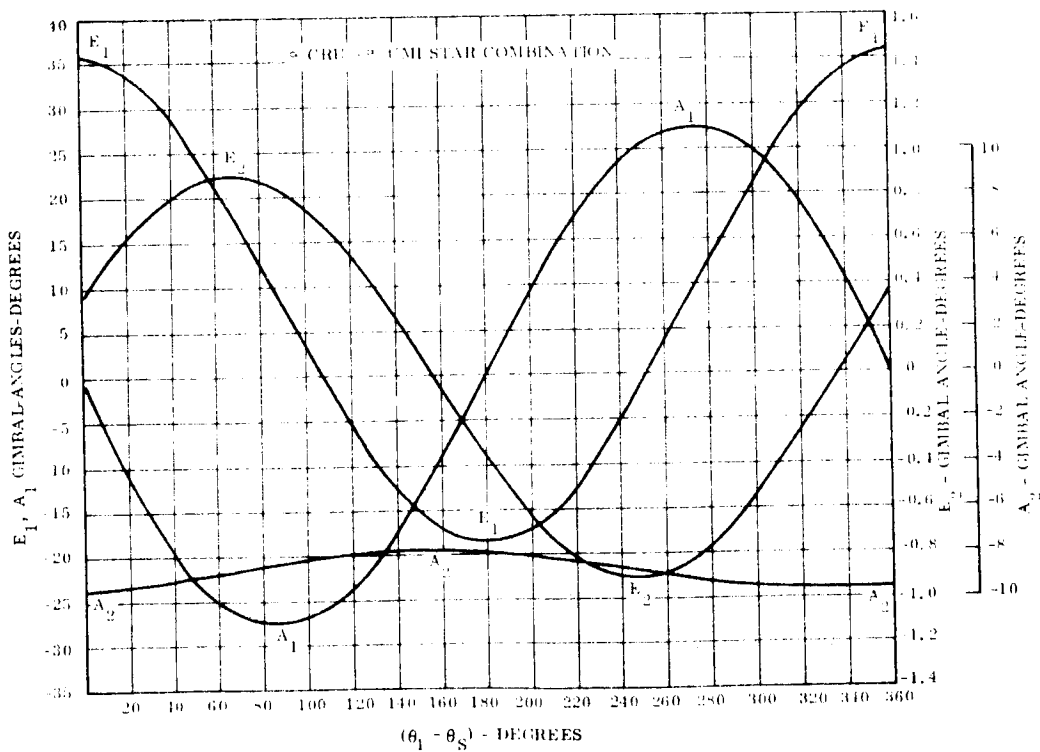


Figure F-15. Gimbal Range Variation - $\phi_T = 81.5$, $(\alpha_T - \alpha_S) = 0$

F. 3 POINTING ANGLE ERROR STUDY

The purpose of this section is to present and discuss the results of a pointing angle error analysis. Also, control system errors due to momentum storage will be derived.

Three types of errors are considered.

- a. Attitude sensor errors. These include measurement errors due to non-orthogonality effects in the star trackers, misalignment, gimbal readout error, drift, threshold, etc.
- b. Errors due to uncertainties in knowledge of spacecraft and target locations.
- c. Errors due to sensor output noise and control electronics noise.

The spacecraft is nominally in a synchronous equatorial orbit and it is required that the antenna, assumed aligned with the vehicle yaw control axis, is to be capable of being pointed to any specified point on the earth surface in view of the spacecraft, to within an accuracy of 0.1 degrees.

F. 3.1 ATTITUDE SENSOR ERRORS

The mean square pointing error ($\overline{\xi_M^2}$) is the sum of the squares of pitch and roll errors, for small errors. The pitch and roll errors, in turn, are functions of sensitivity coefficients are partial derivatives of pitch and roll errors with respect to gimbal angles (such as the partial derivative of pitch error with respect to the outer gimbal angle of tracker No. 1). Gimbal measurement errors are a function of boresight error, sensor/control axis misalignments (prior to launch, due to launch effects, and due to orbit environment), drifts, command angle resolution, gimbal angle pickoff resolution, and tracker threshold.

F. 3.2 POSITION ERROR EFFECTS

This error arises as a result of uncertainties in knowledge of satellite and target locations. The mean square error ($\overline{\xi_c^2}$) is the sum of the squares of pitch and roll errors. The pitch and roll errors, in turn, are functions of sensitivity coefficients and latitude and longitude errors which are indicative of the deviation between the predicted or measured and desired

location of the spacecraft and target. There can also be a timing lag error which occurs when updating gimbal angles to keep the vehicle locked on target. The sensitivity coefficients are partial derivatives of pitch and roll errors with respect to one of the following variables: spacecraft latitude and longitude, target latitude and longitude, distance from earth center to spacecraft and target, and timing lag error, e. g., the partial derivative pitch error with respect to spacecraft latitude.

F. 3. 3 CONTROL SYSTEM ERRORS

Control system errors will occur due to sensor output noise, control electronics noise, and due to momentum storage in the fine wheel. The mean square error due to the first two effects (ξ_{csn}^2) is simply the sum of the individual mean square errors.

The fine wheel speed associated with momentum storage is maintained by applying a certain voltage to the motor terminals. There must then be a system error which is directly related to the speed by the system gain. Star tracker data is summed and averaged by a star tracker signal processor whose gain is a function of the number of trackers in operation, gimbal angle magnitudes, and attitude errors. This gain comprises a portion of the total gain that affects the system error and since it is not a constant, the system error can also vary.

For the two-tracker system under study, the gain associated with roll and yaw axes will vary over the range from approximately 0.75 to 1.0 for any star combination so that system error is essentially a constant for this case. The manner with which pitch information is obtained, however, can be the cause of large gain fluctuations in the star tracker signal processor (STSP) and requires a careful selection of the stars to be tracked by trackers No. 1 and No. 2. The STSP gain is equivalent to the e_{22} coefficient in the error matrix derived in Section F. 2. 2. Thus for pitch attitude errors only,

$$K_{pitch} = 1/2 (\sin^2 A_1 + \sin^2 A_2)$$

System error varies inversely with this gain. Outer gimbal angles in this equation vary over a range which is dependent on the star selection and on the target location. Choosing a star

such as Polaris for one tracker leads to trouble since the outer gimbal of that tracker will fluctuate through small angles (corresponding \sin^2 magnitude will be small) and cause the pitch gain to be very small when the outer gimbal angle corresponding to the other tracker goes through zero.

The error in degrees using the OAO configuration and numbers (10 sec system) can be calculated from the equation

$$\xi_{cs} = 0.00274/K_{pitch}$$

F. 3.4 TOTAL POINTING ERROR

The total pointing error ξ_T is defined as the sum:

$$\xi_T = \xi_{rss} + \xi_{cs}$$

where

$$\xi_{rss} = \left(\overline{\xi_m^2} + \overline{\xi_c^2} + \overline{\xi_{csn}^2} \right)^{1/2}$$

The component ξ_{rss} can be regarded as the sum of two orthogonal components: a pitch and roll component. Both pitch and roll errors may be taken as approaching asymptotically to normal distributions so that the square of the pointing error is the sum of the squares of the two errors. The square root of the resultant is referred to as the rss value which is approximately three times the rms value. On the basis of 3σ values used for random errors, the probability must be at least 99 percent that the pointing error will at no time be greater than the rss value.

F. 3.5 NUMERICAL EVALUATION OF TOTAL POINTING ERROR

An error budget listing numerical values for the error components is given in Table F-3. A digital computer program was devised to compute the total and components of the total pointing error for the two star combinations selected for this study and for several target locations.

Table F-3. Error Budget

The following are design tolerances and are limits of error unless otherwise specified. Star ephemeris errors are neglected.

Boresight Error: $\Delta_{\beta} (A_K) = \Delta_{\beta} (I_K) = 0.003^{\circ}$

Drifts, 3 rmp, all sources: $\Delta_d = 0.007^{\circ}$

Tracker threshold: $\Delta_T = 0.001^{\circ}$

Sensor/Control axis misalignments:

Prior to launch: $\Delta_{V_o} = \alpha_{V_o} = \Delta_{H_o} = \alpha_{H_o} = 0.003^{\circ}$

(tracker/surface/control axis)

Due to launch effects: $\Delta_{V_L} = \alpha_{V_L} = \Delta_{H_L} = \alpha_{H_L} = 0.01^{\circ}$
(bending, etc.)

Due to orbit environment: $\Delta_{V_E} = \alpha_{V_E} = \Delta_{H_E} = \alpha_{H_E} = 0.01^{\circ}$
(temperature, vibration, etc.)

Command Angle Resolution: $\Delta_{r_c} = 0.003^{\circ}$

Gimbal Angle Pickoff Resolution: $\Delta_{r_p} = 0.0015^{\circ}$

Sensor Output Noise, 3σ : $\Delta_n = 0.006^{\circ}$

Control Electronics Noise, 3σ : $\Delta_c = 0.006^{\circ}$

Offset Due to Momentum Storage Device: $\Delta_m = 0.01^{\circ}$

Time Error In Command: $\Delta_t = 1.2$ sec's time (0.005°)

Spacecraft Drift: $\Delta_{\phi_s} \Delta = \Delta_{\theta_s} \Delta = 0.02^{\circ}$
(stationkeeping deadband)

Uncertainty In Knowledge of

Spacecraft Location, Angular, 3σ : $\Delta_{\phi_s} \text{ p} = \Delta_{\theta_s} \text{ p} = 0.03^{\circ}$
(includes effects of tracking site

location and tracking system uncertainties, based on Minitrack net)

Radial Position Uncertainty

of Spacecraft, 3σ : $\Delta_{r_s} = 2.0$ km

Uncertainty of Target Location, Angular, 3σ : $\Delta_{\phi_T} = \Delta_{\theta_T} \cos \phi_T = 0.0045^{\circ}$

Radial Position Uncertainty

of Earth Surface Target Point, 3σ : $\Delta_{r_T} = 0.135$ km

F. 3. 5. 1 α' Cru and ϵ UMa Star Combination

Plots of the three errors ξ_{CS} , ξ_{RSS} , and ξ_T are drawn on Figures F-16, F-17, and F-18 for three target locations as a function of location-in-orbit. The error component ξ_{RSS} has essentially a constant amplitude as it is mainly a function of position error effects (ξ_c) which are independent of the location-in-orbit of the spacecraft. The behavior of the control system error ξ_{CS} is predictable on the basis of the outer gimbal variations plotted on Figures F-9, F-10, and F-11. Thus for any given target latitude the variation of ξ_{CS} is essentially independent of the relative target longitude. There is, however, a considerable change in the variation of ξ_{CS} as the target latitude changes, since the angular variation of one of the outer gimbals changes markedly from its variation at zero latitude (outer gimbal angle A_2 in Figure F-11 as compared to that in Figure F-9).

Maximum total and component errors are plotted on Figure F-19 versus target relative longitude with target latitude as a parameter. The following information can be extracted from these curves:

- a. $\xi_{RSS \max}$ occurs at zero target latitude and zero relative longitude, i. e. local vertical pointing.
- b. $\xi_{CS \max}$ occurs at zero relative longitude and maximum latitude, i. e. horizon pointing.
- c. $\xi_{T \max}$ occurs at zero target latitude and zero relative longitude, i. e., local vertical pointing.

The maximum total pointing error lies within $0.0895^\circ \leq \xi_{T \max} \leq 0.098^\circ$ for all values of target latitude and longitude.

F. 3. 5. 2 α' Cru and α UMi Star Combination

Curves of total and component pointing errors are plotted on Figures F-20, F-21, and F-22 for three target locations. Now, the error ξ_{RSS} is strongly dependent on attitude sensor errors (ξ_m) in contrast with its dependence on position error effects (ξ_c) for the previous star combination. There is a wide transition in waveshape for pointings away from the local

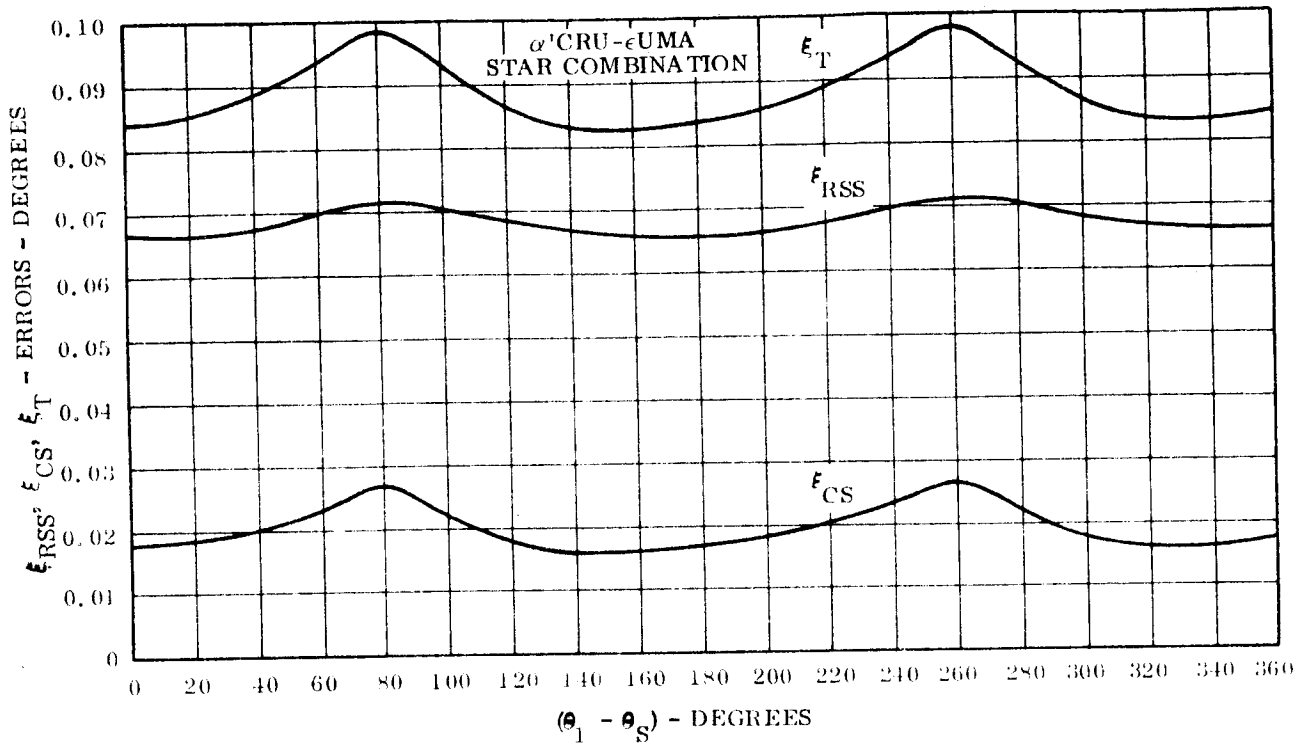


Figure F-16. Pointing Angle Errors - $\phi_T = 0$, $(\theta_T - \theta_S) = 0$

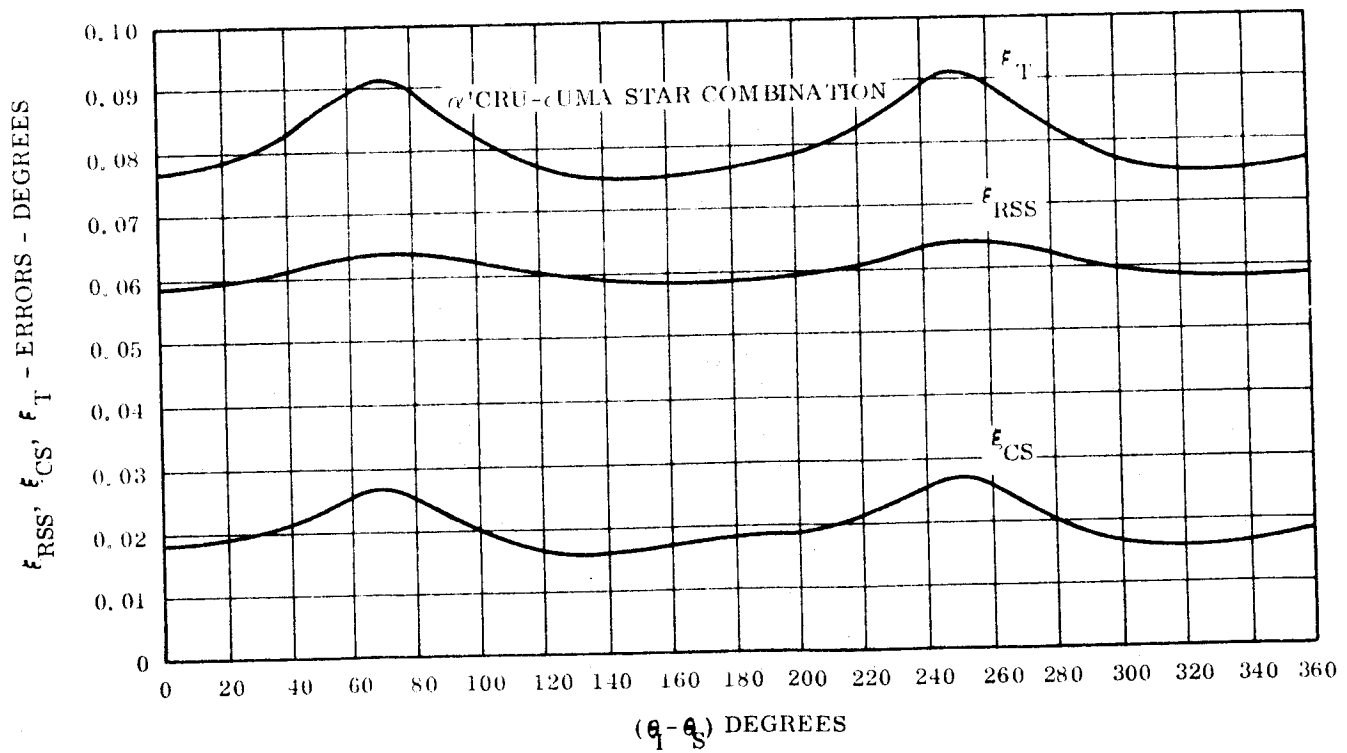


Figure F-17. Pointing Angle Errors - $\phi_T = 0$, $(\theta_T - \theta_S) = 81.5$

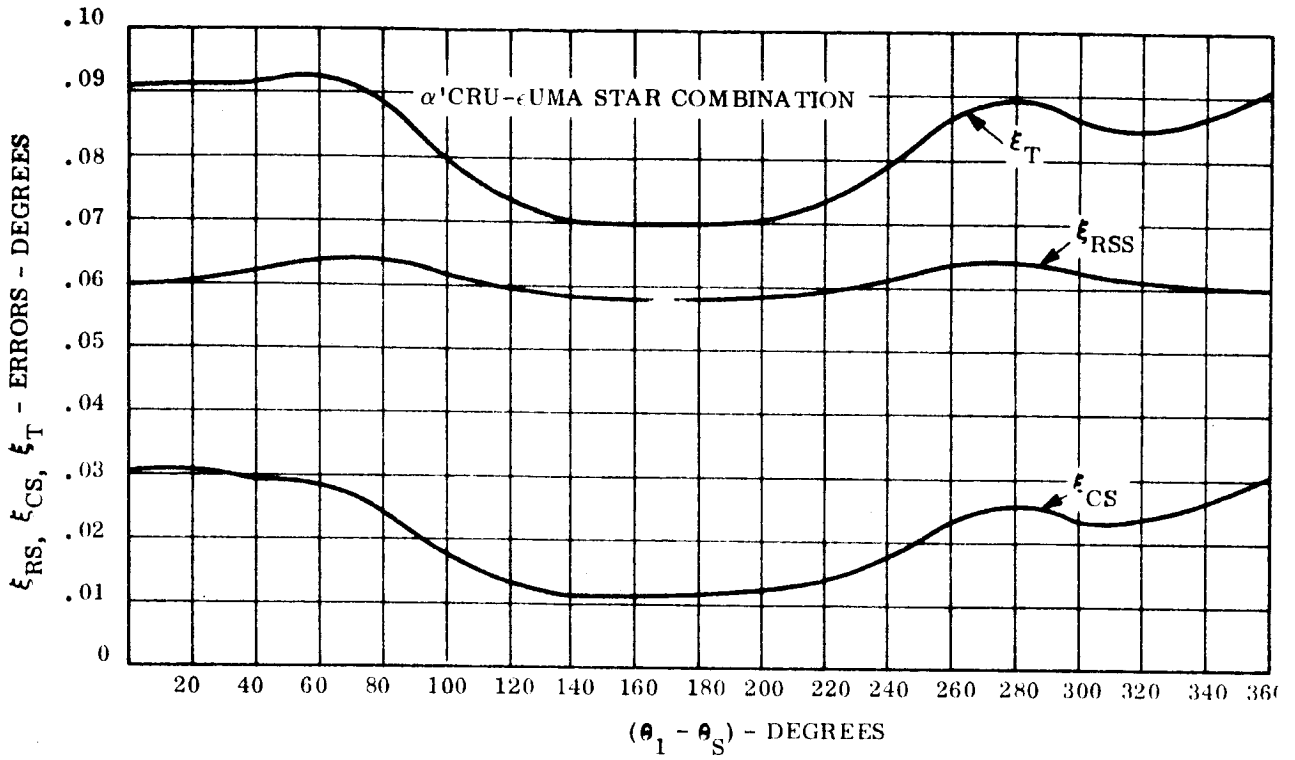


Figure F-18. Pointing Angle Errors - $\phi_T = 81.5$, $(\theta_T - \theta_s) = 0$

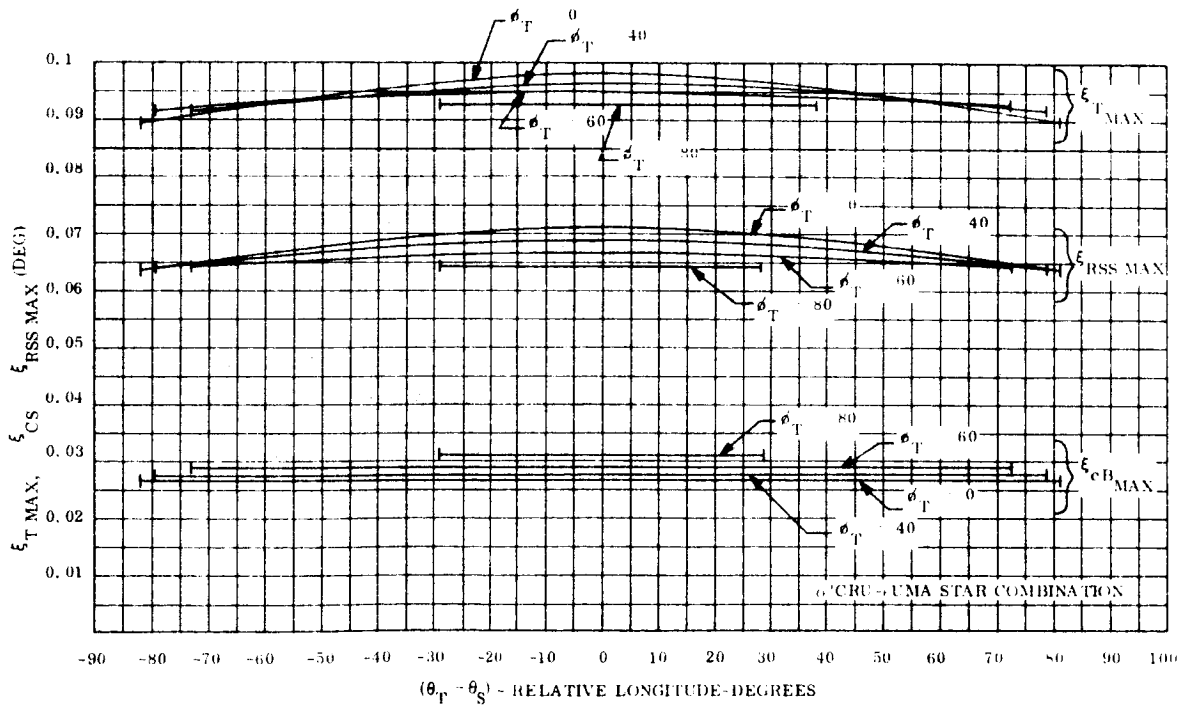


Figure F-19. Curves of Maximum ξ_{RSS} , ξ_{CS} , and ξ_T Error

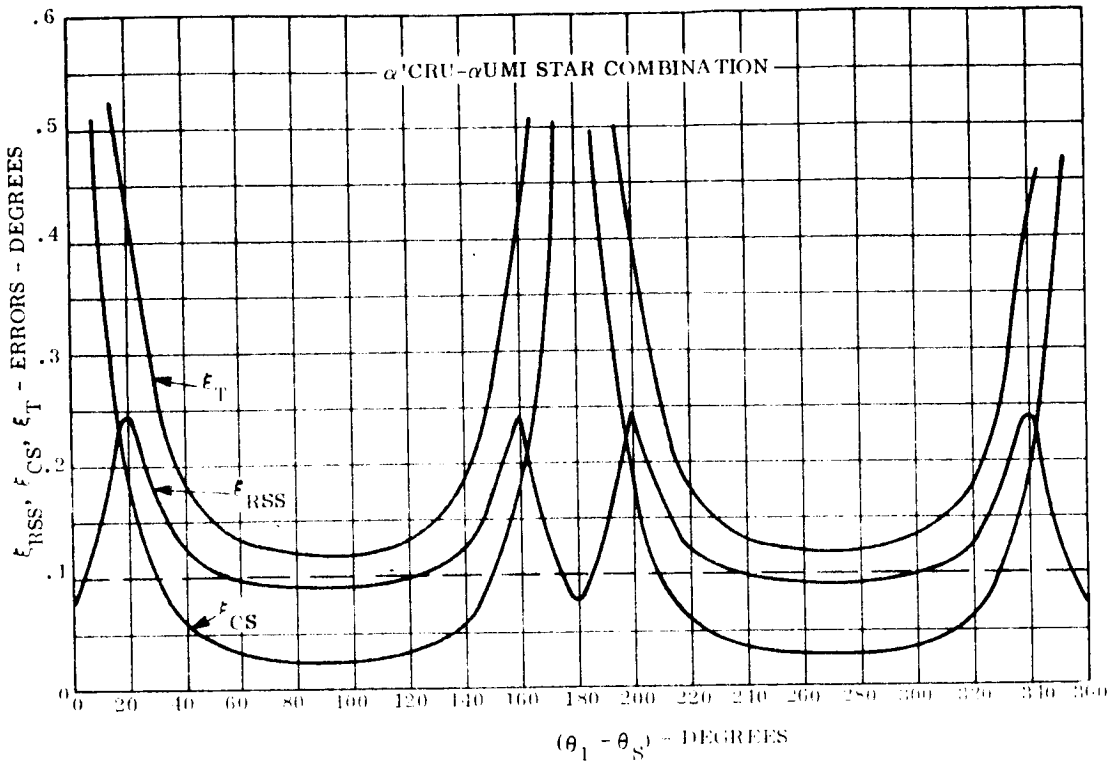


Figure F-20. Pointing Angle Errors - $\phi_T = 0, (\theta_T - \theta_S) = 0$

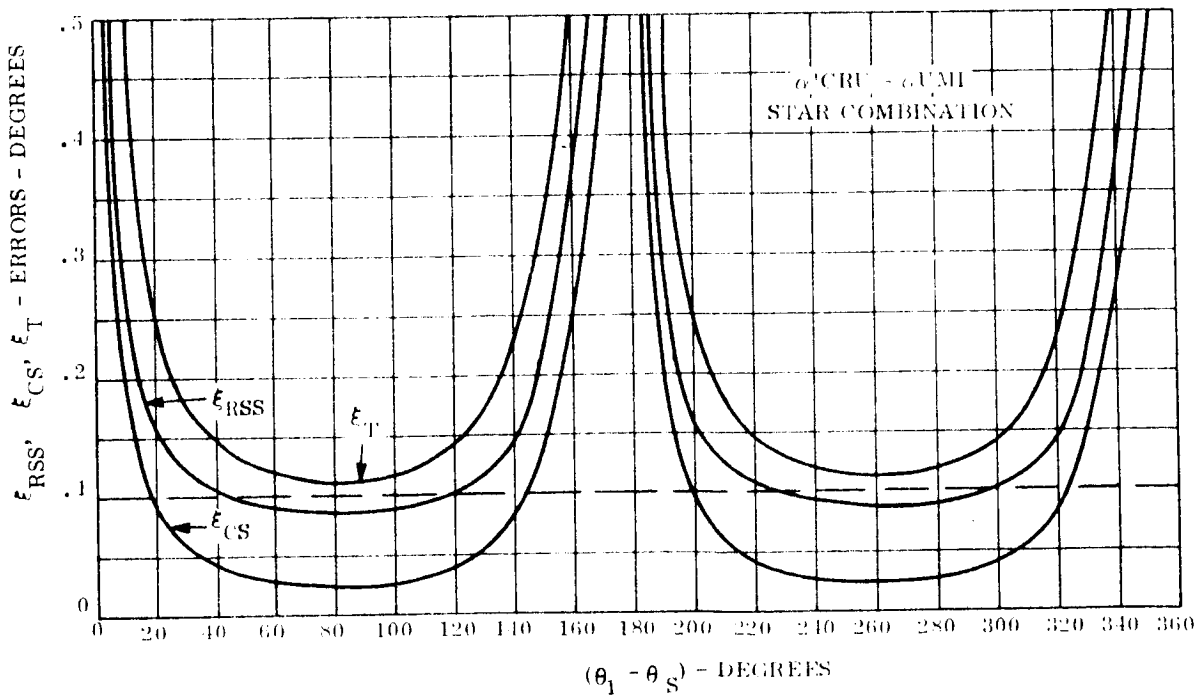


Figure F-21. Pointing Angle Errors - $\phi_T = 0, (\theta_T - \theta_S) = 81.5$

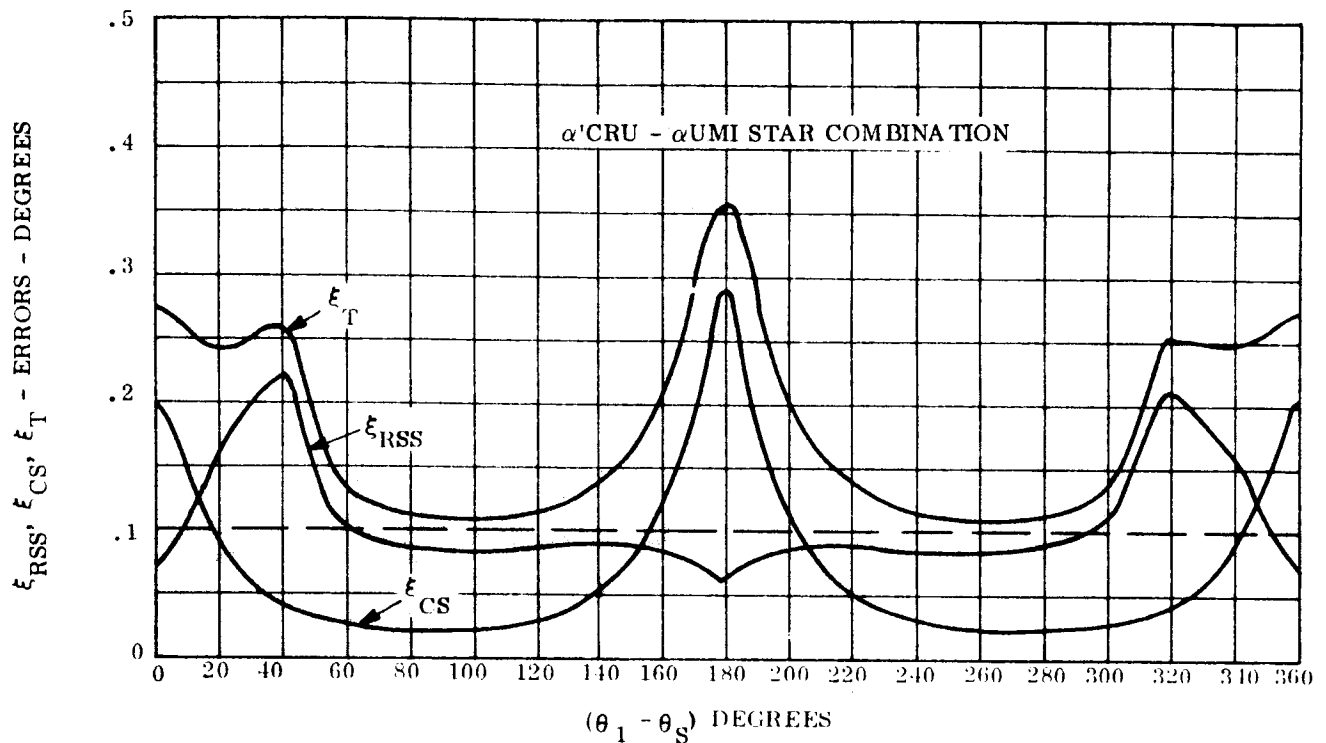


Figure F-22. Pointing Angle Errors - $\phi_T = 81.5$, $(\theta_T - \theta_S) = 0$

vertical. The control system error ξ_{CS} , however, has about the same waveshape for all target pointings.

Peaks in the error ξ_{RSS} do not always occur at the same location-in-orbit for different target pointings. Also, the relative longitude at which $(\xi_{RSS \max})_{\max}$ occurs is a function of the target latitude as is evident from the plot on Figure F-23. At low target latitudes, $(\xi_{RSS \max})_{\max}$ occurs at a longitude corresponding to the horizon line. As the latitude increases the peak in $\xi_{RSS \max}$ now shifts towards zero longitude and again shifts to a longitude approaching the horizon line for still further increases the latitude. At large latitudes the variation of $\xi_{RSS \max}$ becomes essentially independent of longitude.

Curves of maximum control system error $\xi_{CS \max}$ are drawn on Figure F-24 as a function of relative longitude with target latitude as a parameter. Peaks of $\xi_{CS \max}$ occur at zero longitude for the low range of target latitude. This peak shifts towards small positive

longitudes in the high range of target latitude. The variation of $\xi_{cs \max}$ is essentially constant with longitude (except for a small rise near the maximum) for large target latitudes.

Curves of total maximum pointing error $\xi_{T \max}$ are plotted on Figure F-25. Peaks of $\xi_{T \max}$ occur at zero longitude for small target latitude, shift essentially in a symmetrical manner towards positive and negative longitudes as the latitude is further increased, and finally occur at a longitude corresponding to the horizon line for large latitudes. There is also a small variation of $\xi_{T \max}$ with longitude for large latitudes.

The large errors incurred with this star combination exceed the allowable level of 0.1 degree so that this combination is completely unsatisfactory.

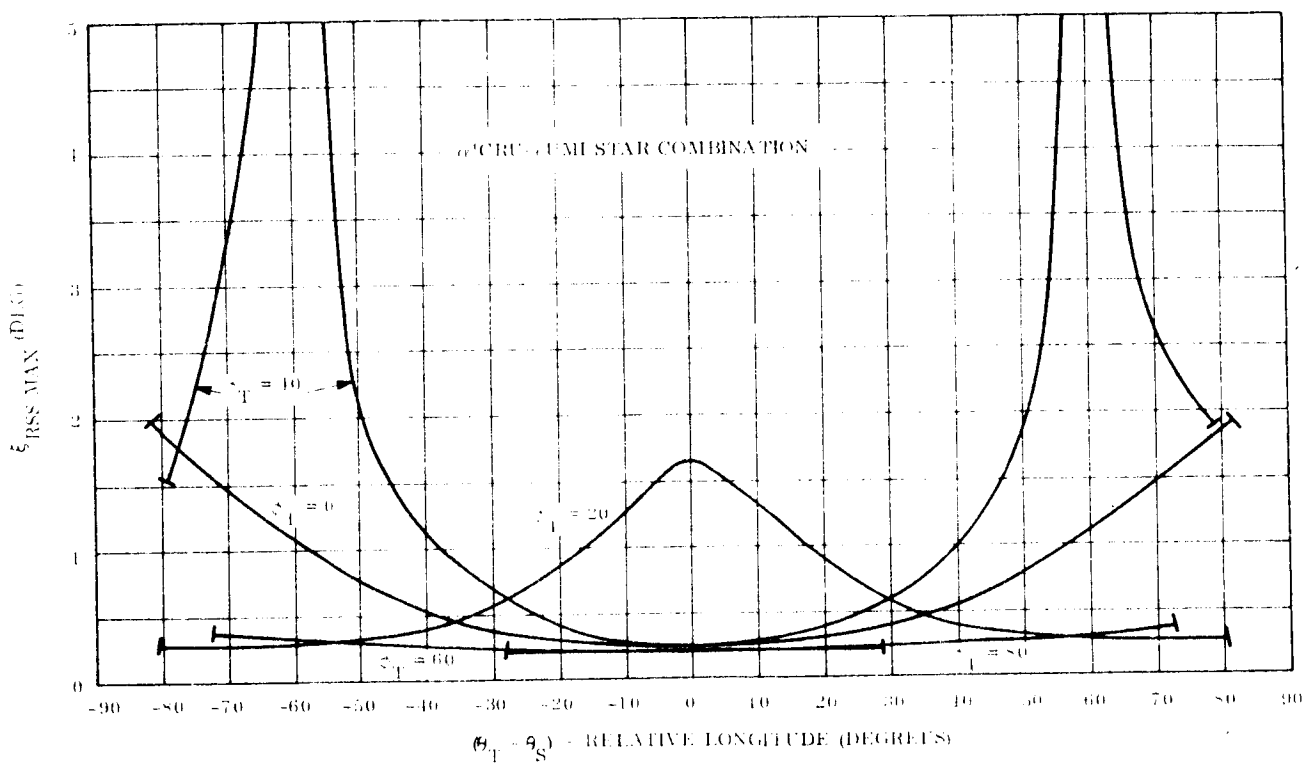


Figure F-23. Curves of Maximum Error ξ_{RSS}

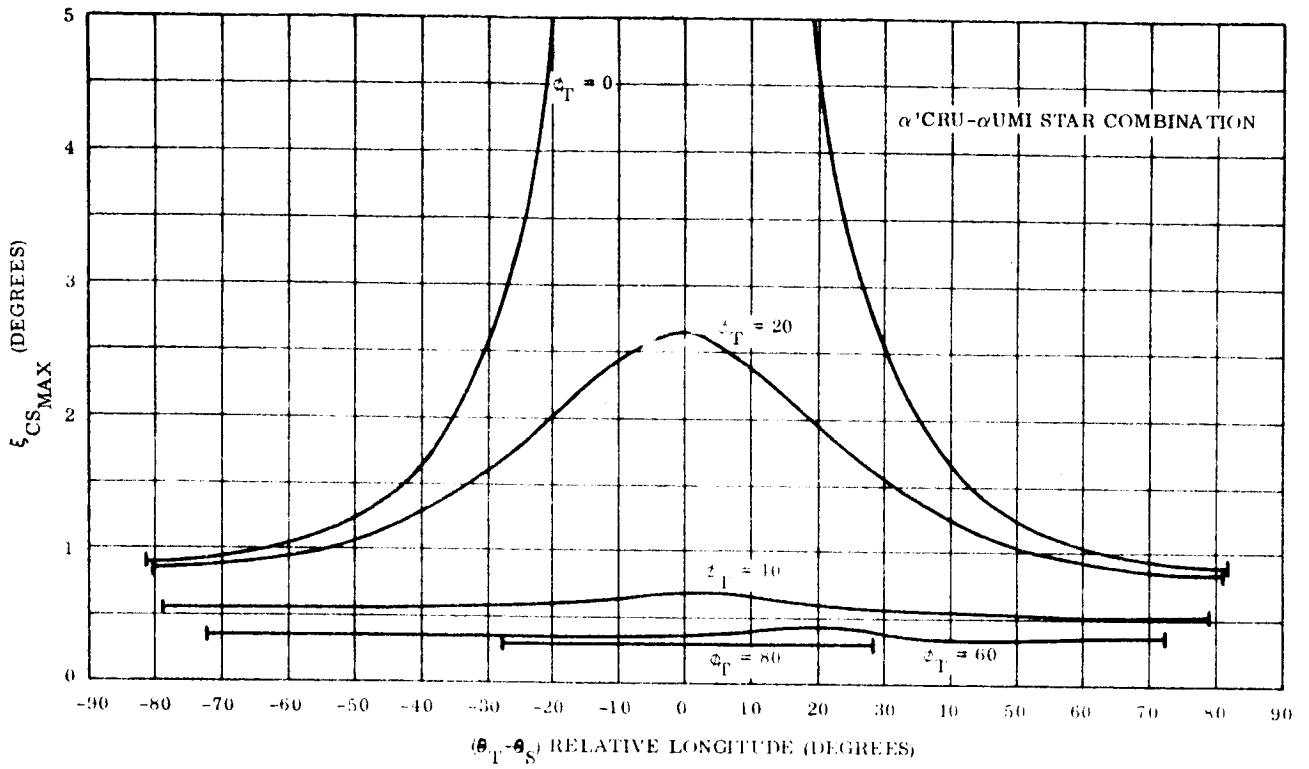


Figure F-24. Curves of Maximum Error ξ_{CS}

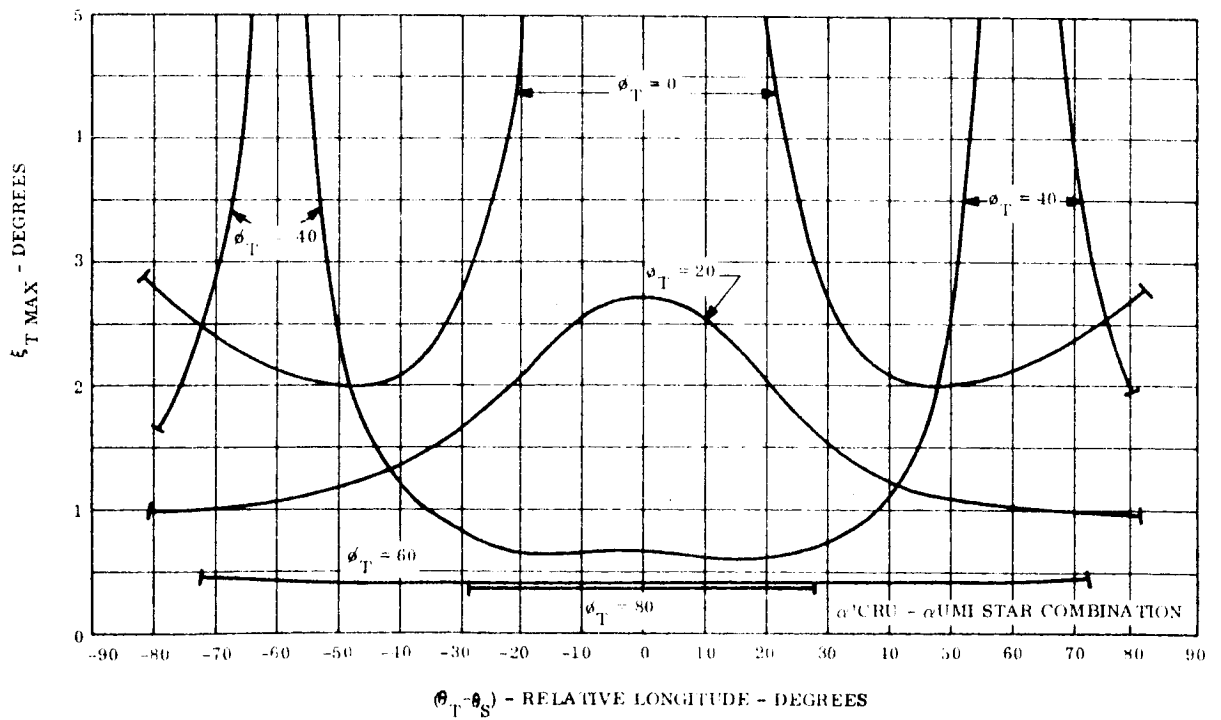


Figure F-25. Curves of Maximum Error ξ_T

APPENDIX G
SOLAR ARRAY COMPUTER PROGRAM

The computer program used to determine the ATS-4 array power output calculates the total current and power output of a solar array taking into account the following parameters:

- a. Solar intensity
- b. Temperature
- c. Angle of solar incidence
- d. Number of cells in series in a series string
- e. Number of cells in parallel in series string
- f. Number of series strings
- g. Basic cell characteristics (efficiency, base resistivity)
- h. Losses and uncertainties

The output of the program is a listing, for each set of input parameters, of voltage versus total current, and voltage versus power. The program calculates the array output based on the characteristics of a single solar cell, multiplying the voltages and currents by the number of cells in series and parallel, respectively, to obtain the voltage-current characteristics of the total array.

The voltage-current characteristics of a single solar cell are represented by the following relation:

$$I = I_{sc} - \frac{V}{R_p} - I_o \left[e^{\frac{K(V + R_s I)}{S}} - 1 \right]$$

where the variables are:

I = Cell current output

V = Voltage on solar cell

and the coefficients are:

I_{sc} = Illumination current (virtually equal to short circuit current)

R_p = Shunt resistance of the cell

I_o = Reverse saturation current of the ideal diode characteristic

K = Coefficient of the exponential

R_s = Series resistance of the cell

The coefficients are further treated as functions of cell temperature, using sixth degree polynomial approximations, to more accurately reflect changes in cell characteristics with temperature. The coefficients in the cell characteristic equation were derived from basic cell V-I curves and are adjusted by a computer input to represent the percent efficient cells desired.

Correction coefficients are added to the above relation to account for various operating and loss factors, and uncertainties. These coefficients are as follows:

CDEG = Short Circuit Current Degradation Factor

and

VDEG = Voltage Degradation Factor

The degradation factors making up the above correction coefficients are listed in detail in Section 5.8.2.4 and are discussed in detail in Section 6.6.4.4.

The resulting cell current-voltage equation appears as:

$$I = CDEG (B) I_{sc} - \frac{V}{R_p} - I_o \left[e^{\frac{K(V + R_s I + V_{oc})(1 - VDEG)}{e}} - 1 \right]$$

where

V_{oc} = Open circuit voltage (also a sixth degree polynomial function of temperature).

The computer program also takes into account the voltage drop due to the blocking diode associated with each series string, and the effects of blocking diode temperature (assumed to be the same as solar panel temperature).

APPENDIX H

RADIATION EFFECTS ON SILICON SOLAR CELLS

H.1 INTRODUCTION

The general effect of energetic particles in solar cells is to cause disordering of the atoms in the crystal structure of the cells. The high efficiency silicon solar cell in use today is made from single crystal material and its energy conversion capability is very dependent on the highly ordered arrangement of the crystal lattice. The disordering caused by charged particles, such as that found in space, creates defects in the crystal lattice which in turn serve as trapping centers for the carriers (electrons or holes) created by the absorption of light energy. Thus, these carriers are absorbed in the solar cell and never appear as electrical output of the cell. The type of defect formed is very dependent upon the type and energy of the incident radiation causing the damage.

However, insofar as the effect on the electrical output of a cell is concerned, the damage caused by one type of monoenergetic particle (say 0.5 Mev electrons) differs from that caused by another type of monoenergetic particle (say 20 Mev protons) by a constant factor relating the total dose of each type of radiation that causes equal damage to the cell. This has been shown by experiments conducted in many laboratories (H. 6.1, H. 6.2). This implies that one can determine the flux of radiation of a given type and energy (here called the equivalent flux) that will cause the same damage to the electrical output of a cell as that due to a complex radiation environment. Also, for cell types that depend upon minority carrier diffusion for the majority of their power output, this equivalence can be established between different cell types. P/N and N/P silicon cells are of this type. An example of this is shown in Figure H-1. Here the effects of one Mev electrons in N/P cells (the actual data is given in Figure H-2) is multiplied by the specified constants and plotted over the effects of 0.5 Mev electrons in P/N cells.

These curves show the decrease in cell short circuit current and open circuit voltage. This cell data is representative of cell degradation under space sun illumination. The P/N data was taken under a carbon arc solar simulator (H. 6.1). The N/P data was derived by a

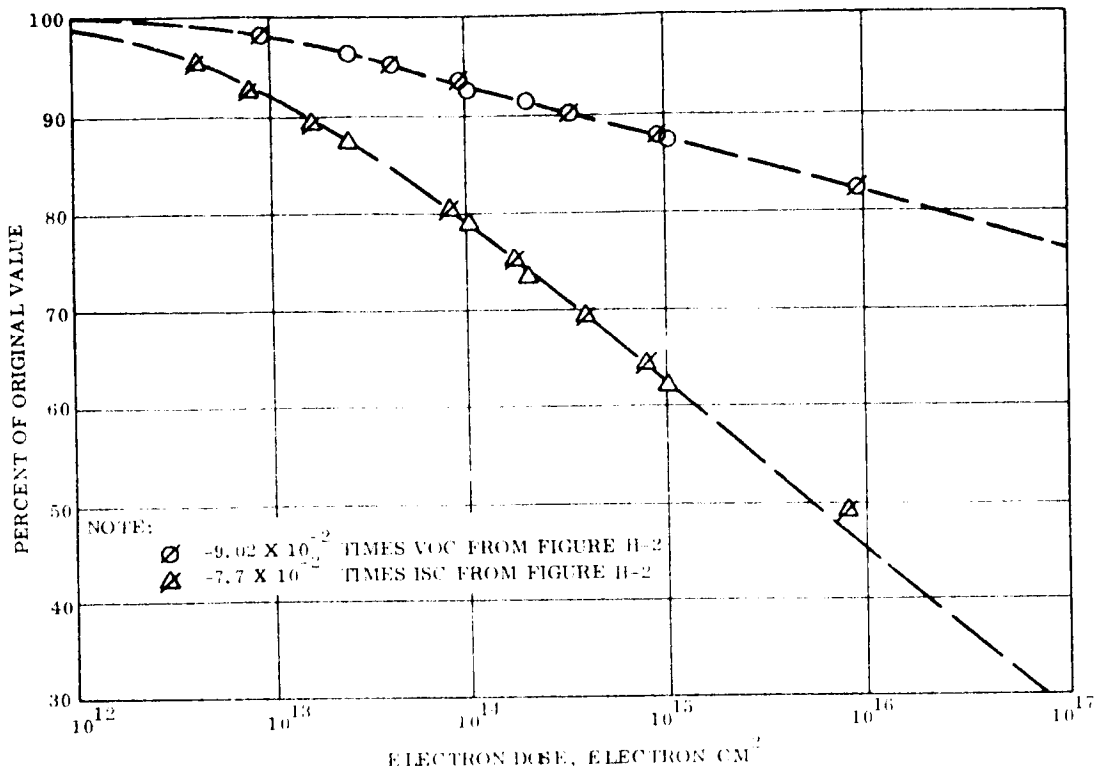


Figure H-1. P/N Solar Cell Characteristics Under 0.5 Mev Electrons

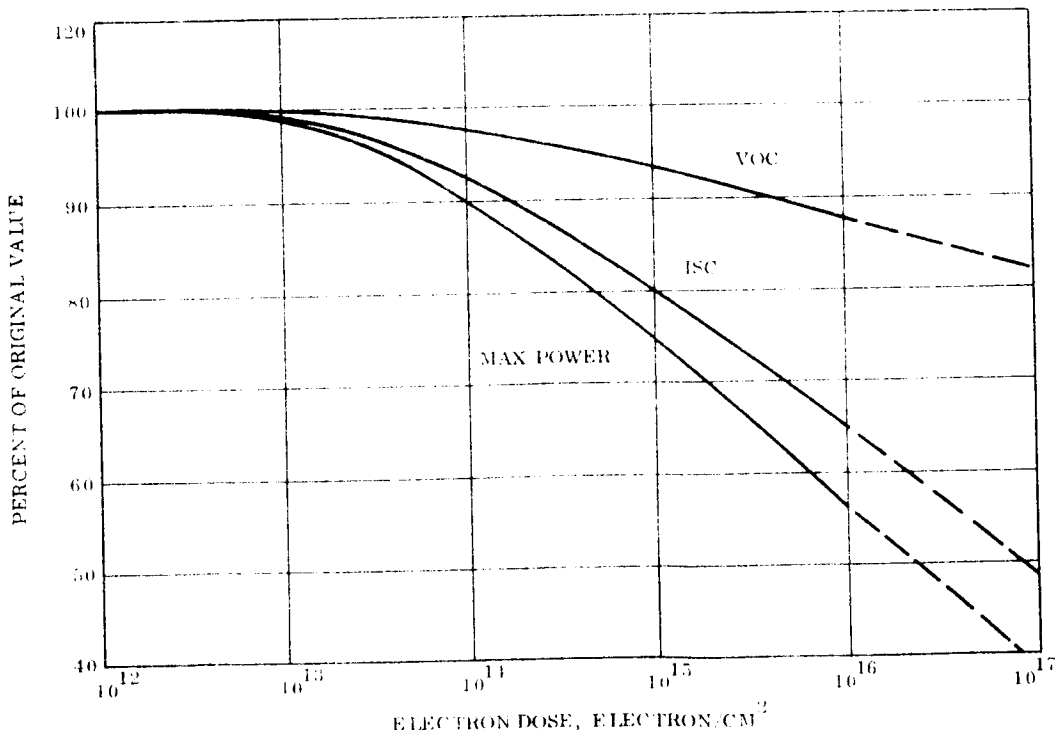


Figure H-2. N/P Solar Cell Characteristics Under 1.0 Mev Electrons

technique which is equivalent to solar illumination (H. 6. 2). This is a very important point to consider if one desires the absolute value of radiation flux for a given decrease in a cell electrical parameter when the cell is to be used in space. The silicon cell is a selective absorber of light energy. The power conversion capability of these cells for incident light in the wavelength region from ~ 0.7 to 1.1 microns is affected more so by the radiation encountered in space than the wavelength region below ~ 0.7 micron. Therefore, the degradation of the electrical output of the cell for a given dose of radiation will be dependent upon the type of light source used to illuminate it for power output measurements. For example, the radiation dose required to decrease the cell short circuit current by 25 percent under space illumination is approximately twice that required under 2800°K tungsten light (H. 6. 3). Therefore, in order to calculate the effects of radiation on satellite photovoltaic power systems, all laboratory measurements must ultimately be referred back to the measurement of the power output of the cell under space illumination.

It has further been shown by extensive laboratory work performed at General Electric (H. 6. 1) that the radiation effect on the voltage-current characteristic of a cell can be defined by a degradation of the cell short circuit current and open circuit voltage, at least for radiation doses up to where the cells are rendered useless for most applications. Therefore, the essence of the radiation effects due to a complex radiation environment on the electrical output of a solar cell of a given type is to calculate the equivalent flux of a reference radiation in some reference type cell. When this is done for both the short circuit current and open circuit voltage, the entire voltage-current characteristic can be defined. Here the equivalent flux is taken as 0.5 Mev electrons, the reference cell type is the standard P/N silicon cell, one ohm-cm, space efficiency > 9 percent. The effect of 0.5 Mev electrons on P/N silicon cells is shown in Figure H-1 for a cell temperature of 85°F . This is taken as the reference decay curve and all radiation effects data due to electrons and protons in P/N and N/P silicon cells is referred to this curve.

The effect of temperature on the damage rate is not considered here, mainly due to lack of data. Some work has been done at General Electric (H. 6. 1) on the damage rate of electrons in P/N cells as a function of temperature. This work indicates that over a temperature

range of $\pm 150^{\circ}\text{F}$, the equivalent fluxes would not vary more than ± 20 percent from that at 85°F . This variation would result in a very small error in the cell damage estimate.

H.2 DEFINITION OF EQUIVALENT FLUXES - N/P CELLS

The equivalent fluxes can be stated mathematically as follows:

$$\Phi_{\text{in}} = \int_t \int_E \phi_P(E, t) D_{\text{pin}}(E) dEdt + \int_t \int_E \phi_e(E, t) D_{\text{ein}}(E) dEdt \quad (1)$$

$$\Phi_{\text{vn}} = \int_t \int_E \phi_P(E, t) D_{\text{pvn}}(E) dEdt + \int_t \int_E \phi_e(E, t) D_{\text{evn}}(E) dEdt \quad (2)$$

where the foregoing symbols have the following meanings:

- D_{pin} = short circuit current proton damage constant
- D_{ein} = short circuit electron damage constant
- D_{pvn} = open circuit voltage proton damage constant
- D_{evn} = open circuit voltage electron damage constant
- Φ_{in} = short circuit current equivalent flux
- Φ_{vn} = open circuit voltage equivalent flux

The units of the equivalent fluxes are electrons (0.5 Mev)/cm²/unit time.

Once the equivalent fluxes are determined for each radiation component in the environment, the total is found by the summation of the components:

$$\Phi_{\text{i Total}} = \sum_j \Phi_{ij}$$

$$\Phi_{\text{v Total}} = \sum_j \Phi_{vj}$$

The damage is found by determining the decay of the short circuit current and open circuit voltage from Figure H-1, based on the total equivalent fluxes. It can further be shown that the maximum power point of the cell voltage-current curve is equal to: (H. 6. 1)

$$P = I^*V^*$$

where:

P = fraction of original power remaining

I* = fraction of original short circuit current remaining

V* = fraction of original open circuit voltage remaining

The damage constants defined above are experimentally-determined functions and are described in detail in Section H-3, below. The differential flux spectra are those incident perpendicular on the cell surface. When a shield material is used, the effect of this shield on the incident spectrum must be taken into account. Also, when the incident particle spectrum is isotropic, the effect of the isotropy must be considered.

H. 3 THE DAMAGE CONSTANTS

Specifically, the damage constants are defined as $\Phi_{yz} = D_{xyz}(E) \phi_x(E)$. That is, if $\phi_x(E)$ is the incident dose of radiation X of energy E on cell type Z and Φ_{yz} is the dose of 0.5 Mev electrons that will cause equal damage to cell parameter Y in P/N cells as $\phi_x(E)$ causes in cell parameter Y in cell type Z, then $D_{xyz}(E)$ is the ratio of these two fluxes. The following describes the damage constants for electrons and protons in N/P, 1 Ω -cm silicon cells. All temperatures are 85^oF.

H. 3.1 PROTONS

The damage constants for protons are based on the decrease of the minority carrier diffusion length (L) in the cell base region as a function of dose. This follows a well-established relation:

$$\frac{1}{L^2} = \frac{1}{L_0^2} + K \phi \text{ for monoenergetic particles.} \quad (3)$$

or

$$\frac{1}{L^2} = \frac{1}{L_o^2} + K(E) \phi(E) dE \text{ for a spectrum of energies.} \quad (4)$$

This relation holds as long as the fraction of the total collected current coming from the cell surface layer is negligible since the diffusion length, and therefore K, are determined by measuring the current output of the cell under electron bombardment. (H. 6. 4) The collection of carriers from the surface layer is not primarily by diffusion, but rather due to electric field considerations. The above relation holds for either electrons or protons.

For one Mev electrons in N/P cells the value of K is 1.7×10^{-10} ; (H. 6. 2) therefore,

$$\frac{1}{L^2} = \frac{1}{L_o^2} + 1.7 \times 10^{-10} \phi \quad (5)$$

where ϕ is the dose of 1 Mev electrons in electrons/cm².

Similarly, if the degradation of L is caused by a spectrum of protons, one can define an equivalent 1 Mev electron flux from Equation 5 as

$$\phi(1 \text{ mev}) \text{ eq} = \left[\frac{1}{L^2} - \frac{1}{L_o^2} \right] \times \frac{10^{10}}{1.7}$$

Using equation (4), this becomes

$$\phi(1 \text{ mev}) \text{ eq} = \frac{10^{10}}{1.7} \int K(E) \phi(E) dE \quad (6)$$

The utility of these relations is the well-known fact that cells with equal diffusion lengths will have the same output regardless of what type of radiation affected the diffusion length. Therefore, if the incident radiation is a spectrum of protons, Equation (6) will define an equivalent 1 Mev electron flux in N/P cells where K(E) is the proper function for protons

and $\phi(E)$ is the incident proton spectrum. The function $K(E)$ for protons in N/P cells is taken from Reference H. 6. 2 and is given in Figure H-3. This function is approximated by the following equations for the specified energy intervals:

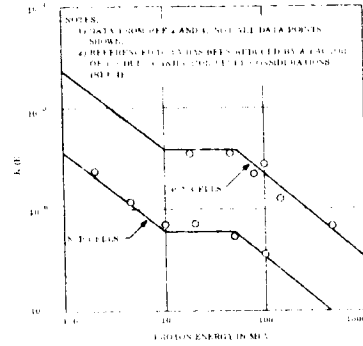


Figure H-3. Degradation Constants for Protons

$$K(E) = 3.53 \times 10^{-6}, E < 1 \text{ Mev} \quad (7)$$

$$K(E) = 3.53 \times 10^{-6}, E^{-0.778}, 1 < E < 10 \quad (8)$$

$$K(E) = 5.88 \times 10^{-7}, 10 < E < 50 \quad (9)$$

$$K(E) = 2.25 \times 10^{-5} E^{-0.914}, 50 < E \quad (10)$$

The value below one Mev is assumed constant since there is no data below this point. It is difficult to say how $K(E)$ would vary at these low energies since these particles are being absorbed in the first few microns of the cell surface. Recent experiments with low energy protons ($E < 1.0$ Mev) indicate that the open circuit voltage is more drastically affected than the short circuit current implying greater junction damage. This problem is somewhat lessened as long as there is some shield material on the cell surface. This would tend to harden the incident spectrum.

Equation 6 can be referred back to the reference decay curve by multiplying Equation 6 by the previously determined constants relating one Mev N/P data to the reference curve.

These are 0.077 for short circuit current and 0.0902 for open circuit voltage. Therefore, the desired damage constants as defined in Equations 1 and 2 are:

$$D_{pin} = 1.6 \times 10^3, E < 1 \text{ Mev} \quad (11)$$

$$= 1.6 \times 10^3 E^{-0.778}, 1 < E < 10$$

$$= 2.67 \times 10^2, 10 < E < 50$$

$$= 1.02 \times 10^4 E^{-0.914}, 50 < E$$

and

$$\begin{aligned}
 D_{pvn} &= 1.87 \times 10^3, E < 1 \\
 &= 1.87 \times 10^3 E^{-0.778}, 1 < E < 10 \\
 &= 3.12 \times 10^2, 10 < E < 50 \\
 &= 1.19 \times 10^4 E^{-0.914}, 50 < E
 \end{aligned}
 \tag{12}$$

H. 3.2 ELECTRONS

The electron damage constants D_{ein} and D_{evn} are derived in a similar fashion as the proton damage constants. Figure H-4 shows the electron damage function versus energy, normalized to one Mev. This data is obtained from References 5 and 6. The damage constants D_{ein} and D_{evn} are then obtained by referring this relative damage function back to the reference decay curves of Figure H-1 by multiplying this function by the constant 0.077 to obtain D_{ein} and by 0.0902 to obtain D_{evn} . The final values for D_{ein} and D_{evn} are shown in Figure H-5.

H. 4 SHIELDING EFFECTS

The previous section defined the damage rate in silicon solar cells in terms of the dose of radiation incident perpendicular to the cell surface. When one has shield material surrounding the solar cell, the change in the radiation spectrum as it passes through the shield and the effect of isotropy (as is

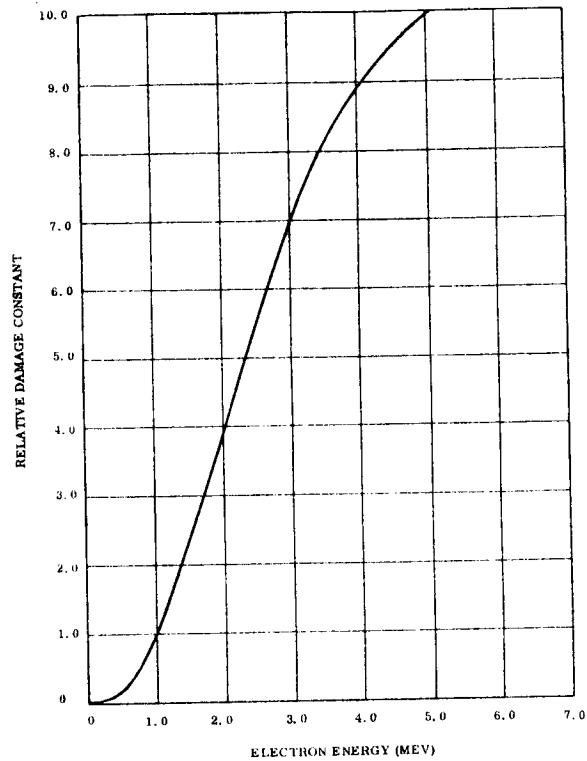


Figure H-4. Relative N/P Damage Constants - Electrons

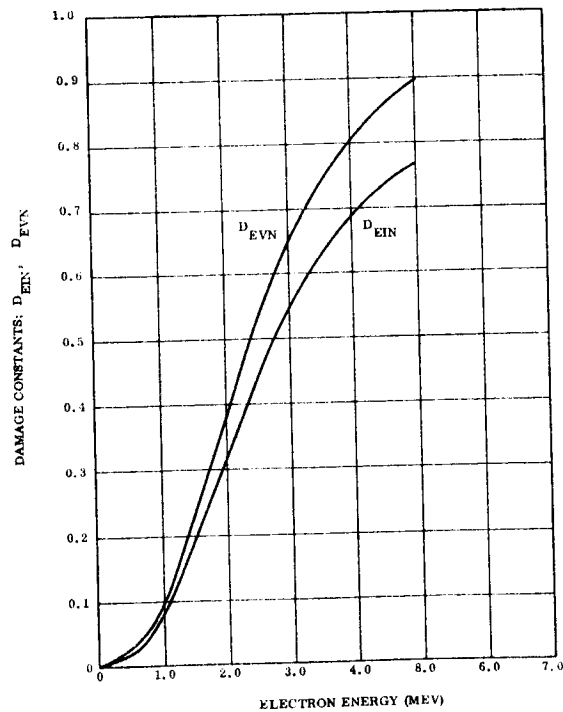


Figure H-5. N/P Damage Constants - Electrons

usually assumed for space radiation) must be properly taken into account in order to apply the previously derived equations. For a given incident isotropic spectrum, one must calculate an equivalent normal spectrum incident on the cell surface that would cause the same cell damage as the isotropic spectrum.

H. 4.1 ELECTRONS

Neglect, for the moment, the effect of isotropy and assume all particles are incident normal to the cell and shield. The residual spectrum of electrons that emerges from the under surface of the shield material can be estimated using range-energy data for aluminum. This method is only an approximate method and ignores the straggling effect of the electrons. However, for thin shields, the net effect of this will be quite small.

The range-energy data is taken from Katz and Penfold ^(H. 6.7). The range curve for energies less than several Mev can be defined by

$$R_o \text{ (gms/cm}^2\text{)} = 0.412 E_o^{1.4} \quad (13)$$

Now the residual range of an electron (i. e., its energy) after it traverses a given thickness of material is

$$R_r = R_o - R_s \quad (14)$$

where

R_r = residual range of the electron corresponding to its residual energy, E_r

R_o = initial range of the electron corresponding to its initial energy, E_o

R_s = thickness of shield in gms/cm²

When applying range-energy data to a continuous spectrum, it is convenient to work in a stepwise fashion. For instance, it is assumed that electrons having average intensity, ϕ_o ,

and average energy, E_o , within an energy interval, ΔE_o , will emerge (providing E_o is larger than the cutoff energy corresponding to R_s) from the other side of the material with intensity, ϕ_r , energy, E_r , and contained within the energy interval, ΔE_r .

Now assuming no absorption of these particles as they traverse the shield, then it follows that:

$$\phi_o \Delta E_o = \phi_r \Delta E_r \quad (15)$$

or

$$\phi_r = \phi_o \frac{dE_o}{dE_r} \quad (16)$$

where ϕ represents the electrons/cm²/Mev so that Equation 15 is the total electrons in the energy interval.

Using Equation 13 and 14, Equation 16 becomes

$$\phi_r = \phi_o \left[\frac{E_r}{E_o} \right]^{0.4} \quad (17)$$

Now the energy that a particle loses in traversing a thickness is

$$\begin{aligned} E_{\text{loss}} &= \int_{R_o - R_s}^{R_o} \left[\frac{dE}{dR} \right] dR \\ &= E_o - 1.885 \left[0.412 E_o^{1.4} - R_s \right]^{0.714} \end{aligned}$$

The residual energy is then

$$E_r = E_o - E_{\text{loss}} = E_o \left(1 - \frac{2.43 R_s}{E_o^{1.4}} \right)^{0.714} \quad (18)$$

Therefore, using Equations 17 and 18 in stepwise fashion from the maximum energy in the spectrum to the cutoff energy, one can calculate the residual spectrum for a shield thickness R_s , where

$$R_s = \rho T,$$

where

$$\rho = \text{gm/cc}$$

$$T = \text{thickness (cm)}$$

(19)

The cutoff energy for electrons is

$$E_c = 1.885 R_s^{0.714} \quad (20)$$

The above discussion does not take into account the effect of isotropy. Consider the diagram in Figure H-6. Here the number of electrons/cm²/sec/Mev incident on the shield and contained between the two cones of semi-aperture θ and $\theta + d\theta$ is equal to

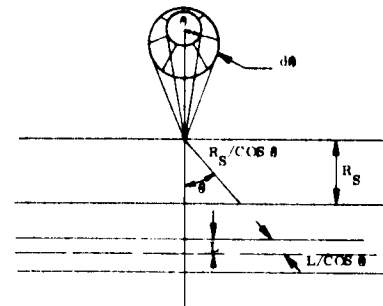


Figure H-6. Geometry for Isotropic Flux

$$\phi_o (E_o) \frac{d\omega}{2\pi}$$

where $d\omega = 2\pi \sin\theta d\theta$ is the solid angle and $\phi_0(E_0)$ is equal to 1/4 the total isotropic flux. The electrons contained in this cone will pass through a distance $R_s/\cos\theta$ in traveling through the shield. Therefore, the energy loss for these particles, using equation (18) is

$$E_r(\theta) = E_0 \left[1 - \frac{2.43R_s/\cos\theta}{E_0^{1.4}} \right]^{0.714} \quad (21)$$

Similarly, these same particles will enter the cell at the same angle θ , assuming the electron path has not deviated appreciably from a straight line. If the particle range, $R(E_r)$, after it passes through the shield is greater than the thickness of the active region of the cell, it will cause more damage than a normally incident particle of the same energy. If the damage is assumed to be proportional to the path length through the active region and this is assumed to be a thickness equal to bulk diffusion length, L , then a particle entering at an angle θ will cause $1/\cos\theta$ times more damage than a normally incident particle of the same energy.

However, the dose received at the cell surface in particles/cm²/sec is reduced to $\phi \cos\theta$ where ϕ is the particles/cm²/sec normal to the direction of the incident particles. Therefore, for particles whose residual range, $R(E_r)$, exceeds the path length through the cell, $L/\cos\theta$, for a given incidence angle, θ , the net effect in the cell is the same as particles entering normal to the cell surface having intensity, ϕ , and energy, E_r , since the damage is proportional to the surface dose times the path length. This has been shown experimentally using one Mev electrons where the cell damage was found to be independent of angle of incidence when the damage is referred to the incident beam intensity.

However, when the angle of incidence and the residual range are such that $R(E_r) < L/\cos\theta$, the damage becomes proportional to $\phi \cos\theta \times R(E_r)/L$ relative to a particle entering normal with range $R(E_r)$. Further, if the incident particles have a residual range which is less than L , the incident particles will have the same range in the cell independent of the angle of incidence. Therefore, the damage when referred to the cell surface dose should decrease with $\cos\theta$.

Based on the preceding remarks, an isotropy-damage function, $\sigma(E_r, \theta)$, can be defined which relates the cell damage for isotropic incidence to cell damage due to normal incidence. If $\phi(E_r, \theta)$ is the particle flux measured normal to the direction of the particle direction then the equivalent normal flux, $\Phi(E_r, \theta)$, which will cause the same cell damage is $\Phi(E_r, \theta) = \sigma(E_r, \theta)$, where $\sigma(E_r, \theta)$ is defined as follows:

$$\begin{aligned}
 R(E_r) < L, \sigma(E_r, \theta) &= \cos \theta \\
 R(E_r) < L/\cos \theta, \sigma(E_r, \theta) &= \frac{R(E_r)}{L} \cos \theta \\
 R(E_r) > L/\cos \theta, \sigma(E_r, \theta) &= 1.0
 \end{aligned}
 \tag{22}$$

The total equivalent - normal flux of energy, E_r , is then, using Equation (17)

$$\Phi(E_r) = \int_0^{\pi/2} \phi(E_o) \left(\frac{E_r}{E_o} \right)^{0.4} \sigma(E_r, \theta) \sin \theta \, d\theta
 \tag{23}$$

Further, letting $\mu = \cos \theta$, $d\mu = -\sin \theta \, d\theta$, and using Equation (21),

$$\Phi(E_r) = \int_0^1 \phi(E_o) \left[\frac{E_r}{\left(E_r^{1.4} + \frac{2.43R_s}{\mu} \right)^{0.714}} \right]^{0.4} \sigma(E_r, \mu) \, d\mu
 \tag{24}$$

where $\sigma(E_r, \mu)$ is:

$$\begin{aligned}
 R(E_r) < L, \sigma &= \mu \\
 R(E_r) < L/\mu, \sigma &= \left(\frac{R(E_r)}{L} \right) \mu \\
 R(E_r) > L/\mu &= 1.0
 \end{aligned}
 \tag{25}$$

If it is also assumed that the environment $\phi(E_o)$ can be defined by a number of line segments of the form $\phi(E_o) = G E_o^{-H}$, where G and H are constants over a specified interval of E_o , then using Equation 21 to define E_o as a function of E_r , Equation 24 becomes

$$\Phi(E_r) = \int_0^1 \frac{G E_r^{0.4} (E_r, \mu) d\mu}{\left(E_r^{1.4} + \frac{2.34R}{\mu} \right)^{0.714 (H + 0.4)}} \quad (26)$$

and $\sigma(E_r, \mu)$ is defined by Equation 25 for each value of E_r and μ .

4.4.2 PROTONS

Identical considerations are used to calculate the equivalent-normal residual proton spectrum as was used for the electrons. The range-energy data is taken from Reference H.6.8. This is approximated by:

$$R \text{ (gm/cm}^2\text{)} = 0.00334 E^{1.73}, \quad E = \text{mev} \quad (27)$$

The resultant equivalent-normal residual proton spectrum is

$$\Phi(E_r) = \int_0^1 \frac{G_p E_r^{0.73} \sigma(E_r, \mu) d\mu}{\left(E_r^{1.73} + \frac{300R}{\mu} \right)^{0.578 (H_p + 0.73)}} \quad (28)$$

Here $\sigma(E_r, \mu)$ has the same definition as given by Equation 25 except the range, $R(E_r)$, now applies to protons in silicon, which is calculated in the same units as the diffusion length, L .

The differential proton spectrum is also assumed to be defined as,

$$\phi_p(E_o) = G_p E_o^{-H_p}, \quad \text{where } G_p \text{ and } H_p \text{ are constants.}$$

Both the electron and proton differential spectra are defined in particles/cm²/Mev/unit-time and represent the dose received per unit time on one side of a flat surface. Therefore, these spectra are equal to 1/4 the total intensity of the isotropic spectra. The equations give the value of flux for a given value of E_r. By repetitively applying these equations for different values of E_r, one can calculate as many points as desired on the residual spectrum for a given shield thickness. The residual spectra, so determined, are then used in Equations 1 and 2 to determine the equivalent fluxes for a particular front shield thickness. The equivalent fluxes are then used in conjunction with Figure H-1 to determine the amount of degradation. For cases where the flux entering the back side of the solar cells must also be considered, the same calculational procedures as above are used in conjunction with the appropriate backside shielding to determine the equivalent fluxes due to backside irradiation. These then are added to the front side equivalent flux on the cells.

H. 5 SOLAR CELL DAMAGE ESTIMATES

The above analytical procedures have been programmed for computer analysis. Utilizing this program and the radiation environment estimates given previously, the N/P, one ohm-cm, silicon solar cell degradation expected at the end of the two-year mission has been determined. These results are shown in Figure H-7 as a function of front shield thickness. The backside shielding for the cells in all cases is taken as 0.3 gm/cm².

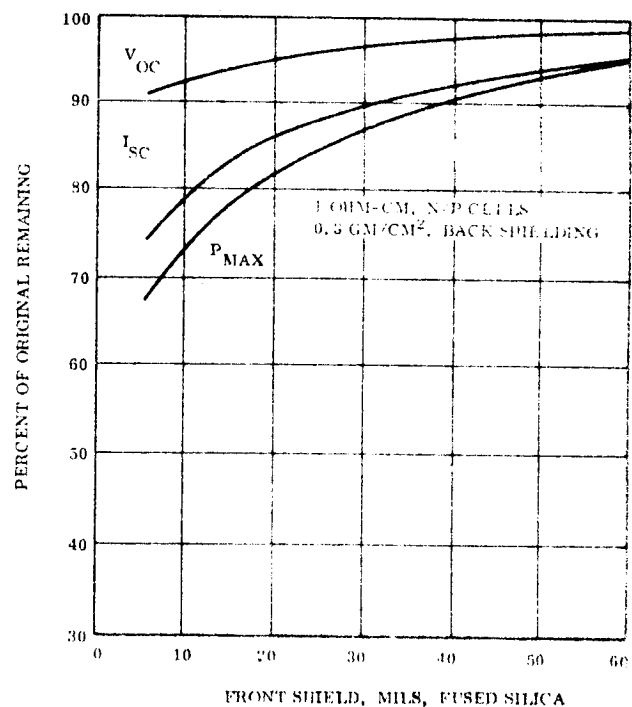


Figure H-7. Solar Cell Degradation After Two Years

H.6 REFERENCES

- H.6.1 Bobone, R., Merchant, B.W., Predicting Damage to Silicon Solar Cells Subject to Complex Radiation Spectra, General Electric Company, AIEE Conference Paper CP-62-1279, AIEE Conference - Denver 1962.
- H.6.2 Smits, F.M. The Degradation of Solar Cells Under Van Allen Radiation, IEEE Transactions on Nuclear Science, Volume NS-10, No. 1, Jan. 1963
- H.6.3 Denny, J.M., Downing, R.G. Charged Particle Radiation Damage in Semiconductors, I: Experimental Proton Irradiation of Solar Cells, Space Technology Laboratories, Inc., Doc. No. 8987-001-RU-000, Sept. 15, 1961
- H.6.4 Smits, F.M. et al, Report of Solar Cell Work at Bell Telephone Laboratories, Proceedings of the Solar Working Group Conference, Interagency Advanced Power Group, PIC-SOL 209/2, Vol. I, April, 1962
- H.6.5 Rosenzweig, W. Radiation Damage Effects, IEEE Photovoltaic Specialists Conference Washington, D.C., April 10-11, 1963
- H.6.6 Cooley, W., and Janda, R. Handbook of Space Radiation Effects on Solar Cell Power Systems, NASA SP-3003, 1963.
- H.6.7 Katz and Penfold, Rev. Mod. Phys., 24, 28 (1952).
- H.6.8 Sternheimer, R.M. Phys. Rev., 115, 137 (1959).

APPENDIX I

BASIC DESIGN DATA FOR SUBSYSTEM COMPARISON

Power conditioning equipment consists of all components required to control the primary and secondary energy sources and to assure that load regulation requirements are satisfied. Components required to perform this function are battery charge regulator, voltage regulators, converters, and inverters. Details of these components such as efficiency and size, are required for a thorough power system tradeoff study of various power system configurations. The effort in this section is to justify the efficiencies used in the analysis of power systems since the efficiency of each component is critical to the size of array and battery.

The conditions for efficiency calculations are identified for each component. The general conditions that apply to all the components under review are:

- a. Components considered are either representative of series dissipative elements or series switching (nondissipative) elements. For a dissipative element, the efficiency is determined as in (b) of this paragraph. For a nondissipative element, the following (b-e of this paragraph) is applied in the component configurations under review.
- b. Rectifiers are silicon diodes having a forward drop of 0.8 volt at the required load current.

The drive efficiency is respectively

$$\left(\frac{V_{\text{out}} - 0.8}{V_{\text{out}}} \right), \text{ and if } V_{\text{out}} = 28 \text{ vdc, then the diode efficiency is approximately } 0.97.$$

- c. Power switches are transistors with a minimum switch gain of $I_c/I_b = 10$ operating from 2000 to 8000 Hz, and saturation voltage drop is 0.5 volt. The losses of a transistor switch are summarized:
 1. Static losses - 0.50 of 0.96 of transistor power output
 2. Switch losses - 0.50 of 0.96 of transistor power output
 3. Drive losses - 1.0 of 0.02 of transistor power output

Therefore, total transistor losses are 0.94 of transistor power output.

- d. Filter and transformer efficiencies are design requirements for those parts. A plus one-percent tolerance may be used without greatly increasing total weight. However, for this analysis, no tolerance is placed on the efficiency number.
- e. Total component efficiency is based on full load design point and minimum input-output voltage difference in order to satisfy the output voltage requirements. Efficiency changes with load are shown in Figure I-1. Efficiency changes as a function of input voltage changes are about 0.4 percent per volt above the minimum input voltage.

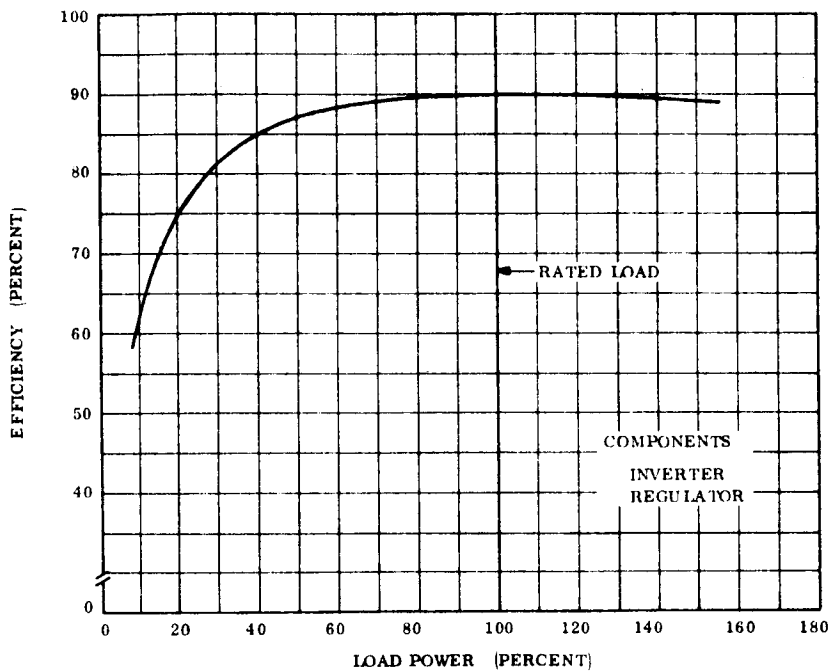


Figure I-1. Load Effects on Efficiency

I.1 BATTERY CHARGE REGULATOR

The battery charge regulator considered for this application is a constant charge current regulator. A series dissipative method was selected; therefore, its efficiency is determined by the input voltage to the regulator and the battery charge voltage. This ratio is the efficiency as identified above (paragraph b).

If input voltage is 41 volts (solar array maximum power voltage at end of life) and the battery charge voltage is 37 to 39 volts, then the efficiency range is 0.95 to 0.90.

For a series nondissipative regulator, the efficiencies used for the PWM regulator apply (paragraph I. 2a. of this appendix).

I. 2 REGULATORS

- a. PWM Buck Regulator - A PWM buck regulator is a switching regulator that periodically interrupts the input voltage through a power switch such that the output voltage is always less than the input voltage. The pulsed output voltage is averaged by a low pass filter. A representative block diagram of a PWM regulator is shown in Figure I-2. The efficiency is the ratio of output power, (P_{out}), to input power, (P_{in}).

$$\eta = \frac{P_{out}}{P_{in}}$$

$$P_{in} = \frac{P_s + 0.025 P_s}{(0.99)}$$

$$P_s = \frac{P_{out}}{(0.96)(0.97)}$$

$$P_{in} = \frac{P_{out}(1.025)}{(0.99)(0.96)(0.97)}$$

$$\frac{P_{out}}{P_{in}} = \frac{(0.99)(0.96)(0.97)}{1.025}$$

$$\eta = \frac{P_{out}}{P_{in}} = 0.90$$

- b. PWM Boost Regulator - A PWM boost regulator is a switching regulator that periodically adds voltage pulses to the input voltage such that the output voltage is always greater than the input for normal operation. The pulsed output voltage is averaged by a low pass filter. Since the voltage pulses are add-on voltages to the input voltage, the power transferred by the power switch and transformer to the output filter is proportioned to the input-output voltage difference. Therefore, the size of power switch, transformer, and filter are relatively small when compared with a PWM buck regulator, because all the power must be transferred and filtered in the PWM buck regulator. A representative block diagram of a PWM boost regulator is shown in Figure I-3. The efficiency is:

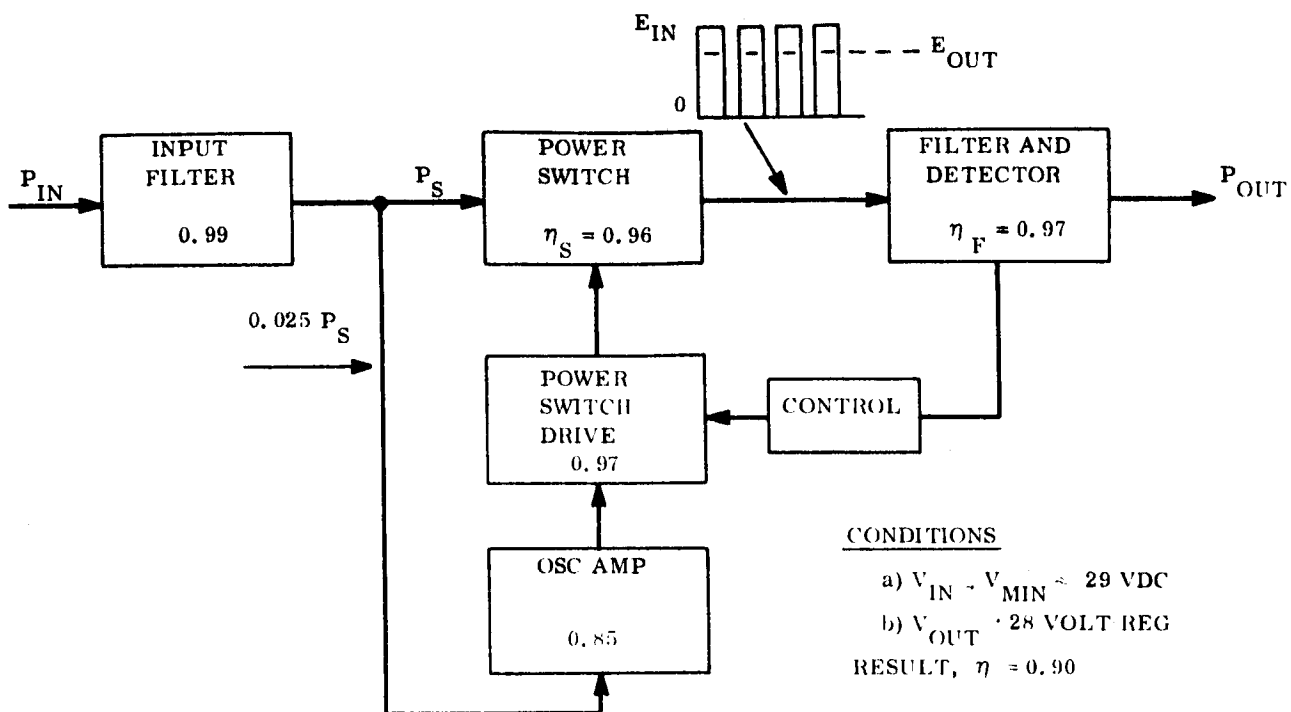


Figure I-2. Efficiency Block Diagram - PWM Buck Regulator

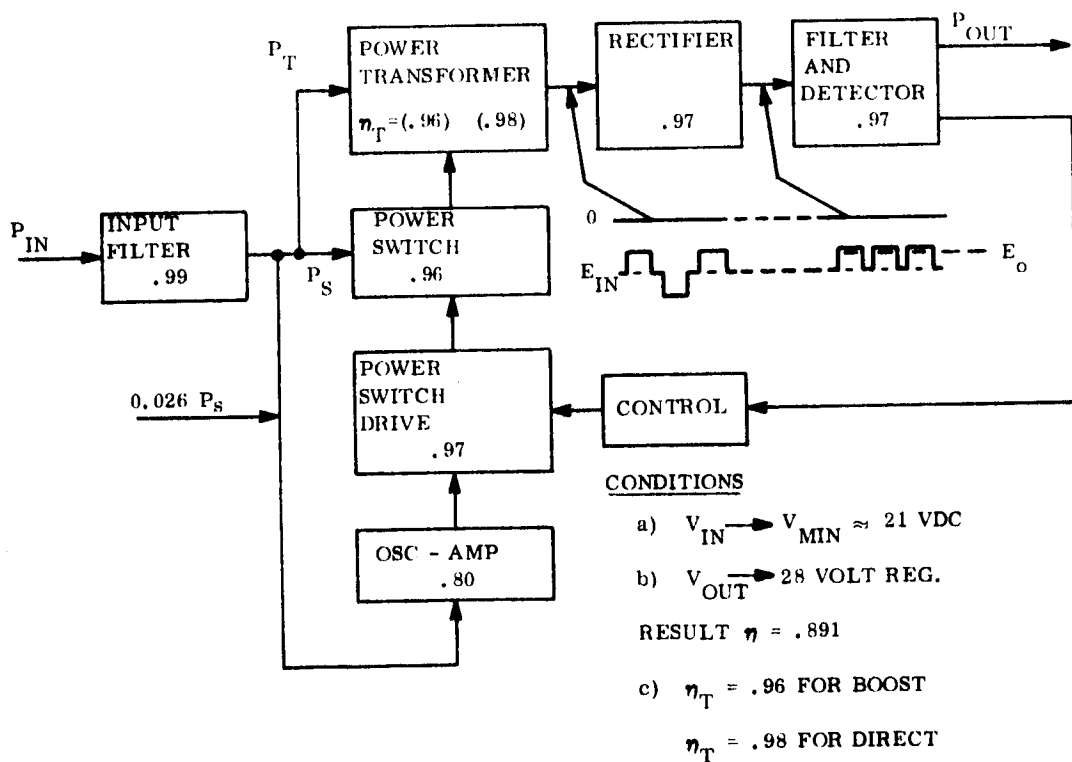


Figure I-3. Efficiency Block Diagram - PWM Boost Regulator

$$\eta = \frac{P_{out}}{P_{in}}$$

$$P_{in} = \frac{P_T + P_S + P_S (0.026)}{(0.99)} = \frac{P_T + P_S (1.026)}{0.99}$$

$$P_T = \frac{P_{out}}{(0.97)(0.97)(0.98)} \times \frac{V_{in}}{V_{out}}$$

$$P_S = \frac{P_{out}}{(0.97)(0.97)(0.96)(0.96)} \times \frac{V_{out} - V_{in}}{V_{out}}$$

$$V_{in} = 21 \text{ volts}$$

$$V_{out} = 28 \text{ volts}$$

$$\therefore \frac{V_{in}}{V_{out}} = 0.75 \text{ and } \frac{V_{out} - V_{in}}{V_{out}} = 0.25$$

$$\begin{aligned} P_T + P_S (1.026) &= P_{out} \left[\frac{0.75}{(0.97)(0.97)(0.98)} + \frac{(1.026)(0.25)}{(0.97)(0.97)(0.96)(0.96)} \right] \\ &= P_{out} (0.814 + 0.296) = P_{out} (1.110) \end{aligned}$$

$$\eta = \frac{P_{out}}{P_{in}} = \frac{0.99}{1.11} = 0.891$$

$$\eta = 0.891$$

I.3 Dc-Dc CONVERTER

A dc-dc converter generates a square wave ac voltage which is transformer coupled at any desired voltage (or multiple voltages) to rectifiers and low pass filter. The filter requirements are minimum since a square wave ac voltage requires filter energy storage only during the short period where both transistors are off and no power is

transferred to the filter. For this reason, the filter efficiency is higher than for the PWM regulators.

If regulation of the output is required, only one output is considered for having a close regulation for dc-dc converter/regulator. Direct regulation may be provided in this configuration through PWM methods similar to those previously discussed in I. 2a except that all power is transferred through a transformer and rectifiers. A representative block diagram of a dc-dc converter is shown in Figure I-4. The efficiency is determined by,

$$\eta = \frac{P_{out}}{P_{in}}$$

$$P_{in} = \frac{P_s + 0.025 P_s}{(0.99)} = \frac{P_s (1.025)}{(0.99)}$$

$$P_s = \frac{P_{out}}{(0.98)(0.97)(0.96)(0.96)}$$

$$P_{in} = \frac{P_{out} (1.025)}{(0.99)(0.98)(0.97)(0.96)(0.96)}$$

$$\eta = \frac{P_{out}}{P_{in}} = 0.847$$

Note: For output voltage less than 28 volts, the rectifier efficiency must be modified according to the general conditions of I. 3b in this appendix).

I. 4 Dc-Ac INVERTER

A dc-ac inverter generates a square wave and applies it to a filter tuned to the operating frequency so that the square wave is converted to a sine wave. If square wave power distribution is acceptable, then the filters may be deleted with a corresponding increase in efficiency. A representative block diagram of a dc-ac inverter is shown in Figure I-5.

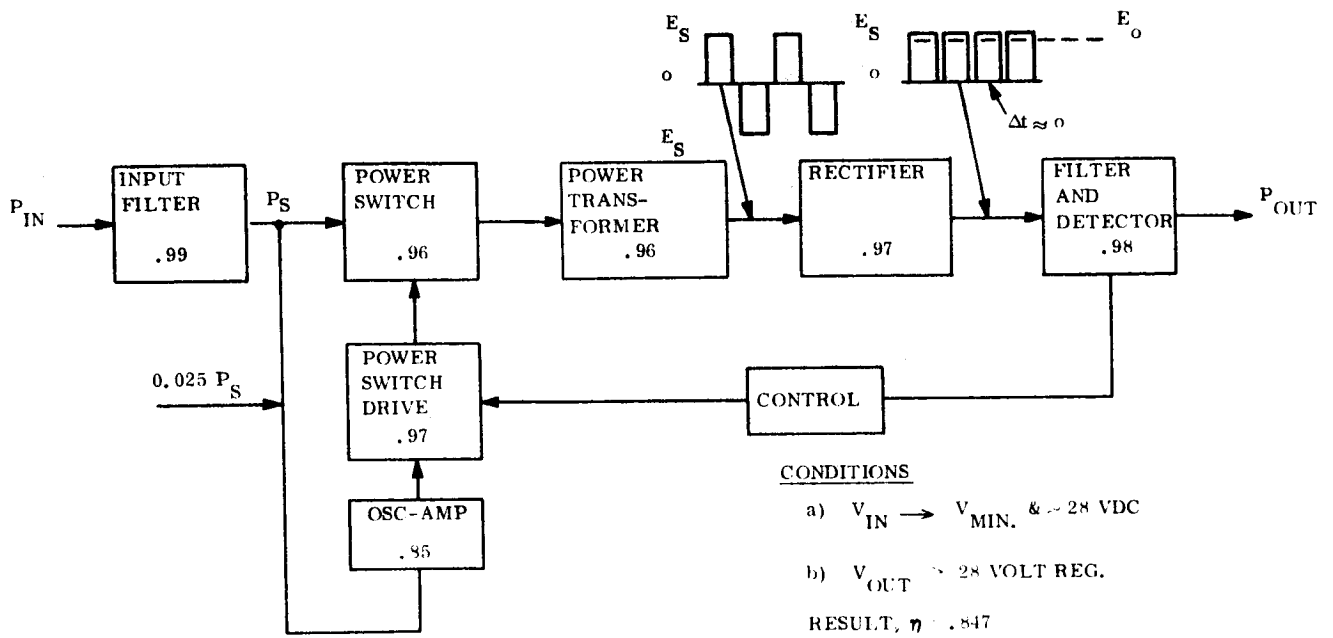


Figure I-4. Efficiency Block Diagram - Dc - Dc Converter/Regulator

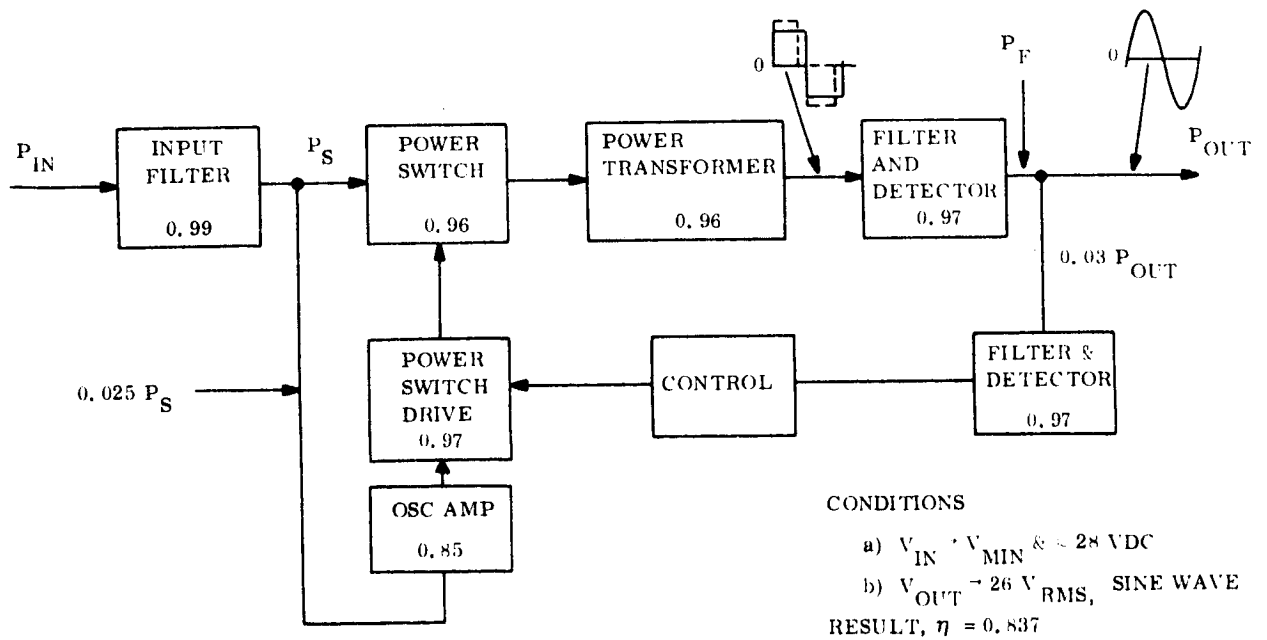


Figure I-5. Efficiency Block Diagram - Dc - Ac Inverter/Regulator

If regulation is provided, then the wave shape into the filter is represented by the dashed line. The efficiency is determined by,

$$\eta = \frac{P_{out}}{P_{in}}$$

$$P_F = P_{out} + 0.03 P_{out} = P_{out} (1.03)$$

$$P_S = \frac{P_F}{(0.97)(0.96)(0.96)}$$

$$P_S = \frac{P_{out} (1.03)}{(0.97)(0.96)(0.96)}$$

$$P_{in} = \frac{P_S + 0.025 P_S}{0.99} = \frac{P_S (1.025)}{0.99}$$

$$P_{in} = \frac{P_{out} (1.03)(1.025)}{(0.99)(0.97)(0.96)(0.96)}$$

$$\eta = \frac{P_{out}}{P_{in}} = 0.837$$

For an ac distribution providing a square wave, the efficiency is,

$$P_{in} = \frac{P_{out} (1.025)}{(0.99)(0.96)(0.96)}$$

$$\eta = 0.890$$

All the above derived efficiencies are tabulated in Table I-1. These base efficiencies are corrected for load variations by use of Figure I-1 and for input voltage variation by 0.4 percent per volt above the minimum. Therefore, the losses may be identified in a power conditioning component for type of component, percent of rated load and input voltage.

Table I-1. Component Efficiency Summary

Component	Efficiency (%)
Regulator, PWM Buck	90.0
Regulator, PWM Boost	89.1
Dc-Dc Converter	84.7
Dc-Ac Inverter, Sine wave	83.7
Dc-Ac Inverter, Square wave	89.0

APPENDIX J

COUPLING OF STRUCTURAL FLEXIBILITY WITH A CONTROL SYSTEM FEEDBACK LOOP

J. 1 INTRODUCTION

Any structural system when acted upon by forces whose rates of variation are the same order as the natural frequencies of the system will respond in both its unconstrained rigid body motion and flexible body motions. Both components of motion can be defined in terms of the applied force. The total motion of any point can be most conveniently determined as the linear superposition of the rigid body motions and the various components of flexible body motion defined by the normal modes of the system.

In the case of the control system incorporated in the ATS-4 structural system it is necessary to consider the flexible (or vibratory) motions of the system in the feedback loop. This appendix discusses the manner in which the structural transfer functions are obtained and the form in which they are incorporated into the control system loop.

J. 2 THE STRUCTURAL SYSTEM

Consider any general linear structural system. Its dynamic equations of motion can be written in matrix form as

$$M\ddot{q} + C\dot{q} + Kq = F(t) \quad (1)$$

where

- M = a matrix of inertias
- C = a matrix of damping coefficients
- K = a matrix of stiffness coefficients
- q = a vector of generalized coordinates
- F(t) = externally applied forces as functions of time

The dots indicate differentiation with respect to time.

The modal equation is

$$M\ddot{q} + Kq = 0$$

$$(M\omega^2 - K)q = 0$$

$$Mq\lambda = Kq \tag{2}$$

where $\lambda = \omega^2$, the eigenvalue

Each solution of Equation (2) for an eigenvalue which satisfies the equation will impose a shape defined by a specific relation between the q's. These are the eigenvectors.

The displacements, q, can be represented by a linear combination of the eigenvectors.

$$q = \phi \xi \tag{3}$$

where ϕ = a rectangular matrix of eigenvectors

ξ = a column vector of modal displacements

Substituting Equation (3) into Equation (1) and premultiplying by ϕ^T , the transpose of ϕ yields

$$\phi^T M \phi \ddot{\xi} + \phi^T C \phi \dot{\xi} + \phi^T K \phi \xi = \phi^T F(t) \tag{4}$$

or

$$M^* \ddot{\xi} + C^* \dot{\xi} + K^* \xi = F^* \tag{5}$$

where

$M^* = \phi^T M \phi$ = a diagonal matrix of generalized masses
(usually normalized to a unit matrix)

$C^* = \phi^T C \phi$ = a diagonal matrix of modal damping (coefficient
to be taken as $2\zeta\sqrt{\lambda_r} = 2\zeta\omega_r$ where ζ is the
fraction of critical damping in the rth mode

$$\begin{aligned}
 K^* &= \phi^T K \phi && = \text{a diagonal matrix of modal stiffness (a diagonal} \\
 &&& \text{matrix of } \lambda \text{ when } M^* \text{ is normalized to unity)} \\
 F^* &= \phi^T F(t) && = \text{the modal forcing function, a vector}
 \end{aligned}$$

The diagonal form of M^* and K^* follow from the property that the eigenvectors satisfy orthogonality relations.

Equation (5) then is a linear set of independent equations in ζ and can be easily solved. For example the equation of the r^{th} mode is

$$\ddot{\xi}_r + 2\zeta_r \omega_r \dot{\xi}_r + \omega_r^2 \xi_r = \phi_r^T F(t) = F_r^* \quad (6)$$

$$\omega_r = \sqrt{\lambda_r}$$

$$\phi_r^T = \text{the } r^{\text{th}} \text{ row of } \phi^T$$

$$\zeta_r = \text{the fraction of critical damping in } r^{\text{th}} \text{ mode}$$

$$F_r^* = \text{is of the form}$$

$$\left[F_r^* = \sum_{i=1}^n V_{ir} F(t)_i \right]$$

where V_{ir} is the i^{th} element of the r^{th} row of ϕ^T and $F(t)_i$ is the force at the i^{th} coordinate of the system

For an impulse, F_r^* (which may be the sum of impulses at several coordinates) the Laplace transform of Equation (6) is

$$\xi_r(s) = \frac{F_r^*}{s^2 + 2\zeta_r \omega_r s + \omega_r^2} \quad (7)$$

the velocity is

$$\dot{\xi}_r(s) = \frac{F_r^* s}{s^2 + 2\zeta_r \omega_r s + \omega_r^2} \quad (8)$$

and the acceleration is

$$\ddot{\xi}_r(s) = \frac{F_r^* s^2}{s^2 + 2\zeta_r \omega_r s + \omega_r^2} \quad (9)$$

The corresponding physical coordinates and velocities are

$$q_r(s) = \phi_r \xi_r(s) = \phi_r \frac{F_r^*}{s^2 + 2\zeta_r \omega_r s + \omega_r^2}$$

or

$$q_{ir}(s) = V_{ir} \xi_r(s) = V_{ir} \frac{F_r^*}{s^2 + 2\zeta_r \omega_r s + \omega_r^2}$$

and

$$\dot{q}_r(s) = \phi_r \dot{\xi}_r(s) = \phi_r \frac{F_r^* s}{s^2 + 2\zeta_r \omega_r s + \omega_r^2}$$

$$\dot{q}_{ir}(s) = V_{ir} \dot{\xi}_r(s) = V_{ir} \frac{F_r^* s}{s^2 + 2\zeta_r \omega_r s + \omega_r^2} \quad (10)$$

$q_r(s)$ and $\dot{q}_r(s)$ are vectors of the displacements and velocities of the r^{th} modal component of response.

$q_{ir}(s)$ and $\dot{q}_{ir}(s)$ are the i^{th} displacement and velocity of the r^{th} modal component of response.

V_{ir} is the i^{th} term of the r^{th} column of ϕ .

ϕ_r is the r^{th} column of ϕ .

Thus, the total physical displacements and velocities are

$$\begin{aligned}
 \mathbf{q}(s) &= \phi \xi(s) = \sum_{r=1}^n \phi_r \xi_r(s) \\
 \dot{\mathbf{q}}(s) &= \phi \dot{\xi}(s) = \sum_{r=1}^n \phi_r \dot{\xi}_r(s)
 \end{aligned}
 \tag{11}$$

$\mathbf{q}(s)$ and $\dot{\mathbf{q}}(s)$ are vectors. If only the i^{th} coordinates are of interest, equation (11) can be written

$$\begin{aligned}
 q_i(s) &= \sum_{r=1}^n V_{ir} \xi_r(s) \\
 \dot{q}_i(s) &= \sum_{r=1}^n V_{ir} \dot{\xi}_r(s)
 \end{aligned}
 \tag{12}$$

The form of the equation shown in Equation 12 is used for the control loop problem where it is convenient to provide a transfer function for each input force (or moment) in each mode and sum the modal transfer functions in the control loop. In this event each individual transfer function is of the form

$$\begin{aligned}
 q_{ir}(s) &= \frac{A_{ir}}{s^2 + 2\zeta\omega_r s + \omega_r^2} F_i(t) \\
 \dot{q}_{ir}(s) &= \frac{A_{ir}s}{s^2 + 2\zeta\omega_r s + \omega_r^2} F_i(t)
 \end{aligned}
 \tag{13}$$

APPENDIX K

CONING CONTROL

K.1 INTRODUCTION

A portion of the ATS-4 flight requires the spacecraft to be spin-stabilized.

After boost phase of flight, the spacecraft will be spun up about its minor axis and allowed to coast prior to thrusting by the apogee motor. Since the spacecraft is spinning about its minor axis any loss in kinetic energy will produce an increase in cone angle of the spinning spacecraft about the momentum vector.

It is important to know the total growth in cone angle before thrusting if no active control system is to be used and the time constant (rate of change of cone angle with respect to time) if an active control system is used.

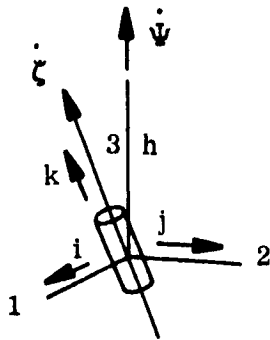
W. T. Thomson, in his book, Introduction to Space Dynamics treats this problem in Section 7.6 pp 212-218. Unfortunately, his example problem does not fit usual spacecraft models.

This report starts with Thomson's work and carries it into the model coordinate description of a structural dynamic system.

The resulting equations are solved for an idealized ATS-4 spacecraft to determine the rate of increase of cone angle.

K.2 THOMSON'S EQUATIONS

Following is a sketch of the coordinate system for an axisymmetric body spinning about its minor axis. Principal axes are 1, 2, 3 with moments of inertia A, A, C respectively. The moment free motion is a steady precession of the spin axis at a constant angle θ about the angular momentum vector(h) which is fixed in space.



For this motion, Thomson presents the following equations:

$$\dot{\psi} = \frac{C \dot{\phi}}{(A-C) \cos \theta} = \frac{C}{A} \frac{\omega_3}{\cos \theta} \quad (1)$$

$$\omega_3 = \dot{\phi} + \dot{\psi} \cos \theta$$

which describe the steady precession for moment free motion of the axisymmetric body.

Next, from the equations for angular momentum (h) and the kinetic energy of rotation (T) he determines the time rate of change

$$\dot{T} = \frac{h^2}{C} \left(\frac{C}{A} - 1 \right) (\sin \theta \cos \theta) \dot{\theta} \quad (2)$$

of the kinetic energy (\dot{T}) as a function of the time rate of change of the cone angle ($\dot{\theta}$). This energy change is produced by dissipation of energy due to damping in the structural dynamic system.

K. 3 ENERGY DISSIPATED PER CYCLE

The work done per cycle in a system under harmonic motion is (Ref. Den Hartog, Mechanical Vibrations):

$$W = \pi \bar{F} \bar{X} \sin a$$

where

W = work

\bar{F} is the force amplitude

\bar{X} is the displacement amplitude

a is the phase angle between the force and displacement.

Let

$$\bar{X}_Q = \bar{X} \sin a$$

Then

$$W = \pi \bar{F} \bar{X}_Q \quad (3)$$

The work done per cycle can be determined once the force amplitude (\bar{F}) and the quadrature displacement amplitude (\bar{X}_Q) are known.

K.4 SOLUTION FOR DISPLACEMENT AMPLITUDE \bar{X}_Q

The matrix equation for a structural dynamic system, including viscous damping, under harmonic motion is

$$(K + i\omega C - \omega^2 M) \bar{X} = \bar{F} \quad (4)$$

where

K is stiffness matrix

C is damping matrix

M is mass matrix

ω is circular forcing frequency

\bar{X} is vector of complex displacement amplitude

\bar{F} is vector of real force amplitude

A more convenient form of this equation can be had by transforming into modal coordinates. The transformation is obtained from the following equations:

$$K \bar{X} = M \bar{X} \lambda \quad (5)$$

$$\bar{X}^T K \bar{X} = \bar{X}^T M \bar{X} \lambda = I \lambda = \lambda$$

where

\bar{X} is the matrix of mode shapes

λ is a diagonal matrix of the modal circular frequencies squared

I is an identity matrix.

The transformation of Equation (4) to modal coordinates is accomplished by substituting:

$$\bar{X} = \bar{X} \bar{\xi} \quad (6)$$

where

$\bar{\xi}$ is vector of modal displacement amplitudes into the equation and premultiplying both sides of the equation by the transpose of matrix of mode shapes (\bar{X}^T).

That is:

$$\bar{X}^T (K + i\omega C^* - \omega^2 M) \bar{X} \bar{\xi} = \bar{X}^T \bar{F}$$

and

$$(\lambda + i\omega C^* - \omega^2 I) \bar{\xi} = \bar{X}^T \bar{F} \quad (7)$$

where

$$C^* = \bar{X}^T C \bar{X}$$

Under the assumption of modal damping, the C^* matrix is a diagonal matrix which completes the uncoupling of the equations and results in a system in "n" single degree of freedom equations of the form:

$$(\lambda_i + i\omega c_i - \omega^2) \bar{\xi}_i = \bar{X}_i^T \bar{F}. \quad (8)$$

Recognizing the complex amplitude $\bar{\xi}_i$, Equation (8) can be written as:

$$\begin{bmatrix} (\lambda_i - \omega^2) & i\omega c_i \\ i\omega c_i & (\lambda_i - \omega^2) \end{bmatrix} \begin{bmatrix} \xi_{r_i} \\ i\xi_{qi} \end{bmatrix} = \begin{bmatrix} \bar{X}_i^T \bar{F} \\ 0 \end{bmatrix} \quad (9)$$

which states the relationship of the real and quadrature components of the displacement to the force.

Solving Equation (9) for the quadrature component of the displacement yields:

$$\bar{\xi}_{qi} = \frac{-\omega c_i}{(\lambda_i - \omega^2)^2 + (\omega c_i)^2} \bar{X}_i^T \bar{F}. \quad (10)$$

Consider for our purpose that modal damping is of the familiar form:

$$c_i = 2\zeta_i \lambda_i^{\frac{1}{2}}$$

where ζ_i is the ratio of viscous damping to critical viscous damping for the i^{th} mode

then

$$\bar{\xi}_{qi} = \frac{-2\omega\zeta_i \lambda_i^{\frac{1}{2}}}{(\lambda_i - \omega^2)^2 + (2\omega\zeta_i \lambda_i^{\frac{1}{2}})^2} \bar{X}_i^T \bar{F}. \quad (11)$$

The displacement amplitude \bar{X}_Q is obtained by use of Equation (6) as:

$$\bar{X}_Q = \sum_1^n \bar{X}_i \xi_{qi} = -\sum_1^n \frac{2\omega \zeta_1 \lambda_1^{\frac{1}{2}}}{(\lambda_1 - \omega^2)^2 + (2\omega \zeta_1 \lambda_1^{\frac{1}{2}})^2} \bar{X}_i \bar{X}_i^T \bar{F} \quad (12)$$

which is the solution for the quadrature component of the displacement amplitude in terms of the force amplitude, frequency and modal parameters.

K. 5 TIME RATE OF ENERGY DISSIPATION

The matrix form of Equation (3) is:

$$W = \pi \bar{F}^T \bar{X}_Q$$

where \bar{F}^T is the transpose of the force amplitude vector.

Substituting Equation (12) into the above yields:

$$W = \sum_1^n W_i = -\pi \sum_1^n \frac{2\omega \zeta_1 \lambda_1^{\frac{1}{2}}}{(\lambda_1 - \omega^2)^2 + (2\omega \zeta_1 \lambda_1^{\frac{1}{2}})^2} \bar{F}^T \bar{X}_i \bar{X}_i^T \bar{F}$$

which is equal to the energy dissipated per cycle.

The time per cycle is:

$$t = \frac{2\pi}{\omega} \quad (13)$$

and

$$\dot{W} = W \frac{\omega}{2\pi} = - \frac{\omega}{2} \sum_1^n \frac{2\omega \zeta_1 \lambda_i^{\frac{1}{2}}}{(\lambda_i - \omega^2)^2 + (2\omega \zeta_1 \lambda_i^{\frac{1}{2}})^2} = \bar{F}^T \bar{X}_1 \bar{X}_1^T \bar{F} \quad (13)$$

where

\dot{W} is the time rate of energy dissipation

K. 6 DETERMINATION OF FORCE AMPLITUDE

The harmonic excitation is the acceleration. Thomson presents the acceleration for a point (ψ_p, z_p) on the structure laying in the plane 1, 0, 3 as:

$$\begin{aligned} a_p = & \omega_0^2 \left[-\psi_p \left(\frac{C}{A}\right)^2 + \psi_p \left(\frac{C}{A}\right)^2 \sin^2 \theta \sin^2 \varphi + \psi_p \left(\left(\frac{C}{A}\right)^2 - 1\right) \right. \\ & \left. + z_p \left(\frac{C}{A}\right)^2 \sin \theta \cos \theta \sin \varphi \right] i \\ & + \omega_0^2 \left[\psi_p \left(\frac{C}{A}\right)^2 \sin^2 \theta \sin \varphi \cos \varphi + z_p \left(\frac{C}{A}\right)^2 \sin \theta \cos \theta \cos \varphi \right] j \\ & + \omega_0^2 \left[-\psi_p \left(\frac{C}{A}\right) \left(\frac{C}{A} - 2\right) \sin \theta \cos \theta \sin \varphi - z_p \left(\frac{C}{A}\right)^2 \sin^2 \theta \right] k. \end{aligned}$$

where

ω_0 is the initial spin rate

It is seen that the periodic component of the acceleration is:

$$A_{p(\phi)} = \omega_0^2 \left(\frac{C}{A}\right)^2 \left\{ \left[\psi_p \sin^2 \theta \sin^2 \varphi + z_p \sin \theta \cos \theta \sin \varphi \right] i \right.$$

$$+ \left[\psi_p \sin^2 \theta \sin \varphi \cos \varphi + z_p \sin \theta \cos \theta \cos \varphi \right] j \\ + \left[-\psi_p \left(1 - 2 \frac{A}{C}\right) \sin \theta \cos \theta \sin \varphi \right] k \left. \right\}$$

which can be separated into:

$$a_{p(\phi)} = \omega_0^2 \left(\frac{C}{A}\right)^2 \left\{ \psi_p \sin^2 \theta \left[\left(\frac{1}{2} - \frac{1}{2} \cos 2\varphi\right) i + \left(\frac{1}{2} \sin 2\varphi\right) j \right] \right. \\ \left. + \sin \theta \cos \theta \left[z_p (\sin \varphi) i + z_p (\cos \varphi) j - \psi_p \left(1 - \frac{2A}{C}\right) (\sin \varphi) k \right] \right\}$$

Which shows that the harmonic acceleration has two frequencies ϕ and 2ϕ . If a centerline model is chosen for the rotating body, ψ_p is zero and the acceleration reduces to:

$$a_{p(\phi)} = \omega_0^2 \left(\frac{C}{A}\right)^2 z_p \sin \theta \cos \theta \left((\sin \varphi) i + (\cos \varphi) j \right) .$$

The lateral acceleration along body axis 1 is:

$$i a_{p(\phi)} = \omega_0^2 \left(\frac{C}{A}\right)^2 z_p \sin \theta \cos \theta \sin \phi t \quad (14) \\ = \bar{a}_p \sin \phi t$$

since $z_p \sin \theta$ is the arm from the spin axis to point p and $\omega_0 \left(\frac{C}{A}\right)$ is a rotational velocity it is seen that the amplitude \bar{a} in the above expression is the centrifugal acceleration of point p resolved by the $\cos \theta$ term into the component normal to the rotating body centerline.

The amplitude of the forcing function can be written for point p as:

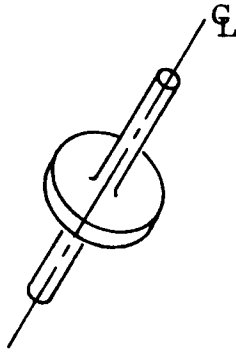
$$\bar{f}_p = m_p \bar{a}_p = \omega_0^2 \left(\frac{C}{A}\right)^2 (\sin \theta \cos \theta) z_p m_p$$

and

$$\bar{F} = \omega_0^2 \left(\frac{C}{A} \right)^2 \sin \theta \cos \theta MZ \quad (15)$$

where Z is a vector of beam locations relative to the center of gravity.

Equation (11) is an approximation and does not include the restoring gyroscopic moment. It is suitable however, for simplified models of the sort shown in Figure K-2. The system is represented as a center line having length, mass and stiffness with rotary inertia concentrated at the center of gravity of the system.



K. 7 EQUATIONS FOR SIMPLIFIED MODEL

It is desirable to bring the above equations to the form:

$$\dot{\theta} = \mathcal{K} \cdot f(\theta)$$

where \mathcal{K} is the time constant

Rewriting Equation (2):

$$\dot{\theta} = \dot{T} \frac{AC}{(C-A)h^2 \sin \theta \cos \theta} \quad (16)$$

letting $\dot{T} = \dot{W}$ and substituting Equation (13) in Equation (16) yields

$$\dot{\theta} = \frac{-AC}{(C-A)h^2 \sin \theta \cos \theta} \frac{\omega}{2} \sum_1^n \frac{2\omega \zeta_1 \lambda_1^{\frac{1}{2}}}{(\lambda_1 - \omega^2)^2 + (2\omega \zeta_1 \lambda_1^{\frac{1}{2}})^2} \bar{F}^T \bar{X}_1 \bar{X}_1^T \bar{F}$$

and substituting for \bar{F} from Equation (15):

$$\dot{\theta} = - \frac{AC}{(C-A)h^2} \omega_0^4 \left(\frac{C}{A}\right)^4 (\sin \theta \cos \theta) \omega^2 \sum_1^n \frac{\zeta_1 \lambda_i^{\frac{1}{2}}}{(\lambda_i - \omega^2)^2 + (2\omega \zeta_1 \lambda_i^{\frac{1}{2}})^2} Z^T M \bar{X}_i \bar{X}_i^T M Z_i \quad (17)$$

It is recognized from Equation (14) that

$$\omega = \dot{\phi}$$

and

$$\dot{\phi} = \omega_0 \left(1 - \frac{C}{A}\right) \cos \theta$$

also

$$h = \omega_0 C$$

substituting into Equation (17) yields:

$$\dot{\theta} = \omega_0^4 \frac{A-C}{A^2} \left(\frac{C}{A}\right)^3 (\sin \theta \cos^3 \theta) \sum_1^n \frac{\zeta_1 \lambda_i^{\frac{1}{2}} Z^T M \bar{X}_i \bar{X}_i^T M Z}{(\lambda_i - \omega_0^2 \left(1 - \frac{C}{A}\right)^2 \cos^2 \theta)^2 + (2\omega_0 \left(1 - \frac{C}{A}\right) (\cos \theta) \zeta_1 \lambda_i^{\frac{1}{2}})^2} \quad (18)$$

Under the condition that the cone angle (θ) is small

$$\cos \theta \approx 1.$$

and Equation (18) becomes:

$$\dot{\theta} = \omega_0^4 \frac{A-C}{A^2} \left(\frac{C}{A} \right)^3 \left(\sum_1^n \frac{\zeta_i \lambda_i^{\frac{1}{2}} Z^T \underline{M} \underline{X}_i \underline{X}_i^T M Z}{\lambda_i - \omega_0^2 \left(1 - \frac{C}{A}\right)^2 + \left(2\omega_0 \left(1 - \frac{C}{A}\right) \zeta_i \lambda_i^{\frac{1}{2}}\right)^2} \right) \sin \theta \quad (19)$$

which is the form desired.

K. 8 SOLUTION OF SIMPLE MODEL

The fundamental frequency of the ATS-4 spacecraft will be above 10 cps and it will be spun at ~ 1 rad/sec. This yields a ratio λ/ω_0^2 of ~ 3600 and it is seen that Equation (19) can be approximated with good accuracy by:

$$\dot{\theta} = \omega_0^4 \frac{A-C}{A^2} \left(\frac{C}{A} \right)^3 \left(\sum_1^n \frac{\zeta_i}{\lambda_i^{\frac{3}{2}}} Z^T \underline{M} \underline{X}_i \underline{X}_i^T M Z \right) \sin \theta. \quad (19a)$$

Let $\omega_0 = 2\pi f_0$
 $\lambda_i = 4\pi^2 f_i^2$

then Equation (19a) is

$$\dot{\theta} = 2\pi f_0^4 \frac{A-C}{A^2} \left(\frac{C}{A} \right)^3 \left(\sum_1^n \frac{\zeta_i}{f_i^3} Z^T \underline{M} \underline{X}_i \underline{X}_i^T M Z \right) \sin \theta \quad (19b)$$

which is an easy form for evaluating.

It is apparent from Equation (19b) that the rate of cone angle will be dominated by the fundamental with higher frequency modes consuming much less energy, therefore only the fundamental (10 Cps) mode need be considered.

Given

$$f_0 = 1 \text{ cps}$$

$$C = \frac{1.62}{386} \times 10^6 \frac{\text{lb-in.}^2 \text{-sec}^2}{\text{in.}} = 0.42 \times 10^4$$

$$\frac{A}{C} = 7.1$$

$$\text{weight} = 4000 \text{ lb}$$

Assume

$$f_i = 10 \text{ cps}$$

$$M_{\text{eff}} = \frac{1200}{386} \frac{\text{lb-in.}^2 \text{-sec}^2}{\text{in.}}$$

$$Z_{\text{eff}} = 8 \times 12 \text{ in.}$$

Since

$$\bar{X}^T M \bar{X} = 1$$

$$\bar{X} = (M_{\text{eff}})^{-1/2}$$

then

$$Z^T \bar{M} \bar{X}^T M Z = 64 \times 144 \times \frac{1200}{386} = 2.86 \times 10^4$$

and

$$\begin{aligned}\dot{\theta} &= \frac{2\pi(7.1-1) \times 0.42 \times 10^4}{(7.1)^2 (0.42 \times 10^4)^2} \left(\frac{1}{7.1}\right)^3 \frac{\zeta}{10^3} 2.86 \times 10^4 \sin \theta \\ &= \frac{2\pi \times 6.1 \times 2.86 \times 10^4}{(7.1)^5 \times 0.42 \times 10^7} \zeta \sin \theta = 1.45 \times 10^{-5} \zeta \sin \theta \\ &0.18 \times 10^5\end{aligned}$$

Converting this result into $^{\circ}$ /hour

$$\begin{aligned}\dot{\theta} \text{ } ^{\circ}/\text{hr} &= \dot{\theta} \text{ rad/sec} \times 57.2 \text{ } ^{\circ}/\text{rad} \times 3600 \text{ sec/hr} \\ &= 1.45 \times 5.72 \times 3.6 \times 10^{-1} \zeta \sin \theta \\ \dot{\theta} &= 2.98 \zeta \sin \theta \text{ } ^{\circ}/\text{hr}.\end{aligned}$$

Damping for a spacecraft such as the ATS-4 may vary from 2 to 10 percent of critical viscous damping. Assuming the high value, (10 percent) yields a time constant of:

$$\mathcal{K} = 0.298 \text{ } ^{\circ}/\text{hr}/\text{radian}.$$

At a cone angle of 10° the cone rate is:

$$\dot{\theta} = 0.0517 \text{ } ^{\circ}/\text{hr}$$

which appears to be a very slow rate.

APPENDIX L

L.1 ELEMENTS OF MONOPULSE

The system under discussion here is a simultaneous lobe comparison system. The term monopulse arose from radar applications. Early precision tracking radars obtained their angle data by means of sequential lobe comparison, using either lobe switching or conical scan techniques. It was found that with either of these techniques, the reflectance of the target and hence the amplitude of the returned echo would vary between the successive lobes (this rapid variation in target reflectance is known as scintillation). Sometimes transmitter power, receiver sensitivity, etc., also varied between one lobe and another. Such variations cause errors in amplitude comparisons and hence in angle measurements. This particular error was overcome by generating all lobes (usually four) simultaneously. By this means a complete angle measurement could be made with one pulse, eliminating all errors caused by time varying parameters; hence the term monopulse.

The value of monopulse techniques for obtaining precise measurement of angles rests on the fact that very small changes in angle cause relatively large changes in the difference pattern, and hence in signal amplitude.

By generating two lobes symmetrical about the electrical axis of an antenna, a system can be obtained in which the signals obtained from a source are equal in the two lobes when and only when the electrical axis of the antenna is pointed (in the plane of the two lobes and the source) directly toward the source. A relatively small change in the direction of the electrical axis will cause the signal to increase in one lobe and decrease in the other. By comparison of amplitudes of the two signals, an error signal can be generated, which can be used either to measure the angle or to drive a control system to point the antenna toward the signal source.

As applied to the ATS-4, the monopulse feed would be incorporated into the feed cluster, probably at one of the frequencies specified for receiver experiments. The necessary signal processing equipment would be incorporated on board the spacecraft. Error signals would

be transmitted to ground by telemetry. In addition, the error signals can be applied, through appropriate filters, gain, and impedance matching circuitry to the attitude control system. In space, once the operational reliability of the system has been demonstrated, it will be possible to close the loop and demonstrate actual pointing of the antenna with the lobe comparison system.

L. 2 ACCURACY

Obtainable accuracy is one of the major characteristics of the monopulse system, and the potential for high accuracy is one of the primary reasons for considering the technique.

A detailed error budget would include all the equipment and propagation errors and is beyond the scope of the present report. A first estimate of such an error budget is presented later in this section. A useful first approximation can be obtained by considering the basic limiting parameters, antenna beamwidth and signal-to-noise (S/N) ratio. By proper system design, the errors from other causes may be restricted to the same order of magnitude.

The thermal noise and beamwidth limitations on angular accuracy are given by:

$$\sigma_t = \frac{\lambda \sqrt{1 + \frac{P_s}{P_n}}}{d_o \left(\frac{P_s}{P_n} \right) \sqrt{2 TW}} \quad (1)$$

where

σ_t = accuracy (to the 1σ point) in radians

$\frac{P_s}{P_n}$ = signal-to-noise power ratio

λ = wavelength

d_o = effective length of the antenna

T = measurement time, in seconds

W = bandwidth, in Hz

For situations in which $\frac{P_s}{P_n} \gg 1$; i. e., where the signal-to-noise ratio is large; one can write:

$$\sigma_t \approx \frac{\tau}{d_o} \frac{1}{\sqrt{\frac{2E}{N_o}}} \quad \text{Radians} \quad (2)$$

where

$E = \text{Signal energy } P_s T$

$N_o = \text{Noise power (cycle per second)} = \frac{P_n}{W}$

For a circular aperture of radius R , $d_o = \pi R$, and:

$$\sigma_t \approx \frac{2}{\pi} \left(\frac{\lambda}{R}\right) \frac{1}{\sqrt{\frac{2E}{N_o}}} \quad (3)$$

Since the beamwidth $\theta_\beta = \frac{\lambda}{R} \frac{1}{\sqrt{\pi}}$ for small θ_β :

$$\sigma_t \approx \frac{\theta_\beta}{\sqrt{\frac{2}{\pi}} \sqrt{\frac{E}{N_o}}} \quad \text{radians}$$

or

$$\frac{\sigma_t}{\theta_\beta} \approx \sqrt{\frac{2}{\pi}} \sqrt{\frac{1}{\frac{E}{N_o}}} \quad (4)$$

The expression $\frac{\sigma_t}{\theta_\beta}$ indicates the improvement in terms of beamwidths. For example, if $\frac{\sigma_t}{\theta_\beta} = \frac{1}{100}$, the angular accuracy of the system as permitted by the thermal noise will be $\frac{1}{100}$ beamwidth.

For $\frac{\sigma}{\theta_{\beta}} = \frac{1}{100}$, one obtains from Equation 4:

$$\begin{aligned} \frac{E}{N_0} &= 6.363 \times 10^3 \\ &= 38 \text{ dB.} \end{aligned}$$

It is presently a fair rule of thumb that $\frac{1}{100}\theta_{\beta}$ is about the limiting thermal accuracy for a good tracking monopulse installation. Improvement beyond this point becomes increasingly difficult; and also increasingly less important, since other errors will begin to predominate.

In the ATS-4 system, a $\frac{\sigma}{\theta_{\beta}}$ of $\frac{1}{100}$ would result in noise-limited accuracies of the order of 0.01 to 0.015° at S-Band and 0.003° or better at X-Band, provided that S/N ratios in the neighborhood of 40 dB can be obtained. Such accuracies are better than required, and in any well designed system will probably not be more than a reasonable share of the total error budget.

A preliminary estimate of errors is shown in Table L-1 below. It must be emphasized that this estimate is based only on a preliminary analysis. For more reliable and precise estimates, a thorough study would be required. It must also be pointed out that these accuracies are "on-boresight" accuracies. Errors within the field of view but off boresight will tend to be somewhat larger.

Table L-1. Estimated Errors for ATS-4 Lobe Comparison System

Source	Estimated Error, Degrees	Estimated Error, mr	Comment
Thermal Noise	3×10^{-3} to 1.5×10^{-2}	5×10^{-2} to 2.5×10^1	$\frac{1}{100}$ Based on experience with operational tracking radars and precision (MISTRAM) interferometers
Microwave Components and Geometric Distortions	3.51×10^{-3}	0.061	
Signal Processing	2.8×10^{-3}	0.048	
Total (rms)	9×10^{-3}	0.083	

L.3 FIELD OF VIEW

The field of view (FOV) of a lobe comparison system is limited to the peaks of the offset lobes. Since the offset at each lobe is usually to about the 2 to 3 dB point, the field of view will be approximately one beamwidth wide.

(The exact FOV for a given system will depend upon quite complex system and equipment considerations. Discussion of the tradeoffs involved is beyond the scope of this report.)

Beyond the lobe peaks, the output of the lobe comparison system may give false readings. It is also possible for a false lock-on to occur on a side lobe, depending of course, upon the side lobe structure.

Because of FOV limitations, the ability of a lobe comparison system to measure offset angles is limited to small angles (of the order of half a beamwidth). Other techniques must be used to measure larger angles, and also to bring the antenna within the operating range of the lobe comparison system, approximately a half-beamwidth either side of the beacon.

L.4 ONBOARD EQUIPMENT REQUIREMENTS

A monopulse system will impose additional onboard equipment requirements in the following areas:

- a. Feeds. Nominally, four feeds are required for lobe comparison, two for each of two orthogonal angles. However, a technique of producing the four lobes with a single feed is available.

The procedure is to excite the TM_{01} mode in a circular horn, comparing its phase and amplitude against two orthogonal components of the TE_{11} mode. When receiving circular polarization the TM_{01} mode effectively produces the difference pattern with a null on boresight. The waveguide and horn must be of sufficiently large electrical diameter to support the TM_{11} mode; dielectric loading may be required to accomplish this.

If such a technique were applied to the ATS-4 system, only the inner horn of the proposed coaxial horn feed structure would be available. This would restrict the monopulse system to the 7-8 GHz range. However, this would probably be the most desirable range. The additional weight of the feed system suggested above would be less than 1 pound, that of a conventional 4-horn feed about 4 pounds.

- b. Rf System. The lobe-comparison modification, whether using the feed system suggested above or four independent feeds, requires at least three and possibly four independent rf channels. In the ATS-4 configuration presently suggested, the physical lengths required for rf conduits can be small. In this configuration, total additional rf weight will probably be 1 to 2 pounds.
- c. Receivers. Nominally, four separate receivers are required for the four independent channels of a lobe comparison system. These may be combined into a single IF if desired. Details will depend upon the design of the system. A conservative estimate for these receivers is approximately 2 pounds each, or a total of 8 pounds, 6 of which are chargeable to the monopulse system. (One receiver would be required for receiver experiments, but the other 3 are required by the lobe comparison experiment).
- d. Signal Processing. The derivation of the error signal requires a signal amplitude comparison. This is essentially a simple procedure. However, the necessity for calibration and/or compensation for drift, nonlinearity, etc., in the electronics will complicate the process considerably.

The weight required for accomplishing the total processing will have to be determined by a design study. However, a reasonable estimate at this point is about 4 pounds. This includes provision for matching to the orientation control system, as well as coupling to the telemetry (TLM) commutator for transmission of error signals to the OCC.

The ground system requirements of the monopulse installation include monopulse beacons of all ground stations which are to be used, and minor additions to displays and computer software.

The beacon requirements for monopulse are quite modest. Link calculations for the monopulse installation for both a large ground station and a low-orbit spacecraft, are shown in Table L-2. Similar requirements for the radio interferometer are included for comparison purposes. A direct comparison of monopulse performance with that of the radio interferometer is given in Table L-3. Summary of the effects on the experiments integration system of the incorporation of monopulse is given in Table L-4.

The possibility exists of substituting the monopulse for the interferometer, rather than adding the monopulse to the system. The advantages of such a substitution would be:

- a. Weight reduction - 20 to 40 pounds
- b. Power reduction - 25 watts
- c. Slight reduction in rf complexity
- d. Reduction in beacon ERP, simplifying the small-station tracking problems
- e. High-accuracy measurement of electrical boresight of parabolic antenna
- f. Demonstration of monopulse

Table I.-2. Link Calculations for Monopulse and Interferometer*

	(With OCC)		(With Low-Orbit Spacecraft)	
	Interferometer	Mono-pulse	Interferometer	Mono-pulse
P_{out}	+ 12 dBw 15.9 watts	- 33 dBw 0.5 mw	+12 dBw 15.9 watts	-13 dBw 50 mw
Transmtr Ant. Gain	+57 dB	+55 dB	+37 dB	+35 dB
ERP	+69 dBw	+22 dBw	+49 dBw	+22 dBw
Miscellaneous System Losses	-3 dB	-3 dB	-3 dB	-3 dB
Net ERP	+66 dBw	+19 dBw	+46 dBw	+19 dBw
Path Loss	-204 dB	-204 dB	-204 dB	-200 dB
Power Density at Receiver Antenna	-138 dBw	-181 dBw	-158 dBw	-181 dBw
Receiver Ant. Gain	+10 dB	+55 dB	+20 dB	+55 dB
Power at Receiver Terminals	-128 dBw	-126 dBw	-138 dBw	-126 dBw
Converter Input	-128 dBw	-126 dBw	-138 dBw	-126 dBw
Receiver Noise Figure	10 dB	10 dB	10 dB	10 dB
Reference	-138 dBw	-136 dBw	-148 dBw	-136 dBw
KTb	-174 dBw	-174 dBw	-174 dBw	-174 dBw
S/N	+36 dB	+38 dB	+26 dB	+38 dB

* Interferometer - 10 GHz
Monopulse - 8 GHz

Table L-3. Estimated Performance Comparison Interferometer and Monopulse

Parameter	Interferometer	Monopulse
Accuracy	0.01°, 1, 10 cps	0.009° to 0.015°, 1 on boresight 1 to 10 cps
Field of View	23.5°	0.3° to 1°
Rf Complexity	Feeds 40-60 λ apart dimensional stability to about 0.01 inch required. Little difficulty anticipated.	Multiple or dielectric loaded feeds, little difficulty anticipated
Parabolic Antenna Efficiency	No effect	Reduction to below required 50% at 7-8 GHz
Equipment Weight	35 pounds basic 55 pounds complete	12 pounds basic 15 pounds complete
Prime Power	50 watts	10 watts
Ground Equipment	High ERP* beacon	Low ERP beacon, but are required for every station worked
Tracking	Difficulty in meeting ERP requirements in small aircraft and spacecraft	Can readily meet ERP requirements in aircraft and spacecraft
Prime Experiment Requirements	As designed can meet experiment requirements	Cannot demonstrate interferometer pointing for non-antenna uses, as required in RFP
Additional	Difficulty with tracking	Readily meets tracking requirements
	Precision yaw angle measurement possible	Not possible
	Synthetic angle generation	Not possible
System Complexity	Minimal; instrument is largely self-contained	Requires considerable support because of limited FOV and possibility of false lock-on

*ERP is effective radiated power; includes transmitter power and transmitter antenna gain

Table L-3. Estimated Performance Comparison Interferometer and Monopulse
(Continued)

Parameter	Interferometer	Monopulse
Angle Measurement	Can measure large angles accurately and work with multiple station	Limited by FOV to small angles and one station, or stations very close together
Cascading of Experiment	Independent	Dependent upon proper operation of parabolic antenna
Feasibility Demonstration	Feasibility of Interferometer	Feasibility of monopulse
Boresight	No boresight determination of antennas	Directly determines electrical boresight of parabolic antenna
Support of antenna pattern and orientation control measurement	Straightforward over entire measurement by accurate measurement of large angles	Limited to small angles by FOV

Table L-4. System Effects of Incorporation of Monopulse System

Characteristics	Effects
Accuracy	Nominal improvement
Field of View	No effect
Rf Complexity	Modest increase in feed and rf lines complexity
*Parabolic Antenna Efficiency	Reduces to < 50% at 7-8 GHz
Equipment Weight	Adds about 12-15 pounds
Prime Power	Adds about 10 watts for some experiments
Ground Equipment	Adds processing requirement for control and evaluation of monopulse experiment; also monopulse beacons.
*Tracking	Reduces aircraft and spacecraft beacon ERP to manageable proportions. If interferometer tracking is incorporated, provides an additional verification and (if lower accuracy must be accepted by the interferometer in the tracking mode because of beacon ERP requirements) monopulse may provide some improvement in accuracy.
*Prime Experiment Requirements	Provides important additional verification of interferometer accuracy and precision in both open and closed loop modes
Additional Interferometer Experiments	No effect
System Complexity	Some increase due to limited FOV and possible false lock-on
Angle Measurement	No effect
Cascading of Experiments	No effect
*Feasibility Demonstration	Both interferometer and monopulse
*Boresight	Excellent measurements, including interferometer/monopulse alignment
Support of Antenna Pattern and Orientation Control Measurements	Considerably improved

* Considered important

The disadvantages would be:

- a. Additional system complexity, to prevent false lock-on, etc.
- b. No support for antenna pattern measurements and Orientation Control measurements.
- c. Inability to meet prime experiment requirements for demonstration of pointing without high-gain antennas.
- d. Reduced FOV
- e. Reduction of antenna efficiency at 8 GHz
- f. No support for additional interferometer experiments
- g. No demonstration of interferometer performance
- h. Cascading of experiments

These effects are listed in detail in Table L-5. Largely because of poor support for Orientation Control measurements and antenna off-boresight lobe analysis, and the fact that no evaluation of a radio interferometer would be obtained, this substitution is not recommended.

Table L-5. Estimated Effects of Substitution of Monopulse for Interferometer

Characteristics	Effects
Support of Antenna Pattern and Orientation Control Measurements	Severely handicapped
Prime Experiment Requirement	Cannot meet stated requirement of investigating interferometer pointing for non-antenna purposes
Accuracy	Nominal improvement (negligible for practical purposes)
Field of View	Drastic reduction (23.5° to 0.3°)
Rf Complexity	Useful reduction - elimination of critical dimensional stability antenna at the expense of modest increase in feed complexity
Parabolic Antenna Efficiency	Reduced to below 50% at 7-8 GHz
Equipment Weight	Reduction of 20 to 40 pounds
Prime Power	Reduction of about 25 watts
Ground Equipment	Reduction of about 30 dB in required ERP - very useful to small mobile terminals
Tracking	Reduction of aircraft and spacecraft tracking to a simple problem so far as ERP is concerned
Additional Experiments	Deleted
System Complexity	Some increase due to limited FOV and possibility of false lock on
Angle Measurement	Cannot measure large angles or work with widely separated multiple stations
Cascading of Experiments	Dependent upon proper operation of parabolic antenna
Feasibility Demonstration	Monopulse instead of interferometer
Boresight	Excellent measurement of parabolic antenna boresight

L.6 GROUND EQUIPMENT REQUIREMENTS

No special additional requirements for ground equipment are immediately apparent. Such requirements may develop as the problem is examined further.

The beacon requirements may be considerably relaxed, according to the link calculations, as compared to the interferometer. This particularly simplifies the beacon problem for small stations.

One limitation is apparent: Since precision measurements of offset angles is not feasible, use of the technique for stations not having a beacon - e.g., to point another antenna at a second station - will not be possible.

L.7 SYSTEM CONSIDERATIONS

There are a number of system considerations in the regard to the monopulse technique, advantages and disadvantages. These are summarized in Table L-4. The importance of these considerations to a particular system will depend upon the mission and system objectives and the system design considerations.

- a. Flexibility. The interferometer will be used, as presently contemplated, to demonstrate the capabilities and limitations of such an instrument in pointing not only the antennas but also the spacecraft and any other instrument (TV cameras, meteorological sensors, etc.) which require precision earth pointing. The lobe comparison system, being dependent on a highly directional antenna, will not be available for precision pointing in the absence of such an antenna, hence might not be as useful in pointing of nonradio instruments, as in meteorological satellites. Thus the lobe comparison system will not entirely fulfill the requirements of the interferometer prime experiment.
- b. Alternate Pointing Techniques. The monopulse will provide a very useful additional pointing technique if used as a supplement to the radio interferometer. It can be used as an additional check on the accuracy and precision of the interferometer, and also to measure precisely the interferometer/antenna boresight alignment.
- c. FOV. The limited FOV of the monopulse system precludes measurement of large angles, work with multiple ground stations simultaneously, etc., if used in place of the interferometer. In addition, a supplementary pointing scheme will be required to point the antenna to within one-half beamwidth of the target point.

d. System Complexity. The complexity of the system procedures required for monopulse will be somewhat greater than that required for the interferometer:

1. The interferometer can home on any point on the visible disc; the monopulse must be pointed within \pm one-half beamwidth.
2. In the interferometer, ambiguity resolution is incorporated; the monopulse in closed loop operation must be supported by a backup system which takes over automatically if the error exceeds one-half beamwidth.

In open loop processing, the monopulse error signal must be compared with the half-beamwidth and checked with the signals from the backup system.

e. Beacon Power. Because of the high gain of the large parabolic antenna, the monopulse can work with a much lower effective radiated power (ERP) on the ground than can the interferometer. This advantage will be at least 30 dB, and may be as high as 45 dB. The relevant link calculations are shown in Table L-2.

f. Tracking. If experimental tracking of a low-orbit spacecraft proves feasible, the gain advantage to the monopulse system described above will considerably simplify the beacon problem. Link calculations bearing on this situation are also shown in Table L-2.

g. Cascading of Experiments. The monopulse system will be incorporated in the parabolic antenna system; therefore, if the monopulse is used in the place of the interferometer, a failure (e. g., deployment abort) of the parabolic antenna will abort both the antenna and the pointing experiments.

h. Feasibility Demonstration. Demonstration of monopulse pointing and investigation of its capabilities and limitations will be a potential benefit of the monopulse experiment whether used in place of or in addition to the interferometer.

i. Boresight. The monopulse system will permit, at the frequency used, extremely precise determination of the electrical boresight of the parabolic antenna, and of boresight misalignments if any, between the antenna, the interferometer, the attitude control sensors, etc.

j. Support of Other Experiments. The interferometer, by its capability for measuring angles, can be used in support of antenna pattern measurements and orientation control measurements. The monopulse system, because of its limited FOV, could not provide this support.

L. 8 SUMMARY AND RECOMMENDATIONS

The estimated effects upon ATS-4 system performance and costs of the incorporation of monopulse are shown in Tables L-3, L-4 and L-5 of the present section. These tables are intended to show the performance and effects of the three major alternatives in regard to monopulse, i. e. :

- a. Reject the monopulse experiments
- b. Substitute the monopulse for the interferometer
- c. Incorporate the monopulse together with the interferometer

Table L-3 compares the estimated performance of the monopulse and interferometer systems.

Table L-4 summarizes the estimated effects upon system performance of incorporating the monopulse as a supplement to the interferometer.

Table L-5 summarizes the estimated effects upon system performance of substituting the monopulse for the interferometer.

As can be seen from the tables, the monopulse could save from 20 to 50 pounds if substituted for the interferometer, but at the cost of some compromise of the primary pointing experiment.

Adding the monopulse experiment would cost approximately 12 pounds, but would permit additional experiments and would provide additional verification in the pointing experiment.

L. 9 REFERENCES

The following references were consulted in assembling the material for this report:

1. Skolnik, M. I., "Introduction to Radar Systems," McGraw-Hill Book Company, Inc., New York, 1962.
2. Rhodes, D. R., "Introduction to Monopulse," McGraw-Hill Book Company, Inc., New York, 1959.

3. Manasse, R. , "Maximum Angular Accuracy of Tracking a Radio Star by Lobe Comparison," IRE Transactions, PGAP, pp. 50-56, January 1960.
4. Watters et al. , "Angle Determination by Means of Radar," IRE Transactions, PGMIL, pp. 317-325, October 1961.
5. Rubin, W. L. , Kamen, S. K. , SCAMP - "A Single-Channel Monopulse Radar Signal Processing Technique," IRE Transactions, PGMIL, pp. 146-152, April 1962.
6. Powell, Thomas H. , Jr. , "Angular Accuracy of Monopulse Radar," Thesis, Drexel Institute of Technology, College of Engineering, Graduate Studies, Department of Electrical Engineering, June 1966.
7. Howard, Dean D. , "Single Aperture Monopulse Radar Multi-Mode Antenna Feed and Homing Device," International Convention on Military Electronics, 1964.
8. Barton, D. K. , Final Report, Instrumentation Radar AN/FPS-16 (XN-2), report from the Radio Corporation of America, Defense Electronics Products, Missile and Surface Radar Division, Moorestown, New Jersey.

APPENDIX M
PLUME CALCULATIONS
FOR
WALTER KIDDE TWO-POUND THRUST NOZZLE
AND FOR A RESISTANCE JET AMMONIA NOZZLE

Method of characteristics nozzle-plume calculations were carried out for two nozzles, an existing two-pound nozzle and a 0.001 pound resistance jet, both exhausting to vacuum. (An existing two-pound nozzle which produces conservative results for a one-pound nozzle was investigated.) Plots of streamlines are presented in Figures M-1 and M-3 to indicate the extent of plume impingement on surfaces adjacent to the nozzle exit. Lines of constant Mach number have been plotted in Figures M-2 and M-4 to permit calculation of forces acting on any objects that might be in the plume. (Since an ideal gas assumption was used, the constant Mach number lines also represent lines of constant pressure, temperature, and density. Values of pressure, temperature and density which correspond to the Mach numbers of Figures M-2 and M-4 appear in Tables M-1 and M-2.

The results show that it is apparent (Figure M-1) that the Kidde plume will not impinge on a surface which is flush with the nozzle exit plane. The turning of the plume boundary is somewhat greater for the ammonia nozzle (Figure M-3), but even there, less than 1/2% of the flow turns far enough to impinge on a surface which is flush with the exit plane.

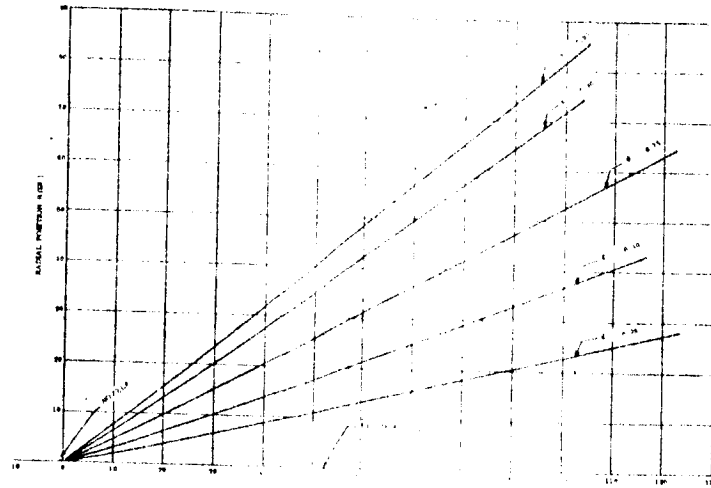
Constant Mach number lines have been plotted (Figures M-2 and M-4) for Mach numbers as large as 60. At such high Mach numbers, pressures are too low to justify continuum calculations. However, the forces which the plume exerts on objects in the high Mach number regions are negligible because the pressures are extremely small as indicated in Tables M-1 and M-2.

Table M-1. Kidde Two-Pound Thrust Nozzle

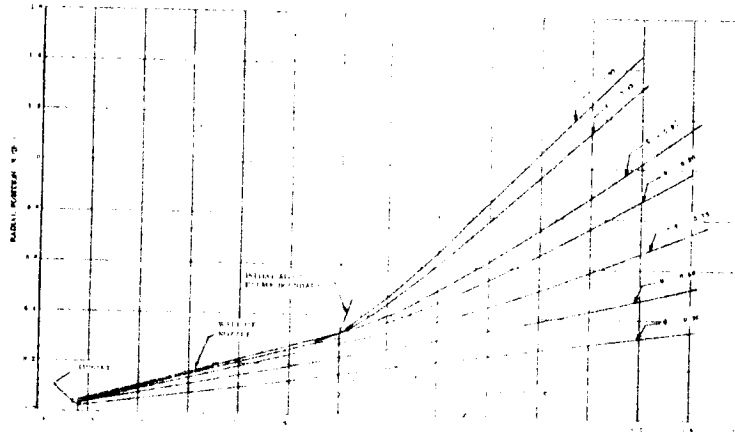
M	P (PSF)	ζ (slugs/ft ³)	T (°R)
2.5	3.360×10^3	7.392×10^{-4}	969.0
5.0	9.108×10^0	5.232×10^{-5}	373.8
10.0	8.388×10^{-1}	1.668×10^{-6}	108.3
15.0	4.404×10^{-2}	1.908×10^{-7}	49.6
20.0	5.316×10^{-3}	4.032×10^{-8}	28.3
30.0	2.544×10^{-4}	4.320×10^{-9}	12.7
40.0	2.880×10^{-5}	8.676×10^{-10}	7.1
50.0	5.148×10^{-6}	2.118×10^{-10}	4.5
60.0	1.308×10^{-6}	8.940×10^{-11}	3.1

Table M-2. Ammonia Nozzle

M	P (PSF)	ζ (slugs/ft ³)	T (°R)
2.5	118.5	0.218×10^{-4}	1330.9
5.0	2.156	0.953×10^{-6}	554.0
10.0	0.874×10^{-2}	0.129×10^{-7}	166.1
15.0	0.241×10^{-3}	0.765×10^{-9}	77.3
20.0	0.192×10^{-4}	0.107×10^{-9}	44.0
30.0	0.502×10^{-6}	0.629×10^{-11}	19.7



a. Unexpanded View



b. Expanded View

Figure M-1. Kidde Two-Pound Thrust Nozzle Constant Streamlines

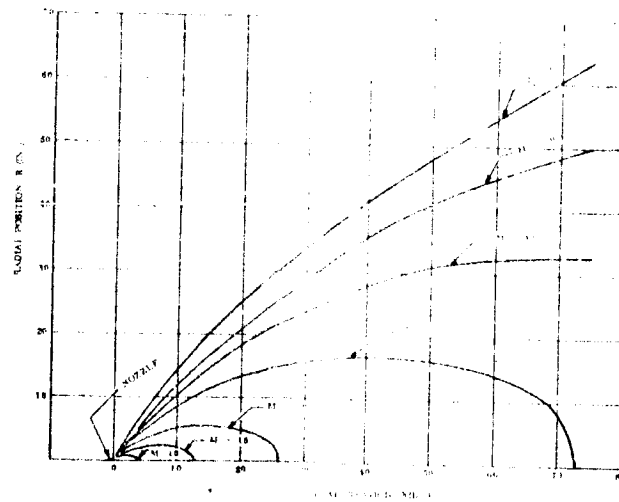
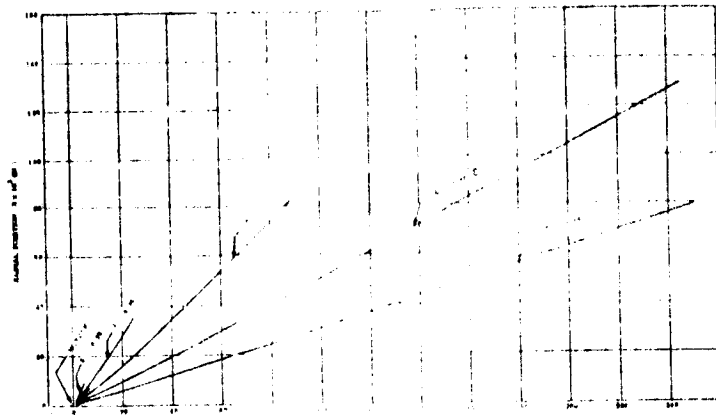
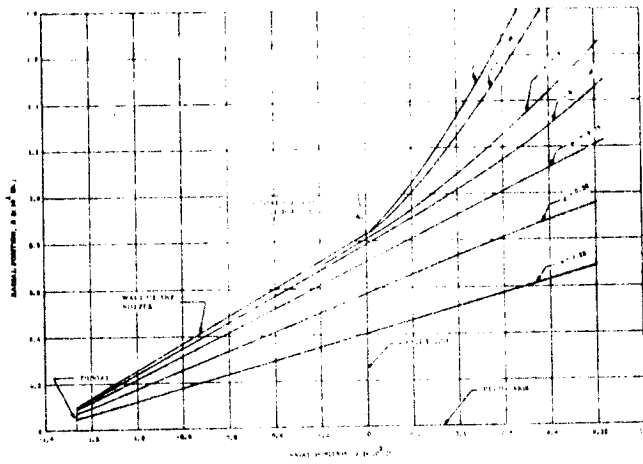


Figure M-2. Constant Mach Number Lines



a. Unexpanded View



b. Expanded View

Figure M-3. Ammonia Nozzle Constant Streamlines

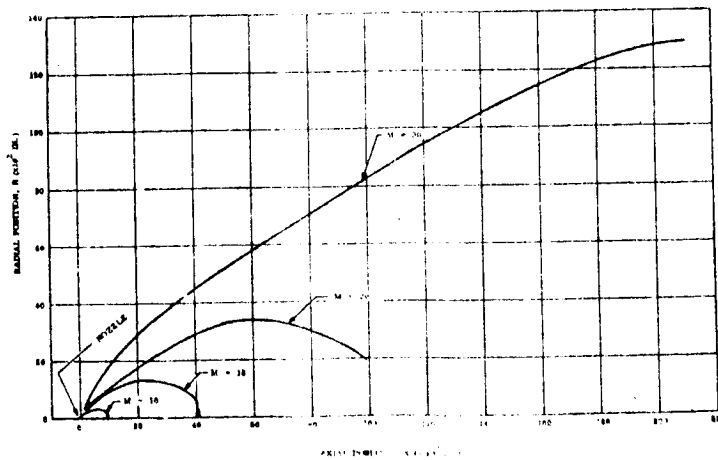


Figure M-4. Ammonia Nozzle Constant Mach Number Lines